



# Hydrological Conceptualisation of the Walyarta Mound Springs

Jasmine Rutherford<sup>1</sup>, Dioni I. Cendón<sup>2</sup>, Camilla Soerensen<sup>3</sup>, Steven Batty<sup>4</sup>, Bart Huntley<sup>1</sup>,  
Lindsay Bourke<sup>1</sup>, Adrian Pinder<sup>1</sup>, Kirsty Quinlan<sup>1</sup>, Val English<sup>1</sup> and Mike Coote<sup>1</sup>

DEPARTMENT OF BIODIVERSITY, CONSERVATION AND ATTRACTIONS

WETLANDS CONSERVATION PROGRAM

July 2018

<sup>1</sup>Department of Biodiversity, Conservation and Attractions

<sup>2</sup>Australian Nuclear Science and Technology Organisation (ANSTO)

<sup>3</sup>CSIRO Mineral Resources

<sup>4</sup>Target Geoscience



Department of **Biodiversity,**  
**Conservation and Attractions**

**BHP**

Department of Biodiversity, Conservation and Attractions  
Locked Bag 104  
Bentley Delivery Centre WA 6983  
Phone: (08) 9219 9000  
Fax: (08) 9334 0498

[www.dbca.wa.gov.au](http://www.dbca.wa.gov.au)

© Department of Biodiversity, Conservation and Attractions on behalf of the State of Western Australia 2018  
July 2018

This work is copyright. You may download, display, print and reproduce this material in unaltered form (retaining this notice) for your personal, non-commercial use or use within your organisation. Apart from any use as permitted under the *Copyright Act 1968*, all other rights are reserved. Requests and enquiries concerning reproduction and rights should be addressed to the Department of Biodiversity, Conservation and Attractions.

This report/document/publication was prepared by Jasmine Rutherford

Questions regarding the use of this material should be directed to:  
Senior Hydrologist  
Wetlands Conservation Program  
Department of Parks and Wildlife  
Locked Bag 104  
Bentley Delivery Centre WA 6983

The recommended reference for this publication is: Rutherford, J.L., Cendón, D.I., Soerensen, C., Batty, S., Huntley, B., Bourke L., Pinder, A., Quinlan, K., Val English and Mike Coote (2018). Hydrological conceptualisation of the Walyarta Mound springs. Department of Biodiversity, Conservation and Attractions, Wetlands Conservation Program, Perth Western Australia.

#### **Disclaimer**

While all reasonable care has been taken in the preparation of the information in this document, the Chief Executive officer of the Department of Biodiversity, Conservation and Attractions and its officers and the State of Western Australia accept no responsibility for any errors or omissions it may contain, whether caused by negligence or otherwise, or any loss, however caused, arising from reliance on, or the use or release of, this information or any part of it.

#### **Acknowledgements**

The following are acknowledged for their assistance at various stages during this project.

We respectively acknowledge the Nyangumarta as the traditional owners of the land on which the spring survey was conducted. We are grateful to you for imparting your cultural knowledge, for introducing us to the springs and wetlands of Walyarta and for assistance in the 2015 and 2016 field surveys.

DBCA Principal Ecologist Val English for requesting the investigation, Glenn Harrington for undertaking the sampling and reporting preliminary results and staff of the Kimberley Region, in

particular Tracy Sonneman and Naomi Findlay, for invaluable advice and assistance in coordinating the field programs.

BHP Billiton for funding this work through the Eighty Mile Beach and Walyarta Conservation Program 2014-17.

Department of Water and Environmental Regulation (DWER) and Department of Primary Industries and Rural Development (DPIRD) and for sharing data collected across the Canning Basin.

*Cover photo is an aerial view of Fern Spring, courtesy of Glenn Harrington*

## Table of contents

1	Report aims and objectives.....	16
1.1	Report structure.....	16
2	Background .....	16
2.1	Geology and structure .....	16
2.2	Hydrogeology.....	17
2.3	Environmental water .....	21
2.4	Research directions.....	22
3	Physical setting.....	22
3.1	Location.....	22
3.2	Geomorphology and surficial geology .....	23
4	Geology .....	23
4.1	Canning Basin scale stratigraphy and structure.....	27
4.2	Mesozoic geology.....	27
4.1	Cenozoic geology and palaeovalleys.....	29
4.2	Canning Basin scale geological structure .....	35
4.3	Walyarta stratigraphy and structure .....	37
4.3.1	Airborne electromagnetic data (AEM).....	37
4.3.2	Airborne magnetic data .....	46
4.3.3	3D Conceptual Geological Model.....	52
5	Climate, vegetation and soils .....	61
5.1	Rainfall .....	61
5.2	Temperature and evaporation.....	61
5.3	Vegetation.....	62
5.3.1	Remote Sensing.....	64
5.3.2	Environmental isotopes .....	67
5.4	Soils .....	68
5.4.1	Remote Sensing.....	68
5.4.2	Environmental isotopes .....	74
5.4.3	Microbiology .....	75
5.4.4	SEM .....	76
6	Hydrology.....	81
6.1	Groundwater.....	81
6.1.1	Quaternary aquifers.....	81
6.1.2	Broome Sandstone Aquifer.....	90



6.1.3	Wallal Sandstone Aquifer.....	91
6.2	Surface water.....	92
6.3	Ecohydrology.....	97
6.3.1	Mound spring riparian vegetation water use and tolerances .....	97
6.3.2	Spring water quality and salt balance.....	98
6.3.3	Spring resilience indicators .....	100
7	Hydrochemistry and environmental tracers.....	101
7.1	Previous investigations .....	101
7.2	Hydrogeochemical interpretation - approach .....	104
7.2.1	Groundwater recharge - chemistry and age.....	104
7.2.2	Aquifer gradients .....	109
7.2.3	Wallal transmissivity and heterogeneity .....	112
7.3	Hydrogeochemical interpretation – results.....	114
7.3.1	Major ion data sourcing, quality assurance and modelling .....	114
7.3.2	Major ions - spatial distribution and trends .....	116
7.1	Major ions – geochemical gradients and mixing .....	124
7.1.1	Environmental isotopes .....	141
7.1.2	Hydrogeochemistry summary.....	158
8	Walyarta conceptual hydrological model .....	163
9	Conclusions and recommendations.....	166
10	References .....	168

## Appendices

Appendix 1 – Mid-Jurassic to Early Cretaceous Isopachs (from Forman and Wales 1981).....	174
Appendix 2 Geophysics – stratigraphic and structural modelling .....	180
Appendix 3 Geophysics (AEM) – interpreted stratigraphy, structure and water quality .....	186
Appendix 4 2015 Spring and Surface water Sampling Metadata .....	208
Appendix 5 Indicative regional Broome and Wallal aquifer water levels: gradients (mAHD) and depth below ground level (mbgl) (from the DWER in prep) .....	213
Appendix 6 AEM conductivity depth profiles for major spring and surface water sites .....	216
Appendix 7 Hydrogeochemical Database .....	220
Appendix 8 Hydrogeochemistry – Correlation Matrices .....	224

## Tables

Table 1 Drill-holes with lithological logging in the Walyarata Conservation Park (data from DWER Water Information Network (WIN)).	37
Table 2 Rainfall statistics for BOM Mandora station (#4019).	61
Table 3 Carbon and Nitrogen isotopes $\delta^{13}\text{C}$ , $\delta^{15}\text{N}$ for major plant species at Fern, Melaleuca and Saunders Springs.	67
Table 4 Fern, Melaleuca and Saunders Springs Peat substrate analyses; Carbon and Nitrogen isotopes $\delta^{13}\text{C}$ , $\delta^{15}\text{N}$ , moisture (%), volumetric water content, EC1:5 and pH.	74
Table 5 Inundation frequency calculated for WOfS sample locations in Figure 49.	95
Table 6 Field groundwater TDS compared with AEM derived TDS measurements for aquifers underlying the springs and surface water sampling sites; major aquifer sustaining springs=blue; field samples indicating evaporation field sample=green; sequential aquifer mixing during discharge=orange, equilibration with surface sediments=yellow, and throughflow-discharge=pink.	99
Table 7 Spring resilience indicators as a function of Wallal Sandstone aquifer hydraulics, lower potential resilience highlighted in red.	101
Table 8 Formations and mineralogy mapped and discussed in Hickman and Gibson (1982), Towner (1982a), Williams (2003) with organic carbon sources highlighted in purple and inorganic carbon sources in blue (see Figures 8 & 9 for geological map and key).	106
Table 9 Environmental isotope data for DBCA spring and surface water sampling (2015 & 2016), samples selected for graphing in Figures 71 to 76 are highlighted in grey (see Appendix 7 for expanded information on location and chemistry) (Note accuracy elevation (mAHD) is derived from the SRTM1s hydrologically corrected DEM).	129
Table 10 Environmental isotopes and Sr and Rb ( $\mu\text{mol/L}$ ) sampling examined in this report	142

## Figures

Figure 1 Location map of Walyarta/Mandora Marsh with information on management and private land holder boundaries (from DPaW 2016).	18
Figure 2: Generalised stratigraphy of the major formations of the Canning Basin (modified from GSWA 2012a).	19
Figure 3: Top; map of the major tectonic elements and structures of the Canning Basin (modified from Parra-García et. al. 2012) and below a pseudo colour perspective view of modelled basement topography for the Canning Basin (from GSWA 2016); red arrow showing the approximate location of the Walyarta mound springs.	20
Figure 4 Location of Walyarta hydrological study area superimposed on SPOT 5 Imagery (2009) with photographs showing the variation in physical environments.	24

Figure 5 SRTM1s DEM and modelled ephemeral drainage (30 metre gridded and hydrologically corrected Shuttle Radar Topography Mission (SRTM) 1 second DEM) .....	25
Figure 6 Regolith mapping in Walyarta (from digital 1:500 000 WA Regolith Map) .....	26
Figure 7 Schematic representation of palaeoenvironments responsible for the transportation and deposition of sediments in the Jurassic era (from Forman and Wales 1981) .....	29
Figure 8 1:250 000 scale mapped geology for the Mandora Sheet (SE/51-13) and the Munro Sheet (SE/51-14) (refer to Figure 9 for the Key), Note digital data are not available and the central white strip marks the join between the two maps sheets. ....	30
Figure 9 Key to mapped Mesozoic and Cenozoic (previously known as Cainozoic) geology in Figure 8 (from Towner 1982a). ....	31
Figure 10 Middle to Late-Eocene palaeogeography showing the location of the Mandora palaeo river in relation to the Walyarta mound springs (adapted from Forman and Wales 1981). ....	32
Figure 11 Regional map of the Canning Basin showing the location of the Mandora and Wallal palaeovalleys and salt lakes (modified from Magee 2009). ....	32
Figure 12 Late Pleistocene to early Holocene palaeogeography during the Flandrian transgression (17 000 to ?8 000 years ago) (adapted from Forman and Wales 1981). ....	33
Figure 13 WASANT palaeovalleys for the CB – WCB, Walyarta Conservation Park and the La Grange area overlain on greyscale image of SRTM1s DEM (modified from Bell et. al. 2012) .....	34
Figure 14a,b&c (left to right) Dominant Australasian stress-strain relationships and geological faulting styles in (a) the Late Carboniferous to Early Permian (b) Late Triassic and (c) Miocene to Recent; Arrows show the major direction of movement, dotted line-work indicates aprox movement extent, rectangle annotation - normal faulting and triangles - thrust faulting (from FrOG Tech 2005). ....	35
Figure 15 Major coarse scale Phanerozoic geological structures interpreted from modelled magnetic and gravity data overlain on greyscale image of SRTM 1s DEM (adapted from Parra-García 2014) ..	36
Figure 16 Location of E-W trending TEMPEST AEM flight lines (2km line spacing blue lines) and drill holes/boreholes with lithological logs in Walyarta and northern WCB (AEM data inverted for this study include data presented in Appendix 3 and closely spaced (50-100 metre spacing) north-south orientated flight lines – coloured purple in the above figure) .....	38
Figure 17 Example of stratigraphic and structural information from TEMPEST AEM flight line L10014 (viewed west to east; see Figure 14 for location and Appendix 3 for key).....	40
Figure 18 Pseudocoloured TEMPEST AEM interval conductivity image (0-10m) showing electrical conductivity variation in the Quaternary Formations (assuming lateral continuity) .....	41
Figure 19 Pseudocoloured TEMPEST AEM interval conductivity image (40-50m) showing electrical conductivity variation in the Broome Sandstone (assuming lateral continuity) .....	42

Figure 20 Pseudocoloured TEMPEST AEM interval conductivity image (140-150m) showing electrical conductivity variation in the Jarlemai Formation (assuming lateral continuity).....	43
Figure 21 Pseudocoloured TEMPEST AEM interval conductivity image (280-300m) showing electrical conductivity variation in the Wallal Sandstone (assuming lateral continuity) .....	44
Figure 22 Broome Sandstone relationship between groundwater TDS (mg/L) and TEMPEST AEM (average EC) in Walyarta (n=68) .....	45
Figure 23 Airborne magnetic 1VD greyscale image overlain by FrOG Tech coarse scale Phanerozoic structural interpretation and Walyarta major fault interpretation.....	47
Figure 24 Airborne magnetic 1VD greyscale and pseudo-colour TMI images overlain by Walyarta interpretation of magnetic features (geological faults, channels and strandlines).....	48
Figure 25 Walyarta major fault interpretation overlain on pseudo-colour AEM conductivity (40-50m – Broome Sandstone) and greyscale SRTM 1s images to understand relationships between major electrical conductivity pattern breaks and geological faults .....	49
Figure 26 Walyarta major fault interpretation overlain on pseudo-colour AEM conductivity (140-150m – Jarlemai Siltstone) and greyscale SRTM 1s images to understand relationships between major electrical conductivity pattern breaks and geological faults.....	50
Figure 27 Walyarta major fault interpretation overlain on pseudo-colour AEM conductivity (280-300m – Wallal Sandstone) and greyscale SRTM 1s images to understand relationships between major electrical conductivity pattern breaks and geological faults.....	51
Figure 28 Schematic example of the Walyarta oblique accommodation zone, coloured pink, direction of relay fault movement denoted by blue arrows (modified from Parra-García et. al. 2014) showing the location of the palaeovalley, palaeo-drainage and DBCA spring and surface water sample sites (location map includes key and scale). .....	53
Figure 29 Transparent cross section through the Walyarta Leapfrog conceptual model showing the SRTM 1s DEM, interpreted and gridded stratigraphic layers and drill-hole lithology (viewed south).56	
Figure 30 Isopach of Quaternary aeolian and sandplain sediments in Walyarta area; (bores with logging information on formation thickness are shown) .....	57
Figure 31 Isopach of Quaternary Formation and Broome Sandstone in Walyarta area (bores with logging information on formation thickness are shown) .....	58
Figure 32 Isopach of Jarlemai Siltstone in Walyarta area; (bores with logging information on formation thickness are shown) .....	59
Figure 33 Isopach of Wallal Sandstone in Walyarta area; ; (bores with logging information on formation thickness are shown) .....	60
Figure 34 Histogram of dry and wet season rainfall (mm) from 1914 to 2016 for BOM Mandora station (#4019); nominal seasonal periods; wet season (Nov-April) and dry season (May-Oct) .....	61

Figure 35 Graph showing average dry (red line work) and wet (blue line work) season temperatures from 1962 to 2016 for BOM Mandora station (#4019); nominal seasonal periods; wet season (Nov-April) and dry season (May-Oct) .....	62
Figure 36 Vegetation communities of the Mandora Marsh Survey 2015 Area, labelled by floristic community group code (see Section 5.4). From Markey 2017.....	63
Figure 37 ASTER VNIR-SWIR green vegetation index (high content is red and low content is blue) with location of mound springs and surface water and bores with stratigraphic information.....	65
Figure 38 ASTER VNIR-SWIR green vegetation index (high content is red and low content is blue) and below, Landsat persistent vegetation overlain on greyscale SRTM 1s image; across all of the eight driest dry seasons (coloured blue) and all but one of the eight driest dry seasons (coloured green); major geological faults in both maps are shown in white .....	66
Figure 39 ASTER MgOH group composition, red=calcite, dark areas represent vegetation and blue=cloud cover – see Figures 37 and 38. ....	69
Figure 40 ASTER MgOH Group Composition overlain on 1:250k geology for Walyarta study area .....	70
Figure 41 ASTER MgOH Group Composition overlain on 1:250k geology for Walyarta Conservation Park (below), showing the location of major springs and surface water sampling sites 2015-2016 ...	71
Figure 42 ASTER – CSIRO Landsat TM regolith ratios; RGB image; R=B3/B2, G=B3/B7 & B=B4/B7, Note; white=vegetation, green=cloud cover, black-dark brown=free water and/or fire scars .....	72
Figure 43 ASTER Opaque Index, red areas represent areas with high concentrations of manganese oxides and/or maghemite gravels .....	73
Figure 44 Eil Eil Spring (previously known as Mandora Swamp) peat core description (0cm equals greatest depth below ground level) (from Wyrwoll et. al. 1986).....	75
Figure 45 Descriptive bar charts of fungal communities from locations (FS=Fern Spring, MS=Melaleuca Spring, SS=Saunders Spring, PSw and NSw are other WA sites) at a depth of 10 cm. OTUs have been coloured by Family. Y axis represents % abundance. 24 bacterial Families each with a mean abundance < 0.01% have been excluded for clarity .....	77
Figure 46 AEM derived water quality map for the Quaternary Formation aquifers (0-10 metres below ground level); Note confidence in map is higher within the western valley floor and coastal areas where depth to groundwater is closer to the ground surface. ....	83
Figure 47 AEM derived water quality map for the Quaternary Formation aquifers (0-10 metres below ground level) overlain on geology mapped at 1:250 000 scale .....	84
Figure 48 AEM derived water quality map for the Broome Sandstone aquifer (40-50 metres below ground level) .....	85
Figure 49 AEM derived water quality map for the Wallal Sandstone aquifer (220 to 240 metres below ground level) .....	86

Figure 50 AEM derived water quality map for the Wallal Sandstone aquifer / Permian Formation aquifers (340 to 360 metres below ground level) .....	87
Figure 51 Schematic diagram for cross section A-A' (perspective view from Figure 6) through the Mandora Palaeovalley; (adapted from Laws (1991), Roach (2010) and DWER (in prep)).....	88
Figure 52 Schematic diagram for cross section A-A' (perspective view from Figure 6) through the Mandora Palaeovalley illustrating main aquifer interactions (adapted from Laws (1991), Roach (2010) and DWER (in prep). .....	89
Figure 53 Inundation frequency of Mandora Lake/Walyarta, including the location of the WOfS mapping sample locations, see Table 5. ....	94
Figure 54 Mandora surface water extent modelling with modelled ephemeral drainage derived from SRTM 1s DEM.....	96
Figure 55. Map of potential carbonate/evaporite regolith units, b. 1:500 000 WA Regolith Map (see Figure 6 for key) and c. to f. remote sensing derived mineral maps (ASTER VNIR-SWIR imagery) ....	107
Figure 56 Map of potential carbonate/evaporite regolith units, b. 1:500 000 WA Regolith Map (see Figure 6 for key) and c. to f. remote sensing derived mineral maps (ASTER VNIR-SWIR imagery) ....	108
Figure 57 Coarse scale geological and hydrogeological controls on compartmentalisation of groundwater flow; increasing complexity from a. to d.; a. WCB tectonic elements (see Figure 3)b. WCB tectonic elements with major NW-SE faults from Parra-García et. al. (2014), c. WCB tectonic elements with major NW-SE and NE-SW faults from Parra-García et. al. (2014), d. WCB tectonic elements with major NW-SE faults from Parra-García et. al. (2014) and potential surficial carbonate / evaporite sources; Note that arrows in b. and c. represent regional and sub-regional groundwater gradients. ....	110
Figure 58 Fine-scale geological and hydrogeological controls on compartmentalisation of groundwater flow; increasing complexity from a. to d.; a. WCB tectonic elements (see Figure 3)b. WCB tectonic elements with major NW-SE faults from Parra-García et. al. (2014), c. WCB tectonic elements with major NW-SE and NE-SW faults from Parra-García et. al. (2014), d. WCB tectonic elements with major NW-SE faults from Parra-García et. al. (2014) and potential surficial carbonate / evaporite sources; Note that arrows in b. and c. represent regional and sub-regional groundwater gradients; Walyarta study area=purple boundary.....	111
Figure 59 Simple block faulted Wallal Sandstone aquifer thickness map based on centre point (metres below ground level mbgl) of the bore inlet screen depth; cross section A-'A shows tectonic element controls on aquifer thickness; a. coarse scale structural/tectonic elements and b. coarse and fine-scale structural/tectonic elements.....	113
Figure 60 WCB, southern La Grange and Walyarta hydrogeochemical database showing the location of bores, spring sites and tectonic element boundaries, with interpretation areas numbered (1=western basin margin, 2=Wallal Embayment, 3=Wallal Platform and 4. Samphire Embayment and Willara sub-basin; see Appendix 7).....	115

Figure 61 A Piper trilinear diagram of groundwater, springs and surface water sampled between 1975 and 2017 (see Appendix 7) (Note groundwater is sampled from the Bossut Fm., Surficial-Broome and Broome sandstone aquifers, Wallal sandstone aquifer and weathered crystalline basement aquifer).....	116
Figure 62 WCB, southern La Grange and Walyarta hydrogeochemical database showing the location of sampling sites in relation to tectonic element boundaries, landform/groundwater flow path and potential carbonate/evaporite regolith map.....	118
Figure 63 WCB, southern La Grange and Walyarta hydrogeochemical database showing a Piper diagram and location of Wallal aquifer sampling sites in relation to landform/groundwater flow path .....	119
Figure 64 WCB, southern La Grange and Walyarta hydrogeochemical database showing a Piper diagram and location of Broome/Surficial aquifer sampling sites in relation to landform/groundwater flow path .....	120
Figure 65 WCB, southern La Grange and Walyarta hydrogeochemical database showing a Piper diagram and location of spring sampling sites in relation to landform/groundwater flow path.....	121
Figure 66 Bivariate log-log plots of various ions against chloride, concentrations are shown in mmol/L and solid black trend line represents seawater concentration .....	122
Figure 67 Bivariate log-log plots of $SO_4/Ca$ , $SAR/Cl$ , $Na/Cl$ vs $Cl/Br$ , $HCO_3/SiO_2$ , $Na/Mg$ and $Na/Cl$ vs $Cl$ , concentrations are shown in mmol/L, solid black and dashed trend line in $SO_4/Ca$ plot represents seawater concentration and gypsum dissolution respectively, blue and red trend lines and arrows in $HCO_3/SiO_2$ plot represent respective carbonate and silicate reactions.....	123
Figure 68 Brine differentiation plots for a. all data, b. Wallal aquifer, springs and surface water, c. Broome and surficial aquifers, springs and surface water and d. data within tectonic element 4 see Figure 60. ....	125
Figure 69 Brine differentiation plot for all spring and surface water sampling.....	126
Figure 70 Piper trilinear diagram for Wallal groundwater sampled in the Wallal Embayment (see Figure 60), labels show bore names (black) and mid screen sampling depth in metres below ground level (red).....	127
Figure 71 (A) Map showing location of Canning Basin, simplified major tectonic element boundaries and Wallal Embayment Transect A'-A and Willara sub-basin Transect B-B', showing the location of bores; bores interpolated onto transects are within red dashed boundaries, apart from NSOKidson; (B) Geological X-Section A'-A, adapted from Meredith et. al. 2018; bores (depth drilled and screened sections) and interpretations of major geological structures and evaporities from report Sections 4.5 and 7.2. ....	128
Figure 72 Scatterplots showing analyte concentrations 1. total dissolved solids (TDS) (mg/L), 2. chloride (Cl) (mmol/L), 3. sodium (Na) (mmol/L) and 4. Na/Cl (mmol/L) against depth sampled (mAHD); a=full dataset, b=Wallal Embayment data & c=Wallal Platform/Sapphire Embayment & Willara sub-basin .....	135

Figure 73 Scatterplots showing analyte concentrations 5. calcium (Ca) (mmol/L), 6. magnesium (Cl) (mmol/L), 7. sulfate (SO <sub>4</sub> ) (mmol/L) and 8. K (mmol/L) with depth sampled (mAHD); a=full dataset, b=Wallal Embayment data & c=Wallal Platform/Samphire Embayment & Willara sub-basin.....	136
Figure 74 Scatterplots showing analyte concentrations 9. Ca/Cl (mmol/L), 10. HCO <sub>3</sub> /Cl (mmol/L), 11. SO <sub>4</sub> /Cl (mmol/L) and 12. SO <sub>4</sub> /Ca (mmol/L) with depth sampled (mAHD); a=full dataset, b=Wallal Embayment data & c=Wallal Platform/Samphire Embayment & Willara sub-basin.....	137
Figure 75 Scatterplots showing analyte concentrations 13. HCO <sub>3</sub> /SiO <sub>2</sub> (mmol/L), 14. SiO <sub>2</sub> (mmol/L), 15. HCO <sub>3</sub> (mmol/L) and 16. modelled chalcedony SI with depth sampled (mAHD); a=full dataset, b=Wallal Embayment data & c=Wallal Platform/Samphire Embayment & Willara sub-basin.....	138
Figure 76 Scatterplots showing 17. pH, 18. alkalinity (mg/L) and analyte concentrations 19. bromine (Br) (mmol/L) and 20. Cl/Br (mmol/L) with depth sampled (mAHD); a=full dataset, b=Wallal Embayment data & c=Wallal Platform/Samphire Embayment & Willara sub-basin.....	139
Figure 77 Scatterplots showing modelled 21. calcite SI, 22. dolomite SI and 23. gypsum SI with depth sampled (mAHD); a=full dataset, b=Wallal Embayment data & c=Wallal Platform/Samphire Embayment & Willara sub-basin .....	140
Figure 78 Bivariate plots of a. δ <sup>2</sup> H vs δ <sup>18</sup> O, showing La Grange wet season Local Meteoric Water Line (LMWL) (δ <sup>2</sup> H =7.5 δ <sup>18</sup> O +9.4 (Harrington and Harrington 2016) and Pilbara Local Evaporation Line (LEL) (Dogramaci et. al. 2012) and b. δ <sup>18</sup> O vs. log Cl (mmol/L) (observations sourced from δ <sup>2</sup> H and δ <sup>18</sup> O data in Table 10; note that Wallal upland bores are shown as blue squares) .....	144
Figure 79 Wallal Embayment geological X-Section A'-A (from Figure 71) showing the location of the sub set of bores sampled for stable water isotopes, δ <sup>18</sup> O results from Table 10, arrows showing the direction of groundwater and soil water movement, piezometric surface from Meredith et. al. 2018 and bivariate plot δ <sup>18</sup> O vs depth sampled (mAHD) (all data Table 10).....	146
Figure 80 Bivariate plots of a. log Rubidium (Rb) vs log Strontium Sr (mmol/L) and b. log Strontium Sr (µmol/L) vs log Cl (mmol/L) .....	147
Figure 81 Bivariate plots of a. Ca/Sr (mg/L) vs δ <sup>87</sup> Sr, b. log chloride (Cl) vs Ca/Sr (mg/L) and c. log 1/Sr (mmol/L) vs <sup>87</sup> Sr/ <sup>86</sup> Sr (solid blue line with arrow in c. represents Wallal aquifer groundwater flow path & increasing depth sampled).....	149
Figure 82 Wallal Embayment geological X-Section A'-A (from Figure 71) showing the location of the sub set of bores sampled for δ <sup>87</sup> Sr results from Table 10, arrows showing the direction of groundwater and soil water movement, piezometric surface from Meredith et. al. 2018 and bivariate plots of Sr (µmol/L), Cl/Sr (mmol/L) and δ <sup>87</sup> Sr vs depth sampled (mAHD) (all data Table 10). .....	150
Figure 83 Wallal Embayment geological X-Section A'-A (from Figure 71) showing the location of the sub set of bores with <sup>14</sup> C age determination from Meredith et. al. (2018), arrows showing the direction of groundwater and soil water movement, piezometric surface from Meredith et. al. 2018 .....	156



Figure 84 Wallal Embayment geological X-Section A'-A (from Figure 71) showing the location of the sub set of bores sampled for  $\delta^{14}\text{C}_{\text{DIC}}(\text{‰})$  results from Table 10, arrows showing the direction of groundwater and soil water movement, piezometric surface from Meredith et. al. 2018 and bivariate plots of  $\delta^{13}\text{C}(\text{‰})/^{14}\text{C}$  (pMC) and  $^{14}\text{C}$  (pMC) vs depth sampled (mAHD) (all data Table 10). 157

Figure 85 Predictive hydrological conceptual model for the Walyarta study area, see Figure 71 (A) for location and Figures 28, 51 and 52 for context ..... 164

Figure 86 Schematic showing shallow aquifer dynamics in the wet and dry seasons and physico-chemical changes that occur and impede the collection of robust spring discharge samples ..... 165

## Executive Summary

Major geological and hydrogeological investigations have taken place in the Canning Basin since the early 1900's as the basin is prospective for hydrocarbons, base metals and groundwater. In the west Canning Basin (WCB), groundwater demand from both the unconfined Broome and confined Wallal aquifers has increased over the last decade, which has created a need to undertake rapid assessments of the sustainability of groundwater resources. The major conclusion of recent groundwater resource modelling in the western part of the Basin is that insufficient data have been collected to understand how the aquifers will respond to groundwater abstraction over time.

The west Canning Basin also contains unique environmental assets that have high heritage and ecological values, including the Ramsar listed Mandora Marsh mound spring and wetland system, which are located in the Walyarta Conservation Park. The artesian mound spring system hosts unique phreatophytic vegetation communities and perennial and ephemeral water bodies inhabited by fish and invertebrates.

The springs are not thought to represent a significant part of the west Canning Basin water balance, but they are broadly understood to be sustained by groundwater discharge along discrete geological faults. Predictions from past and recent groundwater assessments appear contradictory, one advising springs in the western basin margin are likely to be sensitive to groundwater level changes in the confined Wallal aquifer and another advising there will be limited Wallal aquifer drawdown in the Walyarta study area. This is of concern for two main reasons. The first reason being there is a high degree of uncertainty on how the Wallal aquifer will respond to groundwater abstraction and the second is, groundwater contributions from the Wallal aquifer to the Walyarta mound springs have not been assessed.

These concerns prompted the Department of Biodiversity, Conservation and Attractions (DBCA) to undertake a study of the hydrological processes that support perennial groundwater discharge in the Walyarta mound springs and surface water systems. The approach concentrated on developing a three dimensional understanding of hydrological processes, with data mining (sourcing and interpretation) used to develop evidence for transferring the results to areas with less information.

The four most important conclusions from this study are that;

- In the WCB, groundwater in the Wallal and Broome aquifers generally has a spatially distinct and consistent hydrogeochemistry and its variability is predictable with depth. Patterns also exist along flow paths, where the Wallal aquifer also increases in thickness. This allows for the transfer of knowledge gained to areas like the Walyarta study area where there is sparse bore data, but information on formation thicknesses,
- Slow rates of lateral groundwater movement are inferred from groundwater radiocarbon ages along flow paths and appear to have assisted in the preservation of subtle fault zone hydrogeochemical fingerprints. Available evidence indicates that faults;
  - exist in the near surface (propagate to the land surface from depth representing reactivated basement structures),
  - can be mapped both geophysically and hydrogeochemically,

- constrain formation thicknesses at a basin scale, but do not appear to physically compartmentalise groundwater flow (limited stratigraphic offsets noted in Broome and Wallal aquifers), and
- Represent zones where there is greater vertical groundwater mixing and water-rock interactions.
- Long-lived, perennial springs are located within roughly sub vertical (possible high angle shallow dip to the west) geological fault zones and are sustained by perennial groundwater moving vertically, to the ground surface, along these zones. A large amount of sampling is required to obtain spring discharge samples that represent deeper groundwater and are not affected by overprinting caused by increased aquifer mixing/connectivity and unsaturated zone processes. Three of the twenty three DBCA spring samples (aprox 15%) sampled fault conduits with higher flow rates and confirm that discharge water in perennial springs is sourced from the Wallal aquifer at depths of around 200 metres below ground level and
- Perennial surface water is likely to have a similar origin to the long lived mound springs but this is unable to be verified due to insufficient sampling and overprinting of unsaturated zone processes.

The major outcome of this study is an improved understanding of how the Walyarta mound springs and perennial surface water function under natural conditions. However, the behaviour of groundwater flow under changed conditions, in particular the larger scale abstraction of groundwater from the Wallal aquifer, is unknown.

Questions that need to be answered about the Wallal aquifer are how, under increased and prolonged groundwater abstraction, will aquifer hydraulic heads be maintained in fault zones, do we know enough about aquifer heterogeneity to predict aquifer depressurisation patterns and if depressurisation is anisotropic, will depressurisation propagate preferentially along fault zones and decrease spring discharge rates.

Further work is required to answer these questions and reduce uncertainty and should include verification of the DBCA hydrological conceptual model of the mound springs by;

- Undertaking numerical modelling to provide a proof of concept on the role of geological faults,
- Increase hydrogeological information within and upgradient of the Walyarta mound springs and
- Improve targeting of future Walyarta mound spring and surface water sampling programs (water, soils and formations) by using non-invasive methods to acquire robust information on the sub-surface.

## 1 Report aims and objectives

The Walyarta Conservation Park (Figure 1) is located in the west Canning Basin and is host to unique environmental assets that have high heritage and ecological values, including the Ramsar listed Mandora Marsh mound spring and wetland system.

The main aim of the work undertaken in this study is to develop a three dimensional framework that explains the hydrological processes that support perennial groundwater discharge in the Walyarta mound springs and surface water systems.

The approach adopted involved data mining, which first covered sourcing data and information and was then followed by the production of an integrated interpretation and development of a conceptual model. The uncertainty of the conceptualisation varying according to the availability of verification data sources.

### 1.1 Report structure

The report has nine sections. Section one covers the intent and approach taken in the interpretation and reporting of the work. Section two summarises background material drawn on for the interpretation and sets the research directions. Sections three to five report on the physical setting (e.g. geomorphology and surficial geology), geology (e.g. information obtained from drilling and geophysics) and climate, vegetation and soils. Section six and seven provides information on the hydrology and hydrogeochemistry and sections eight and nine detail the Walyarta conceptual hydrological model and the conclusions and recommendations.

Datasets are integrated progressively throughout the report, Sections three to seven, to produce the Walyarta conceptual hydrological model in Section 8.

## 2 Background

### 2.1 Geology and structure

Major geological investigations in the Canning Basin (CB) since the early 1900's have focused on exploration for hydrocarbons and have provided information on the broad scale distribution of geological materials and the structural discontinuities that separate them. The CB is a large sedimentary basin located in northern Western Australia and is extensive, with an onshore area of around 530 000 km<sup>2</sup>. Stratigraphic units present in the basin comprise a sequence of Cenozoic (Quaternary and Tertiary), Cretaceous, Jurassic and Permian sediments that overlie Archaean and Proterozoic aged basement (e.g. GSWA 2012a) (Figure 2).

The stratigraphy and the paleoenvironments responsible for the deposition and preservation of sediments in the CB have been described by many authors including Foreman and Wales (1981) and Towner and Gibson (1983).

The basin geology is summarised in GSWA (2012) as being covered by low-lying Cenozoic sandplains, with longitudinal seif dunes forming the dominant geomorphic features, rising to 30 metre in height. Precambrian cratons form the west and north CB boundaries, including pre-Permian outcrop in the north, while scattered Permian and Mesozoic outcrop occur in the south.

Drilling and the modelling of coarse scale geophysical data has defined two pairs of northwest trending sub-basins (Fitzroy and Gregory sub-basins and the Kidson and Willara sub-basin) separated by a basement high and containing sediments to a thickness of 10km (Figure 3). The CB has a complex tectonic and depositional history and recent modelling of geophysical data indicates that at a finer scale these coarse scale basin elements are evident at smaller dimensions, with high angle faults and basement highs separating 20-40km wide grabens and half grabens in the southwestern CB (Parra-García et al. 2014).

Basement structures are thought to be important in the formation of basins as they follow the major CB northwest structural grain. Many faults propagate to the land surface due to the normal reactivation of existing faults (Jurassic growth structures) during the Miocene to Recent periods (Early Miocene, Late Miocene and Late to Early Pliocene) as southeast Asia and the northwest and northern margins of Australia collided (FrogTech 2005). Similar to the tectonic elements, coarse scale structural styles repeat at finer scales.

## 2.2 Hydrogeology

In the 1970's the Western Australian Geological Survey carried out a groundwater resource investigation over an area known as the West Canning Basin (WCB), which covers the area Wallal Embayment, Wallal Platform and Samphire Embayment tectonic elements (Figure 3). This study covered the coastline to approximately 50km inland and included the mapping and assessment of aquifer water storages, gradients and identifying processes that underpin their sustainability (Leech 1979).

This study reported on two sedimentary aquifers that contained potential groundwater resources, the deeper confined Jurassic aged Wallal Sandstone aquifer and a younger and shallower unconfined Cretaceous Broome Sandstone aquifer. In the WCB the Jarlemai Siltstone forms an aquitard and generally confines the Wallal aquifer, apart from where it has been subjected to erosion to the south. Overlying the Broome Sandstone aquifer is a thin surficial aquifer comprised of Tertiary aged sediments. In the WCB the confined Wallal aquifer is the most prospective resource. The Broome aquifer generally contains variable quality water and the surficial aquifer has small supplies of groundwater best suited for local stock water use. At a regional scale groundwater flow in all aquifers is roughly east to west, or in the WCB south to north, with discharge occurring at the ocean. At a local scale gradients may be more variable. Groundwater recharge to unconfined aquifers is constrained by seasonal climatic patterns, in particular the likelihood of receiving cyclonic rainfall. Higher recharge to the Wallal aquifer arises where the Jarlemai Siltstone is absent or thin, in the WCB this is the area to the south near the Pilbara Craton boundary.

In the 2000's more detailed studies on the sustainability of WCB water resources were carried out using numerical models in response to increased water demand for public water supplies and mining and agriculture needs (Aquaterra 2010 and NTEC 2012). The focus of these models was the Wallal aquifer and the results indicated that based on the current data and information the aquifer was capable of providing a staged water supply with a maximum draw of 20GL/yr for a up to ten years (NTEC 2012). Other investigations during this period included researching the use of geochemistry and environmental tracers to understand groundwater recharge, aquifer connectivity and sustainability (Meredith et. al. 2014).

# HYDROLOGICAL CONCEPTUALISATION OF THE WALYARTA MOUND SPRINGS

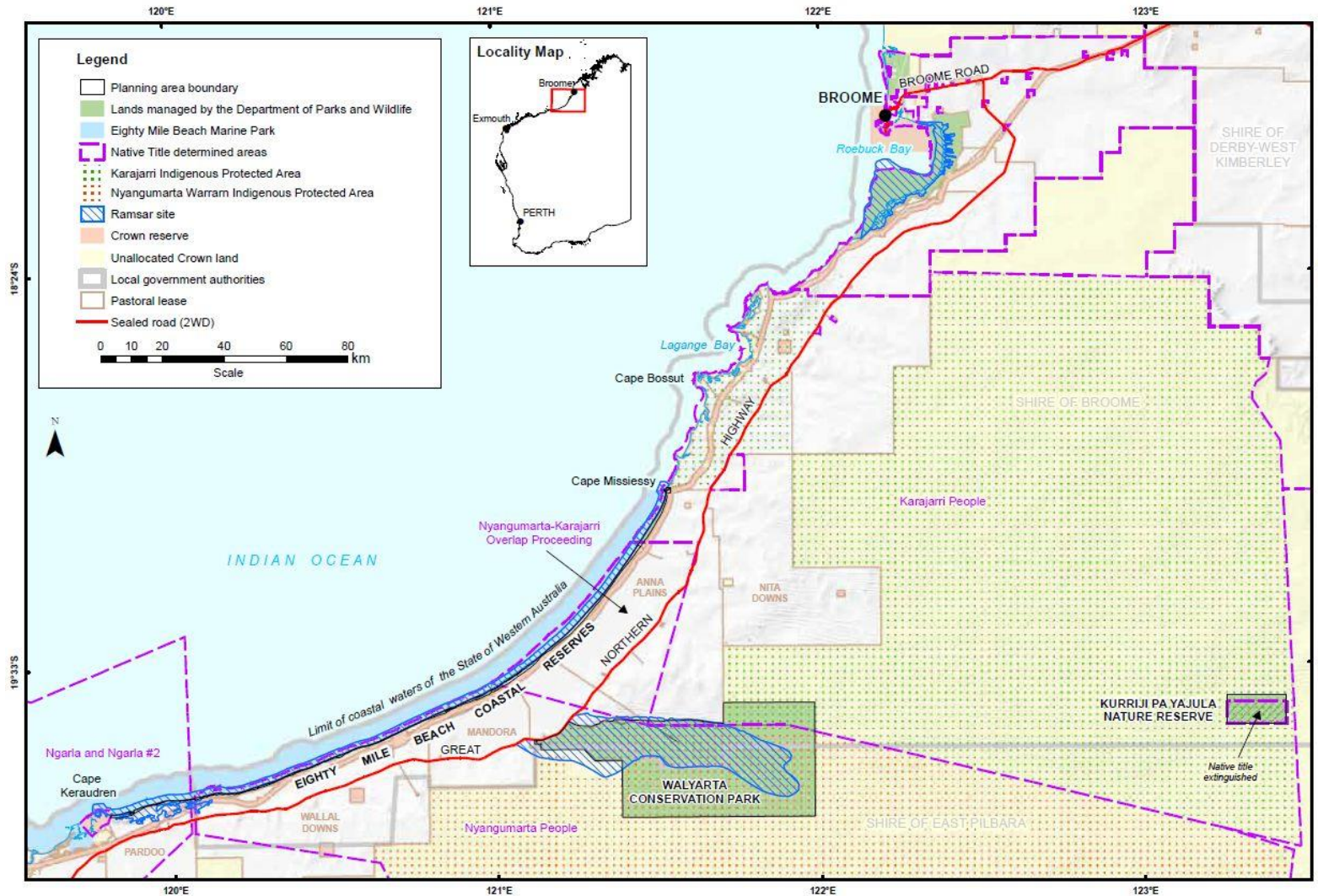


Figure 1 Location map of Walyarta/Mandora Marsh with information on management and private land holder boundaries (from DPaW 2016)

HYDROLOGICAL CONCEPTUALISATION OF THE WALYARTA MOUND SPRINGS

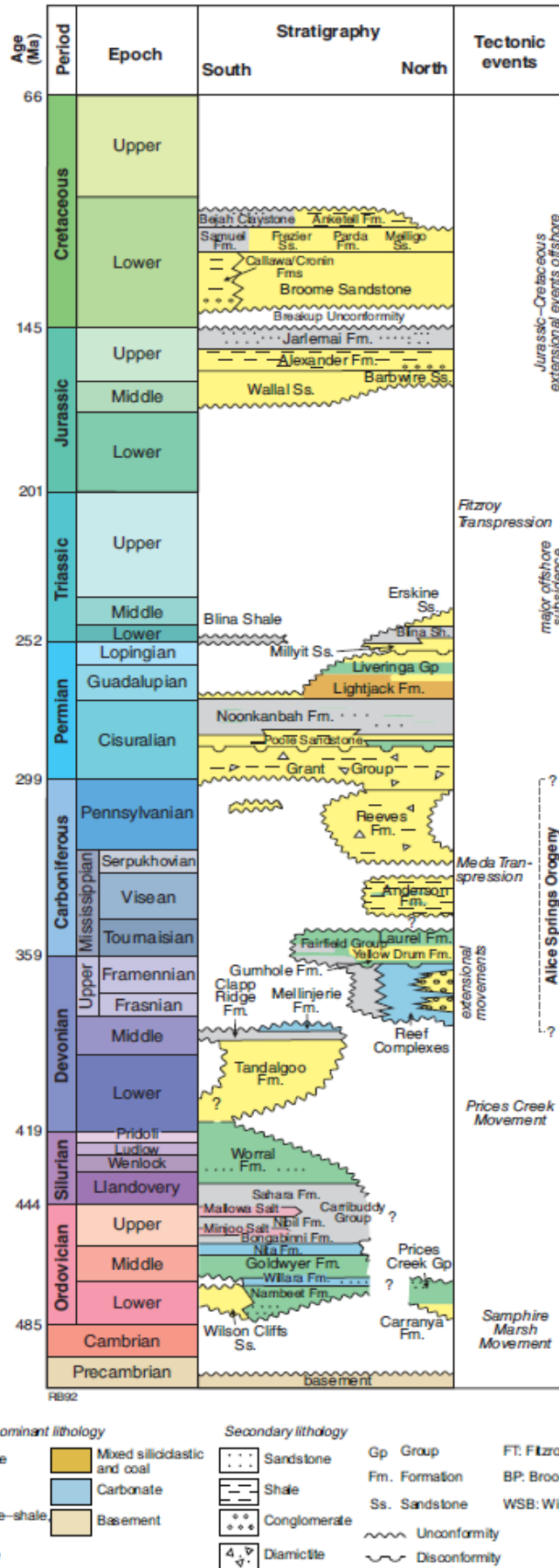


Figure 2: Generalised stratigraphy of the major formations of the Canning Basin (modified from GSWA 2012a)



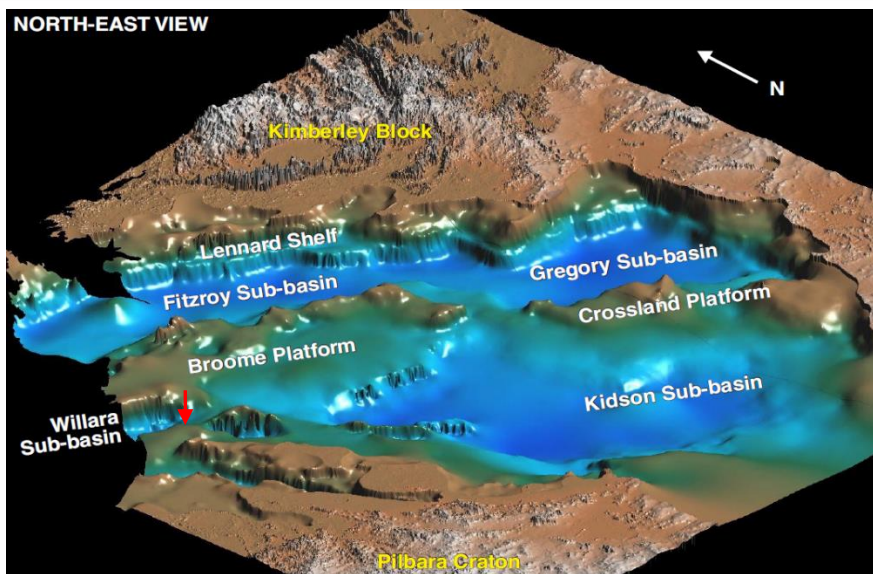
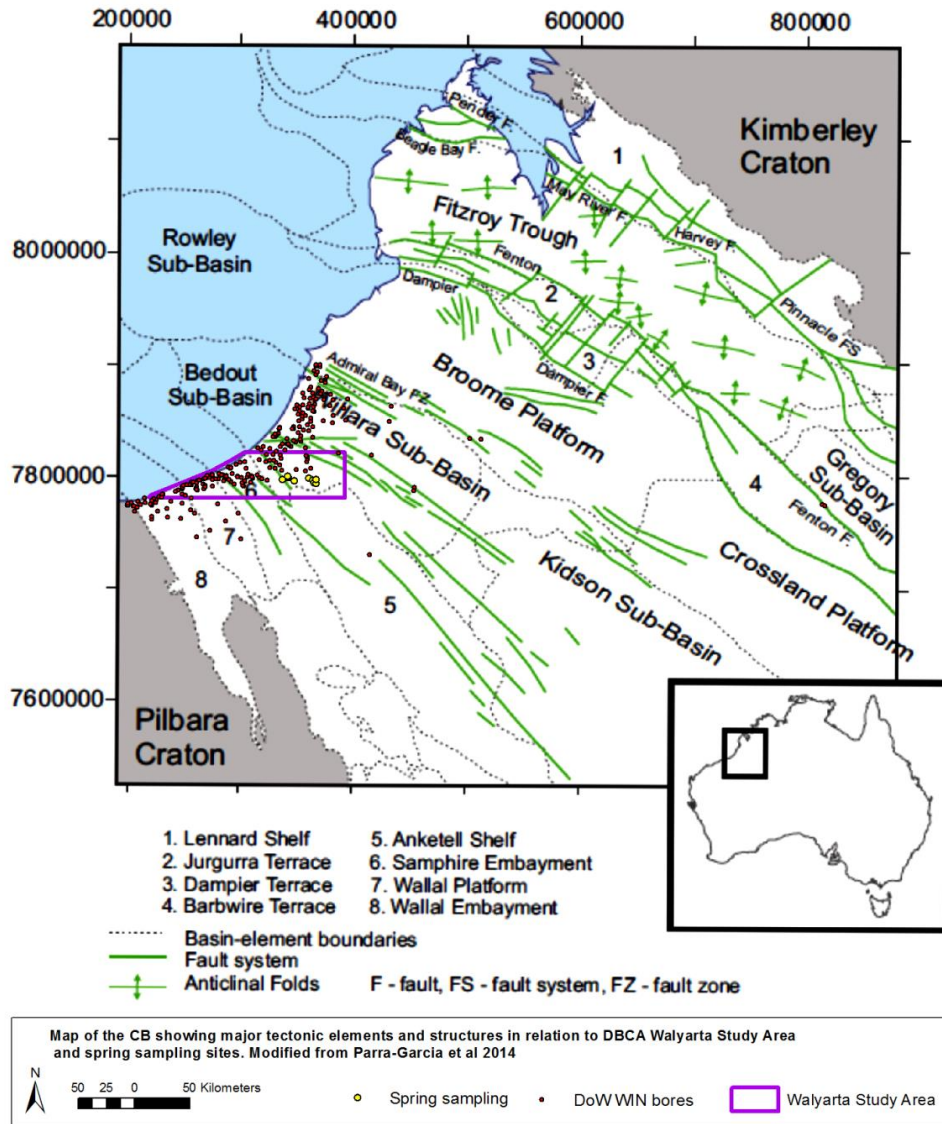


Figure 3: Top; map of the major tectonic elements and structures of the Canning Basin (modified from Parra-García et. al. 2012) and below a pseudo colour perspective view of modelled basement topography for the Canning Basin (from GSWA 2016); red arrow showing the approximate location of the Walyarta mound springs.



Results reported showed that combined hydrochemical and isotopic techniques could be used to identify and assess episodic (cyclonic) recharge events (Meredith et al 2018). Other hydrology research in the WCB re-evaluated conceptual models through the exploration of geological and hydrogeological ideas interpreted from airborne geophysical data and terrain modelling. Ideas tested with numerical models developed from more complex, heterogenous conceptual models, appear to provide improved model calibrations (Hanna 2014).

Based on these findings, to increase confidence in mapping aquifers airborne geophysical data (electromagnetics) were acquired over the WCB and the southern margin of the Willara sub-basin in 2015. Inversions of these data were used to map the location of the salt water interface in addition to the base of the Wallal aquifer and the top of the Jarlemai Siltstone. Other hydrogeological features identified included minor faults and one major basement fault, the latter creating an uplifted fault block in the Wallal sub-basin, resulting in the base of the Wallal (which is also the top of the Permian) moving upwards by approximately 250 metres (Mira Geoscience 2016). Ideas were also put forward that palaeochannels may have developed along the downthrown fault block, with major channels likely to show inheritance characteristics (e.g. be present as low lying areas in the contemporary landscape).

In 2013 the Department of Agriculture and Food, now the Department of Primary Industries and Rural Development (DPIRD) undertook a review of groundwater resources in the Willara sub-basin, north of the WCB (Paul et al. 2013). This area has limited geological and hydrogeological information due to drilling being limited to only a few deeper petroleum wells and many shallow unlogged bores (less than 50mbl) drilled for stock and farm water supply.

Hydrogeological investigations carried out as a result of the review indicated the Broome Sandstone aquifer was a suitable resource for horticulture due to having suitable quality groundwater, physical parameters (saturated thickness, hydraulic conductivity and transmissivity) and sustainability, with isotopic tracers estimating groundwater recharge at around 5% of average annual rainfall (Harrington and Harrington 2016). Aquifer gradients are relatively flat and likely to be disrupted by both the internal heterogeneity within the Broome Sandstone sediments as well as the location of palaeovalley sediments. Areas mapped as suitable for horticultural development are mainly located near the coast (east of the Great Northern Highway and approximately 30km from the coastline) and where depth to groundwater is closer to the ground surface (Wright et al 2016).

### 2.3 Environmental water

Leech (1979) was one of the first investigators in the WCB to identify that the Broome and Wallal aquifers had different hydrochemical fingerprints (e.g. Broome-surficial aquifer has elevated concentrations of bicarbonate over chloride ions). In this study aquifer chemistry were compared with groundwater levels to assess aquifer mixing, map groundwater flow paths and propose environmental water requirements.

Fresh to brackish perennial-ephemeral wetlands and springs were mapped at the coast and to a distance of around fifty kilometres inland. The coastal wetlands known as the Eighty Mile Beach wetlands are Ramsar listed, as is the internationally significant Mandora Marsh (now known as Walyarta Conservation Park (DPaW 2016), which includes suites of mound springs (CALM 1999, V&C Semeniuk 2000, DoW 2010 & 2012 & Storey et. al. 2011). Groundwater discharge and throughflow

from the Broome aquifer is recognised as supporting coastal wetland systems, phreatophytic vegetation at the coast and in river alluvium (e.g. De Grey River) (e.g. Leech 1979, DoW 2012).

Some ephemeral wetlands were also thought to be perched where the wetland substrate has low permeability sediments, in particular those located on the tidal flats and within inter-dunal swales (V & C Semeniuk 2000). Geomorphology, geology and hydrology were identified as being important in grouping wetlands and ideas were proposed on what hydrological processes are likely to support them.

Aquifer water quality fingerprinting has also been used to assess the source of local spring groundwater, with data showing discharge water was aligned with the deeper confined Wallal aquifer (Leech 1979). Aquaterra (2010) also reported on the springs and advised that where fault zones propagate to the ground surface, through the Wallal aquifer, Jarlemai aquitard and Broome and surficial aquifers) they form a conduit to discharge Wallal groundwater and form mound springs. Aquaterra (2010) put forward that the wetlands and springs were unlikely to form a significant part of the overall WCB water balance and the springs could form useful indicators of the changes in groundwater pressure in the Wallal aquifer. DoW (2012) reports that the sources of water supporting the coastal wetlands springs is unclear but results from numerical modelling indicate they will not be affected by the current allocated levels of groundwater abstraction.

## 2.4 Research directions

The area of scientific interest to the Department of Biodiversity, Conservation and Attractions is the Walyarta Conservation Park, located on the southern margin of the Willara sub-basin. The conservation park includes the Mandora Marsh with its Ramsar listed wetlands and mound springs.

Environmental water research and reporting over the past forty years has identified a range of hydrological processes are likely to be important but there is high uncertainty in confirming which processes are the most important. The lack of hydrological monitoring data impedes progress on this research and as the area has high heritage values it is important to develop low impact non-invasive techniques to study the hydrology and reduce uncertainty.

Problems identified that required more work included understanding spatial connectivity of the Broome and Wallal aquifers, groundwater gradients in the Wallal aquifer and past and current processes responsible for the location of poorer quality water.

Work undertaken in this study focuses on extracting geological and hydrogeological information from past and recent airborne geophysical and hydrochemical data, with interpretations integrated to identify critical hydrological processes sustaining the springs and wetlands in the Walyarta Conservation Park (in this report identified as the Walyarta study area; abbreviated to Walyarta).

# 3 Physical setting

## 3.1 Location

The Walyarta hydrology study area is located in north-western Australia approximately 1700km north of Perth (DPaW 2016). The study area covers approximately 516800ha, encompassing the

Walyarta Conservation Park and part of the Eighty Mile Beach coastal reserves and Marine Park (Figure 4).

### 3.2 Geomorphology and surficial geology

The physiography of the West Canning Basin (WCB) has been described by others investigating the geology, hydrogeology and hydrology (Leech 1979; Semeniuk 2000). The variation in relief generally increases from the coast to inland areas (Figure 5). The highest available resolution topographic data (30 metre gridded and hydrologically corrected Shuttle Radar Topography Mission (SRTM) 1 second DEM (<http://www2.jpl.nasa.gov/srtm/>)) show the coastal margin maintains an elevation of around 10m AHD; 50km inland. Variation in relief in the valley slowly increases from 50 to 80km inland, with topographic gradients remaining low at generally less than one percent.

Gradients into the upper valley approximately 50-80km inland (location of East Lake and Lake Walyarta) are higher than those downgradient. Changes in relief combined with episodic rainfall will result in infrequent transport and deposition of sediments and this is reflected in the patterns of mapped alluvium and lacustrine sediments (Figure 6).

The coastal margin comprises a coastal plain, subdued landscape comprising major coastal and tidal regolith units (e.g. thin beach dune sands and tidal mud salt flats) and post Pleistocene sand dunes (DMP 2010) (Figure 6). Inland and to the south east the variation in relief increases, with weathered and transported sediments forming a sand plain, with a high density of fixed seif dunes orientated to either north-west or east-west prevailing winds. In the upper valley an evaporative sequence, including halite and carbonates, has formed at the surface and beneath thin Quaternary valley-fill sediments. The development of this sequence is thought to have occurred in the Pleistocene during the last major sea level high stand (V&C Sememiuk Research Group 2000).

In the WCB the main river courses are the De Grey River and Pardoo Creek (located to the west of Figures 3-5) and they are located in the southern WCB and drain in a northerly direction. In the Walyarta study area east-west and north-west trending ephemeral drainages develop following cyclonic rainfall events and often follow the general direction of seif and longitudinal dunes (Figure 5). Topographic gradients are lower on the coastal plain, which encourages a network of discrete and deeply incised river channels that may follow a break of slope along the sandplain margin.

## 4 Geology

The Canning Basin contains a sequence of sediments ranging in age from Ordovician to Recent (e.g. up to approximately 480 million years old) (Magee 2009). Sediments overly crystalline basement rock have been deposited through marine, fluvial, lacustrine and aeolian processes following changes in climate (e.g. rainfall, sea level etc.) and tectonic activity (e.g. elevation changes such as compression induced uplift and downwarping due to rifting). These processes have been active over the last 480Ma and have influenced the formation, preservation and resultant physico-chemical properties of sediments.

HYDROLOGICAL CONCEPTUALISATION OF THE WALYARTA MOUND SPRINGS

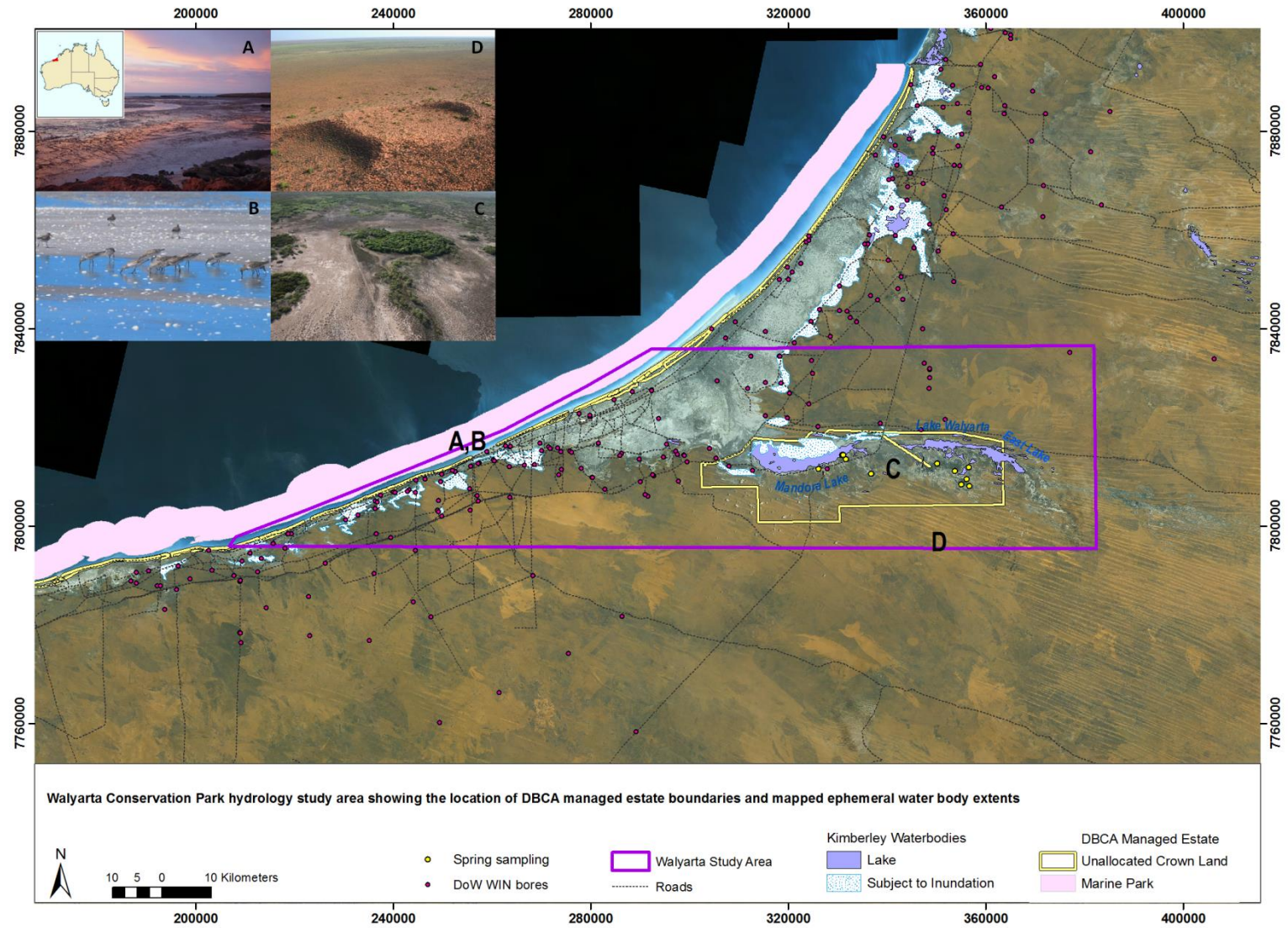


Figure 4 Location of Walyarta hydrological study area superimposed on SPOT 5 Imagery (2009) with photographs showing the variation in physical environments



HYDROLOGICAL CONCEPTUALISATION OF THE WALYARTA MOUND SPRINGS

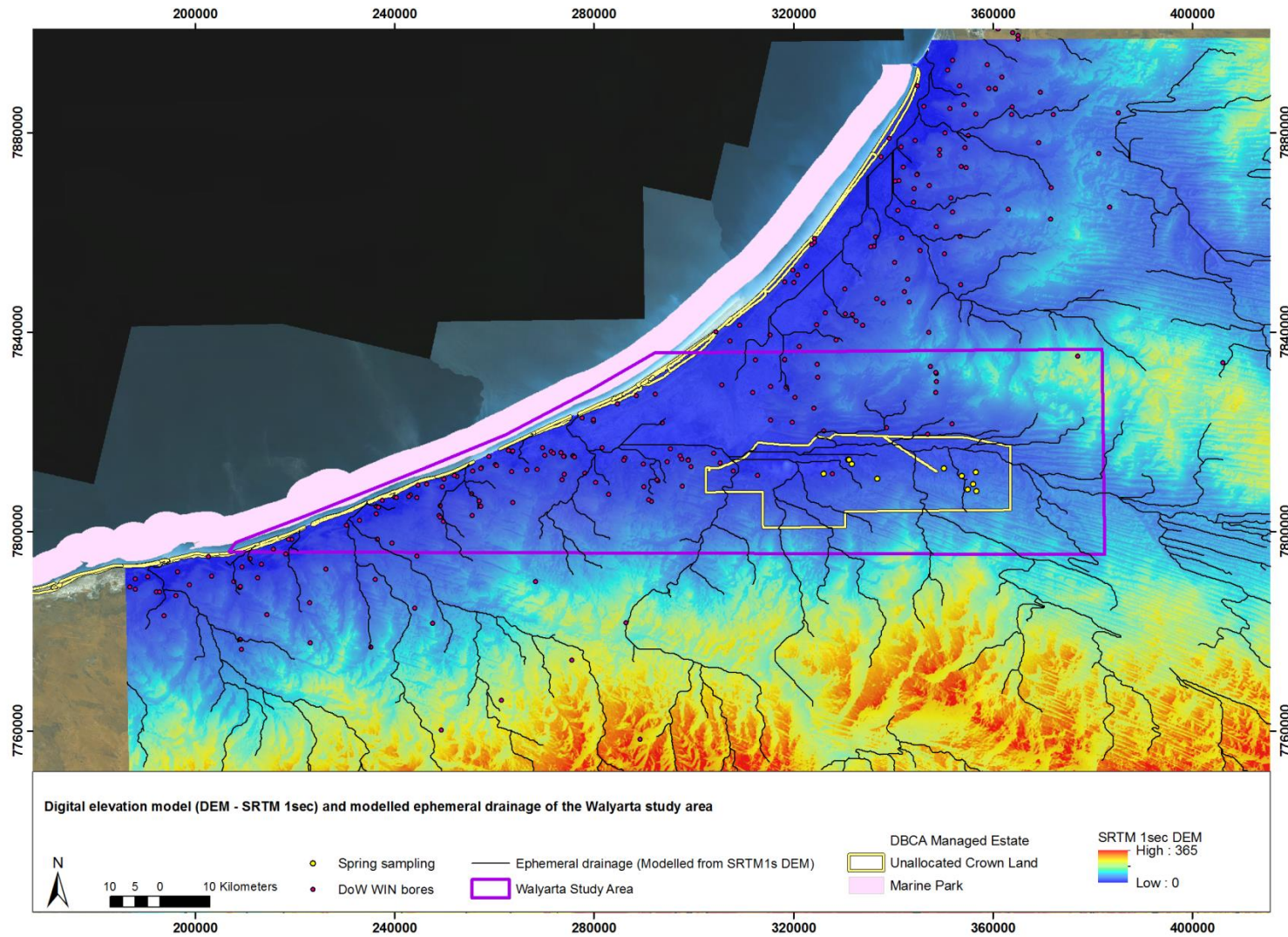


Figure 5 SRTM1s DEM and modelled ephemeral drainage (30 metre gridded and hydrologically corrected Shuttle Radar Topography Mission (SRTM) 1 second DEM)

HYDROLOGICAL CONCEPTUALISATION OF THE WALYARTA MOUND SPRINGS

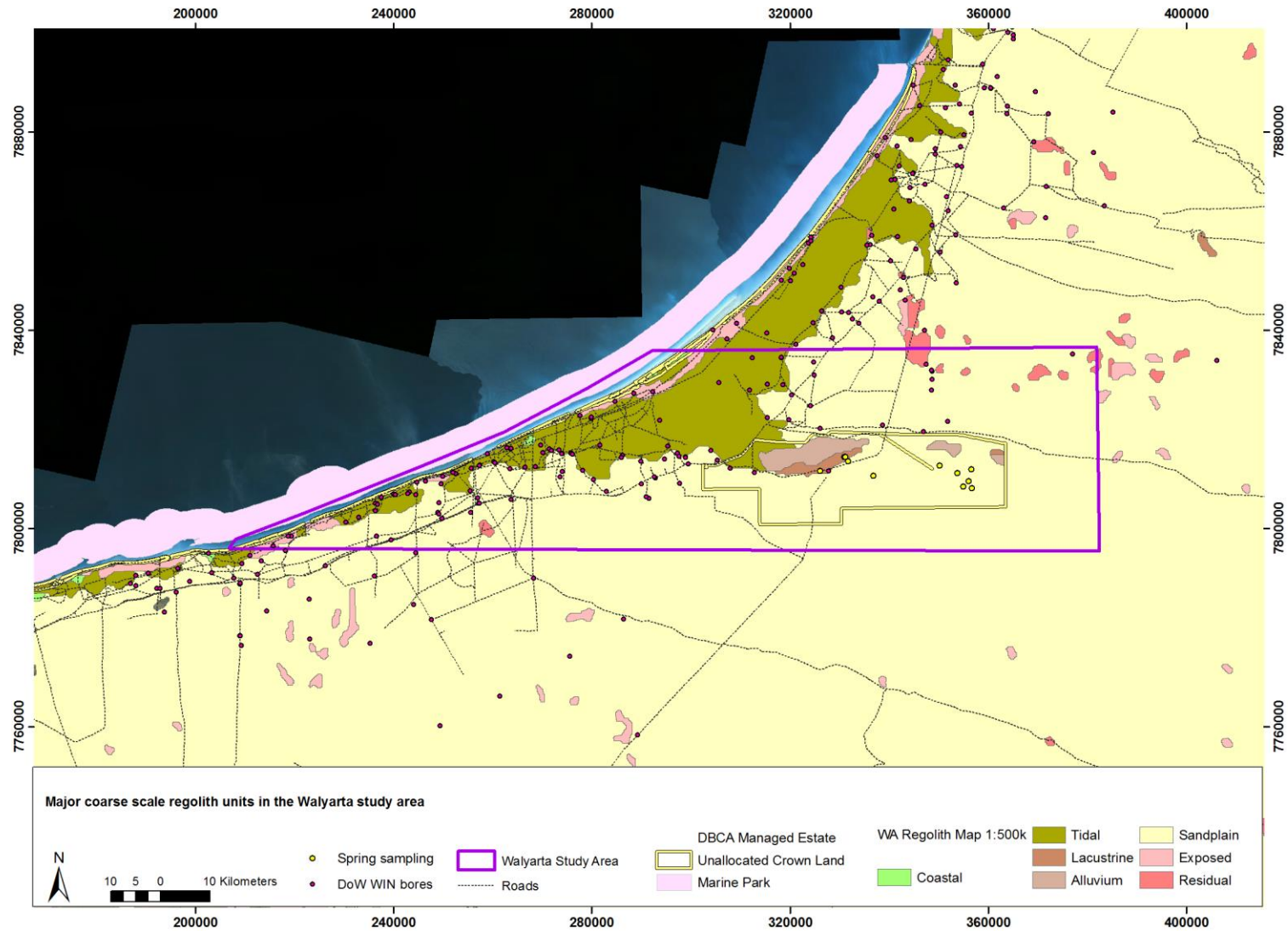


Figure 6 Regolith mapping in Walyarta (from digital 1:500 000 WA Regolith Map)

#### 4.1 Canning Basin scale stratigraphy and structure

The acquisition of airborne (magnetics and electromagnetics) and ground geophysical (seismic) data has helped develop a three dimensional understanding of structural controls that have controlled the distribution of geological formations across the basin. An interpretation of these data divides the CB into a number of distinct tectonic elements (Figure 3). The variation in the distribution and thickness of sediments in these domains is the result of varying basin wide depositional and tectonic processes.

A detailed history of the basin sedimentation and deformation is provided in Forman and Wales (1981) and Towner and Gibson (1983). A brief summary of historical events reported for the tectonic elements is outlined below (refer Figures 2 and 3 for stratigraphy and spatial information):

- Precambrian to the Ordovician: development of north-south trending decollement faults in the Willara sub basin and Fitzroy Trough and gentle downwarping in the Kidson sub-basin; marine transgression deposits sediments and evaporates (sandstone, limestone & shale); regression deposits dolomite, anhydrite and red shale; erosion, followed by uplift and erosion and marine transgression produces evaporates (dolomite, anhydrite, gypsum and halite),
- Devonian: regression and deposition thick dune sands, minor lacustrine and marginal marine sedimentation,
- Carboniferous: marine transgression and uplift,
- Late Carboniferous to Permian: glaciation, erosion, rifting and emplacement igneous intrusives,
- Triassic: marine transgression and deposition of clastic sediments; development of braided river network depositing coarse clastic sediments in the Fitzroy Trough and red beds with minor carbonates,
- Late Triassic to Early Jurassic: sedimentation followed by uplift, major folding and faulting (likely basement right-lateral wrenching in the Fitzroy Trough, east trending en-echelon anticlines and synclines and northwest trending faults, folding probably assisted by deep salt movement and decollement from salt pillows within Carribuddy Formation within the Willara sub-basin); deep basin wide erosion,
- Early Jurassic, broad scale delta (Lower and mid Jurassic) with major tilting and faulting to the southwest; transgression in the late Jurassic depositing clastic sediments (sandstone, siltstone and mudstone),
- Early Cretaceous; regression and deposition thick marine sands to the east; faulting due to rifting (separation of Indian and Australian continents); transgression and sedimentation (fine sands, clay and mud (fine grain size material may be marine origin),
- Early Palaeocene: shallow sea with thin sediment sequence (foraminiferal glauconitic mud, calcilutite, claystone and siltstone),
- Late Palaeocene: transgression and sedimentation (gypsum, dolomite bioclastic carbonate and minor clay),
- Mid to late Eocene: sedimentation (carbonate clay and dolomite) (seaward migration of barriers sheltering a possible sabkha environment),
- Oligocene to Early Miocene: aridity, weathering and possible lateritisation,
- Miocene: regression and deformation/diastrophism,
- Pliocene to Pleistocene; continuation of regression and aridity under lower temperatures,
- Holocene: transgression and sedimentation due to eustatic fluctuation (coastal calcareous and fossiliferous marine sediments); onshore deposition dependent on effectiveness of perennial streams, minor uplift/marine regression and subsequent aridity.

#### 4.2 Mesozoic geology

Forman and Wales (1981) identified major synclines and produced sediment thickness/isopach maps noting the Willara sub-basin formed an irregular synclinal zone. The Walyarta study area is located

near the southern boundary of the Willara sub-basin (Figure 3) and due to limited drilling in this area interpreted sediment thickness distributions form an important initial conceptual model.

Of particular interest for the management of Walyarta is the distribution of the uppermost 500 metres of sediments as this Mid-Jurassic to Recent sediment package contains the main aquifers that sustain groundwater dependent ecosystems. Isopach maps for the Mid-Late Jurassic (Wallal Sandstone, Alexander Formation, Jarlemai Siltstone and Callawa Formation) to Early Cretaceous (Broome Sandstone) sediments are shown in relation to the Walyarta Conservation Park and the mound springs in Appendix 1 (Map1-6).

In the Mid-Late Jurassic palaeoenvironments transporting and depositing sediments in Walyarta ranged from fluvial, proximal deltaic plain to marine transgressive settings (Figure 7; Appendix 1). Fluvial systems were important in the Jurassic as extensive rivers drained into large deltaic platforms, depositing materials ranging from shale to conglomerate. The onshore spatial distribution of different sedimentary facies is noted as variable, fining upward sequences being common with coarser material at the source area margins of the CB (e.g. Pilbara and Kimberley Blocks and eastern edge of Jurassic sedimentation) (Forman and Wales 1981).

The Mid-Late Jurassic Wallal Sandstone has a mixed fluvial/aeolian, proximal to distal delta origin, with sediments sourced from the central CB. The formation is a very coarse to fine grained poorly consolidated sandstone that contains traces of carbonaceous material, pyrite and heavy minerals. Quartz grains show variable maturity and a conglomerate forms a basal layer is likely to represent an unconformable surface, overlying older rocks (e.g. Permian sediments or Archean crystalline basement). Isopachs produced by Forman and Wales (1981) show the formation to range in thickness in Walyarta from approximately 150 to 350 metres, with thickness increasing from the south-west (WCB) to the north-east (Appendix 1 Maps1&2).

A marine transgression in the Late-Jurassic resulted in the deposition of finer grained sediments through the reworking of existing sediments and the deposition of fine sediments in deeper water. Formations deposited at this time include the Alexander Formation, Jarlemai Siltstone and Callawa Formation. In Walyarta respective thickness ranges for these formations are 40-80, 50-100 and 0-40 metres, with the Alexander Formation and Jarlemai Siltstone increasing in thickness near the current coastline (Appendix 1 Maps 3, 4&5). The overlying Alexander Formation contains reworked deltaic sands, while the overlying Jarlemai Siltstone has characteristic low energy marine silts and clay sediments containing glauconite. In the WCB Higher energy palaeoenvironments were active during the deposition of the Alexander and Callawa Formations and this is influenced by the basin's proximity to the Pilbara Craton. Beach/barrier and fluvial processes respectively provided input to the Alexander and Callawa Formations, resulting in a thinner sequence of fine-grained marine sediments east to south east of the current coastline.

The Early Cretaceous (Neocomian) Broome Sandstone is characterised by both coarsening and fining upward sedimentary sequences indicating palaeoenvironments ranged from deltaic (progradation sequences) to fluvial (channel fill) (Forman and Wales 1981). Thicknesses of Broome Sandstone across Walyarta range from 100 metres to the north and current coastline, to 50 metres in the southwest and potentially absent to the south-east (Appendix 1 Map6).



#### 4.1 Cenozoic geology and palaeovalleys

The Broome Sandstone is overlain by a thin, up to thirty metres thick, sequence of generally Quaternary age or younger sediments comprising colluvium, alluvium, aeolian sands, beach deposits, intertidal and mangrove swamp deposits, evaporitic and pedogenic calcretes, lateritised Mesozoic sediments, salt lakes and claypans (Towner 1982a&b) (Figures 8 and 9).

Towner (1982a) noted that most of the mapped Cenozoic geological units grade into one another, with ferruginous and siliceous duricrust remnants cropping out in the uplands, grading to residual lateritic soils and pedogenic or fluvio-lacustrine calcretes on low rises. In the lower landscape, older erosional features (e.g. ephemeral lakes and drainages) contain mixed colluvial and alluvial sands, silt and minor gravels, with some lakes having a thin crust of evaporite minerals (e.g. gypsum).

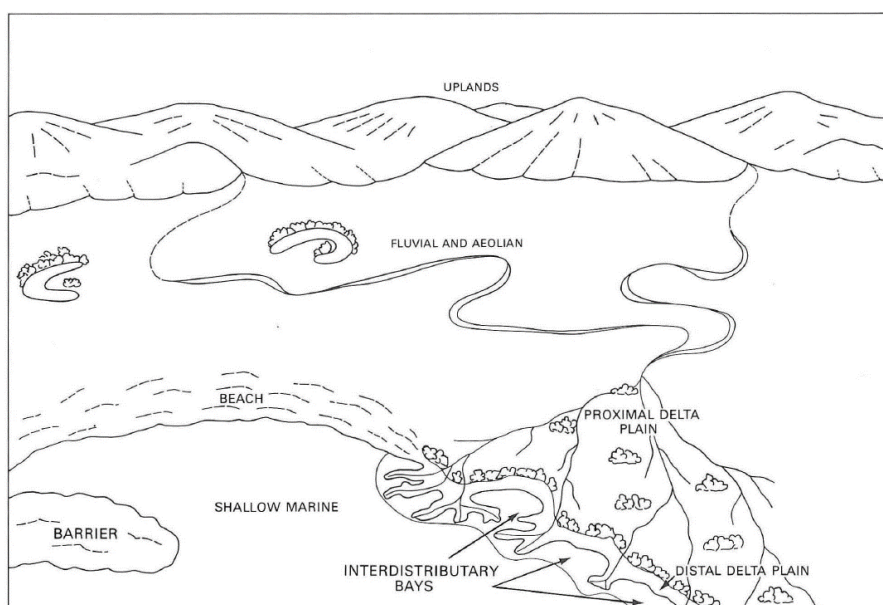


Figure 7 Schematic representation of palaeoenvironments responsible for the transportation and deposition of sediments in the Jurassic era (from Forman and Wales 1981)

Terrestrial dominated sediments merge into coastal tidal (supratidal) flats, which are Holocene in age and characterised by mixed sediment including grey clay, silt, sand and organic material on the eastern margin. Coastal dunes (Bossut Formation Qpb, see Figure 9) contain quartzose calcarenite and calcilutite and have a physiographic expression as well as underlying and interfingering with the tidal flats (Towner 1982a).

The hiatus in onshore sedimentation from the Cretaceous to the Quaternary is thought to have occurred in response to climate, topography and the location of the coastline/ocean. Rainfall was variable and low average annual rainfall promoted aridity, internal drainage and evaporation. This described the overall climatic behaviour through to the latter part of the Cenozoic (late Miocene) as the Australian continent moved southward. During this time salt lakes developed, evaporate deposits formed in lower lying areas, onshore sands were retained in the uplands and reworked by aeolian processes and gravity and ephemeral fluvial systems moved and preserved sands and alluvium in channel and valley systems (Figures 6, 10 & 11).



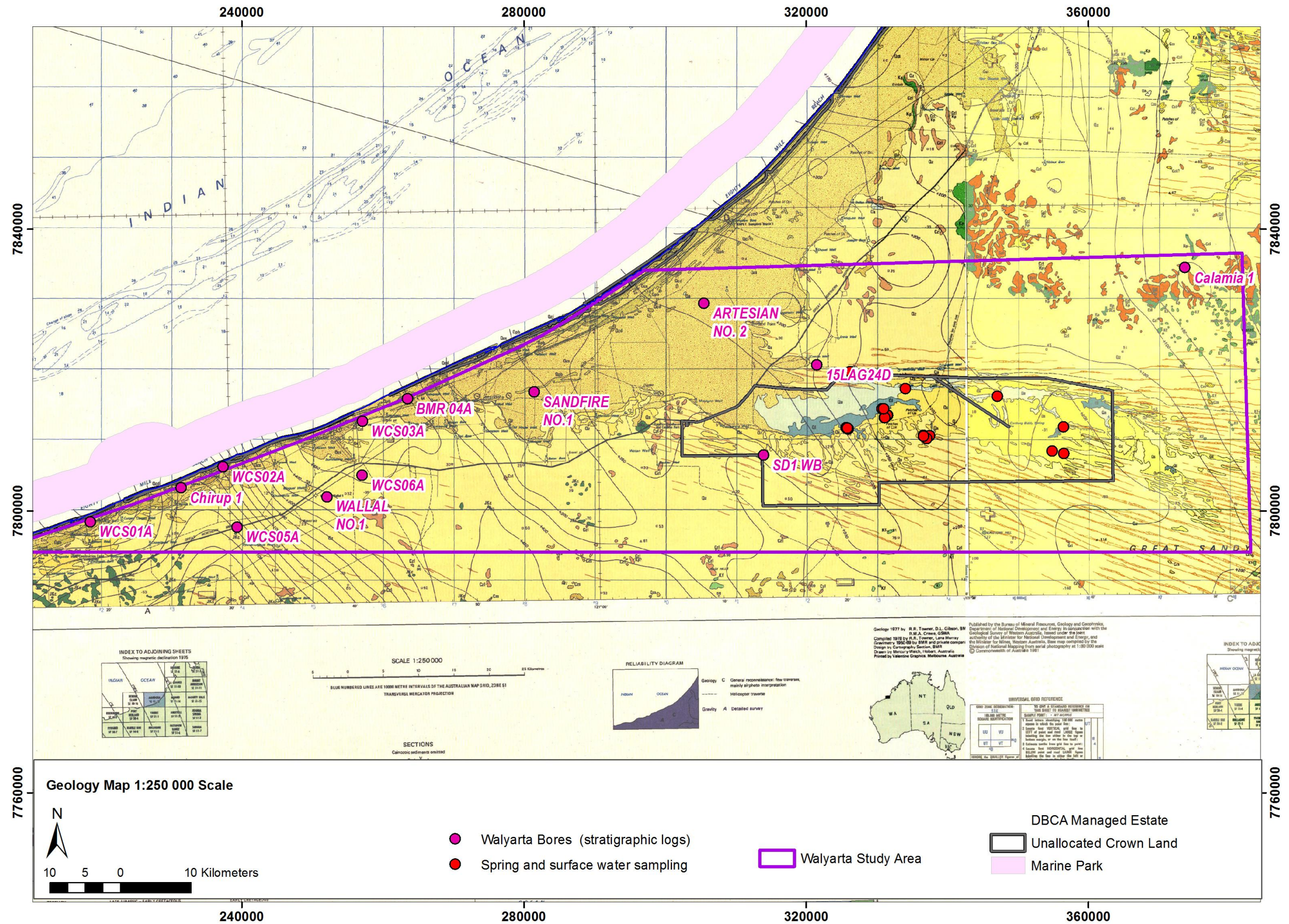


Figure 8 1:250 000 scale mapped geology for the Mandora Sheet (SE/51-13) and the Munro Sheet (SE/51-14) (refer to Figure 9 for the Key), Note digital data are not available and the central white strip marks the join between the two maps sheets.



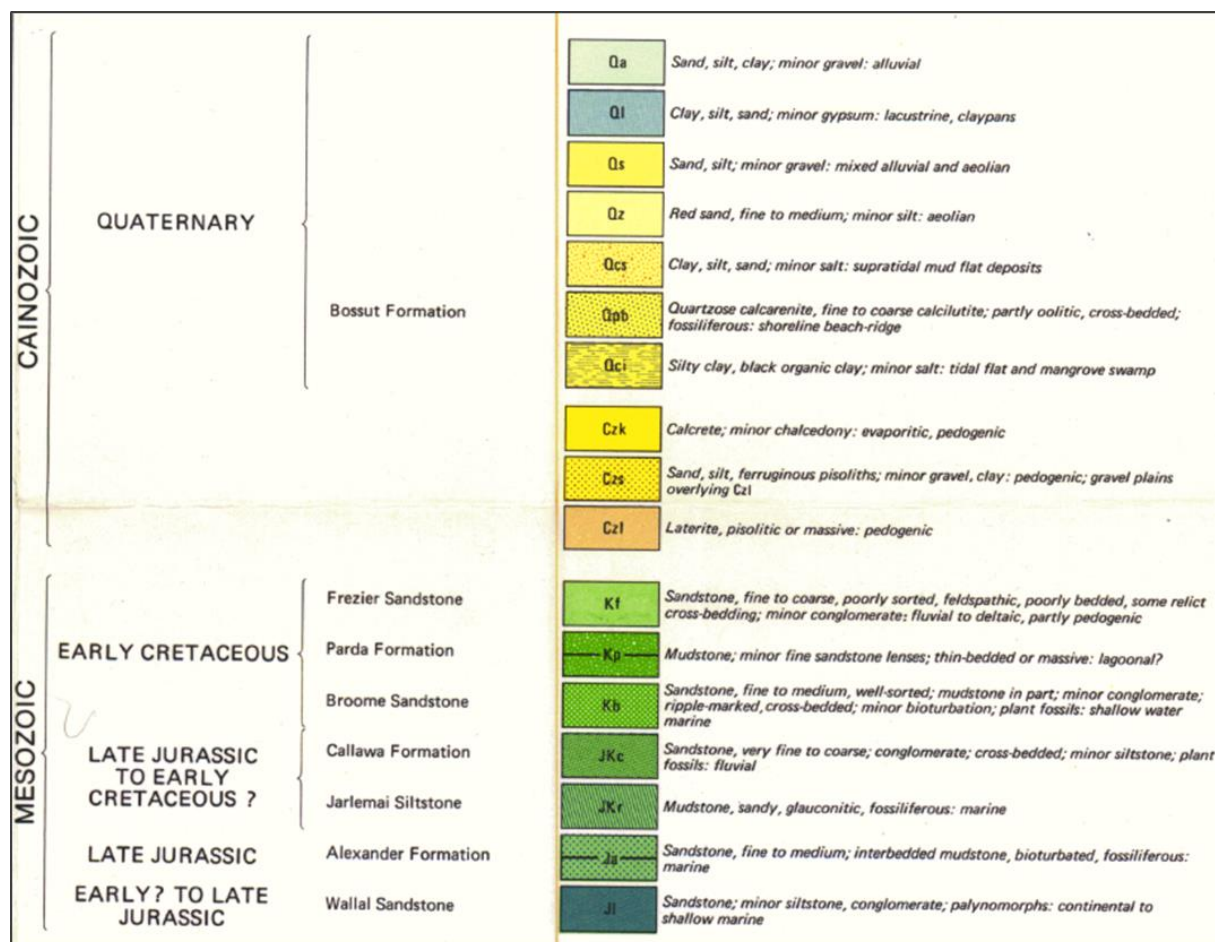


Figure 9 Key to mapped Mesozoic and Cenozoic (previously known as Cainozoic) geology in Figure 8 (from Towner 1982a).

The location of palaeovalley and palaeochannel sediments has been the subject of debate and research since the 1970's (Magee 2009). Two main watersheds were put forward by Beard (1973) who suggested that post Cretaceous uplift and above average Cenozoic rainfall encouraged the development of incised drainage lines (variation in relief of up of up sixty metres). These included the northern Mandora River, which drained the Mandora Palaeovalley (supported by tentative evidence), and the southern Canning River, which flowed through a chain of salt lakes, including Lake Dora and Lake Waukarlycarly before linking with the Oakover and De Grey Rivers (Forman and Wales 1981) (Figures 10 & 11).

Mulcahy and Bettany (1972) argued that despite higher average annual rainfall in the early Tertiary (now Palaeogene), rivers were likely to be short lived in flow due to the high permeability of surficial sediments and suggested that to the north of the Canning River the CB may have been internally draining, with no outlet to the sea. These authors put forward an outlet location for the northern drainage, located to the north of Wallal Downs; near bore WCS03 (see Appendix 3, Figure 16). This was speculative as offshore bathymetry data showed no evidence of a channel at the Early Tertiary coastline, which was located approximately 160km offshore. Others argue that during this period onshore erosion was dominant and sedimentation was predominantly off shore.

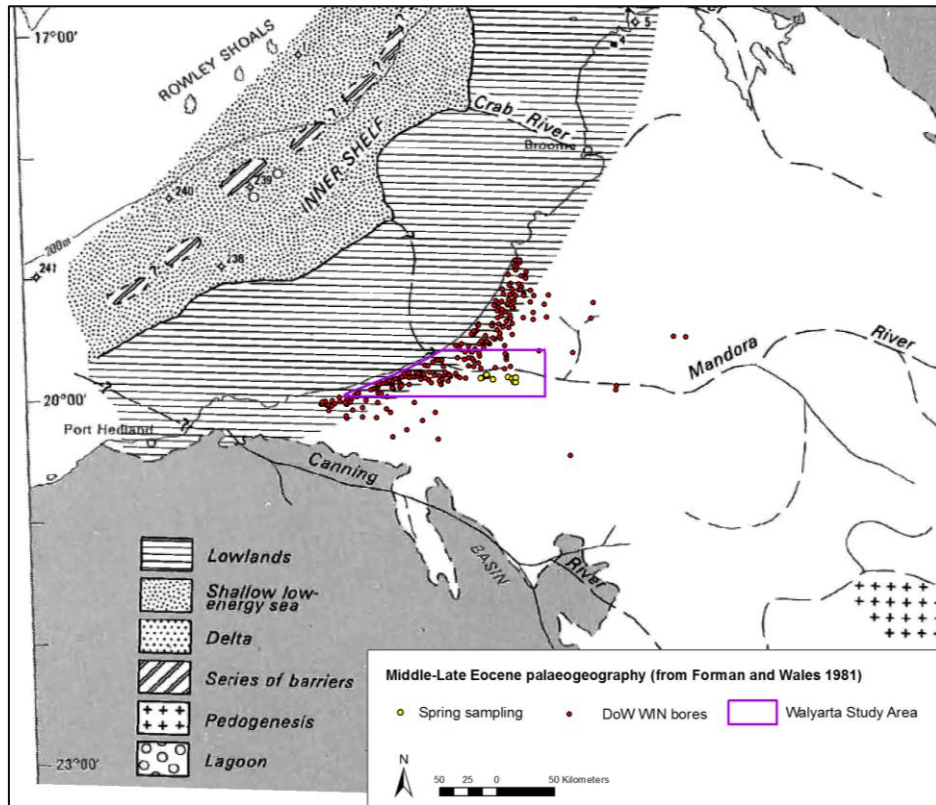


Figure 10 Middle to Late-Eocene palaeogeography showing the location of the Mandora palaeo river in relation to the Walyarta mound springs (adapted from Forman and Wales 1981).

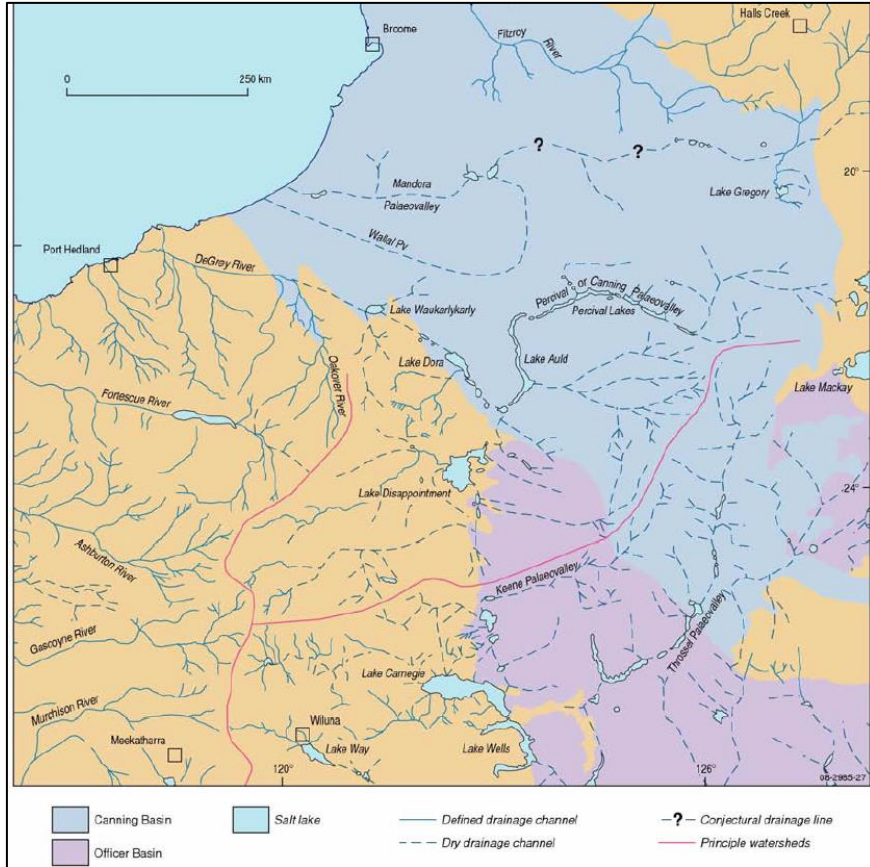


Figure 11 Regional map of the Canning Basin showing the location of the Mandora and Wallal palaeovalleys and salt lakes (modified from Magee 2009).

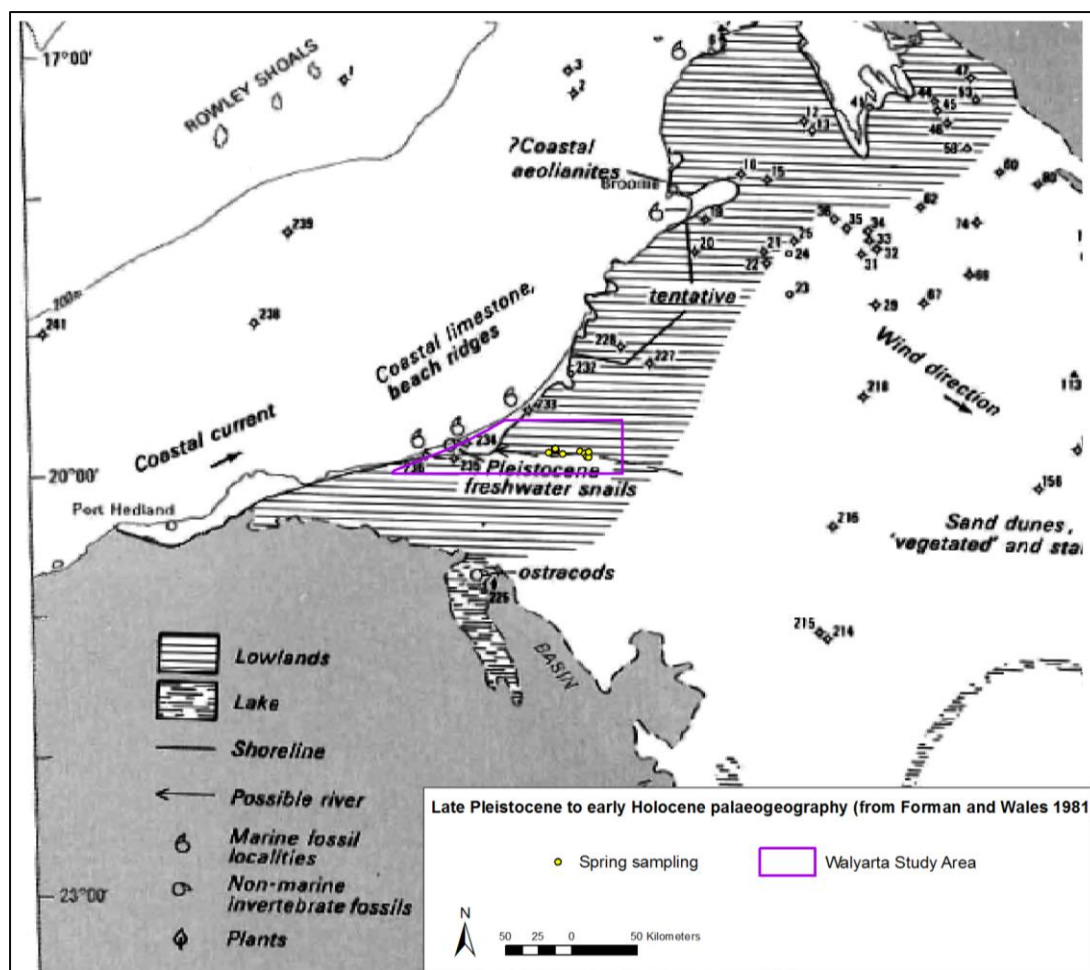


Figure 12 Late Pleistocene to early Holocene palaeogeography during the Flandrian transgression (17 000 to ~8 000 years ago) (adapted from Forman and Wales 1981).

In the Late Pleistocene (17 000 to ~8 000 years ago) beach ridges and fossils indicate that the shoreline in the Mandora Palaeovalley was approximately 30km inland from its current position, with over time coastal processes likely to have assisted onshore erosion and deposition (Figure 12)(Forman and Wales 1981). The location of major drainage networks were recognised as being coincident with major north-west trending geological structures that were likely to have assisted in generating the deeper incisions (Van der Graaff et al. 1977). The Wallal Palaeovalley is a good example of a north-west trending palaeovalley (Figure 11).

In 2012 Geoscience Australia published the WASANT Palaeovalley map, which employed terrain analysis (MrVBF, see Gallant and Dowling 2003) to assess valley flatness and produce a model of palaeovalley extents. The hypothesis that underpins this model is that the contemporary landscape has inherited geomorphic characteristics from the geologic past (Bell et al. 2012). The WASANT palaeovalley extents in Walyarta area are shown in Figure 13 and include the northern Cudalgarra palaeovalley. This approach was used by Hanna (2014) in the WCB who employed MrVBF data to hypothesise where palaeochannels may exist, if they were incised and if they were what geological formations comprised their infill. In this study Late Jurassic formations (Alexander, Jarlemai and Callawa Formations) were substituted by younger, Early Cretaceous sediments.



HYDROLOGICAL CONCEPTUALISATION OF THE WALYARTA MOUND SPRINGS

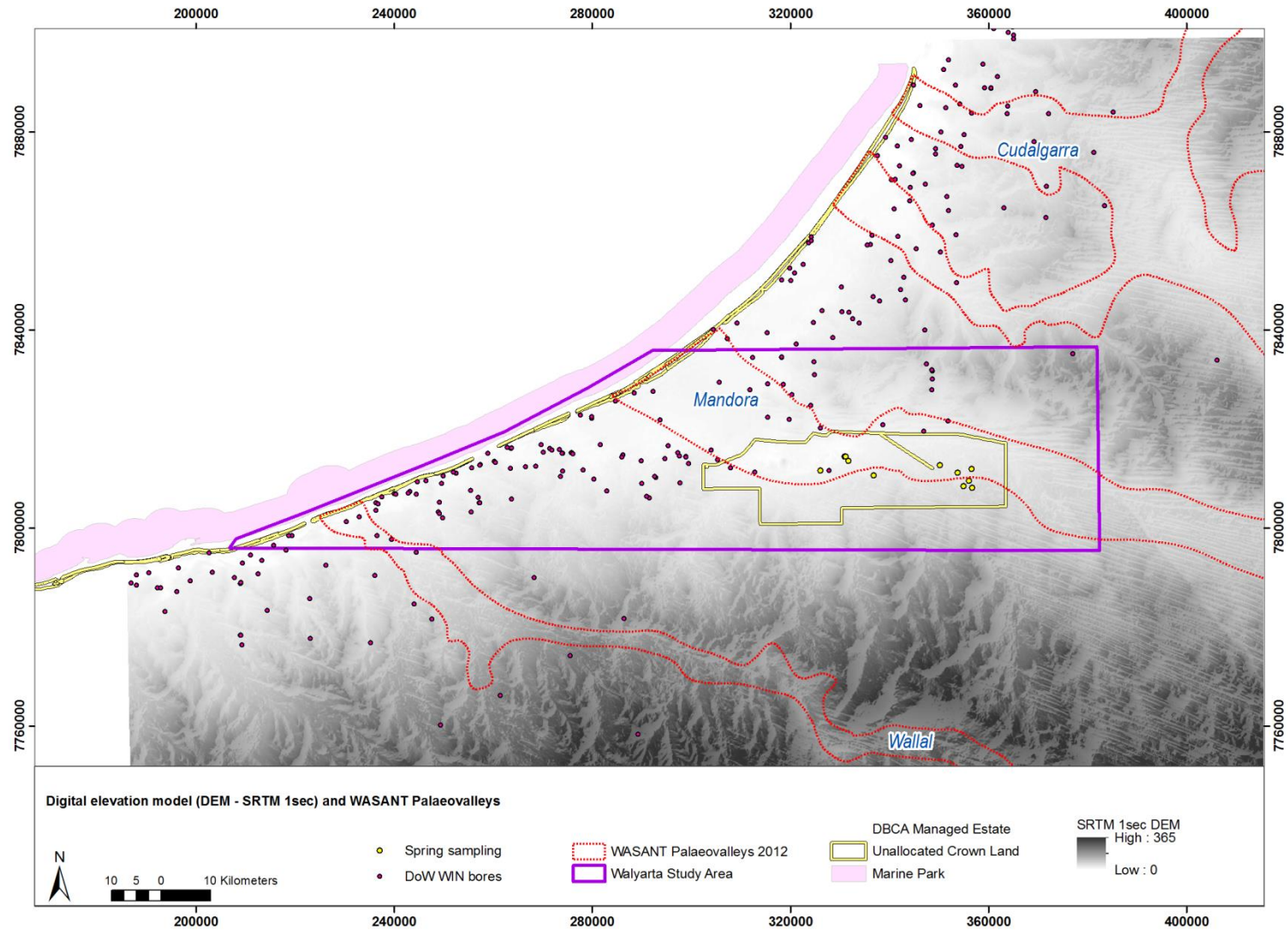


Figure 13 WASANT palaeovalleys for the CB – WCB, Walyarta Conservation Park and the La Grange area overlain on greyscale image of SRTM1s DEM (modified from Bell et. al. 2012)

The location and ideas on three dimensional extents of palaeovalleys in the CB have undergone refinement but to date there has been little verification of mapping models. This includes the nature of the valleyfill sediments (e.g. age and physical and chemical properties) and their relationships with geological structures and coastal processes over time.

#### 4.2 Canning Basin scale geological structure

Major tectonic events that influence structural styles in the CB have been summarised by FrOG TECH (2005) in their Australia wide basin scale study. This work involved interpreting coarse scale structural trends evident in available geophysical data. For the CB the following major structural trends were reported;

1. Late Carboniferous to Early Permian (306-268 Ma) NW-SE extension with the development of NE trending normal faults and NW trending relay zones; development of sub basins and reactivation of older NW-trending sinistral fracture and transfer zones (Figure 14a);
2. Late Triassic (220-210 Ma) local development of pull-apart and pop-up structures due to the reactivation of NW and NE trending dextral transpressional and sinistral wrench zones; dextral shear induced new fault extensions produced N-S trending normal faults and E-W trending folds (Figure 14b);
3. Miocene to Recent (21-5 Ma) collision SE Asian microcontinental fragments with NW Australia produced complex fault reactivation during Early Miocene, Late Miocene and Late-Early Pliocene; reactivation of normal faults in sinistral transtensional convergent margin (Figure 14c).

Mapped normal, transfer and undifferentiated faults interpreted to be Phanerozoic (post Proterozoic and more likely to be important in Walyarta) are depicted on Figure 15.

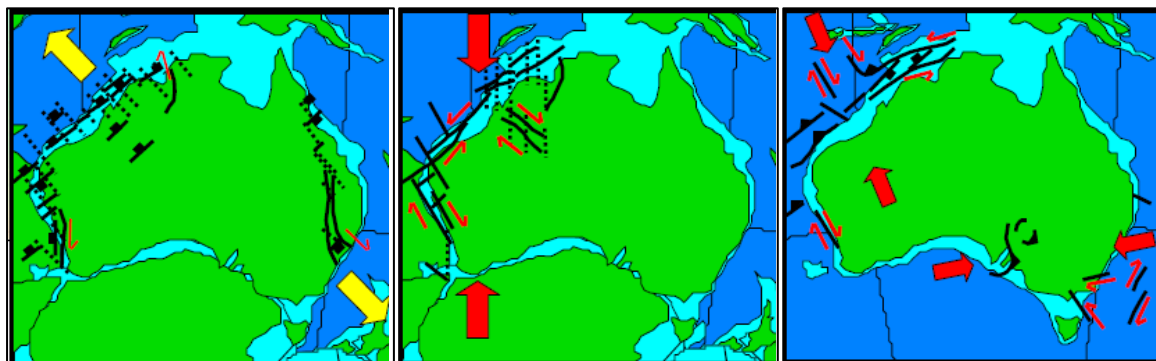


Figure 14a,b&c (left to right) Dominant Australasian stress-strain relationships and geological faulting styles in (a) the Late Carboniferous to Early Permian (b) Late Triassic and (c) Miocene to Recent; Arrows show the major direction of movement, dotted line-work indicates aprox movement extent, rectangle annotation - normal faulting and triangles - thrust faulting (from FrOG Tech 2005).

In 2014, available CB geophysical data were reprocessed and modelled and major trends reported (Parra-García et al. 2014). The study mainly focused on tectonic settings north of and including the Willara sub-basin. For some geophysical datasets this limits their application to the south of Walyarta and the WCB, although the bouger gravity data map major troughs and basins as well as intervening basement highs, with Walyarta located on a basin wide high (Appendix 2 Map1).

This is verified with results of CB depth to magnetic source modelling, which was carried out using dRTP (differentially reduced-to-pole) magnetic data (Appendix 2 Maps 2&3). These maps show Walyarta spring sampling sites are closer to the depth to magnetic sources (crystalline basement and/or Permian sediments) than areas to the west, north and north-east, within the Willara sub-basin, as well as the deeper basins / troughs (as shown in Figure 3).

HYDROLOGICAL CONCEPTUALISATION OF THE WALYARTA MOUND SPRINGS

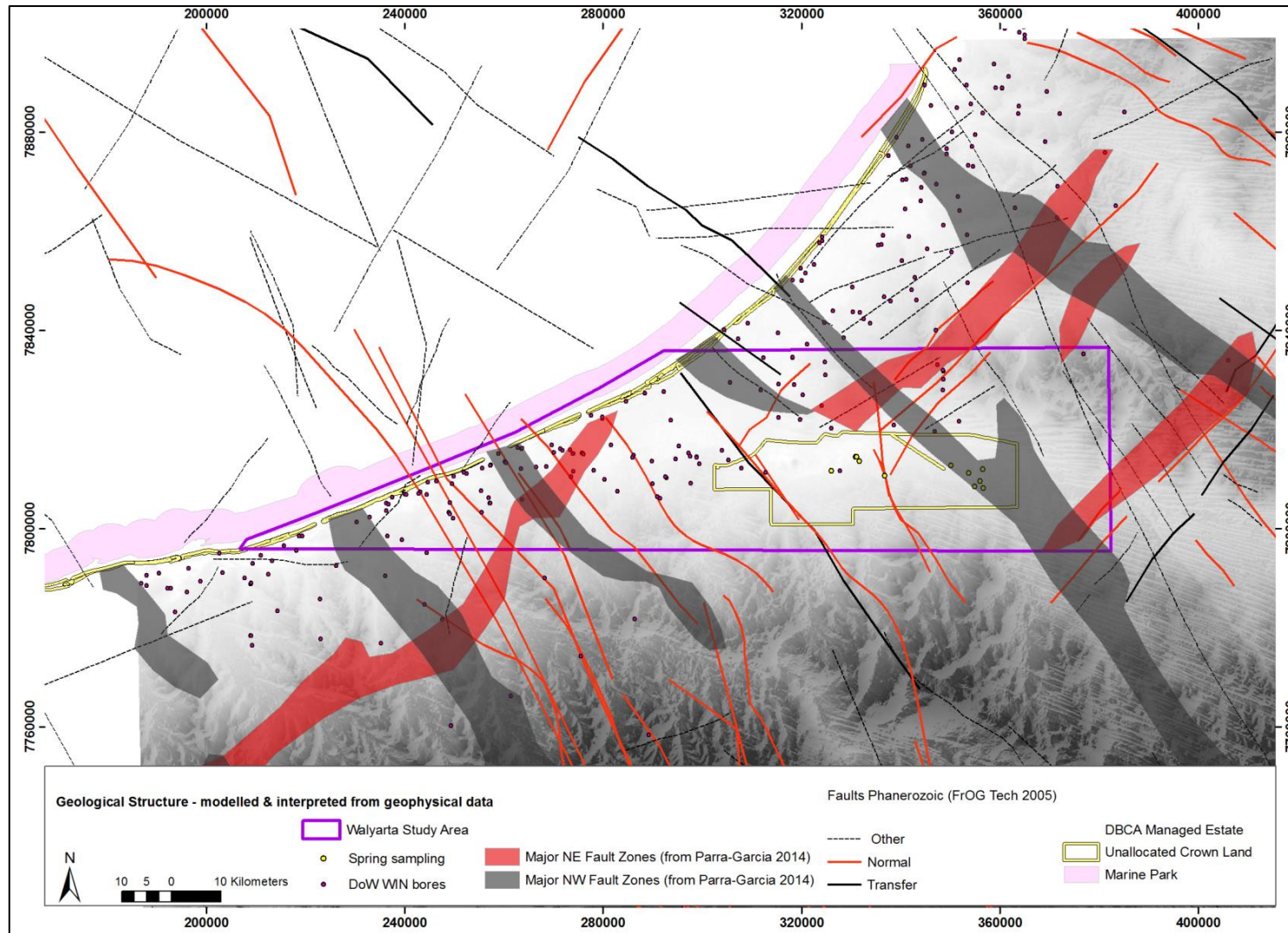


Figure 15 Major coarse scale Phanerozoic geological structures interpreted from modelled magnetic and gravity data overlain on greyscale image of SRTM 1s DEM (adapted from Parra-García 2014)



Mapping and enhancement of geological structures was undertaken by Fathom Geophysics using magnetic and isostatic residual gravity data. Results reported in Parra-García (2014) resolve important structural boundaries for the Willara sub-basin and Walyarta (see Figure 15; Appendix 2 Maps 5, 6 and 7).

### 4.3 Walyarta stratigraphy and structure

Information on stratigraphy provided by drilling in the Walyarta Conservation Park is provided by thirteen drill-holes that were drilled primarily for groundwater and petroleum exploration (Table 1, Figure 14). Stratigraphic information collected is highest for the Broome Sandstone, with little information collected on the full stratigraphic thickness of the Wallal Sandstone (Table 1). Spatial confidence is highest from the current coastline to approximately 15km inland where most of the bores have been drilled (Figure 16). Only one bore (SD1 WB) is located within the Walyarta Conservation Park and this drill-hole provides information on the Broome Sandstone.

Drillhole/Bore Name	Purpose/Asset owner	Depth drilled (metres below ground level)	Quaternary	Broome Sandstone	Jarlemai Siltstone	Wallal Sandstone
15LAG24D	Groundwater investigation/DPIRD (DAFWA)	96	Y	Y		
ARTESIAN NO. 2	Groundwater investigation/	357	Y	Y	Y	*
BMR 04A Mandora	Petroleum exploration/Geoscience Australia	549	Y	Y	Y	Y
Calamia 1	Petroleum exploration/Oil Comp Aust	1671	Y	Y	Y	Y
Chirup 1	Petroleum exploration/WAPET	762		Y	Y	Y
SANDFIRE NO.1	Groundwater investigation/	276		Y	Y	
SD1 WB	Groundwater investigation/Pittston Aust Min Exp Pty Ltd	62		Y		
WALLAL NO 1	Petroleum exploration/Wallal Station (prev WAPET)	309		Y	Y	
WCS01A	Groundwater investigation/DWER (DoW/GSWA)	318	Y	Y	Y	*
WCS02A	Groundwater investigation/DWER (DoW/GSWA)	375	Y	Y	Y	*
WCS03A	Groundwater investigation/DWER (DoW/GSWA)	350	Y	Y	Y	*
WCS05A	Groundwater investigation/DWER (DoW/GSWA)	289	Y	Y	Y	*
WCS06A	Groundwater investigation/DWER (DoW/GSWA)	310	Y	Y	Y	*

\*indicates full thickness of the Wallal Sandstone was not drilled/sampled

**Table 1 Drill-holes with lithological logging in the Walyarta Conservation Park (data from DWER Water Information Network (WIN)).**

#### 4.3.1 Airborne electromagnetic data (AEM)

To improve understanding on the distribution of sediments and potential groundwater resources, (see Section 6) in 2012-2013 the Department of Water and Environmental Regulation (DWER) (previously Department of Water) and Department of Primary Industries and Rural Development (DPIRD) (previously Department of Agriculture and Food WA) sourced funding to acquire airborne geophysical (electromagnetics) (AEM) data over the respective WCB and the Willara sub-basin areas.

Data (TEMPEST AEM) were acquired in 2013-2014. In 2015 all available AEM data were merged, reprocessed and modelled (inverted) into a coverage that extended across the WCB and Walyarta Conservation Park (Figure 16) (Mira Geoscience 2016). The main electrical targets generated were interpreted to be the top of the Jarlemai Siltstone and the salt water interface (Mira Geoscience 2016). The work showed that within the project area, AEM could resolve sediment electrical conductivity structure to depths of up to 700 metres below ground level, with depth of investigation (DOI) decreasing where there were thick evaporite deposits and/or high concentrations of solutes entrained in sediments.

HYDROLOGICAL CONCEPTUALISATION OF THE WALYARTA MOUND SPRINGS

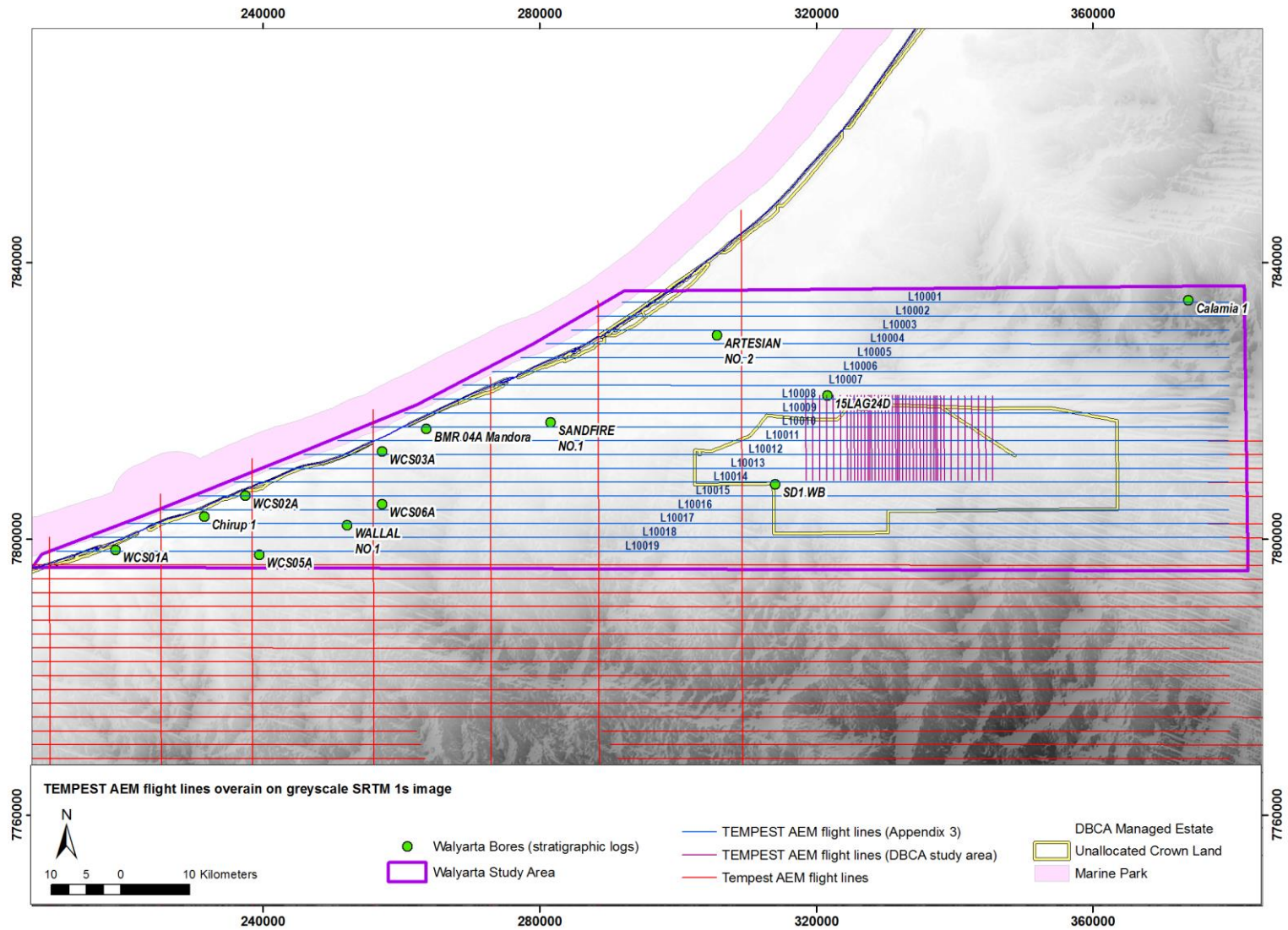


Figure 16 Location of E-W trending TEMPEST AEM flight lines (2km line spacing blue lines) and drill holes/boreholes with lithological logs in Walyarta and northern WCB (AEM data inverted for this study include data presented in Appendix 3 and closely spaced (50-100 metre spacing) north-south orientated flight lines – coloured purple in the above figure)

Walyarta proved to be a challenging area to resolve variation in electrical conductivity due to higher solute storages in the tidal flat calcilutite deposits and Quaternary, or older, lacustrine and alluvial sediments. An investment had been made in acquiring coarse east-west and finer scale north-south orientated AEM data over Walyarta (Figure 16) and these data were reprocessed (inverted) in 2016 to optimise the extraction of fine-scale, near surface geological and hydrogeological data plus information on the deeper aquifer geometry (Soerensen et. al. 2017).

The technical rationale for this work, including specifications of the TEMPEST AEM system, is described in Soerensen et. al. (2017). In brief, the study involved application of a non-linear inversion of raw TEMPEST data using a 1D model assumption to produce of a smooth layered (25 layer) laterally constrained inversion (LCI) using AarhusInv 1D inversion code (Auken et al. 2005).

The thickness of the first layer in the smooth layer inversion was 5m, with layer thicknesses increasing logarithmically to the last layer boundary at a depth of 500 metres below ground level. Of note in this approach is the potential complication in selecting layer boundaries due to the gradational change in conductivity produced by the large number of layers. The LCI is characterised by its ability to allow prior information from adjacent AEM soundings (e.g., the expected geological variability of the area) to migrate along the flight lines. This aids geological interpretation as it enhances the connection of layer parameters and encourages the definition of laterally continuous conductive layers. The study also determined the depth of investigation (DOI) to understand at what depth below ground level the AEM system will reliably map or resolve the electrical character of the geology and hydrogeology. This was found to be highly variable and the DOI for inverted data from the nineteen 2km spaced, east-west orientated flight lines (Figure 16) is shown on conductivity depth sections in Appendix 3; defined by an opaque overlay.

Measurements of the electromagnetic response were converted to a modelled ground conductivity and results presented in formats that allowed their interpretation against existing or new ground data and information. This process is known as inversion and generates outputs that allow for the visualisation and mapping of subsurface conductivity in three dimensions (e.g. Lane 2000).

Comparisons of inversion outputs showed that overall the modelled structure is comparable, with the AarhusInv LCI resolving more near surface conductivity variation and use of the 1D approach was vindicated, with no obvious artefacts observed as a result of the complex conductivity structure and geometries (e.g. contemporary salt water interface, salt storage, fault conduits and fault blocks with contrasting groundwater quality – see Figure 17).

Interval conductivity images were generated for 26 layers, 16 at 10 metre intervals (from 0 to 160 metres below ground level) and 10 at 20 metre depth intervals (from 160 to 360 metres below ground level) and gridded at a cell size of 400m. Drill-hole and borehole stratigraphy in Table 1 were examined to assess layers that were intersecting the main formations discussed in Section 2. Representative interval conductivity images were selected for the Quaternary Formations (depth 0 to 10m below ground level; Figure 18), Broome Sandstone (depth 40 to 50m below ground level; Figure 19), Jarlemai Siltstone (140 to 150m below ground level; Figure 20) and the Wallal Sandstone (280 to 300m below ground level; Figure 21).

HYDROLOGICAL CONCEPTUALISATION OF THE WALYARTA MOUND SPRINGS

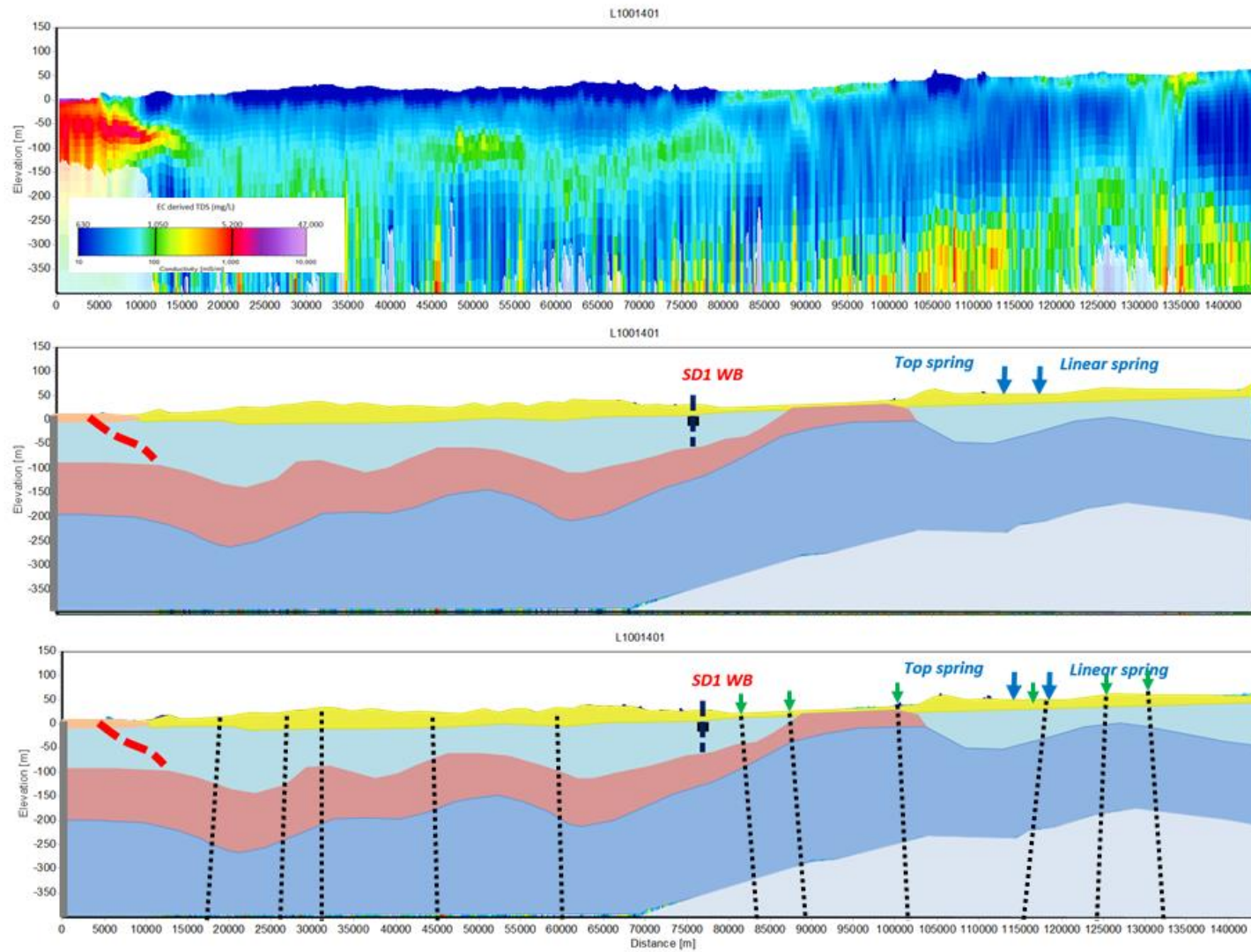


Figure 17 Example of stratigraphic and structural information from TEMPEST AEM flight line L10014 (viewed west to east; see Figure 14 for location and Appendix 3 for key)



HYDROLOGICAL CONCEPTUALISATION OF THE WALYARTA MOUND SPRINGS

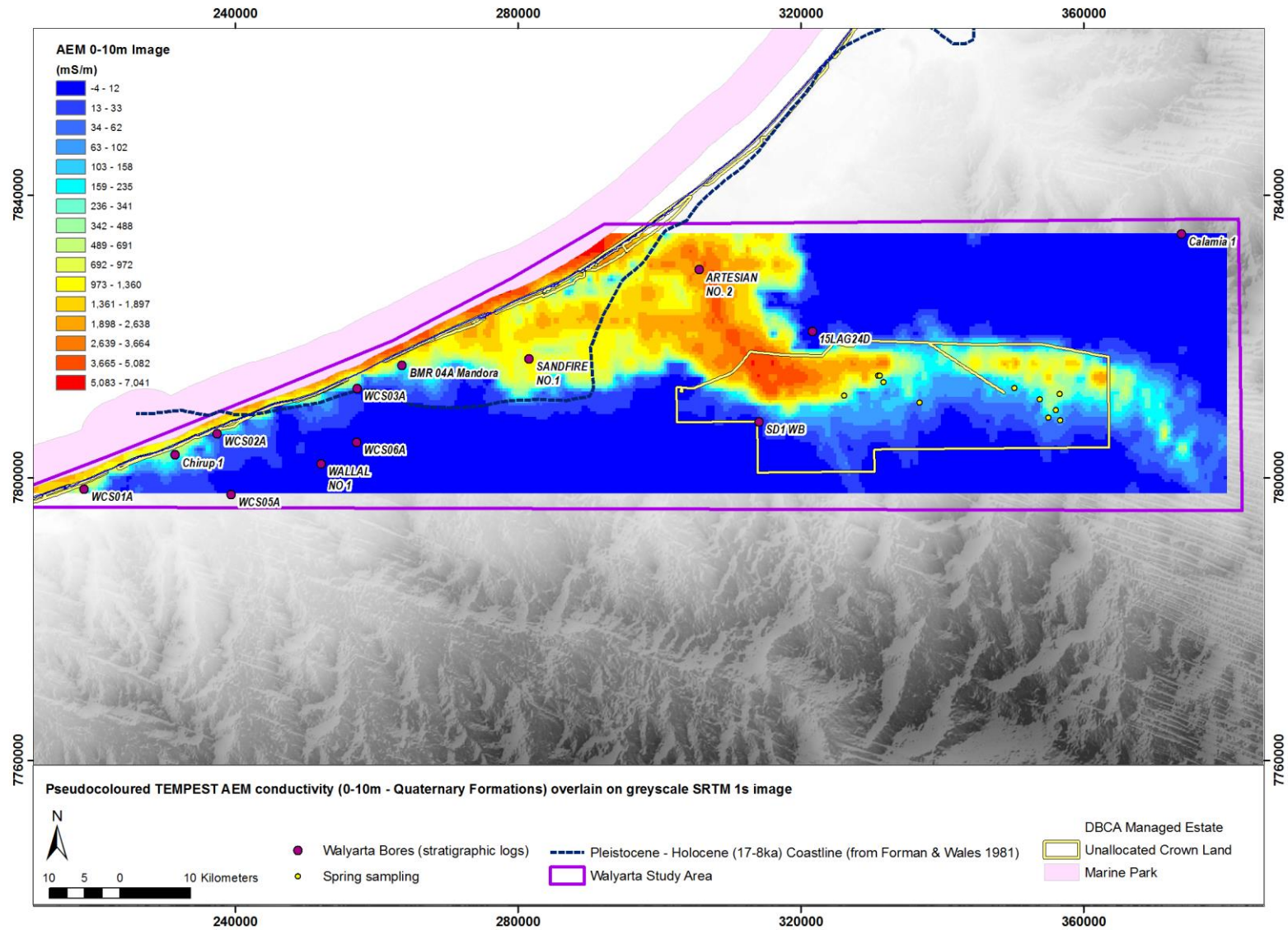


Figure 18 Pseudocoloured TEMPEST AEM interval conductivity image (0-10m) showing electrical conductivity variation in the Quaternary Formations (assuming lateral continuity)

HYDROLOGICAL CONCEPTUALISATION OF THE WALYARTA MOUND SPRINGS

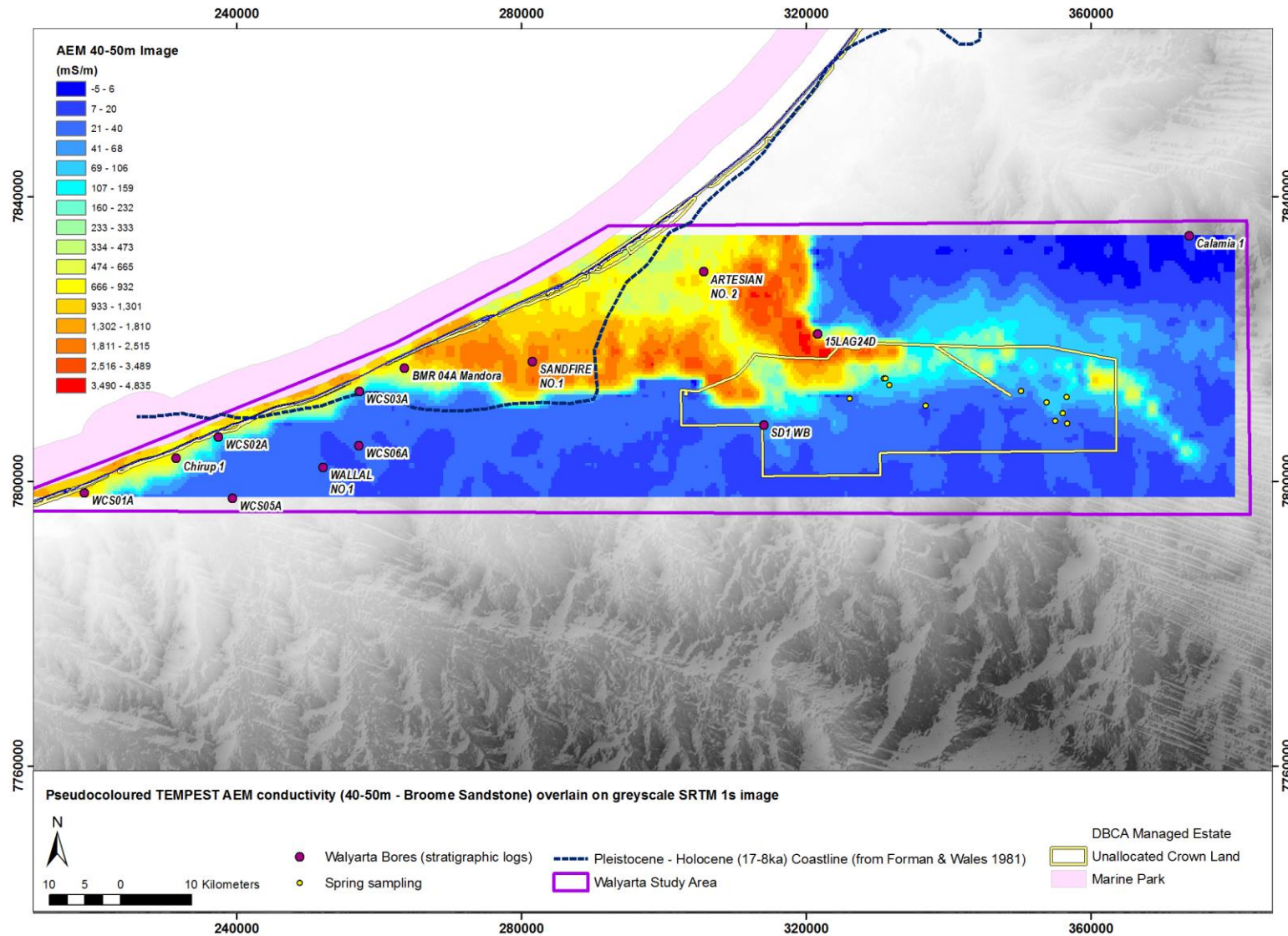


Figure 19 Pseudocoloured TEMPEST AEM interval conductivity image (40-50m) showing electrical conductivity variation in the Broome Sandstone (assuming lateral continuity)

HYDROLOGICAL CONCEPTUALISATION OF THE WALYARTA MOUND SPRINGS

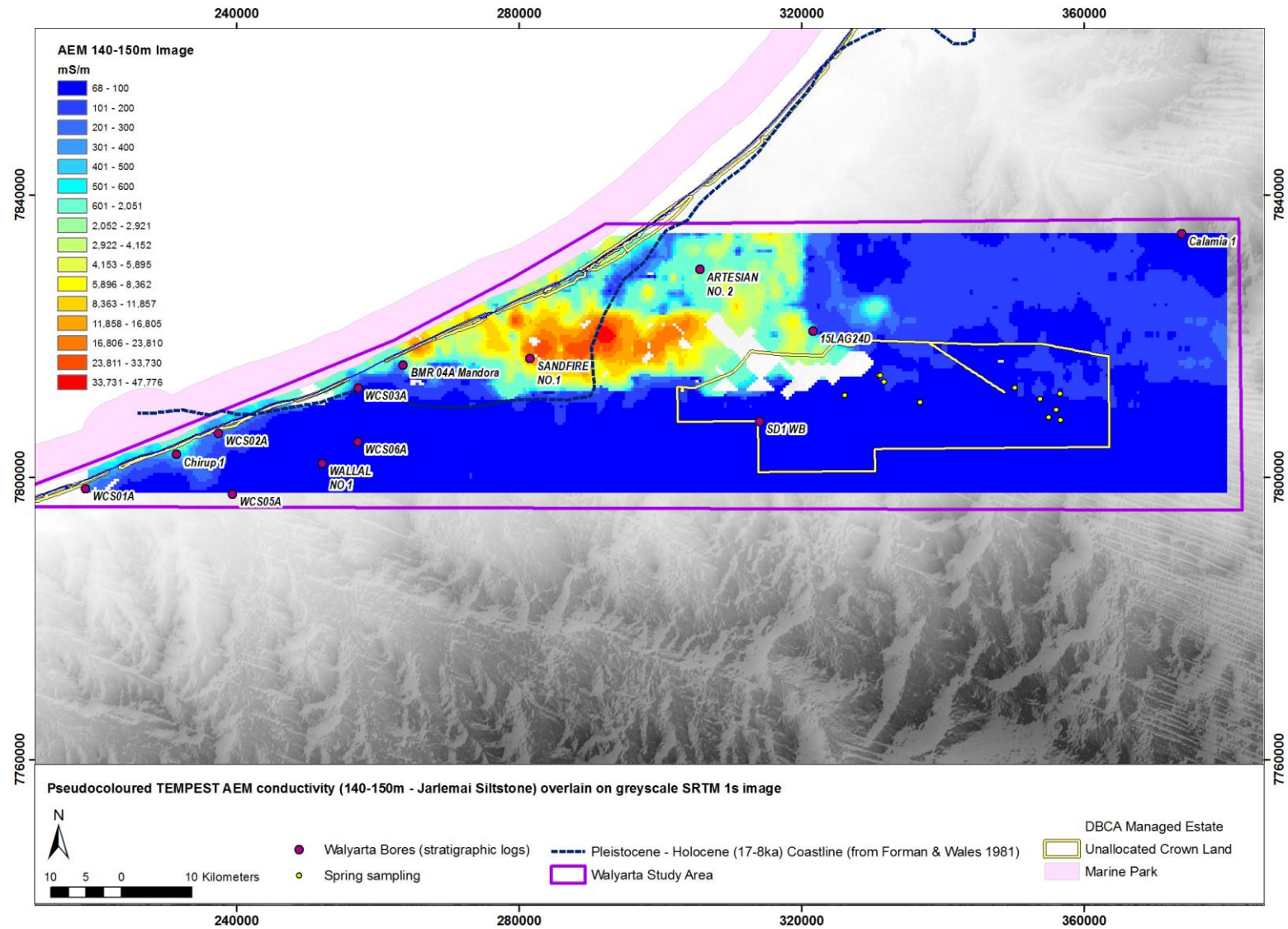


Figure 20 Pseudocoloured TEMPEST AEM interval conductivity image (140-150m) showing electrical conductivity variation in the Jarlemai Formation (assuming lateral continuity)



HYDROLOGICAL CONCEPTUALISATION OF THE WALYARTA MOUND SPRINGS

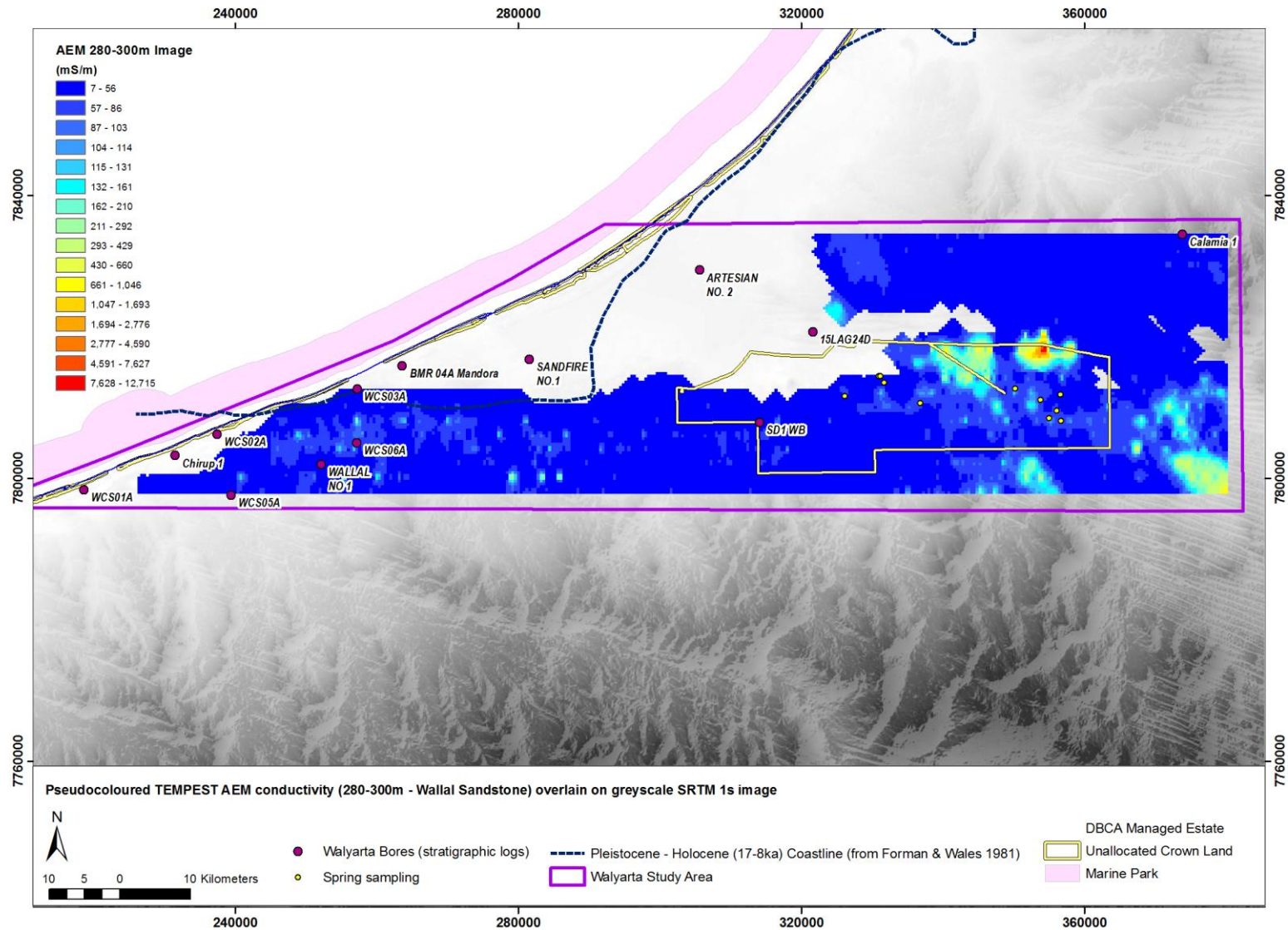
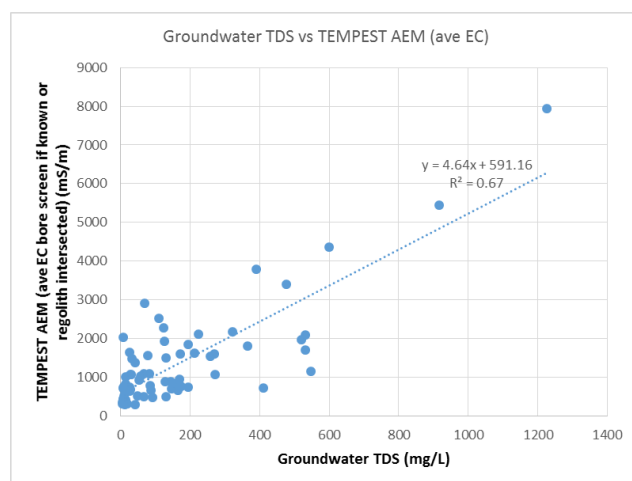


Figure 21 Pseudocoloured TEMPEST AEM interval conductivity image (280-300m) showing electrical conductivity variation in the Wallal Sandstone (assuming lateral continuity)

Patterns observed in all interval conductivity images (Figures 18 to 21) and conductivity depth sections (Appendix 3) concur, in part, with observations reported by Mira Geoscience (2016), specifically that the salt water interface (past and present) and the top of the Jarlemai Siltstone are the dominant conductivity features (conductivity threshold of 300 mS/m), which allows them to be mapped spatially (Appendix 3). The AEM data can determine the combined thickness of formations overlying the Jarlemai Siltstone where the conductivity contrasts are clear. However, as Figure 17 shows, this is not always clear in Walyarta, particularly in the central to eastern parts of the study area (Figure 20).

Mira Geoscience (2016) noted that median electrical conductivity (EC) data from thirteen bore hole induction logs did not reveal large conductivity contrasts between the sandstone formations and formations with higher percentage of clay-sized material (e.g. top of Broome and Wallal Sandstone approx. median EC (13 to 16 mS/m respectively) and top of Jarlemai, Permian and Basement approx. median EC (41, 44 & 36 mS/m respectively) (note that induction log conductivity distributions were skewed or have multiple populations in the case of the Permian and Basement formations).

Induction logging was undertaken where bores were prospective for fresh to brackish groundwater supplies and is therefore unlikely to provide an accurate representation of the range of conductivities for these formations. In Walyarta conductivity ranges are large and this is due to the wide range of groundwater quality in all formations mapped by the TEMPEST AEM. The Broome and Wallal Sandstone conductivity EC ranges are (0 to 5000 and 13000 mS/m respectively) and top of Jarlemai (70 to 48000 mS/m) (Figures 19 to 21). The small variation in borehole induction electrical conductivity reported by Mira Geoscience (2016) can be interpreted to indicate that formation conductivity is driven by the total dissolved solids (TDS) in the entrained groundwater rather than the conductive response of formation minerals (e.g. clays). This is not uncommon in these materials and settings and is supported by the relationship between groundwater quality and TEMPEST AEM (average conductivity) for bores sampling the Quaternary Formation and Broome Sandstone within and in close proximity to Walyarta (Figure 22). This discussion is expanded in Section 6.



**Figure 22 Broome Sandstone relationship between groundwater TDS (mg/L) and TEMPEST AEM (average EC) in Walyarta (n=68)**

Interpretations of formation thickness are further complicated for the Jarlemai Siltstone and Wallal Sandstone Formations due to the AEM system DOI, which is shown as an opaque overlay in

Appendix 3 and null values (white in colour) in Figures 20 and 21. These figures show that the DOI limits the use of AEM data for the generation of isopachs for the central and north-western quadrant of Walyarta, the Jarlemai Siltstone and Wallal Sandstone respectively.

As conductivity patterns show similar pattern breaks to the coarse scale geological structure these data and airborne magnetic data can help refine faulting and landscape processes and can be used to provide additional evidence to the likely preservation and thickness of formations in Walyarta.

#### 4.3.2 Airborne magnetic data

Recent interpretations of airborne magnetic data in the WCB and Walyarta area had reported that there were no significant geological faults present in the Mesozoic and Quaternary sediments, with the exception of one north-east trending fault located near to and immediately south of the southernmost mound springs (Mira Geoscience 2016). This fault zone was also noted to be associated with the uplift of Permian sediments and potential development of a palaeochannel.

As the breaks within the different AEM conductivity depth images appear to be fault controlled (Figures 18 to 21) it was considered necessary to re-investigate the geological information present in the airborne magnetic data. Consequently, airborne magnetic data were sourced from the Geological Survey of Western Australia (GSWA) and Geoscience Australia (GA) in gridded (40m cell size) and imaged formats. An interpretation of the magnetic data helped to understand the distribution of coarse scale magnetic features and in-particular, the application of a first vertical derivative (1VD) filter sharpened textural image was used to interpret and integrate with the AEM data to determine geological structures and shallow palaeo-drainage features.

Assessment of 1VD magnetic imagery indicates that the structural grain interpreted by FrOG Tech (2005) exists at a finer scale (Figure 23). Major NW-SE trending transfer faults break up the geology into a series of fault blocks, with reactivation of left lateral strike slip structures producing both strike slip and normal displacement. The WSW-ENE normal faults also have an element of strike slip displacement. The reduced to pole (TMI-RTP) and 1VD magnetic images in Figure 24 shows several distinct NW-SE trending units with significantly different magnetic response (amplitude and wavelength). From the magnetic response it can be inferred that the high amplitude and high wavelength areas have a shallow depth to magnetic source (e.g. closer to the land surface, with the magnetite source inferred to be either Permian or Basement) in the south-west and south-eastern areas of Walyarta. The areas with a low amplitude and low wavelength response in the central northern area (blue shading in Figure 24) are inferred to have a deep magnetic source (approx. 50 to 150 metres below ground level – nominally termed Eocene in Figure 24). Palaeo-drainage channels located west and south of the Walyarta springs are associated with a very high amplitude high frequency magnetic response and partial dendritic pattern. In the valley floor linear, high-frequency (shallow – near surface) magnetic responses correspond with younger beach/ slope deposits and strandlines, which are likely to be related to the last major sea level high stand in the Pleistocene – Holocene as they show good correlation with ideas on where these coastlines were located in this period (Figure 24) (Semeniuk 2000). Shallow interpreted channel features in the central Walyarta area correspond to relay displacement along NE-SW trending normal faults and these are noted to be in close proximity to some springs, which is expected as there is generally a relationship between Palaeo-drainage networks and major structural trends (Van der Graff 1977).

HYDROLOGICAL CONCEPTUALISATION OF THE WALYARTA MOUND SPRINGS

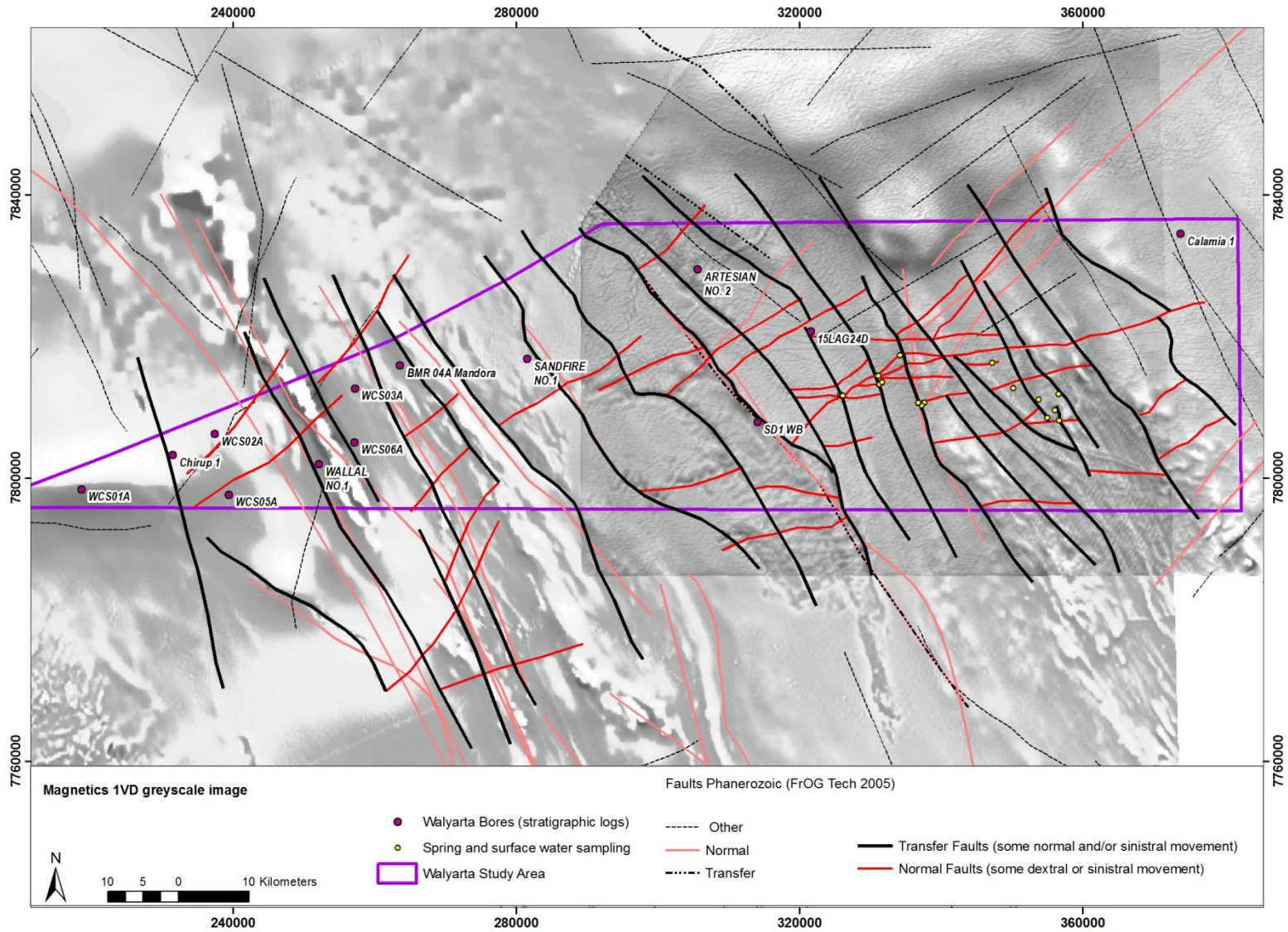


Figure 23 Airborne magnetic 1VD greyscale image overlain by FrOG Tech coarse scale Phanerozoic structural interpretation and Walyarta major fault interpretation



HYDROLOGICAL CONCEPTUALISATION OF THE WALYARTA MOUND SPRINGS

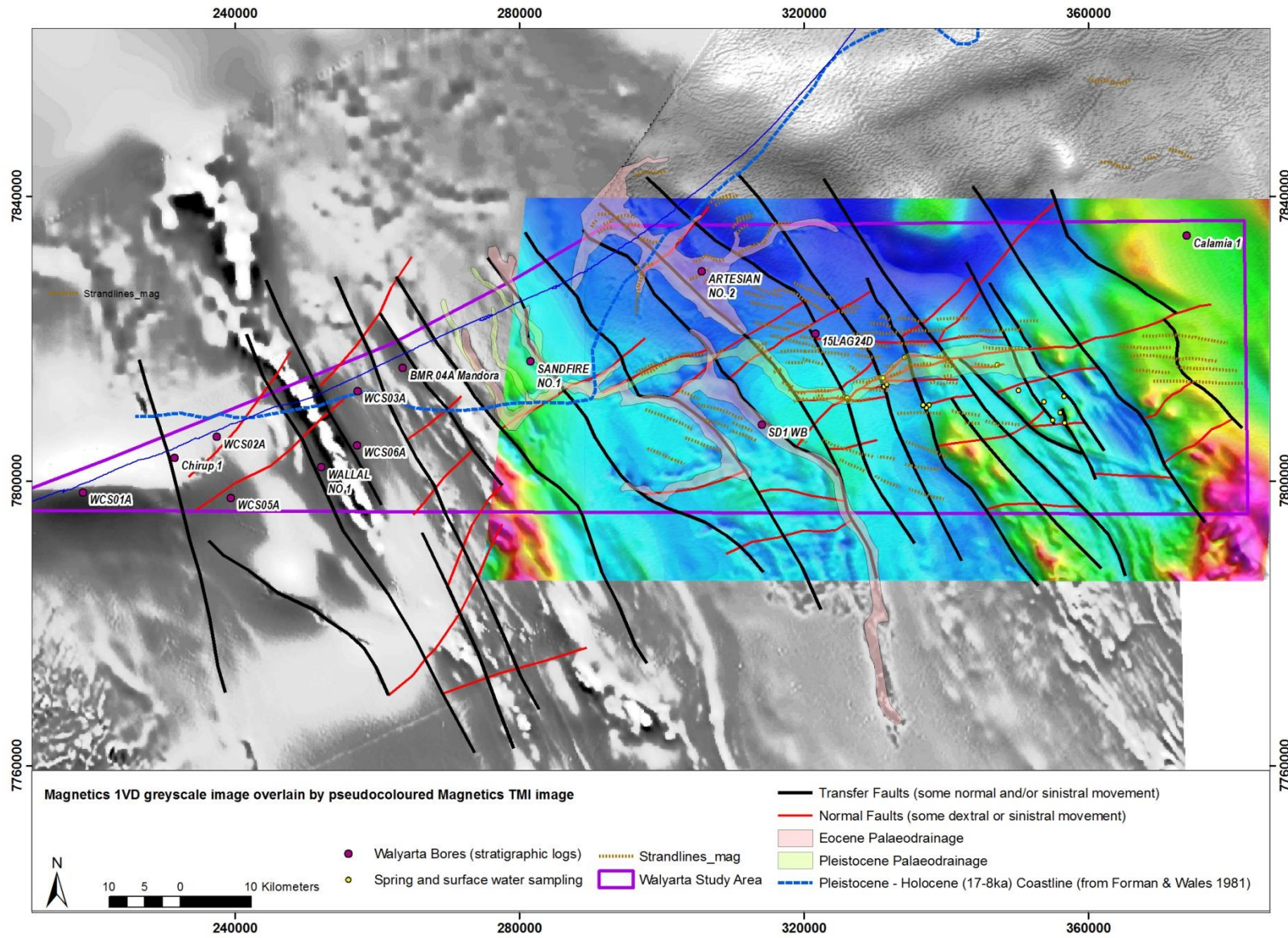


Figure 24 Airborne magnetic 1VD greyscale and pseudo-colour TMI images overlain by Walyarta interpretation of magnetic features (geological faults, channels and strandlines)

HYDROLOGICAL CONCEPTUALISATION OF THE WALYARTA MOUND SPRINGS

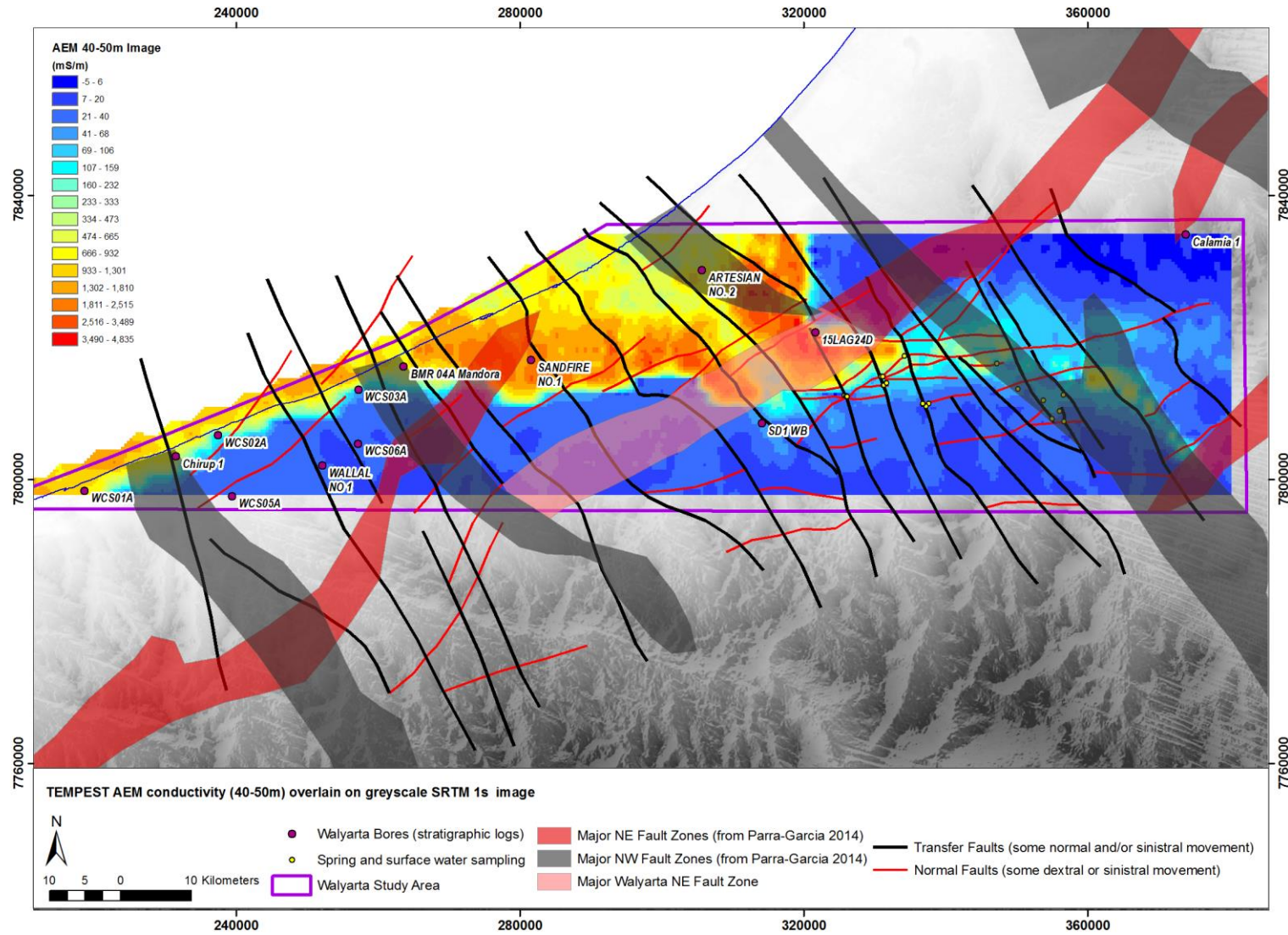


Figure 25 Walyarta major fault interpretation overlain on pseudo-colour AEM conductivity (40-50m – Broome Sandstone) and greyscale SRTM 1s images to understand relationships between major electrical conductivity pattern breaks and geological faults



HYDROLOGICAL CONCEPTUALISATION OF THE WALYARTA MOUND SPRINGS

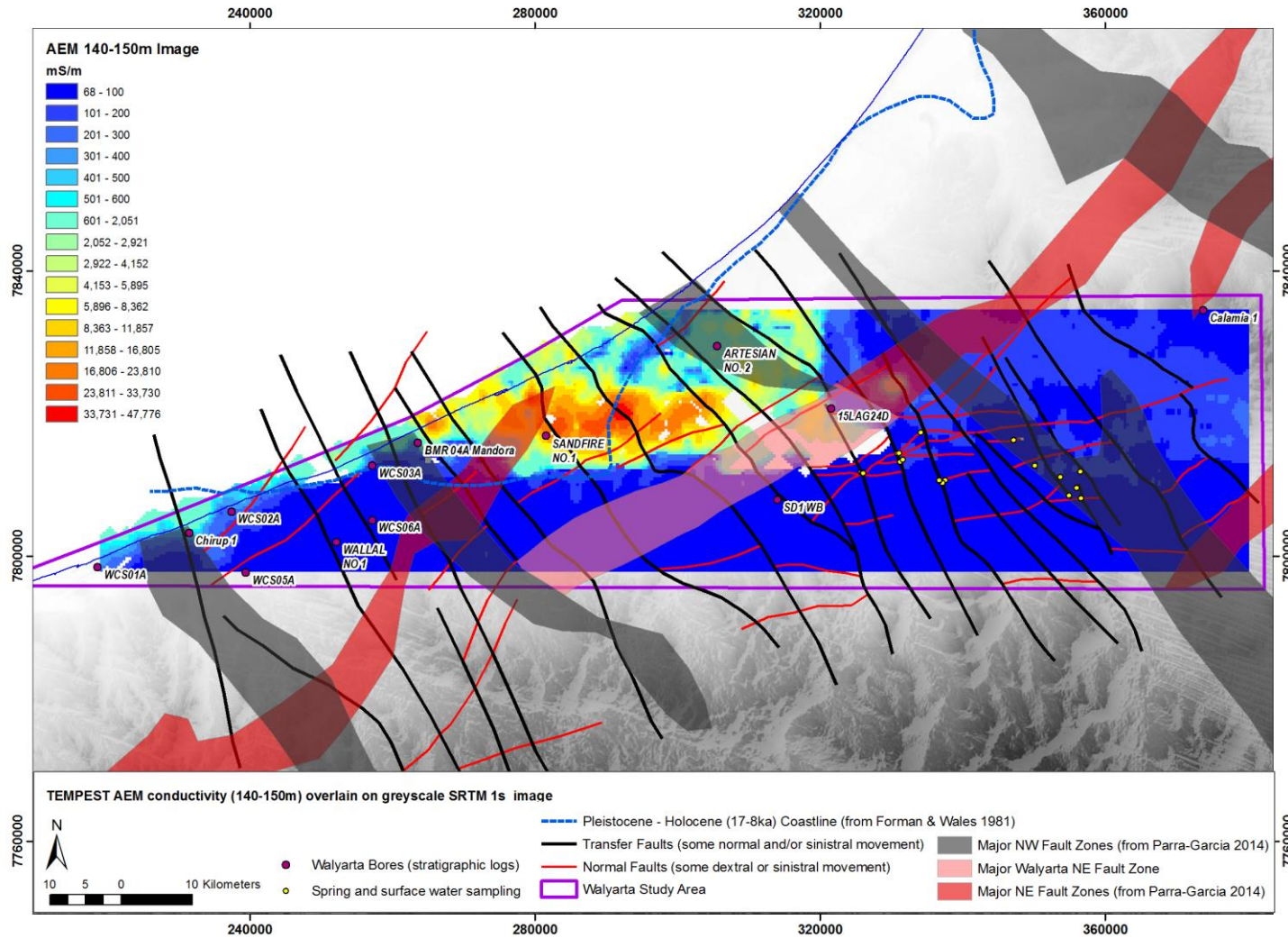


Figure 26 Walyarta major fault interpretation overlain on pseudo-colour AEM conductivity (140-150m – Jarlemai Siltstone) and greyscale SRTM 1s images to understand relationships between major electrical conductivity pattern breaks and geological faults



HYDROLOGICAL CONCEPTUALISATION OF THE WALYARTA MOUND SPRINGS

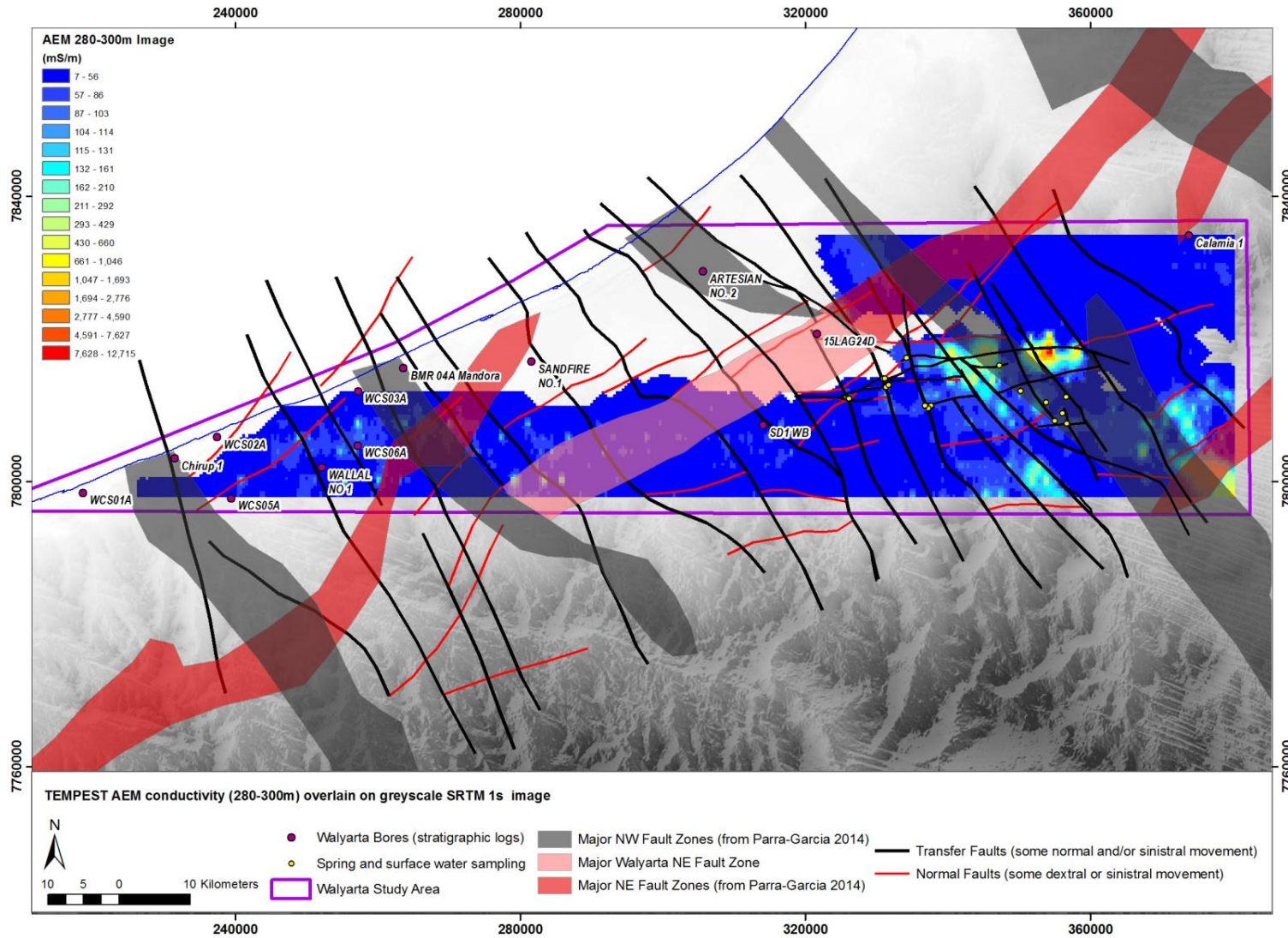


Figure 27 Walyarta major fault interpretation overlain on pseudo-colour AEM conductivity (280-300m – Wallal Sandstone) and greyscale SRTM 1s images to understand relationships between major electrical conductivity pattern breaks and geological faults

Integrating the Walyarta geological structural interpretation from the airborne magnetic data with AEM conductivity data shows a very close association of pattern breaks implying that the electrical conductivity pattern breaks are associated with the same structural controls. NW-SE pattern breaks coincident with transfer faults and interpreted Palaeo-drainage channels are evident in both the Broome Sandstone (40-50m) and Jarlemai Siltstone (140-150m), with changes likely to represent different channel sediments, preferential flushing of higher salinity groundwater (remnant of the Pleistocene – Holocene transgression) and/ or localised uplift and erosion (Figures 25 and 26).

Coarse scale fault modelling using gravity data, undertaken by Fathom Geophysics (Parra-García et al. 2014), follows the same structural grain as the Walyarta magnetic interpretation, with major NW trending structures marking the location of springs in the eastern Walyarta area. Deeper conductivity patterns in the Wallal Sandstone (280-300m) in the south-eastern Walyarta area follow NW trends, coincident with geological faults from the magnetic and modelled gravity datasets (Figure 27). Trends in this area are patchy and correspond with a shallower depth to magnetic source indicating a thinner sedimentary sequence due to a change in depositional environment, or uplift and erosion.

The relay faults form important hydrogeological controls, marking electrical conductivity pattern breaks from the land surface to over 300 metres below ground level (Figures 25 to 27). This change is aligned with, and forms a south-western extension of, major fault zones modelled in Parra-García et al. (2014). The surface orientation of the relay faults change across the Walyarta area, from an east-west trend (central area) to east south-east to the east (inclusive of transfer faults with a normal fault component). Similar trends are observed in the Fitzroy Basin and are separated by an oblique accommodation zone (Parra-García et al. 2014). In Walyarta a similar structural style can explain the fault geometry (Figure 28). The change in relay ramp orientation together with depth to magnetic source to the east concurs with observations of FrOG TECH (2005) that oblique rifting has produced shortening (transpression) across the major strike-slip faults resulting in the formation of a northeast trending push-up basin in the central to eastern Walyarta area.

This appears to be in contrast with the adjoining western area where the sigmoidal extent of Mandora Lake and valley sides are more indicative of a pull-apart basin. Laboratory and modelling experiments show that both sub-basin styles (geometry) can occur within the same larger basin and stress regime over time, controlled by temporal and spatial basin migration as well as stressors, with the Dead Sea Basin being a useful analogue (e.g. Smit et al. 2008 and van Wijk in press).

This 2.5D information was incorporated into the development of a schematic block model (Figure 28) and the ideas tested in the development of a 3D conceptual geological and hydrogeological model (see Section 4.5.3).

#### 4.3.3 3D Conceptual Geological Model

Geological formation tops and top of formation surfaces and thicknesses (isopachs) were produced in the 3D conceptual geological model Leapfrog Geo™. The 3D conceptual modelling involved importing AEM interval conductivity images and conductivity depth sections, along with drill hole/borehole and topographic data into the Leapfrog Geo™ software programme. Major stratigraphic horizons were interpreted along 2km spaced AEM flight lines within Leapfrog Geo™, with the finer AEM flight line spaced survey used for interpretation quality assurance. Resultant modelled surfaces formed the 3D model and this model was used to export 400m cell size gridded

surfaces and isopachs for use in numerical saturated flow and solute transport models (see Section 8).

- 1 Stromatolite Pool
- 2 Salt Creek
- 3 Stockyard Spring
- 4 Saunders Spring
- 5 Fern & Melaleuca Springs
- 6 Brett, Eil Eil & Little Eil Eil Spring
- 7 Dingo Spring
- 8 Linear & Top Spring
- 9 Friday Well

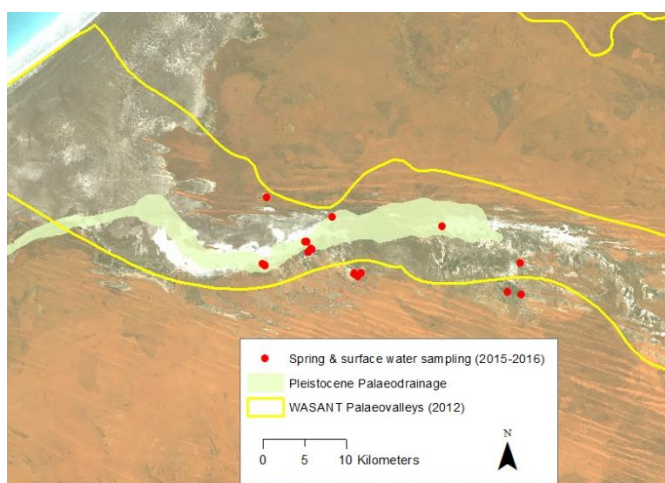
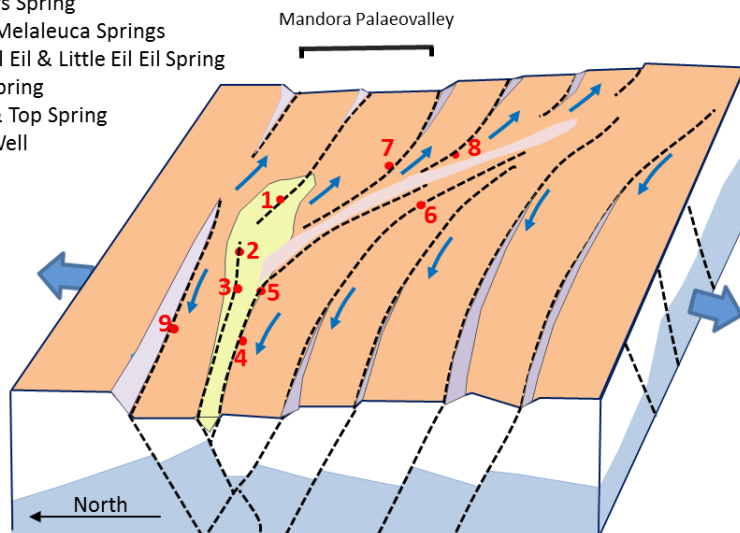


Figure 28 Schematic example of the Walyarta oblique accommodation zone, coloured pink, direction of relay fault movement denoted by blue arrows (modified from Parra-García et. al. 2014) showing the location of the palaeovalley, palaeo-drainage and DBCA spring and surface water sample sites (location map includes key and scale).

The 3D modelling was undertaken to improve understanding of the likely distribution of aquifers, groundwater levels and gradients and assess major hydrogeological controls on the Walyarta springs (see Section 6).

Information from previous geological mapping was employed as a straw model (e.g. Forman and Wales 1981, Appendix 1), with the 2.5D interpretation of AEM and airborne magnetic data used to support the location of major structures that form fault block boundaries where the blocks are characterised by major changes in depositional and erosional conditions.

#### 4.3.3.1 *Quaternary Formations*

Electrical conductivity variation in the upper ten metres of Quaternary aged sediments is variable, ranging from highly resistive to 7,000 mS/m (rainwater and/or unsaturated sands to ~33, 000 mg/L). Higher conductivities tend to correlate with tidal sediments located close to the current coastline and approximately 30km inland within Lake Mandora (Figures 6 and 18). The thickness of the tidal sediments is difficult to map due to the electrical conductivity of the tidal sediments being similar to the conductivity of the salt water interface in the underlying Broome Sandstone.

Circular and/or elongate electrically resistive bodies ranging in diameter from approximately 1 to 5km in diameter occur in the conductive tidal sediments in the north-western area (Flight lines 1 to 5; Appendix 3 & Figure 18). These features appear to form part of palaeo-drainage systems and/or coastal ephemeral wetlands and little is known about their mineralogical composition as previous investigations, including drilling, have not intersected and described them. They produce a strong conductivity contrast to the underlying conductive tidal sediments and salt water interface and are mapped in cross sections where they are more extensive in thickness, bordering the conductive tidal sediments to the south (Flight lines 9 to 12; Appendix 3). Sandplain sediments upgradient of the palaeovalley are generally electrically resistive, which makes the formation base (e.g. top of Broome Sandstone, Callawa Formation or Jarlemai Formation) a clear AEM mapping target in the southern Walyarta area.

The thickness of the tidal sediments was given a nominal thickness of 20 metres in cross sections (Appendix 3) and along with the coastal palaeo-drainage sediments they were not included in the Leapfrog conceptual 3D model. The interpolated sandplain sediment isopach is verified by drilling information from nine bores and ranges in thickness from 0 to over 60 metres, with thinner cover in topographically low lying areas and thick sands in the north-east dune systems. Areas of thin patchy cover overlying tidal sediments were not included in the Leapfrog conceptual 3D model. Uncertainty in modelled sandplain thickness cover reduces where there is information from drilling (Figure 30).

#### 4.3.3.2 *Broome Sandstone*

In Walyarta, the Broome Sandstone was anticipated to range in thickness from a maximum 100 metres in the north, 50 metres to the south-west and potentially absent in the south-east (Appendix 1). The top of the Jarlemai Siltstone provided a strong electrical conductivity contrast to overlying sediments, which includes the Callawa Formation, Broome Sandstone and Quaternary Formation sediments. Previous work on assessing the electrical responses of the Callawa Formation and Broome Sandstone found them to be similar and therefore they were not separated in this study (Mira Geoscience 2016).

Confidence in mapping the base of the Broome Sandstone with AEM data increased in areas where there was no salt water intrusion and the Jarlemai Siltstone provided a clear conductivity contrast (e.g. western Walyarta area) (Appendix 3). The interpolated combined Quaternary Formation and Broome Sandstone isopach is verified by drilling information from thirteen bores and ranges in thickness from 0 to over 176 metres (Figure 31). Thinner cover on east-west trending relay faults, near mound spring locations, with thicker cover to the north-east and reduced uncertainty where there is drill-hole information (Figure 31).

#### 4.3.3.3 *Jarlemai Siltstone*

Mapping the top of the Jarlemai Siltstone using AEM data was essential to map the Broome Sandstone and this is discussed above, Section 4.5.3.2. Using AEM data to map the thickness and lateral extent of the Jarlemai Siltstone was more challenging. The electrical response of the Jarlemai Siltstone decreases across the Walyarta survey area (Appendix 3), from west to east and appears thin or absent on relay faults (near mound springs) in south-eastern Walyarta where airborne magnetic data indicate there is uplift in the Permian formations (e.g. depth to magnetic source decreases).

Similar to the Broome Sandstone, confidence in mapping the thickness of the Jarlemai Siltstone using AEM data increased in areas where there was no salt water intrusion and the Jarlemai Siltstone provided a clear conductivity contrast (e.g. western Walyarta area) (Appendix 3). The isopach produced is verified by drilling information from eleven bores and ranges in thickness from 0 to approximately 300 metres (Figure 32).

The thickness of the Jarlemai Siltstone is thicker at the coast and there is higher confidence in this area as this is where the majority of drilling has taken place (Figure 32). In the central and eastern areas the siltstone thins and this is not dissimilar with the depositional straw model presented by Forman and Wales (1981). The deposition and/or preservation of the Jarlemai Siltstone across relay structures are difficult to predict, as well as resolve using electrical conductivity data. If the uplift of the Permian in the southern Walyarta area is approximately 200 metres this event may have removed the Jarlemai Siltstone if this occurred following its deposition. To understand if this is likely the quality assurance of the Jarlemai Siltstone and Wallal Sandstone were carried out concurrently.

#### 4.3.3.4 *Wallal Sandstone*

The thickness of the Wallal Sandstone was anticipated to range from 150 to 350 metres from the south-west to the north-east (Appendix 1 Maps 1&2).

The Wallal Sandstone has a similar electrical response to the Broome Sandstone and where it is underlain by Permian sediments or crystalline basement there is a mappable conductivity contrast (Mira Geoscience 2016). In Walyarta, Permian sediments are intersected for Petroleum wells Calamia 1, BMR 04A and Chirup 1, with the AEM DOI at Calamia covering the top of the Permian and showing a mappable conductivity contrast (Table 1 Appendix 1&3). Using this information, together with the structural interpretation from Section 4.5.2, the top of Permian sediments / base of Wallal Sandstone were mapped for AEM Flight lines 8, 9 and 11-19 in Appendix 3, with surfaces interpolated to adjoining lines where the AEM DOI was unable to resolve deeper conductivity structures. The east-west trending, 2km spaced flight lines are either parallel or oblique to relay structures creating sinusoidal patterns (Flight lines 10 to 14 Appendix 3). The 200 metre maximum uplift of interpreted Permian sediments to the south agreed with observations reported by Mira Geoscience (2016). The uplift decreased from south to north, which assisted in defining the east-west relay structures (Appendix 3).

As only three bores intersect the full thickness of the Wallal Sandstone there is higher uncertainty in the mapped surfaces and modelled isopach (Figure 33). The resultant range in thickness is 130 to 320 metres, increasing thickness spatial trends matching those of the straw model.



HYDROLOGICAL CONCEPTUALISATION OF THE WALYARTA MOUND SPRINGS

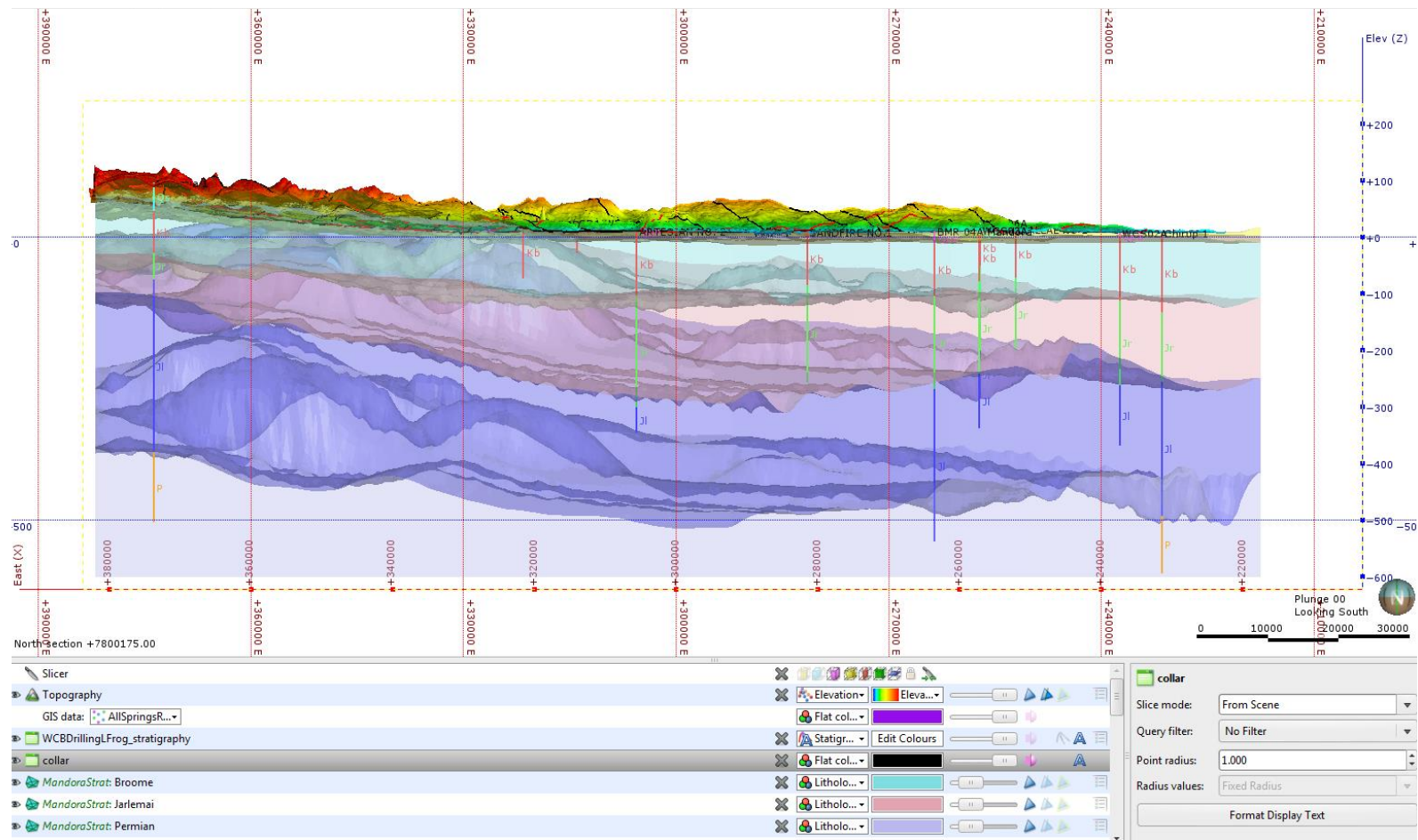


Figure 29 Transparent cross section through the Walyarta Leapfrog conceptual model showing the SRTM 1s DEM, interpreted and gridded stratigraphic layers and drill-hole lithology (viewed south)

HYDROLOGICAL CONCEPTUALISATION OF THE WALYARTA MOUND SPRINGS

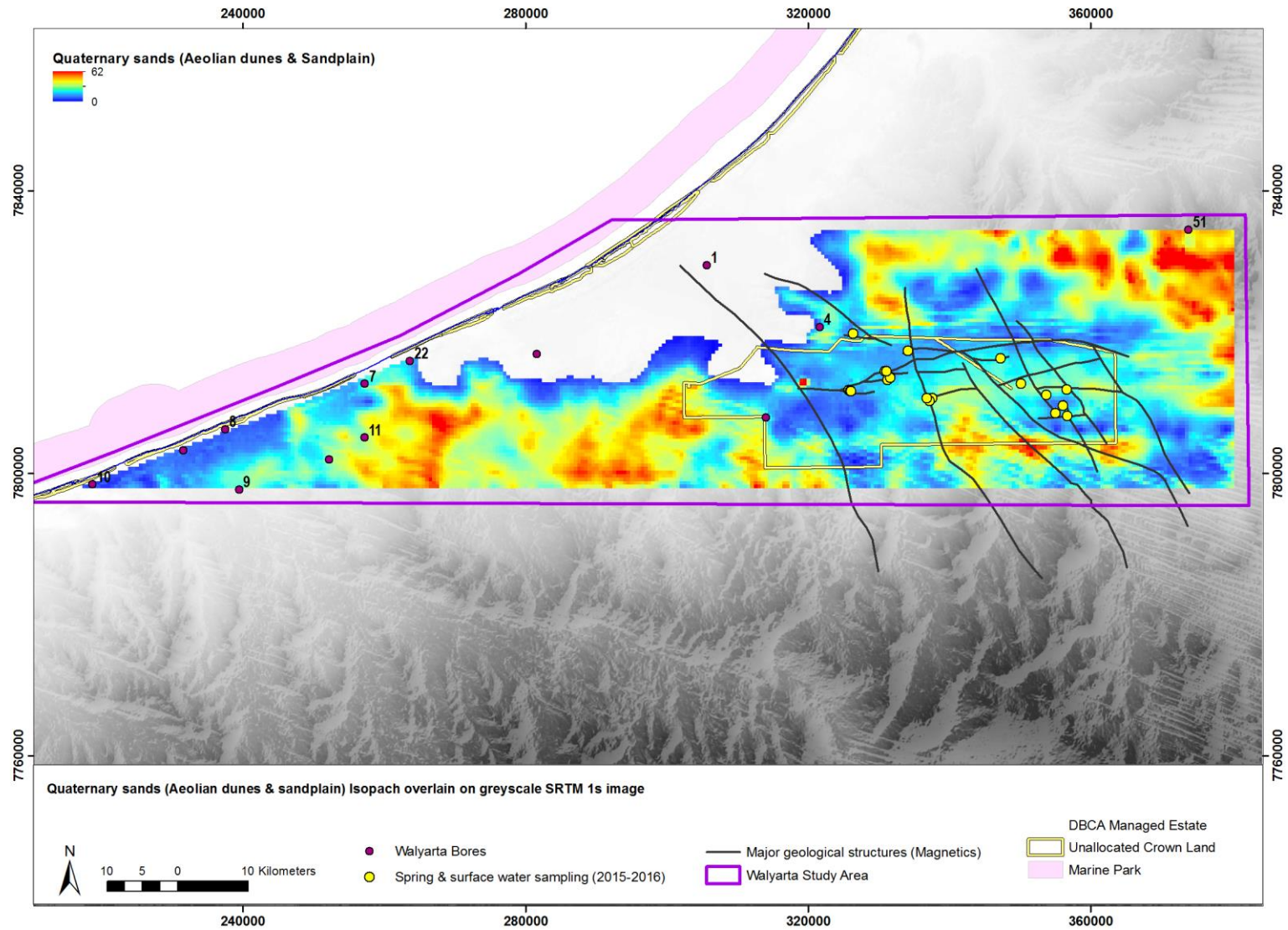


Figure 30 Isopach of Quaternary aeolian and sandplain sediments in Walyarta area; (bores with logging information on formation thickness are shown)



HYDROLOGICAL CONCEPTUALISATION OF THE WALYARTA MOUND SPRINGS

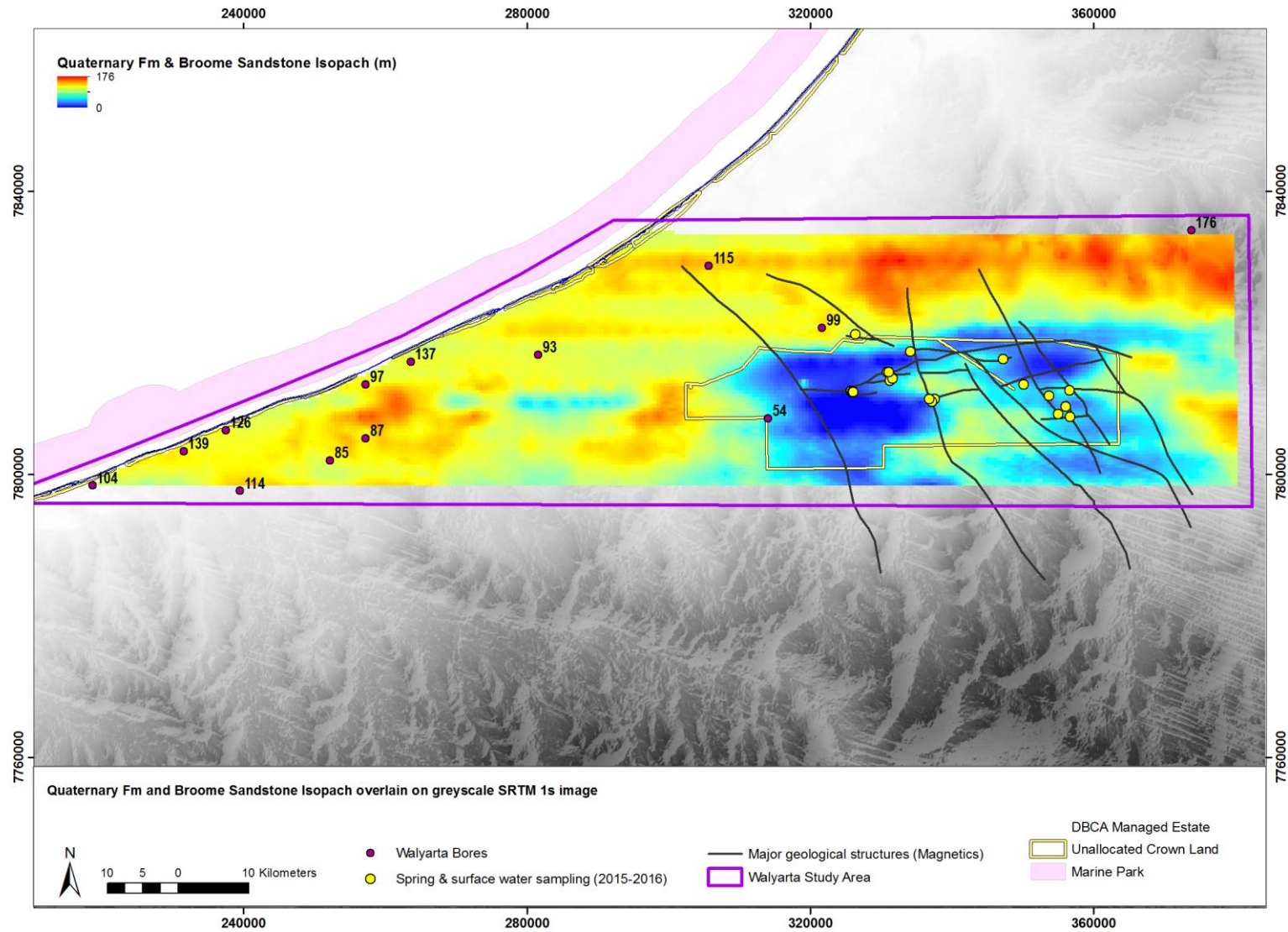


Figure 31 Isopach of Quaternary Formation and Broome Sandstone in Walyarta area (bores with logging information on formation thickness are shown)

HYDROLOGICAL CONCEPTUALISATION OF THE WALYARTA MOUND SPRINGS

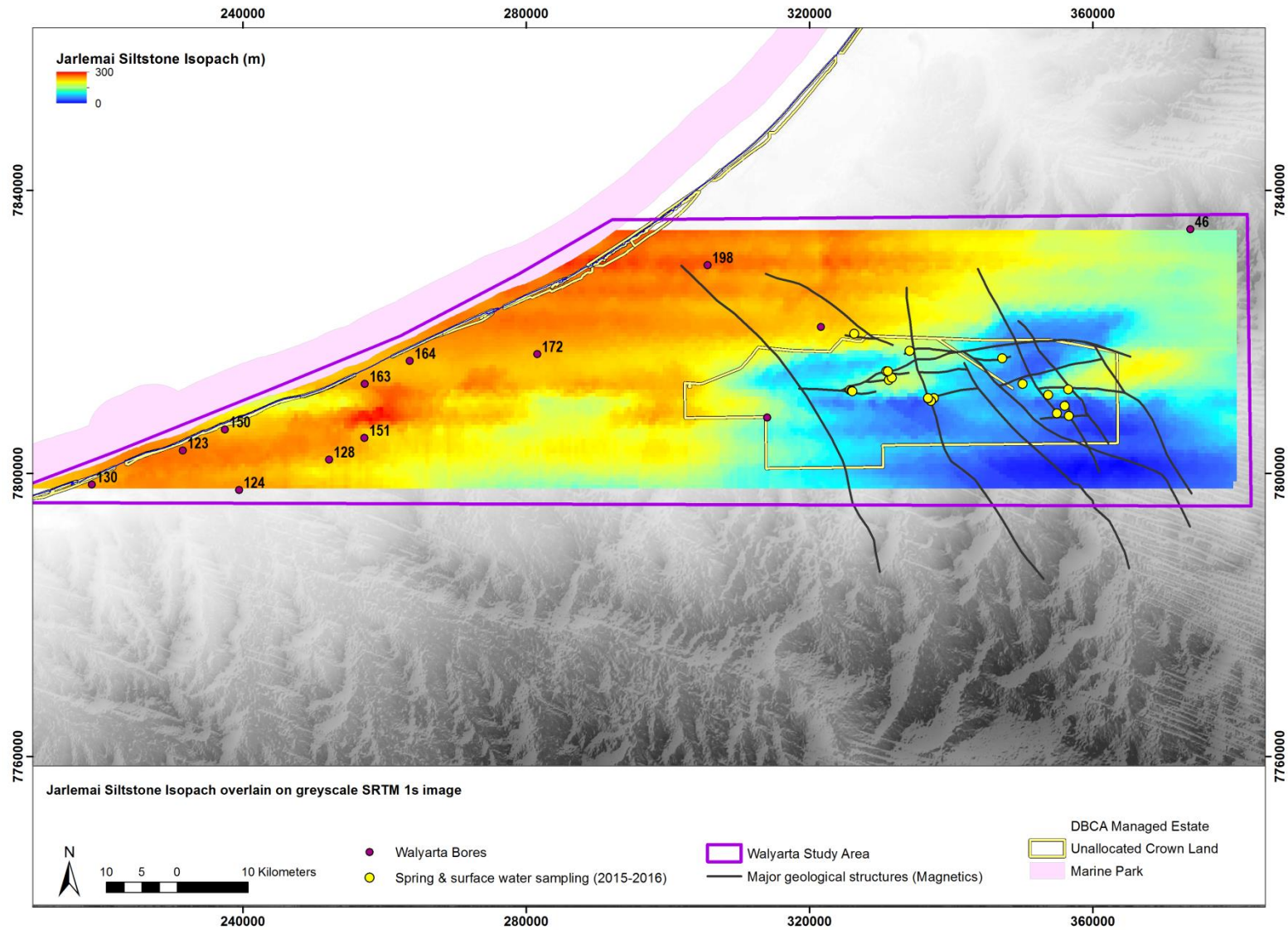


Figure 32 Isopach of Jarlemai Siltstone in Walyarta area; (bores with logging information on formation thickness are shown)

HYDROLOGICAL CONCEPTUALISATION OF THE WALYARTA MOUND SPRINGS

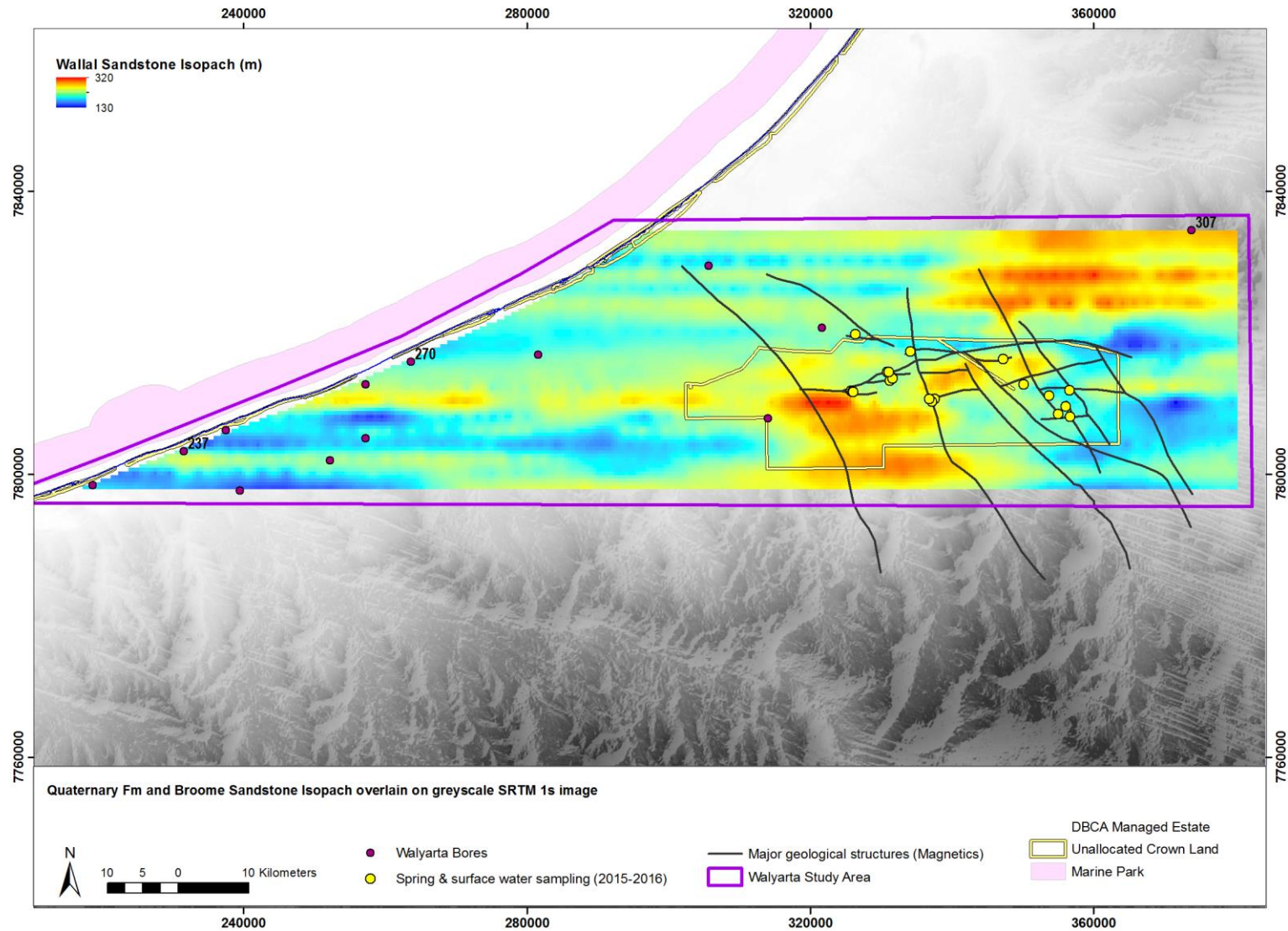


Figure 33 Isopach of Wallal Sandstone in Walyarta area ; (bores with logging information on formation thickness are shown)



## 5 Climate, vegetation and soils

### 5.1 Rainfall

Walyarta is located inland from 80-mile Beach, with Mandora Station being the closest Bureau of Meteorology (BOM) weather station. Table 2 displays statistics of the average monthly mean maximum temperature and mean rainfall (1913 to 2016). Average annual daily temperatures are around 35 C with slightly lower average temperatures in the months of June and July.

Rainfall patterns reflect seasonal cyclonic trends, with highest rainfall in the wet season months of January through to March (Figure 34). The rainfall gradient across the WCB decreases from north to south; highest average annual rainfall near Broome (~500mm) and lowest near Pardoo (~300mm) (Figure 1). Isohyets are orientated roughly east-west, with average annual rainfall around Mandora Station and the Walyarta Springs area of around 300mm (Table 2).

BOM Station 004019 MANDORA	Jan	Feb	March	April	May	June	July	Aug	Sept	Oct	Nov	Dec	Annual
Mean maximum temperature (Degrees C)	36	35.7	36.9	36.1	32.1	29	28.9	30.8	33.8	36	36.6	36.8	34.1
Mean rainfall (mm)	83.8	103.1	72.9	19.3	25.2	17.6	9	2.4	1	1.1	6.5	33.9	376

Record length: 1913-2016; Latitude 19.74 Degrees South, Longitude: 120.84 Degrees East, Elevation 8m

Table 2 Rainfall statistics for BOM Mandora station (#4019)

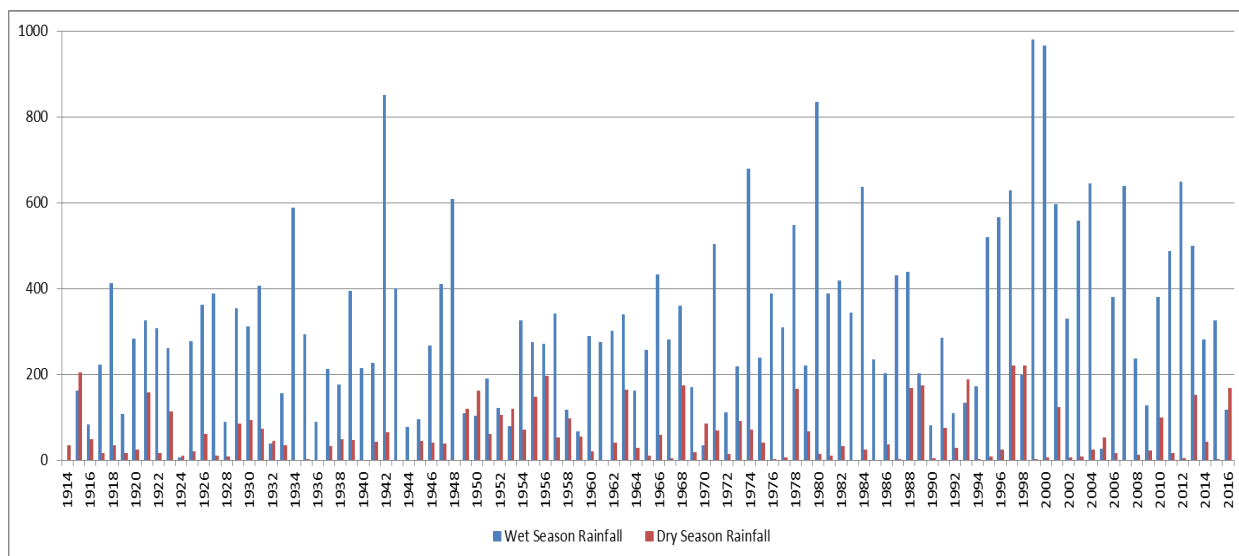


Figure 34 Histogram of dry and wet season rainfall (mm) from 1914 to 2016 for BOM Mandora station (#4019); nominal seasonal periods; wet season (Nov-April) and dry season (May-Oct)

### 5.2 Temperature and evaporation

Daily and monthly temperature data are available for BOM Mandora station for the period since January 1962. Average dry season temperatures are increasing while wet season average temperature trends are more variable (Figure 35).

Evaporation data are not available for BOM stations in the Walyarta area. Evaporation data from weather stations in Port Hedland, in the southern WCB, generally exceeds rainfall each month of the year unless cyclonic rainfall is received.



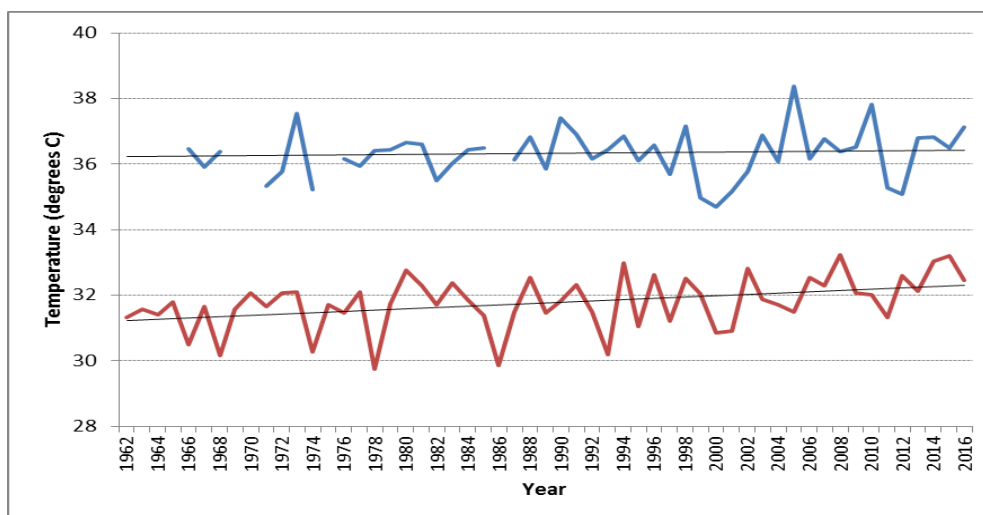


Figure 35 Graph showing average dry (red line work) and wet (blue line work) season temperatures from 1962 to 2016 for BOM Mandora station (#4019); nominal seasonal periods; wet season (Nov-April) and dry season (May-Oct)

Leech (1979) pointed out the importance of the current rainfall deficit in relation to assessing groundwater recharge to WCB aquifers and suggested that coastal areas in the WCB were likely to experience similar high rates of evaporation, with lower levels in inland areas due to reduced humidity.

Water discharging from the Walyarta mound springs was sampled by DBCA (Figure 1) in the dry season of 2015 and 2016. In 2015 the sampling took place in the first week of September following a wet season characterised by above average rainfall, BOM Mandora station rainfall for Nov 2014 to April 2015 totalling 325.8mm. Below average rainfall was received in the following dry season (2.5mm). In 2016 conditions were reversed, with sampling carried out after a dry wet season (117 mm) and a wetter dry season (167.4mm).

### 5.3 Vegetation

Broad scale vegetation patterns of the WCB are described by Leech (1979) as mainly comprising sandplain grasses, spinifex and deep rooted perennials, which are particularly common in dune swales and along river and creek beds. Within creek lines on the tidal flats the change in water quality promotes mangroves, with halophytes (samphires) on coastal salt flats.

In Walyarta vegetation communities and general condition were investigated and reported as part of a land management assessment in 1999 (Calm 1999). This exercise was repeated in September 2015 (English et. al. 2017 and Markey 2017.). Markey (2017) describes eight main floristic communities that occupy the main landforms and they are itemised below and shown in Figure 36;

- (A) sand dune *Acacia* shrublands and *Triodia* grasslands,
- (B) *Acacia* shrublands and *Triodia* grasslands on sand dunes/flats,
- (C) *Triodia* hummock grasslands on plain,
- (D) *Melaleuca alsophila* shrublands on calcretes,
- (E1) Tall mound spring *Melaleuca* woodlands,
- (E2) Tall *Sesbania* / *Melaleuca* mound spring woodlands over ferns,
- (F) *Melaleuca alsophila* shrublands over samphires on loamy flats and
- (G) Samphires on salt lake flats.

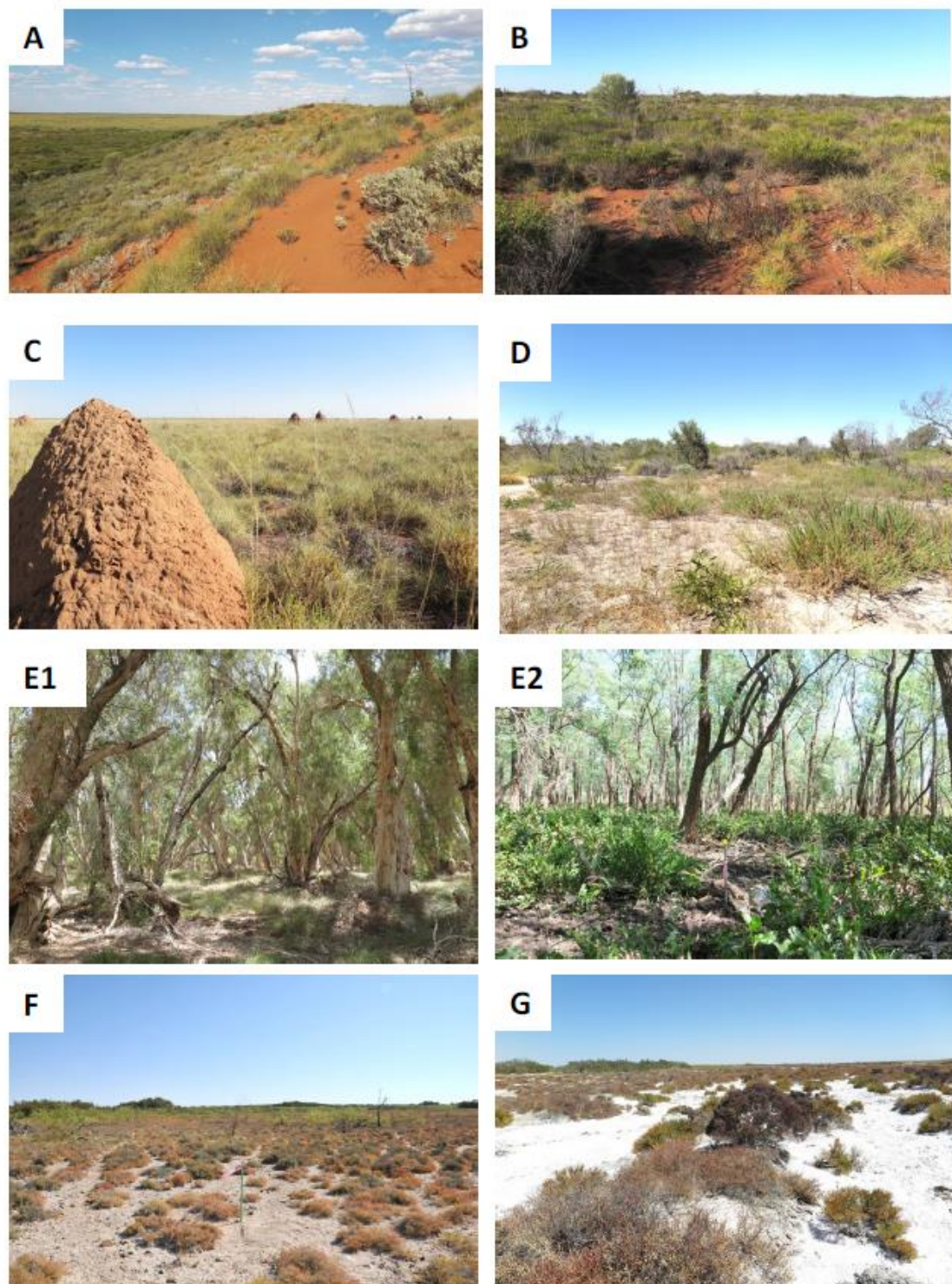


Figure 36 Vegetation communities of the Mandora Marsh Survey 2015 Area, labelled by floristic community group code (see Section 5.4). From Markey 2017.

Spatial patterns within floristic communities have been documented with mound springs having distinctive zonation that includes a central (topographic high point) peat mound with a forest of riparian vegetation (e.g. *Sesbania Formosa* and scattered *Melaleucas*; *M. alsophila*, *M. leucadendra* and *M. cajuputi* over a dense ground cover of *Acrostichum speciosum*, with stands of *Typha domingensis* and sedgeland dominated by *Schoenoplectus* spp. with *Fimbristylis* spp., along with

patches of *Sporobolus virginicus*) (English et. al. 2016). Ephemeral open water bodies (moats) occur on the margins of the central peat mound and have variable vegetation coverage (species and condition), which is likely due to variable fine-scale landforms, rate of groundwater discharge at the spring vent, surface water movement into and through the spring (e.g. spring moat hydroperiod and overland flow), in addition to water and soil chemistry (see Sections 6, 7 & 8). English et. al. (2016) also noted that there is a change to terrestrial vegetation communities outside the moats, consisting of a shrubland of *Acacia ampliceps* and various understorey species. Springs fringing Lake Mandora trending to a transitional environment denoted by floristic community F and springs upgradient (to the south) transitioning to floristic communities A and B (Markey 2017).

Salt Creek is located in floristic community type F (Markey 2017). The creek supports a unique occurrence of inland mangroves (*Avicennia marina*), a species which is traditionally located in marine-estuarine habitats characterised by brackish or saline water (Beard 1967). Perennial saline groundwater discharging into salt creek enables sustains the unique mangrove community, in addition to a diverse range of fish, with two native fish species recorded by Storey *et al.* (2011); spangled perch (*Leiopotherapon unicolor* (Günther)) and a new species of goby (*Acentrogobius* sp. nov).

#### 5.3.1 Remote Sensing

Vegetation coverage over Walyarta is sparse reflecting the low average rainfall and high temperatures. Remote sensing data were sourced from two different satellites (ASTER and Landsat) to map the spatial distribution of green vegetation (cellulose), with the understanding that this will be effective at mapping riparian vegetation where there is minimal signal interference from iron oxides, dry vegetation and aerosols (GSWA 2012b).

ASTER data (Advanced Spaceborne Thermal Emission and Reflectance Radiometer - <http://asterweb.jpl.nasa.gov>) of green vegetation coverage was sourced from GSWA and is shown in Figure 37 and 38. The methodology and limitations of the ASTER processing are detailed in GSWA 2012b. USGS Landsat scenes (<http://glovis.usgs.gov/>) were downloaded over Walyarta (path row 111/074) for the period 1988 to 2014 and a stack of annual September imagery selected and processed to assess spatio-temporal change in perennial vegetation at the end of dry season. Landsat TM spectral bands selected for the Walyarta perennial vegetation coverage were (band 3 + band 5)/2, also known as 3+5 (Huntley 2015). Processed data were calibrated with on ground spectral measurements and limitations to mapping changes in cellulose identified. For the 26 years assessed, data for the eight driest September months were selected and classified spatially according to presence in each of the eight driest seasons. Figure 38 shows results for the distribution of vegetation across all of the eight driest dry seasons (coloured blue) and all but one of the eight driest dry seasons (coloured green).

Green vegetation coverage for both ASTER and Landsat show similar patterns (Figure 38), with perennial (riparian) vegetation patterns tending to be localised, constrained by geological and geomorphological features, in particular dune swales within palaeo-drainage channels mapped in the airborne magnetic data (Figure 37; western to central Walyarta) and along ENE-WSW trending relay faults near mound springs (Figure 38).



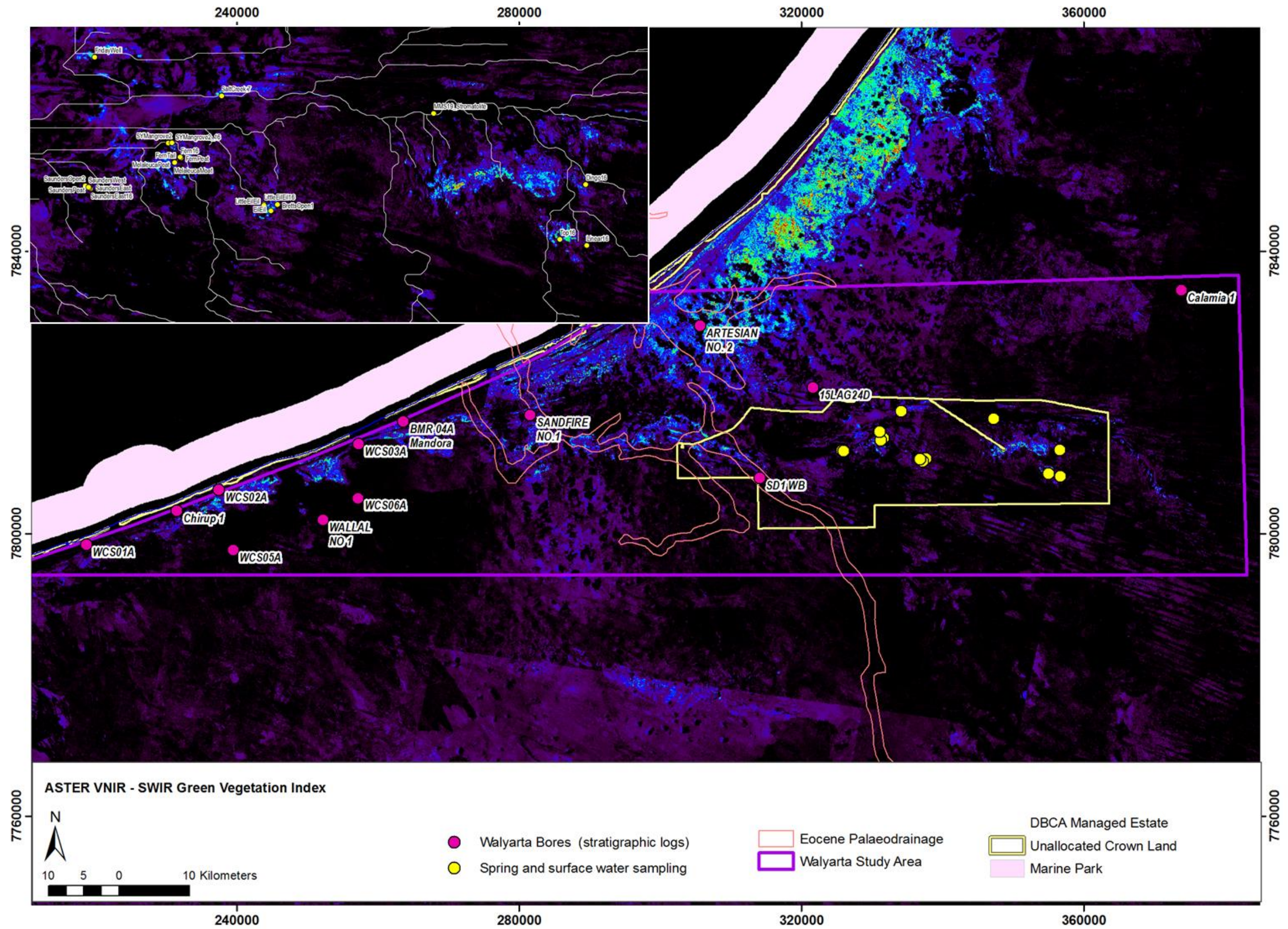


Figure 37 ASTER VNIR-SWIR green vegetation index (high content is red and low content is blue) with location of mound springs and surface water and bores with stratigraphic information



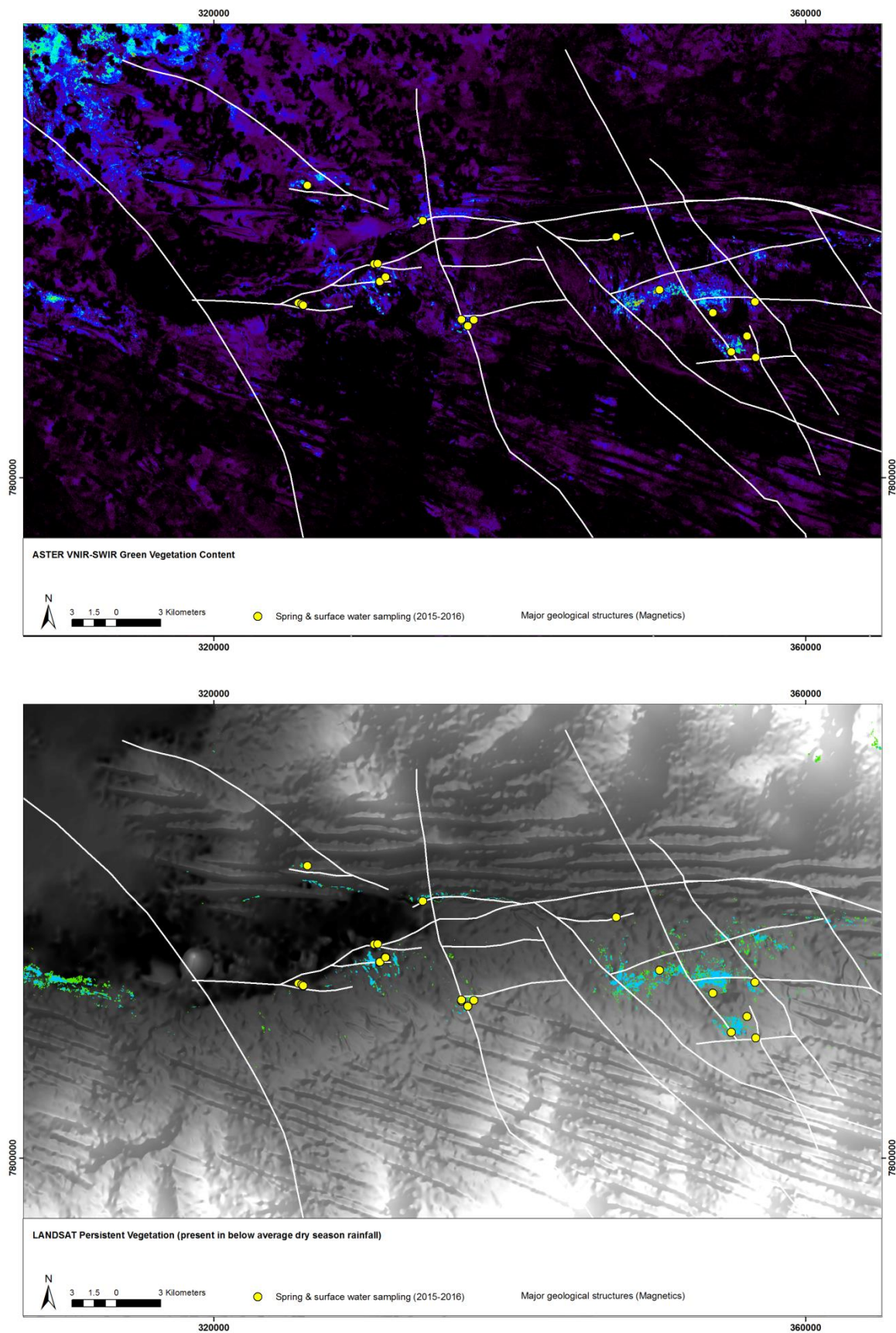


Figure 38 ASTER VNIR-SWIR green vegetation index (high content is red and low content is blue) and below, Landsat persistent vegetation overlain on greyscale SRTM 1s image; across all of the eight driest dry seasons (coloured blue) and all but one of the eight driest dry seasons (coloured green); major geological faults in both maps are shown in white

The similarity of the ASTER and Landsat coverages, along with the persistence of the vegetation patterns over time suggests some areas are resilient to changes in climate, including the physical effects of cyclones and bushfires. The major limitation with mapping spatially discrete mound spring vegetation with freely available satellite data is the resolution of data capture and resultant gridded cell size, which is around 30 meters for both the ASTER and Landsat data; this is discussed further in Section 6.

### 5.3.2 Environmental isotopes

Dominant species from three mound springs (Fern, Melaleuca and Saunders springs; Figure 1) were sampled and analysed for carbon and nitrogen isotopes ( $\delta^{13}\text{C}$ ,  $\delta^{15}\text{N}$ ) using a Finnigan Delta Plus XP continuous flow inlet isotope ratio mass spectrometer at The University of Western Australia Biogeochemistry Centre. Normalisation procedures were carried out according to Skrzypek (2013).

These analyses were undertaken to collect a baseline dataset to assess contemporary vegetation carbon contribution to dissolved inorganic carbon in groundwater and the peat mound substrate, as well as provide an insight into abiotic and biotic variation between the springs. The majority of vegetation species in Walyarta are believed to be C3 species (pers comm. Dr. Pauline Grierson) apart from spinifex grasses (McWilliam and Mison 1974). Plants take carbon directly from the atmosphere, with carbon isotopic composition reflecting changes in the energy budgets of leaves. This means that C3 plants growing under water-stressed conditions are expected to be enriched in  $\delta^{13}\text{C}$  (e.g. Ma et. al. 2012) compared to plants growing under optimal to waterlogged conditions (e.g. Ladd et. al. 2009). A comparison of  $\delta^{13}\text{C}$  for the same species between springs was possible for the main fern species and results show similar  $\delta^{13}\text{C}$  levels as do dragon tree sampled at Fern and Saunders springs (Table 3). Results for Melaleuca sampled at Melaleuca and Saunders springs exhibit the main variation, suggesting that Melaleuca species may be less stressed at Saunders compared with Melaleuca Spring (Table 3). Although due to the limited dataset, further sampling is required to verify this interpretation.

Spring	Species	$\delta^{15}\text{N}$ [‰ AIR]	$\delta^{13}\text{C}$ [‰ VPDB]	N [wt %]	C [wt %]	C/N [wt]
Fern	Acrostichum speciosum (fern)	-0.14	-28.33	1.7	40.7	24.1
Fern	Sesbania Formosa (dragon tree)	0.35	-27.19	3.5	42.7	12.1
Fern	Acacia ampliceps	0.70	-31.08	2.3	40.6	17.7
Melaleuca	Acrostichum speciosum (fern)	3.05	-28.45	1.1	40.8	38.4
Melaleuca	Melaleuca	3.31	-31.69	1.1	48.0	42.3
Saunders	Sesbania Formosa (dragon tree)	0.49	-30.71	3.6	44.4	12.4
Saunders	Acrostichum speciosum (fern)	2.01	-29.94	1.5	42.2	27.3
Saunders	Melaleuca	3.76	-12.30	0.5	38.6	72.6

Table 3 Carbon and Nitrogen isotopes  $\delta^{13}\text{C}$ ,  $\delta^{15}\text{N}$  for major plant species at Fern, Melaleuca and Saunders Springs

Plant and soil nitrogen isotopic composition ( $\delta^{15}\text{N}$ ) is related to the availability of nutrients and water, which makes it a useful spatio-temporal indicator of ecosystem nutrient cycling. In arid, oxic and/or high nitrogen available environments, isotopically depleted nitrogen  $^{14}\text{N}$  is preferentially lost from the ecosystem through the processes of  $\text{NH}_3$  volatilization, denitrification and leaching of  $\text{NO}_3$ , resulting in enrichment of soil nitrogen and leaf  $\delta^{15}\text{N}$  (Ma et. al. 2012). Under low nitrogen availability and/or wetter, anoxic environments plants are more likely to depend on N-fixing mycorrhizal fungi for nitrogen acquisition, which produces a plant depleted in  $\delta^{15}\text{N}$ .

Given these environmental factors, we expect that the Walyarta spring peat mounds to receive constant groundwater discharge and would therefore be anoxic, with most plant species sourcing nitrogen from mycorrhizal fungi. Results from Table 3 should show depleted in  $\delta^{15}\text{N}$  and high C/N ratios and this is observed for Melaleuca species where it was sampled at Saunders and Melaleuca springs.  $\delta^{15}\text{N}$  content in fern species is low in Melaleuca spring, increasing in Saunders and Fern springs but due to limited sampling it is unknown if this is statistically significant. For dragon trees,  $\delta^{15}\text{N}$  content at both Fern and Saunders springs is high resulting in low C/N ratios. It is possible this is due to their location in the peat mounds (e.g. marginal to the peat mound and/or fault conduit) or their metabolic processes (e.g. timing of photosynthesis in relation to sampling). These results are examined in relation to soil and microbe analyses in Sections 5.4.3 and 5.4.4.

## 5.4 Soils

Spatial coverage of soils and shallow regolith units across Walyarta is limited to the 1:500k scale surficial geology mapping (Figure 6) and 1:250k geology mapping (Figures 8 & 9), both of which were heavily reliant on interpretations of satellite imagery and aerial photography (see Section 3.2, DMP 2010 & Towner 1982a).

During vegetation mapping in 2015 Markey (2017) identified three main soil types, alkaline soils sampled at calcrete sites in the palaeovalley, soils with elevated carbon, nitrogen and phosphorus within organic mound spring sites and sandplain soils characterised by depleted carbon, nitrogen and phosphorus. Soils noted during spring and surface water sampling were in agreement with those described by Markey (2017) (Appendix 4).

Upscaling the soil type observations to deduce a mapped extent of soil units across Walyarta has not been possible with the point measurement data collected in 2015 or earlier. Mapping near surface organic carbon could provide information on moisture content (e.g. higher soil moisture - water retention) and help understand surface water – groundwater interactions of the mound springs. Mapping near surface inorganic carbon (carbonates) is important as it would improve knowledge of hydrological and hydrochemical processes and better define uncertainty associated with using carbon isotopes as environmental tracers in Walyarta (e.g. spatial extent of carbonate materials that can provide additional carbon input to groundwater besides rainfall – carbon recycling). To achieve this mapping aim mineralogical information from ASTER data were examined and interpretations assessed.

### 5.4.1 Remote Sensing

ASTER coverages across Walyarta contain artefacts due to the mosaicing of data acquired at different times under changing ground and atmospheric conditions (GSWA 2012b). These are observed by the presence of NE-SW orientated striping across the images (see subtle striping in Figure 39) and these features are aligned with the satellite flight path/swaths.

ASTER products that provided spatial information on carbon included carbonate mineralogy from the MgOH group composition (red=calcite, Figures 39 to 41), CSIRO Landsat TM regolith ratios (turquoise=carbonates and/or clay minerals, Figure 42 and the opaque index (red=manganese oxides, carbon and/or maghemite gravels, Figure 43) (GSWA 2012b).



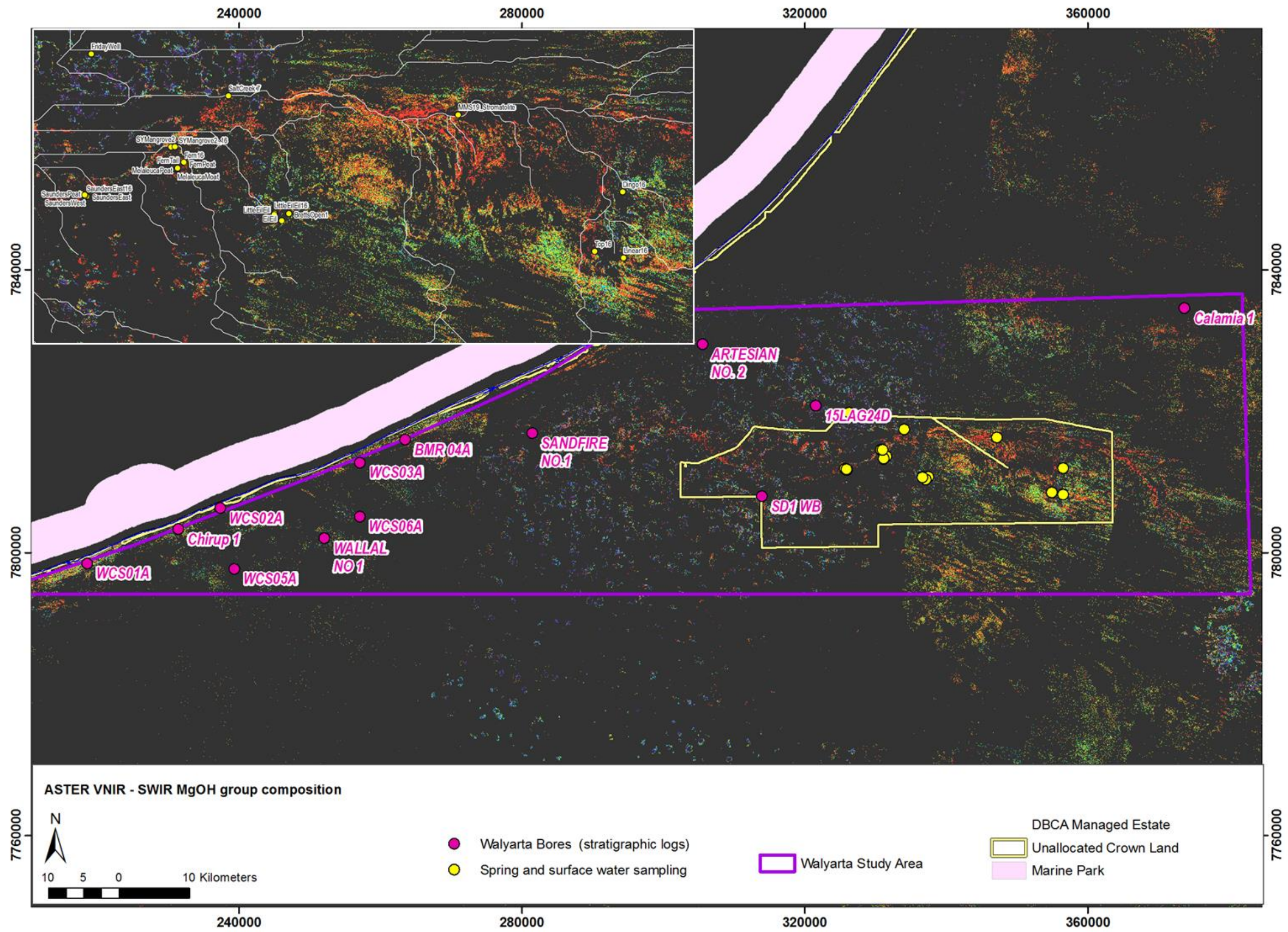


Figure 39 ASTER MgOH group composition, red=calcite, dark areas represent vegetation and blue=cloud cover – see Figures 37 and 38.



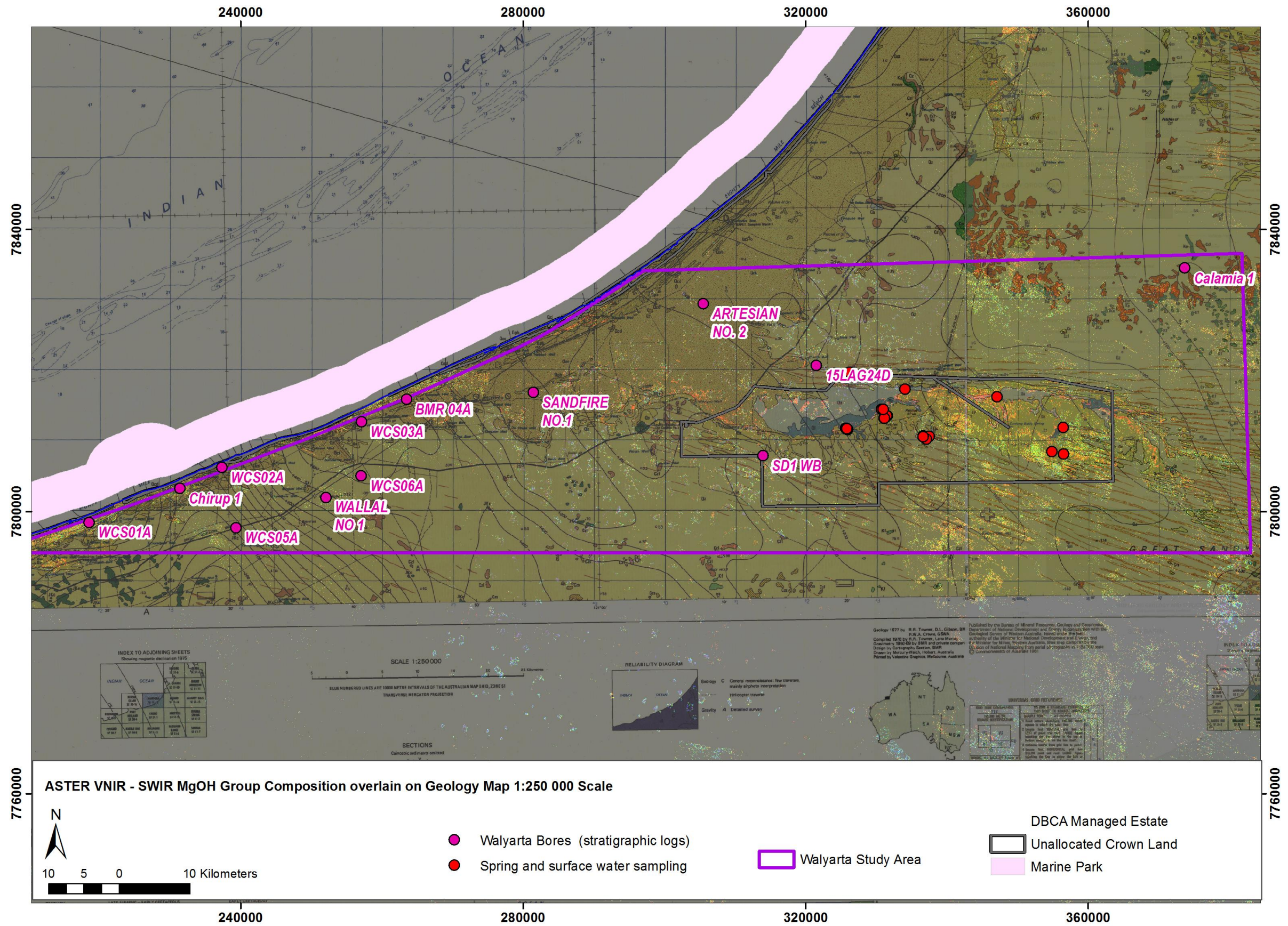


Figure 40 ASTER MgOH Group Composition overlain on 1:250k geology for Walyarta study area



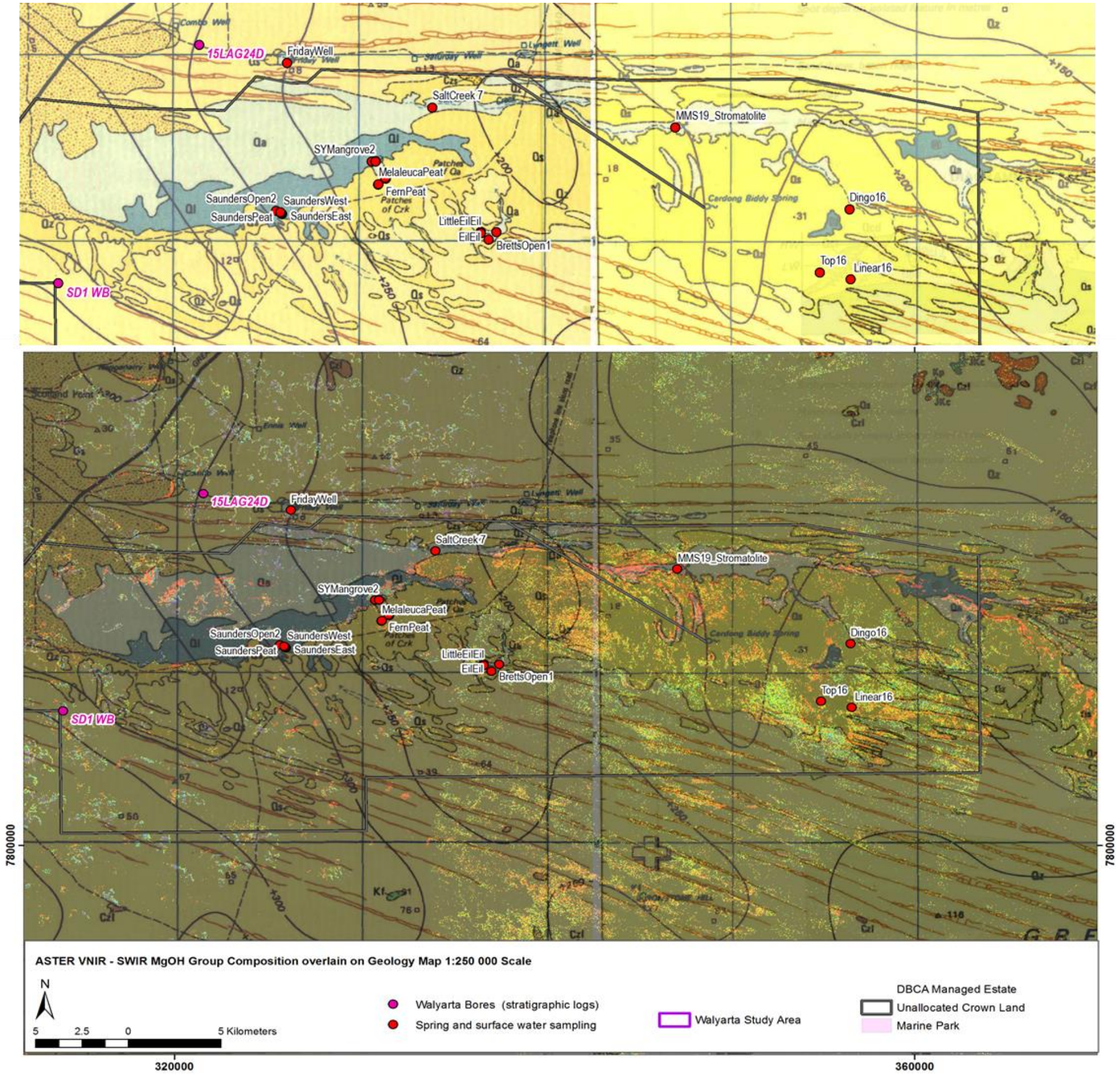


Figure 41 ASTER MgOH Group Composition overlain on 1:250k geology for Walyarta Conservation Park (below), showing the location of major springs and surface water sampling sites 2015-2016



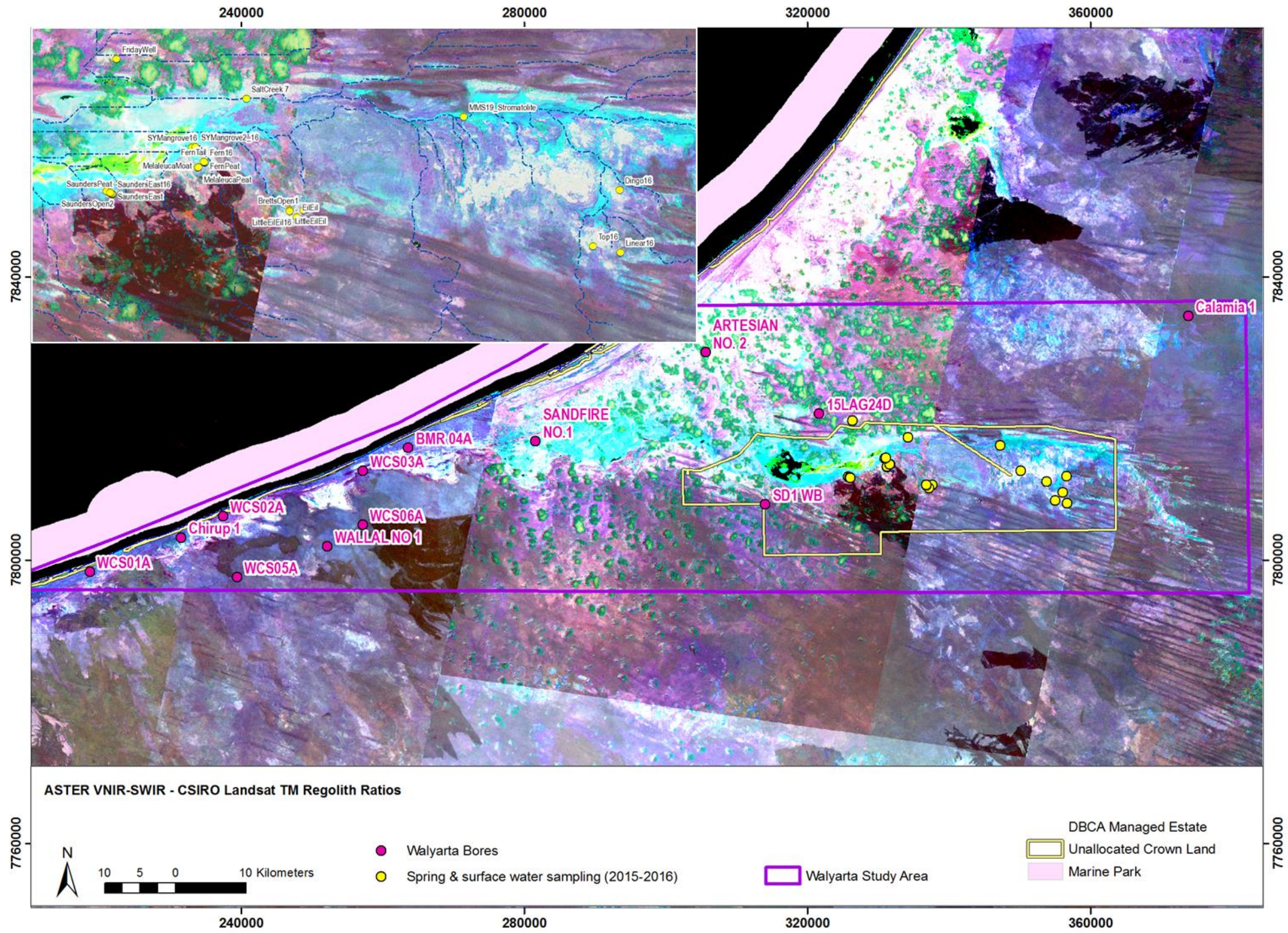


Figure 42 ASTER – CSIRO Landsat TM regolith ratios; RGB image; R=B3/B2, G=B3/B7 & B=B4/B7, Note; white=vegetation, green=cloud cover, black-dark brown=free water and/or fire scars



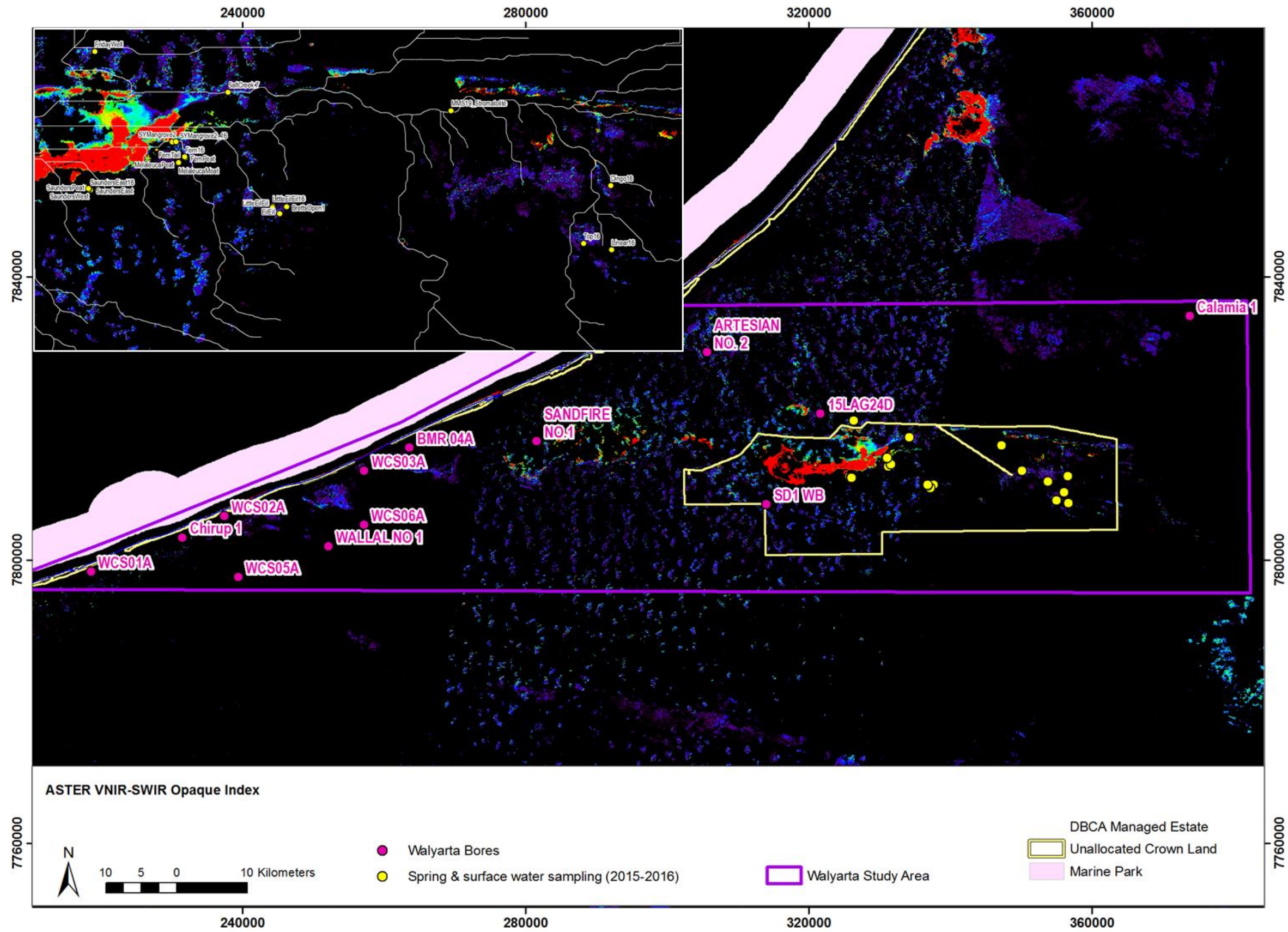


Figure 43 ASTER Opaque Index, red areas represent areas with high concentrations of manganese oxides and/or maghemite gravels



The MgOH group composition together with the CSIRO Landsat TM regolith ratio data indicate that carbonates are concentrated within sections of the Mandora palaeovalley floor, as well as occurring upgradient in narrow ephemeral channels (shown in inset map Figures 39 to 42) and dune swales, often mapped bordering or covering mound springs.

Towner (1982a) identified a number of surficial geology units that were likely to have a carbonate component. As the boundaries of these units were described as gradational it is not unsurprising to see the interpreted ASTER carbonates are present across Quaternary alluvium, lake and tidal flat deposits (Qa, Ql, Qcs and Qpb), in addition to discrete outcrop of lateritised Mesozoic Parda Formation (Kp, Cz1) to the north of the Mandora Palaeovalley, near Munro Spring (see Paul et. al. 2013 for the location of Munro Spring) (Figures 40, 41, 42 and (Figure 9 for key).'

It is important to reaffirm that the spatial coverage of carbonates shown in Figures 39 to 42 is an underestimate due to the vegetation cover appearing as black and white respectively in the ASTER MgOH and CSIRO Landsat TM regolith ratio datasets.

For organic carbon, the opaque index results didn't appear to resolve organic carbon-rich soils as the main feature mapped was the southern margin of Lake Mandora where surficial carbon stores have not been mapped. Elevated opaque mineral responses occur in geologically older drainage features (e.g. lakes and drainage lines; coastal wetlands and Lake Mandora). It is therefore more likely that high opaque mineral concentrations represent manganese oxides and/or maghemite gravels that have been deposited and concentrated within topographically low lying areas through fluvial and lacustrine processes (Figure 43).

The spatial patterns in the ASTER datasets examined do show some alignment with deeper geological faults (e.g. abrupt NW-SE pattern breaks) (Figures 39 to 42). This is discussed further in Sections 6 and 7.

#### 5.4.2 Environmental isotopes

Peat soil samples were taken from three mound springs (Fern, Melaleuca and Saunders springs; Figure 1) and analysed for carbon and nitrogen isotopes ( $\delta^{13}\text{C}$ ,  $\delta^{15}\text{N}$ ) using a Finnigan Delta Plus XP continuous flow inlet isotope ratio mass spectrometer at The University of Western Australia Biogeochemistry Centre. As described in Section 5.3.2, normalisation procedures were carried out according to Skrzypek (2013).

Analyses of  $\delta^{13}\text{C}$  and  $\delta^{15}\text{N}$  from peat substrate at depths of between 10 and 20cm below ground level are similar as are peat soil water content, salinity and pH, with peat soil water being neutral and relatively low in stored solutes (Table 4). The similarity in results for all three springs suggests hydrological processes (groundwater and surface water interactions) within peat mounds at these springs sites are the same, or similar. This is discussed in more detail in Section 6.3.

Spring	$\delta^{15}\text{N}$ [‰ AIR]	$\delta^{13}\text{C}$ [‰ VPDB]	N [wt %]	C [wt %]	C/N [wt]	Moisture (%)	Volumetric water content (%)	EC (mS/m)	*TDS (mg/L)	pH
Fern	2.87	-28.11	2.1	39.3	19.1	90	18	258.2	1789	6.81
Melaleuca	4.15	-29.60	2.2	35.7	16.0	80	16	135.15	1218	7.06
Saunders	4.04	-28.61	1.3	28.6	22.8	86	17	48.7	817	6.76

\*Derived from relationship Figure 22; volumetric water content calculated using ave bulk density 0.2 (g/cm<sup>3</sup>)

**Table 4 Fern, Melaleuca and Saunders Springs Peat substrate analyses; Carbon and Nitrogen isotopes  $\delta^{13}\text{C}$ ,  $\delta^{15}\text{N}$ , moisture (%), volumetric water content, EC1:5 and pH**

The thickness of the peat substrate in the Walyarta mound springs is not well understood. Limited coring at Eil Eil Spring (previously known as Mandora Swamp) in the 1980's by Wyrwoll et. al. (1986) suggests the thickness is between 0.5 and 1.0 metres, with higher carbon stores within a matrix of alkaline clay sized material in the upper part of the profile (Figure 44). Underlying the peaty marl horizon are medium to fine textured sands that appear to have the same origin as the nearby sand dunes. Carbon dating ( $^{14}\text{C}$ ) of the basal peat material sampled by coring at Eil Eil estimates the peat substrate is approximately 7,000 years BP and is Holocene in age and therefore the underlying Aeolian sands are 7,000 years BP or older.

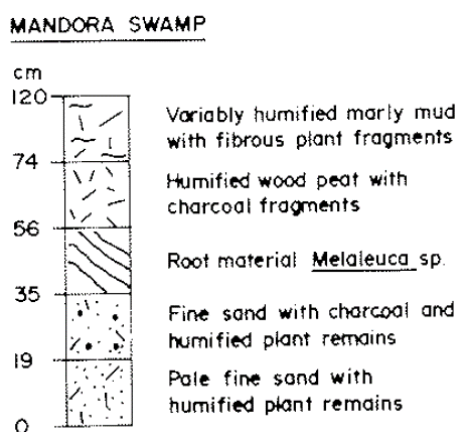


Figure 44 Eil Eil Spring (previously known as Mandora Swamp) peat core description (0cm equals greatest depth below ground level) (from Wyrwoll et. al. 1986).

### 5.4.3 Microbiology

DBCA is a contributor to the Global Peat Microbiome Project (Lamit et. al. in prep), which investigates the role of fungi in peat wetland carbon dynamics (Lamit et. al. 2017). In September 2015 mound spring peat samples from Fern, Melaleuca and Saunders Springs were sampled at depths of approximately 10cm and forwarded to Michigan Technological University for metagenomic sequencing. The aim of this work was to gain an understanding of peat microbial community composition and identify and diagnose variation between springs sampled.

Changes thought to be important in changing spring microbe community composition were changes in spring water balance (surface water and/or groundwater) as well as the introduction of nutrients through agricultural practices (e.g. grazing of cattle). Where organic springs were functioning under constant discharge and low disturbance (anoxic and nutrient limited) it is expected that the peat profile organisms would include those with roles in sulfur-cycling and N-fixing (e.g. mycorrhizal fungi, see Section 5.3.2). In Walyarta cattle disturbance in springs is common, with increasing disturbance noted for Fern, Melaleuca and then Saunders springs. The least disturbed site (Fern Spring) was set as a community base-line to which Melaleuca and Saunders Springs were compared.

Metagenome data were retrieved from the Joint Genome Institute (JGI) (<https://jgi.doe.gov/>) and a methodology developed to cover data complication, quality assurance and interpretation (Wood 2017). The key findings of the interpretation include;

- increasing bacterial Shannon diversity across mound spring ecosystems with increased disturbance,
- communities appear to be characterised by an enrichment of diverse sulfur-cycling organisms,
- Chromatiales bacteria (photosynthetic bacteria) dominated mound spring communities and

- plant-fungal interactions show Saprotrophic family Hypocreaceae is dominant and is involved in plant-microbe interactions.

Comparisons of the least disturbed (Fern Spring) communities to the more disturbed Melaleuca and Saunders Spring communities, indicate that major taxonomic changes between the Springs are related to vegetation dynamics (at least for depth 10 cm):

- Fungal communities from springs were dominated by the Sordariomycetes, specifically the Family Hypocreaceae (parasites and saprobes) (Figure 45). Sub-dominant Soradimycete families changed from Clavicipitaceae (obligate parasites of plants, insects or fungi) at Fern Spring to Ophiostomataceae (plant pathogens) at Saunders and Melaleuca Springs. The turn-over in sub-dominant plant-pathogen related taxa is likely to be driven by changes in vegetation dynamics and host specificities.
- Fungal taxa that engage in plant symbioses also changed between spring sites: Whilst the Family Ambisporaceae (a member of the arbuscular mycorrhizal forming Glomeromycetes), were highly dominant at Saunders Spring, Glomeromycota were not prevalent at Fern or Melaleuca Springs. However, Fern and Melaleuca Springs each contained different major sub-dominant groups that form ectomycorrhizal associations with plants. At Fern Spring, the Tricholomataceae were a major sub-dominant order. Members of this order often form ectomycorrhizal associations with coniferous or board-leaved plants. At Melaleuca Spring, the Thelephoraceae were a sub-dominant order, some members of which form ectomycorrhizal associations.
- There was a turnover in the dominance of N – cycling bacteria. Whilst nitrite oxidising Nitrospiraceae were predominant at Fern and Melaleuca Springs, ammonia oxidising Nitrosomonadaceae were more prevalent at Saunders Spring. These results likely reflect varying input of nitrogen from cattle.

Peat microbiology results were in agreement with the expectations set prior to sampling and analysis. This indicates that environmental conditions, in particular water quantity and quality, are stable and under the current climate and water use regimes the main pressure on spring resilience is disturbance by cattle.

#### 5.4.4 SEM

Little is known on the mineralogical content and origin of sediments within the spring peat substrates. Suggestions put forward for Eil Eil springs indicate a carbonate component is present in the upper part of the profile (Section 5.4.2). ASTER and on ground soil observations suggest carbonates could be forming from the ponding and evaporation of surface water and/or from groundwater discharge.

Prior to assessing the hydrological process responsible it is important to understand if carbonate minerals are present in the peat profiles. Mineralogy from peat substrate cores sampled from central peat mounds in Fern (20cm below ground level) Melaleuca (30cm below ground level) and Saunders Springs (80cm below ground level) were analysed using scanning electron microscopy (SEM). Samples were analysed by Microanalysis Australia using a Carl Zeiss EVO50 scanning electron microscope (SEM) fitted with an Oxford INCA X-Max energy dispersive spectrometer (EDS).

HYDROLOGICAL CONCEPTUALISATION OF THE WALYARTA MOUND SPRINGS

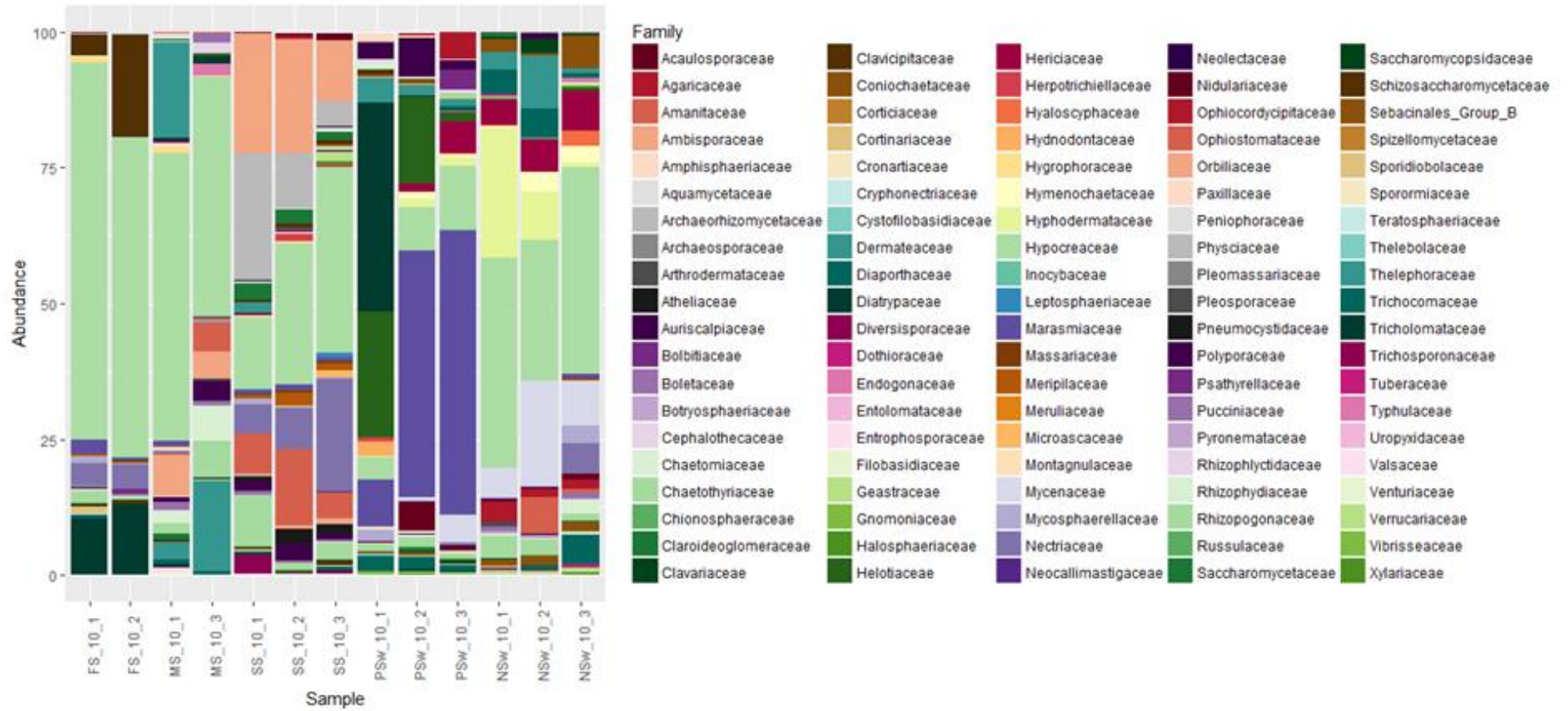


Figure 45 Descriptive bar charts of fungal communities from locations (FS=Fern Spring, MS=Melaleuca Spring, SS=Saunders Spring, Psw and NSW are other WA sites) at a depth of 10 cm. OTUs have been coloured by Family. Y axis represents % abundance. 24 bacterial Families each with a mean abundance < 0.01% have been excluded for clarity



Results for Fern peat (10cm);

- Major quantities of particles (~ 1 µm to ~ 35 µm) containing primarily oxygen and silicon with varying trace concentrations of aluminium, sulfur, chlorine, potassium, sodium, iron and calcium (possible diatoms and quartz);
- Major quantities of particles (~ 20 µm to ~ 200 µm) containing primarily carbon and oxygen with varying trace concentrations of silicon, sodium, calcium, sulfur, chlorine, aluminium, magnesium, potassium, phosphorus and nitrogen (possible organic)
- Minor quantities of particles (~ 1 µm to ~ 10 µm) containing primarily oxygen, sulfur and iron with varying trace concentrations of sodium, chlorine, calcium, silicon, phosphorus and aluminium (possible pyrite);
- Minor quantities of particles (~ 2 µm to ~ 110 µm) containing primarily oxygen, sulfur and calcium with varying trace concentrations of sodium, chlorine, magnesium, silicon, aluminium, aluminium and potassium (possible gypsum);
- Trace quantities of particles (~ 10 µm) containing primarily oxygen and silicon with minor concentrations of aluminium, iron, magnesium and potassium and trace concentrations of calcium, sulfur, titanium and chlorine (possible mica);
- Trace quantities of particles (~ 9 µm) containing primarily iron, sulfur, arsenic and oxygen with trace concentrations of chlorine and calcium (possible arsenopyrite);
- Trace quantities of particles (~ 6 µm) containing primarily oxygen and silicon with minor concentrations of aluminium and potassium and trace concentrations of sodium, sulfur and chlorine (possible feldspar);
- Trace quantities of particles (~ 6 µm) containing primarily oxygen, silicon and aluminium with trace concentrations of sodium, iron, potassium, titanium, calcium and chlorine (possible aluminosilicate); and,
- Trace quantities of particles (~ 4 µm) containing primarily oxygen, sulfur, nickel and iron with trace concentrations of magnesium, silicon, sodium, aluminium and calcium (possible bravoite).

For Melaleuca peat (10cm);

A range of particle sizes from ~ 1 µm to ~ 70 µm were observed in the following distinct compositions –

- Major quantities of particles (~ 3 µm to ~ 70 µm) containing primarily oxygen and silicon with varying trace concentrations of magnesium, iron, sulfur, sodium, phosphorus, chlorine, aluminium and potassium (possible diatoms and quartz);
- Minor quantities of particles (~ 1 µm to ~ 10 µm) containing primarily oxygen, sulfur and iron with varying trace concentrations of silicon, sodium, chlorine, aluminum and potassium (possible pyrite);
- Trace quantities of particles (~ 2 µm to ~40 µm) containing primarily oxygen and silicon with varying minor concentrations of iron and aluminium and varying trace concentrations of sodium, chlorine, sulfur, calcium, titanium and potassium (possible mica); and,
- Trace quantities of particles (~ 2 µm to ~40 µm) containing primarily oxygen and silicon with minor concentrations of potassium and aluminium and varying trace concentrations of sodium, chlorine and sulfur (possible feldspar).
- For Melaleuca peat (30cm);

A range of particle sizes from ~ 1 µm to ~ 55 µm were observed in the following distinct compositions –

- Major quantities of deposits containing primarily oxygen and silicon with minor concentrations of aluminium and varying trace concentrations of calcium, sodium, sulfur, iron, magnesium and potassium;
- Major quantities of particles (~ 2 µm to ~ 55 µm) containing primarily oxygen and silicon with varying trace concentrations of sodium, aluminium, calcium, iron and potassium (possible quartz);
- Minor quantities of particles (~ 1 µm to ~ 10 µm) containing primarily oxygen and titanium with varying minor concentrations of iron and varying trace concentrations of silicon, aluminium, magnesium and calcium;
- Trace quantities of particles (~ 2 µm to ~ 30 µm) containing primarily oxygen, sulfur and barium with varying trace concentrations of silicon, aluminium, calcium, sodium and strontium (possible baryte);
- Trace quantities of particles (~ 20 µm) containing primarily oxygen and silicon with minor concentrations of aluminium and sodium (possible albite);
- Trace quantities of particles (~ 15 µm) containing primarily oxygen and silicon with minor concentrations of aluminium and potassium (possible feldspar);
- Trace quantities of particles (~ 1 µm) containing primarily sulfur, iron and oxygen with trace concentrations of silicon, sodium and aluminium (possible pyrite).

For Saunders peat (10cm);

A range of particle sizes from ~ 1 µm to ~ 100 µm were observed in the following distinct compositions –

- Major quantities of particles (~ 5 µm to ~ 60 µm) containing primarily oxygen and silicon with varying trace concentrations of calcium, sodium, chlorine, sulfur, potassium, magnesium and aluminium (possible quartz and diatoms);
- Minor quantities of particles (~ 20 µm to ~ 100 µm) containing primarily carbon and oxygen with varying trace concentrations of sulfur, silicon, sodium, chlorine, iron, calcium, magnesium, potassium and aluminium (possible organic);
- Minor quantities of particles (~ 1 µm to ~ 11 µm) containing primarily oxygen, sulfur and iron with varying trace concentrations of sodium, chlorine, sulfur, calcium, magnesium and aluminium (possible pyrite);
- Trace quantities of particles (~ 9 µm to ~ 16 µm) containing primarily oxygen and silicon with minor concentrations of potassium and aluminium and varying trace concentrations of sodium, chlorine and sulfur (possible feldspar); and,
- Trace quantities of particles (~ 2 µm) containing primarily oxygen, titanium and iron with trace concentrations of sodium, zinc, chlorine, silicon, sulfur, calcium, magnesium, aluminium and manganese (possible ilmenite).

For Saunders peat (80cm)

A range of particle sizes from ~ 1 µm to ~ 170 µm were observed in the following distinct compositions –

- Major quantities of deposits containing primarily oxygen and silicon with varying minor concentrations of aluminium, calcium and magnesium and varying trace concentrations of sulfur, iron, potassium and titanium;
- Major quantities of particles (~ 10 µm to ~ 170 µm) containing primarily oxygen and silicon with varying trace concentrations of aluminium (possible quartz);
- Minor quantities of particles (~ 5 µm to ~ 30 µm) containing primarily oxygen and silicon with minor concentrations of aluminium and potassium (possible feldspar);
- Minor quantities of particles (~ 1 µm to ~ 5 µm) containing primarily sulfur, iron and oxygen with varying trace concentrations of silicon and aluminium (possible pyrite);

- Trace quantities of particles (~ 2 µm to ~ 10 µm) containing primarily oxygen and titanium with varying minor concentrations of iron and varying trace concentrations of manganese, silicon and aluminium (possible titanium oxide);
- Trace quantities of particles (~ 12 µm to ~ 70 µm) containing primarily oxygen and silicon with minor concentrations of aluminium and varying trace concentrations of magnesium, iron and potassium (possible aluminosilicate);
- Trace quantities of particles (~ 2 µm to ~ 5 µm) containing primarily oxygen, sulfur and barium with varying trace concentrations of silicon, aluminium and calcium (possible baryte); and,
- Trace quantities of particles (~ 40 µm) containing primarily oxygen, zirconium and silicon (possible zircon).

The results of this work suggest that carbonates are present as trace elements and the major mineral in sediments within the central peat mounds of Fern, Melaleuca and Saunders springs is quartz and possibly tectosilicates such as feldspar, with variable aluminosilicates (clay minerals) and sulfides (pyrite and arsenopyrite). However, acquiring SEM data is subjective as data collected are dependent on the technician's selection of a site that is representative and then analysing the range of minerals present within that site. SEM results are followed up with hydrogeochemical modelling of surface water and groundwater samples in Section 7.



## 6 Hydrology

### 6.1 Groundwater

The hydrogeology of the WCB has been reported by Leech (1979), Haig (2009), Aquaterra (2010) and Department of Water and Environmental Regulation (DWER) (in prep). As there is limited drilling and fine-scale hydrogeological information in Walyarta these investigations either limit their studies to the southern boundary, or produce a theoretical model for Walyarta through an interpolation of the WCB conceptualisation.

The main aquifers of interest in Walyarta occur in Quaternary (in particular palaeovalley and palaeochannel sediments) and Mesozoic (Broome and Wallal Sandstones) geological formations. The Broome and Wallal Sandstone aquifers are generally separated by the Jarlemai Siltstone aquitard, where it is present. In Walyarta there is limited lithology information from drill holes (Table 1) and less information on aquifer groundwater levels and gradients. Monitoring bores with higher levels of confidence limited to those constructed for this purpose (e.g. the five WCS series bores in Table 1).

The lack of groundwater monitoring data along with the variable and patchy distribution of Quaternary and Broome Sandstone sediments (Section 4.5.3) prohibits the development of reliable saturated thickness maps and aquifer flow nets. In the absence of this information the following approach was taken to develop the conceptual hydrogeology of Walyarta;

- Selected AEM interval conductivity data were converted to water quality maps to interpret their spatial variation in relation to both the variation in the physico-chemical properties of sediments and hydrogeological processes (e.g. vertical and lateral gradients). Maps were produced for the Quaternary formation aquifers, as well as Broome and Wallal Sandstone aquifers using the relationship determined in Figure 22 (Figures 46 to 50).
- Two schematic diagrams for cross sections along the Mandora Palaeovalley were constructed to illustrate the main aquifer geometries and interactions in Walyarta (Figures 51 and 52). These figures were developed using additional information from Laws (1991), Roach (2010) and DWER (in prep).

Information obtained from this work was incorporated into the numerical modelling (Section 8).

#### 6.1.1 Quaternary aquifers

In Walyarta only one bore maps the presence and thickness of surficial cover and there is sparse information on aquifer materials, saturated thickness or soil water content.

Quaternary sediments outcrop on the land surface and form unconfined aquifers that receive groundwater recharge from rainfall, with groundwater movement generally following topographic gradients. The Quaternary formations contain groundwater but as they are relatively thin and spatially discrete resources they have not been the subject of thorough investigations. Aquifers are more likely to form where sediments have higher porosities and permeability's (e.g. higher percentage of quartzose sands and/or development of secondary porosity). Towner (1982a) described the Quaternary sediments as grading into one another, with the likelihood of secondary cementation in sediments occurring in depressions (e.g. ephemeral lakes and drainage channels). As these sediments differ in mineralogy, physical properties and water quality this reduces their ability to form effective aquifers for stock and domestic supplies.

Shallow AEM derived water quality maps (0-10m below ground level, Figure 46) resolve large variations in water quality from the coast to the uplands. For the coastal, tidal flat, mixed calcilutite and calcarenite sediments groundwater quality ranges from fresh to saline. Elevated salinities (>20,000 mg/L) are interpreted to occur where the calcilutite is intersected and entrained saline groundwater is close to the ground surface, which promotes discharge and evapotranspiration. Fresh to saline groundwater (>500 to 6,000 mg/L) in coastal areas (e.g. aprox. 5km west of Artesian No2 in Figures 46 & 47) appears to resolve the mixed response of partly saturated coastal dune sediments (e.g. Bossut Formation (Qpb) that store lower salinity groundwater but overlie saline tidal flat sediments (also see Figures 8, 9, 51 & 52).

In the WCB the Bossut Formation is the most prospective Quaternary aquifer for small stock water supplies. The sediments attain a thickness of up to 25 meters and they consist of lithified coastal dunes, characterised by fresh to brackish groundwater with high boron, fluoride and nitrate (Leech 1979). In Walyarta little is known of the Bossut Formation apart from its mapped extent (Towner 1982a). The formation may store and discharge groundwater within tidal flat swales, which may explain spatial coastal linear responses in the ASTER green vegetation index map (Figures 37 and 52).

The Mandora Palaeovalley in Walyarta is characterised by higher soil and groundwater salinities with geological faults marking electrical conductivity pattern breaks. The major north-west AEM pattern break (approximately 10km east of 15LAG24D) is aligned to the interpreted oblique accommodation zone (Figures 46, 47 & 28). To the west of the accommodation zone groundwater salinities are higher and are aligned to another north-west trending fault that is coincident with interpreted contemporary ephemeral drainage lines, *shallow* (~30 to 50 metres below ground level) Pleistocene and Eocene palaeo-drainages and the southern boundary of Mandora Lake (Figures 46, 47 & 24). This area is interpreted to mark the extent of the Pleistocene-Holocene (17,000-8,000 yrs BP) marine transgression (Figure 18), with the higher electrical conductivities/groundwater salinities likely to represent areas of 'stored/unflushed' solutes. This area also receives perennial saline discharge from Salt Creek, the latter occupying a steeply incised and spatially discrete east-west trending drainage line (see Section 6.3). Combined the hydrogeology, contemporary ephemeral drainage and the palaeohydrology help maintain near surface groundwater levels and as a result perennial groundwater discharge, evaporation and high salt stores.

HYDROLOGICAL CONCEPTUALISATION OF THE WALYARTA MOUND SPRINGS

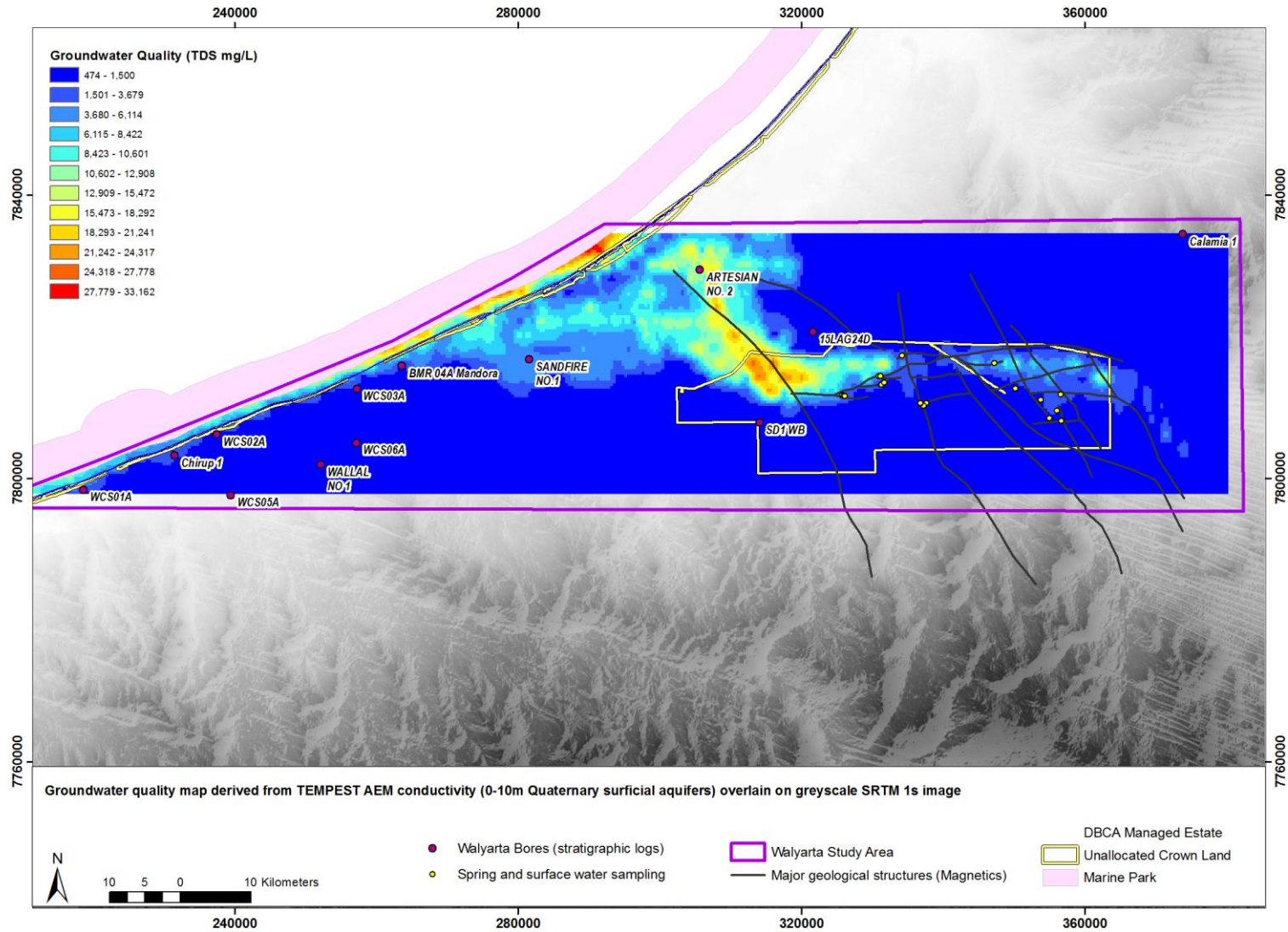


Figure 46 AEM derived water quality map for the Quaternary Formation aquifers (0-10 metres below ground level); Note confidence in map is higher within the western valley floor and coastal areas where depth to groundwater is closer to the ground surface.



HYDROLOGICAL CONCEPTUALISATION OF THE WALYARTA MOUND SPRINGS

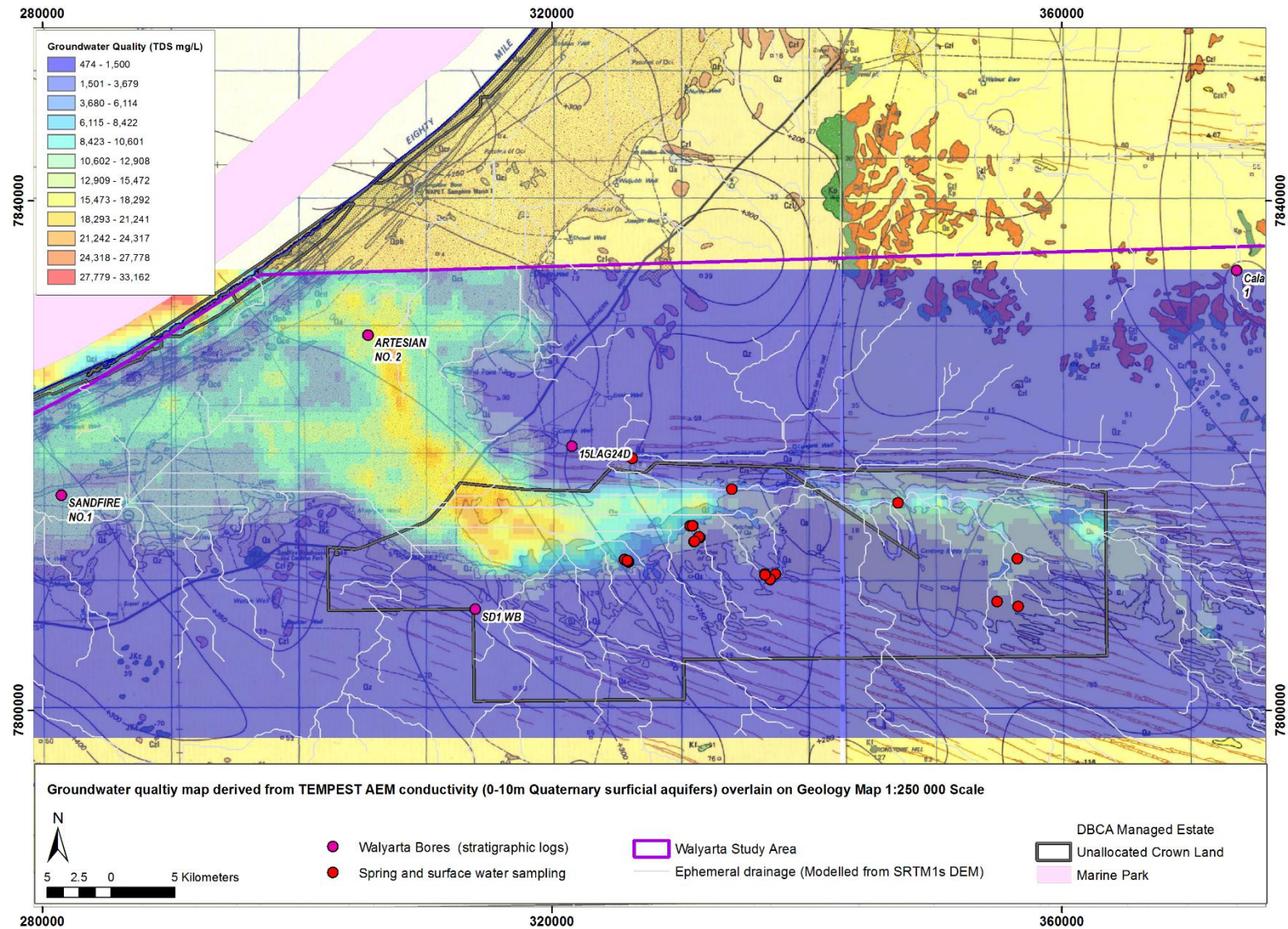


Figure 47 AEM derived water quality map for the Quaternary Formation aquifers (0-10 metres below ground level) overlain on geology mapped at 1:250 000 scale

HYDROLOGICAL CONCEPTUALISATION OF THE WALYARTA MOUND SPRINGS

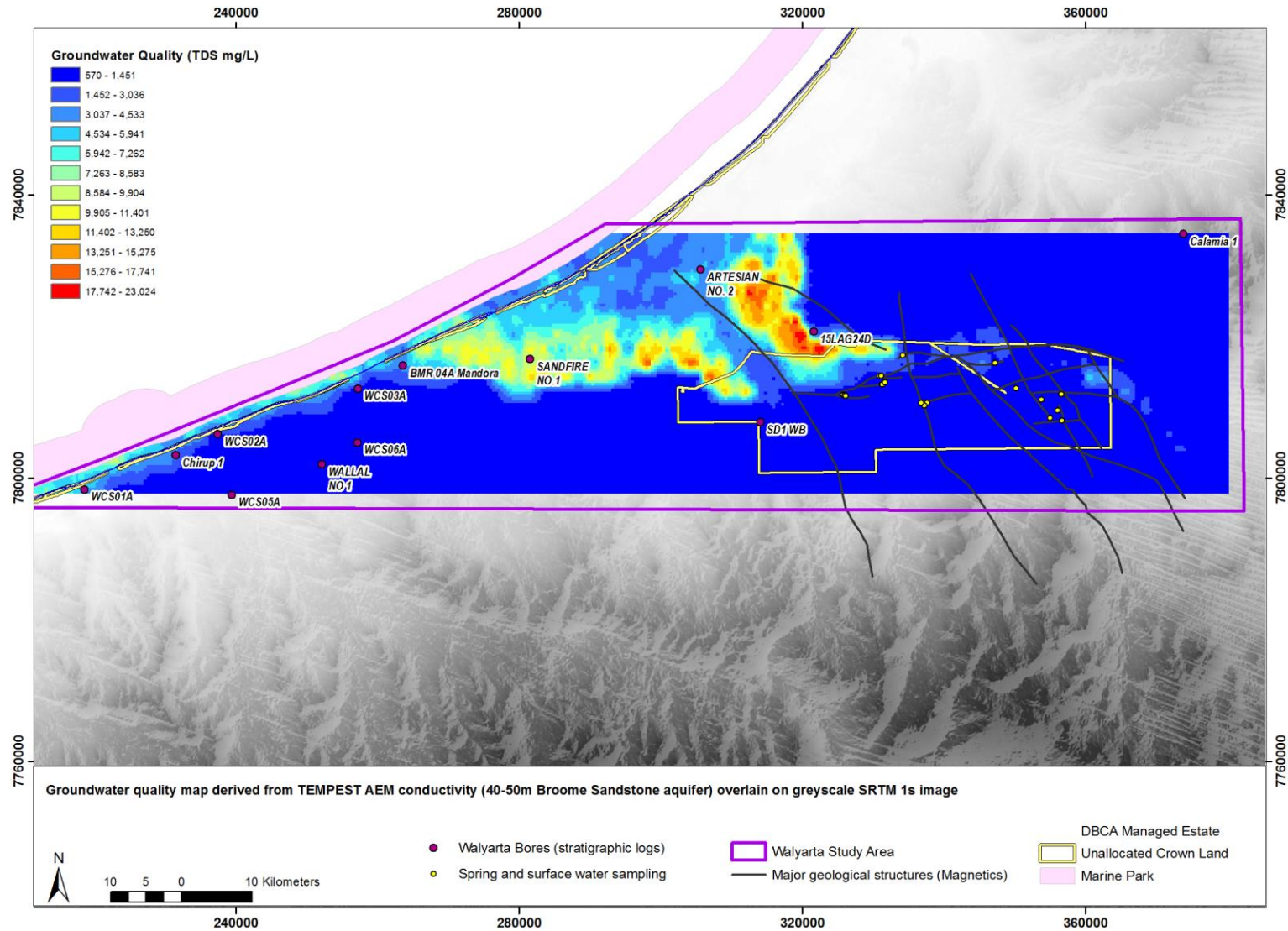


Figure 48 AEM derived water quality map for the Broome Sandstone aquifer (40-50 metres below ground level)



HYDROLOGICAL CONCEPTUALISATION OF THE WALYARTA MOUND SPRINGS

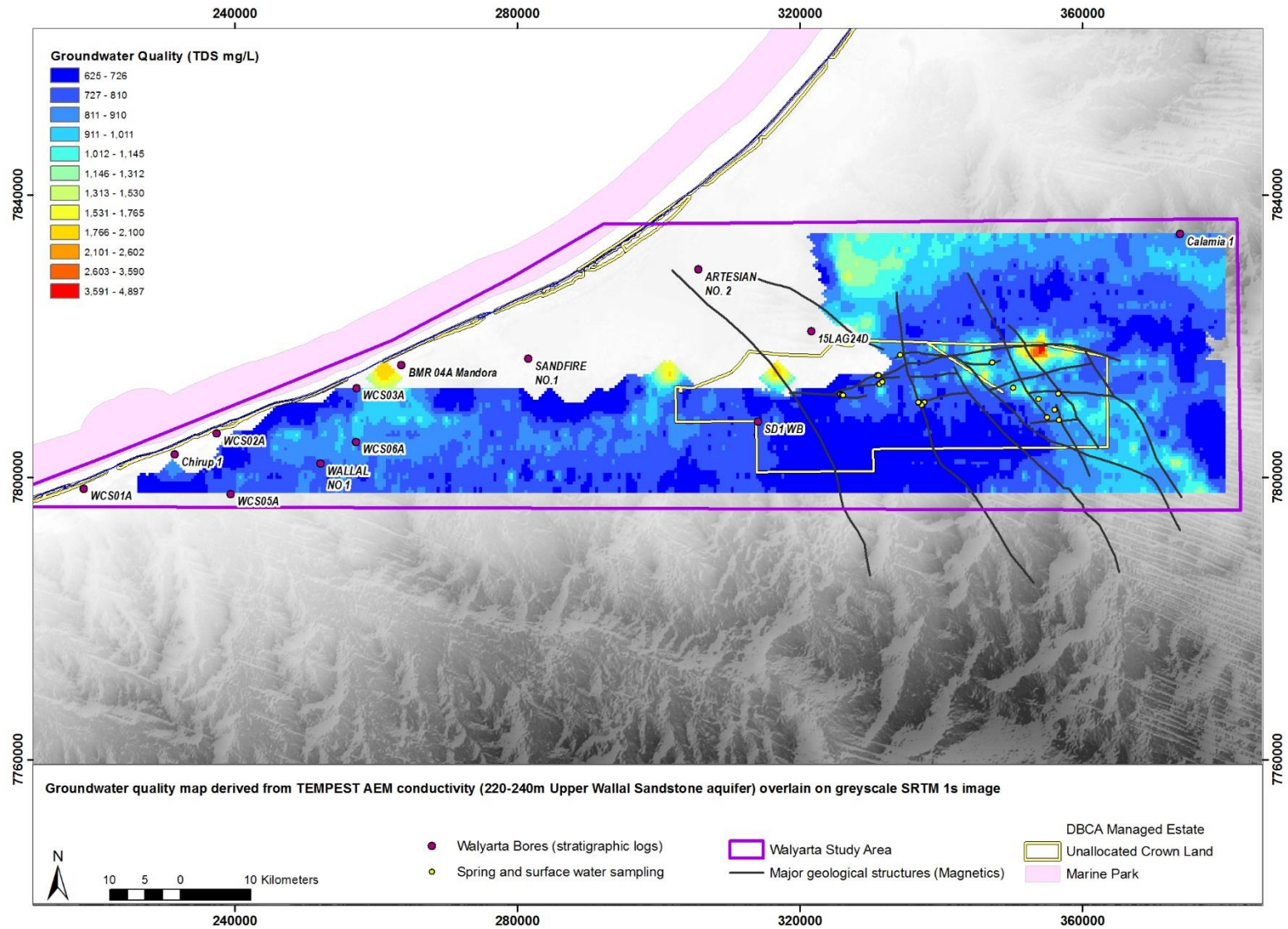


Figure 49 AEM derived water quality map for the Wallal Sandstone aquifer (220 to 240 metres below ground level)



HYDROLOGICAL CONCEPTUALISATION OF THE WALYARTA MOUND SPRINGS

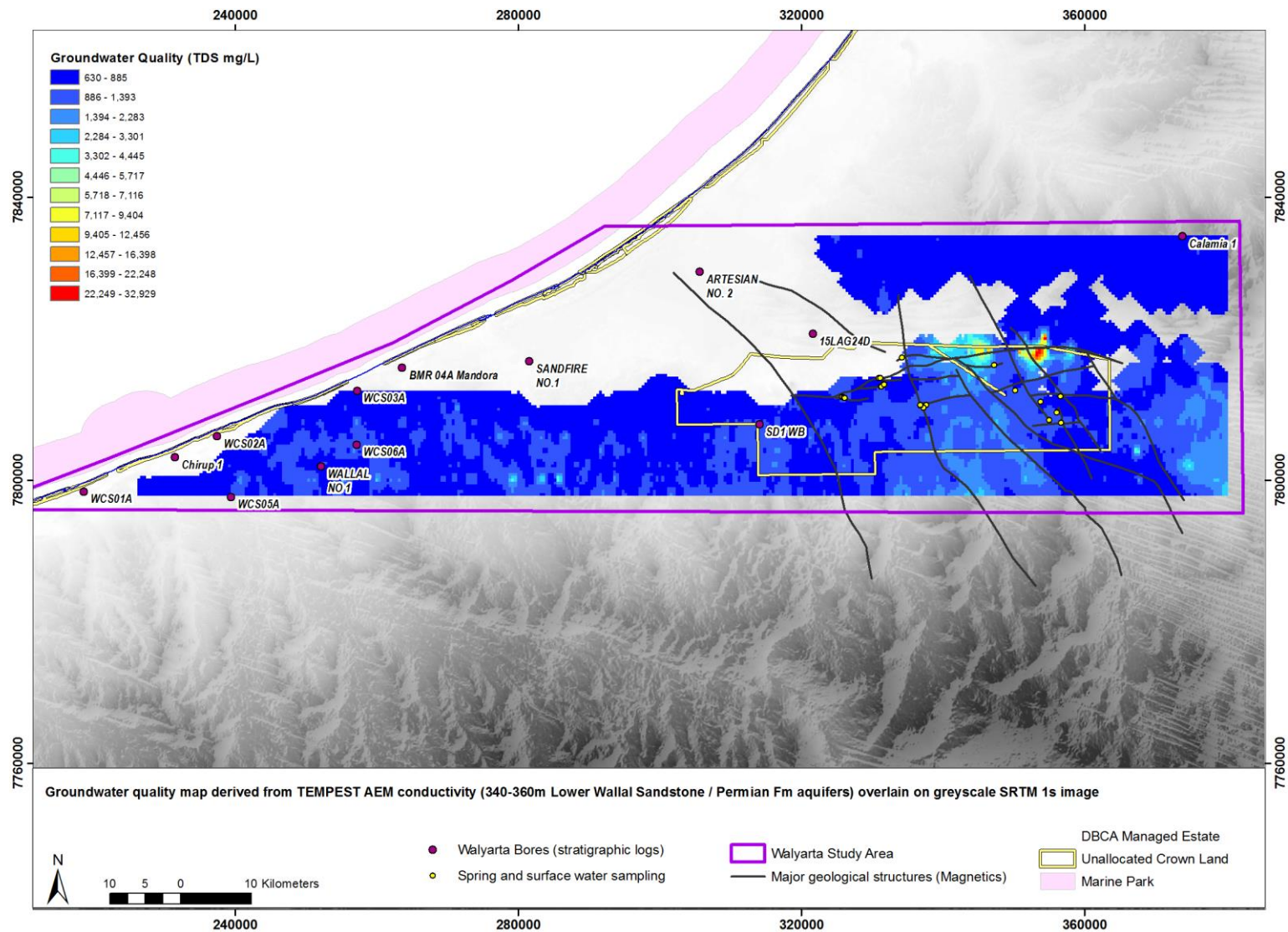
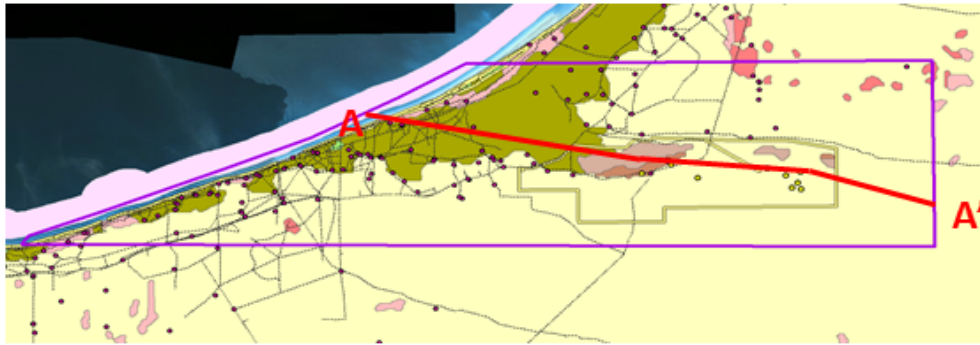


Figure 50 AEM derived water quality map for the Wallal Sandstone aquifer / Permian Formation aquifers (340 to 360 metres below ground level)

HYDROLOGICAL CONCEPTUALISATION OF THE WALYARTA MOUND SPRINGS



Note: indicative Wallal Aquifer Hydraulic Head is estimated @ 50 to 75 mAHD

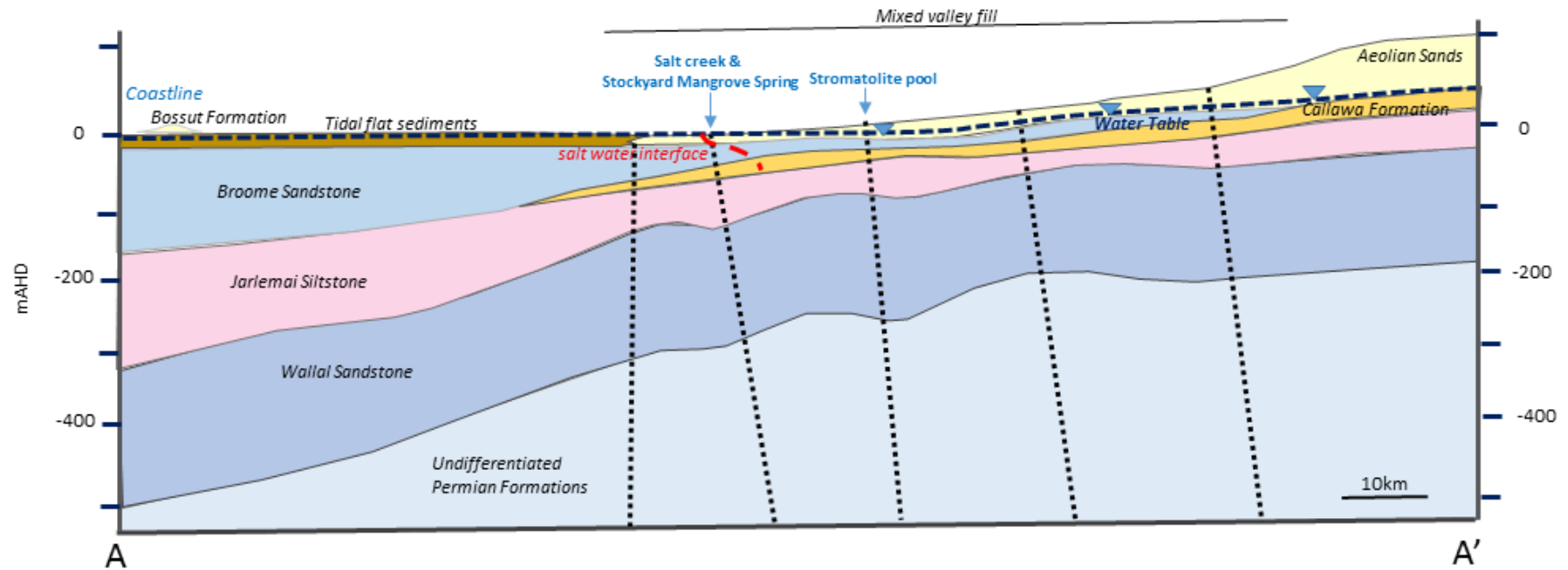


Figure 51 Schematic diagram for cross section A-A' (perspective view from Figure 6) through the Mandora Palaeovalley; (adapted from Laws (1991), Roach (2010) and DWER (in prep)).

HYDROLOGICAL CONCEPTUALISATION OF THE WALYARTA MOUND SPRINGS

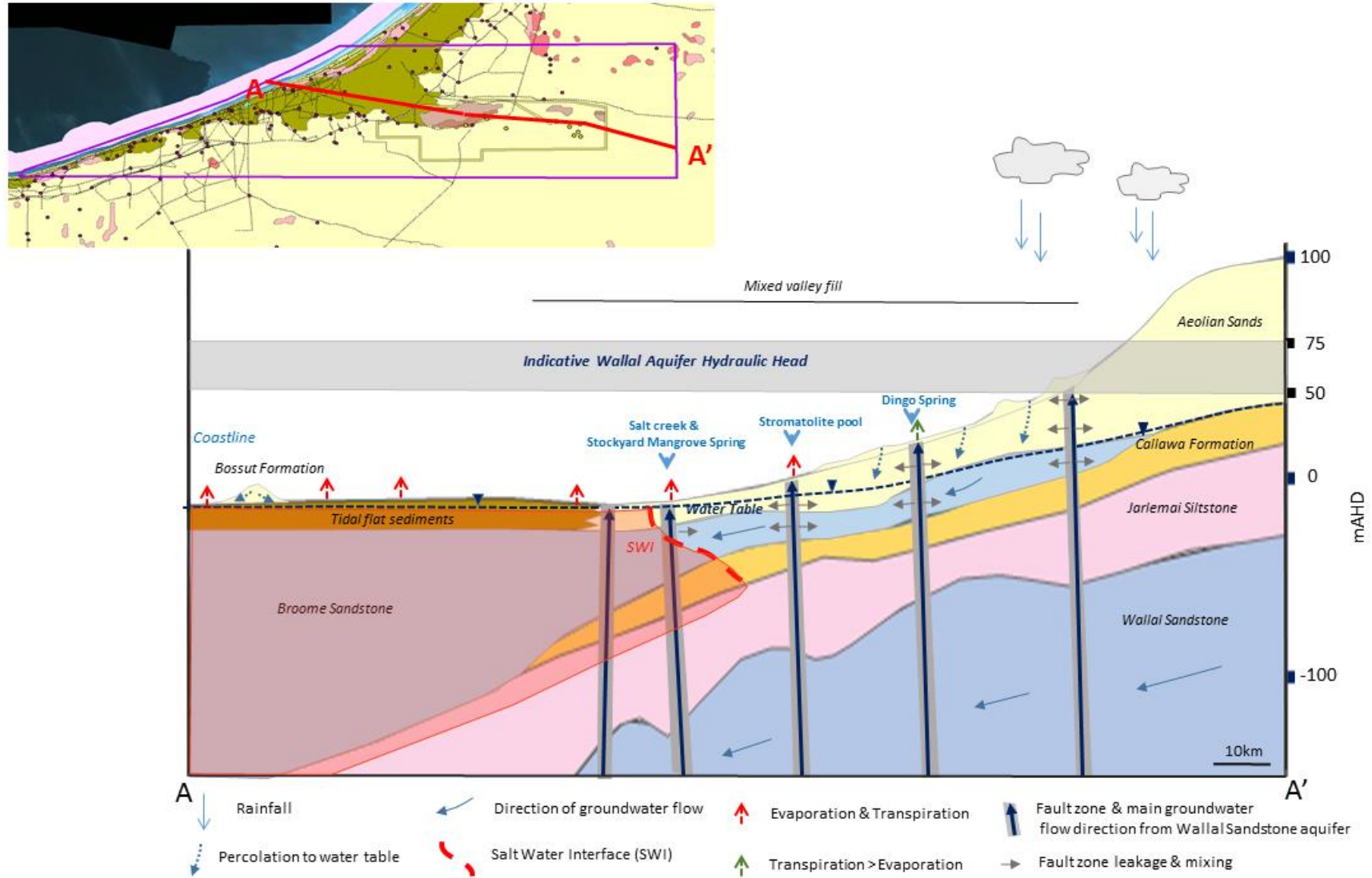


Figure 52 Schematic diagram for cross section A-A' (perspective view from Figure 6) through the Mandora Palaeovalley illustrating main aquifer interactions (adapted from Laws (1991), Roach (2010) and DWER (in prep)).



In the eastern section of the palaeovalley electrical conductivities are lower and more variable. Elevated salinities, brackish to saline groundwater (~5,000 to 10,000 mg/L), occur within valley floor alluvial deposits (Qa) and are connected by the contemporary ephemeral drainage lines (Figures 46 & 47). Immediately upgradient of the valley floor alluvium, groundwater salinities are fresh to brackish (~500 to 3,000 mg/L) indicating that groundwater discharge and evaporation is a minor process (Figures 46 & 47). The areal extent of these zones includes ephemeral drainage confluences and persistent vegetation cover (Figure 37) providing evidence that the most likely processes maintaining low to moderate salinities are episodic surface water flows and transpiration (Figure 47 & 37).

The low and variable shallow electrical conductivities suggest that for large areas of the eastern palaeovalley groundwater levels in the unconfined Quaternary aquifers may be greater than 10 meters below ground level. Therefore the major process taking place in the Quaternary sediments is seasonal groundwater recharge, with groundwater moving vertically and laterally to replenish storage within local and downgradient Quaternary surficial aquifers, as well as the underlying Broome Sandstone aquifer (Figures 51 & 52).

Aeolian dune sands are located upgradient of the coastal tidal flats and the Mandora Palaeovalley sediments. The dune sands are estimated to range in thickness from approximately 0 to 60 metres and appear to be more extensive in Walyarta, compared to the WCB (see Section 4.5.3.1 (Figures 30, 51 & 52). They receive recharge from rainfall and groundwater gradients follow topography and are thought to have thick unsaturated zone, which is supported by the low groundwater and/or soil water salinities derived from AEM data (Figures 46 & 47).

Groundwater in aeolian dune sands moves vertically and either recharges and mixes with underlying aquifers (e.g. Broome Sandstone aquifer), or moves laterally via throughflow prior to discharging in coastal sediments and dune swales (Figure 52). Spatially discrete curvilinear patterns in the ASTER green vegetation content map supports the proposal that groundwater discharge occurs in swales where they are coincident with interpreted Eocene and Pleistocene palaeo-drainage channels (Figures 24 & 37).

### 6.1.2 Broome Sandstone Aquifer

The combined thickness of the Quaternary and Broome Sandstone formations increases from the north-east to the west south-west and is thin or absent in the south-eastern quadrant of Walyarta (see Section 4.5.3, Figure 31). The isopach map was verified using lithology information from thirteen drill holes. The saturated thickness of the Broome Sandstone aquifer is not well constrained as groundwater monitoring bores were only installed in five of these drill holes and they are all located near the coastal margin.

In the absence of local scale information, coarse scale Broome Sandstone groundwater level maps produced by DWER (in Prep) (Appendix 5) are used as an indication of the likely aquifer gradients (mAHD) and depth to groundwater (metres below ground level). Maps in Appendix 5 showing Broome Sandstone aquifer groundwater gradients in Walyarta mimic topography with flow from east to west (approximately 20mAHD to 0mAHD at the coast). Walyarta Broome Sandstone groundwater levels decrease from the north-east to west, showing a maximum of approximately 60 metres below ground level in the north-east, while coastal groundwater levels are at the land surface (Appendix 5).

Groundwater level information from Appendix 5 was included in Figures 51 and 52, with the water table also representing the Broome Sandstone aquifer groundwater levels in the Walyarta Mandora Palaeovalley. Figures 51 and 52 depict the Callawa Formation to be present and the Broome Sandstone to be absent near the south eastern boundary of Walyarta. The Callawa Formation is included to align the conceptualisation with information provided in Forman and Wales (1981) and to fill interpretation gaps that the AEM data could not provide (e.g. the Callawa Formation does not have a distinctive electrical response in AEM data (see Appendix 3)).

In Walyarta the Broome Sandstone aquifer receives groundwater recharge from the Quaternary formation aquifers and from the Wallal Sandstone aquifer where major geological faults have produced advective flow resulting in upward leakage and mixing (Figure 51). Discharge will occur via Quaternary sediments, downgradient towards the coast where groundwater levels are close to the ground surface.

Broome Sandstone aquifer groundwater salinities, at 40-50 metres below ground level, are predominantly fresh to brackish (~1,000 to 3,000 mg/L), with elevated salinities (~5,000 to 20,000 mg/L) on the Mandora Palaeovalley coastal margins (Figure 48). Lowest salinities correspond to north-west trending faults that have assisted in the development of *shallow* (~30 to 50 metres below ground level) Pleistocene and Eocene palaeo-drainages (e.g. ~2km north of bore SD1WB, Figure 48). High salinities bordering the low salinity area, particularly to the east represent areas of 'stored/unflushed' solutes from the Pleistocene-Holocene (17,000-8,000 yrs BP) marine transgression (Figure 18). The AEM data here providing combined information on mapped geological materials and hydrogeological processes within the Broome Sandstone aquifer. The north-west trending palaeo-drainage system may contain a mixture of Broome Sandstone and reworked Broome Sandstone and Quaternary sediments that under a 'wetter' climate were efficient at discharging water and entrained solutes into the paleo-coastline.

### 6.1.3 Wallal Sandstone Aquifer

The Wallal Sandstone aquifer in Walyarta has less geological and hydrogeological information than the Broome Sandstone, resulting in higher uncertainty, particularly inland from coastal areas (Section 4.5.3). In the absence of local scale information, the same approach was adopted for the Wallal as the Broome Sandstone aquifer in Section 6.1.2.

Groundwater level maps produced by DWER (in Prep) (Appendix 5) were used as an indication of the likely aquifer gradients (mAHD) and depth to groundwater (metres below ground level). Maps in Appendix 5 show Wallal Sandstone aquifer groundwater gradients in Walyarta are similar to those in the Broome Sandstone aquifer, as they follow the coarse scale topographic, east to west, gradients (approximately 75mAHD in the east to 51mAHD at the coast) (Figures 51 & 52). Wallal Sandstone aquifer hydraulic head is thought to be highest in the central Mandora Palaeovalley (approximately 50 metres above ground level) decreasing to around 25 metres above ground level to the west, north and south (Appendix 5; Figures 51 & 52).

In Walyarta, the Wallal Sandstone aquifer head interpretations presented in Appendix 5 are unable to be verified due to the absence of bore data. Aquifer geometry and relationships that constrain

groundwater recharge and discharge processes in the Wallal aquifer are also theoretical and require verification. In Walyarta the AEM DOI is limited to the ground surface in coastal areas and between 50 to 100 metres below ground level for Mandora Lake and some adjoining areas. Where the AEM data does provide information groundwater quality maps were produced and the information interpreted (Figures 49 & 50).

Groundwater quality in the Wallal Sandstone aquifer at depths around 220 to 240 metres below ground level is interpreted to be fresh (~600 to 1,500 mg/L), with higher salinities associated with an east-west trending relay ramps located to the west of the oblique accommodation zone (Figures 49 & 28). Spatially discrete high salinity zones (>3,000 mg/L) occur within valley floor relay NE-NW fault intersections, potentially representing leakage of deeper, higher salinity groundwater along fault zones (Figures 49, 51 & 52). Groundwater quality patterns are similar at depths of 340 to 360 metres below ground level (close to the interpreted top of the Permian Formations in south-eastern Walyarta area) (Figure 50). At this depth the oblique accommodation zone is characterised by higher salinities, potentially in response to AEM measuring physico-chemical changes in the Permian sediments. Groundwater in the Wallal Sandstone aquifer, along east-west trending relay structures, is fresh (<1,000 mg/L), while spatially discrete high salinity zones along NE-NW valley floor fault intersections show an increase in salinity (~7,000 to >30,000 mg/L) (Figure 50).

Patterns within the AEM interval conductivity images and derived water quality maps presented in this section and Section 4.5.1 provide corroborative information that the interpreted Walyarta structural framework propagates through the Wallal and Broome Sandstone aquifers as well as Quaternary Formations (Figures 46 to 50). Despite this connection the lower groundwater salinities in overlying aquifers in eastern Walyarta indicates that if the elevated Wallal Sandstone aquifer hydraulic heads exist, the presence and integrity of the Jarlemai Siltstone aquitard and/or Callawa Formation (the latter forming an aquitard in Walyarta, see Section 4.2) constrains groundwater discharge (Figures 51 and 52). This may not be the case in within and west of Mandora Lake and this is discussed further in Section 6.2.

Another important feature resolved in the AEM are the potentially deeper, higher salinity, recharge sources to the Wallal sandstone aquifer within the valley floor. These features are likely to represent advective flow along fault systems as they are discrete and become less saline at shallow depths indicating mixing with fresher formation groundwater occurs. Advective flow and mixing along fault zones are mapable in AEM data where there is a salinity contrast. Springs in Walyarta are located where there is generally not a strong salinity contrast, with either shallow or deeper aquifers (Figures 46 to 50, see Section 6.3). The use of hydrogeochemical methods to verify fault controlled discharge from deeper aquifers within springs is discussed in Section 7.

## 6.2 Surface water

Heavy wet season rains fill numerous small claypans on supratidal flats. Inland, other depressions (e.g. Mandora Lake, Lake Walyarta and East Lake (Figure 4)) appear to have formed within a relict drainage system that developed during the previous pluvial period in the Palaeogene (see Section 4.3). These depressions are thought to only hold water intermittently (Towner 1982a).



V&C Semeniuk Research Group (2000) undertook an investigation to assess the role of surface water in supporting springs and wetlands in Walyarta and the WCB. Results from this study indicate that most wetlands and springs were sustained by groundwater, the exception being the perched claypan systems that hold water due to the ponding/ perching of meteoric water.

The role of relict ephemeral drainages to connect to and fill depressions (e.g. perched and groundwater connected wetlands and lakes) remains unknown, as are the surface water body hydroperiods (frequency and length of inundation).

As no instrumentation exists to measure potential inflows or lake water levels in Walyarta a study was undertaken to trial using remote sensing data to (approximately) map historical lake water level extents (Vogwill and Callow 2017). The study trialed data from a number of satellites for the study and for the modelling chose the Landsat Water Observations from Space (WOfS) product created by Geosciences Australia (Mueller et al., 2016). The period modelled was from May 1987 to October 2015.

The study results showed that

1. Filling of the main wetland basins of Walyarta occurs during high rainfall wet seasons, particularly those with multiple cyclonic events (with the study presenting information that Walyarta (Mandora Station) is in an area that statistically receives more than one cyclone a year);
2. Walyarta proximal cyclonic activity however does not guarantee large inflow events, as was observed in 1995;
3. Three Walyarta wide inflow events have occurred in 1997, 2004 and 2007;
4. The largest inflow event estimated using this technique was approximately 53500 ML and this affected the whole extent of Walyarta; and
5. Mound springs appear to be disconnected from the main basins during all inflow events observed through the investigation period.

The spatial coverage of the inundation frequency for Walyarta in Figure 53 demonstrates the surface water drainages and depressions operate as per the description of Towner 1982a. The apparent chain of lakes and incision of some drainage channels does not reflect the current climate or hydrological processes.

The inundation frequency was calculated for sample locations in Figure 53 and the results tabulated in Table 5. The landscape within the southern boundary of Mandora Lake/Walyarta is relatively, consistently flat (sample locations Pt1, Pt2, Pt3 and Pt 5). Lake bathymetry is slightly elevated and variable in the north and north eastern areas of the lake and as a result is inundated only when the southern section has sufficient water to promote overflow. The western margin is rarely inundated as it forms a local high area, bounding the main road, the Great Northern Highway (Figure 6) and the eastern margin is connected to the Salt Creek inflow and elevations here are around 0.5 metres higher than Mandora Lake's southern margin (see Pt 4 Table 5). Sample location Pt 4 is close to DBCA 2015 salt creek sample location, which is located in a gaining section (perennial groundwater discharge section) of salt creek (Figure 54)

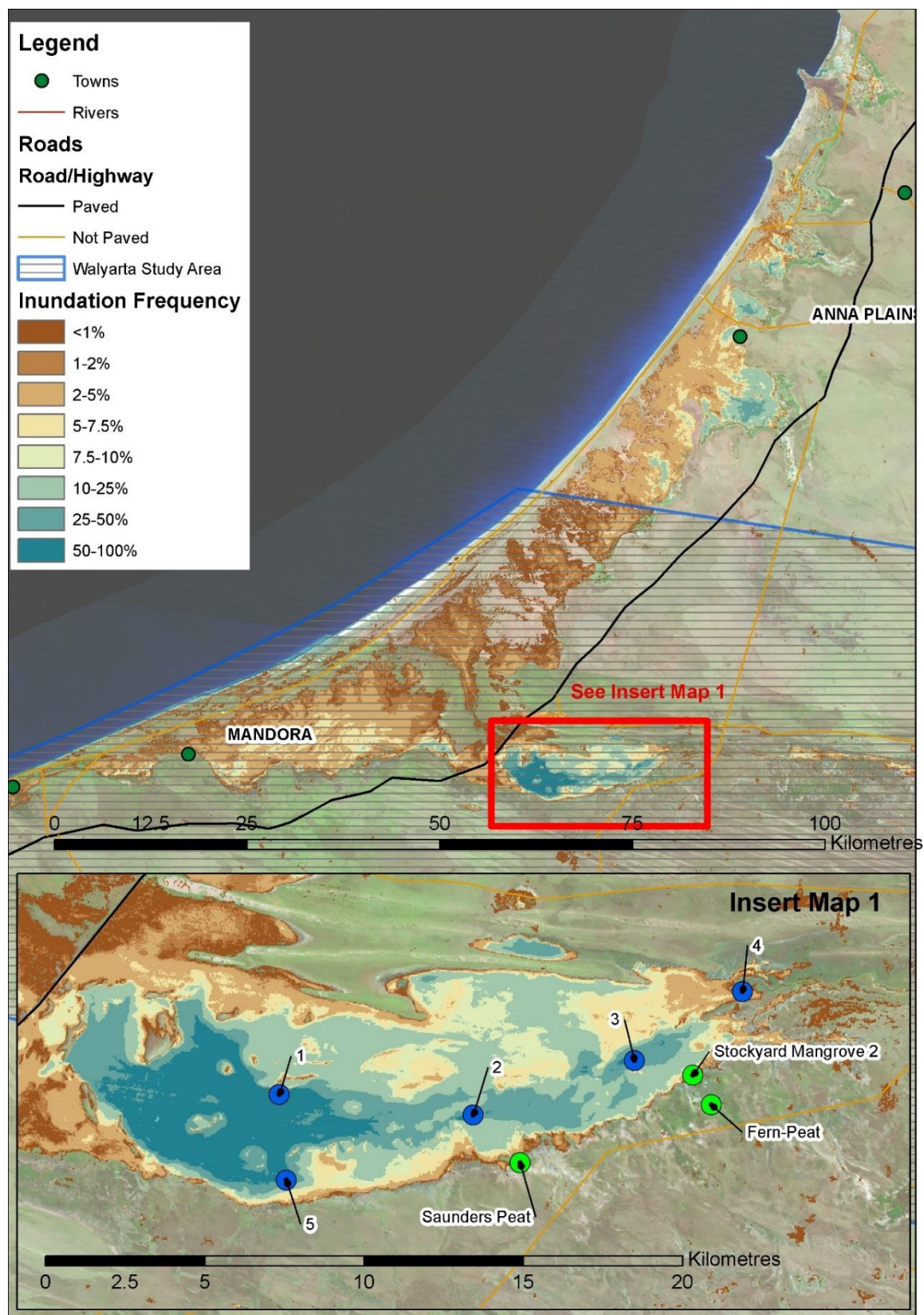


Figure 53 Inundation frequency of Mandora Lake/Walyarta, including the location of the WofS mapping sample locations, see Table 5.

Point Identification	Easting_MGA51	Northing_MGA51	Inundation Frequency (%)	Elev (m)*
Pt 1 (Deepest Point)	318833.7	7813720.0	63.4	5.26
Pt 2 (Local Low)	324581.1	7813144.8	59.9	5.27
Pt 3 (Local Low)	329333.4	7814881.3	53.9	5.3
Pt 4 (Inflow of Tributary)	332510.7	7817069.0	8.1	5.8
Pt 5 (Local Low)	319067.6	7811054.8	52.2	5.31
Stockyard Mangrove Spring	331067.0	7814450.0	0	*
Fern Spring	331614.0	7813532.0	0	*
Saunders Spring	325974.0	7811660.0	0	*
*Value estimated using ICESat elevation data				

**Table 5** Inundation frequency calculated for WOfS sample locations in Figure 49.

Other information gained from this work is derived from the spatial information in the section of Mandora Lake/Walyarta where the frequency of inundation is greater than 25%. This zone, which extends along the southern margin of the lake, coincides with the interpreted shallow Pleistocene Palaeo-drainage channel, (Figure 54) and high concentrations of opaque minerals in ASTER data (Figure 43). The Palaeo-drainage channel was mapped by the spatial location of high frequency (shallow ~50 to 100 meter depths) curvilinear features (e.g. magnetic strandlines) in airborne magnetic data, which may indicate the opaque mineral in the ASTER data may have a similar origin and therefore be maghemite. The magnetite and/or maghemite deposited and concentrated through combined gravitational and fluvial-lacustrine processes. However, the opaque mineral may also be manganese oxide, precipitation as a result of biogeochemical processes in areas that are more frequently inundated due to surface water ponding, as well as groundwater discharge. The inundation zone where sample location points 1 and 5 are located may also represent an area receiving groundwater discharge from the Wallal Sandstone aquifer, due to the Jarlemai Siltstone and Callawa Formation aquitards being thin or absent (Section 6.1.3).

The variation in relief indicates that flow could occur in channels and connect depressions, as demonstrated by the modelling of the ephemeral drainage channels in Figure 5. The presence of concentrated magnetic minerals at the surface and at shallow depths within the depressions (ephemeral wetlands and lakes) indicates that fluvial systems operating in previous pluvial periods (e.g. Neogene) were more effective, which means for example that they had higher energy and/or were longer lived.

The connectivity of surface water flows appears to be infrequent under the current climate, or at least since the 1980's when remote sensing imagery was available and at a resolution to assess the presence of surface water. Although infrequent, an episodic event may benefit the biodiversity value of mound springs by facilitating the connection of surface flows and resulting in the distribution of species between mound spring pools and moats. If these translocated species can adapt and survive to their new environments this could increase species richness, as observed by Quinlan et. al. (2016). This is discussed in more detail in Section 6.3.



HYDROLOGICAL CONCEPTUALISATION OF THE WALYARTA MOUND SPRINGS

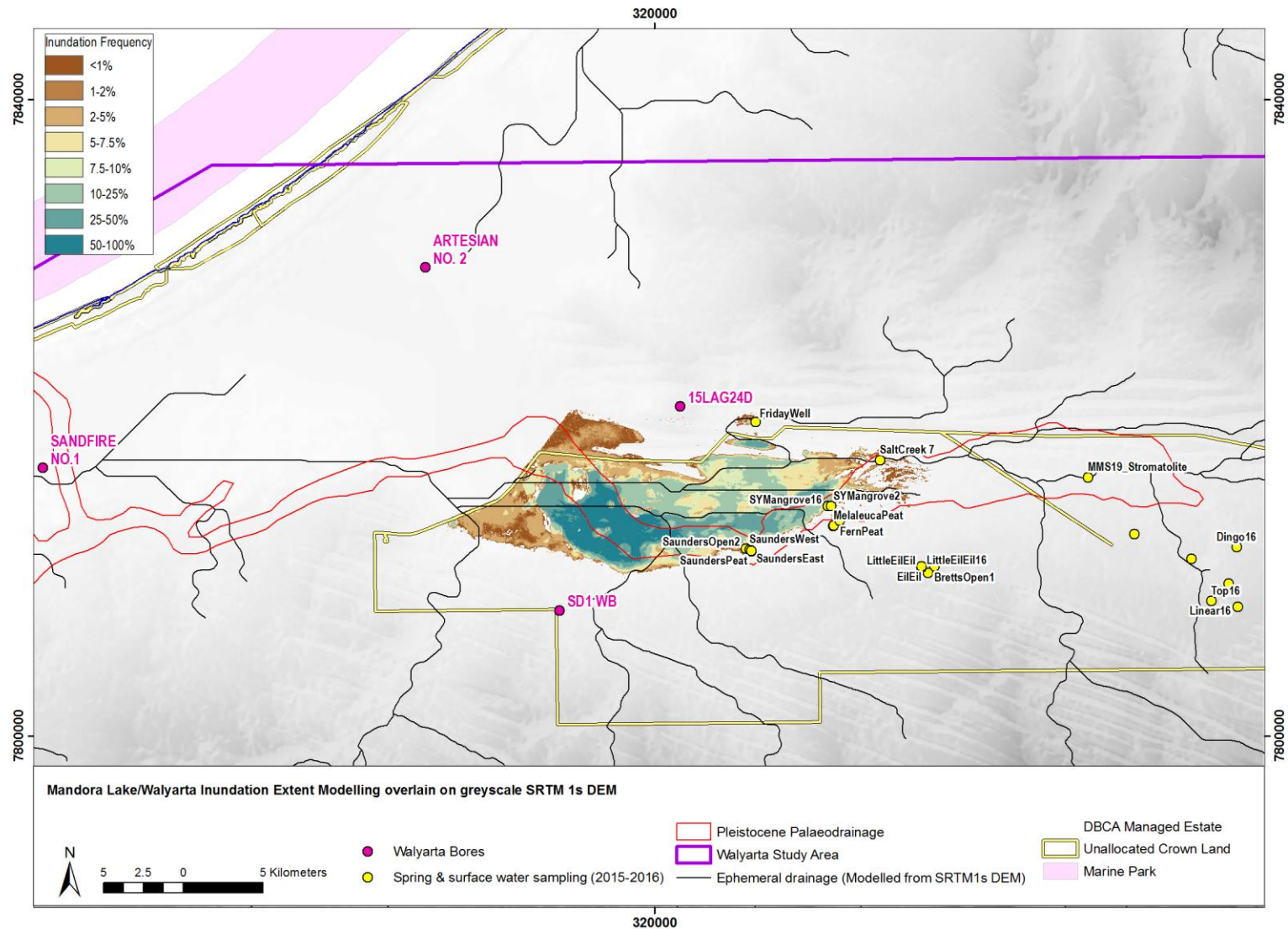


Figure 54 Mandora surface water extent modelling with modelled ephemeral drainage derived from SRTM 1s DEM

### 6.3 Ecohydrology

Developing an understanding of the water requirements of unique flora and faunal communities identified within the springs and the Salt Creek perennial valley-floor surface water flow system is complicated by the campaign style of data collection. Two major biological surveys have been undertaken in the last fifteen years, the survey described by CALM (1999) and Storey et. al. (2011) followed by the 2015 investigation reported to date in English et. al. (2016), Quinlan et. al. (2016) and Markey (2017). All biological investigations have included the collection of water quality data to characterise the variation in habitat physico-chemical conditions.

In this section a conceptual model is developed for the springs to identify the main aquifers sustaining groundwater flow to the springs. The resilience of the springs to changes in the groundwater flow regime is then assessed.

#### 6.3.1 Mound spring riparian vegetation water use and tolerances

In the absence of site specific studies, work undertaken on riparian vegetation in the Pilbara region by Loomes (2010) was identified as an appropriate surrogate for tree species identified in mound springs (pers comm Val English).

Vegetation communities are discussed in Section 5.3, where the main riparian species are identified. Within the mound spring communities, similar to Loomes (2010), the main species recognised as groundwater dependent are riparian trees and macrophytes. Groundwater dependent species of interest are;

1. *Riparian trees; Sesbania formosa (Dragon trees) and Melaleuca leucadendra,*
2. *Macrophytes; Typha domingensis and Sedges; Schoenoplectus spp., Fimbristylis spp., and Sporobolus virginicus, and Acrostichum speciosu (Mangrove Fern).*

For riparian trees, Loomes (2010) reports on *Melaleuca argentea* (similar to *M. leucadendra*; Val English pers comm) and *Sesbania formosa*. Statistics for four Pilbara study sites yield a mean maximum (greatest) depth to water for *M. argentea* and *Sesbania formosa* respectively of 4.88 metres below ground level (mbgl) and 3.44mbgl, under the current climate, increasing to 3.86mbgl and 3.06mbgl over the past 20 years. Absolute maximum groundwater levels decrease to around 8mbgl and 5mbgl for *Melaleuca argentea* and *Sesbania formosa* indicating in tropical climates these species root below 5 and 4 mbgl, with a maximum rooting depth of 9 and 5mbgl. Tolerances to changes in water quality are unknown but as they tend to be located in landscape positions that are regularly flooded, it is likely they have a low tolerance to higher salinity water.

Macrophytes include typha, sedges and ferns. Loomes (2010) reports *Typha domingensis* and sedge species *Cyperus vaginatus* (similar to sedge species within the mound springs). Statistics reported for these species show mean maximum groundwater levels beneath *Typha domingensis* and *Cyperus vaginatus* are around 2.5mbgl and 4mbgl respectively. Respective absolute maximum groundwater levels decrease to around 5 and 6mbgl. Rooting depths for these species would appear to be optimal at around 3-4mbgl, with the possibility that they extend to around 6mbgl.

Information on *Acrostichum speciosu* (Mangrove Fern) is unavailable from existing studies and it is thought the rooting depths are shallower than both typha and sedge species extending to around 2mbgl (Val English pers comm). Mangrove fern is a recommended species to plant in waterlogged soils and although is known to be tolerant of saline soils, it prefers a habitat where it is not frequently inundated by seawater (<https://florafaunaweb.nparks.gov.sg/special-pages/plant-detail.aspx?id=1535>)

In the absence of groundwater level data at the springs, and site specific information on vegetation water use, it is suggested that combined visual and remote sensing vegetation vigor datasets are advising that the spring vegetation communities have constant access to groundwater of suitable quality. Due to the substantial size of the riparian trees, in particular the *Melaleuca argentea*, it is likely the trees act as groundwater pumps. Accessing high volumes of groundwater, with minimal energy expended, with a high groundwater throughput required to extract required nutrients to support the production and consistent retention of biomass (Mike Lyons pers comm). Information provided by Loomes (2010) suggests groundwater levels may be maintained at approximately 2-4mbgl for macrophytes, with riparian trees potentially being able to tolerate lower groundwater levels at around 4-5mbgl.

From a salt balance perspective riparian tree rooting depths allow for the separation of water balance parameters transpiration and evaporation. Macrophyte predicted optimal rooting depths are shallower (2-4mbgl) making the separation of transpiration and evaporation difficult and producing higher soil, shallow regolith, salinities in the near surface. This is discussed further in the Section 6.3.2.

### 6.3.2 Spring water quality and salt balance

One of the major aims of this work undertaken in this report is to identify the aquifer, or aquifers, that are sustaining the springs (Section 1). In the absence of monitoring bores to sample and analyse the groundwater chemistry of aquifers underlying the springs, the initial step involved assessing the quality of near surface discharging groundwater. The hypothesis underpinning this work is that resilient springs, with vegetation cover in good condition, should be in balance with the discharging groundwater, that is spring discharge is keeping pace with transpiration, which in turn out paces evaporation.

AEM derived water quality for aquifers beneath the springs and perennial surface water sites have been constructed and compared with near surface (not greater than 0.2 metres below ground level) groundwater salinity measurements collected in the DBCA 2015-2016 field program. Results from this assessment are then compared with predicted depth to aquifer hydraulic head to determine the aquifer pressures required to transmit groundwater to the surface and as a consequence assess spring resilience.

Conductivity depth profiles were produced for major spring and surface water sites shown in Figure 54. Data for individual sites were graphed, with electrical conductivity (mS/m) plotted against depth below ground level (to a maximum of 400 metres below ground level) (Appendix 6). Average AEM electrical conductivities were converted to average total dissolved salt (TDS mg/L) measurements for the major aquifers as well as the Jarlemai Siltstone and Permian Formations. Results are tabulated in Table 6.



Spring/Surface water sampling sites	Field sampling (2015-2016)	Near Surface sediments (0-10m bgl)	Quaternary / Broome Aquifers	Jarlemai Siltstone	Wallal Sandstone Aquifer	Permian Formations	Low or High salinity groundwater/soil water zone 1	Low or High salinity groundwater/soil water zone 2
	(mg/L)	(mg/L)	(mg/L)	(mg/L)	(mg/L)	(mg/L)	(mg/L) (depth range mbgl)	(mg/L) (depth range mbgl)
Top	840	929	806		731	996		
Linear	580	930	851		726	945		
Dingo	2400	3334	1594	1108	858	863		
Little Eil Eil	714	960	855		735	939		
Eil Eil	1600	963	841		705	879		
Bretts Open	2920	1023	892		713	904		
Saunders Peat & East	800	3398	3398	1047	710	929		
Saunders Open	627	4521	4520	1035	692	921		
Fern	4300	1769	1325	1241	860			
Melaleuca	6000	1876	1323	1103	869			
Stockyard Mangrove	1700	4409	2537	1122	798			
Salt Creek	34400	2756	2226	1755	956	904	2400 (50-60mbgl)	
Stromabilite pool	31900	5647	3314	1142	859	1283		
Friday Well	1475	1579	4066	1394			1470 (10-20mbgl)	7600 (40-70mbgl)

TDS (mg/L) determined from relationship in Figure 22

**Table 6 Field groundwater TDS compared with AEM derived TDS measurements for aquifers underlying the springs and surface water sampling sites; major aquifer sustaining springs=blue; field samples indicating evaporation field sample=green; sequential aquifer mixing during discharge=orange, equilibration with surface sediments=yellow, and throughflow-discharge=pink.**

Soils and shallow regolith near the spring and surface water sites are characterised by a thin (~0.5 to <3 metres) veneer of marly clays and surface precipitates (e.g. gypsum and halite) that are controlled by local processes occurring in the Walyarta Mandora Palaeovalley (Section 5.4). This means that if a deeper, fault controlled spring discharge vent is sampled then the water is unlikely to have geochemically equilibrated (mixed) with the near surface sediments and possibly deeper aquifers (e.g. sample is likely to have a lower salinity and different hydrochemistry).

Sampling was undertaken at the end of the dry season (September 2015 and November 2016) to ensure there was limited mixing with recently recharged rainfall from the previous wet season. Field and AEM electrical conductivity measurements were converted to TDS (mg/L) and field results compared semi-quantitatively to AEM data to see if trends could be identified within the different suites of springs sampled. Discharge spring water and aquifer fingerprinting/connection were determined where salinities were within an arbitrary value of 20% of the field readings.

This approach allowed for the identification of four spring suites (Table 6);

- Wallal Sandstone aquifer discharge (formation is <50 metres from ground surface, flow rates are conducive & sample location successful),
- Mixing during discharge (Wallal Sandstone Quaternary/Broome aquifer discharge, further hydrochemical evidence required),
- Evaporation fingerprint (non-optimal sample location, further hydrochemical evidence required) and
- Equilibration with near surface sediments (further hydrochemical evidence required).

Wallal aquifer discharge sites (e.g. Linear, Little Eil Eil and Saunders Springs; Table 6) were identified by discharging spring groundwater having significantly lower salinities compared with the surface sediments and underlying Quaternary and Broome aquifers. At these springs groundwater discharge is more aligned with water quality of the Wallal Sandstone aquifer; the top of this aquifer is interpreted to be at 50, 30 and 30 metres below ground level at these respective spring sites (Appendix 3 & 6).

Mixing during discharge describes Dingo and Stockyard Mangrove Springs, where the field sampling salinities are likely to have evolved through the mixing of groundwater from different underlying

aquifers during discharge. At these sites the Wallal Sandstone aquifer is interpreted to be deeper, located at around 130 metres below ground level (Appendix 3 & 6).

Spring groundwater discharge that cannot be assigned aquifers or processes due to field salinities being affected by evaporation (e.g. having a higher derived TDS than the near surface sediments and underlying aquifers) include Eil Eil, Bretts, Fern and Melaleuca Springs (Table 6). Evaporation appears to increase groundwater salinities within the discharge mounds at these springs. Brett's Spring was sampled at a depth of 5cm below ground level near an open water body and therefore salinities were likely to be influenced by interactions with evaporated surface water. For Fern and Melaleuca Springs, their peat substrate salinities were analysed at sample depths of 10-20cm below ground level (Table 4) with results aligning with AEM electrical conductivities at depths of 0-10 metres below ground level at Fern Spring and 20-30 metres below ground level for Melaleuca Spring. Field samples were sampled at a different site to the soil site and this disparity may mean that more sampling is required to determine a more representative sample of near surface soil and groundwater salinities.

Conversely groundwater sampled discharging from Friday Well also has a lower salinity than the average water quality of the combined Quaternary and Broome aquifers. However, in this case the discharge is likely to represent groundwater quality at 0-10 and/or 10-20 metres below ground level. The interpreted local north-east to south-west Broome Sandstone aquifer gradients promoting throughflow, localised discharge and limited mixing with saline water at 40 metres below ground level (Appendix 6).

Developing further lines of evidence to fingerprint aquifers is discussed further in Section 7. Potential sources of saline groundwater that can sustain perennial flow in Salt Creek and Stromatolite pool is also reviewed.

### 6.3.3 Spring resilience indicators

Results from Section 6.3.2 indicate the Wallal Sandstone aquifer is important in sustaining spring flows and fingerprinting the Wallal aquifer using surface sampling was possible where the depth to the top of the Wallal Sandstone was interpreted to be between 50 to 30 metres below ground level. Mixing at the surface was observed to be more likely, with increasing depth to the top of the Wallal Sandstone.

Resilience indicators can be developed from combining these results with Wallal Sandstone aquifer hydraulic head predictions in Section 6.1 (Table 7).

Spring sampling sites	Surface elevation (mAHD) from SRTM 1s DEM	*Interpreted depth to top Wallal (mbgl)	*Interpreted depth to top Wallal (mAHD)	**Predicted metres hydrostatic head Wallal aquifer (based on consistent 50mAHD Wallal hydraulic head surface)	**Predicted metres hydrostatic head Wallal aquifer (based on consistent 75mAHD Wallal hydraulic head surface)
		Resilience#1	Resilience#2	Resilience#3	Resilience#4
Top	48	60	-12	<b>2</b>	27
Linear	52	50	-2	<b>-2</b>	23
Dingo	37	50	-2	<b>13</b>	38
Little Eil Eil	35	30	18	<b>15</b>	40
Eil Eil	40	30	18	<b>10</b>	35
Bretts Open	35	30	18	<b>15</b>	40
Saunders Peat & East	11	30	18	39	64
Saunders Open	11	30	18	39	64
Fern	14	<b>150</b>	<b>-102</b>	36	61
Melaleuca	15	<b>150</b>	<b>-102</b>	35	60
Stockyard Mangrove	10	<b>130</b>	<b>-82</b>	40	65

\*From Appendix 6 \*\*From Figure 52

Table 7 Spring resilience indicators as a function of Wallal Sandstone aquifer hydraulics, lower potential resilience highlighted in red.

Increased depth to the top of the Wallal Sandstone aquifer could be considered a resilience indicator, with spring resilience decreasing with greater depth to the top of the Wallal aquifer (e.g. greater pressure required to maintain the high hydraulic head elevations for Fern, Melaleuca and Stockyard Mangrove Springs, Resilience #1 & #2 Table 7). The spring land surface elevation is also an important factor given the Wallal aquifer depth to hydraulic head elevation is predicted to occur at between 50 to 75 mAHD (Figure 52). Topographic elevations for springs in the upper landscape exceed or are close to 50mAHD, which means if the Wallal aquifer hydraulic head elevation is the predicted minimum, springs such as Top, Linear, Dingo, Little Eil Eil, Eil Eil and Bretts would be affected by a change in hydraulic head (Resilience indicator #3 Table 7).

If the Wallal aquifer hydraulic head elevation is at the predicted maximum (75mAHD) the same group of springs would be considered less resilient but the hydrostatic head buffer increases (Resilience indicator #3 & #4 Table 7).

This conceptualisation is expanded on in Section 8 in the development of the numerical fault block model to test the Wallal Sandstone aquifer pressures and fault conduit groundwater flow rates required to sustain the springs.

## 7 Hydrochemistry and environmental tracers

### 7.1 Previous investigations

In the 1970's Leech (1979) sampled and analysed major ions in groundwater from twenty seven Wallal Sandstone aquifer bores, eight wells intersecting the Broome Sandstone aquifer, one bore constructed in the Bossut Formation and three WCB mound springs. This work was undertaken to assess the potential uses for the groundwater resources and to verify groundwater processes (e.g. groundwater recharge, gradients and aquifer mixing).



Results from this study identified both the Broome and Wallal aquifers contained potable groundwater suitable for domestic consumption but the nitrate and sodium levels in the Broome aquifer made it less prospective. Elevated salinities in the Wallal aquifer occur in the north-western part of the WCB, where they are recharged by poorer quality water. The hydrogeochemistry of the Wallal Sandstone aquifer was found to be predominantly sodium-chloride in type, with increased bicarbonate in bores sampled in the eastern recharge areas, where rainfall recharging groundwater reacts with unsaturated zone  $\text{CO}_2(\text{g})$  to produce  $\text{HCO}_3^-$ , which then drives cation exchange reactions with aquifer minerals. The unconfined Broome Sandstone aquifer chemistry is mainly sodium-bicarbonate-chloride.

Water sampled from the three WCB springs was found to be NaCl type water and therefore reported to be aligned geochemically to the Wallal Sandstone aquifer, rather than the Broome Sandstone aquifer. The absence of surface carbonate precipitates, travertine or tufa, was noted and this indicates changes in geochemical gradients may be subtle and/or there are geochemical inhibitors preventing their precipitation and/or the discharging groundwater is low in suitable cations and  $\text{CO}_2(\text{g})$ . Recommendations from Leech (1979) included undertaking radiometric dating of groundwater to assess the sources and processes controlling aquifer salinity levels at the coast.

Following Leech (1979) a number of finer scale hydrogeochemical studies were carried out to investigate groundwater abstraction from the Wallal Sandstone aquifer for town water supplies and mining and agricultural purposes. The next broad scale investigation took place in the 2008 and 2012 when the Australian Nuclear Science and Technology Organisation (ANSTO) sampled and analysed groundwater from twenty five recently installed WCB bores as well as some bores installed in the Leech (1979) investigation (Meredith et. al. 2009, 2014 & 2018). The main objective of this work was to develop an isotopic and hydrogeochemical approach to improve the understanding of groundwater processes. This study measured major and minor ions, trace elements, Rare Earth Elements (REE) and environmental isotopes ( $^{14}\text{C}_{\text{DIC}}$ ,  $^3\text{H}$ ,  $\delta^2\text{H}$ ,  $\delta^{18}\text{O}$ ,  $^{13}\text{C}_{\text{DIC}}$ ,  $^{13}\text{C}_{\text{DOC}}$ ,  $^{87}\text{Sr}/^{86}\text{Sr}$ ,  $^{36}\text{Cl}/\text{Cl}$ ,  $\delta^{34}\text{S}_{\text{SO}_4}$ ,  $\delta^{18}\text{O}_{\text{SO}_4}$ ). Of the twenty eight bores sampled, four sampled the Broome Sandstone aquifer and twenty four sampled the Wallal aquifer.

Results reported focus on the Wallal aquifer and resolve three main groups within bores drilled within approximately 20km from the coastline. These groups show different recharge and flow regimes, resulting in different chemistry. REE increase in concentration along flow paths, with radiogenic strontium ratios of  $^{87}\text{Sr}/^{86}\text{Sr}$  signifying the dominance of silicate weathering. Groundwater in the Broome aquifer and near recharge areas is less radiogenic. Groundwater in the Wallal aquifer, particularly at greater depths, or at the end of flow paths near the coast, is more radiogenic providing information on the evolution of groundwater along flow paths and aquifer mixing where vertical processes dominate.

Recharge assessments using stable water isotopes  $\delta^2\text{H}$ ,  $\delta^{18}\text{O}$  showed they were depleted, demonstrating groundwater recharge occurs through intense episodic events (cyclones) where recharge is relatively rapid. These results were corroborated with corrected  $^{14}\text{C}_{\text{DIC}}$  data that indicate the beginning of the flow path groundwater to be sub-modern (>60 to ~500yrs), increasing in age (around 5,000yrs) along north trending flow paths. This is in agreement with results from saturated flow modelling (Aquaterra 2010), although Wallal aquifer gradients in this model trend east-north east rather than to the north. A statistical analysis of carbon isotopes in groundwater predicted that

aquifer systems ranged from open to closed, the contribution of soil carbon dioxide was small due to rapid recharge and was derived from a mix of C3 and C4 vegetation types. Dissolved inorganic carbon is believed to be added through the oxidation of organic material in the aquifer, carbonate dissolution and indirectly via silicate weathering reactions.

Sampling and analysing water from the Mandora Marsh/Walyarta mound springs and Salt Creek flows occurred in 1999 and is reported in Storey et. al. (2011). The major aim of the hydrogeochemical component of that study was to characterise the habitat of the unique flora and fauna. This survey took place when Walyarta and surrounds were inundated with surface water and following five years of above average rainfall (1994 to 1999) due to the land fall of annual cyclones (Storey et. al. 2011 & Quinlan et. al. 2015). Major ions were analysed at twelve sites and results showed the water type at most locations is NaCl in type, apart from three sites with high HCO<sub>3</sub> and Ca, and these sites comprise the carbonate base Coolabah claypan and upland springs Linear and Top. The change in the ionic composition to the HCO<sub>3</sub> enriched water was attributed to the influence of “limestone aquifers”, which may represent increased input from the Broome-surficial aquifer.

In 2015 DBCA designed an expanded hydrogeochemical sampling program for the Walyarta mound springs and Salt Creek to determine the aquifer(s) sustaining the springs and assess their resilience. The work included analysing for major and minor ions, trace elements, Rare Earth Elements (REE) and environmental isotopes (<sup>14</sup>C<sub>DIC</sub>, δ<sup>2</sup>H, δ<sup>18</sup>O, <sup>13</sup>C<sub>DOC</sub>, <sup>87</sup>Sr/<sup>86</sup>Sr). Fifteen sites were sampled in September 2015 and a subset of data collected are presented and reported in Harrington and Harrington (2017). Discussion from this report advises that major ion chemistry indicates the Wallal Sandstone aquifer was likely to be a source of water for the springs. However this was not definitive due to supporting environmental isotope results (<sup>14</sup>C<sub>DIC</sub>, δ<sup>2</sup>H, δ<sup>18</sup>O, <sup>13</sup>C<sub>DOC</sub>) being overprinted by near surface geochemical processes/reactions (e.g. H/O isotopic enrichment/evaporation, precipitation of calcite and/or interactions with soil and atmospheric CO<sub>2</sub>(g)).

Sampling in 2015 took place following a wet season characterised by above average rainfall (see Section 5.2). Similar to results from Storey et. al. (2011) this encouraged the dissolution and mobilisation of carbonates, which increased the bicarbonate component of water sampled. To test this theory and collect a dataset more representative of spring discharge DBCA designed a repeat sampling program in November 2016, which followed a “dry” wet season. The 2016 program was undertaken by helicopter, which allowed for five of the 2015 sites to be resampled and the following additional work to be added;

- Sampling water and vegetation at sites that were inaccessible in 2015 (Top Spring, Linear Spring and Sporobolus Spring),
- Assessing potential spring discharge sites identified in ASTER VNIR-SWIR green vegetation index and Landsat persistent vegetation (see Figure 38),
- Opportunistic sampling water and vegetation where springs were observed from the helicopter and determined to be discharging groundwater when investigated on the ground,
- Installing data loggers at Eil Eil spring to measure barometric pressures, spring moat water levels and shallow groundwater levels at the spring mound and,
- Search for bore SD1 for DWER.

Details on the installation of data loggers and collection and field physico-chemical results of the eight spring sampled are reported in Harrington (2016).

Reports are currently in preparation for hydrogeochemical investigations that have been carried out by DPIRD in the La Grange area and DWER in the WCB. While reports are being prepared hydrogeochemical data collected by the three agencies (DBCA, DWER and DPIRD) has been shared to ensure individual agency interpretations are made with the knowledge and opportunity to use the full dataset collected across the WCB and southern La Grange areas. The location of hydrogeochemical data examined in this report is shown in Figure 62.

## 7.2 Hydrogeochemical interpretation - approach

The main challenge is to identify the key hydrogeochemical indicators that can be used to map the hydrogeochemical evolution of groundwater in Broome and Wallal Sandstone aquifers, from groundwater recharge, through to discharge areas. In this study the geological model developed in Sections 4, 5 and 6 for Walyarta is used to understand formation thicknesses, as well as areas with potential for increased aquifer connectivity and recharge.

Information gained from previous hydrogeochemical studies in Section 7.1 indicates that the main aquifers, the Broome and Wallal Sandstone aquifers have a similar mineralogical composition, hydrogeochemistry and flow path/aquifer gradients. Aquifer gradients following topography in the WCB, from recharge to discharge areas, with flow paths being shorter in areas to the west (e.g. Meredith et. al. 2018).

The Broome aquifer is unconfined, characterised by younger groundwater than the underlying Wallal aquifer, and therefore based on observations of Meredith et. al. (2014 and 2018) typified by lower radiocarbon ages. Upgradient of discharge areas the Broome aquifer chemistry may reflect interactions with surficial carbonate / evaporite sediments and shallow hydrological processes (e.g. contemporary evapotranspiration and rainfall resulting in an evaporation fingerprint in  $\delta^2\text{H}$ ,  $\delta^{18}\text{O}$  isotopic data).

Examining aquifer hydraulics was beyond the scope of work in this study. Instead spatial patterns in the hydrogeochemistry were interpreted to increase understanding in the vertical and lateral movement of groundwater. The approach adopted here involves expanding the hydrogeochemistry study to assess recharge water quality, the direction of groundwater flow, geological constraints that may disrupt flow and aquifer stratification (limited vertical mixing). This is undertaken at both coarse and fine-scales to understand the evolution of groundwater and the mound spring chemistry.

### 7.2.1 Groundwater recharge - chemistry and age

Previous work advises that the dominant ionic constituents in groundwater, spring and surface water are chloride, bicarbonate, sodium and calcium. Sodium and chloride are generally sourced from rainfall within the main aquifer systems, the siliceous Broome and Wallal sandstone aquifers.

Harrington and Harrington (2016) describe departure from the sodium chloride rainfall water type in the Broome aquifer in the La Grange area (within and north of the Mandora Palaeovalley) to occur due to minor water-rock reactions due to the weathering of pedogenic carbonates in the Pindan soil unit. As the Broome aquifer contains shallow marine units (Towner 1982a) it is likely that there is  $^{14}\text{C}$  dilution along flow paths due to the dissolution of carbonates, or near the coast where elevated



bicarbonate exists due to the continued flushing of saline water sourced from the Holocene intrusion (e.g. as evidenced in Jordan Rift Valley and reported by Mercado 1985). In the Wallal aquifer Meredith et. al. 2018 report that bicarbonate and calcium are sourced from partial carbonate dissolution processes and weathering of primary and secondary silicate minerals.

Groundwater age determination by means of  $^{14}\text{C}$  requires a conceptualisation that covers input concentrations from the soil/vadose zone (e.g. carbonate minerals and  $\text{CO}_2$  gas) and change along flow paths that occur due to decay and dilution from both inorganic sources (e.g. carbonate dissolution and silicate mineral weathering) and organic carbon sources (e.g. sulfate reduction and methanogenesis). In the WCB Wallal aquifer age determinations using  $^{14}\text{C}$  conclude that dilution takes place, but keeps pace with decay along flow paths (Meredith et. al. 2018). Processes in the Broome aquifer flow paths are likely to be more complex but due to limited sampling they are not well understood.

Information on geological formations that contain carbonate material is included in 1:250 000 scale geological mapping (Towner et. al. 1982a, Hickman and Gibson 1983, Williams 2003). A summary of this information is presented in Table 8. At a finer and more spatially intensive scale, ASTER remote sensing data was shown to effectively map surficial carbonate and evaporite sediments in Walyarta (see Section 5.4.1, Figures 39 to 43). In Walyarta formations mapped include localised outcrop and sub-crop of the carbonate-rich Parada Formation. This unit was deposited under shallow-marine conditions and is mapped in recharge areas in the northeast quadrant of the study area. Pedogenic carbonates are interpreted to the south east and may be broadly distributed, reflecting palaeoclimatic conditions and forming a sizeable sink for carbon (e.g. as discussed in other low rainfall areas in the U.S.A. in Retallack 2005, Breecker et al 2009). Downgradient, evaporite deposits within discrete ephemeral lakes, wetlands and drainage lines of the Mandora Palaeovalley are resolved, while towards the coast in discharge tidal flat discharge areas are clearly mapped within different ASTER datasets. Tidal flat areas near the Mandora Palaeovalley representing areas that are continuing to flush saline water that infiltrated sediments and aquifers in the Holocene marine transgression.

In this semi-arid environment, gravitational, aeolian and fluvial processes mobilise and redistribute pedogenic and evaporite carbonate-rich materials, with lateral movement encouraging surface water supersaturated in evaporites to concentrate in topographically low lying areas. The latter is supported by observations from Towner (1982a) who noted that most of the mapped Cenozoic, mainly Quaternary, geological units grade into one another, to form a broader, but shallow evaporite body.

Information gained from the interpretation of the Walyarta ASTER datasets (presented in Figure 55) underpins the development of a potential carbonate/evaporite regolith unit map (Figure 55). This map can be used to interpret groundwater recharge chemistry in both the Wallal and Broome aquifers. Although it is important to note that Meredith et. al. (2018) report that cyclonic events provide the greatest sources of groundwater recharge to the Wallal aquifer, and under these conditions recharge is thought to be relatively rapid, resulting in limited soil-water-gas interactions and subsequent dissolution and mobilisation of pedogenic or evaporite carbon sources.

Interactions along flow paths, where groundwater recharge moves via throughflow may react with, and mobilise, in-situ carbon sources, which for the Wallal Sandstone and underlying Triassic and Permian formations are localised beds of deltaic carbonaceous sediments (purple text in Table 8).

Formation	Age & thickness (m) (from Towner 1982a)	Mineralogy
<b>Qa</b> Alluvium	<i>Quaternary (3)</i>	sand, silt, clay, minor gravel
<b>Ql</b> Salt lakes and claypans	<i>Quaternary (5)</i>	clay, silt, sand and minor gypsum
<b>Qs</b> Mixed alluvial and aeolian	<i>Quaternary (5)</i>	sand, silt, minor gravel
<b>Qz</b> Sandplain aeolian dunes	<i>Quaternary (5±)</i>	fine to medium grained red quartz sand, minor silt
<b>Qcd</b> Coastal aeolian dunes	<i>Quaternary (5±)</i>	calcareous sand, partly oolitic
<b>Qci</b> Intertidal and mangrove swamps	<i>Quaternary (10±)</i>	silty clay, black organic clay and minor salt
<b>Qbp</b> Bossut Formation; shoreline beach-ridges	<i>Quaternary (10±)</i>	quartzose calcarenite and calcilutite
<b>Qcs</b> Supratidal mud flats	<i>Quaternary (10±)</i>	clay, silt, sand and minor salt
<b>Czk</b> Evaporites and pedogenic	<i>Quaternary (3)</i>	calcrete and minor chalcedony
<b>Czs-Czl</b> Ferricrete	<i>Quaternary (5)</i>	sand, silt, ferruginous pisoliths, minor gravel and clay
<b>Kp</b> Parda Formation	<i>Early Cretaceous (0-10)</i>	mudstone with minor fine sandstone lenses
<b>Kb</b> Broome Sandstone	<i>Early Cretaceous (0-50)</i>	fine to medium sandstone, with a well-sorted mudstone facies and minor conglomerate
<b>Jkc</b> Callawa Formation	<i>Late Jurassic-Early Cretaceous (3-50)</i>	very fine to coarse sandstone, conglomerate and minor siltstone
<b>Jkr</b> Jarlemai Siltstone	<i>Late Jurassic-Early Cretaceous (0-100)</i>	mudstone, with sandy sections, glauconite & minor pyrite
<b>Ja</b> Alexander Formation	<i>Late Jurassic (0-30+)</i>	sandstone, fine to medium interbedded mudstone
<b>Jl</b> Wallal Sandstone	<i>Early-Late Jurassic (0-500)</i>	sandstone, minor siltstone, conglomerate and traces of carbonaceous material, pyrite and heavy minerals
<b>Rb</b> Blina Shale	<i>Triassic (0-25)</i>	siltstone, shale (grey, micaceous & carbonaceous with thin sandstone lenses)
<b>Pi</b> Chirup Formation	<i>Late Permian (0-40)</i>	shale, grey to black sandy carbonaceous; interbedded sandstone, fine to conglomeratic
<b>Pg</b> Grant Group	<i>Early Permian (0-100)</i>	sandstone, fine to coarse mudstone, minor conglomerate
<b>Sc</b> Carribuddy Formation	<i>Late Ordovician-Early Devonian (0-100)</i>	dolomite, dolomitic siltstone, shale, halite, anhydrite, minor sandstone

Table 8 Formations and mineralogy mapped and discussed in Hickman and Gibson (1982), Towner (1982a), Williams (2003) with organic carbon sources highlighted in purple and inorganic carbon sources in blue (see Figures 8 & 9 for geological map and key).

The Walyarta observations lend themselves to being up-scaled to resolve similar formations for the broader WCB (Figure 56).

HYDROLOGICAL CONCEPTUALISATION OF THE WALYARTA MOUND SPRINGS

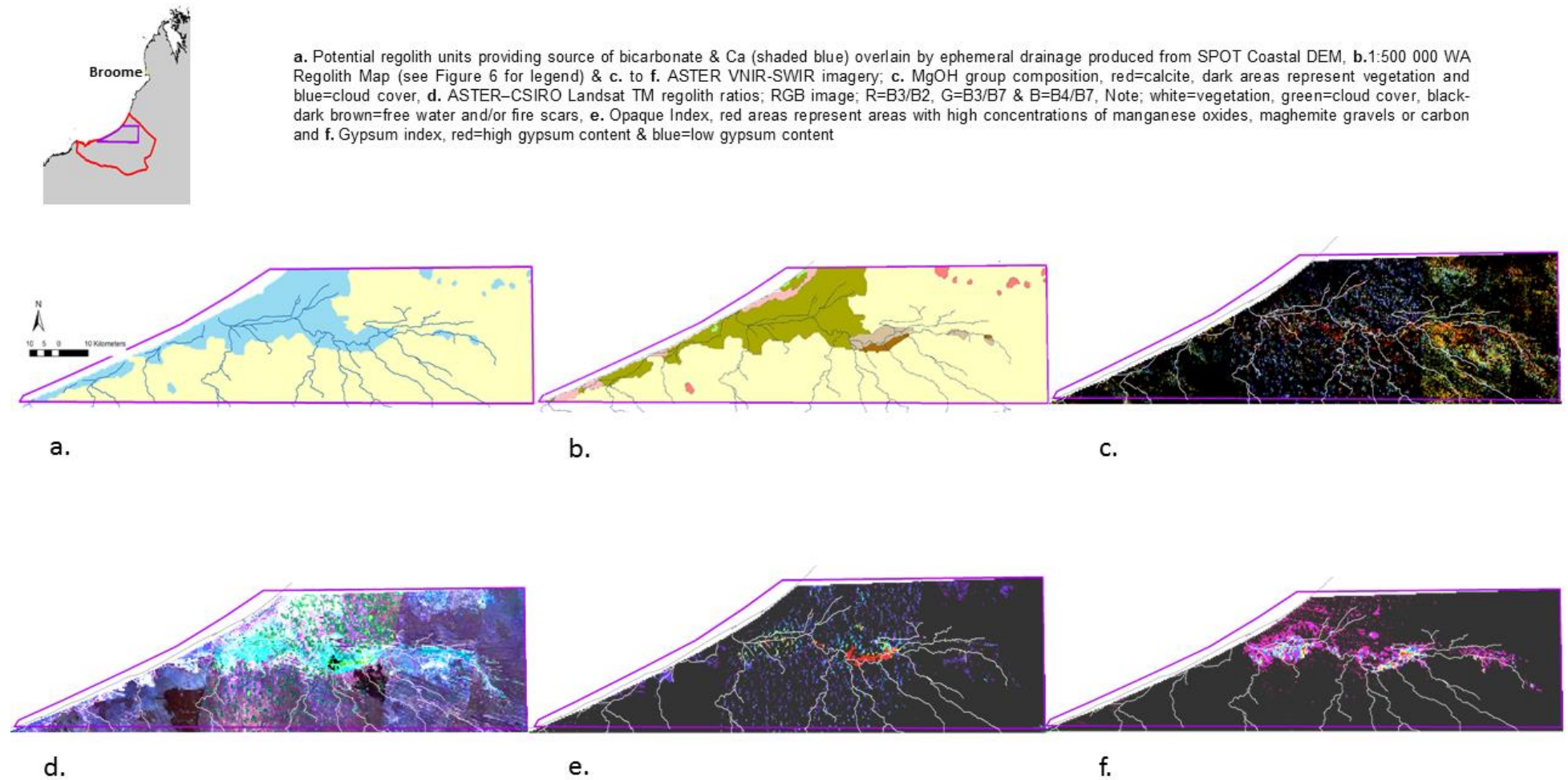


Figure 55. Map of potential carbonate/evaporite regolith units, b. 1:500 000 WA Regolith Map (see Figure 6 for key) and c. to f. remote sensing derived mineral maps (ASTER VNIR-SWIR imagery)



# HYDROLOGICAL CONCEPTUALISATION OF THE WALYARTA MOUND SPRINGS



a. Potential regolith units providing source of bicarbonate & Ca (shaded blue) overlain by ephemeral drainage produced from SPOT Coastal DEM, b. 1:500 000 WA Regolith Map (see Figure 6 for legend) & c. to f. ASTER VNIR-SWIR imagery; c. MgOH group composition, red=calcite, dark areas represent vegetation and blue=cloud cover, d. ASTER-CSIRO Landsat TM regolith ratios; RGB image; R=B3/B2, G=B3/B7 & B=B4/B7, Note; white=vegetation, green=cloud cover, black-dark brown=free water and/or fire scars, e. Opaque Index, red areas represent areas with high concentrations of manganese oxides, maghemite gravels or carbon and f. Gypsum index, red=high gypsum content & blue=low gypsum content

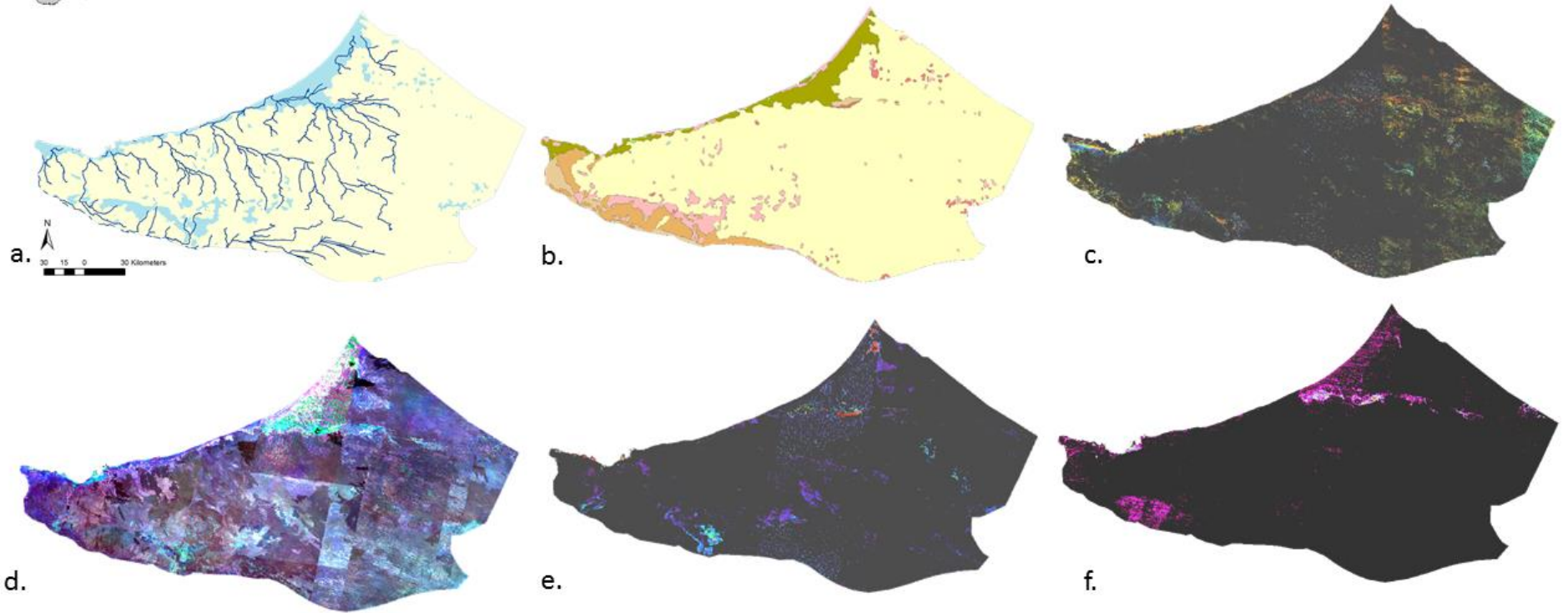


Figure 56 Map of potential carbonate/evaporite regolith units, b. 1:500 000 WA Regolith Map (see Figure 6 for key) and c. to f. remote sensing derived mineral maps (ASTER VNIR-SWIR imagery)

Figures 56c&d shows the MgOH group composition and CSIRO Landsat TM regolith ratio data indicate that carbonates are concentrated within sections of the Mandora palaeovalley floor, sections of the Oakover River (south western WCB boundary), narrow ephemeral channels and more broadly within Quaternary alluvium, lake and tidal flat deposits (Qa, Ql, Qcs and Qpb) as well as discrete outcrop of lateritised Mesozoic Parda (Kp, Czl) (Towner 1982a and Williams 2003) and Callawa Formation (Hickman and Gibson 1982). Elevated opaque mineral responses (Figure 56e) remain constrained to drainage features (e.g. lakes and drainage lines; coastal wetlands and Lake Mandora) in the northwest and are likely to represent manganese oxides and/or maghemite gravels deposited through fluvial and lacustrine processes.

Intermediate responses also occur within older geological formations on the margin of the WCB and marginal to the Oakover River. Higher values within the gypsum index are restricted to the Mandora palaeovalley and tend to border the southern palaeovalley and tidal flat margin (Figure 56f).

At a coarse scale ASTER data show that in addition to carbonate and evaporite deposits mapped in the Walyarta area, evaporite deposits are also concentrated on the south western WCB margin. The latter generally corresponding to mapped Mesozoic units that are located in upland recharge areas due to their resistance to weathering (categorised as exposed regolith units in the 1:500 000 WA Regolith Map) (Hickman and Gibson 1982 and Williams 2003). Here the Parda Formation has a similar response in the Walyarta area, which verifies the interpretation and production a coarse scale potential carbonate/evaporite regolith unit map (Figure 56a). In these areas they have potential to influence the quality and chemistry of groundwater recharge, while carbonates/evaporites downgradient will influence groundwater chemistry where groundwater levels permit vertical recharge.

### 7.2.2 Aquifer gradients

The interpretation of airborne electromagnetic (AEM) data in Section 6 demonstrated that both coarse and fine-scale geological structures constrain aquifer electrical conductivity (related to total dissolved salts, salinity) patterns in the Broome and Wallal aquifers. At a coarse scale these structures are also likely to have influenced the deposition and preservation of sediments. Consequently, they will also affect flow rates in aquifers through their influence on hydraulic properties, notably hydraulic conductivity and transmissivity.

The main challenges to using hydrogeochemistry and environmental tracers in isolation to aquifer water levels are the likelihood of non-unique hydrogeochemical responses. In particular, problems associated with misinterpreting pattern variation as a result of limited understanding of stratigraphy and facies changes, delayed flushing of post Holocene salt storages in clay rich and/or secondary cemented regolith materials, vertical groundwater mixing (e.g. deep and shallow faults / Palaeo-drainage channels) and recycling of carbon (Meredith et. al. 2014 & 2018).

In this study tectonic element boundaries (Figure 3) and geological faults are used as a framework to interpret spatial and temporal changes in aquifer hydrogeochemistry and determine if groundwater flow is compartmentalised (Figure 57). A good alignment exists between tectonic element boundaries and major north-west fault structures reported in Parra-García et. al. (2014). As the tectonic elements represent deeper crustal features they were modified slightly to align with structures modelled from magnetic and gravity data (Figure 57b).

HYDROLOGICAL CONCEPTUALISATION OF THE WALYARTA MOUND SPRINGS

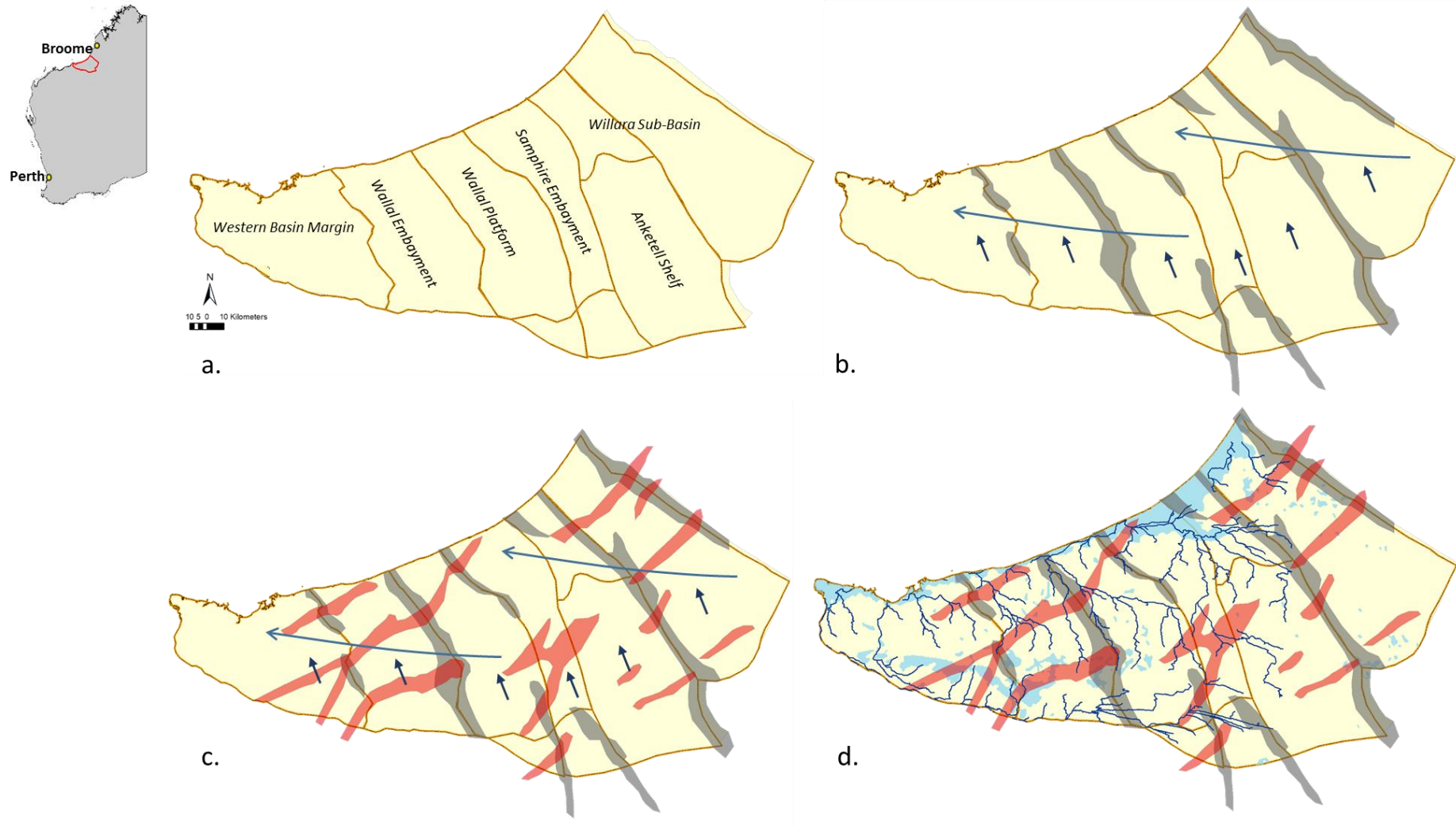


Figure 57 Coarse scale geological and hydrogeological controls on compartmentalisation of groundwater flow; increasing complexity from a. to d.; a. WCB tectonic elements (see Figure 3)b. WCB tectonic elements with major NW-SE faults from Parra-García et. al. (2014), c. WCB tectonic elements with major NW-SE and NE-SW faults from Parra-García et. al. (2014), d. WCB tectonic elements with major NW-SE faults from Parra-García et. al. (2014) and potential surficial carbonate / evaporite sources; Note that arrows in b. and c. represent regional and sub-regional groundwater gradients.

HYDROLOGICAL CONCEPTUALISATION OF THE WALYARTA MOUND SPRINGS

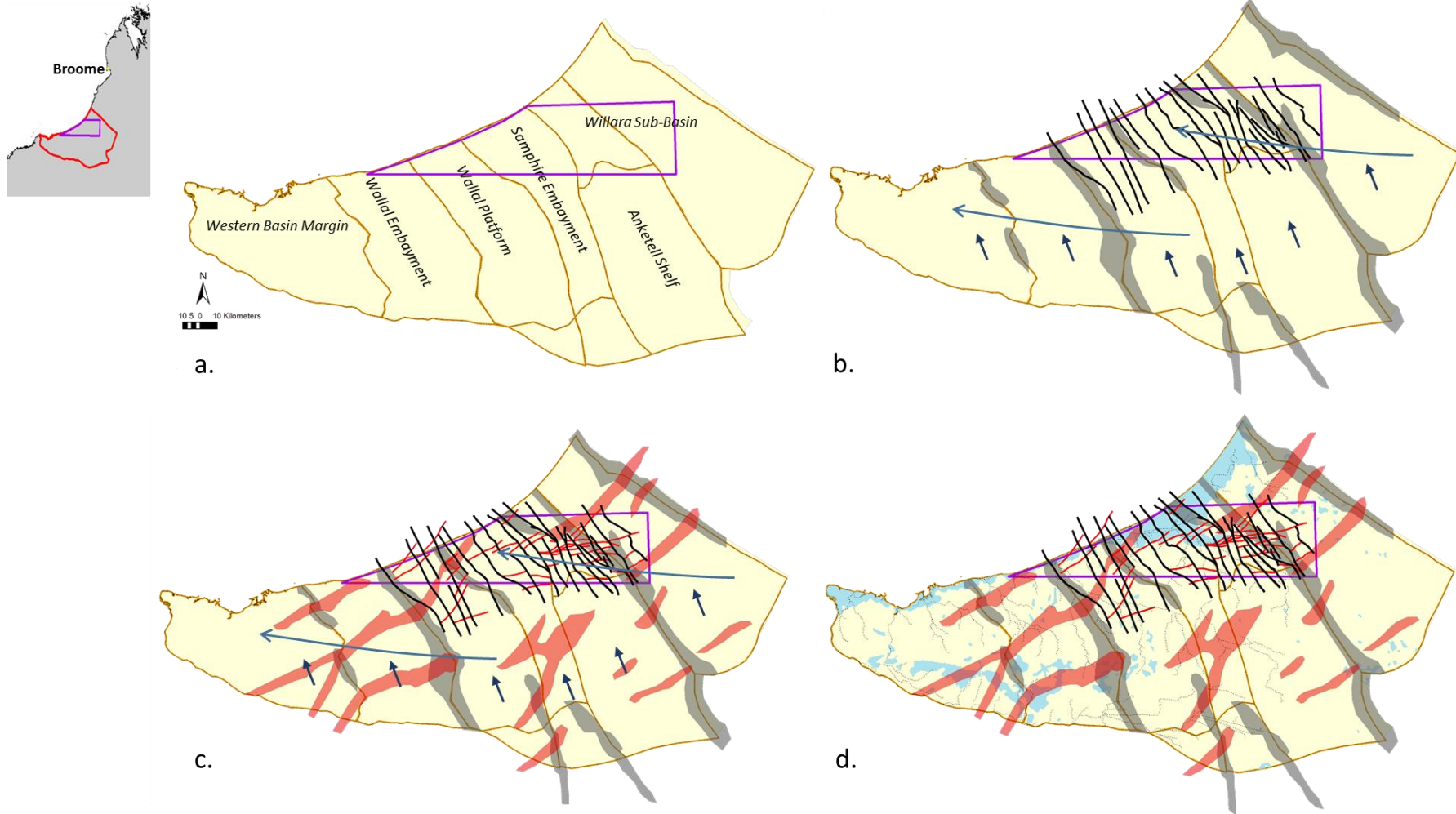


Figure 58 Fine-scale geological and hydrogeological controls on compartmentalisation of groundwater flow; increasing complexity from a. to d.; a. WCB tectonic elements (see Figure 3)b. WCB tectonic elements with major NW-SE faults from Parra-García et. al. (2014), c. WCB tectonic elements with major NW-SE and NE-SW faults from Parra-García et. al. (2014), d. WCB tectonic elements with major NW-SE faults from Parra-García et. al. (2014) and potential surficial carbonate / evaporite sources; Note that arrows in b. and c. represent regional and sub-regional groundwater gradients; Walyarta study area=purple boundary.



Arrows show the dominant regional and sub regional flow directions, with regional flow trending east north east and sub-regional flow north-west. Additional complexity may occur where north east structures reported in Parra-García et. al. (2014) interrupts groundwater flow paths (Figure 57c). Figure 57d shows the distribution of potential carbonate/evaporite regolith units that may modify groundwater chemistry in recharge or discharge areas.

To assess the potential flow path complexity at a finer scale the Walyarta fine-scale geological structure mapping is included in Figure 58. Overlaying the fine-scale fault structures demonstrates the repeatability of fine and coarse scale trends. The structural constraints on electrical conductivity and the tidal flat regolith unit, noted in Section 6, are visible within the fine-scale data at the coarse viewing scale in Figure 58.

Contemporary topography is likely to play a role for both the Wallal and Broome aquifers at a coarse and fine-scale. Therefore all bores are assigned to a tectonic element as well as a regolith landform unit that also defines their location along sub-regional flow paths (Appendix 7). The hydrogeochemistry is assessed against both frameworks in Section 7.3.

### 7.2.3 Wallal transmissivity and heterogeneity

Reports covering the numerical modelling of the WCB Mesozoic sediments discuss stratigraphic variation within (e.g. upper and lower Wallal), above (Alexander Formation) and below (various) the Wallal Sandstone aquifer (Aquaterra 2010, Hanna 2014 and PSM 2017). These reports use hydraulic data to debate the importance of the stratigraphic variation within the aquifer and how this may alter the water balance and sustainability of the aquifer. PSM (2017) recognise the Wallal Sandstone Aquifer is widely heterogeneous and anisotropic, but quote vertical stratigraphic connection under short term pump test conditions as a justification to model the formation as a single aquifer.

An assessment of Wallal Sandstone lithology logs, assignment of facies and evaluation of bore construction and facies screened and sampled was beyond the scope of this report. Instead, hydrogeochemistry and environmental tracers are employed to identify if different flow patterns exist where changes in the Wallal aquifer thickness and transmissivity are apparent. An internally consistent approach was adopted, where for the eighty two Wallal bores sampled, the centre point of the bore inlet/mid screen (MOS mbgl, see Appendix 7)) was used as an indicator of the average thickness of the Wallal Sandstone. The resultant population is skewed and applying a geometric interval resolves three classes; 55 to 106, 107 to 212 and 213 to 429 metres below ground level in Figure 59.

Results presented in Figure 59 indicate that within around twenty kilometres from the coastline the thickness of the Wallal Sandstone generally increases from the south west to the north east, from the western basin margin to the Willara sub-basin (Figures 57, 58 and 59). Tectonic elements resolve patterns in the thickness of the Wallal sandstone that correspond to neotectonic normal faulting resulting the production of half grabens within the coarse scale tectonic elements (e.g. Parra-García et. al. 2014). Fault displacement and Wallal Sandstone thickness both increase from the south east to the north-west. In the Walyarta study area the thickness of the Wallal Sandstone varies according to fine-scale structural controls (Section 4.5) and these are shown on Figure 59b.

HYDROLOGICAL CONCEPTUALISATION OF THE WALYARTA MOUND SPRINGS

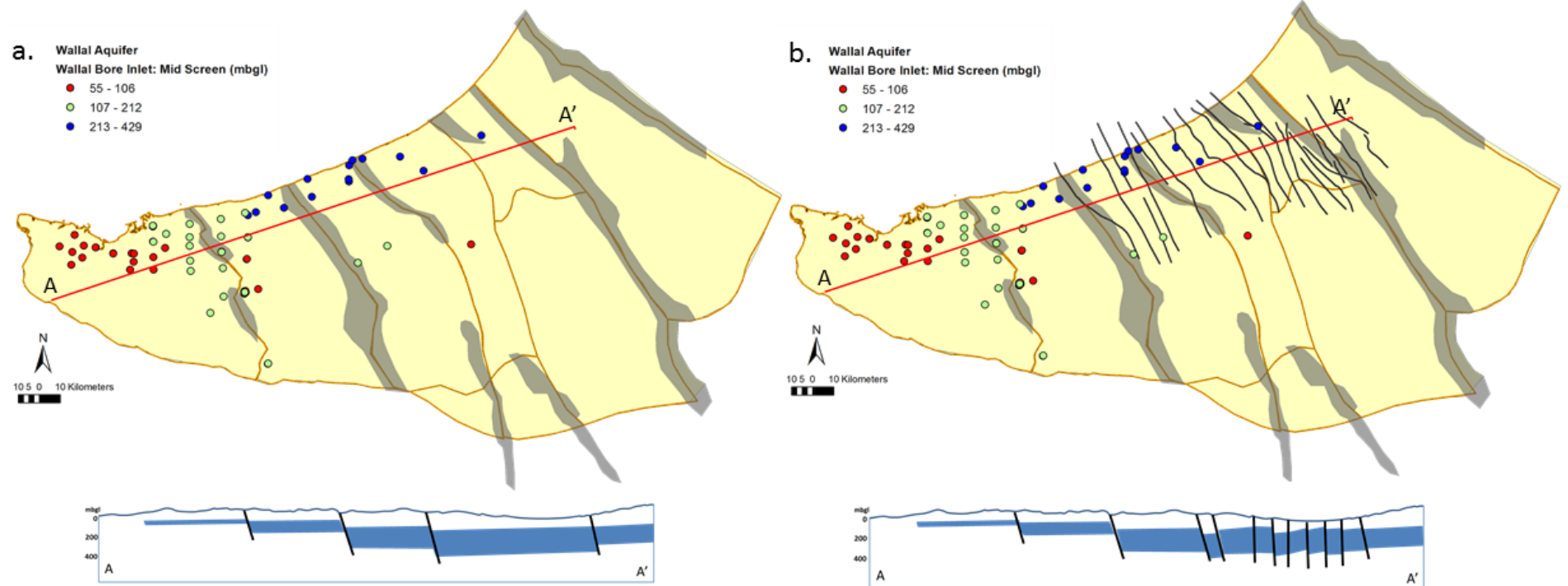


Figure 59 Simple block faulted Wallal Sandstone aquifer thickness map based on centre point (metres below ground level mbgl) of the bore inlet screen depth; cross section A-A' shows tectonic element controls on aquifer thickness; a. coarse scale structural/tectonic elements and b. coarse and fine-scale structural/tectonic elements.

The cross sections in Figure 59a&b depict the coastal area where the Wallal sandstone aquifer is saturated and variation in depth to hydraulic head suggests there is hydraulic connection (Appendix 5). Fine-scale structures and displacement information may produce a more realistic representation of connectivity and transmissivity, as influenced by fault offsets, particularly across the western basin margin and Wallal Embayment (Figures 58 and 59).

A number of shallow bores have been drilled through the Wallal aquifer further inland. These bores don't intersect the full thickness of the Wallal aquifer and this is probably due to budget constraints and reduced demand for Wallal groundwater inland from the coast.

### 7.3 Hydrogeochemical interpretation – results

#### 7.3.1 Major ion data sourcing, quality assurance and modelling

Groundwater major ion analyses form the largest and most consistent hydrogeochemical dataset collected in the WCB. To minimise error primary hydrogeochemical data were sourced from original investigation reports (e.g. Leech 1979, Storey et. al. 2011, Meredith et. al. 2009 & 2014) and entered into a spreadsheet database (Appendix 7). Additional data were sourced from DPIRD who provided hydrogeochemical data from thirty six bores that mainly sample Surficial-Broome Sandstone aquifers in the southern La Grange area. DWER provided sixteen samples from their March 2017 WCB sampling campaign and remaining data were sourced from quality assured DWER Water Information Network (WIN) data reported in Harrington and Harrington (2017). The combined hydrogeochemical database used in this study contains 184 samples and includes a small number of repeat measurements from bore and spring station sites (Figure 60; Appendix 7).

Field sampling and laboratory analysis methods for data examined are detailed in Leech (1979), Storey et. al. (2011), Meredith et. al. (2009 & 2014), Harrington and Harrington (2016) and Harrington (2017).

Following the input and compilation of hydrogeochemical data to a central spreadsheet database the stations were assigned to a tectonic element and landform (Section 7.2.2 and 7.2.3).

Major and minor ions were converted to the common measurement unit (mg/L) and where bicarbonate and carbonate data were missing they were modelled from alkalinity data using the WATEQ4F thermodynamic database within the PHREEQC programme (Parkhurst and Appelo 1999). The charge balance error percentage (CBE) was assessed for accuracy, with results showing that of the 184 samples, 40 (~21%) exceed the acceptable  $\pm 5\%$  range, with 14 (~7%) samples exceeding  $\pm 8 < 10\%$  range. These samples are highlighted in yellow in Appendix 7 and their data and modelling results are considered with caution in the interpretation.

Data were imported into the AquaChem™ 2014.2 software programme to undertake data reliability checking, determine water type/facies and produce Piper Trilinear Diagrams. Saturation indices (SI) were then modelled using the WATEQ4F thermodynamic database within PHREEQC, with mineralogical outputs including, but not limited to, calcite, chalcedony, dolomite, gypsum and quartz, as well as ionic concentrations of carbonate [ $\text{CO}_3^{2-}$ ] and bicarbonate [ $\text{HCO}_3^-$ ]. For each of the 184 samples, chemistry data, along with the station sample location, source information, water type and mineralogical saturation indices are tabled in Appendix 7.

HYDROLOGICAL CONCEPTUALISATION OF THE WALYARTA MOUND SPRINGS

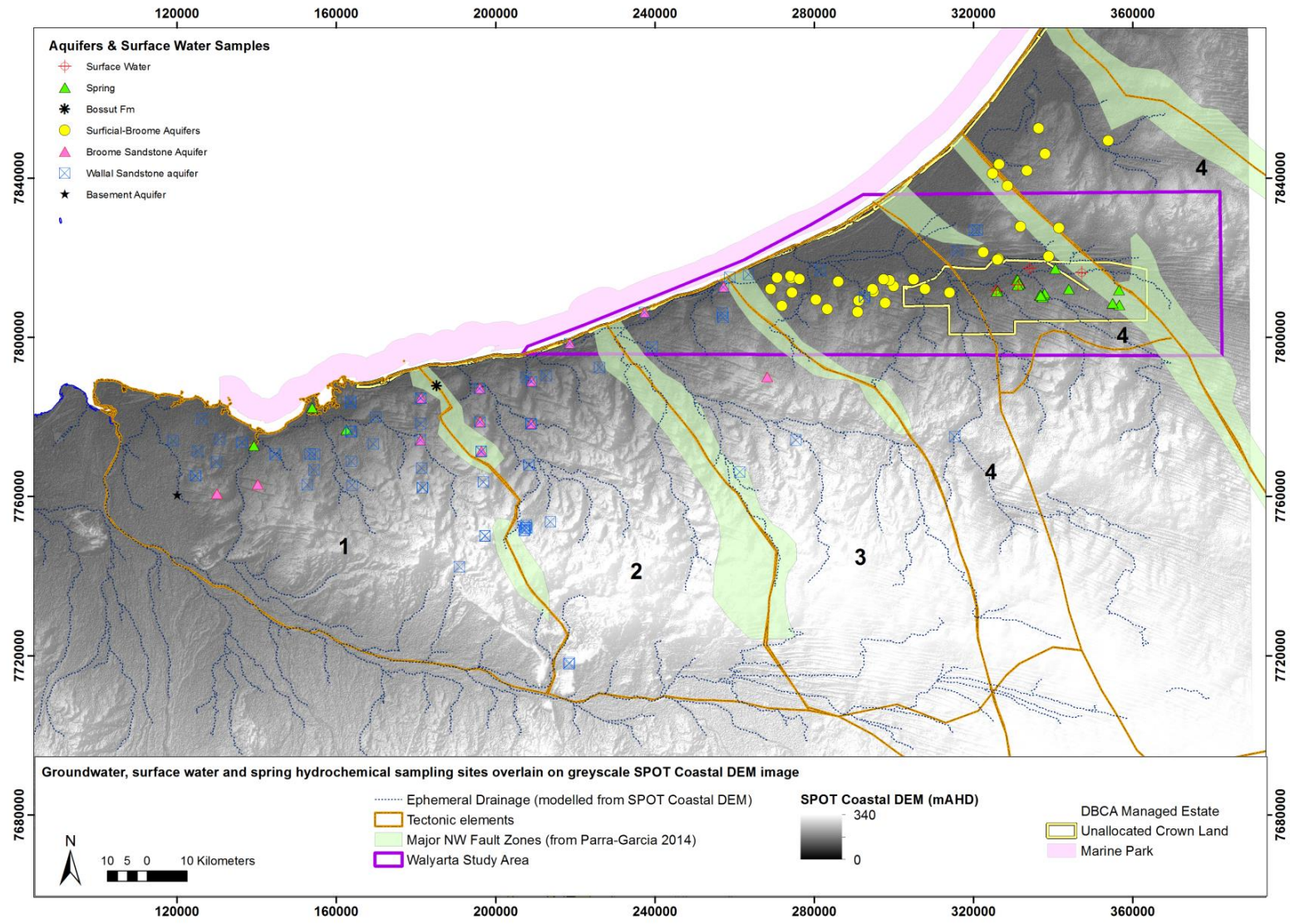


Figure 60 WCB, southern La Grange and Walyarta hydrogeochemical database showing the location of bores, spring sites and tectonic element boundaries, with interpretation areas numbered (1=western basin margin, 2=Wallal Embayment, 3=Wallal Platform and 4. Sapphire Embayment and Willara sub-basin; see Appendix 7)



### 7.3.2 Major ions - spatial distribution and trends

The spatial distribution of groundwater and spring sampling sites are shown in relation to tectonic elements in Figure 60. This figure shows a spatial sampling bias that occurs due to the Wallal aquifer being more prospective in the south west where the aquifer generally contains potable water and artesian conditions means pumping is not required. Conditions change to the north east of Walyarta, where potable water resources exist in the unconfined Broome/Surficial-Broome aquifers.

Despite the sampling bias a Piper trilinear diagram in Figure 61 resolves hydrogeochemical fingerprints and trends for the main aquifers. Observations concur with those reported in previous work (Sections 7.1 and 7.2), with all aquifers showing the hydrogeochemistry to range from Ca-Mg-HCO<sub>3</sub>, to Ca-SO<sub>4</sub>-Cl and then NaCl water and spring sampling generally characterised by lower concentrations of bicarbonate and carbonate relative to chloride and sulfate (Figure 61).

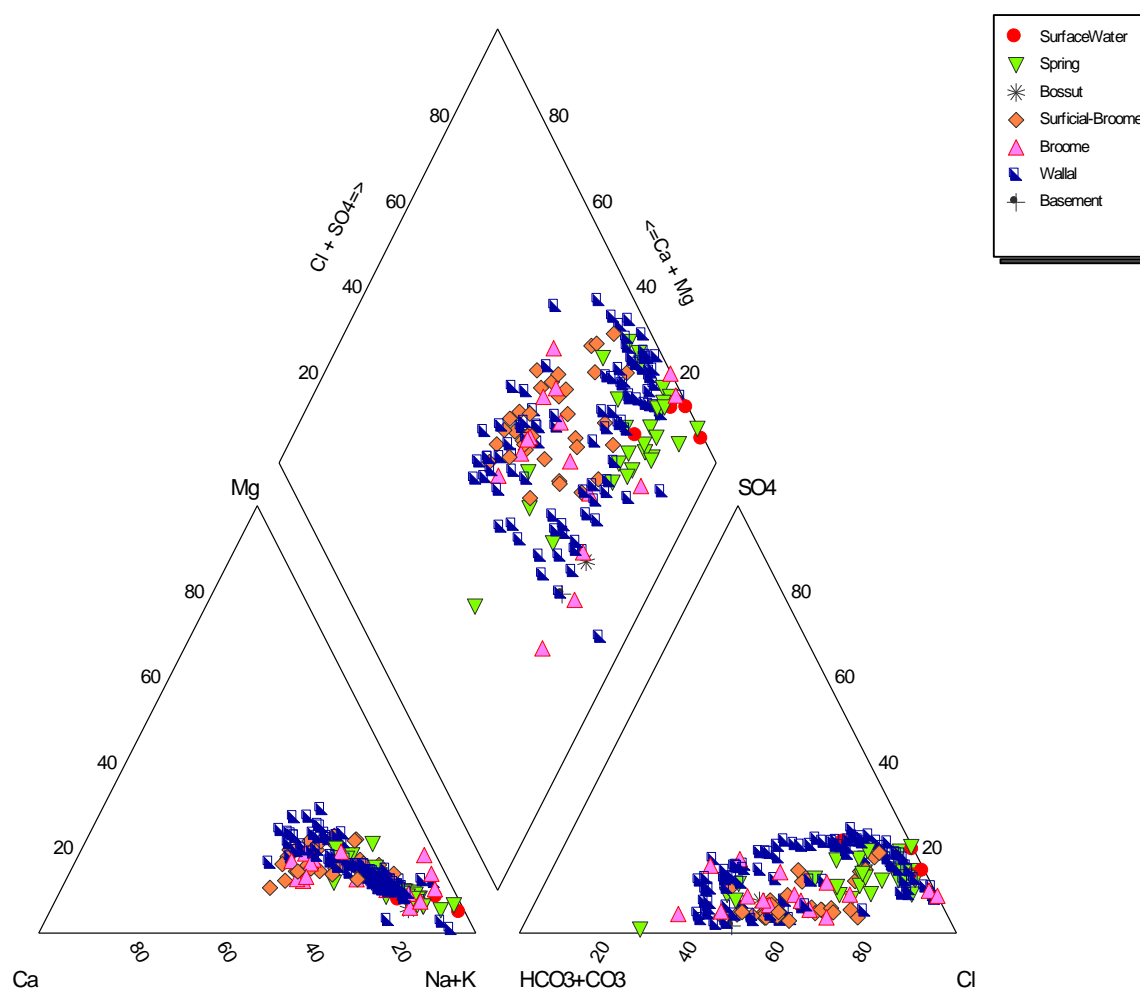


Figure 61 A Piper trilinear diagram of groundwater, springs and surface water sampled between 1975 and 2017 (see Appendix 7) (Note groundwater is sampled from the Bossut Fm., Surficial-Broome and Broome sandstone aquifers, Wallal sandstone aquifer and weathered crystalline basement aquifer)

Previous hydrogeochemical assessments examined the evolution of groundwater against distance from the coast, which in the WCB mimics topographic gradients (Meredith et al. 2018). A similar approach is adopted here and shown in Figure 62, with bores located at a distance of around ten

kilometres from the coast classified as coastal bores and those greater than twenty five kilometres from the coast as upland bores. Bores in the area between these classes are given the nominal midflow path term. Landforms change in Walyarta and bores are classified according to their location in relation to the tidal flats, the palaeovalley and upgradient locations (e.g. midflow path and uplands).

Figure 62 also shows the location of bores in relation to potential changes in recharge chemistry due to contributions from surficial carbonate / evaporite deposits. In the WCB area potential carbonates / evaporite deposits are located on catchment divides and in close proximity to some upland bores, while downgradient they are located along the coastline and extend with the tidal flats into the Mandora Palaeovalley. Based on this conceptualisation it is expected that the groundwater chemistry of aquifers sampled from upland bores in recharge areas of the WCB, and discharge bores and springs in the Mandora Palaeovalley and tidal flats, will be elevated in calcium, magnesium and bicarbonate compared with chloride. Data presented in piper diagrams in Figures 63 to 65 indicate that this model holds for the Wallal aquifer but variation is more complex in the Broome and surficial aquifers and springs and surface water sampling. The palaeovalley spring sampling in particular indicates limited interactions with carbonate / evaporites (Figure 65).

These trends were explored further in bivariate plots in Figures 66 and 67, which resolves variation within and between aquifers. In Figure 66 ion to chloride ratios show calcium (in particular within the Broome and surficial aquifers) and potassium and sodium (especially within the Wallal aquifer and spring sampling) tend to be either slightly elevated or in equal ratios to seawater. Although elevated concentrations are less apparent at chloride concentrations exceeding 50mmol/L (Figure 67).

Apart from the Broome aquifer which shows variable magnesium, magnesium is generally slightly depleted compared to chloride and the depletion increases with increasing chloride concentration. Conversely for sulfate, concentrations in the Wallal aquifer are depleted relative to chloride where sulfate levels are less than 0.1mm/L and this relationship changes as to relative enrichment compared to chloride increases between sulfate levels of 0.1 to approximately 5mm/L. Broome and surficial aquifer samples are generally depleted in sulfate relative to chloride, with spring and surface water samples tending to mimic either the seawater trend line or the Wallal aquifer trends (Figure 67). The Wallal bicarbonate signature compared to chloride exhibits a distinct population and trend with bicarbonate decreasing as chloride increases. Sampling for other aquifers and springs tends suggests bicarbonate increases against chloride (Figure 67).

Apart from  $SO_4/Ca$ , most other ion ratios are examined in Figure 68 show overprinting of aquifer populations and generally a wide variation in spring sampling chemistry. The  $SO_4/Ca$  data indicate that sulfate and calcium are at concentrations that infer gypsum dissolution occurs in most spring and surface water sampling and the Wallal aquifer, at sulfate concentrations above 0.2mmol/L. Most Broome and surficial aquifer sampling is characterised by elevated calcium over sulfate, forming a more distinct population beneath the dashed gypsum dissolution line. Disparate Broome and surficial sampling exhibiting similar trends to the Wallal aquifer and springs is likely in connection with the Wallal aquifer.

HYDROLOGICAL CONCEPTUALISATION OF THE WALYARTA MOUND SPRINGS

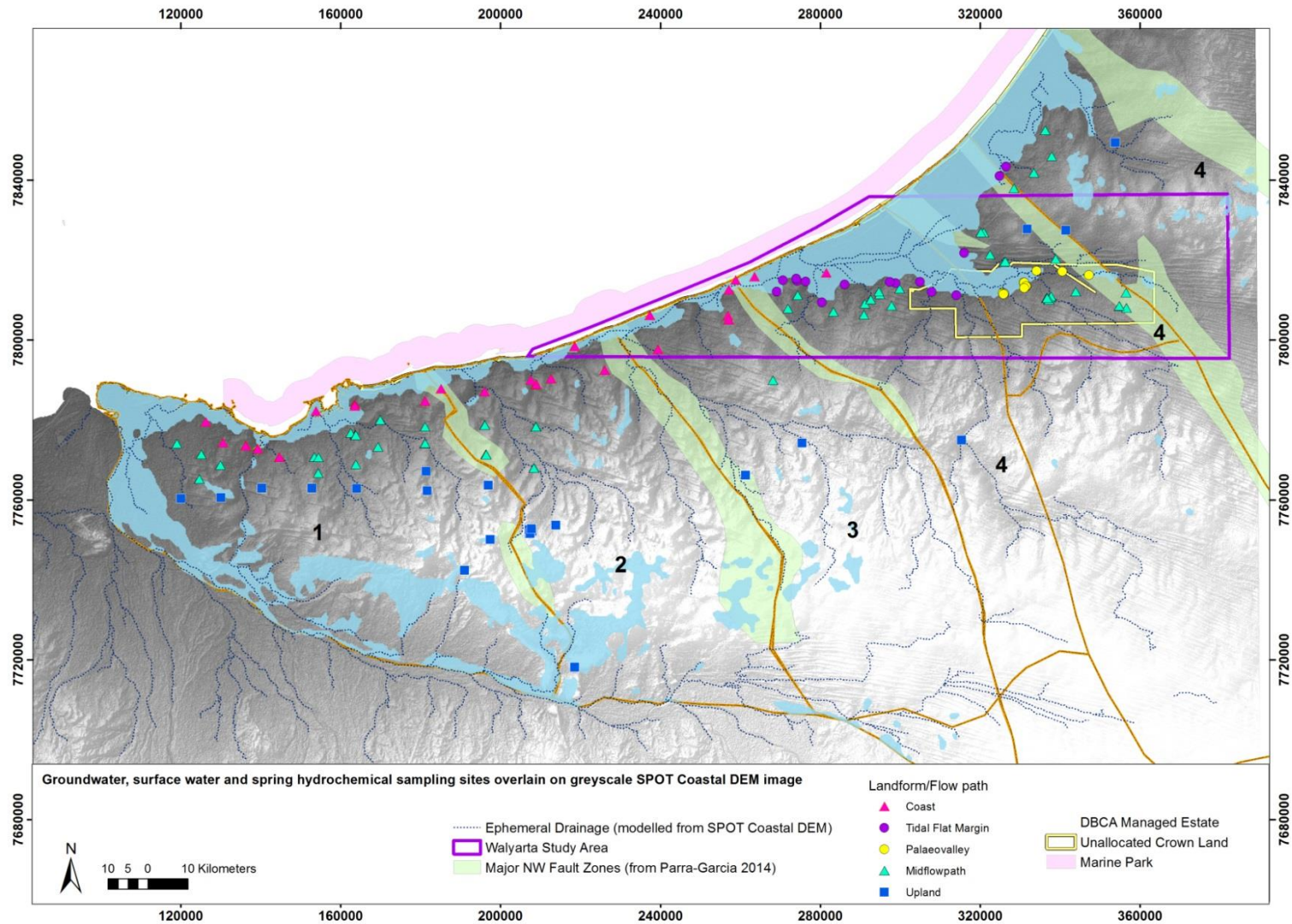


Figure 62 WCB, southern La Grange and Walyarta hydrogeochemical database showing the location of sampling sites in relation to tectonic element boundaries, landform/groundwater flow path and potential carbonate/evaporite regolith map

HYDROLOGICAL CONCEPTUALISATION OF THE WALYARTA MOUND SPRINGS

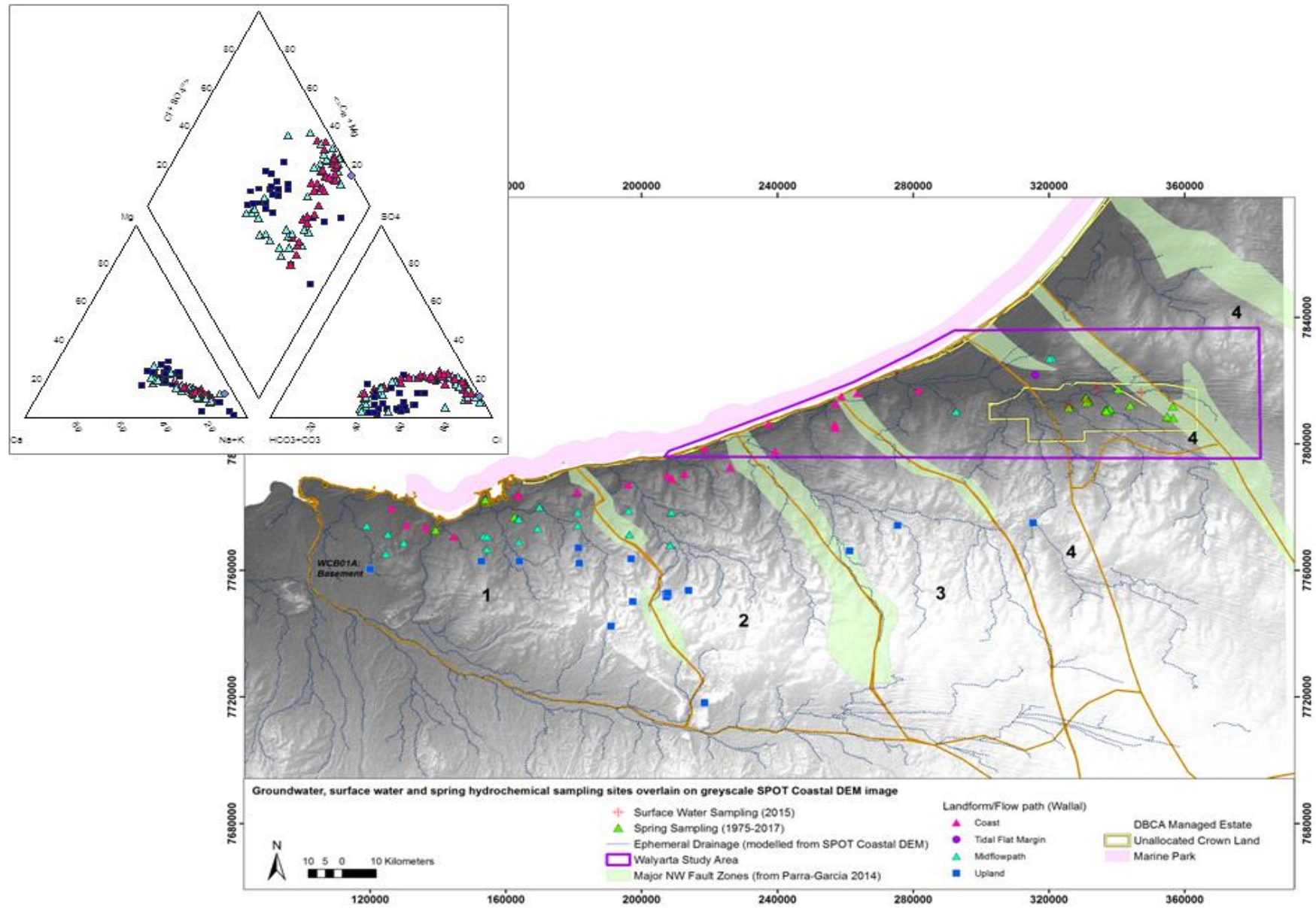


Figure 63 WCB, southern La Grange and Walyarta hydrogeochemical database showing a Piper diagram and location of Wallal aquifer sampling sites in relation to landform/groundwater flow path



HYDROLOGICAL CONCEPTUALISATION OF THE WALYARTA MOUND SPRINGS

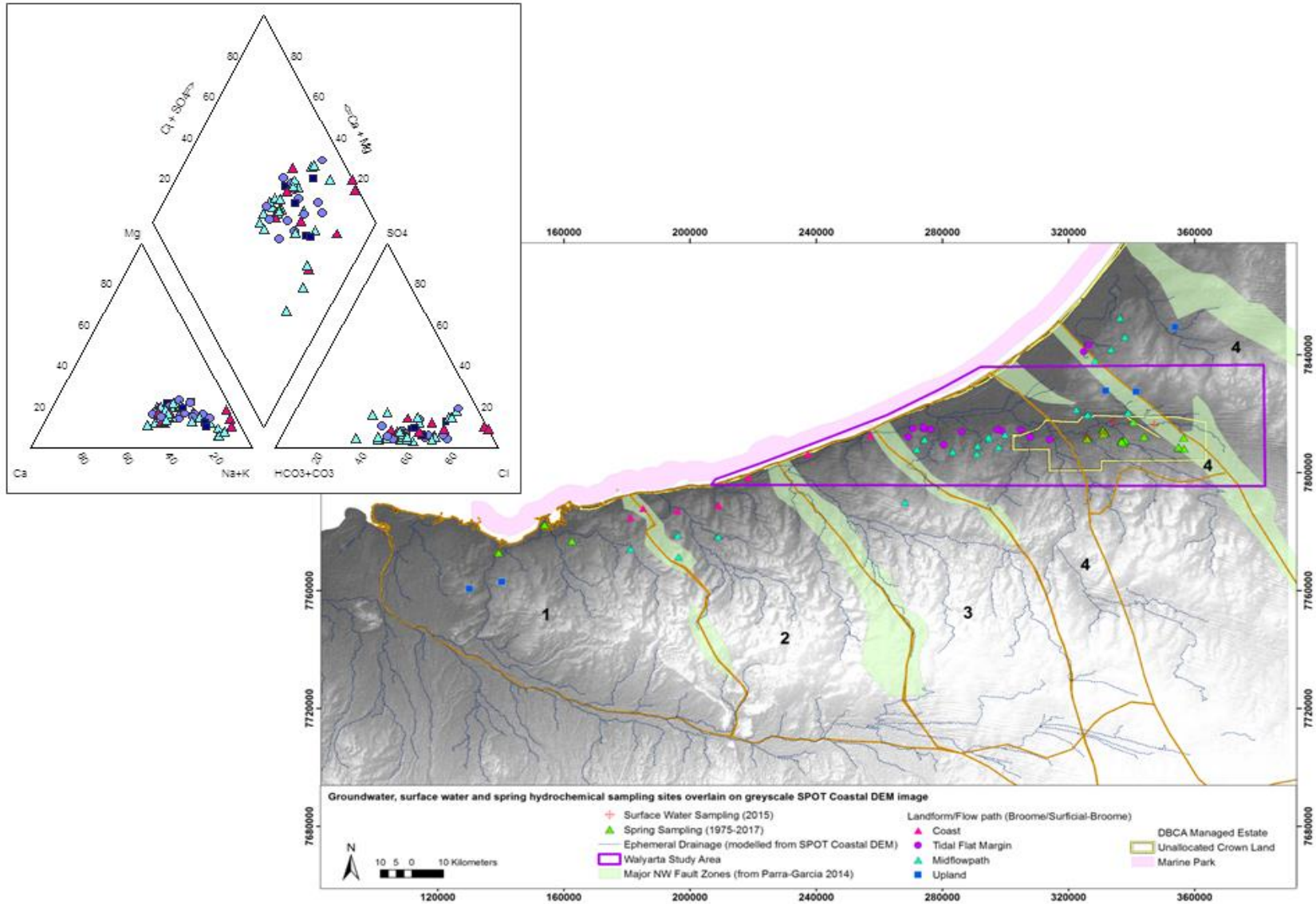


Figure 64 WCB, southern La Grange and Walyarta hydrogeochemical database showing a Piper diagram and location of Broome/Surficial aquifer sampling sites in relation to landform/groundwater flow path

HYDROLOGICAL CONCEPTUALISATION OF THE WALYARTA MOUND SPRINGS

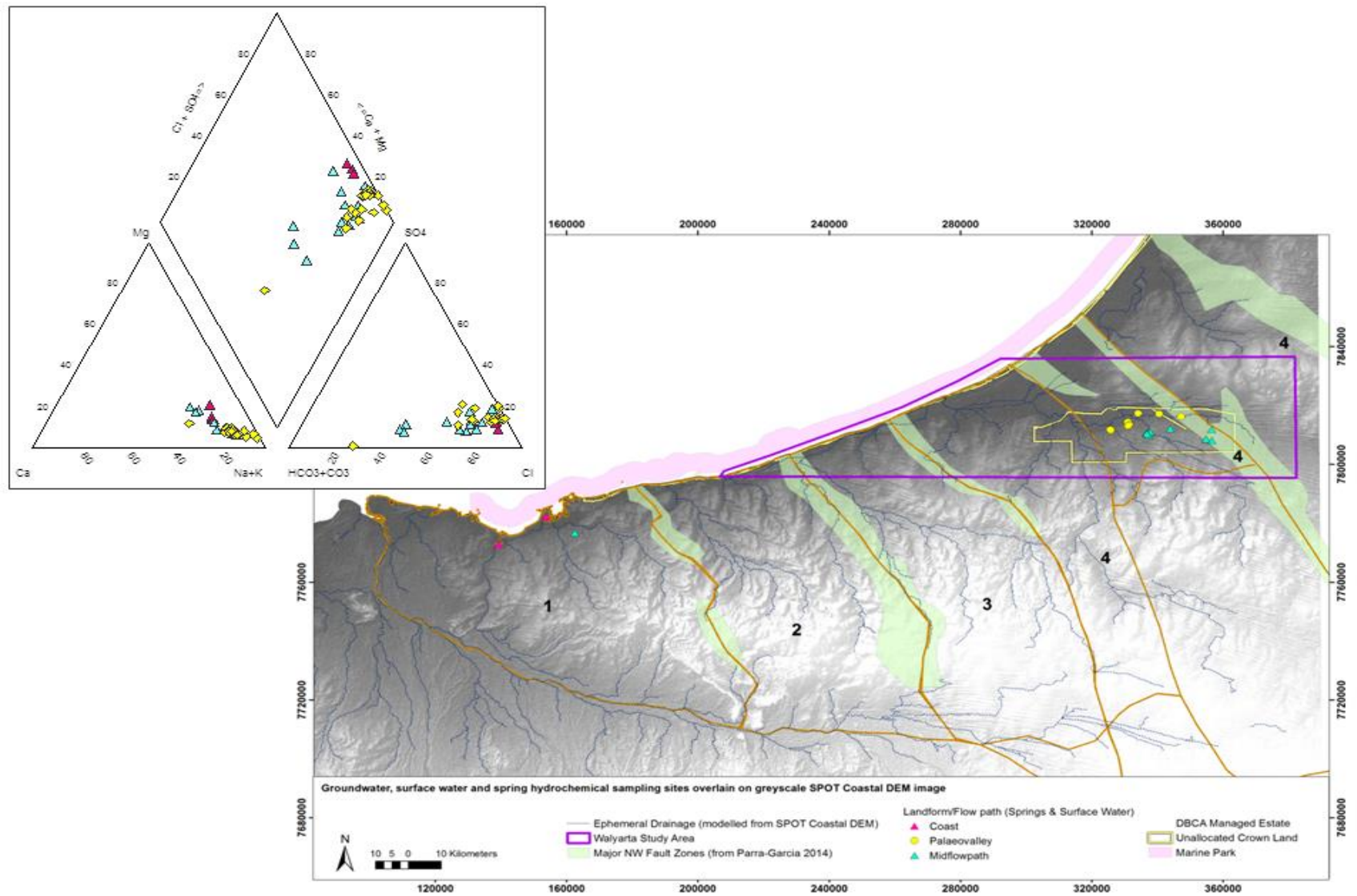


Figure 65 WCB, southern La Grange and Walyarta hydrogeochemical database showing a Piper diagram and location of spring sampling sites in relation to landform/groundwater flow path

HYDROLOGICAL CONCEPTUALISATION OF THE WALYARTA MOUND SPRINGS

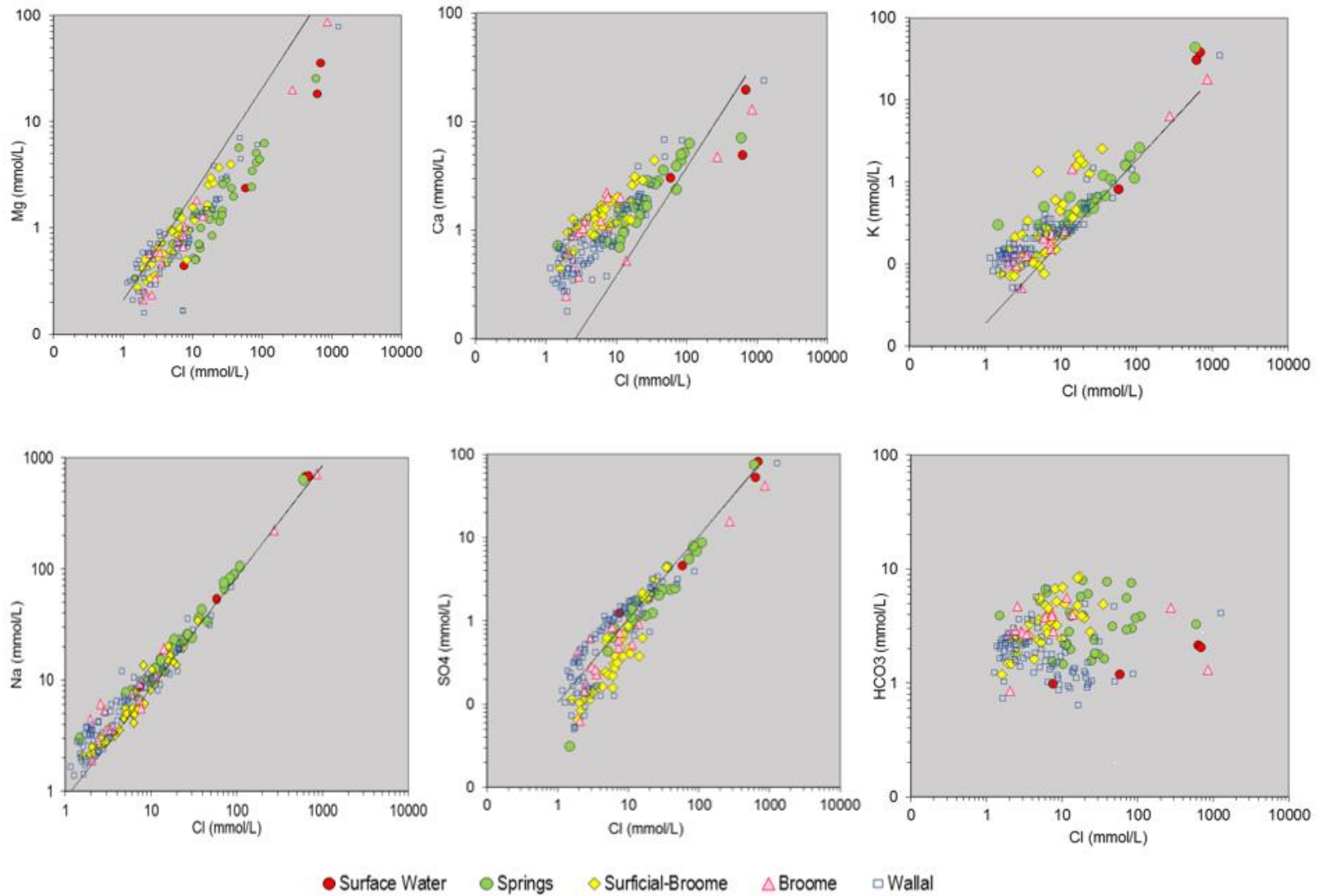


Figure 66 Bivariate log-log plots of various ions against chloride, concentrations are shown in mmol/L and solid black trend line represents seawater concentration

HYDROLOGICAL CONCEPTUALISATION OF THE WALYARTA MOUND SPRINGS

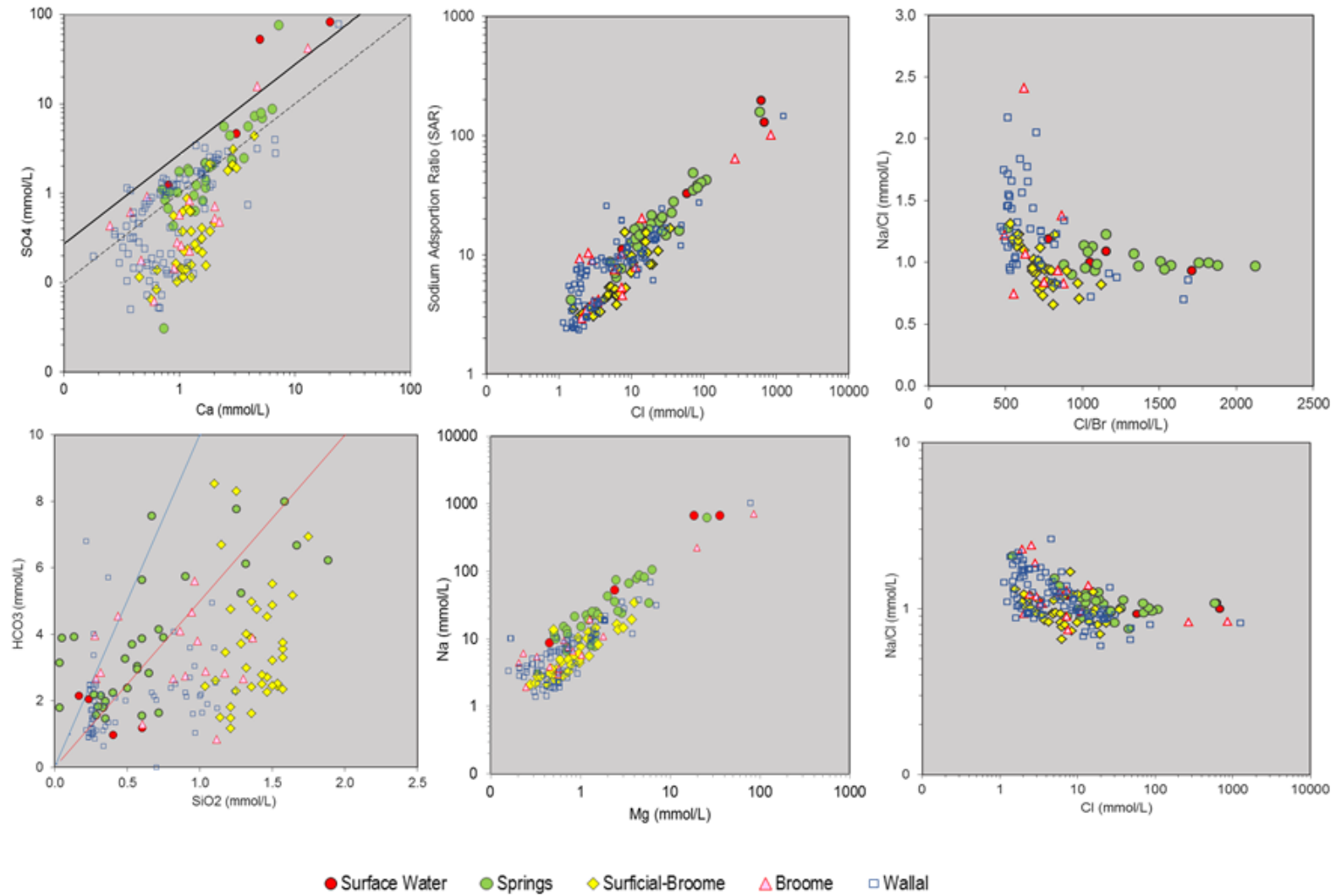


Figure 67 Bivariate log-log plots of SO<sub>4</sub>/Ca, SAR/Cl, Na/Cl vs Cl/Br, HCO<sub>3</sub>/SiO<sub>2</sub>, Na/Mg and Na/Cl vs Cl, concentrations are shown in mmol/L, solid black and dashed trend line in SO<sub>4</sub>/Ca plot represents seawater concentration and gypsum dissolution respectively, blue and red trend lines and arrows in HCO<sub>3</sub>/SiO<sub>2</sub> plot represent respective carbonate and silicate reactions.



Combined piper and bivariate plot trends resolve that the Wallal aquifer and springs sampling is similar in hydrogeochemical character above chloride concentrations around 5mmol/L (e.g. recharge areas), with generally lower calcium and higher sodium and sulfate compared to the Broome and surficial aquifers. Where the Wallal aquifer has chloride concentrations less than or around 5mmol/L it is also characterised by higher Ca/Cl, HCO<sub>3</sub>/Cl and lower SO<sub>4</sub>/Cl indicating the aquifer chemistry may be influenced by the dissolution of surficial carbonate / evaporite deposits during recharge.

Correlation matrices were also constructed for hydrogeochemical data using Pearson's correlation coefficient to measure the strength of the association between analytes. Results provide an objective assessment and are in agreement with bivariate plot observations (Appendix 8).

To help discriminate between the calcium and sodium rich groundwater derived from evaporite dissolution and alkali lakes data were plotted on brine differentiation plots developed by Boschetti (2011) (Figures 68 and 69). Results resolve distinct populations that are in part constrained by tectonic element boundaries and landform/flowpath locations. Spring samples extend outside the evaporite (evap. In Figures 68 and 69) and data potentially resolve four different spring suites. Midflow path springs (e.g. Eil Eil, Bretts, Top and Linear) characterised by higher concentrations of calcium, with Top and Linear Springs also displaying elevated sodium. Saunders Spring is characterised high sodium together with low calcium, which plots close to potential alkali lake type waters (e.g. Salt Creek and MMS Stromatolite Pool) (Figure 68 and 69). Other spring sampling appears to be less distinct. This could be due to reduced/slower groundwater discharge rates or sampling locations not being positioned near the spring vent, with both processes encouraging discharging groundwater to mix with shallow formation and soil water. Alternatively the groundwater flow gradients and mixing may be spatially and temporally different for different spring suites. Insufficient geochemical and physical data exists to model discharge rates. A three dimensional understanding of aquifer hydrogeochemistry is undertaken in Section 7.3.3.

### 7.1 Major ions – geochemical gradients and mixing

A three dimensional hydrogeological model has been produced for the Walyarta study area as part of this project (Figure 4). A coarse scale model for the broader area (Figures 56 & 59) has been produced by the DWER (DWER in prep). In the absence of available three dimensional representations of the coarse scale geology and hydrogeology cross sections are used in this report to interpret hydrogeochemical data. Recent work by Meredith et al (2018) describes how the hydrogeochemistry evolves along roughly south to north trending groundwater flow paths. The same data and cross section are used here, and are expanded to cover new data collection, as well as an interpretation of what is controlling changes in hydrogeochemistry with increasing depth below ground level.

Data for the Wallal aquifer presented in Figure 63 shows that the same evolution in groundwater chemistry (e.g. from Ca-Mg-HCO<sub>3</sub> to Na-SO<sub>4</sub>-Cl) occurs at the coast as well as midway along the flow path. This duplication makes it difficult to assess groundwater recharge, identify changes in chemistry due to geochemical reactions within the aquifer or groundwater mixing and understand the dominance of vertical and lateral gradients, as defined by the hydrogeochemistry.

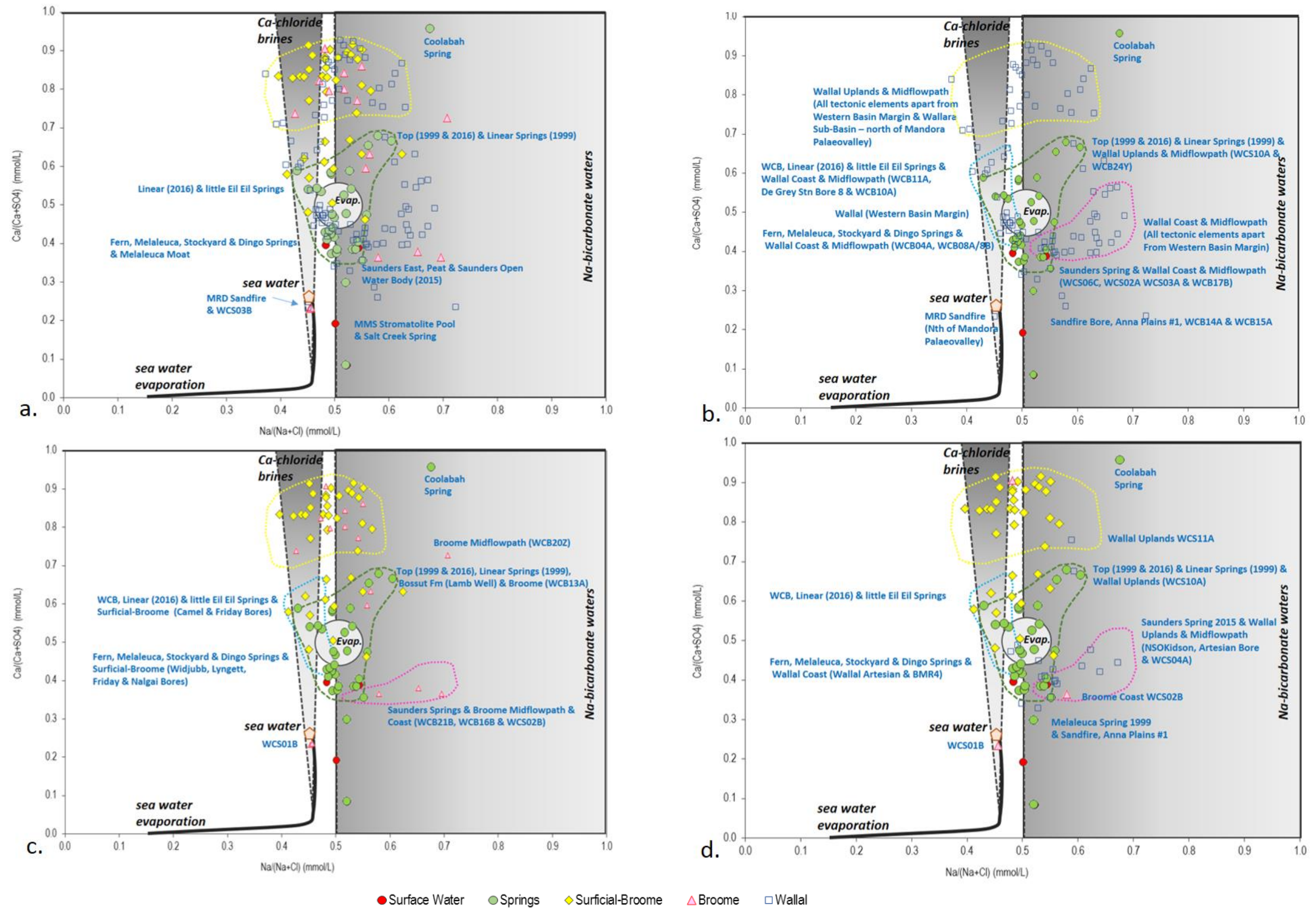


Figure 68 Brine differentiation plots for a. all data, b. Wallal aquifer, springs and surface water, c. Broome and surficial aquifers, springs and surface water and d. data within tectonic element 4 see Figure 60.

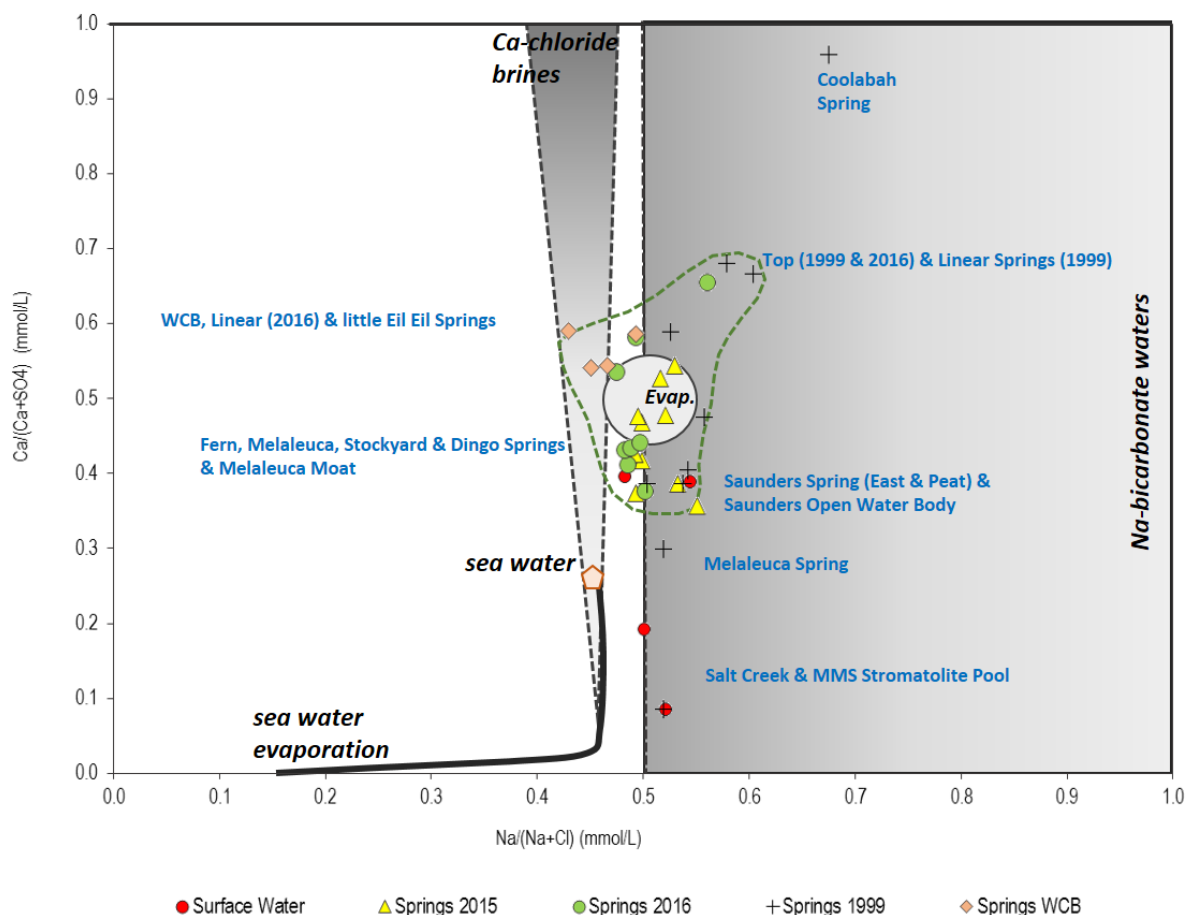


Figure 69 Brine differentiation plot for all spring and surface water sampling

However, when Wallal aquifer data from the Wallal Embayment are examined in a Piper diagram they exhibit a very clear groundwater evolution, with Mg-Ca-HCO<sub>3</sub>-Cl type groundwater in upland areas evolving downgradient to a Ca-Mg-HCO<sub>3</sub>-SO<sub>4</sub> water and a Na-SO<sub>4</sub>-Cl water type near coastal discharge areas (Figure 70). The *capture zone* for data graphed in Figure 70 is shown on Figure 71, in a perspective view as well as a geological cross-section (A-A') adapted from Meredith et. al. 2018. Figure 71 also has the location of a cross-section in Walyarta (cross-section B-B') to test the transferability of the hydrogeochemical evolution of groundwater in the Wallal aquifer.

Transferability was assessed by graphing analytes and ratios against the depth they were sampled. Bore screen details were available for 110 bores, with 78 (71%) sampling the Wallal aquifer and the remaining 32 (29%) sampling the Broome aquifer, with roughly 50% of bores being located in the Walyarta study area and sampled as part of the DPIRD La Grange (LG) Water for Food project (Appendix 7). To investigate vertical geochemical patterning individual analytes were plotted against bore mid screen sample depths (in mAHD). Three graphs were produced for each analyte examined; (a.) all data, (b.) data for the Wallal Embayment cross-section (A-A') and (c.) available data east northeast of cross-section A-A' (Figure 71 to 77). Graphs b. and c. display the Broome LG aquifer bore (Coolgardie Well), which is the closest shallow bore to the Walyarta spring sites (located approximately 11.5km west of Saunders Spring).

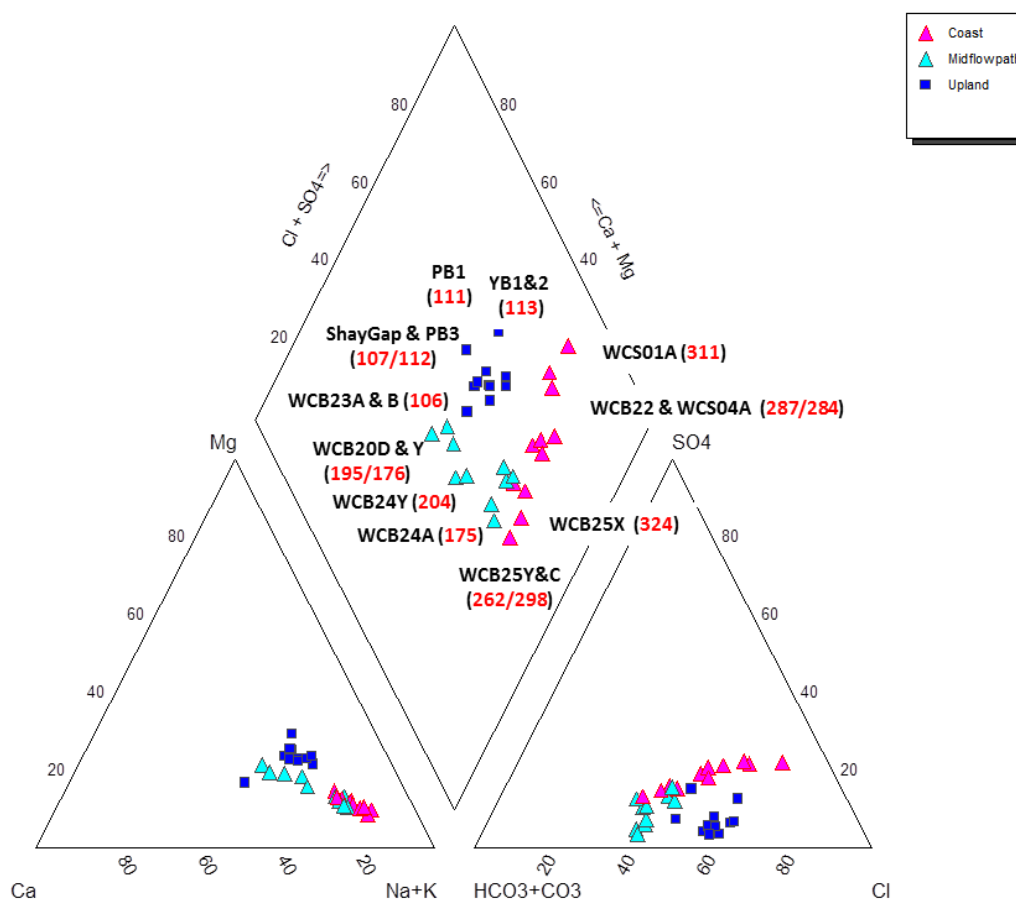


Figure 70 Piper trilinear diagram for Wallal groundwater sampled in the Wallal Embayment (see Figure 60), labels show bore names (black) and mid screen sampling depth in metres below ground level (red).

Three spring water samples containing the lowest  $^{14}\text{C}_{\text{DIC}}$  pmc concentrations and one surface water sample from Salt Creek (Figure 37) were selected to be graphed to assess similarities between spring and surface water hydrogeochemistry and the range in analyte concentrations in the underlying aquifers (Table 9). For the spring selection, the three lowest  $^{14}\text{C}_{\text{DIC}}$  pmc concentrations were graphed, as the current conceptual model advises these samples are likely to represent the oldest water discharging from the confined Wallal aquifer (Harrington and Harrington 2017 & Meredith et al. 2018).

Determining the hydrochemical fingerprint of the aquifer, or aquifers, discharging at springs is an important first step in calculating spring discharge rates, which is required to manage the spring’s ecological water requirements. In the Wallal aquifer, total dissolved solids, chloride and sodium are generally low (TDS;  $\sim 500\text{mg/L}$ ) all show a weak increase in concentration with depth. Higher concentrations (TDS;  $>1000\text{mg/L}$ ) occur in the Walyarta study area at below depths of  $-200\text{mAHD}$  (Figure 72; graphs c.) and between 10 and  $-100\text{mAHD}$  in the western basin margin, where the groundwater is older (Meredith et al. 2018). The Broome aquifer (Broome and LG) shows a wide range of TDS, Cl and Na concentrations, with higher concentrations (TDS; 2000 to 3000 mg/L) in Broome LG bores located on the margin of the tidal flats (Figure 64).



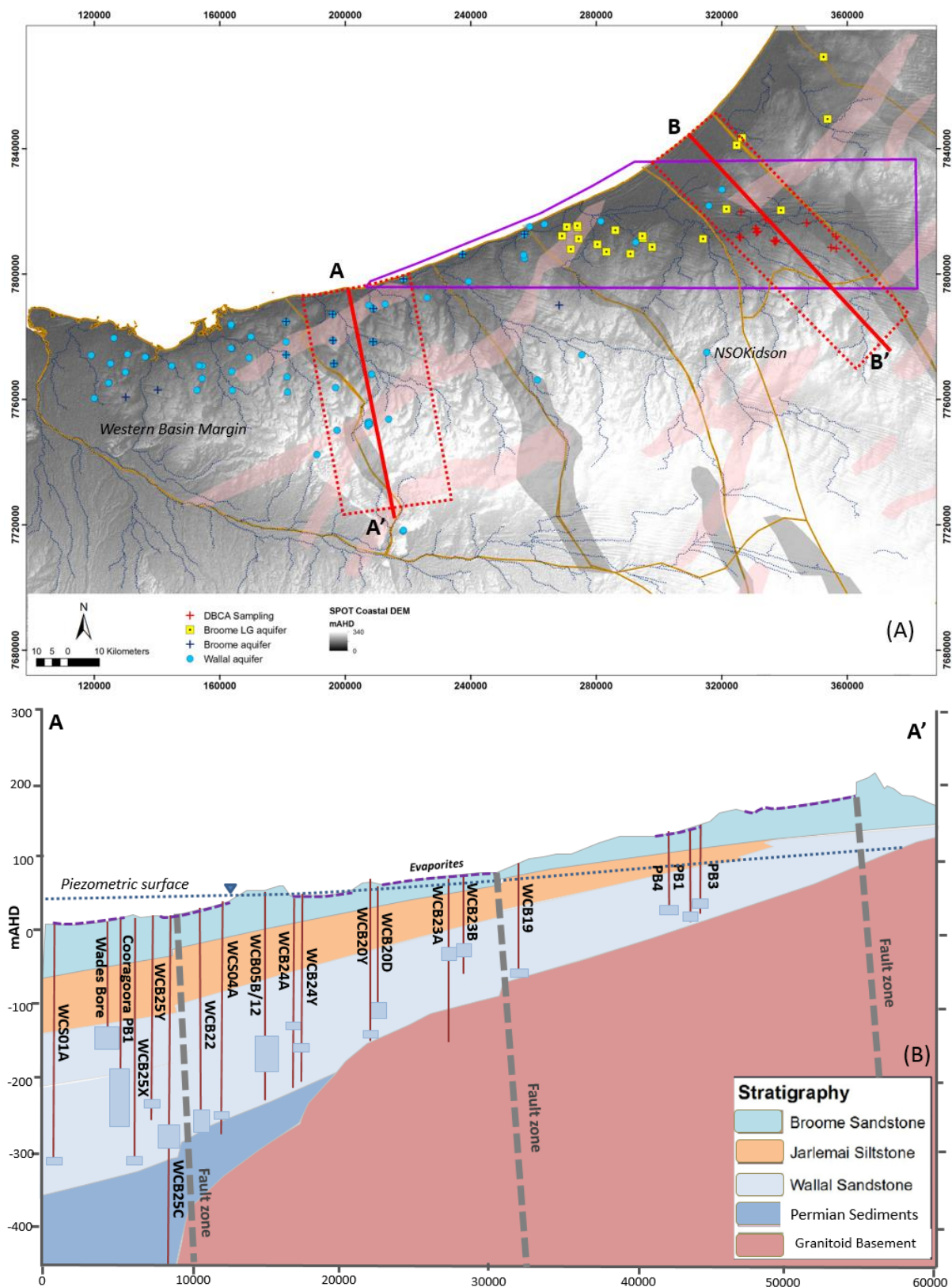


Figure 71 (A) Map showing location of Canning Basin, simplified major tectonic element boundaries and Wallal Embayment Transect A'-A and Willara sub-basin Transect B-B', showing the location of bores; bores interpolated onto transects are within red dashed boundaries, apart from NSOKidson; (B) Geological X-Section A'-A, adapted from Meredith et. al. 2018; bores (depth drilled and screened sections) and interpretations of major geological structures and evaporities from report Sections 4.5 and 7.2.

Spring ID	Date sampled	Elevation mAHD	$\delta^{13}\text{C}_{\text{DIC}}$ ‰	$\delta^{14}\text{C}_{\text{DIC}}$ pmc	$\delta^2\text{H}$ ‰	$\delta^{18}\text{O}$ ‰	$\delta^{87}\text{Sr}$ ‰
Dingo_Spring_2016	24/11/2016	37	-14.8 +/- 0.1	51.96 +/- 0.16	-56.3	-7.74	8.86
Fern_Peat_2016	25/11/2016	14	-16.8 +/- 0.2	71.77 +/- 0.21	-54.8	-7.06	7.18
Linear_Spring_2016	24/11/2016	48	-11.9 +/- 0.1	76.61 +/- 0.21	-55.9	-7.64	7.94
Little_EilEil_2016	24/11/2016	31	-12.6 +/- 0.1	71.39 +/- 0.24	-52.3	-7.61	7.22
Saunders_East_2016	25/11/2016	11	-13.2 +/- 0.1	64.86 +/- 0.24	-53.7	-7.16	8.05
Stockyard_Mangrove_2016	25/11/2016	10	-11.7 +/- 0.1	16.36 +/- 0.09	-55.0	-7.48	9.43
Stockyard_Mangrove2_2016	25/11/2016	10	-13.4 +/- 0.1	50.82 +/- 0.21	-56.6	-7.17	10.59
Top_Spring_2016	24/11/2016	52	-13.7 +/- 0.1	92.36 +/- 0.25	-51.8	-6.67	7.59
Bretts_Open_1	2/09/2015	35	-13.3 +/- 0.1	93.39 +/- 0.27	-43.86	-5.49	6.92
EilEil_Spring	2/09/2015	40	-11.5 +/- 0.1	94.63 +/- 0.27	-45.45	-5.74	7.14
Fern_Peat_2015	3/09/2015	17	-16.4 +/- 0.1	70.67 +/- 0.22	-48.37	-6.26	9.01
Fern_Tail	3/09/2015	15	-7.7 +/- 0.1	101.65 +/- 0.30	-44.15	-5.49	9.07
Friday_Well	31/08/2015	10	-8.7 +/- 0.1	93.05 +/- 0.26	-51.43	-7.36	5.61
Little_EilEil_2015	2/09/2015	35	-11.4 +/- 0.1	41.43 +/- 0.16	-56.12	-8.23	7.14
Melaleuca_Moat	3/09/2015	15	-10.9 +/- 0.1	85.97 +/- 0.24	-41.91	-4.99	7.90
Melaleuca_Peat	3/09/2015	17	-14.4 +/- 0.1	85.74 +/- 0.24	-50.00	-6.87	7.91
MMS19_Stromatolite	1/09/2015	20	-14.1 +/- 0.1	92.62 +/- 0.26	-7.02	2.62	10.25
Salt_Creek_7	1/09/2015	15	-12.4 +/- 0.1	95.91 +/- 0.26	10.03	6.20	10.41
Saunders_Open_2	3/09/2015	15	-9.7 +/- 0.1	65.12 +/- 0.22	-36.9	-4	7.78
Saunders_East_2015	3/09/2015	17	-10.4 +/- 0.1	55.94 +/- 0.17	-51.79	-7.10	7.91
Saunders_Peat	3/09/2015	17	-15.5 +/- 0.1	83.76 +/- 0.24	-52.59	-7.21	7.92
Saunders_West	3/09/2015	15	-12.4 +/- 0.1	87.50 +/- 0.24	-50.06	-7.09	7.89
Stockyard_Mangrove2_2015	4/09/2015	15	-11.5 +/- 0.1	75.01 +/- 0.23	-48.86	-6.79	10.61

**Table 9 Environmental isotope data for DBCA spring and surface water sampling (2015 & 2016), samples selected for graphing in Figures 71 to 76 are highlighted in grey (see Appendix 7 for expanded information on location and chemistry) (Note accuracy elevation (mAHD) is derived from the SRTM1s hydrologically corrected DEM).**

Spring TDS, Cl and Na concentrations tend to fall within near surface (0 to -50mAHD) chemistry of the Broome aquifer. To depths of around -50mAHD, the Wallal bore with chemistry most similar to the spring samples graphed is upland bore WCB15A (screened at -19mAHD) (Figure 72; graphs a.). However, it is important to note that in the Wallal Embayment, Wallal upland bores PB1 and PB3 are screened at similar elevations to the Walyarta springs, depths of 21 and 27mAHD respectively, and evapotranspiration could result in their chemistry evolving to that of the springs.

Ratios of Na relative to Cl show most Wallal, Broome and spring samples, above 0mAHD, exhibit rainfall signatures of 1:1 (Figure 72). Between 40 to -20mAHD, increased Na over Cl occurs in samples from upland Wallal bores and midflowpath Broome bores, with highest values evident in Broome LG samples located in a shallow palaeochannel near the tidal flat margin. Increases in Na relative to Cl in upland and midflow path areas are likely to results from silicate weathering (e.g. evidence of , including cation exchange reactions where clay minerals prefer to take larger cations, such as Ca and Mg, into their lattice and release smaller cations (e.g. Na) (e.g. Anand et. al. 1985 & Singh and MacKinnon 1996). At depth, between -100 to -200mAHD, Na/Cl ratios vary and then below -200mAHD observe a weak decline from elevated Na relative to Cl to unity (rainfall concentrations).

Graphing partial datasets for the Wallal Embayment gives the impression of improved correlations of analyte trends (TDS, Na and Na/Cl) with depth, as outlier values are removed (Figure 72; graphs b). This relationship does not hold for Cl data, which displays elevated values in bores located near mapped major geological faults (Figures 58 and 60). In these locations system conditions may be variable, encouraging aquifer mixing (connectivity with Permian sediments and/or basement) and different water-rock interactions. In contrast plotting data from tectonic elements to the north east of the Wallal Embayment displays similar trends but data gaps (between -30 to -244mAHD) prevents a robust interpretation of spatial relationships (Figure 72; graphs c.).

Other major ions, Ca, Mg, SO<sub>4</sub> and K, sampled are displayed with depth on Figure 73. In the Broome aquifer (exclusive of Broome LG), Ca, Mg SO<sub>4</sub> and K all increase with depth (from a depth range of 7 to -82mAHD). Samples from the Wallal aquifer, between 46 to -78mAHD and including the western basin margin, exhibit a similar relationship as does graphed spring discharge water. This similarity covers analyte concentration range and relationship with depth for both the Broome and Wallal (including western basin margin) populations suggests the aquifers are, or have in the past, been hydraulically connected to depths of around -100mAHD. It also infers there are common processes that have influenced the geochemical evolution of the groundwater, which for these analytes is likely to result from the dissolution of evaporites that are likely to include calcite, dolomite, gypsum and sylvite.

The relationship is more convincing in the Broome aquifer by the inclusion of higher analyte concentrations sampled in groundwater from the more recent installation of coastal bores in the Wallal Platform (e.g. bores WCS03B and WCS01B). These bores are located close to the salt water interface (Figure 25) and the groundwater chemistry is interpreted to be sea water in type (Figure 68). As the Broome aquifer is unconfined it also receives some lower salinity groundwater recharge from the vertical movement of groundwater as well as throughflow. Coastal areas, close to the salt water interface, mark the end of the groundwater flow path in the Broome aquifer, and here changes in groundwater density may slow groundwater discharge, resulting in higher concentrations of dissolved solutes.

In the Walyarta area the Broome LG samples from the tidal flat margin and at depths exceeding the estimated evapotranspiration depth (>6m below ground level) also display a small increase in analyte concentrations (Ca, Mg, SO<sub>4</sub> and K) with depth sampled. This is expected as the Broome groundwater chemistry is controlled by the same physical and chemical processes at the coast as well as inland marginal to the saline tidal flats. As the Wallal aquifer western basin margin groundwater chemistry displays similar patterning it is likely to reflect past recharge from the dissolution of evaporites and where salinities are higher near the coast, the delayed flushing of past sea water incursions.

In the Wallal aquifer below depths -100mAHD, concentrations of Ca, Mg, SO<sub>4</sub> and K tend to mimic chloride trends, which agree with trends observed in bivariate plots (Figures 66 & 67). Concentrations of SO<sub>4</sub> increase with depth, as do Ca, Mg and K, although the latter group show more variation. Increases in sulfate at these depths may be sourced from the oxidation of pyrite (FeS<sub>2</sub>), in addition to the dissolution of gypsum as supported by ANSTO unpublished X-Ray diffraction (XRD)

data. ANSTO mineralogical interpretations of Wallal Embayment drill core XRD analyses indicates the Alexander Formation and Upper Wallal Sandstone may contain up to five percent sulphur, stored in pyrite, between depths of ~100 to 275 metres below ground level. Up to ten percent Siderite ( $\text{FeCO}_3$ ) was identified across a similar depth range as pyrite in XRD analyses, which confirms conditions are currently anoxic, and were also likely to be anoxic at the time of deposition. The presence of both pyrite and siderite at similar depths in the profile is likely to mark a change in diagenetic environment. Pyrite precipitating in a sulfide producing environment (e.g. anoxic marine sediments rich in organics) and siderite in a sulfate environment (e.g. anoxic, non-marine environment where pyrite production through sulfate reduction of organics is exhausted and carbonate then produced from organics through bacterial methanogenesis). In both cases dissolved ferrous iron is derived from the reduction of fine-grained detrital iron oxide minerals, with organic material acting as the reductant. The presence of relatively substantial quantities of these minerals is important in understanding the aquifer carbon balance and dating, as well as assessing longer term water quality, in particular maintaining alkalinity and aquifer buffering capacity under changed redox conditions. Work required to assess this is discussed in Section 8.

Graphing partial datasets produces different results to those reported for Figure 72. Correlations are not convincing for both the Wallal Embayment and combined tectonic elements north east of the Wallal Embayment (Figure 73; graphs b and c).

Ionic ratios  $\text{Ca}/\text{Cl}$ ,  $\text{HCO}_3/\text{Cl}$ ,  $\text{SO}_4/\text{Cl}$  and  $\text{SO}_4/\text{Ca}$  were plotted with depth in Figure 74 and show different trends.  $\text{Ca}/\text{Cl}$  generally increases from 46 to 0 mAHD for the Wallal and Broome aquifers, and then displays a gradual decrease against depth sampled. Broome LG sampling are characterised by elevated  $\text{Ca}/\text{Cl}$ , with highest Ca relative to Cl evident in two coastal bores (circled in Figure 74) located within the palaeochannel interpreted to be incised into the Broome Sandstone and Jarlemai Siltstone (Section 4.5). Salt Creek and spring  $\text{Ca}/\text{Cl}$  ratios are different from Broome LG, tending to be aligned with upland Wallal aquifer sampling (e.g. WCB18, PB4 and NSOKidson). Elevated  $\text{Ca}/\text{Cl}$  at depths below -200mAHD occurs in fault zones (e.g. WCB17 and WCB22).

Ratios of  $\text{HCO}_3/\text{Cl}$  in the Wallal aquifer are mainly relatively high and uniform with depth. A separate population exists, with lower  $\text{HCO}_3/\text{Cl}$  below depths of -250mAHD, as well as in bores located at around -120mAHD, installed in potential evaporites within the Wallal Embayment (Figure 62). The Broome aquifer shows declines in  $\text{HCO}_3/\text{Cl}$  with depth, while samples in the Broome LG are highest in the two coastal palaeochannel bores and lowest in shallow bores (<5 metres below ground level). Salt Creek has very low  $\text{HCO}_3/\text{Cl}$  and ratios are low for all springs, being similar to the shallow Broome LG bores, one of which (Lyngetts Well) is located on the northern Walyarta palaeovalley margin, to the north east of Salt Creek. For  $\text{Ca}/\text{Cl}$  and  $\text{HCO}_3/\text{Cl}$ , the western basin margin sampling tends to form a distinct population, with lower Ca and  $\text{HCO}_3$  relative to chloride.

In the Wallal aquifer ratios of  $\text{SO}_4/\text{Cl}$  and  $\text{SO}_4/\text{Ca}$  show similar increasing trends with depth from ~0 to -150mAHD (Figure 74), while the Broome aquifer sampling displays no obvious trends and has a broader range of ratios. About half of the Wallal upland bores (sampling depths up to -30mAHD) have elevated  $\text{SO}_4$  with respect to Cl and Ca. The upland Wallal is interpreted to be in connection with the overlying Broome aquifer where there is elevated sulfate. The western basin margin  $\text{SO}_4/\text{Cl}$  ratios tend to align with the lower Wallal aquifer trends and conversely the higher Broome aquifer



SO<sub>4</sub>/Ca ratios. This is likely to be the result of longer lived evapotranspiration processes increasing Cl relative to SO<sub>4</sub> and contemporary recharge processes maintaining SO<sub>4</sub>/Ca ratios generally at parity, which is indicative of gypsum dissolution. Below depths of around -150mAHD both ratios are relatively uniform and this suggests system conditions are mainly anoxic and stored sulfides (pyrite) are not oxidising under the current aquifer dynamics and releasing significant additional SO<sub>4</sub> to the groundwater chemistry. Broome LG, as well as Salt Creek and spring SO<sub>4</sub>/Cl ratios are variable, possibly due to overprinting of past salt water incursions and contemporary evapotranspiration processes. In contrast SO<sub>4</sub>/Ca ratios for the springs are elevated and clustered, being similar to the Wallal aquifer upland sampling (e.g. NSOKidson and WCB18), as well as Wallal aquifer sampling below ~-100mAHD. A small subset of Broome aquifer samples exhibit similar ratios, but these samples occur in fault zones and may represent a mix of Wallal and Broome groundwater.

Graphing partial datasets produces similar correlations for the Wallal Embayment and inconclusive trends for the combined tectonic elements north east of the Wallal Embayment (Figure 74; graphs b and c).

Meredith et.al. (2018) reported on the decrease in SiO<sub>2</sub> along groundwater flow paths and presented data from a transect located within the Wallal Embayment (Figure 71). To understand the mobility of silica within these sandstone aquifers Figure 75 displays graphs of SiO<sub>2</sub>, HCO<sub>3</sub>, HCO<sub>3</sub>/SiO<sub>2</sub> and modelled chalcedony saturation indices (SI) against depth sampled. Chalcedony is chosen to be graphed over quartz as cryptocrystalline silica is more likely to be more active within these sedimentary aquifer systems than quartz (Robertson 1996).

Results show that in the Wallal aquifer, HCO<sub>3</sub>/SiO<sub>2</sub> increases with depth, with higher HCO<sub>3</sub> over SiO<sub>2</sub> evident in bores intersecting fault zones (e.g. WCB25X, WCB22 and WCB17). These patterns are constrained by SiO<sub>2</sub> concentrations, which are high in the upper part of the profile and decrease with depth (around -190mAHD), prior to becoming uniform. In contrast HCO<sub>3</sub> displays a slight increase with depth, with greater variation in concentration below -200mAHD. Both datasets resolve the same elevated values, within fault zones, that appear in the ratio dataset. Chalcedony SI data in the Wallal aquifer show the aquifer is saturated with respect to chalcedony in the upper part of the profile, to depths of approximately -100mAHD (Figure 75). Below this depth the system changes and is slightly under saturated with respect to chalcedony, indicating SiO<sub>2</sub> may go into solution. The important information to pick up from examining these analytes and modelling with depth, is assessing profile zonation that represents changes in aquifer system conditions, mixing and reactions. Data for the Wallal aquifer resolve a major change in SiO<sub>2</sub> and chalcedony SI at around -200mAHD, while the Broome aquifer is consistently under saturated in chalcedony and displays generally high SiO<sub>2</sub> and variable HCO<sub>3</sub>. Salt creek surface water and springs have a different fingerprint, having both low HCO<sub>3</sub> and SiO<sub>2</sub> and are slightly under saturated in chalcedony.

Graphing partial datasets produces similar correlations for SiO<sub>2</sub> and chalcedony SI in the Wallal Embayment, but data gaps complicate interpreting trends for the combined tectonic elements north east of the Wallal Embayment (Figure 75; graphs b and c).

Graphs of pH, alkalinity, Br and Cl/Br with depth are shown in Figure 76 and trends with depth exist for alkalinity and Br, although Br was not routinely measured (particularly in the western basin

margin) and is therefore not available for the full dataset. The pH ranges from neutral to alkaline and shows a similar range of values in the Broome, Broome LG and Wallal aquifers, with Salt Creek and spring sampling being generally alkaline. Alkalinity in Wallal aquifer upland bores has generally lower alkalinities. These values mainly show a small increase below 0m AHD, and then apart from higher values in major fault zones (e.g. WCB17 and WCB22), are relatively uniform with depth. Wallal sampling within the western basin margin is generally characterised by lower alkalinity, with the exception of bores at site WCB02, which are very high. The Broome and Broome LG aquifer sampling has a wider range of alkalinities that show no relationship with depth sampled. The highest alkalinity is sampled in a shallow (approximately 15 metres deep) Broome LG bore (circled in Figure 76; graph 18a) located within the palaeochannel interpreted to be incised into the Broome Sandstone and Jarlemai Siltstone in the Walyarta study area. Salt Creek and spring samples have lower alkalinities compared with the Broome and most Broome LG sampling and are more aligned with upland Wallal aquifer sampling (e.g. WCB18A, PB3 and NSOKidson). Rationale underpinning this patterning in these predominantly sandstone aquifers that contain acid producing minerals at depth, is conditions at depth are predominantly anoxic, and past and contemporary recharge water contains a component of ions sourced from the weathering of surficial evaporites, which increases pH and alkalinity and improves aquifer buffering capacity.

Increasing concentrations of Br with depth are apparent for both the Broome and Wallal aquifers. This trend is not persistent in Cl/Br with depth as variation in all sampling is noted to be reduced, with most samples having ratios indicating marine derived rainfall is the common source (e.g. close to ratio of 655). Samples that don't fit this trend are from the Broome LG and the Wallal aquifer sampling in the western basin margin, where variation and ratios increase. Salt Creek and spring samples display a range of Br concentrations and Cl/Br ratios. For Cl/Br, one spring sample (Saunders East 2015) plots close to samples from upland Wallal aquifer bores, while a spring sample noted to be influenced by near surface evaporation (Little Eil Eil 2015) has high Cl/Br ratios, similar to the western basin margin Wallal sampling. Meredith et. al. 2014 noted that a sub-set of samples from the Wallal aquifer in western basin margin were characterised by high Cl/Br and low Na/Cl ratios and interpreted them to be diagnostic of mixing from the overlying Broome aquifer or upward heads in the underlying basement rocks.

Graphing partial datasets impedes the interpretation of trends for both the Wallal Embayment and combined tectonic elements north east of the Wallal Embayment (Figure 76; graphs b and c).

To assess the likelihood of the precipitation or dissolution of evaporites in groundwater, modelled saturation indices are presented for calcite, dolomite and gypsum in Figure 77. Graphing results show that in the Wallal aquifer groundwater is uniformly under saturated in calcite and dolomite and that these minerals are more likely to be in solution. Conversely, for the Broome aquifer a weak trend from under saturated to saturated, is present from depths of 0 to -45m AHD, with calcite and dolomite potentially in solution at higher elevations and in equilibrium, or precipitating at depth. Some Wallal aquifer samples from the western basin margin show similar trends to the Broome aquifer. Spring data graphed show a weak increase in saturation with sampling depth and display the best alignment with Wallal, at various depths, and upland Broome aquifer sampling.

For gypsum, a trend exists for the springs, as well as the Wallal and Broome aquifers where gypsum is under saturated, and the degree of under saturation decreases with depth. Similar to trends observed with calcite and dolomite, the Wallal aquifer western basin margin sampling is more aligned with trends in the Broome than the Wallal aquifer. The Broome LG sampling shows no apparent trends with depth for calcite, dolomite and gypsum, with approximately 50% of the calcite and dolomite samples being either under saturated or saturated. The surface water sample graphed, (Salt Creek) is consistently saturated with respect to calcite, dolomite and gypsum.

Graphing partial datasets impedes the interpretation of trends for both the Wallal Embayment and combined tectonic elements north east of the Wallal Embayment (Figure 77; graphs b and c). In summary the graphing of analytes with depth (Figures 72 to 77) provides an important three dimensional appreciation of patterning to assess hydrogeological processes (e.g. connectivity, mixing and water-rock interactions).

Results of interpreting the graphing show that the Broome aquifer hydrogeochemical fingerprint perseveres for different analytes (e.g. Ca, Mg, K,  $\text{SO}_4$  and  $\text{SiO}_2$ ) and ratios (e.g.  $\text{SO}_4/\text{Cl}$  and  $\text{SO}_4/\text{Ca}$ ) to depths of -50 to -100mAHD, and possibly deeper in fault zones. The Broome LG aquifer sampling tends to at a discrete depth range, close to 0mAHD, and is characterised by a broad range of analyte, ratio and modelled mineral SI values, but compared with the Broome aquifer generally has elevated Na, Ca, Mg, Ca/Cl,  $\text{SO}_4/\text{Cl}$  and  $\text{SiO}_2$  and in shallow palaeochannels, Na, Ca,  $\text{HCO}_3$ ,  $\text{SO}_4/\text{Cl}$ , and alkalinity. The Wallal aquifer displays five main trends with depth, and consequently flow path, and they are;

- connectivity/mixing with the Broome aquifer (-50 to -100mAHD) (as per above),
- uniform ( $\text{HCO}_3$ , pH, alkalinity, Cl/Br, calcite and dolomite SI),
- increasing (TDS, Na,  $\text{SO}_4$ , K,  $\text{HCO}_3/\text{SiO}_2$ , Br),
- decreasing (Ca/Cl, gypsum SI) and
- stratification below  $\sim$ -200mAHD (Cl, Na/Cl, Ca,  $\text{HCO}_3/\text{Cl}$ ,  $\text{SO}_4/\text{Cl}$ ,  $\text{SO}_4/\text{Ca}$ ,  $\text{SiO}_2$ , chalcedony SI).

Elevated values in fault zones below -100mAHD are apparent in TDS, Cl, Na, Ca, Mg, K, Ca/Cl, and  $\text{HCO}_3/\text{SiO}_2$ .

This information indicates that hydrogeochemically the Wallal aquifer in upland locations (46 to 22mAHD) could contribute to spring discharge. This is due to similarities in hydrogeochemistry and the likelihood the aquifer chemistry evolves along the flow path, with increasing depth (mAHD), in response to system conditions in the uplands promoting the timely recharge and mixing with the Broome aquifer groundwater. Noting that in this conceptualisation the discharge from the Wallal aquifer at depth up to -100mAHD may share hydrogeochemical characteristics of the Broome aquifer.

HYDROLOGICAL CONCEPTUALISATION OF THE WALYARTA MOUND SPRINGS

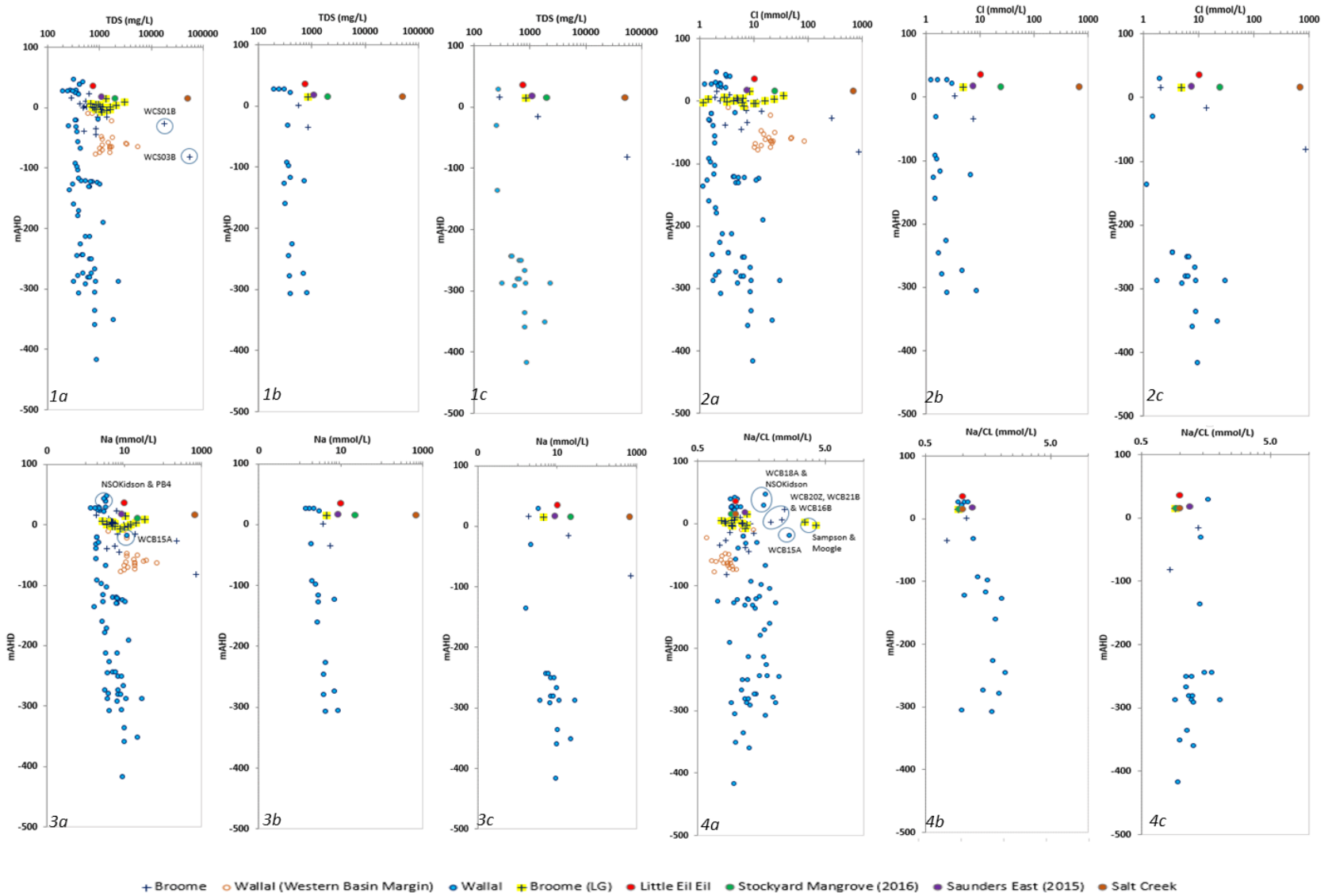


Figure 72 Scatterplots showing analyte concentrations 1. total dissolved solids (TDS) (mg/L), 2. chloride (Cl) (mmol/L), 3. sodium (Na) (mmol/L) and 4. Na/Cl (mmol/L) against depth sampled (mAHD); a=full dataset, b=Wallal Embayment data & c=Wallal Platform/Samphire Embayment & Willara sub-basin



HYDROLOGICAL CONCEPTUALISATION OF THE WALYARTA MOUND SPRINGS

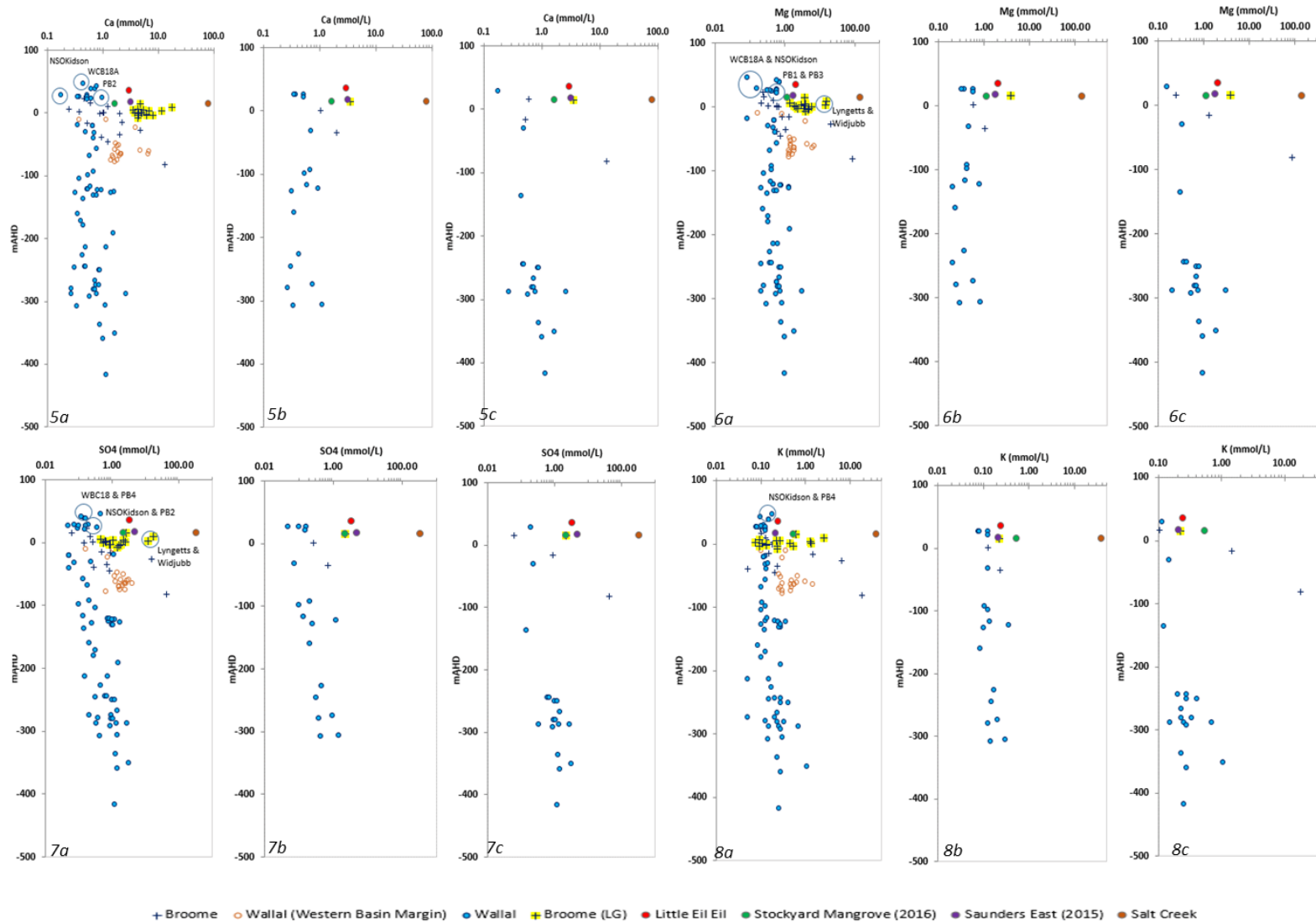


Figure 73 Scatterplots showing analyte concentrations 5. calcium (Ca) (mmol/L), 6. magnesium (Mg) (mmol/L), 7. sulfate (SO<sub>4</sub>) (mmol/L) and 8. K (mmol/L) with depth sampled (mAHD); a=full dataset, b=Wallal Embayment data & c=Wallal Platform/Samphire Embayment & Willara sub-basin

HYDROLOGICAL CONCEPTUALISATION OF THE WALYARTA MOUND SPRINGS

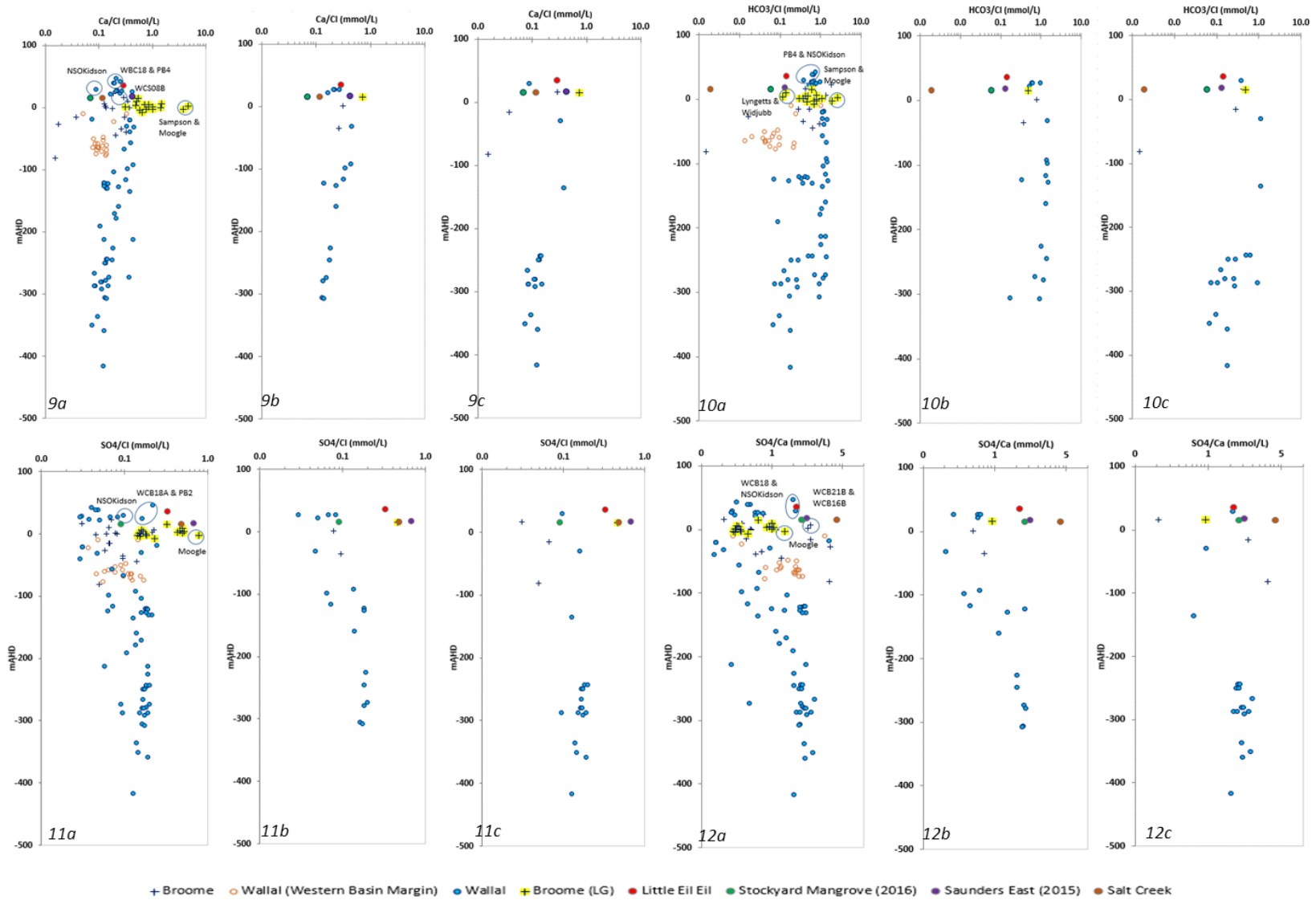


Figure 74 Scatterplots showing analyte concentrations 9. Ca/Cl (mmol/L), 10. HCO<sub>3</sub>/Cl (mmol/L), 11. SO<sub>4</sub>/Cl (mmol/L) and 12. SO<sub>4</sub>/Ca (mmol/L) with depth sampled (mAHD); a=full dataset, b=Wallal Embayment data & c=Wallal Platform/Samphire Embayment & Willara sub-basin

HYDROLOGICAL CONCEPTUALISATION OF THE WALYARTA MOUND SPRINGS

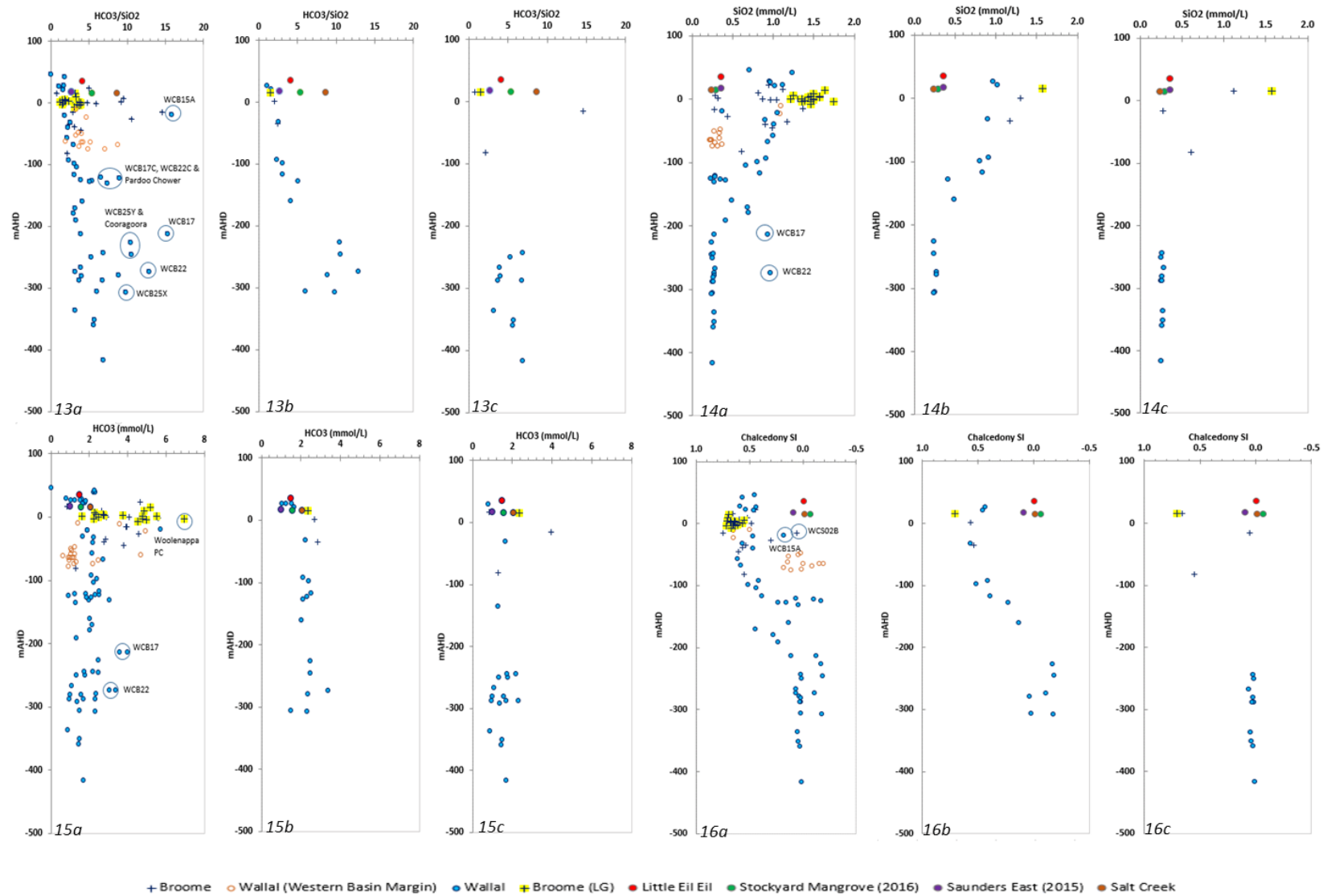


Figure 75 Scatterplots showing analyte concentrations 13. HCO<sub>3</sub>/SiO<sub>2</sub> (mmol/L), 14. SiO<sub>2</sub> (mmol/L), 15. HCO<sub>3</sub> (mmol/L) and 16. modelled chalcedony SI with depth sampled (mAHD); a=full dataset, b=Wallal Embayment data & c=Wallal Platform/Samphire Embayment & Willara sub-basin

HYDROLOGICAL CONCEPTUALISATION OF THE WALYARTA MOUND SPRINGS

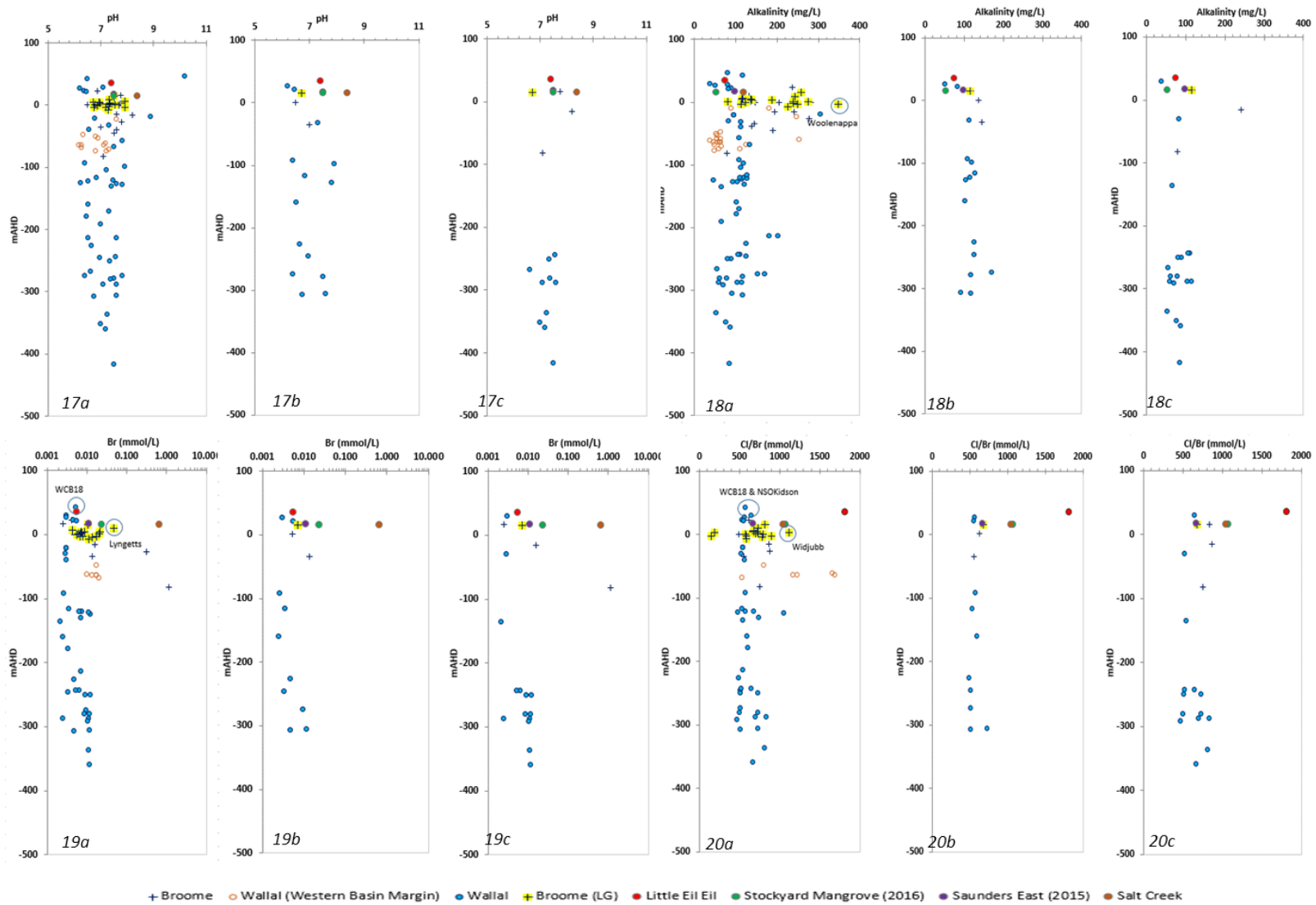


Figure 76 Scatterplots showing 17. pH, 18. alkalinity (mg/L) and analyte concentrations 19. bromine (Br) (mmol/L) and 20. Cl/Br (mmol/L) with depth sampled (mAHID); a=full dataset, b=Wallal Embayment data & c=Wallal Platform/Samphire Embayment & Willara sub-basin



HYDROLOGICAL CONCEPTUALISATION OF THE WALYARTA MOUND SPRINGS

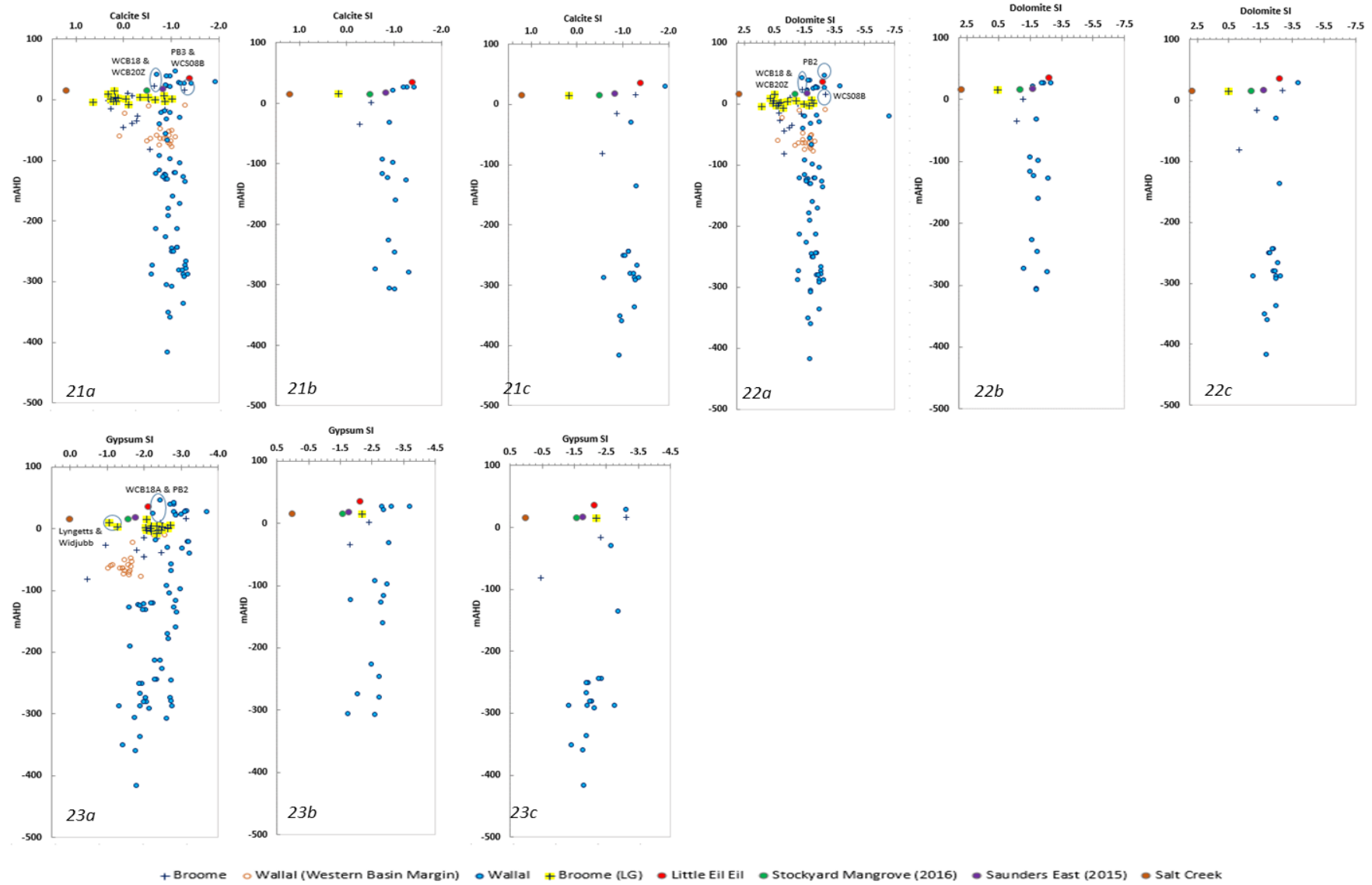


Figure 77 Scatterplots showing modelled 21. calcite SI, 22. dolomite SI and 23. gypsum SI with depth sampled (mAHD); a=full dataset, b=Wallal Embayment data & c=Wallal Platform/Samphire Embayment & Willara sub-basin

Analytes, ratios and modelled mineral SI's diagnostic for the Wallal aquifer (depths greater - 100mAHD) contributing to spring discharge are under saturation in chalcedony, low  $\text{SiO}_2$ ,  $\text{HCO}_3$ ,  $\text{HCO}_3/\text{Cl}$ , alkalinity and elevated  $\text{Cl}/\text{Br}$ ,  $\text{SO}_4$  and  $\text{SO}_4/\text{Ca}$ . However, these Wallal indicators may also be near surface reaction indicators. Changes in the near surface environment (e.g. pressure, temperature, Eh-pH, and biogeochemical changes) could be influencing spring chemistry. Supporting evidence from environmental isotopes is therefore required to strengthen the identification of hydrogeochemical indicators and this is covered in Section 7.3.4.

An important outcome of work in this section is, in the WCB the Wallal aquifer shows consistency in hydrogeochemistry with depth sampled, and along flow paths where this corresponds to a thickening of the Wallal Formation. This increases confidence in using the results to predict the Wallal aquifer hydrogeochemistry, where there is sparse bore data by on formation thickness.

### 7.1.1 Environmental isotopes

Hydrological information from environmental isotopes sampled from ninety bore and spring sites are discussed in this report (Table 10). These data were sourced from three main programs of work undertaken by state government agencies. The Department of Biodiversity, Conservation and Attractions (DBCA; previously DPAW) undertook spring sampling between 2015 and 2016. ANSTO sampled and reported on environmental isotope results from existing and redrilled bores in the West Canning Basin for the Department of Water and Environmental Regulation (DWER; previously DOW) between 2008 and 2014. Further drilling and sampling was undertaken by DWER between 2015 and 2017 (Table 10) and during the same period the Department of Primary Industry and Rural Development (DPIRD; previously DAFWA) also sampled mainly shallow Broome aquifer bores within and to the north of the Walyarta study area. Sampling and analyses methods are outlined in Meredith et. al. 2014, Harrington and Harrington 2016 and 2017.

#### 7.1.1.1 Stable Water Isotopes (SWI's: $\delta^{18}\text{O}$ and $\delta^2\text{H}$ )

Over the past decade stable water isotopes have been collected in the West Canning Basin in order to understand processes controlling groundwater recharge and the evolution of water along groundwater flow paths.

Work undertaken in 2015 in the La Grange area, north of the Walyarta study area, identified rainfall has a wet and dry season stable isotope signature (Harrington and Harrington 2016). Results report that from a limited dataset ( $n < 12$ ) the wet season rainfall is more depleted in heavy isotopes (e.g. more negative  $\delta^2\text{H}$  and  $\delta^{18}\text{O}$ ), which is important for groundwater recharge studies as the wet season generally provides the greater amount of rainfall (Harrington and Harrington 2016).

Meredith et. al. (2018) also notes that other rainfall isotopic studies in northern Australia have found that cyclonic systems are typically more depleted in  $\delta^{18}\text{O}$  compared with  $\delta^2\text{H}$  depletion of heavy isotopes in rainfall. The regression equation developed for the La Grange wet season Local Meteoric Water Line ( $\delta^2\text{H} = 7.5 \delta^{18}\text{O} + 9.4$ ) is noted to be similar to that developed for heavy rain events (rainfall  $> 20\text{mm}$ ) in the Pilbara region by Dogramaci et. al. 2012 ( $\delta^2\text{H} = 7.03 \delta^{18}\text{O} + 4.78$ ;  $n = 8$ ).

HYDROLOGICAL CONCEPTUALISATION OF THE WALYARTA MOUND SPRINGS

Bore and Spring ID	Date sampled	Sample Custodian	Aquifer	Elevation mAHD	$\delta^{13}C_{DIC}$ ‰	$\delta^{14}C_{DIC}$ ‰	$\delta^2H$ ‰	$\delta^{18}O$ ‰	$\delta^{87}Sr$ ‰	Sr $\mu mol/L$	Rb $\mu mol/L$
WCB21Z	22/05/2012	DWER	Broome	38	-10.49	72.27	-57.20	-8.07	6.45	2.7	0.09
WCB24Z	21/05/2012	DWER	Broome	44	-12.80	84.07	-56.90	-7.87	5.49	5.9	0.15
WCB25Z	6/06/2012	DWER	Broome	16	-11.22	60.56	-55.60	-7.67	7.02	9.6	0.27
WCB20Z	22/05/2012	DWER	Broome	78	-11.77	93.49	-55.60	-7.62	3.83	2.4	0.08
15LAG21D	17/11/2015	DPIRD	Broome	37			-50.60	-7.32			
15LAG21S	17/11/2015	DPIRD	Broome	37			-54.30	-7.90			
15LAG24D	17/11/2015	DPIRD	Broome	22	-4.40	27.98					
15LAG24S	17/11/2015	DPIRD	Broome	22	-9.30	79.62					
MRD gravel pit bore		DPIRD	Broome	18			-56.40	-7.84			
MRD Teds bore		DPIRD	Broome	33			-56.40	-7.84			
WCB10B	4/12/2008	DWER	Wallal	24	-14.60	0.50	-55.25	-7.59		9.2	0.28
WCB04B	4/12/2008	DWER	Wallal	17	-12.30	0.70	-56.40	-7.79	12.40	13.7	0.47
WCB04B_R	8/06/2012	DWER	Wallal	17	-15.40	0.30	-59.32	-7.71		14.0	0.54
WCB08C	12/03/2008	DWER	Wallal	17	-12.40	3.80	-56.00	-7.13		7.8	
NSOKidson	13/11/2015	DWER	Wallal	119			-57.40	-7.93			
NMCA03E	25/05/2013	DWER	Wallal	125	-10.98	73.17	-57.10	-7.94	9.13	2.3	0.08
WCB23B	25/05/2013	DWER	Wallal	13	-12.31	48.29	-57.80	-8.02	6.73	2.2	0.08
WCB15Y	5/06/2012	DWER	Wallal	88	-12.20	69.70	-58.60	-8.32	7.32	2.6	0.07
PB3	2/12/2008	DWER	Wallal	139	-12.20	81.70	-61.18	-8.20		2.4	0.07
PB1	2/12/2008	DWER	Wallal	134	-13.10	77.30	-60.95	-8.35		3.3	0.09
WCB18	23/05/2013	DWER	Wallal	161	-10.00	89.00	-57.00	-8.15	7.23	3.2	0.06
WCB09E	12/03/2008	DWER	Wallal	11	-17.80	0.05	-58.33	-7.95		8.2	0.30
WCB17C	12/03/2008	DWER	Wallal	19	-10.60	22.50	-56.15	-7.65		2.7	
Pardoo-Chower	7/06/2012	DWER	Wallal	20	-9.40	12.90	-53.70	-7.40	12.92	4.0	0.18
WCB08A	12/03/2008	DWER	Wallal	17	-12.40	3.80	-56.00	-7.13		7.8	0.27
WCB19	23/05/2013	DWER	Wallal	110	-12.90	61.60	-57.80	-8.19	7.09	2.2	0.07
WCS10A	11/11/2015	DWER	Wallal	124			-57.10	-8.04			
WCS11A		DWER	Wallal	20			-58.00	-8.56			
WCB20Y	24/05/2013	DWER	Wallal	78	-11.00	54.80	-58.40	-7.98	8.49	1.9	0.11
WCB24Y	21/05/2013	DWER	Wallal	44	-12.40	44.60	-57.20	-8.02	9.27	1.6	0.08
WCB21Y	22/05/2013	DWER	Wallal	38	-10.50	45.00	-57.70	-7.98	9.69	2.0	0.09
WCB17	3/12/2008	DWER	Wallal	19	-10.60	22.50	-56.20	-7.65		2.7	0.18
CooragooPB1	7/06/2012	DWER	Wallal	13	-10.30	27.30	-56.80	-7.94	13.70	2.4	0.13
WCB25Y	6/06/2012	DWER	Wallal	16	-10.90	29.90	-56.20	-7.95	13.50	1.7	0.13
WCS04A	15/11/2015	DWER	Wallal	40			-59.30	-7.70			
WCS04A_R	22/03/2017	DWER	Wallal	40			-56.40	-7.79			
WCB22	12/03/2008	DWER	Wallal	13	-10.80	16.80	-54.81	-7.58		4.1	0.34
WCS06A_R	15/11/2015	DWER	Wallal	21			-53.20	-7.51			
ArtesianBore	25/11/2014	DWER	Wallal	17			-55.99	-7.48			
WCS01A	20/03/2017	DWER	Wallal	5			-54.50	-7.27			
WCB25X	6/06/2012	DWER	Wallal	16	-11.10	32.20	-56.70	-8.08	11.88	1.5	0.13
WCS02A	20/03/2017	DWER	Wallal	5			-53.20	-7.20			
WCS05A		DWER	Wallal	27			-54.30	-7.51			
WCS06C		DWER	Wallal	19			-54.00	-7.56			
WCS12A		DWER	Wallal	121			-59.00	-8.32			
WCS13A		DWER	Wallal	198			-57.40	-8.29			
WCS07A		DWER	Wallal	83			-55.10	-8.14			
WCS08A		DWER	Wallal	87			-57.70	-8.41			
WCS09A		DWER	Wallal	140			-56.10	-7.89			
MRD Sandfire	22/03/2017	DWER	Wallal	17	-10.20	11.41	-52.50	-7.79			
MRD Sandfire	16/11/2015	DPIRD	Wallal	17	-6.00	13.24					
Corbetts bore new		DPIRD	Broome	33.6						2.4	
Coolgardie well		DPIRD	Broome	7.2						1.5	
MANDORA_Bakers bore		DPIRD	Broome	21.0						2.7	
Tafts new bore		DPIRD	Broome	28.5						5.9	
Moojan bore		DPIRD	Broome	7.2						9.6	
Moogle bore		DPIRD	Broome	12.3						3.3	
Sampson well		DPIRD	Broome	19.4						2.4	
House bore west		DPIRD	Broome	9.6						13.7	
Dellas bore		DPIRD	Broome	16.0						8.2	
Garden bore solar		DPIRD	Broome	7.7						9.2	
Walnut bore		DPIRD	Broome	31.4						3.0	
Woolenappa bore		DPIRD	Broome	12.1						4.1	
House garden well		DPIRD	Broome	6.8						6.4	
Lyngetts well		DPIRD	Broome	14.7						8.3	
Nalgi well		DPIRD	Broome	6.1						5.8	
Widjubb Bore 2		DPIRD	Broome	7.7						5.8	
Friday_Well	31/08/2015	DBCA	Broome	10	-8.7	93.05	-51.43	-7.36	5.61	24.2	0.70
Dingo_Spring_2016	24/11/2016	DBCA		37	-14.8	51.96	-56.3	-7.74	8.86	25.8	0.69
Fern_Peat_2016	25/11/2016	DBCA		14	-16.8	71.77	-54.8	-7.06	7.18	37.7	1.06
Linear_Spring_2016	24/11/2016	DBCA		48	-11.8	76.61	-55.9	-7.64	7.94	10.0	0.22
Little_EilEil_2016	24/11/2016	DBCA		31	-11.4	41.43	-52.3	-7.61	7.14	8.6	0.17
Saunders_East_2016	25/11/2016	DBCA		11	-13.2	64.86	-53.7	-7.16	8.05	8.4	0.21
Stockyard_Mangrove_2016	25/11/2016	DBCA		10	-11.6	16.36	-55.0	-7.48	9.43	17.5	0.41
Stockyard_Mangrove2_2016	25/11/2016	DBCA		10	-13.4	50.82	-56.6	-7.17	10.59	17.0	0.50
Top_Spring_2016	24/11/2016	DBCA		52	-13.7	92.36	-51.8	-6.67	7.59	19.5	0.27
Bretts_Open_1	2/09/2015	DBCA		35	-13.3	93.39	-43.86	-5.49	6.92	30.1	0.53
EilEil_Spring	2/09/2015	DBCA		40	-11.5	94.63	-45.45	-5.74	7.14	17.5	0.44
Fern_Peat_2015	3/09/2015	DBCA		17	-16.4	70.67	-48.37	-6.26	9.01	39.1	1.55
Fern_Tail	3/09/2015	DBCA		15	-7.7	101.65	-44.15	-5.49	9.07	54.8	1.92
Little_EilEil_2015	2/09/2015	DBCA		35	-12.6	71.39	-56.12	-8.23	7.22	10.5	0.21
Melaleuca_Moat	3/09/2015	DBCA		15	-10.9	85.97	-41.91	-4.99	7.90	34.9	0.77
Melaleuca_Peat	3/09/2015	DBCA		17	-14.4	85.74	-50.00	-6.87	7.91		0.00
MMS19_Stromatolite	1/09/2015	DBCA		20	-14.1	92.62	-7.02	2.62	10.25	73.7	14.05
Salt_Creek_7	1/09/2015	DBCA		15	-12.4	95.91	10.03	6.20	10.41	216.8	17.21
Saunders_Open_2	3/09/2015	DBCA		15	-10.4	55.94	-36.9	-4	7.78	7.5	0.79
Saunders_East_2015	3/09/2015	DBCA		17	-9.7	65.12	-51.79	-7.10	7.91	9.4	0.28
Saunders_Peat	3/09/2015	DBCA		17	-15.5	83.76	-52.59	-7.21	7.92	11.5	0.48
Saunders_West	3/09/2015	DBCA		15	-12.4	87.5	-50.06	-7.09	7.89	9.1	0.37
Stockyard_Mangrove2_2015	4/09/2015	DBCA		15	-11.5	75.01	-48.86	-6.79	10.61	15.4	0.53

Table 10 Environmental isotopes and Sr and Rb ( $\mu mol/L$ ) sampling examined in this report

Dogramaci et. al. (2012) also reports a Local Evaporation Line (LEL) ( $\delta^2\text{H} = 15.6 \delta^{18}\text{O} - 14.37$ ;  $n=189$ ) and the Pilbara LMWL and LEL have been used previously to report results in the West Canning Basin (e.g. Meredith et. al. 2014 and 2018).

Figure 78 displays stable isotope data presented in Table 10 ( $n=71$ ) in bivariate plots of  $\delta^2\text{H}$  vs  $\delta^{18}\text{O}$  and compares data against the Harrington and Harrington (2016) LMWL and LEL from Dogramai et. al. (2012). Overall the interpretation of data presented in Figure 78 are in agreement with those reported by Meredith et. al. 2014 and 2018.

Data in Figure 78a. show groundwater in the Wallal and Broome aquifers is similar to rainfall and has undergone enrichment, with negative values indicative of vadose zone soil-water evaporation taking place prior to recharge, rather than open water body evaporation (Meredith et. al. 2018). Greater depletion in heavy isotopes occurs within upland Wallal aquifer sampling and this may be explained by more rapid recharge to groundwater due to the Wallal Formation being closer to the ground surface and the Jarlemai Siltstone aquitard being thin or absent (Appendix 1).

The Wallal and Broome aquifer groundwater and spring and surface water all align with the LEL. As spring samples were collected at, or just below, the ground surface in the dry season this provides evidence of groundwater discharge supporting the springs. Some springs show more negative values than others (e.g. upgradient spring Little Eil Eil 2015, Figure 78a) and plot near the samples collected from upland Wallal aquifers. Seasonal constraints are also evident for Little Eil Eil, where sampling on consecutive years (2015 and 2016), with 2016 being a drier, dry season, results in stable isotope enrichment and alignment with a deep Wallal bore and shallow Broome well in the Walyarta study area as well as a deeper Broome bore in the La Grange area (e.g. 15LAG21D) (Figure 78a.). Surface water evaporation enriches stable isotope values of water sampled in perennial pools and drainages (e.g. MMS Stromatolite Pool and Salt Creek, not graphed see Table 10). Enrichment is also noted in spring moat samples and to a lesser degree samples within springs with peat substrates that are characterised by higher water retention and as a consequence evaporation.

To gain a better understanding of evaporation processes on stable isotope enrichment  $\delta^{18}\text{O}$  data are graphed over chloride in Figure 78b. Results show that in the Wallal aquifer there is a good correlation between increasing chloride and  $\delta^{18}\text{O}$  enrichment, where chloride concentration doesn't exceed 10 mmol/L. No relationships are evident for the Broome, Broome LG and Wallal western basin margin (e.g. WCB04 and WCB10) or Wallal bores in the Walyarta study area (e.g. MRD Anna Plains & MRD Sandfire) (Figure 78b. & Table 10). A relationship exists for the complete spring and surface water sampling dataset as the higher values produced by open water evaporation influence the correlation. However, the range of chloride concentrations below stable isotope  $\delta^{18}\text{O} < -7\text{‰}$  values is high for the Wallal, Broome, Broome LG and spring datasets and further interrogation of the data in three dimensional space is required to assess and fingerprint the aquifer(s) supporting the springs.

To progress this,  $\delta^{18}\text{O}$  stable isotope data are plotted on the Wallal Embayment geological cross section using data from bores in Figure 71. Stable isotope data exist for a subset of bores in Figure 71 (Table 10) and they are plotted on Figure 79, together with a bivariate plot of  $\delta^{18}\text{O}$  against depth sampled in mAHD.



HYDROLOGICAL CONCEPTUALISATION OF THE WALYARTA MOUND SPRINGS

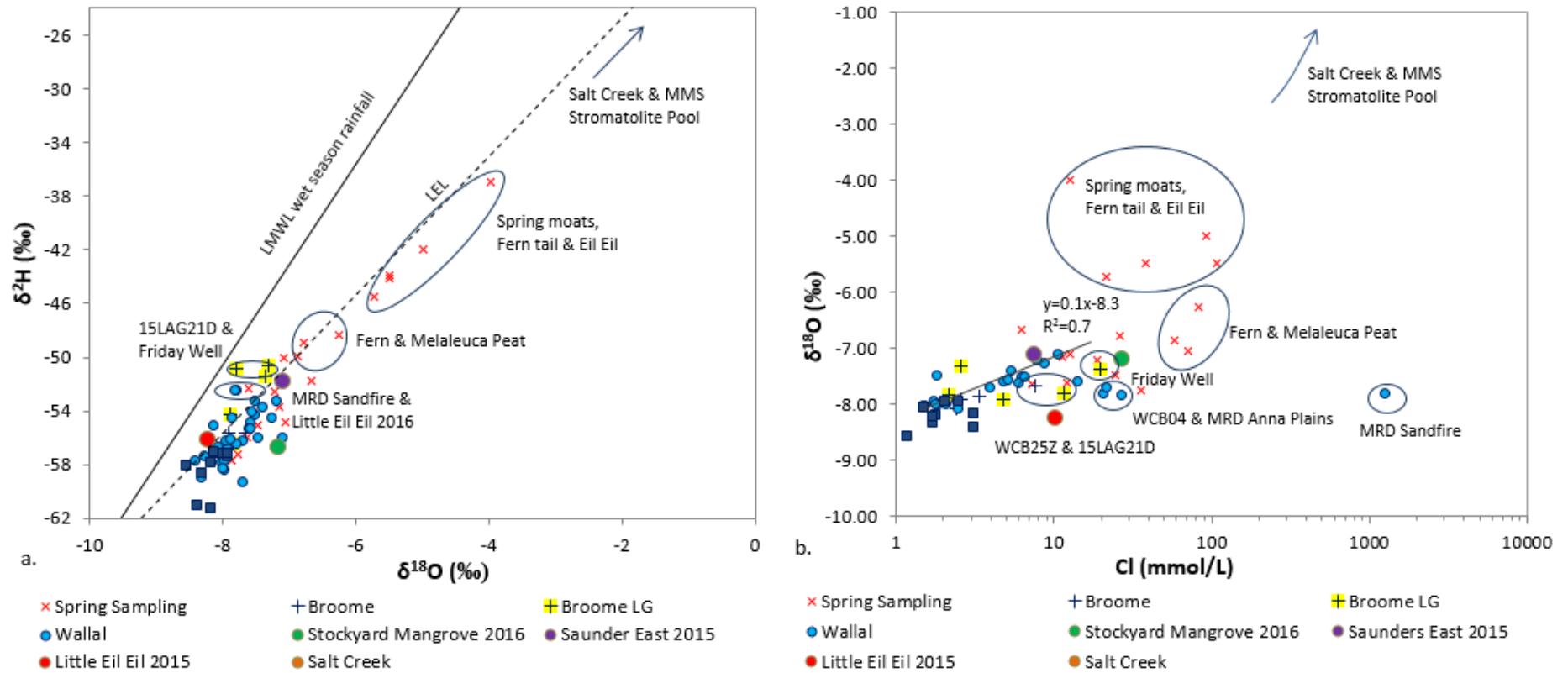


Figure 78 Bivariate plots of a.  $\delta^2\text{H}$  vs  $\delta^{18}\text{O}$ , showing La Grange wet season Local Meteoric Water Line (LMWL) ( $\delta^2\text{H} = 7.5 \delta^{18}\text{O} + 9.4$  (Harrington and Harrington 2016) and Pilbara Local Evaporation Line (LEL) (Dogramaci et. al. 2012) and b.  $\delta^{18}\text{O}$  vs. log Cl (mmol/L) (observations sourced from  $\delta^2\text{H}$  and  $\delta^{18}\text{O}$  data in Table 10; note that Wallal upland bores are shown as blue squares)

Data presented in the Figure 79 cross section show stable isotope enrichment increases with depth sampled. Stable isotope  $\delta^{18}\text{O}$  data within fault zones show subtle isotopic enrichment, suggesting a different stable isotope signature is preserved here. Greatest stable isotope enrichment occurs in the deeper Wallal aquifer and depth of sampling tends to coincide with length along the groundwater flow path and increases in aquifer hydraulic head. As deeper drilling doesn't screen and sample the overlying upper Wallal aquifer and Alexander Formation, the degree of mixing in the Wallal aquifer remains unverified near the coast.

Spatial data gaps increases interpretation uncertainty, as does not knowing the isotopic composition of historical rainfall and the role of contemporary landscapes and climate. Although, global scale modelling undertaken by Jasechko et al. (2015) predicts rainfall in the Last Glacial Maximum (LGM) was more enriched (0.5 to 1‰) while recent stable isotope modelling by Hollins et. al. (in press) develops and reports on Australian isoscapes and identifies other criteria that influence the stable isotope composition of rainfall (e.g. distance from the coast, topographic elevation, temperature and latitude). More sampling and interrogation of existing data required in the WCB to verify new models.

Plotting stable isotope data with depth for the full dataset (Table 10) shows a linear relationship exists, with  $\delta^{18}\text{O}$  increasing with depth sampled. Less variation is observed below depths of around -150mAHD and above this depth sub populations occur at two distinct depth intervals, around -20 to -80mAHD and -90 to -130mAHD, which show small increases with depth that also correspond to increases in chloride at depth and may verify the existence of broader scale stratification (Figure 72).

Spring samples from Little Eil Eil (2015) and Stockyard Mangrove (2016) are enriched compared to upland Wallal bores sampled. This infers spring discharge is unlikely to be directly derived from these aquifers and isotopic data are influenced/overprinted by recent cyclonic events. Springs appear to have a greater commonality with stable isotope enrichment ( $\delta^{18}\text{O}$ ) within three population trends. The western basin margin Wallal groundwater sampled at WCB08B or Pardoo Chowder, at respective depths of ~-69mAHD and -127mAHD and Wallal groundwater sampled within fault zones in the Wallal Embayment or Willara sub-basin (e.g. WCB22 & MRD Sandfire at depth ~-275mAHD). Other environmental tracer data is required to reduce uncertainty on the more likely depth that Wallal groundwater is discharging at the springs and this is explored in the following sections.

#### **7.1.1.2 Strontium**

Strontium (Sr), Rubidium (Rb) and strontium ( $\delta^{87}\text{Sr}$ ) isotopic data were analysed in work undertaken by ANSTO for DWER (Table 10, Appendix 7), as well as DBCA spring and surface water investigations (Table 10, Harrington and Harrington 2017).

Meredith et. al. 2018 report that correlations exist between strontium, rubidium and chloride, indicating a common source and process is responsible for their distribution, for the latter this is likely to point to evapotranspiration and uniform mixing along groundwater flow paths.

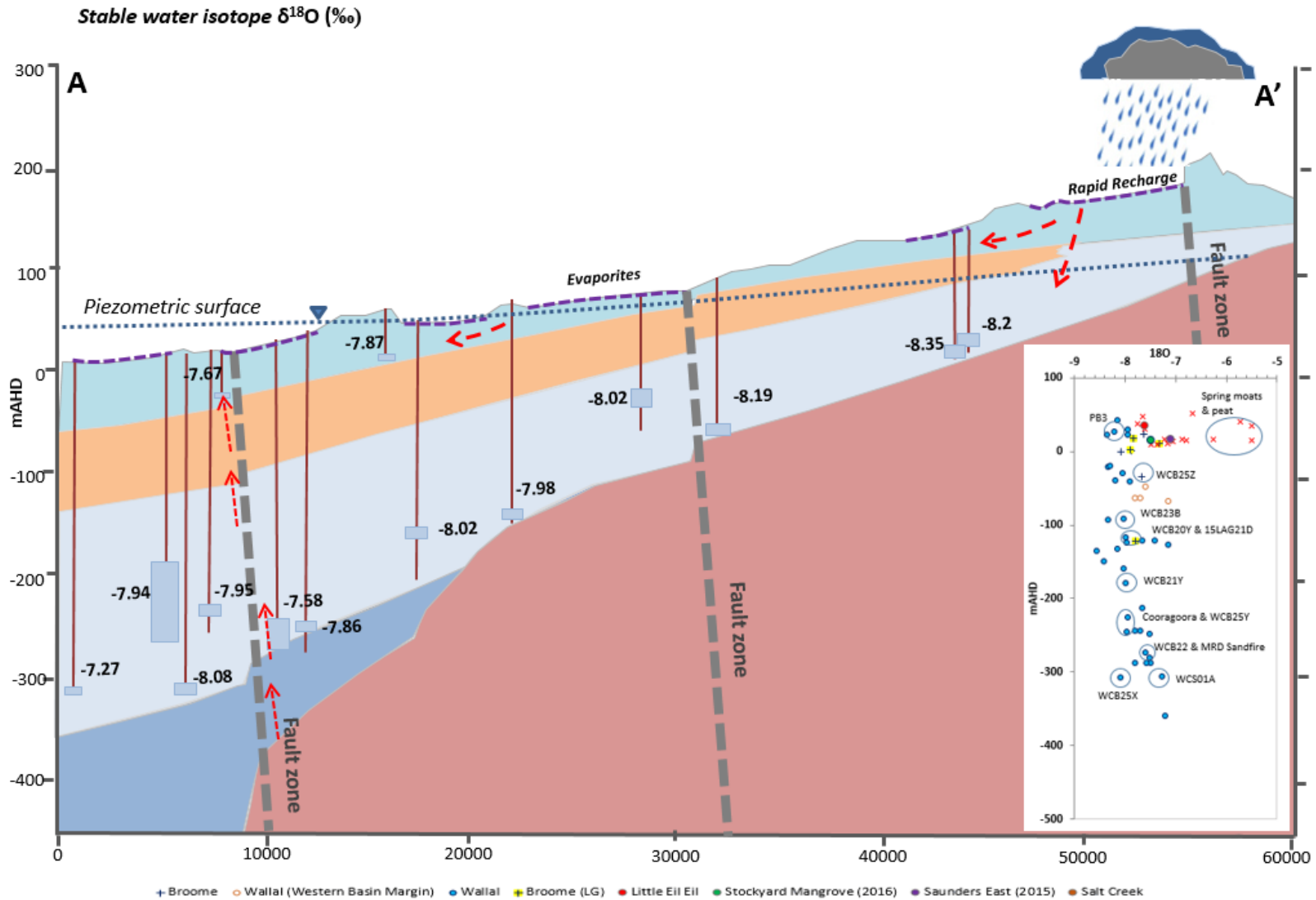


Figure 79 Wallal Embayment geological X-Section A'-A (from Figure 71) showing the location of the sub set of bores sampled for stable water isotopes,  $\delta^{18}\text{O}$  results from Table 10, arrows showing the direction of groundwater and soil water movement, piezometric surface from Meredith et. al. 2018 and bivariate plot  $\delta^{18}\text{O}$  vs depth sampled (mAHd) (all data Table 10).

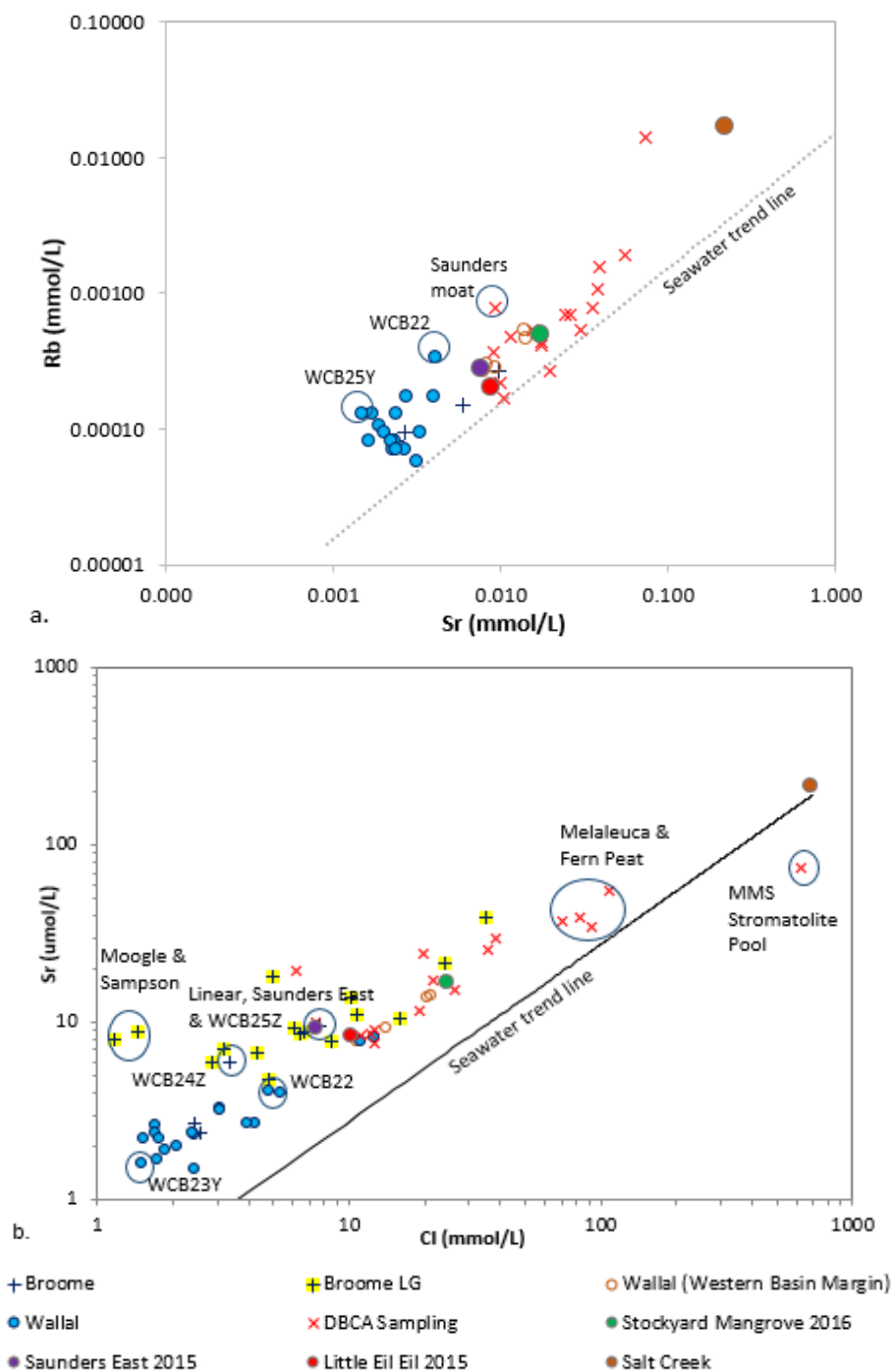


Figure 80 Bivariate plots of a. log Rubidium (Rb) vs log Strontium Sr (mmol/L) and b. log Strontium Sr (µmol/L) vs log Cl (mmol/L)

The respective average and median values for Rb/Sr ratios for data presented in Figure 80 from Table 10 is 0.04 and 0.035. This is higher than the average carbonate sedimentary rock (e.g. <0.01) but low compared to values for shales, granitoid rocks and clay minerals produced from the chemical weathering of granitoids (Dogramaci and Skrzypek 2015).

These relationships were examined within a larger dataset, with Rb vs Sr and Sr vs Cl plotted in Figure 80. Results show an overall correlation exists for the full population graphed in both bivariate



plots. The Rb against Sr dataset shows common enrichment in Rb compared to seawater and elevated Rb over Sr where sampling occurs in mapped fault zones (e.g WCB22 and WCB25Y) as well as DBCA surface water sampling in Salt Creek, MMS stromatolite pool and Saunders moat (Figure 80). However, quantitative relationships for sub populations, different aquifers, are not convincing, which may reflect that concentrations are close to limits of detection (LOD) (Table 10) and/or there are different source rocks and/or there is insufficient sampling to assess trends (Figure 80).

Graphing Sr against Cl produces similar overall trends but different relationships for sub populations, with large variation noted for the Broome LG aquifer (Figure 80). DBCA surface water samples from Salt Creek, Melaleuca moat and MMS stromatolite pool are either the same, or close to, seawater concentrations. Broome LG, as well as Wallal aquifer and spring samples display elevated Sr with respect to chloride (Figure 80). There is a relatively wide range of Sr concentrations, with higher values noted to occur in faults zones mapped in this report, some of which are coincident with interpreted shallow palaeochannels incised into the Jarlemai Siltstone aquitard.

Technically, strontium in primary silicate minerals will be taken into clay lattices during weathering. Cation exchange reactions are likely to follow resulting in clay minerals substituting strontium for other bivalent ions (e.g. calcium and magnesium), or vice versa. Strontium may also replace calcium in carbonates, with Ca/Sr ratios having potential to discriminate strontium sources and mobility. Dogramaci and Skrzypek (2015) use Ca/Sr ratios to develop mixing calculations for the three main sources of solutes in groundwater (e.g. precipitation, carbonates and shales and clays). This work was carried out in the Pilbara Region, which is characterised by older and more radiogenic lithologies (e.g. higher Rb/Sr,  $^{87}\text{Sr}/^{86}\text{Sr}$  and  $\delta^{87}\text{Sr}$ ). A comparable approach is trialled here in younger, less radiogenic geology. Although it is important to note that as strontium concentrations are low, near surface interpretations need to be treated with caution due to the potential for past marine sources of strontium to contribute and overprint relationships/trends.

Work in the previous sections of this report show calcium concentrations in the Broome and Wallal aquifer are generally higher in the near surface (upper 50 metres) and variable with depth (~50 to 400 metres below ground level) (Figure 73). Calcium concentrations, with respect to chloride, generally decrease with depth and show less variation (Figure 74). Ratios of calcium over strontium are plotted in relation to chloride and  $\delta^{87}\text{Sr}$  in Figure 81 to assess if calcium and strontium have a common source and process that mobilises and concentrates both ions. These results are then compared with strontium isotope values to understand if common or different trends are apparent.

Data presented in Figure 81 a. and c. show the Broome aquifer is typified by low to moderate Ca/Sr (50 to 100 mg/L), lower  $\delta^{87}\text{Sr}$  (<7 ‰) and  $^{87}\text{Sr}/^{86}\text{Sr}$  isotopic values. The Wallal aquifer is different, with increasing  $\delta^{87}\text{Sr}$  and  $^{87}\text{Sr}/^{86}\text{Sr}$  correlated with decreasing Ca/Sr and 1/Sr (mmol/L). For the Wallal aquifer the most radiogenic groundwater is located in a mapped fault zone where deeper bores are in closer connection to Permian sediments (e.g. shales) and weathered crystalline basement rocks (Figure 82). DBCA springs and surface water samples are also more radiogenic compared with the Broome aquifer (in particular Stockyard Mangrove 2016 and Salt Creek; Figure 81a.) and form a distinct population with low Ca/Sr (<50 mg/L). Spatial trends in the Broome aquifer Ca/Sr dataset are unclear and this is likely to be due to calcium having a dual source (e.g. sourced from silicate as well as carbonate reactions).

HYDROLOGICAL CONCEPTUALISATION OF THE WALYARTA MOUND SPRINGS

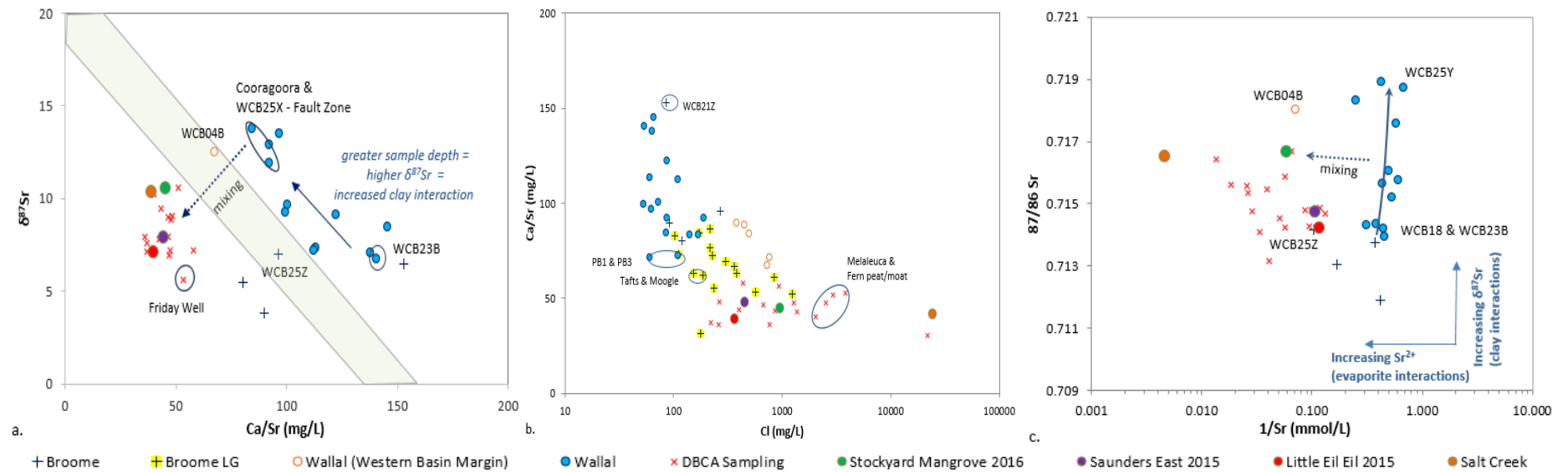


Figure 81 Bivariate plots of a. Ca/Sr (mg/L) vs  $\delta^{87}\text{Sr}$ , b. log chloride (Cl) vs Ca/Sr (mg/L) and c. log 1/Sr (mmol/L) vs  $^{87}\text{Sr}/^{86}\text{Sr}$  (solid blue line with arrow in c. represents Wallal aquifer groundwater flow path & increasing depth sampled)

HYDROLOGICAL CONCEPTUALISATION OF THE WALYARTA MOUND SPRINGS

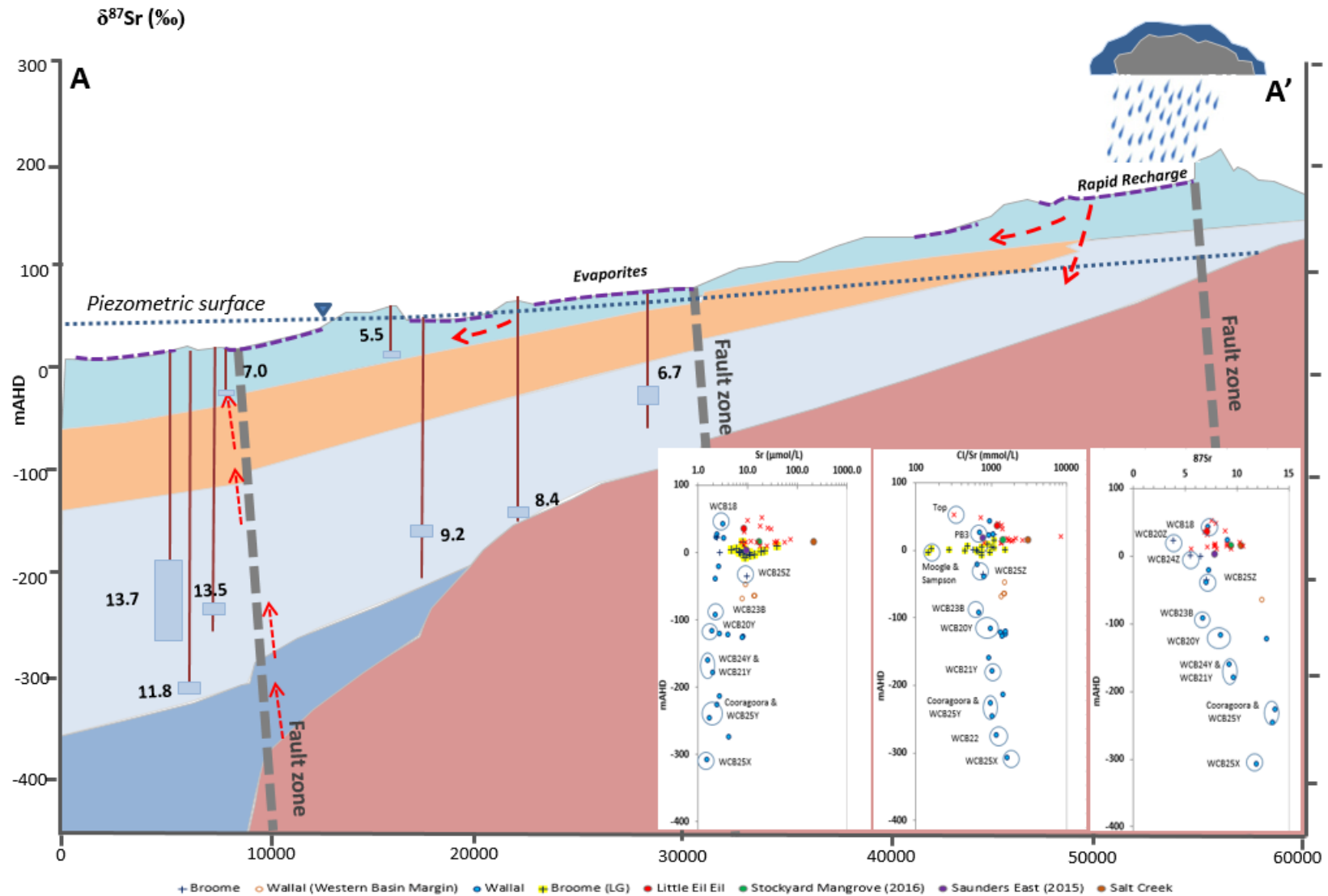


Figure 82 Wallal Embayment geological X-Section A'-A (from Figure 71) showing the location of the sub set of bores sampled for  $\delta^{87}\text{Sr}$  results from Table 10, arrows showing the direction of groundwater and soil water movement, piezometric surface from Meredith et. al. 2018 and bivariate plots of Sr ( $\mu\text{mol/L}$ ), Cl/Sr (mmol/L) and  $\delta^{87}\text{Sr}$  vs depth sampled (mAHd) (all data Table 10).

A Wallal groundwater sample from the Western Basin Margin (bore WCB04B) has the lowest Ca/Sr. This bore is noted to be in close connection to weathered crystalline basement rocks (Meredith et.al. 2014), as well as being connected with potential surficial carbonate/evaporite deposits mapped in Figure 62. Bore WCB04B is screened in the Wallal aquifer, at a depth of around -65mAHD, and therefore higher strontium concentrations may be due to receiving groundwater recharge from either, or both, the overlying evaporites and underlying weathered basement rocks. At that depth and chemistry, WCB04B may be a suitable upper Wallal aquifer proxy to explain the evolution of Walyarta spring discharge. This is explored further in this section of the report.

A larger dataset is available to graph Ca/Sr against Cl and resultant trends show the Broome and Wallal aquifer are similar. The Broome LG distribution connects the Wallal and Broome aquifers with DBCA spring sampling, which infers that a common evolutionary process, such as mixing along a consistent groundwater flow path, is responsible for the evolution of these waters (Figure 81b.). However, there is a poor relationship with decreasing Ca/Sr against chloride and all groundwater flow path parameters examined here, such as aquifer, depth sampled and location along flow path, which indicates the variables are independent. Graphing strontium concentration (1/Sr (mmol/L) against radiogenic  $^{87}\text{Sr}/^{86}\text{Sr}$  isotopic values (Figure 81c.) resolves similar patterns in the Wallal aquifer to those in Figure 81a., where increasing sample depth corresponds with elevated radiogenic  $^{87}\text{Sr}/^{86}\text{Sr}$  isotopic values sourced from interactions with clay minerals from Wallal argillaceous sediments, Permian sediments and/or weathered basement. In Figure 81c., the Wallal aquifer shows little variation in strontium concentration compared the Broome aquifer and DBCA spring sampling. The increases in strontium are likely to result from recharge and discharge groundwaters being enriched in strontium sourced from evaporites, as elevated strontium occurs where sampled within mapped potential evaporites (Figure 62). Similar to Figure 81a., the data presented in Figure 81c., suggest a simple mixing model may explain the hydrogeochemistry of the springs, whereby  $^{87}\text{Sr}/^{86}\text{Sr}$  provides a source Wallal groundwater depth range and relative increases in strontium represent the degree of Broome aquifer (evaporite Broome aquifer e.g. WCB25Z) or Wallal western basin margin (WCB04B) mixing.

The information gained from graphs presented Figures 80 and 81 was applied in a spatial context in Figure 82, where strontium concentrations are shown at depth and compared with Cl/Sr and  $\delta^{87}\text{Sr}$  data, with  $\delta^{87}\text{Sr}$  data also plotted on geological X-Section in Figure 71. Results show DBCA springs have greatest similarity with strontium concentrations sampled within the Broome LG aquifer, Broome bore WCB25Z and groundwater sampled in the Wallal western basin margin. Strontium concentrations are generally lower in the Wallal aquifer and no trends are apparent with depth. Ratios of Cl/Sr resolve some different trends. A weak increasing trend with depth occurs in the Wallal aquifer and the separation of low Cl/Sr in the Broome LG aquifer from shallow fault controlled palaeochannels (e.g. Taft and Moogle bores) (Figure 82). DBCA spring sampling remains aligned with Broome LG and Wallal western basin margin sampling. These trends are less apparent when  $\delta^{87}\text{Sr}$  data are examined as there is a good correlation between the Wallal aquifer  $\delta^{87}\text{Sr}$  values. DBCA spring  $\delta^{87}\text{Sr}$  data are variable, higher  $\delta^{87}\text{Sr}$  values sampled in the palaeovalley (e.g. Stockyard Mangrove (2016) and Salt Creek; Table 10) are similar to Wallal groundwater sampled at depths of between around -300 and -180mAHD (e.g. WCB25X & WCB21Y, Figure 82). Up gradient springs (e.g. Little Eil Eil (2015), Figure 82) is aligned with upland Wallal aquifer sampling (e.g. WCB18, Figure 82),



where groundwater is sampled at a higher landscape elevation, at depth of around 120 metres below ground level.

Strontium isotope  $\delta^{87}\text{Sr}$  data were not analysed and are therefore not available for the Broome LG aquifer. As a result the role of  $\delta^{87}\text{Sr}$  data in helping understand hydrological processes sustaining mound springs and perennial surface water in Walyarta cannot be fully developed. It is likely that as per observations of Broome aquifer data presented in Figure 81, that the Broome LG aquifer will have variable strontium concentrations that relate to access/connectivity to evaporites and the dominance of evapotranspiration processes. And where lower  $\delta^{87}\text{Sr}$  values exist in the Broome aquifer, this indicates shallower aquifers are not in connection with the deeper Wallal aquifer. To summarise, this means elevated  $^{87}\text{Sr}/^{86}\text{Sr}$  isotopic values are sourced from deeper Wallal aquifer groundwater that has some connection to clay material strontium sources (e.g. shales (Wallal and Permian sediments) and/or weathered crystalline basement rock). Data presented in Figure 82 show this can occur in upland Wallal bores, near the south western spatial extent that is closer to the limit of the presence of the Wallal Sandstone (e.g. WCB18) and within deep fault zones (e.g. WCB25X and Cooragoora PB1). From the limited sampling this means the  $\delta^{87}\text{Sr}$  radiogenic response in DBCA spring and surface water samples is likely to develop discretely through throughflow in the deeper Wallal aquifer followed by discharge via fault systems and variable mixing with upper Wallal and Broome groundwater.

#### 7.1.1.3 Carbon

Carbon dating of groundwater and spring water has been undertaken to understand groundwater recharge and discharge and assess the physical properties of aquifers. Methodologies on sampling analysis, data processing and modelling were developed from Cendón et. al. 2014 and are detailed in Meredith et. al. 2014 & 2018, Harrington and Harrington 2016 & 2017.

Reliable Carbon-14 age assessments require a qualitative and quantitative understanding of the carbon cycle, in particular the location and decay of different carbon sources along groundwater flow paths (Meredith et. al. 2016). A brief description the carbon cycle is detailed here and applied to geological information in Towner (1982a) to identify WCB and Walyarta carbon sources, as well as predict water type (Table 8; Appendix 7).

Starting with a top down approach, atmospheric carbon dioxide is converted to cellulose, starch and carbohydrates through the process of photosynthesis. In the soil zone vegetation respiration and decay produce carbon dioxide through the following reaction;



Carbon dioxide is stored in the unsaturated zone for relatively short periods of time with mean residence times estimated at 10 to 100 years (Appelo and Postma 2006). The main export pathways for unsaturated zone carbon dioxide are to the atmosphere, precipitation as surficial pedogenic calcretes or moving into aquifers with recharging rainwater. The amount carbon dioxide produced varies according to vegetation cover, species (dominance of C3 and C4 plants, see Section 5.3.2), soil type and climate and although volumes produced are higher under tropical, forested conditions, investigations have shown that low carbon dioxide storage in sparsely vegetated areas with sandy

soils is significant, being an order of magnitude higher than the atmosphere. Seasonal changes in evapotranspiration and climate affect unsaturated zone carbon dioxide storages, with storages decreasing when vegetation growth cycles slow and soils dry, promoting the release of carbon dioxide and precipitation of pedogenic carbonate (Breecker et al 2009). Most pedogenic carbonate is contemporary in age, with the main processes driving their development being increases in calcium concentration in groundwater and/or soil water, decreases in soil  $p\text{CO}_2$  pressures and increases in soil temperature. Formation in semiarid or arid regions has been noted as a useful surrogate for C4-biased vegetation and average precipitation more generally, which provides useful information on palaeoclimate and palaeobiomes (Retallack 2005, Breecker et al 2009).

Processes that mobilise carbon into groundwater include chemical reactions along groundwater flow paths and/or through geological fractures, which may involve chemical reactions with silicates, carbonates and sulfates (Deng et. al. 2015). Carbon dioxide reacts in water to form carbonic acid, bicarbonate and carbonate according to the following reversible equations;



The relative concentrations of carbonic acid, bicarbonate and carbonate are controlled by pH. The production of carbonic acid will occur and reduce pH but this will be buffered by water rock reactions in the saturated and unsaturated zone (e.g. dissociation of carbonates, silicates, microbial mediated reactions). The commonly accepted model of the evolution of aqueous carbon species along groundwater flow paths advises that with no additional carbon inputs other aquifer reactions will rapidly convert carbonic acid to bicarbonate and hydrogen ions. Although recent research is suggesting that carbonic acid is stable at higher temperatures and pressures and has potential to provide additional carbon under closed system conditions, which poses the question what happens at intermediate pressures and temperatures (Wang et. al. 2016).

Another potential source of carbon in groundwater is organic carbon, which during methanogenesis will react and increase carbon dioxide, resulting in a decrease in pH that in turn encourages further aquifer reactions. Factors to consider when assessing carbon fluxes are that the dissolution of carbonates releases bivalent cations (e.g. calcium, magnesium and strontium) and increases pH, particularly if system conditions are closed. Other processes, such as salt water intrusion and flushing, may create carbon balance artefacts, particularly where the aquifer cation exchange capacity is variable (Mercado 1985). This occurs due to time lags in the buffering responses of aquifers, producing depleted bicarbonate due to carbonate precipitation during intrusion and elevated bicarbonate due to calcite dissolution during flushing. In both cases, within silicate dominated aquifers, cations adsorption and release is assisted by silicate reactions (e.g. generally clay minerals).

To explicitly map sources of carbon and conceptualise processes that are exacerbating or delaying carbon fluxes along flow paths would be a considerable exercise for an area as large as the WCB. The interpretation of data in this report confirms carbon sources are spatially variable, for example there;

1. are areas in the near surface that are likely to encourage the development (e.g. derived through fluvial and/or vegetation-soil processes) of mainly thin evaporites,

2. is incomplete flushing of saline groundwater from past sea water incursions in the Walyarta tidal flats and palaeovalley,
3. is no local information or data on vadose zone soil  $\text{CO}_{2(g)}$ ,
4. C4 (e.g. spinifex) and C3 plants occur in the WCB,
5. organic carbon sources exist at depth in the Wallal aquifer and the near surface (Table 8),
6.  $\text{HCO}_3$  is released during carbonate weathering/dissolution which occurs mainly in the Broome aquifer and where it is connected to the Wallal aquifer it mixes and overprints the Wallal aquifer chemistry (e.g. major process from the surface to depths -100mAHD),
7.  $\text{HCO}_3$  is released during silicate weathering in the Broome and Wallal aquifers at various depths with  $\text{SiO}_2$  data and PHREEQC SI modelling (chalcedony and quartz) suggest this is a major process from the ground surface to depths of -150mAHD where silica is over saturated and
8. PHREEQC SI modelling indicates groundwater in most aquifers is under saturated in carbonates and where they are present they may dissolve.

To reduce uncertainty in the interpretation of Carbon-14 data, and not to be overcome by this complexity, a strategic approach needs to be developed for sampling, which ensures sufficient spatio-temporal data are collected to improve understanding, which may include modelling where appropriate information exists (Suckow 2014). In the WCB, this approach was adopted by Meredith et. al. (2014 & 2018) where carbon isotope sampling was undertaken in the WCB to understand the evolution of coastal groundwater and the processes controlling groundwater evolution along a geological transect in the Wallal Embayment (as depicted in Figure 71).

In this investigation, Meredith et. al. (2014) notes that groundwater is more enriched in  $\delta^{13}\text{C}_{\text{DIC}}$  than expected in a C3 vegetation environment and suggests enrichment through carbonate dissolution is a possibility. Although this process would not be applicable to Wallal sampling in the western basin margin (e.g. WCB04B) due to these samples generally showing greater depletion. Limited sampling in the Broome aquifer was shown to have higher  $^{14}\text{C}_{\text{DIC}}$  activities, while distance to recharge areas was identified as a control on  $^{14}\text{C}_{\text{DIC}}$  activities in the Wallal aquifer, with  $\delta^{13}\text{C}_{\text{DIC}}$  not following the same trends. This work was refined in Meredith et. al. (2018) where a conceptual model for the dissolved inorganic carbon was developed. Parameters with higher uncertainty included system conditions and specific information on carbon sources (e.g. soil  $\text{CO}_2$  and the distribution and reactivity of evaporites and organic carbon). A statistical model of groundwater age for the Wallal aquifer was presented for sampling undertaken in the WCB western basin margin and Wallal Embayment (as shown in Figure 71). The outputs were generated through an iterative conceptual and numerical modelling process, which included undertaking forward and inverse modelling as well as a sensitivity analysis. The final groundwater age results showing good agreement with previous numerical modelling, with Wallal aquifer groundwater age increasing along the flow path (Figure 83).

In the WCB La Grange area, to the north of the Walyarta study area, groundwater tracers, including radiocarbon, were collected to understand groundwater recharge to the Broome aquifer (Harrington and Harrington 2016). Data collected showed significant variation, which was ultimately attributed to the hydrogeological heterogeneity of the Broome aquifer (e.g. complex gradients and delays in

mixing, following episodic/cyclonic rainfall events), with the averaging of results producing what was considered as realistic overall estimates for the La Grange area.

In the Walyarta study area Harrington and Harrington 2017 report that all spring and surface water sampling was enriched in  $\delta^{13}\text{C}_{\text{DIC}}$ , with the expectation this was the result of carbonate weathering. As spring samples were collected at or within 10cm of the ground surface and are mainly undersaturated with respect to carbonates (Appendix 7) isotopic exchange with  $\text{CO}_2$  gas in the vadose zone was identified as the most likely cause of  $\delta^{13}\text{C}_{\text{DIC}}$  enrichment in the mound springs, with evapotranspiration also being an important process for surface water sampling. For surface and near surface water this was attributed to the equilibration of surface water with the atmosphere. Harrington and Harrington 2017 advise that the complex interplay of processes and likelihood of significant carbon recycling prohibits the correcting of the apparent  $^{14}\text{C}$  ages using conventional chemical and/or isotope mass balance methods. Recommending further investigations to age date spring discharge should consider how seasonal and chemical constraints may prohibit the collection of suitable samples.

To address the issues outlined in Harrington and Harrington 2017 additional sampling was undertaken in November 2016 following a year of below average rainfall Harrington and Harrington 2017. Samples collected during this program should have addressed the atmospheric equilibration issues discussed in Harrington and Harrington 2017. However, results show that sampling improved for only one of the four repeat sampling sites (e.g. Stockyard Mangrove) indicating the problem is more complex than that outlined in Harrington and Harrington 2017.

What becomes apparent from the WCB radiocarbon work is that uncertainty is reduced where there is more information on the 3D geometry and heterogeneity of geological formations and aquifers, in addition to groundwater and surface water dynamics, especially gradients, aquifer responses and surface-groundwater interactions (inclusive of vadose/unsaturated zone characterisation). In the WCB this is best achieved for the confined to semi-confined Wallal aquifer in the WCB western basin margin and Wallal Embayment as temporal data have been collected for both the Broome and Wallal aquifers since the 1980's. Collecting radiocarbon or other environmental isotope data from other areas in the WCB tends to result in a pattern matching exercise, either with or without setting a prior hypothesis on if the data is likely to mimic trends, or not. As transferability requires the characterisation of aquifers and a 3D understanding, the argument leads back to the need to develop a 3D framework prior to designing a hydrogeochemical sampling programing and interpreting the results.

Developing a 3D model is especially challenging in the case of the Walyarta study area, where there is little bore information and no information on the dynamics of the unsaturated zone and shallow aquifer (surficial-Broome aquifer). Therefore how the unsaturated zone varies in three dimensions seasonally, in relation to average dry and wet season rainfall, is unknown. Given this fact and the sampling caveats outlined in Harrington and Harrington (2017), it is likely significant investment would be required to sample spring mound discharge water in the near surface (upper 5 to 10 metres) and identify modelling end members (e.g. ten percentiles) for different analytes and environmental tracers.



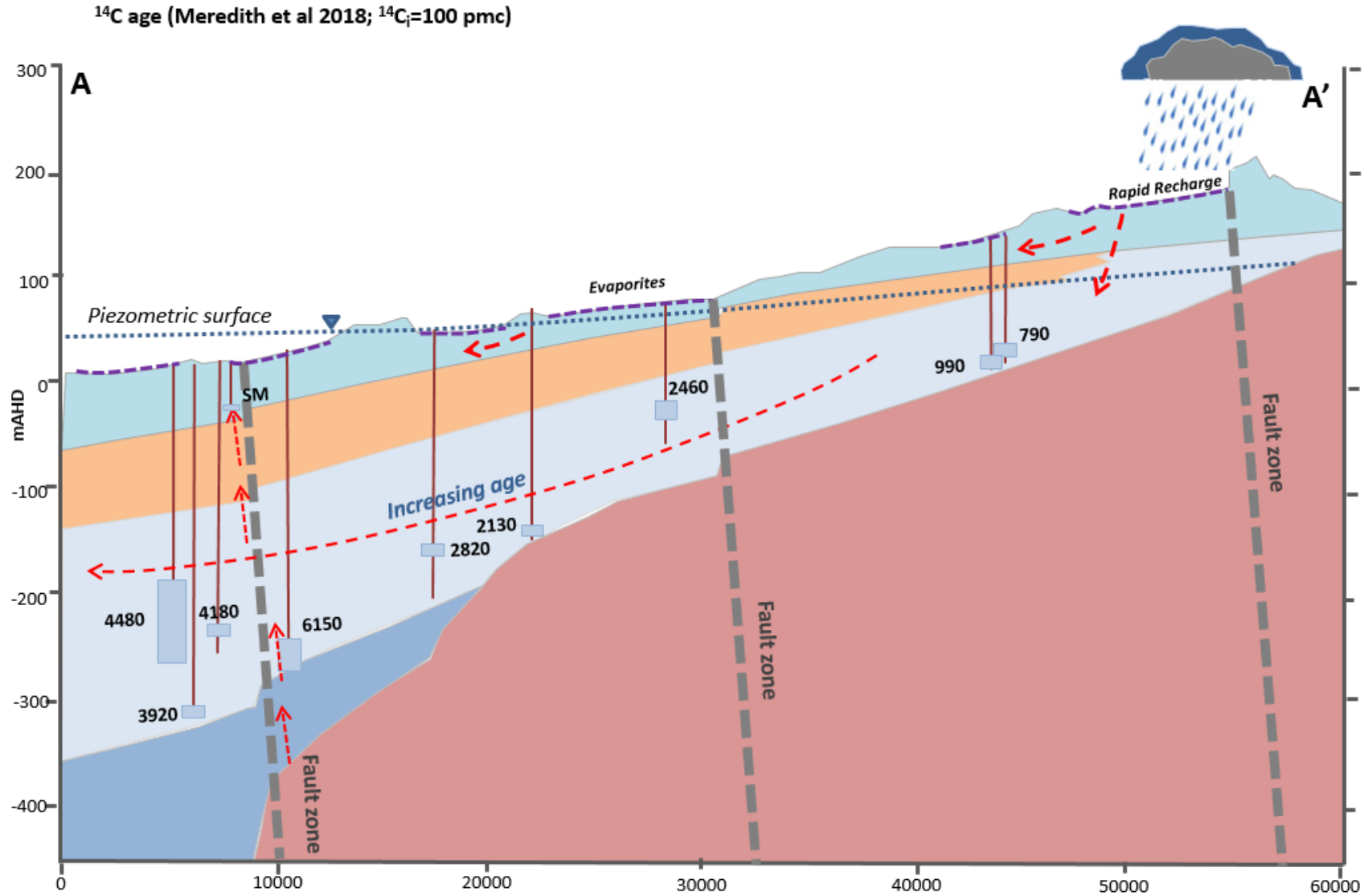


Figure 83 Wallal Embayment geological X-Section A'-A (from Figure 71) showing the location of the sub set of bores with <sup>14</sup>C age determination from Meredith et. al. (2018), arrows showing the direction of groundwater and soil water movement, piezometric surface from Meredith et. al. 2018

HYDROLOGICAL CONCEPTUALISATION OF THE WALYARTA MOUND SPRINGS

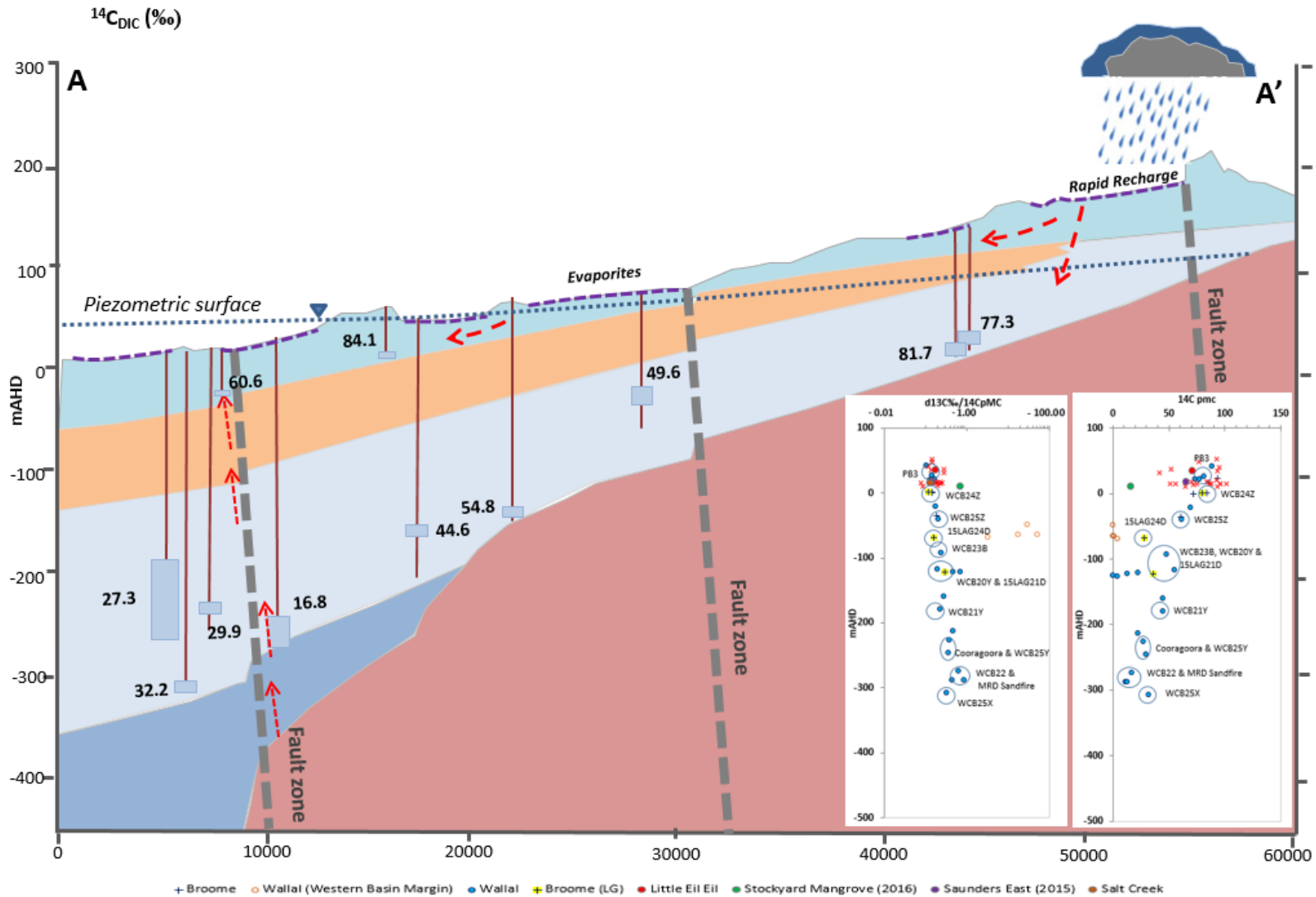


Figure 84 Wallal Embayment geological X-Section A'-A (from Figure 71) showing the location of the sub set of bores sampled for  $\delta^{14}\text{C}_{\text{DIC}}$ (‰) results from Table 10, arrows showing the direction of groundwater and soil water movement, piezometric surface from Meredith et. al. 2018 and bivariate plots of  $\delta^{13}\text{C}(\text{‰})/^{14}\text{C}$  (pMC) and  $^{14}\text{C}$  (pMC) vs depth sampled (mAHN) (all data Table 10).

Although this exercise would be interesting, and obviously an attractive proposition for scientists undertaking the work, it is likely to require a significant investment of time and money and arguably not a sound investment if interpreted in the absence of a local 3D geological and hydrogeological model (unverified or verified with limited controlled drilling).

Therefore the carbon discussion of this report is different from others in the WCB and examines the Walyarta springs  $\delta^{13}\text{C}_{\text{DIC}}$  and  $^{14}\text{C}_{\text{DIC}}$  data in relation to radiocarbon results from other WCB groundwater data and their sample depths (Figure 84). Data in this figure are dominated by the WCB, Western Basin Margin and Wallal Embayment, but do include five samples from the Willara sub-basin (15LAG21D, 15LAG24D & 15LAG24S (DPIRD) and two MRD Sandfire artesian samples (DWER & DPIRD)) to assess spatial continuity of trends. Results show that the three springs selected as representative of robust spring sampling (e.g. Stockyard Mangrove 2016, Saunders East and Little Eil Eil (2015) all display lower  $^{14}\text{C}_{\text{DIC}}$  percentage modern carbon (pmc) values compared to both upland Wallal and Broome aquifer data. Stockyard Mangrove 2016 shows the greater  $^{14}\text{C}_{\text{DIC}}$  depletion, with values similar to Wallal aquifer sampled to depths of around -120mAHD in the WCB western basin margin.

Data for  $^{14}\text{C}_{\text{DIC}}$  pmc decreases at depth which tends to infer an aging of water (e.g. lack of mixing with modern, generally near surface water enriched in carbonates), possibly due to longer flow paths. Sampling from the Willara sub-basin generally follows these trends, within the variation of the larger dataset.

At a coarse scale, ratios of  $\delta^{13}\text{C}_{\text{DIC}}$  (‰) against  $^{14}\text{C}_{\text{DIC}}$  (pmc) data increase with depth sampled and variation observed to depths of around -120mAHD is generally normalised. The overall trend indicates carbonate dissolution and/or organic carbon methanogenesis is an active process that increases with depth sampled (Figure 84). Reactions in the vadose, or unsaturated zone, where the springs were sampled show the most variation and the reasons for this are complex and outlined in Meredith et. al. 2016 and Harrington and Harrington 2017. The notable exceptions that display higher values are, DBCA spring sample Stockyard Mangrove 2016, and WCB western basin margin bores. Both having higher relative  $\delta^{13}\text{C}_{\text{DIC}}$  (‰) values compared to  $^{14}\text{C}_{\text{DIC}}$  (pmc), suggesting a different source of  $\delta^{13}\text{C}_{\text{DIC}}$  (e.g. carbonate/evaporite recycling) is involved in the evolution of Wallal groundwater in the western basin margin and that similar processes may occur in the Walyarta study area, which influences the discharge chemistry of the springs and surface water.

### 7.1.2 Hydrogeochemistry summary

Work undertaken in Section 7 includes a summary of previous work, the construction of broad scale physical and chemical constraints to assess WCB hydrogeochemical data and environmental tracers and the development of aims to assess their application. The main aims being to;

1. Construct a broad scale framework to interpret the hydrogeochemistry and environmental tracer data,
2. identify the key hydrogeochemical indicators that can be used to assess the water and solute balance at coarse scales (e.g. map the hydrogeochemical evolution of groundwater in

Broome and Wallal Sandstone aquifers, from groundwater recharge, through to discharge areas),

3. identify the key hydrogeochemical indicators that can be used to assess the water and solute balance at finer scales (e.g. role of geological constraints that may disrupt lateral and vertical flow (e.g. faults and aquifer stratification (limited vertical mixing)),
4. assess spring hydrogeochemistry data to understand if discharge rates are sufficient to preserve groundwater signatures, or if hydrogeochemical reactions such as precipitation, dissolution, mixing and/or fractionation occurs and dilutes the spring discharge signal and
5. use the interpretation framework and results to the Walyarta study area to develop a hydrogeochemical conceptual model and document limitations and uncertainty.

#### 7.1.2.1 *Hydrogeochemical interpretation framework*

Tectonic element boundaries and major north-west and south east geological faults are aligned and influence the hydrogeomorphology. This is shown to effect the development of surficial evaporites, which has the potential to change aquifer recharge chemistry and the carbon balance (Figures 57 to 59).

Tectonic boundaries also influence the deposition and preservation of Mesozoic sediments and this constrains spatial variations in the thickness of the Wallal Sandstone aquifer (Figure 59). This alters aquifer hydraulic properties, which is known to occur as Wallal Sandstone Aquifer pump tests confirm the formation is widely heterogeneous and anisotropic.

Groundwater in the Wallal and Broome aquifers has a distinct hydrogeochemical signature that provides information on the flow paths, mixing and water-rock interactions (Figures 70 and 71 to 77).

#### 7.1.2.2 *Coarse scale hydrogeochemical indicators*

The main chemical reactions controlling the 4D evolution of groundwater chemistry in the WCB at a coarse scale are;

- a. Evaporation; strong correlations with increasing chloride and other major and minor ions, with most increasing in concentration along the seawater trend line (demonstrating solutes are sourced from oceanic aerosols and evaporation is an important process in controlling water quality (e.g. bivariate plots and correlation matrices (Figures 66 & 67, Appendix 8)). These relationships are more complex and generally don't exist when examined in three dimensions (Figures 72 to 77) due to aquifer heterogeneity (variable aquifer interactions and fluxes), which complicates interpreting aquifer interactions and predicting water quality along groundwater flow paths,
- b. Precipitation of evaporites (calcite and dolomite); Mineral saturation indices range from super saturated to saturated to in equilibrium. Potential to occur in Broome LG aquifer at depths of around 0mAHD,
- c. Dissolution of evaporites (calcite and dolomite); correlations between increasing bivalent cation concentrations (e.g. Ca and Mg) and bicarbonate. Occurs in Broome aquifer and Wallal (western basin margin) to depths of -50 to -100mAHD and observed in major and minor (e.g. Sr) ion relationships and environmental tracers  $^{14}\text{C}_{\text{DIC}}$ ,



- d. Dissolution of evaporites (gypsum); correlations between increasing bivalent cation concentrations (e.g. Ca and Mg) and sulfate. Occurs in Broome aquifer and Wallal (western basin margin) to depths of -50 to -100mAHD, Wallal aquifer from 0 to -200mAHD and observed in major ion relationships,
- e. Silicate weathering and ion exchange reactions (e.g. weathering feldspar and clay mineral ion exchange reactions); (e.g. release of ions and/or exchange monovalent for bivalent ions), correlations between bivalent cations (e.g. Ca and Mg) and silica, increases in both parameters in the Broome aquifer to depths of -50mAHD (weathering is dominant reaction). Variable cation concentrations correspond to decreases in silica (cation exchange is dominant reaction) in the Wallal aquifer to depths of around -200mAHD (very low silica below -200mAHD). Overprinting may occur in the Broome aquifer where both silicate weathering and dissolution of evaporites occurs and
- f. Isotopic enrichment and depletion; (e.g. stable isotopes  $\delta^2\text{H}$  and  $\delta^{18}\text{O}$ , strontium  $\delta^{87}\text{Sr}$  and  $^{14}\text{C}_{\text{DIC}}$ ), in the Wallal aquifer, between 20 to -300mAHD, there is enrichment in stable isotopes and strontium isotopes. In contrast  $^{14}\text{C}_{\text{DIC}}$  (pmc) shows variation but a general trend of isotopic depletion with depth sampled. Less variation observed in ratios of  $\delta^{13}\text{C}_{\text{DIC}}/^{14}\text{C}_{\text{DIC}}$ . Limited sampling in the Broome aquifer shows no trends exist for stable isotopes, but the Broome aquifer does mimic the same trends as the Wallal for strontium and  $^{14}\text{C}_{\text{DIC}}$  (pmc) between depths of around 20 to -40mAHD.

Results indicate that all aquifers show a degree of hydrogeochemical stratification that reflects physico-chemical heterogeneity, as well as system conditions and location along flow path. The same general hydrogeochemical trends occur across the WCB tectonic elements demonstrating that hydrogeochemical data can be used at a coarse scale to fingerprint aquifers and the depth (mAHD) sampled.

Applying hydrogeochemistry to understand the location along flow path is not able to be determined with confidence as when formations such as the Wallal Sandstone aquifer have a greater thickness, groundwater tends to be sampled from depth and groundwater from the upper stratigraphy (e.g. Alexander Formation and Upper Wallal) is not sampled and characterised. Although results presented here suggest there is limited mixing within the Wallal aquifer below -200mAHD (groundwater is older and hydrogeochemically different).

Groundwater in the Wallal Sandstone aquifer in the western basin margin is hydrogeochemically different as it shows an association with both the Broome and Wallal aquifers. Major ion trends generally aligned to the Broome aquifer, due to a history of receiving recharge through surficial sediments characterised by carbonate dissolution, and environmental tracers data showing a greater similarity to the Wallal aquifer.

### **7.1.2.3 Finer scale hydrogeochemical indicators**

Variation within the coarse scale trends discussed in Section 7.3.5.3 tend to correspond to finer scale geological/hydrogeological features that due to their relative extent in the WCB they have been under sampled. These features include geological faults, palaeochannels, salt water intrusion (contemporary and historical/partial flushing) and shallow groundwater discharge. As insufficient data exists to assess the variation attributed to faults, palaeochannels and shallow discharge

statistically (e.g. either descriptively or quantitatively) they are discussed below under the same headings as Section 7.3.5.2.

Chemical reactions controlling the 4D evolution of groundwater chemistry in fine-scale features are outlined below. Noting that fault zones are long lived (e.g. there is a long history of activation) they may also represent zones of stratigraphic heterogeneity, where there may be the preferential deposition and preservation of fine grained sediments and organic materials that then influence local hydrogeochemistry.

- a. Evaporation; geochemical variation due to faulting and/or long term connectivity to shallow palaeochannels is most evident in the Wallal aquifer through either higher or lower total dissolved solids and chloride concentrations (dependent on water quality in underlying aquifer). Similar trends in the Broome aquifer represent salt water intrusion,
- b. Precipitation of evaporites (calcite and dolomite); Mineral saturation indices range from super saturated to saturated to in equilibrium. Potential to occur in Broome LG aquifer at depths of around 0mAHD,
- c. Dissolution of evaporites (calcite and dolomite); resolved when ionic concentrations are compared to chloride (e.g. Ca/Cl and Mg/Cl) against depth sampled. Higher values apparent in fault zones (Wallal aquifer) and palaeochannels (Broome LG aquifer) and lower values associated with the salt water interface (Broome aquifer),
- d. Dissolution of evaporites (gypsum); identified when specific ionic ratios are examined (e.g.  $\text{SO}_4/\text{Cl}$  and  $\text{SO}_4/\text{Ca}$ ) against depth sampled. Higher values observed in fault zones (Wallal aquifer) and palaeochannels (Broome aquifer) and lower values associated with the contemporary salt water interface (Broome aquifer),
- e. Silicate weathering and ion exchange reactions (e.g. weathering feldspar and clay mineral ion exchange reactions); resolved when ionic concentrations and specific ionic ratios are examined (e.g.  $\text{SiO}_2$ ,  $\text{HCO}_3$  and  $\text{HCO}_3/\text{SiO}_2$ ), with higher silica, bicarbonate and  $\text{HCO}_3/\text{SiO}_2$  concentrations in fault zones (Wallal aquifer). Lower silica with respect to higher bicarbonate and  $\text{HCO}_3/\text{SiO}_2$  associated with the contemporary salt water interface (Broome aquifer) and,
- f. Isotopic enrichment and depletion; (e.g. stable isotopes  $\delta^2\text{H}$  and  $\delta^{18}\text{O}$ , strontium  $\delta^{87}\text{Sr}$  and  $^{14}\text{C}_{\text{DIC}}$ ), there is less stable isotope data available compared to major ions and as a consequence less outliers are noted. For the stable isotope data examined in this report the main outlier occurs in a fault zone within the Wallal aquifer at depths exceeding -200mAHD.

Finer scale geological heterogeneity was not readily resolved in bivariate plots and piper trilinear diagrams, notable exceptions being identifying salt water intrusion in the Broome aquifer. Graphing hydrogeochemical data against depth sampled provided a suitable framework to assess variation within fault zones but not shallow palaeochannels due to limited sampling. The higher or lower concentrations or values within fault zones representing the hydrogeochemical fingerprint of deeper groundwater, with the degree of groundwater mixing at the current depth sampled controlled by vertical (advective) flow rates.

#### **7.1.2.4 Walyarta mound spring hydrogeochemistry**

The Walyarta mound springs are sustained by perennial groundwater flow along geological faults. The hydrogeochemistry of fault zones are reported in Section 7.3.5.3, with results confirming that

fault zone chemistry is distinct and resolvable following groundwater mixing via the process of throughflow. Resolving a deeper groundwater fingerprint at springs requires discharge rates to outpace hydrogeochemical changes that occur in the unsaturated zone.

Chemical reactions noted to affect the 4D evolution of groundwater chemistry in mound springs sampled at the ground surface are outlined below;

- a. Evaporation; variable concentrations of total dissolved solids and chloride that reflect a combination of near surface evaporation (dry season sampling) and mixing with variable quality of near surface groundwater and soil water (e.g. higher concentrations of solutes in soil water due to evapotranspiration),
- b. Precipitation of evaporites (calcite and dolomite); Mineral saturation indices are variable and range from super saturated to under saturated. Saturation increasing with higher solute concentrations,
- c. Dissolution of evaporites (calcite and dolomite); bivalent ion concentrations are similar to the Broome and Broome LG aquifers but when normalised with chloride (e.g. Ca/Cl and Mg/Cl) springs tend to have lower values. The spring water sample with the oldest uncorrected radiocarbon age (Stockyard Mangrove 2016) shows alignment with Wallal aquifer Ca/Cl values sampled at depths around 100 metres below ground level,
- d. Dissolution of evaporites (gypsum); sulfate concentrations and  $SO_4/Cl$  values are similar to the Broome LG aquifer. Spring tend to show higher  $SO_4/Ca$  which tend to be more characteristic of the Wallal aquifer sampling at depths of 100 metres below ground level,
- e. Silicate weathering and ion exchange reactions (e.g. weathering feldspar and clay mineral ion exchange reactions); springs are characterised by low silica, bicarbonate and  $HCO_3/SiO_2$ , which could align the samples to the Broome, Broome LG or Wallal aquifers. Spring water is in equilibrium with chalcedony, which tends to be a deeper Wallal aquifer fingerprint (~100m below ground level) and
- f. Isotopic enrichment and depletion; (e.g. stable isotopes  $\delta^2H$  and  $\delta^{18}O$ , strontium  $\delta^{87}Sr$  and  $^{14}C_{DIC}$ ), spring stable isotope data exhibit a range of values that show enrichment where near surface evaporation has influenced the collection of robust spring samples. Compared to coarse scale trends, the three spring samples with the oldest uncorrected radiocarbon ages are aligned with Wallal aquifer data collected at depths of over 200 metres below ground level. Similarly, comparing the spring water sample with the oldest uncorrected radiocarbon age (Stockyard Mangrove 2016) with coarse scale strontium isotope  $\delta^{87}Sr$  and carbon  $^{14}C_{DIC}$  (pmc) and  $\delta^{13}C_{\text{‰}}/^{14}C_{DIC}$  (pmc) trends the spring sample is also aligned with Wallal aquifer data collected at depths of over 200 metres below ground level.

A few major ion trends in the spring sampling indicate the hydrogeochemistry is dissimilar to shallower aquifer results from the Broome and Broome LG aquifers. As the trends involve calcium, silica and all major anions (chloride, sulfate and bicarbonate) overprinting is likely, with calcium potentially being sourced from all reactions making the trends less reliable as indicators of spring discharge. Results from environmental tracers were more definitive, although this could in part be due to the limited number of groundwater samples interpreted here.

It is also important to note that of the twenty three spring and surface water samples collected over consecutive years (2015 and 2016), only three effectively sampled a spring vent and yielded suitable

data to assess as spring discharge in this report. The limitations of collecting robust samples at the near surface that represent advective groundwater flow and discharge in known heterogeneous materials is discussed in the following section.

## **8 Walyarta conceptual hydrological model**

Data and information presented in Section 7 confirms that groundwater in the Wallal and Broome aquifers in the WCB generally has a spatially consistent and therefore predictable hydrogeochemistry with depth, and along flow paths, where the Wallal aquifer also increases in thickness. This allows for the development of a predictive schematic hydrogeochemical conceptual model where there is sparse bore data, such as the Walyarta study area (Figure 85), using the three dimensional geological model constructed in this report Section 4.5.3 and Figures 28, 29, 51 & 52. The schematic in Figure 85 includes annotations overlaid on cross sections exported from the three dimensional model produced in Leapfrog Geo™, with the major annotation being the arbitrary division of the Wallal aquifer into the Alexander Formation/Upper Wallal and Lower Wallal. Other important factors to note is the high uncertainty for the presence and thickness of the Jarlemai Siltstone aquitard (due to lack of drilling and variable geophysical response), the base of the Wallal Formation and positive identification of the underlying Permian and crystalline basement formations (due to the depth of investigation of the geophysical data interpreted to produce the three dimensional model).

Based on this conceptualisation the Walyarta groundwater flow path is around 40km in length from the recharge (e.g. location of NSOKidson bore; superimposed at similar landscape elevation), to spring discharge areas (e.g. springs Stockyard Mangrove, Saunders and Little Eil Eil). This is a similar flow path length presented in the Wallal Embayment cross section (Figure 71; bores PB1 to WCB25X). Variation from this flow path may occur if the Wallal hydraulic head is lower than estimated and/or the Jarlemai Siltstone is less extensive (as shown in Figure 32). If this is the case recharge may also occur in areas immediately up gradient of Little Eil Eil spring, near the north eastern boundary of the Willara sub-basin (Figure 85). In the absence of drilling and aquifer hydraulic information, a 'thin' Jarlemai Siltstone aquitard, that effectively confines the Wallal aquifer and allows discrete groundwater discharge from faults, is conceptualised (Figure 85). The evolution of groundwater chemistry mimicking Figure 71, with spring chemistry evolving from depths of around 200 meters below ground level (bores WCB25X or WCB25Y). Variation from this fingerprints representing the degree of mixing with the Alexander Formation/Upper Wallal and Broome-surficial aquifers Section 7.

As discussed in Section 7, the preservation of a deeper groundwater fingerprint at the springs is dependent on sampling sections of fault conduits that provide a faster groundwater flow rate and minimal near surface reactions. Near surface sampling introduces the greatest uncertainty as it requires the identification and characterisation of a number of end member waters, soils and formations to develop a mass balance that includes hydrogeochemical sources and fluxes, some of these are outlined in Figure 86 and are discussed in relation to flood plain dynamics in a semi-arid zone in Meredith et. al. 2016. Figure 86 also outlines limitations of seasonal sampling, as well as known data and information gaps in the Walyarta study area.



HYDROLOGICAL CONCEPTUALISATION OF THE WALYARTA MOUND SPRINGS

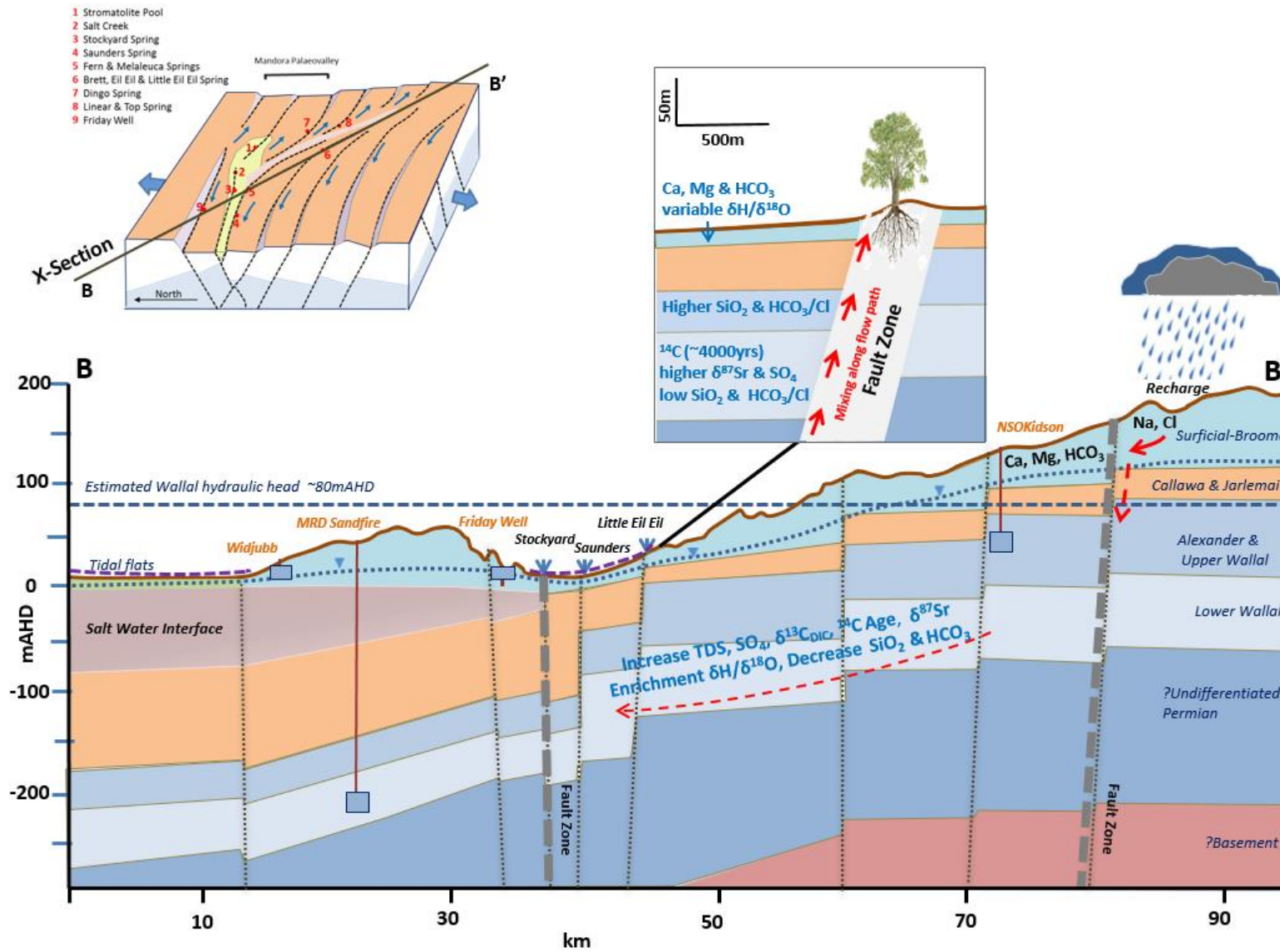
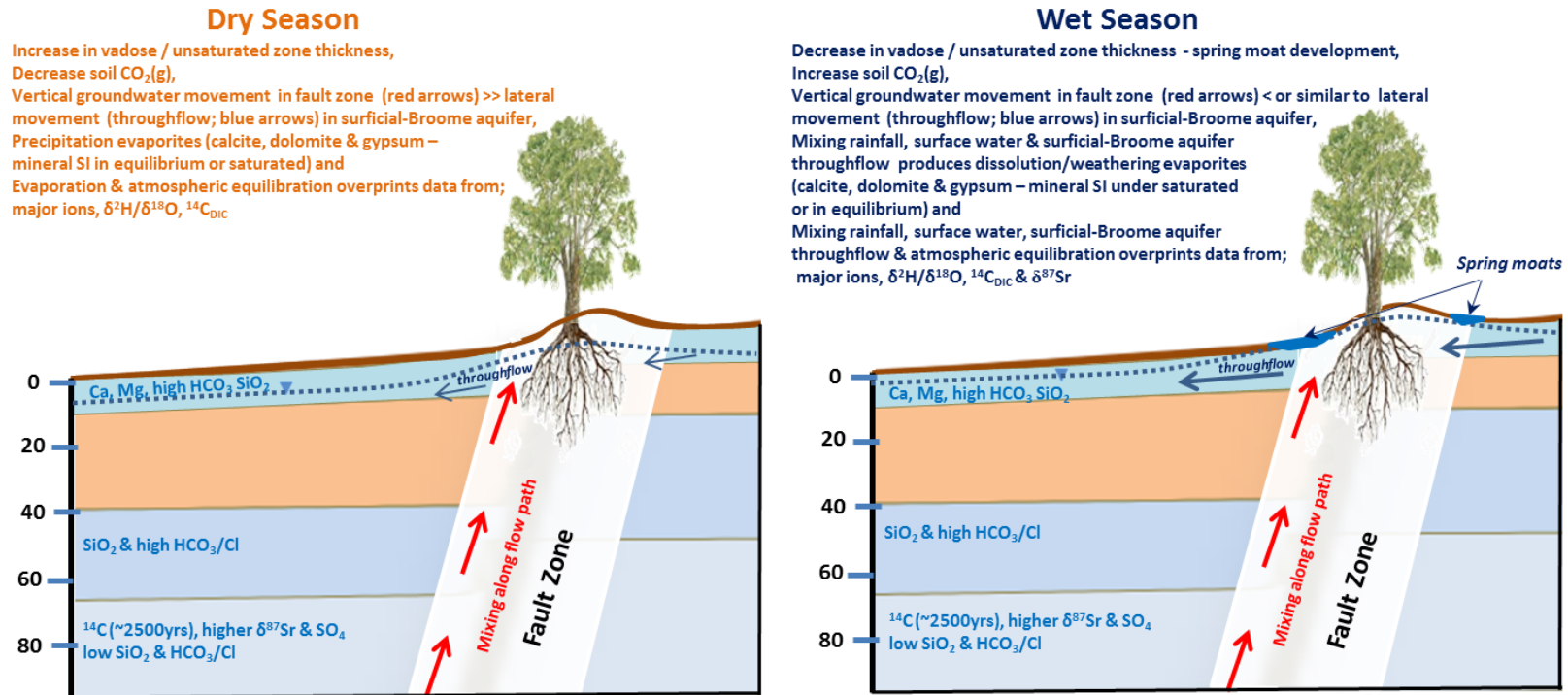


Figure 85 Predictive hydrological conceptual model for the Walyarta study area, see Figure 71 (A) for location and Figures 28, 51 and 52 for context



Limitations of near surface sampling of springs and surface water in the Walyarta study area

No spatio-temporal data or information on;

1. Wallal aquifer groundwater levels and quality,
2. surficial/Broome aquifer groundwater levels and quality,
3. finer scale soil mapping (extent and thickness),
4. saturated hydraulic conductivity of soils,
5. soil saturated water moisture content,
6. soil-water holding capacity,
7. vegetation rooting depths and water use in fault zones,
8. vegetation transpiration (temporal constraints / seasonality)
9. vegetation tolerance (water quality)
10. variation in soil and vegetation parameters (above) across springs and surface water systems
11. variation in soil and vegetation parameters (background values and mapping across Walyarta study area)

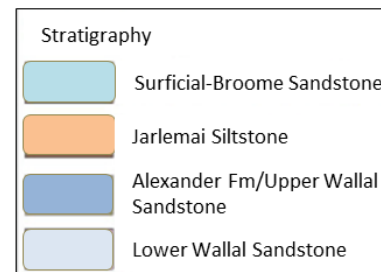


Figure 86 Schematic showing shallow aquifer dynamics in the wet and dry seasons and physico-chemical changes that occur and impede the collection of robust spring discharge samples

The characterisation and inverse modelling of seasonal spring discharge water and/or perennial surface water, in isolation, and without addressing limitation gaps, requires significant investment (financial and time) and is unlikely to yield definitive results. Uncertainty will remain highest in the absence of information on the hydrogeology upgradient of the Walyarta study area. Without this information, and local background data on hydrogeochemical sources and fluxes, the information in the spring data cannot be fully appreciated and the springs effectively managed.

## 9 Conclusions and recommendations

As outlined in Aquaterra (2010), springs in the WCB are not thought to represent a significant part of the WCB water balance, but could form useful indicators of Wallal aquifer groundwater pressure changes. This may mean springs could be sensitive to these changes and arguably it is important to investigate how they function.

A significant amount of geological and hydrogeological data has been collected in the WCB since the 1970's. Variation in spatial and temporal data collection reflects the size of the basin and changes in water demand over time. The approach undertaken in this study was to mine the existing available data and develop a basis for transferring the knowledge and information gained to areas with less information.

The four most important conclusions from this study are that;

- In the WCB, groundwater in the Wallal and Broome aquifers generally has a spatially distinct and consistent hydrogeochemistry and its variability is predictable with depth. Patterns also exist along flow paths, where the Wallal aquifer also increases in thickness. This allows for the transfer of knowledge gained to areas like the Walyarta study area where there is sparse bore data, but information on formation thicknesses,
- Slow rates of lateral groundwater movement are inferred from groundwater radiocarbon ages along flow paths and appear to have assisted in the preservation of subtle fault zone hydrogeochemical fingerprints. Available evidence indicates that faults;
  - exist in the near surface (propagate to the land surface from depth representing reactivated basement structures),
  - can be mapped both geophysically and hydrogeochemically,
  - constrain formation thicknesses at a basin scale, but do not appear to physically compartmentalise groundwater flow (limited stratigraphic offsets noted in Broome and Wallal aquifers), and
  - Represent zones where there is greater vertical groundwater mixing and water-rock interactions.
- Long-lived, perennial springs are located within roughly sub vertical (possible high angle shallow dip to the west) geological fault zones and are sustained by perennial groundwater moving vertically, to the ground surface, along these zones. A large amount of sampling is required to obtain spring discharge samples that represent deeper groundwater and are not affected by overprinting caused by increased aquifer mixing/connectivity and unsaturated zone processes. Three of the twenty three DBCA spring samples (aprox 15%) sampled fault conduits with higher flow rates and confirm that discharge water in perennial springs is sourced from the Wallal aquifer at depths of around 200 metres below ground level and

- Perennial surface water is likely to have a similar origin to the long lived mound springs but this is unable to be verified due to insufficient sampling and overprinting of unsaturated zone processes.

The major outcome of this study is an improved understanding of how the Walyarta mound springs and perennial surface water function under natural conditions. However, the behaviour of groundwater flow under changed conditions, in particular increased and prolonged abstraction of groundwater from the Wallal aquifer, is unknown. Questions that need to be answered are how Wallal aquifer hydraulic heads will be maintained in fault zones and will aquifer depressurisation due to groundwater abstraction be anisotropic (e.g. likely to propagate preferentially along fault zones and as a result decrease spring discharge rates).

Further work is required to answer these questions and reduce uncertainty and should include verification of the DBCA hydrological conceptual model of the mound springs by;

- Undertaking numerical modelling to provide a proof of concept on the role of geological faults. Numerical modelling should be undertaken to provide a proof of concept in relation to aquifer hydraulics. This should include testing model sensitivities to a range of Wallal hydraulic heads and fault zone physical properties required to deliver groundwater to the springs from 200 metres below ground level. Solute transport modelling, using conservative tracers (e.g. chloride) is required to verify saturated flow modelling results, which may prove challenging due to aquifer overprinting issues and the existence of older, less mobile, and spatially complex salt storages in the Mandora palaeovalley.
- Increasing hydrogeological information upgradient of the Walyarta mound springs. The most pressing issue is to increase hydrogeological information (e.g. stratigraphy (Wallal and Broome aquifers), water levels and quality (hydrogeochemistry and environmental tracers)) upgradient of the Walyarta mound springs and
- Improving targeting of future Walyarta mound spring and surface water sampling programs through the use of non-invasive methods to acquire robust information on the sub-surface. There is a need to investigate ways of improving the hit rate of point sampling and obtaining fine scale spatial information that can assist with hydrogeochemical mass balances. Therefore more robust three dimensional information of the sub surface is required to help design spring and surface water sampling programs (water, soils and formations). To address this, the use of other non-invasive, ground geophysical fine-scale mapping techniques in the Walyarta study area should be investigated (e.g. shallow seismic, electromagnetic and magnetotelluric methods).



## 10 References

Aquaterra, 2010. West Canning Basin Modelling Project. Report to the Western Australian Department of Water by Aquaterra Consulting Pty Ltd.

Anand, R.R., Gilkes, R.J., Armitage, T.M., Hillyer, J.W., 1985. Feldspar weathering in lateritic saprolite, *Clays and Clay Minerals*, v.33, no. 1, 31-43pp.

Auken, E., Christiansen, A. V., Jacobsen, Bo. H., Foged, N. and Sørensen, K.I., 2005. Piecewise 1D laterally constrained inversion of resistivity data. *Geophysical Prospecting*, 53, 497–506.

Appelo, C.A.J., and Postma, D., 2006, *Geochemistry, groundwater and pollution*. 2<sup>nd</sup> Edition. A.A Balkema Publishers 649

Beard, J.S. 1967. An Inland Occurrence of Mangrove. *Western Australian Naturalist* 10: 112–115.

Beard, J.S., 1973. The elucidation of palaeo-drainage patterns in Western Australia. *Vegetation Survey of Western Australia, Occasional Paper No 1*. Vegmap Publications, Perth, 17pp.

Bell, J.G., Kilgour, P.L., English, P.M., Woodgate, M.F., Lewis, S.J. and Wischusen, J.D.H. (compilers) 2012. WASANT Palaeovalley Map – Distributions of Palaeovalleys in Arid and Semi-arid WA-SA-NT (First Edition), scale 1:4 500 000. Geoscience Australia Thematic Map (Geocat No 73980)

Boschetti, T., 2011. Application of brine differentiation and Langlier-Ludwig plots to fresh-to-brine waters from sedimentary basins: Diagnostic potentials and limits, *Journal of Geochemical Exploration*, 108:126-130.

Breecker, D.O., Sharp, Z.D. and McFadden, L.D., 2009. Seasonal bias in the formation and stable isotopic composition of pedogenic carbonate in modern soils from central New Mexico, USA., *Geological Society of America Bulletin*; March/April 2009; V. 121; no. 3/4; p. 630-640.

Cendón, D.I., Hankin, S.I., Williams, J.P., Van der Ley, M., Peterson, M., Hughes, C.E., Meredith, K., Graham, I.T., Hollins, S.E., Levchenko, V. and Chisari, R. 2014. Groundwater residence time in a dissected and weathered sandstone plateau: Kulnura–Mangrove Mountain aquifer, NSW, Australia. *Australian Journal of Earth Sciences* 61, 475-499.

Cloetingh, S., and Ben-Avraham, Z., 2008. Pull-apart basin formation and development in narrow transform zones with application to the Dead Sea Basin, *Tectonics*, 27, TC6018

Deng, H., Fitts, J.P., Crandall, D., McIntyre, D. and Peters, C.A. 2015. Alterations of Fractures in Carbonate Rocks by CO<sub>2</sub>-Acidified Brines. *Environmental Science & Technology* 49, 10226-10234.

Department of Biodiversity, Conservation and Attractions (DBCA) 2017. Interim Recovery Plan 2017-2022 for Assemblages of the organic springs and mound springs of Mandora Marsh area and inland mangroves community of Salt Creek. Interim Recovery Plan No. (to be advised). Department of Biodiversity, Conservation and Attractions, Western Australia.

Department of Conservation and Land Management (CALM), 1999. A Land Management Assessment of Mandora Marsh and its Immediate Surrounds. Ed G. Graham. Department of Conservation and Land Management Perth. Unpublished report.

Department of Mines and Petroleum (DMP), 2010. 1:500 000 regolith map (500 metre grid) of Western Australia, Department of Mines and Petroleum WA

Department of Parks and Wildlife (DPaW), 2016. Parks and reserves of the south-west Kimberley and north-west Pilbara – Draft joint management plan 2016. Department of Parks and Wildlife, Perth.

Department of Water (DoW), 2010. La Grange groundwater allocation plan. Department of Water, Water Resource allocation and planning report series Report no. 25

Department of Water (DoW), 2012. West Canning Basin groundwater allocation limit report – Background information and method used to set an allocation limit for aquifers in the West Canning Basin. Department of Water, Water Resource allocation and planning report series Report no. 52

Department of Water and Environmental Regulation (DWER), in prep. West Canning Basin – Sandfire, Hydrogeological Conceptualisation Report. Department of Water Hydrogeological Report Series Report No. (to be advised)

Dogramaci, S., Skrzypek, G., Dodson, W., Grierson, P.F. 2012. Stable isotope and hydrochemical evolution of groundwater in the semi-arid Hamersley Basin of subtropical northwest Australia. *Journal of Hydrology* 475, 281-293.

Dogramaci, S. and Skrzypek, G. 2015. Unravelling sources of solutes in groundwater of an ancient landscape in NW Australia using stable Sr, H and O isotopes. *Chemical Geology* 393-394, 67-78.

English, V., Luu, R., & Coote, M. 2016. Survey of Mandora Mound Springs and Salt Creek, Walyarta. Department of Parks and Wildlife, WA.

Forman, D.J. & Wales, D.W., 1981. Geological evolution of the Canning Basin, Western Australia, Bulletin 210 Bureau of Mineral Resources, Geology and Geophysics. Australian Government Publishing Service Canberra.

FrOG Tech 2005. OZ SEEBASE™ v1 2005. Structural GIS <http://www.frogtech.com.au/seebase-range/>

Gallant, J.C., Dowling, T.I., 2003. A multi-resolution index of valley bottom flatness for mapping depositional areas. *Water Resources Research* 39:12

Geological Survey of Western Australia (GSWA), 2012a. Prospectivity of State Acreage Release Areas L12-8 and L12-9, Canning Basin, Western Australia: Geological Survey of Western Australia, 10p.

Geological Survey of Western Australia (GSWA), 2012b. Satellite ASTER GEoscience Produce Notes for Australia: Geological Survey of Western Australia, 26p.

Haig, T., 2008. The Pilbara Coast Water Study, Department of Water, Hydrogeological Series, Report HR 267, 184 pp.

Haig, T., 2009. The Pilbara coast water study, Department of Water, Hydrogeological Record Series, HG34, 173pp.

Hanna, J., 2014 Influence of Conceptual Model Uncertainty on Recharge Processes for the Wallal Aquifer System in the West Canning Basin, Western Australia. Unpublished University of Western Australia Master of Science (Hydrogeology) Thesis.

Harrington, G.A., & Harrington, N.M., 2016. A hydrochemical assessment of groundwater recharge and flow in the Broome Sandstone Aquifer, La Grange Area, Western Australia. A report prepared for Department of Agriculture and Food, Western Australia by Innovative Groundwater Solutions.

Harrington, G.A. & Harrington, N.M., 2017. Hydrochemistry of peat mound springs within Mandora Marsh, West Canning Basin, WA. A report prepared for Department of Parks and Wildlife, Western Australia by Innovative Groundwater Solutions.

Harrington, G.A. 2017. Hydrochemical data collection report Mandora Springs, November 2016. A report prepared for Department of Parks and Wildlife, Western Australia by Innovative Groundwater Solutions.

Hickman, A.H., & Gibson, D.L. 1982, Port Hedland-Bedout Island, W.A. (2nd edition): Western Australia Geological Survey, 1:250 000 Geological Series Explanatory Notes, 28p.

Hollins, S.E., Hughes, C.E., Crawford, J., Cendón, D., Meredith, K.M. in press. Rainfall isotope variations over the Australian continent - Implications for hydrology and isoscape applications. *Science of the Total Environment*.

Huntley, B. 2015 Walyarta-Preliminary Remote Sensing Report Department of Parks and Wildlife, Perth WA.

Jasechko, S., Lechler, A., Pausata, F.S.R., Fawcett, P.J., Gleeson, T., Cendón, D., Galewsky, J., LeGrande, A.N. Risi, C., Sharp, Z.D., Welker, J., Martin, M., Yoshimura, K. 2015. Late-glacial to late-Holocene shifts in global precipitation  $\delta^{18}\text{O}$ . *Climate of the Past* 11(10): 1375-1393

Ladd, B., Bonser, S.P., Peri, P.L., Larsen, J.R., Laffan, S.W., Pepper, D.A. and Cendón, D.I. 2009. Towards a physical description of habitat: quantifying environmental adversity (abiotic stress) in temperate forest and woodland ecosystems. *Journal of Ecology* 97, 964-971.

Lane, R., Green, A., Golding, C., Owers, M., Pik, P., Plunkett, C., Sattel, D., Thorn, B., 2000, An example of 3D conductivity mapping using the TEMPEST airborne electromagnetic system: *Exploration Geophysics*, 31, 162-172.

Lamit, J.L. , Romanowicz, K.J., Potvin, L.R., Rivers, A.R., Singh, K., Lennon, J.T., Tringe, S.J., Kane, E.S., Lilleskov, E.S. 2017. Patterns and drivers of fungal community depth stratification in sphagnum peat. *FEMS Microbiology Ecology*, 93, 14p.

Lamit, J.L. and others in prep, Global patterning of fungal communities in peat systems - implications for climate change

Laws, A.T., 1991. 1:250 000 Geological Series – Explanatory Notes: Broome Western Australia Sheet SE/51-6 International Index. Bureau of Mineral Resources, Geology and Geophysics and Geological Survey of Western Australia. 37pp.

Leech, R.E.J., 1979. Geology and groundwater resources of the Southwestern Canning Basin, Western Australia. Geological Survey of Western Australia. Record 1979/9. Perth 1979. ISBN No. 072448034X..

Loomes, R., 2010. Determining water level ranges of Pilbara riparian species, Environmental water report series, Report No. 17, Department of Water, Government of Western Australia, Perth.

Ma, J-Y., Sun, W., Liu, X-N., Chen, F-H., 2012. Variation in the Stable Carbon and Nitrogen Isotope Composition of Plants and Soil along a Precipitation Gradient in Northern China. PLoS ONE 7(12): e51894. DOI:10.1371/journal.pone.0051894

Magee, J.W., 2009. Palaeovalley Groundwater Resources in Arid and Semi-Arid Australia – A Literature Review. Geoscience Australia Record 2009/03. 224 pp.

McWilliam, J.R., & Mison, K., 1974. Significance of the C4 Pathway in *Triodia irritans* (Spinifex), a Grass Adapted to Arid Environments. Aust. J. Plant Physiol., 1974, 1, 171-5

Mercado, A., 1985. The use of hydrogeochemical patterns in carbonate sand and sandstone aquifers to identify intrusion and flushing of saline water. Groundwater v 23 no. 5: 635-645pp

Meredith, K.T. 2009. Radiocarbon dating groundwaters of the West Canning Basin, Western Australia. ANSTO-C-1038. A commercial report prepared for the Government of Western Australia, Department of Water. March 2009.

Meredith, K.T., Cendon, D., Hankin, S., Peterson, M. & Hollins, S., 2014. Assessment of the aquifers in the West Canning Basin-Pardoo - application of isotopic and hydrochemical techniques. ANSTO-C-1362. A commercial report prepared for the Government of Western Australia, Department of Water. March 2014.

Meredith, K.T., Han, L.F., Hollins, S.E., Cendon, D., Jacobsen, G.E., and Baker, A., 2016. Evolution of chemical and isotopic composition of inorganic carbon in a complex semi-arid zone environment: Consequences for groundwater dating using radiocarbon. *Geochimica et Cosmochimica Acta* v188: 352-367pp

Meredith, K.T., Han, L.F., Cendon, D.I., Crawford, J., Hankin, S., Peterson, M, & Hollins, S.E., 2018. Evolution of dissolved inorganic carbon in groundwater recharged by cyclones and groundwater age estimations using the <sup>14</sup>C statistical approach. *Geochimica et Cosmochimica Acta* v220: 483-798pp

Mira Geoscience, 2016. Inversion and preliminary interpretation of airborne electromagnetic data from the West Canning Basin - Sandfire TEMPEST survey. A report prepared for the Government of Western Australia, Department of Water. February 2016

Mulcahy, M.J. and Bettenay, E. 1972. Soil and landscape studies in Western Australia, the major drainage divisions. *Journal of the Geological Society of Australia*. 18(4):349-357.

Mueller, N., Lewis, A., Roberts, D., Ring, S., Melrose, R., Sixsmith, J., Lymburner, L., McIntyre, A., Tan, P. & Curnow, S, 2016. Water observations from space: Mapping surface water from 25years of Landsat imagery across Australia. *Remote Sensing of Environment*, 174, 341-352.

Nance, W.B., and Taylor, S.R., 1976, Rare earth element patterns and crustal evolution 1.— Australian Post Archaean sedimentary rocks. *Geochimica et Cosmochimica Acta* v40: 1539-1551pp



NTEC Environmental Technology (NTEC) 2012. West Canning Basin Groundwater Model: Northstar Magnetite Project. Report for Fortescue Metals Group (FMG) Ltd. June 2012

Parkhurst, D.L., Appelo, C.A.J., (1999) User's guide to PHREEQC (Version 2) : a computer program for speciation, batch-reaction, one-dimensional transport, and inverse geochemical calculations USGS Water-Resources Investigations Report 99,-4259.

Parra-García , M, Sanchez, G, Dentith, MC and George, AD 2014, Regional structural and stratigraphic study of the Canning Basin, Western Australia: Geological Survey of Western Australia, Report 140, 215p.

Paul, R,J, George, R,J & Gardiner, P,S 2013, A review of the Broome Sandstone aquifer in the La Grange area, Resource Management technical report 387, Department of Agriculture and Food, Perth.

Pells Sullivan and Meynink (PSM) 2017, West Canning Basin Groundwater Model Report, a report to Department of Water and Environmental Regulation Perth Western Australia, 394p.

Pers comm. Val English, Principal Ecologist, Department of Biodiversity, Conservation and Attractions

Pers comm. Mike Lyons, Senior Research Scientist, Department of Biodiversity, Conservation and Attractions

Pers comm. Dr Pauline Grierson, Director West Australian Biogeochemistry Centre

Quinlan, K., Pinder, A., & Lewis, L. 2016. Aquatic Fauna Survey at Mandora Marsh (Walyarta) in September 2015: Prepared for Parks and Wildlife's Kimberley Region. Department of Parks and Wildlife, Kensington, Western Australia.

Retallack, G.J., 2005, Pedogenic carbonate proxies for amount and seasonality of precipitation in paleosols: *Geology*, v. 33, p. 333-336.

Roach, I. C. ed. 2010. Geological and energy implications of the Paterson Province airborne electromagnetic (AEM) survey, Western Australia. *Geoscience Australia Record* 2010/12, 318 pp.

Robertson, I.D.M., 1996. Rock weathering, fabrics and bedrock identification. CSIRO Division of Exploration Geoscience.

Singh, B. and MacKinnon, I.D.R., 1996. Experimental transformation of kaolinite to halloysite, *Clays and Clay Minerals*, Vol. 44, no. 6, 825-834pp.

Skrzypek G., 2013, Normalization procedures and reference material selection in stable HCNOs isotope analyses – an overview. *Analytical and Bioanalytical Chemistry* 405: 2815-2823.

Soerensen,C.C., Munday, T.J., Rutherford, J.L. and Cahill, K. 2017. Processing and Inversion of Mandora Marsh AEM Data : Enhanced TEMPEST data processing and interpretation. CSIRO Technical Report EP 178999; CSIRO, Australia.

Storey, A.W., Halse, S.A., Shiel, R.J. & Creagh, S. 2011, Aquatic fauna and water chemistry of the mound springs and wetlands of Mandora Marsh, north-western Australia. *Journal of the Royal Society of Western Australia*, 94: 419-437

Suckow, A. 2014, The age of groundwater – Definitions, model and why we do not need this term. *Applied Geochemistry*, 50: 220-230

Towner, R.R., 1982a, 1:250 000 Geological Series – Explanatory Notes: Mandora Western Australia Sheet SE/51-13 International Index. Bureau of Mineral Resources, Geology and Geophysics and Geological Survey of Western Australia. 22pp.

Towner, R.R., 1982b. 1:250 000 Geological Series – Explanatory Notes: Munro Western Australia Sheet SE/51-14 International Index. Bureau of Mineral Resources, Geology and Geophysics and Geological Survey of Western Australia. 22pp.

Towner, R.R., and Gibson, D.L., 1983. Geology of the onshore Canning Basin, Western Australia: Bureau of Mineral Resources, Geology and Geophysics, Bulletin 215, 51p.

Van der Graff, W.J.E, Crowe, R.W.A, Bunting, J.A. and Jackson, M.J. 1977. Relict early Cenozoic drainages in arid Western Australia. *Zeitschrift fur Geomorphologie*, NF 21:379-400.

van Wijk, J., Axen G., and Abera R. (in press) Initiation, evolution and extinction of pull-apart basins: Implications for opening of the Gulf of California, Tectonophysics.

V&C Semeniuk Research Group 2000. Wetlands of the north-western Great Sandy Desert, unpublished. Perth

Vogwill, R., & Callow, N., 2017. Mandora Marsh Surface Water Mapping by Remote Sensing. A report prepared for the Department of Biodiversity, Conservation and Attractions Kensington WA.

Wang, H., Zeuschner, J., Eremets, M., Troyan, I., & Williams, J., 2016. Stable solid and aqueous H<sub>2</sub>CO<sub>3</sub> from CO<sub>2</sub> and H<sub>2</sub>O at high pressure and high temperature. *Nature Scientific Reports* 6:19902, 8pp

Williams, I.R., 2003, Yarrie, W.A. (3rd edition): Western Australia Geological Survey, 1:250 000 Geological Series Explanatory Notes, 84p.

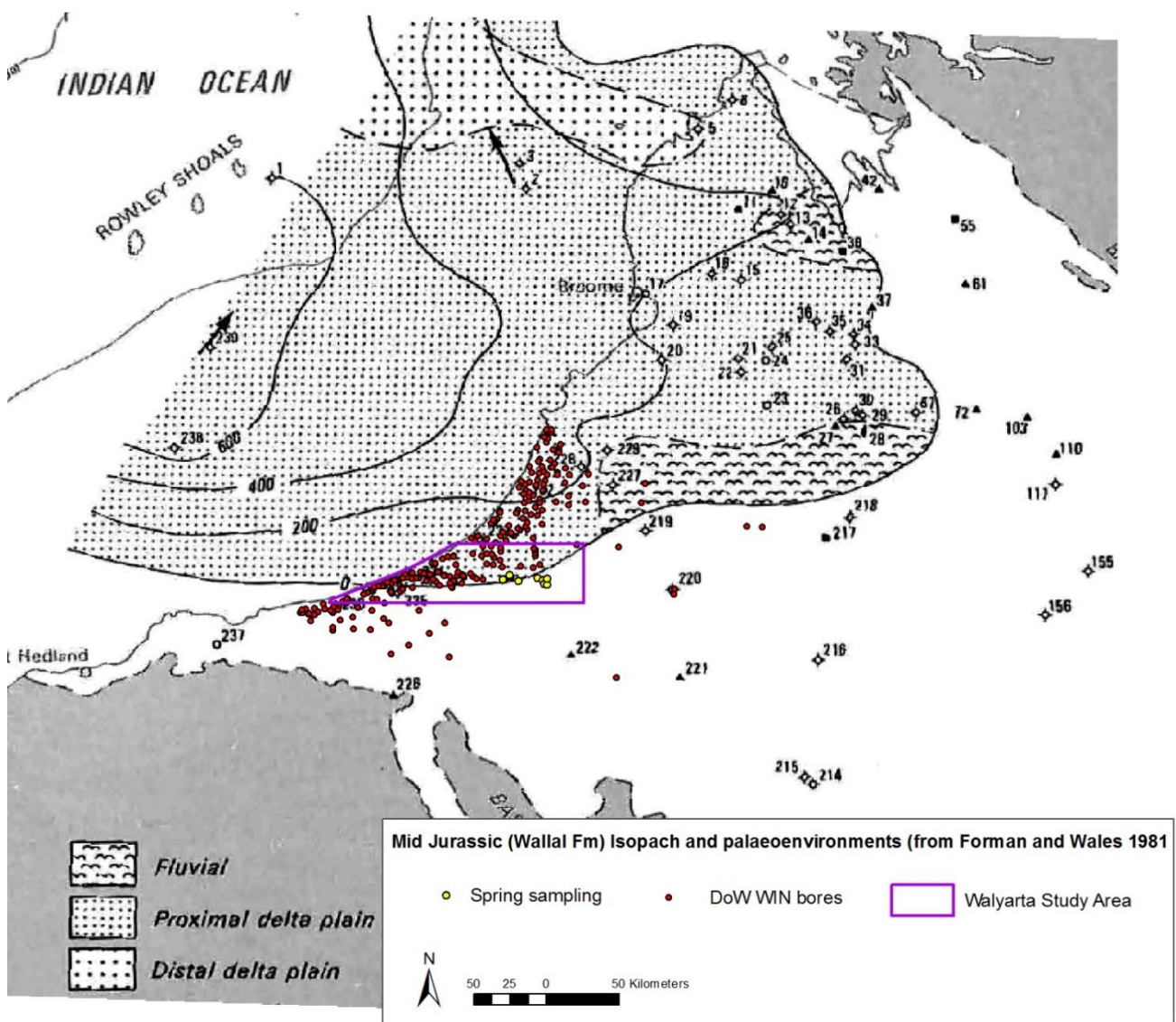
Wood, J.L., 2017. Report for Wetlands and Mound Spring microbial investigation.

Wright, N, George R, Paul, R & Raper, GP 2016. Identifying groundwater dependent wetlands of the Broome Sandstone aquifer in the La Grange groundwater area, Western Australia, Resource management technical report 397, Department of Agriculture and Food, Western Australia, Perth.

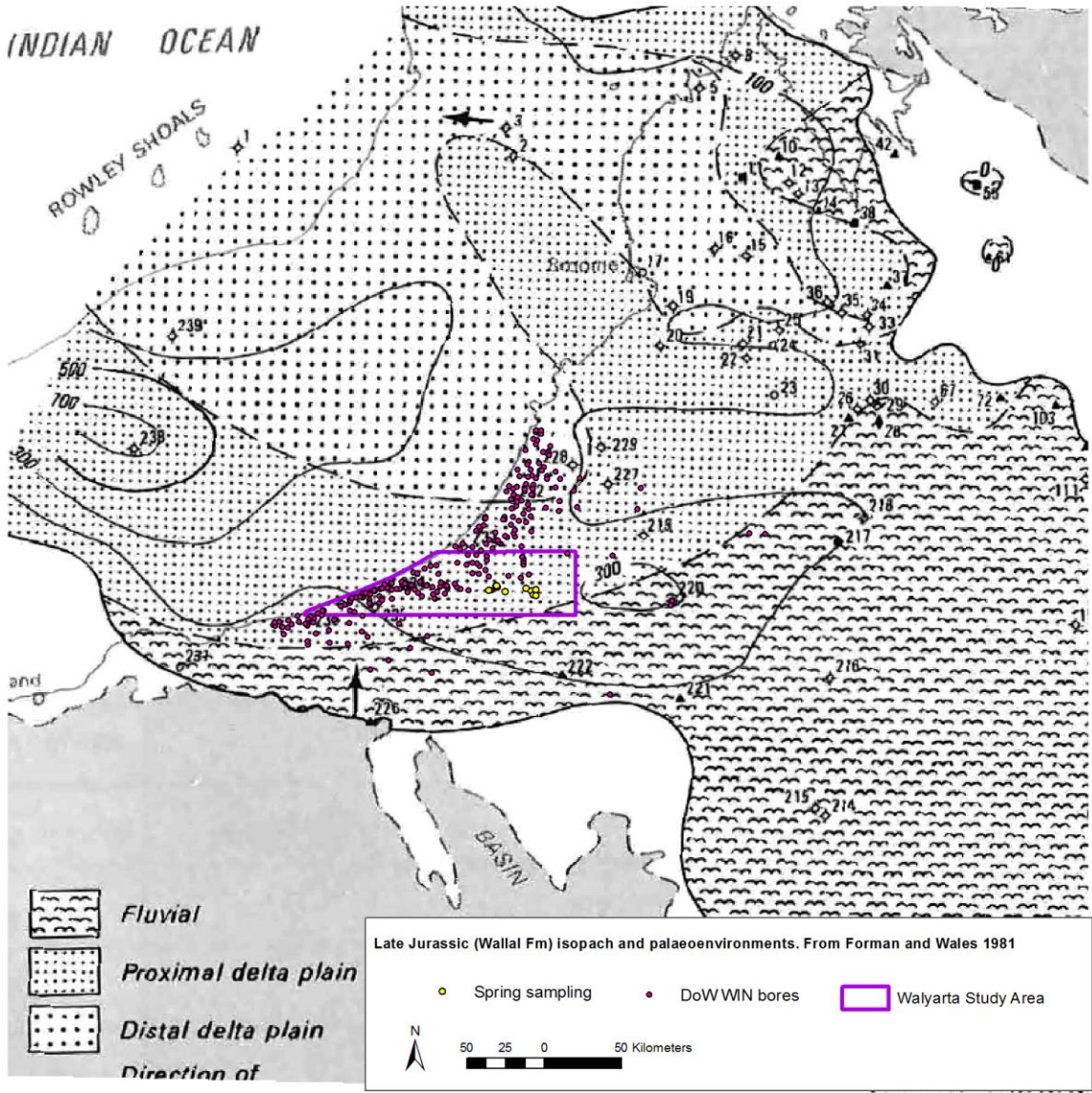
Wyrwoll, H., McKenzie, N.L., Pederson, B.J. & Tapley, I.J. 1986. The Great Sandy Desert of northwestern Australia: the last 7000 years. *Search* 17: 208–210.

## Appendix 1 – Mid-Jurassic to Early Cretaceous Isopachs (from Forman and Wales 1981)

Map 1

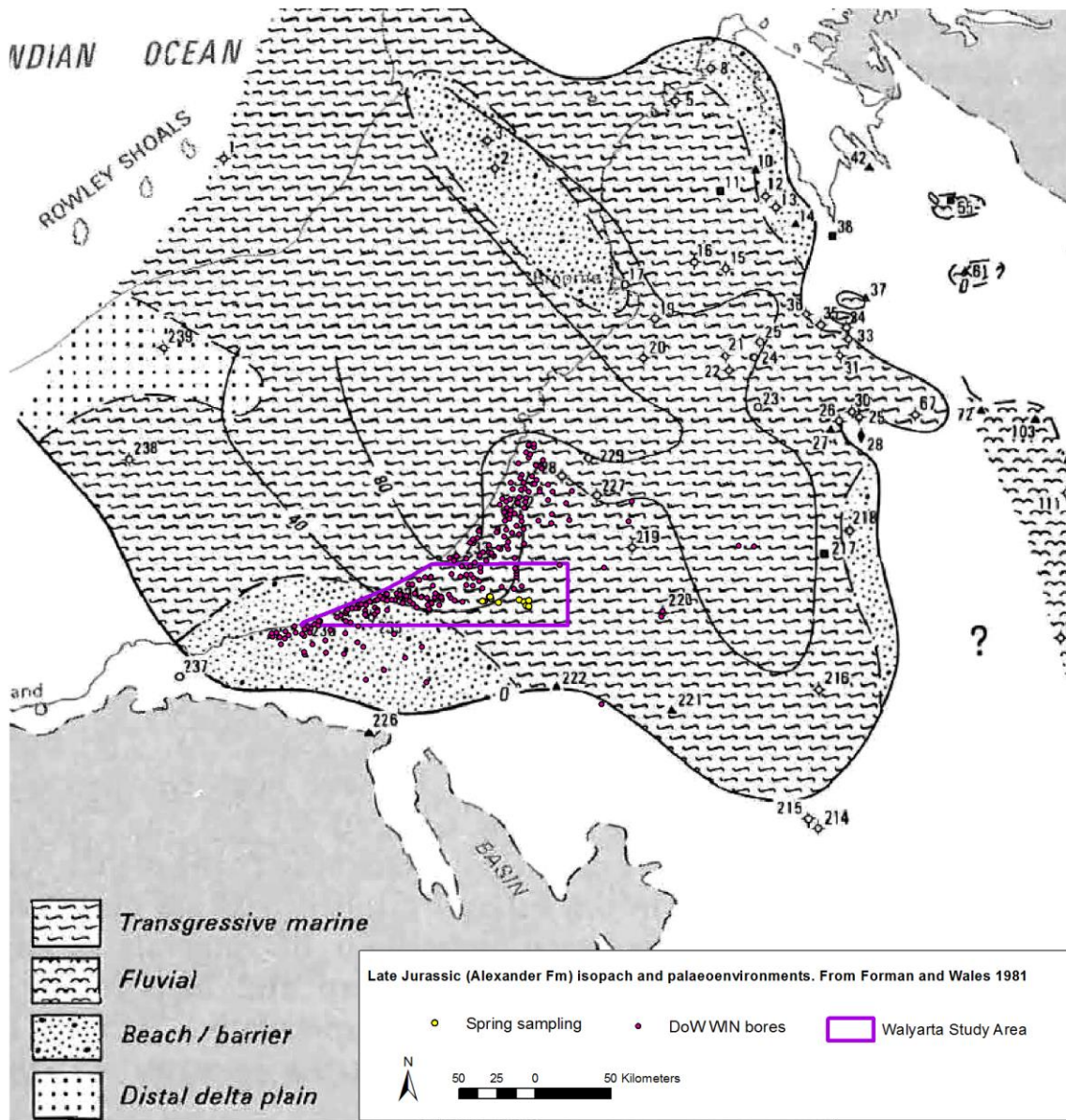


Map 2

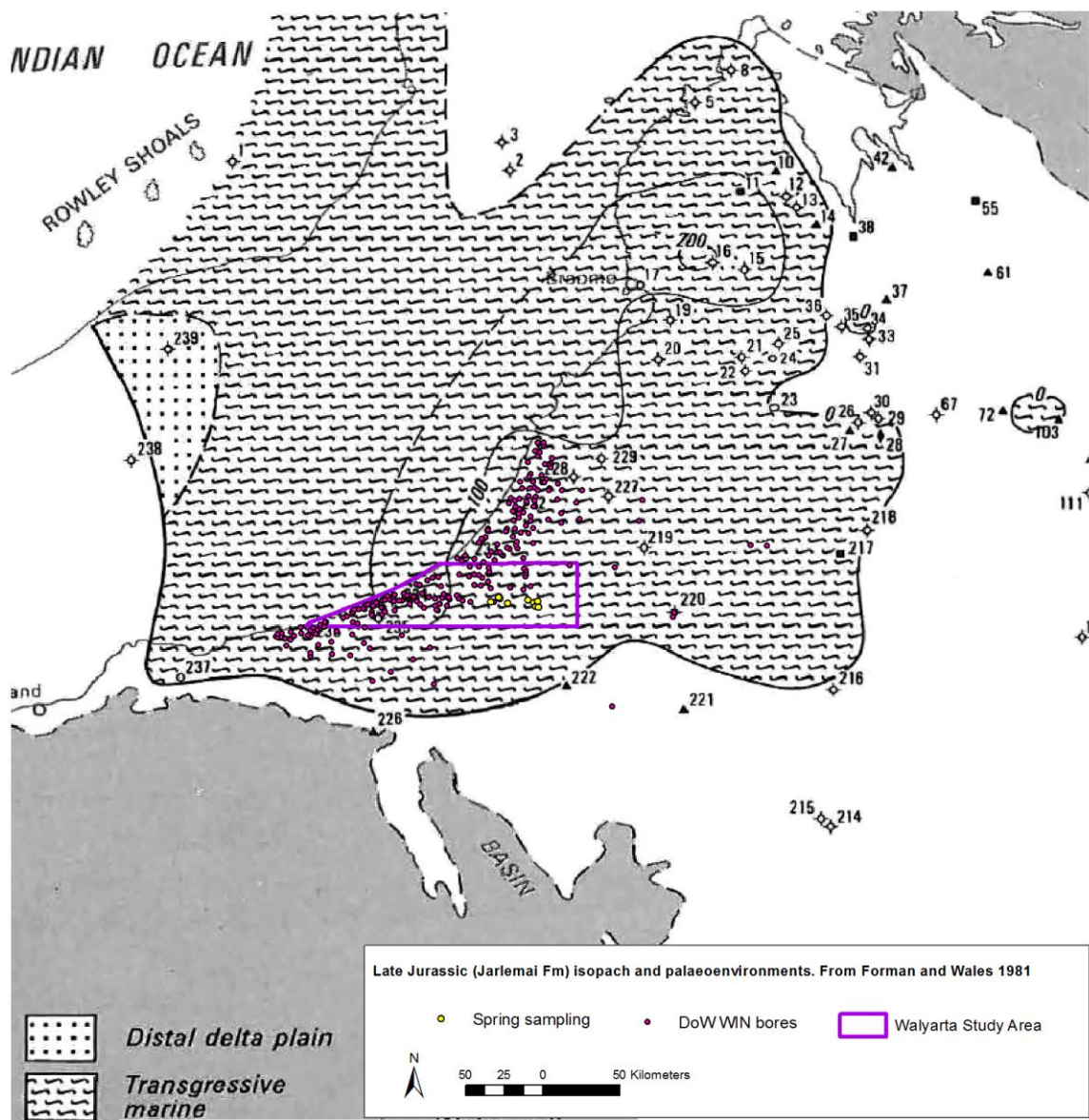




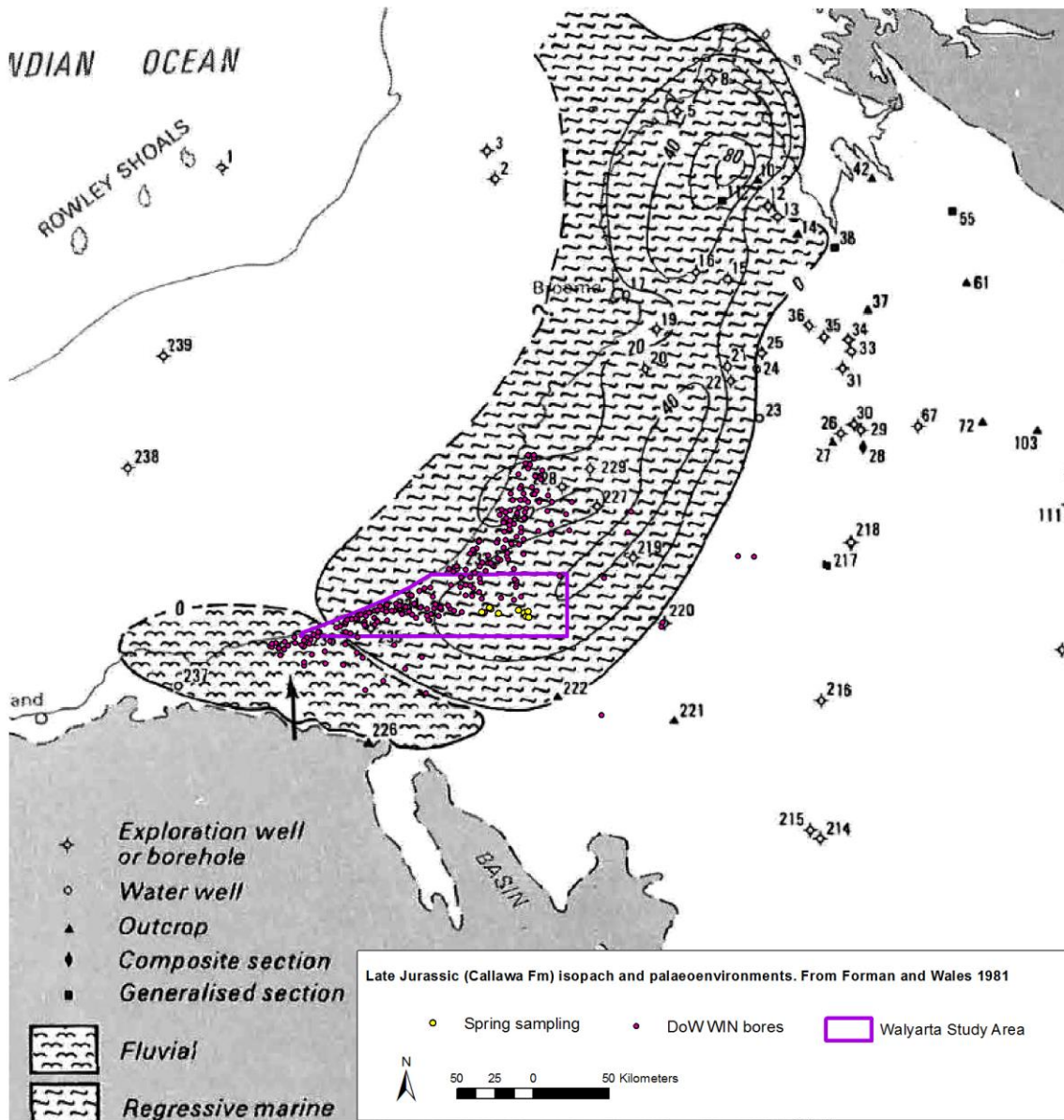
Map 3



Map 4

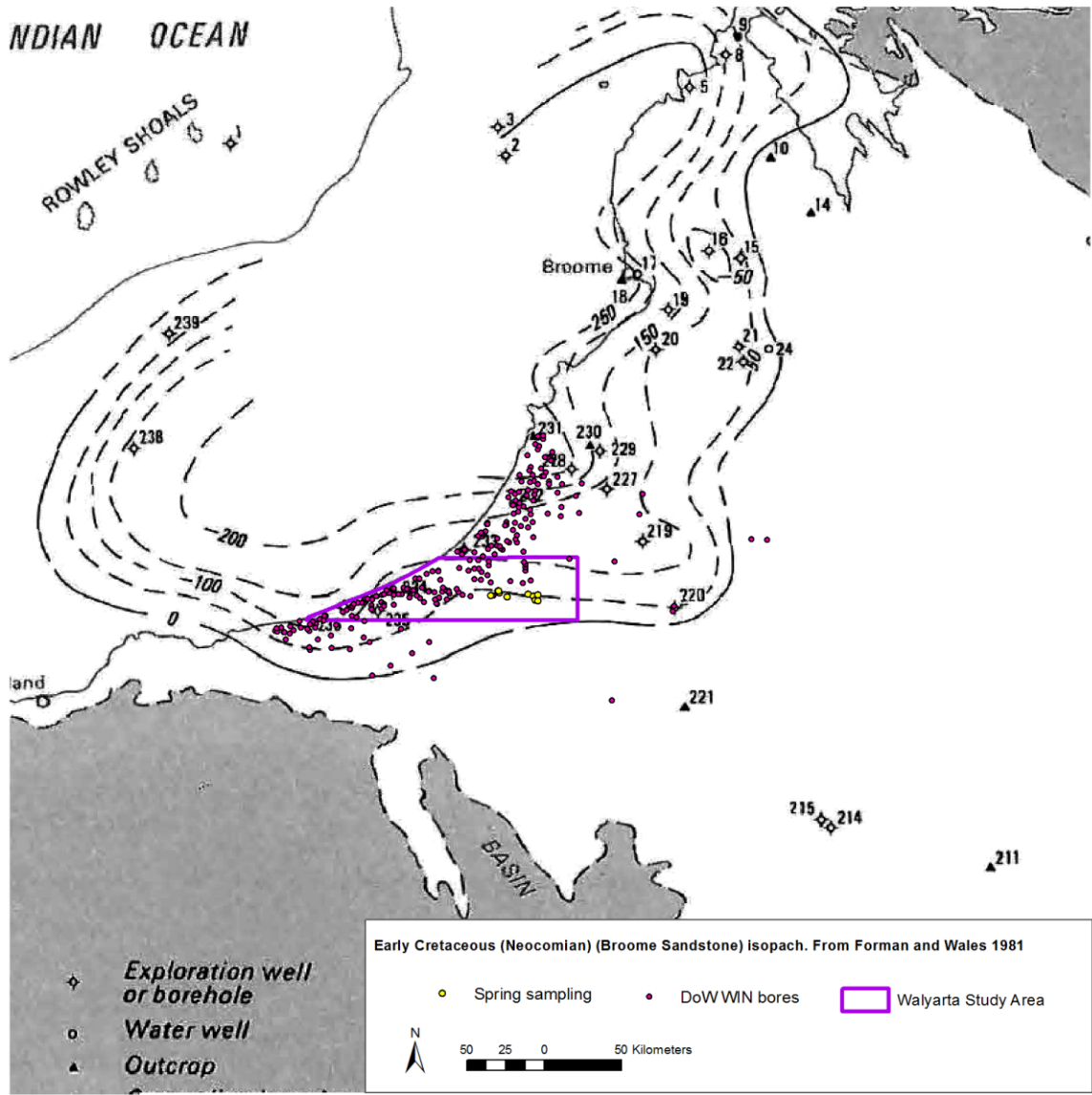


Map 5





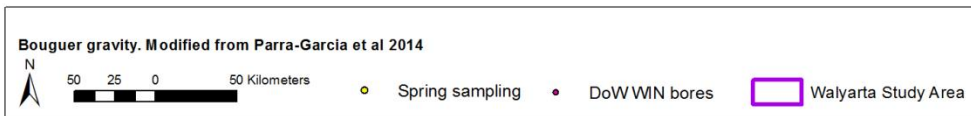
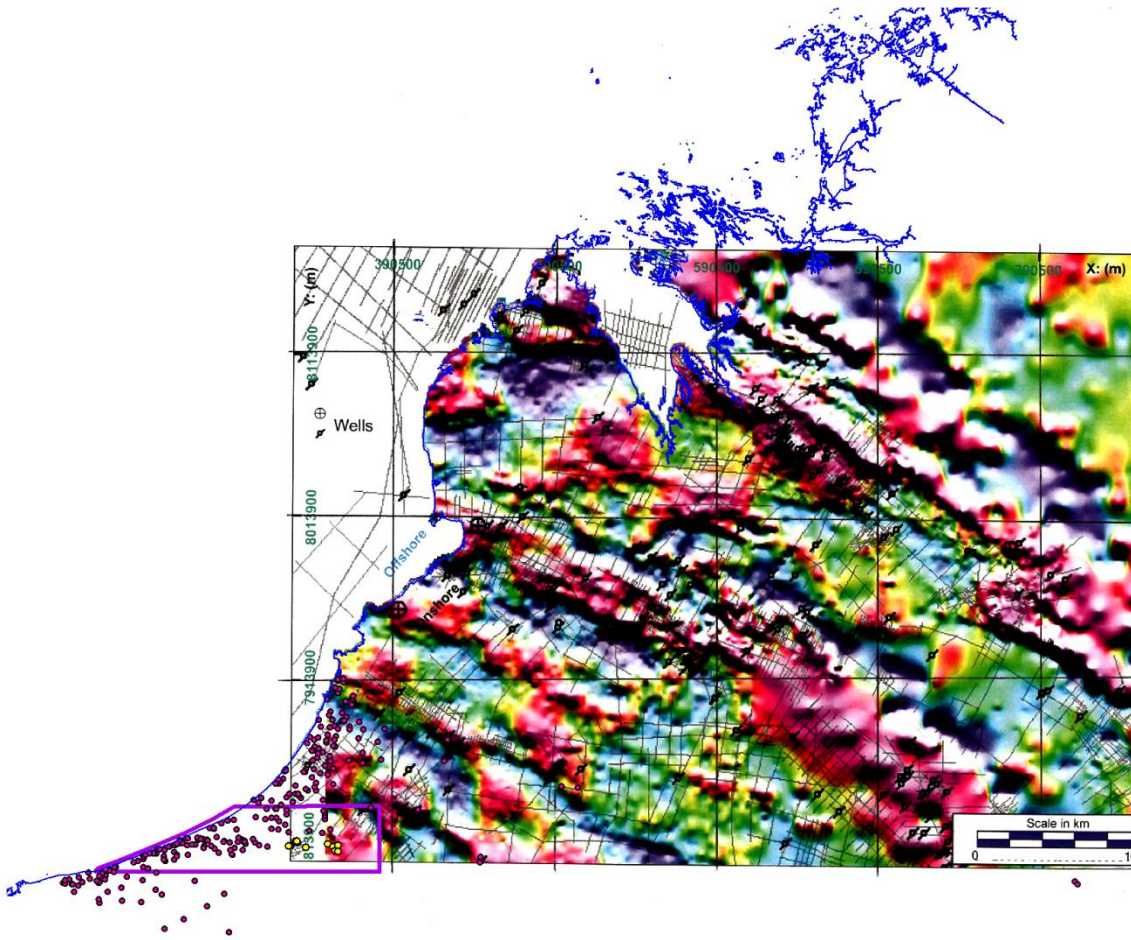
Map 6



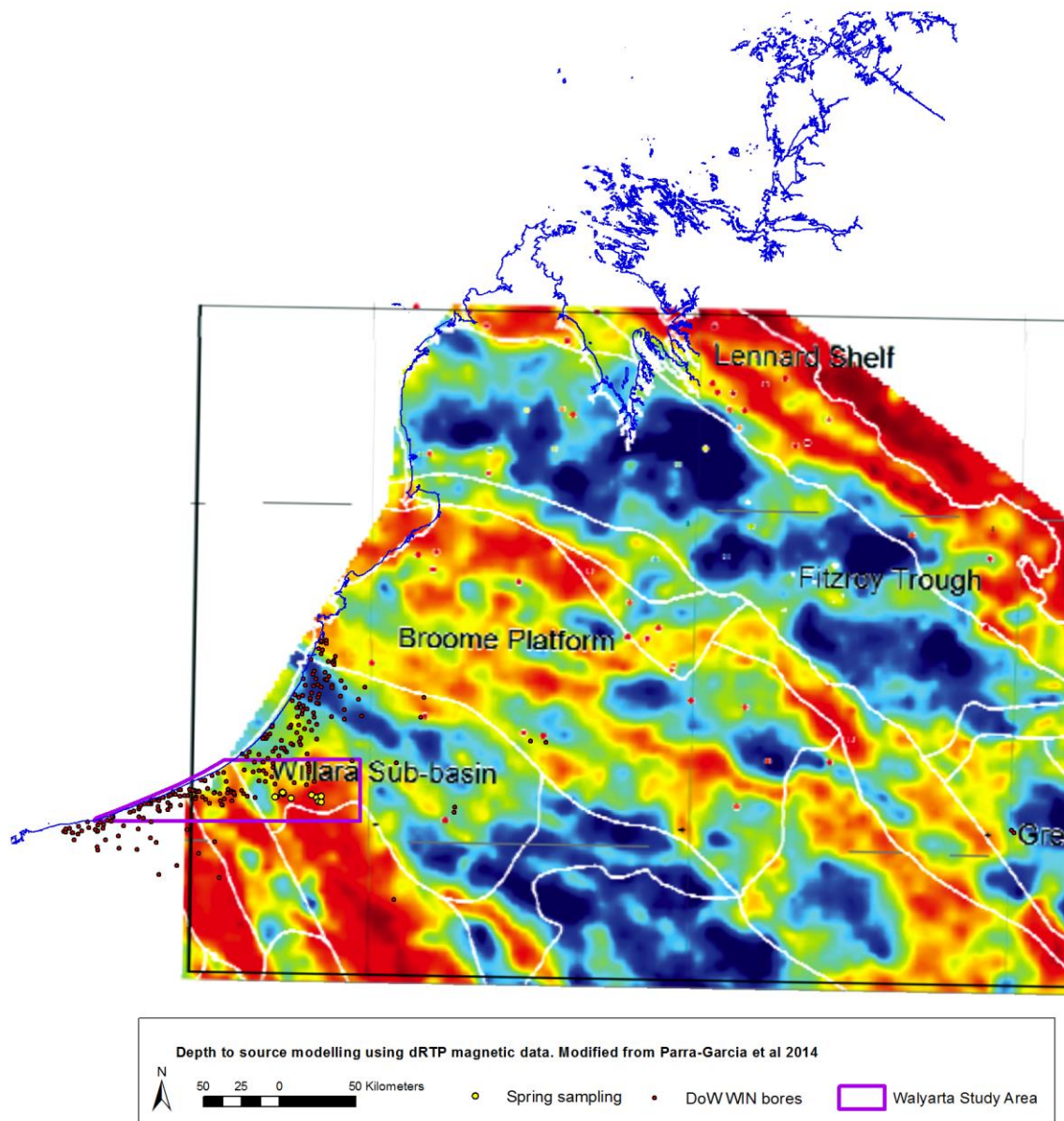


## Appendix 2 Geophysics – stratigraphic and structural modelling

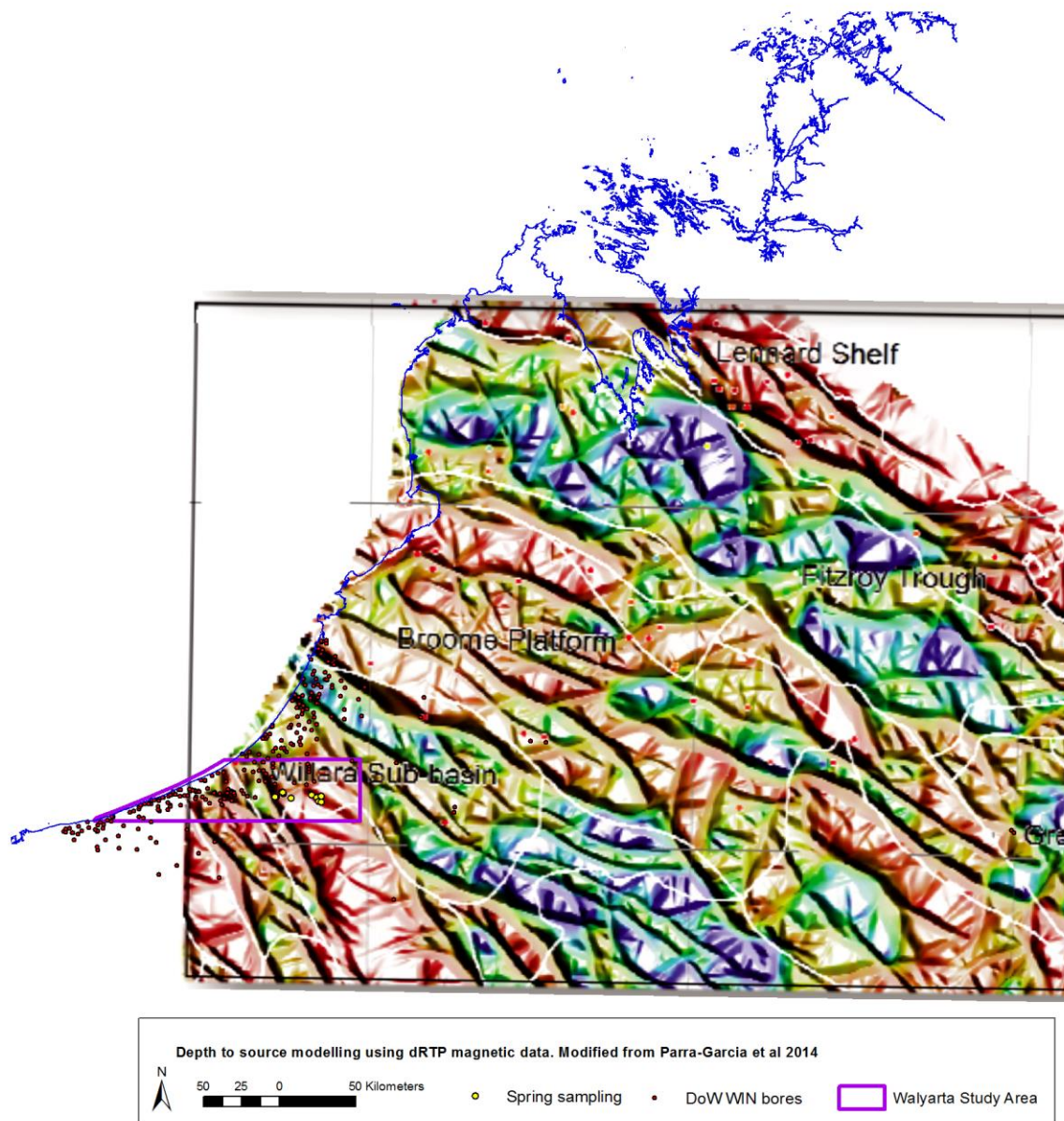
### Map 1



Map 2

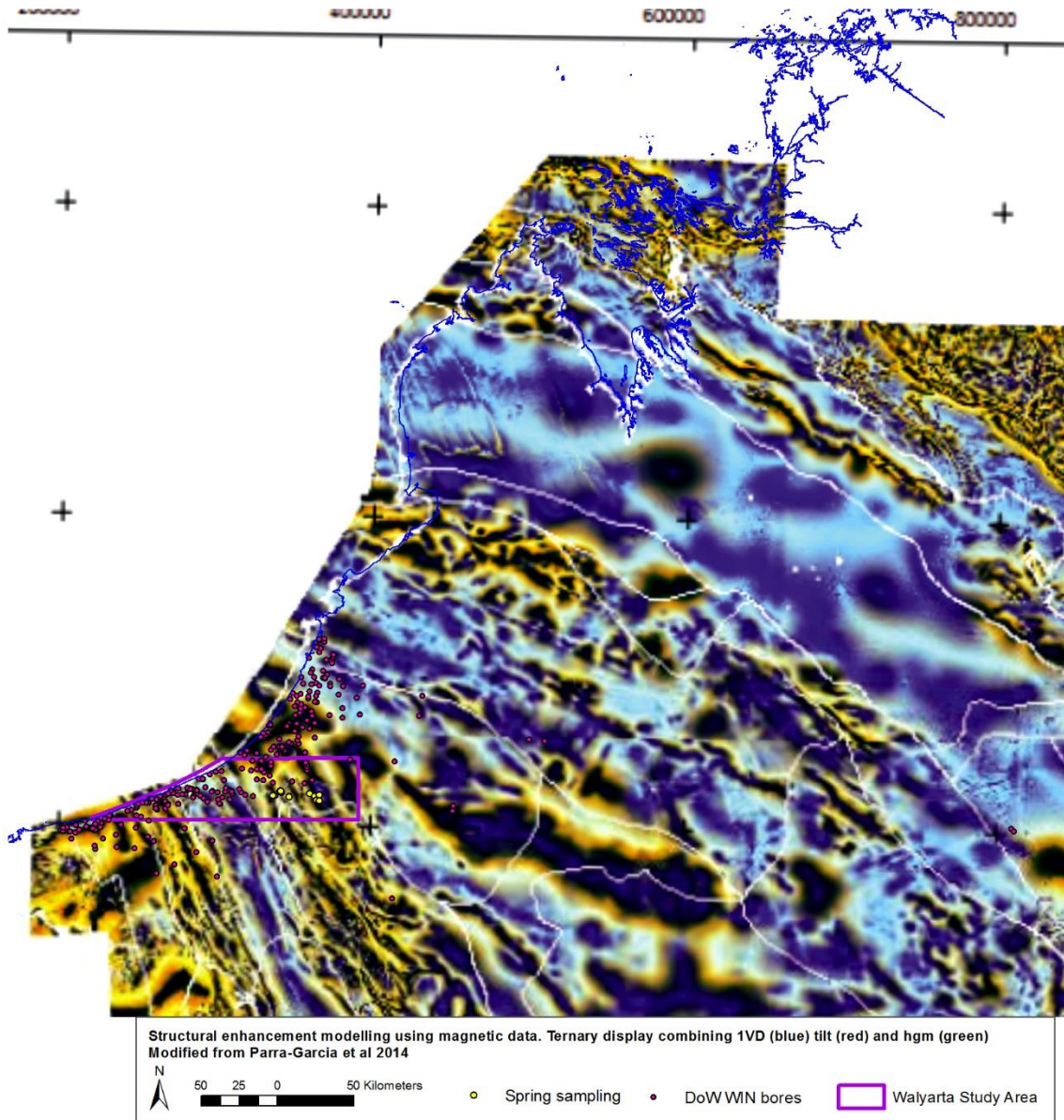


Map 3



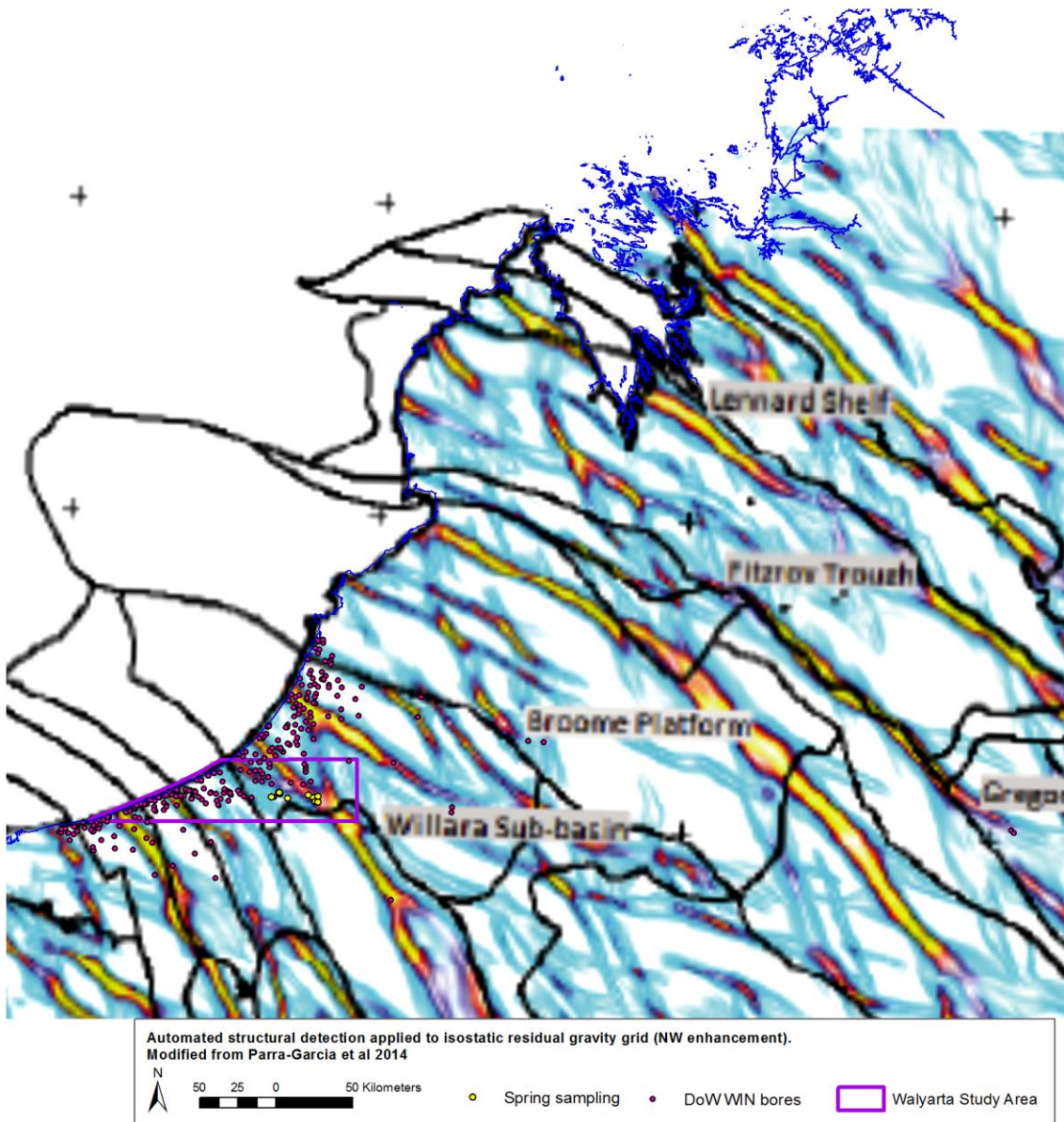


Map 4

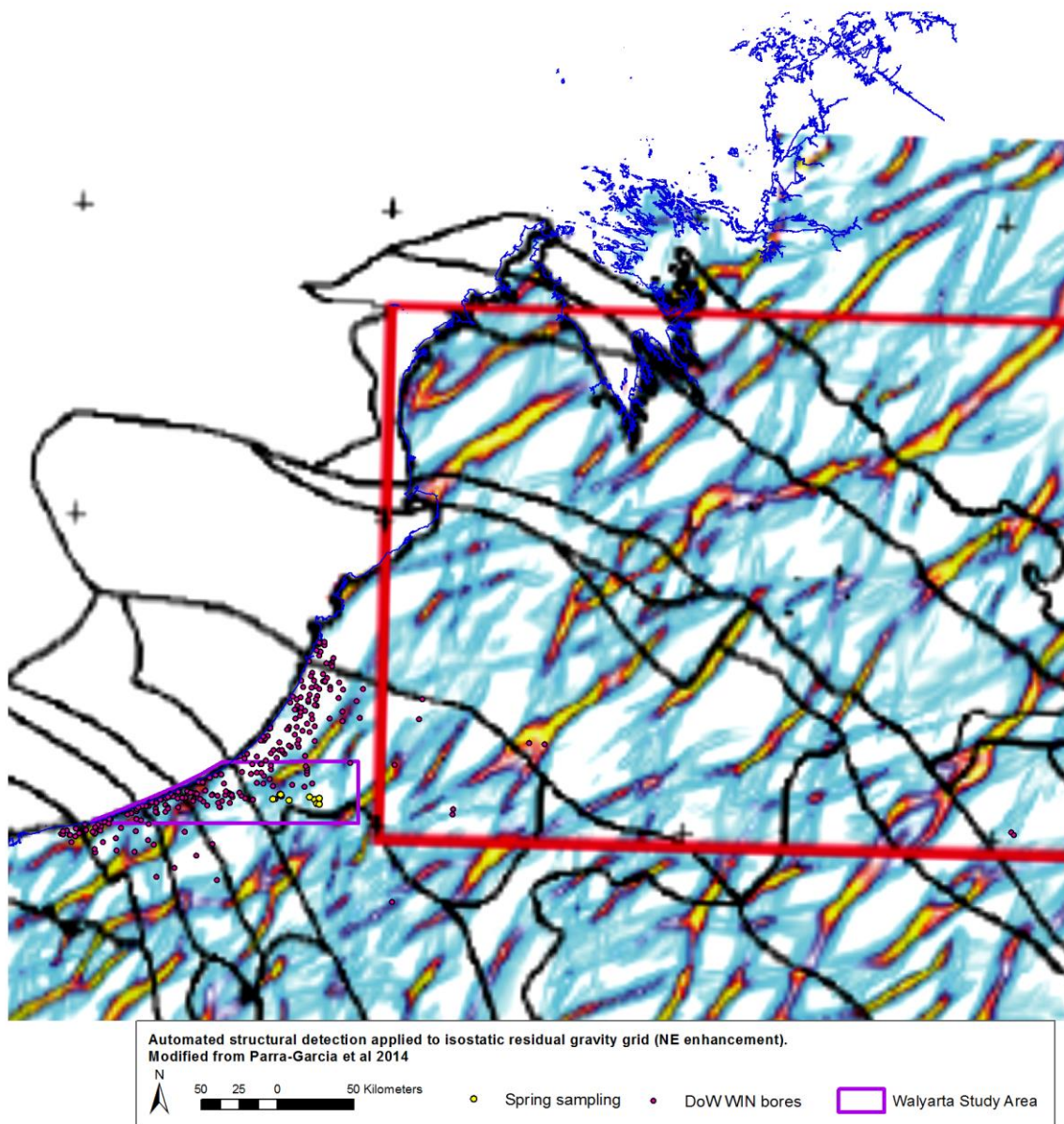




Map 5



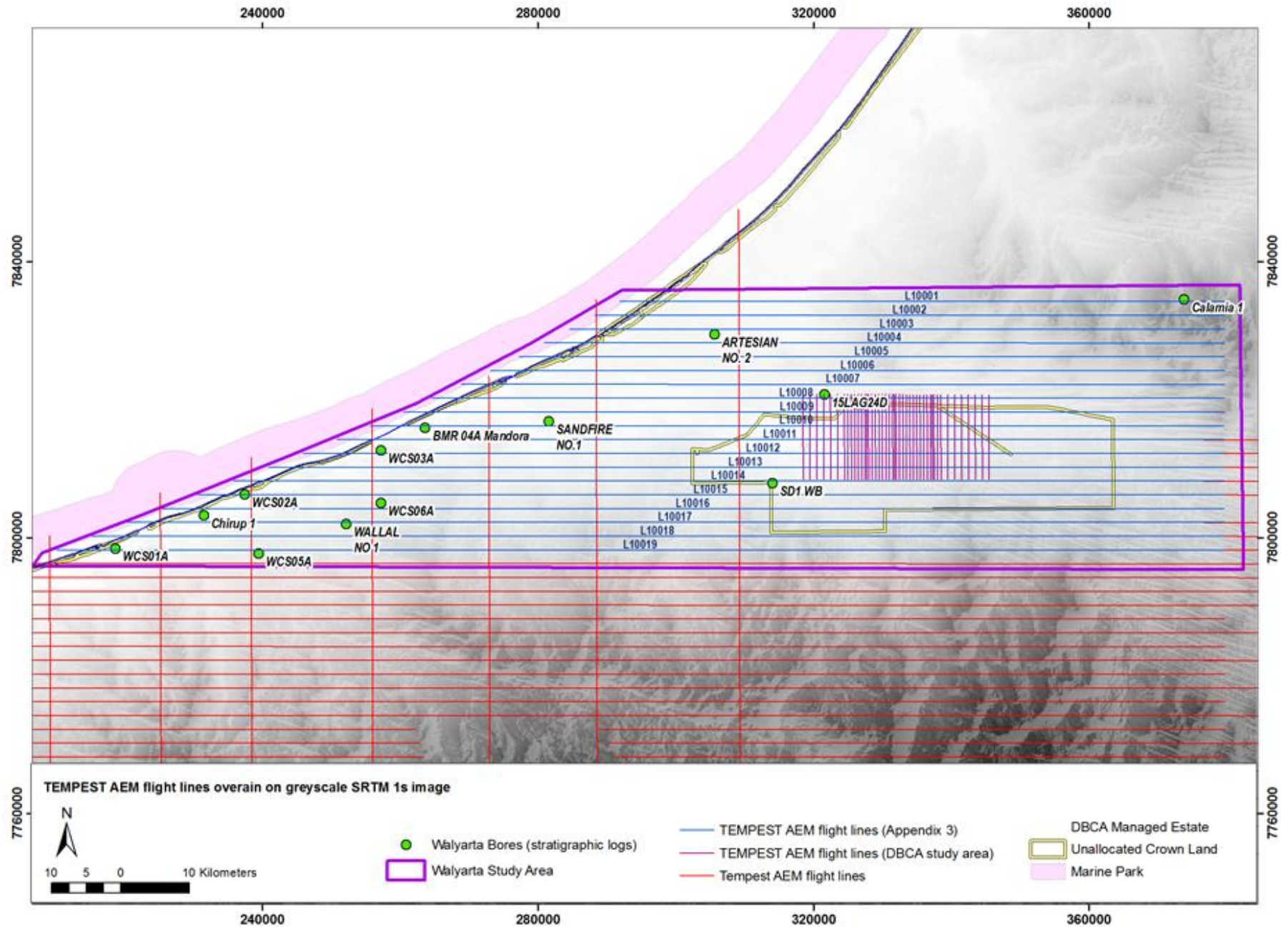
Map 6



## **Appendix 3 Geophysics (AEM) – interpreted stratigraphy, structure and water quality**


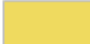




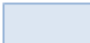






HYDROLOGICAL CONCEPTUALISATION OF THE WALYARTA MOUND SPRINGS

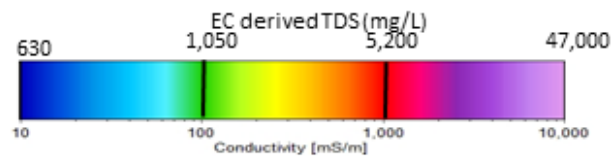




### Key

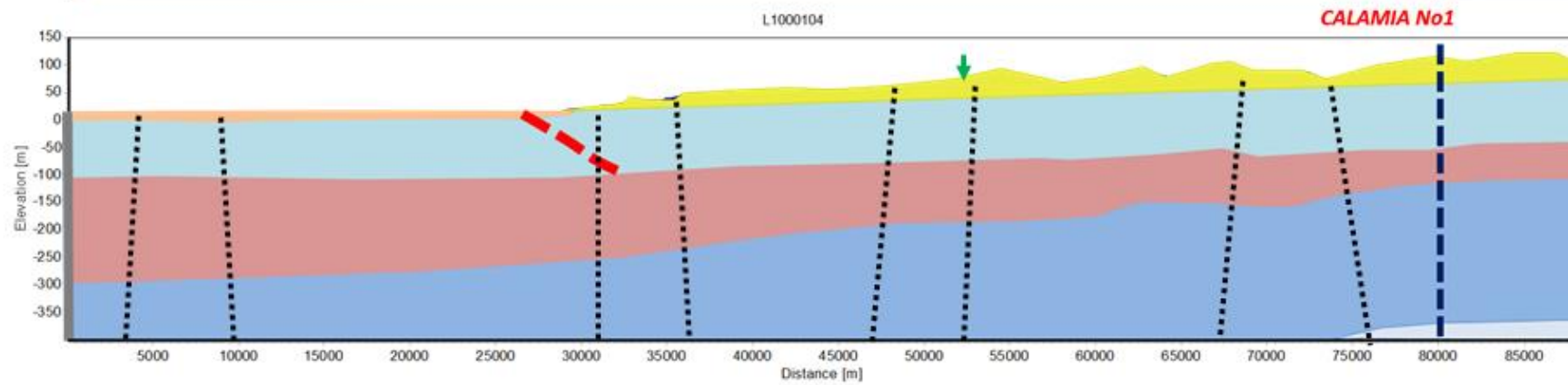
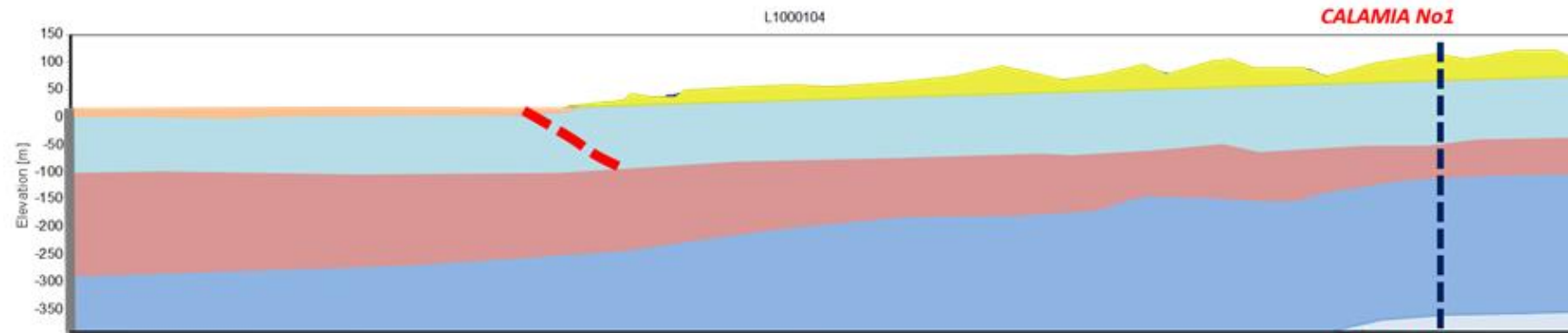
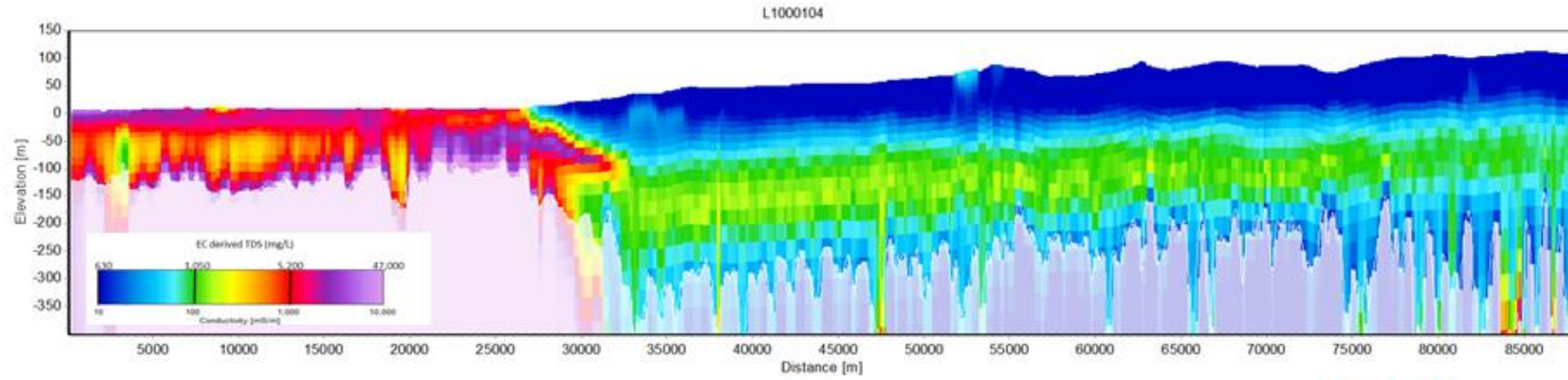
-  Sandplain sediments (DMP/GSWA 1:500k WA regolith map)
-  Palaeodrainage sediments (Pleistocene / Eocene)
-  Tidal sediments (DMP/GSWA 1:500k WA Regolith map)
-  Broome Sandstone (Cretaceous – may include 10-20m Callawa Fm (Late Jurassic at base))
-  Jarlemai Siltstone (late Jurassic) (? maybe present)
-  Wallal Sandstone (mid-late Jurassic)
-  Undifferentiated Permian sediments / ? Crystalline basement

-  Drill hole/bore
-  Evapotranspiration (EVT)
-  Salt water interface (SWI)
-  Geological fault

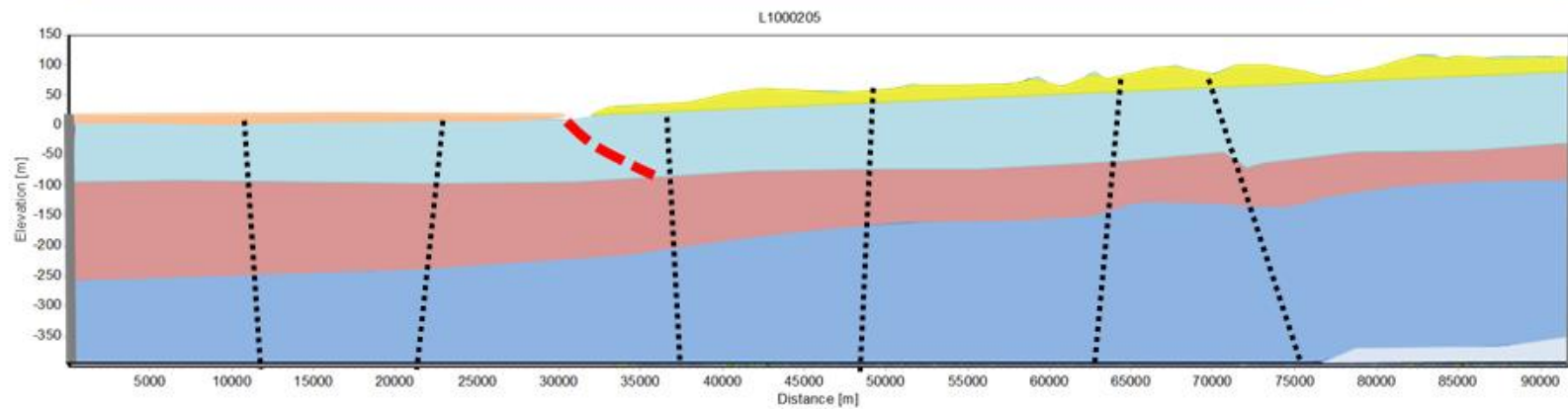
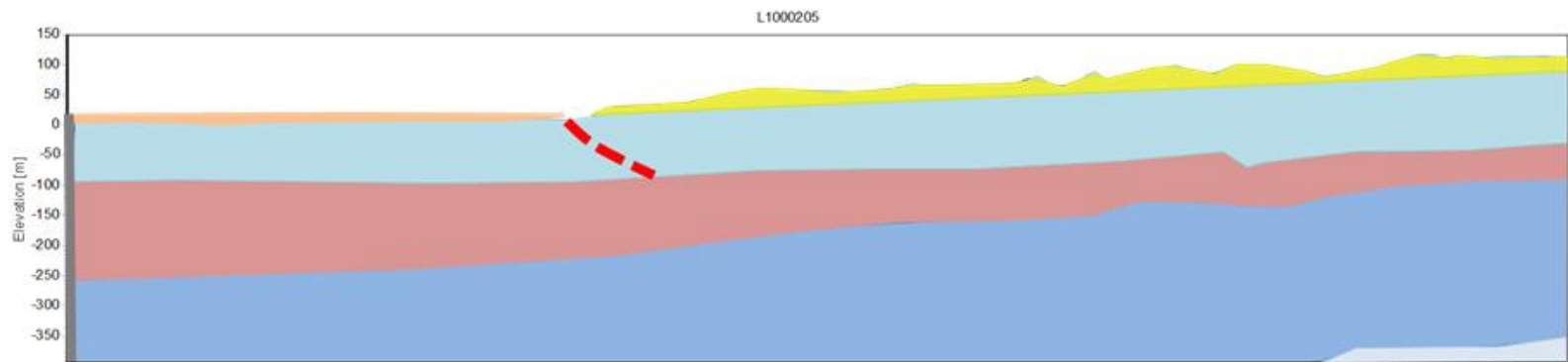
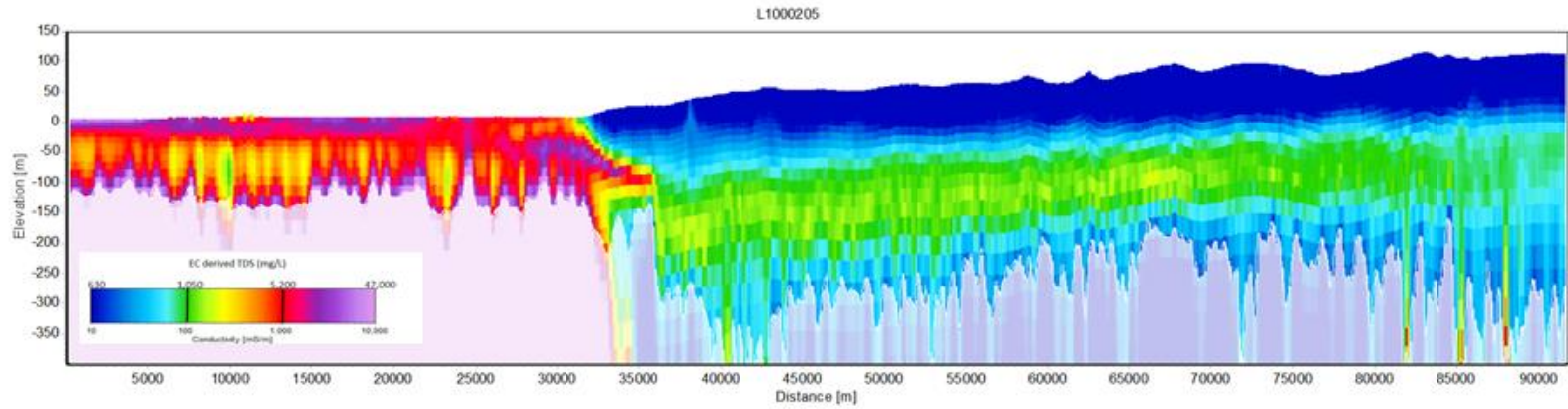


TEMPEST AEM conductivity – depth section scale bar

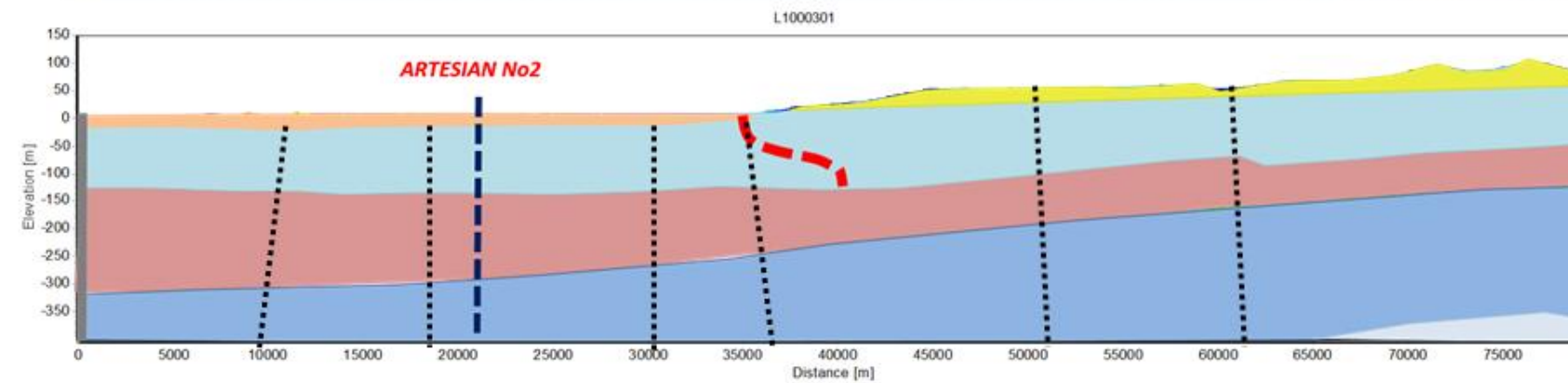
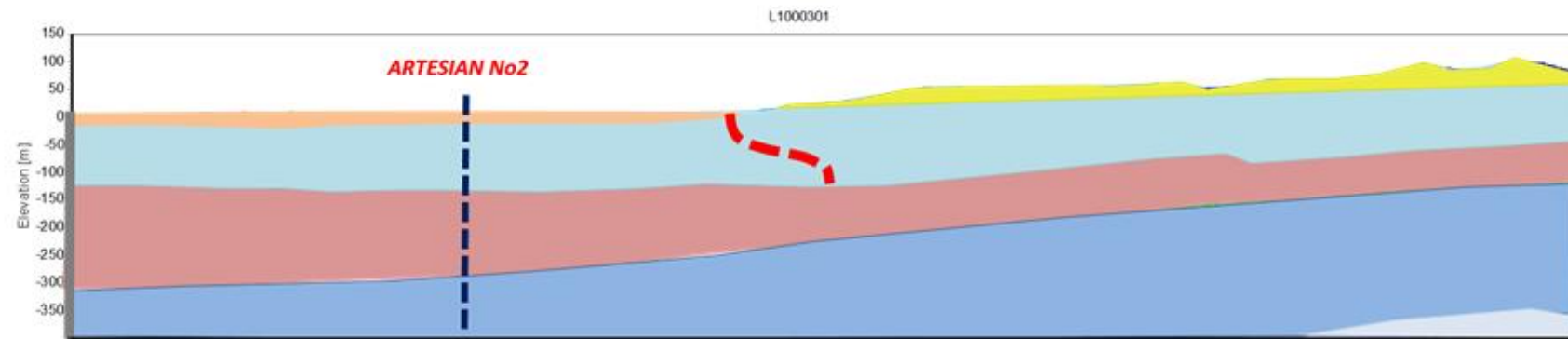
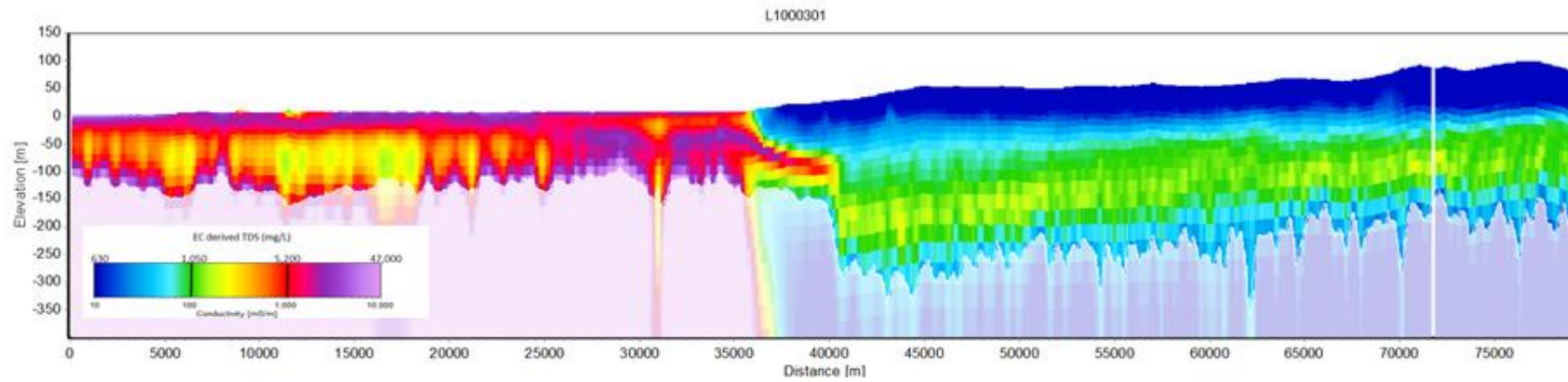
# HYDROLOGICAL CONCEPTUALISATION OF THE WALYARTA MOUND SPRINGS



HYDROLOGICAL CONCEPTUALISATION OF THE WALYARTA MOUND SPRINGS

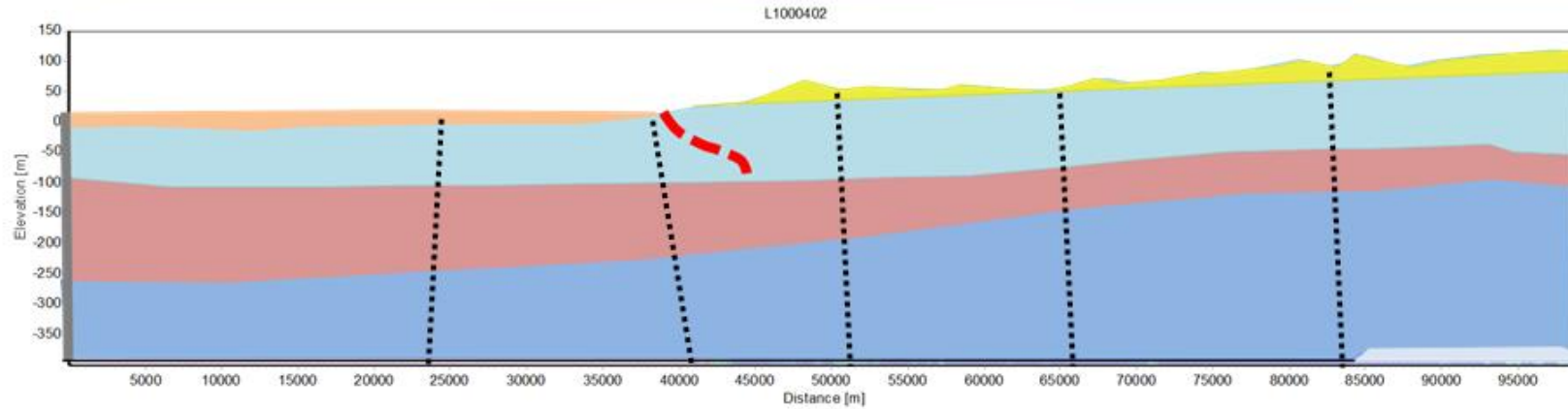
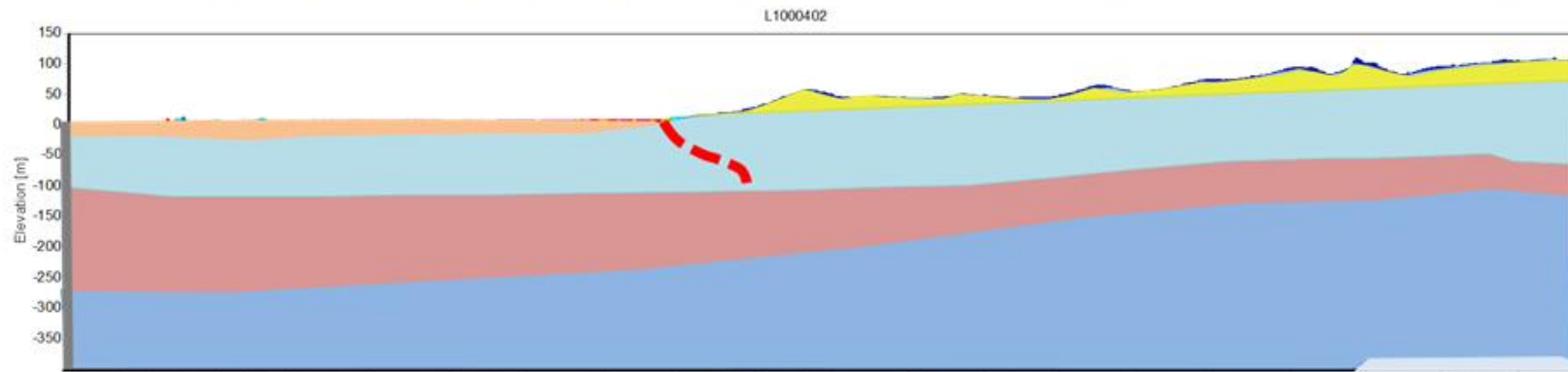
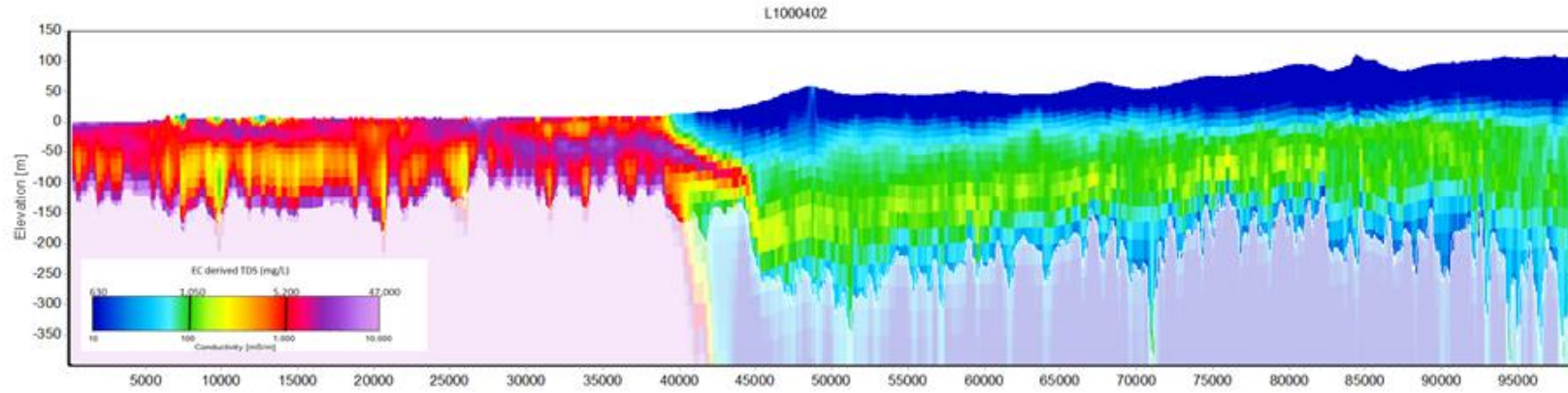


# HYDROLOGICAL CONCEPTUALISATION OF THE WALYARTA MOUND SPRINGS

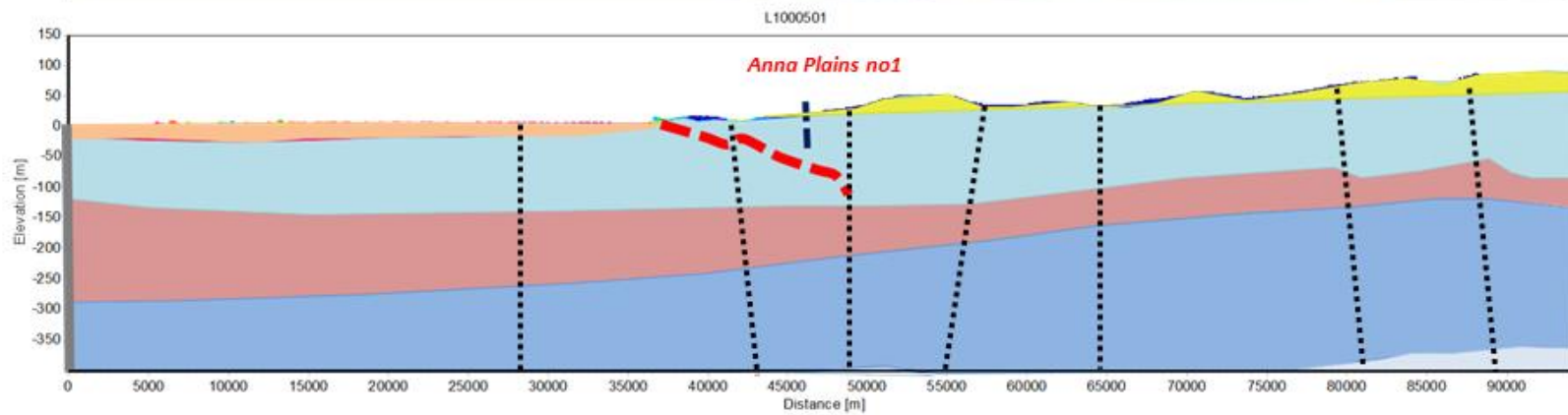
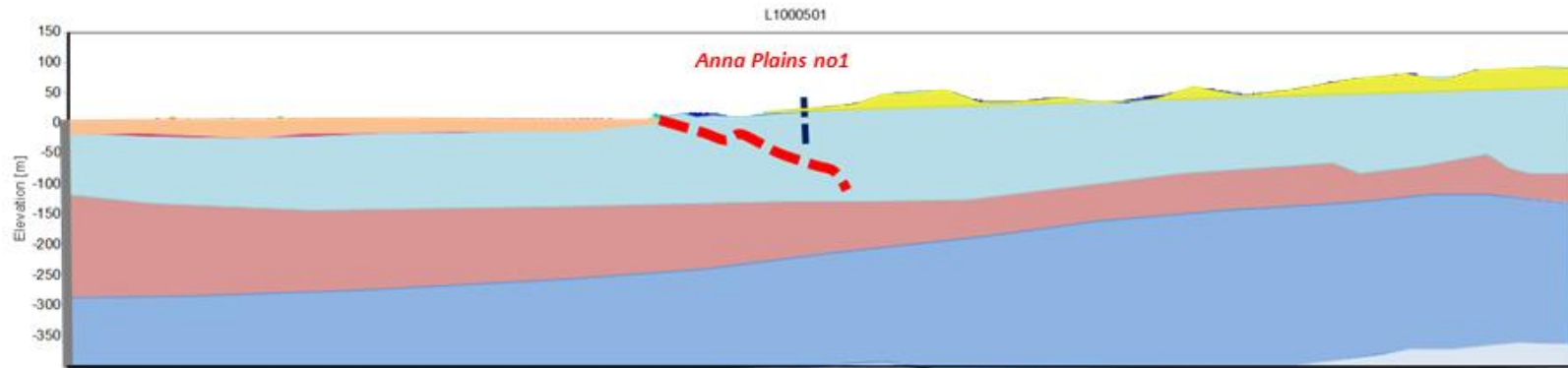
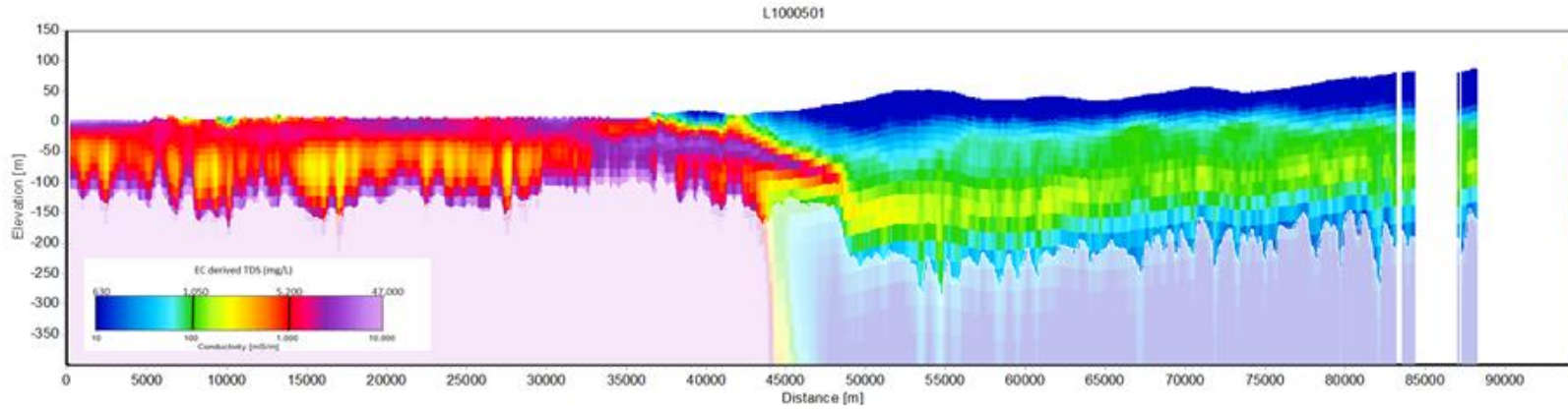




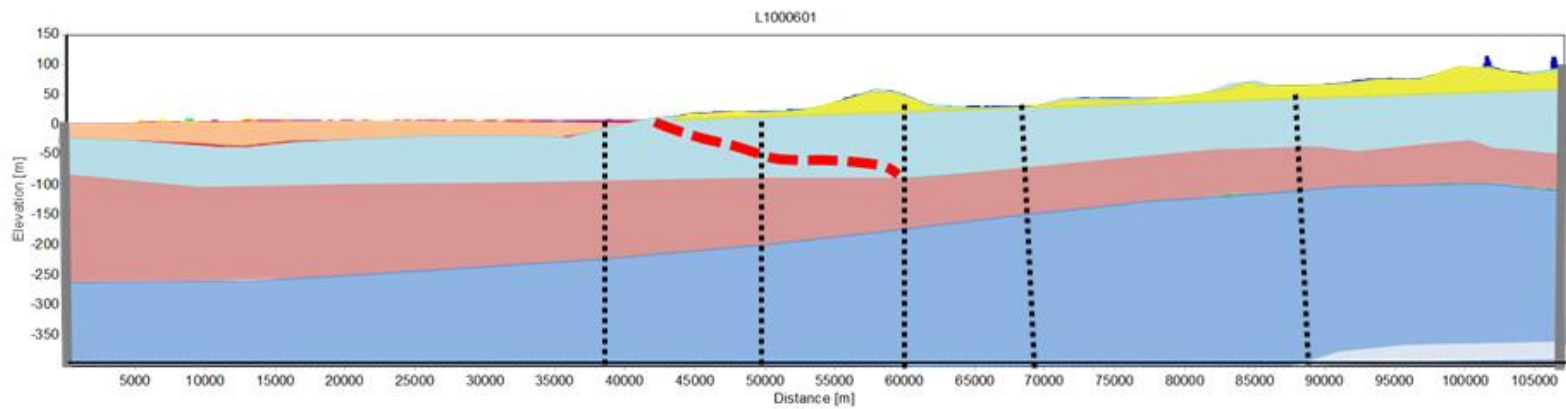
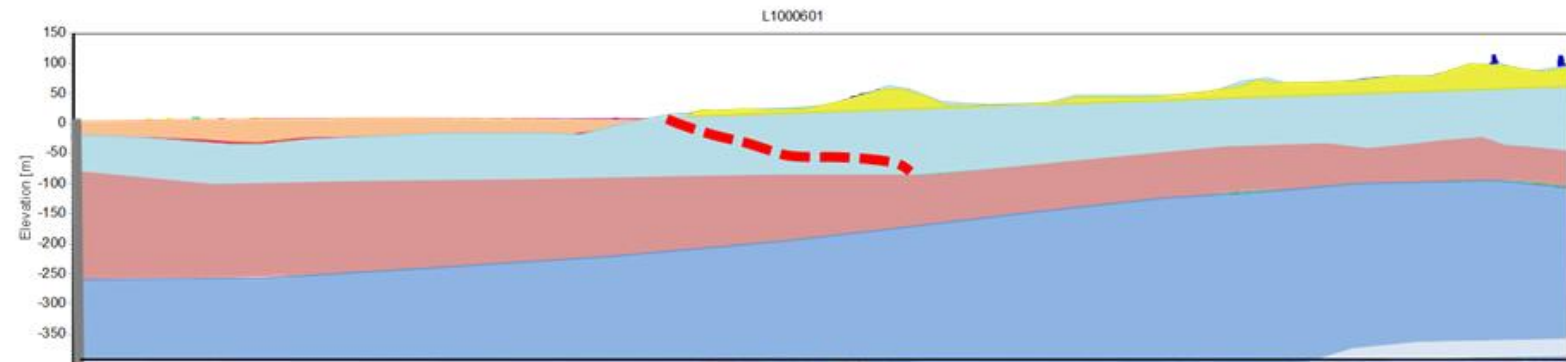
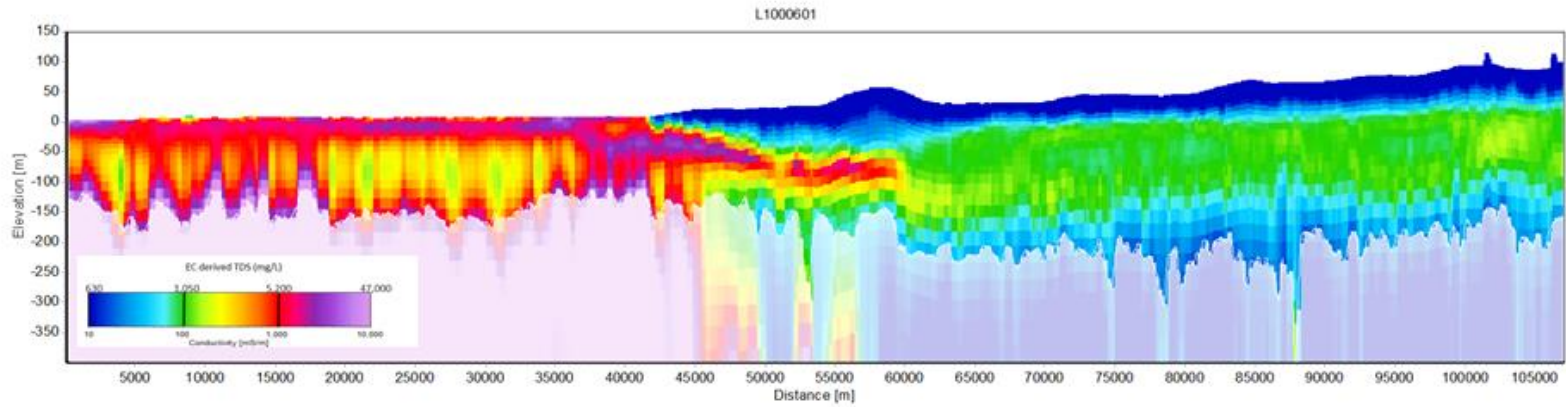
HYDROLOGICAL CONCEPTUALISATION OF THE WALYARTA MOUND SPRINGS



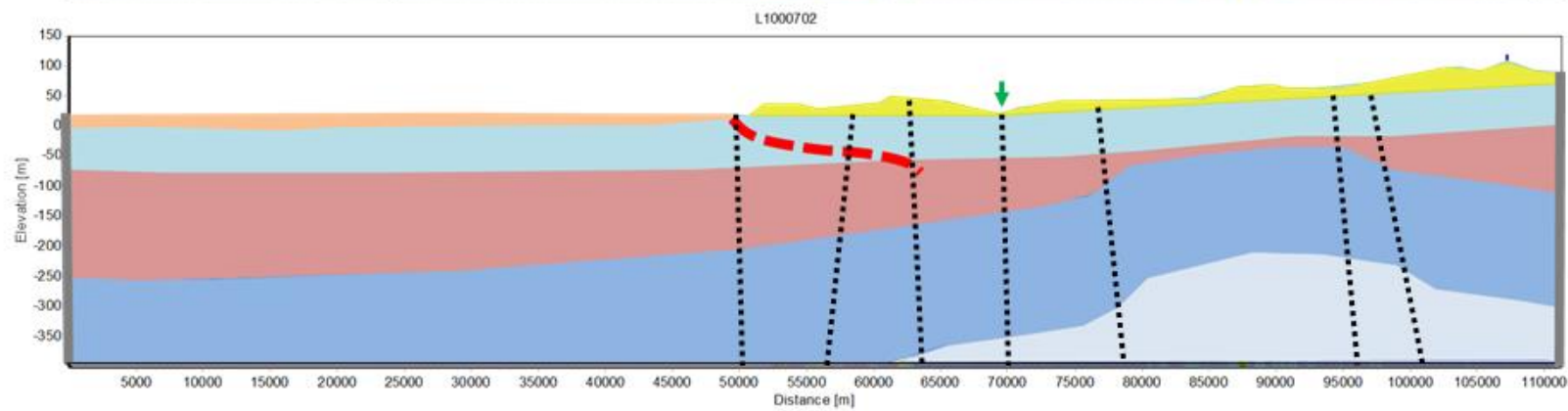
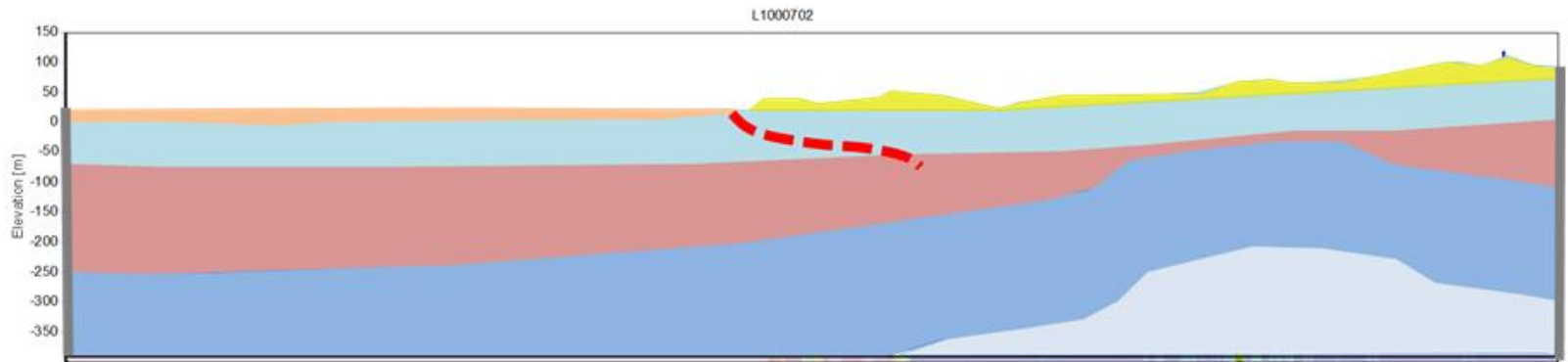
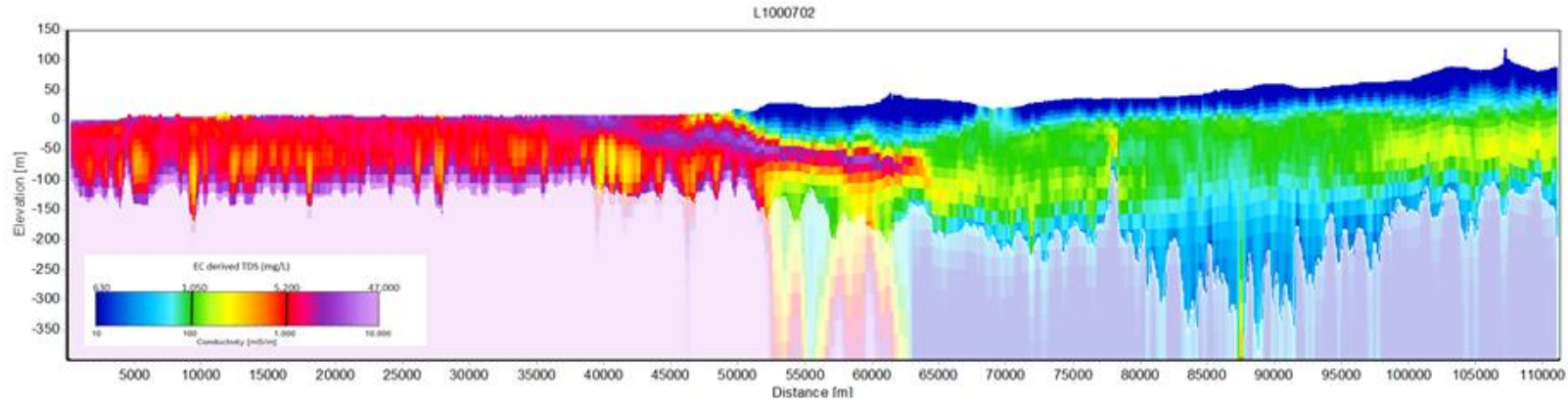
HYDROLOGICAL CONCEPTUALISATION OF THE WALYARTA MOUND SPRINGS



HYDROLOGICAL CONCEPTUALISATION OF THE WALYARTA MOUND SPRINGS

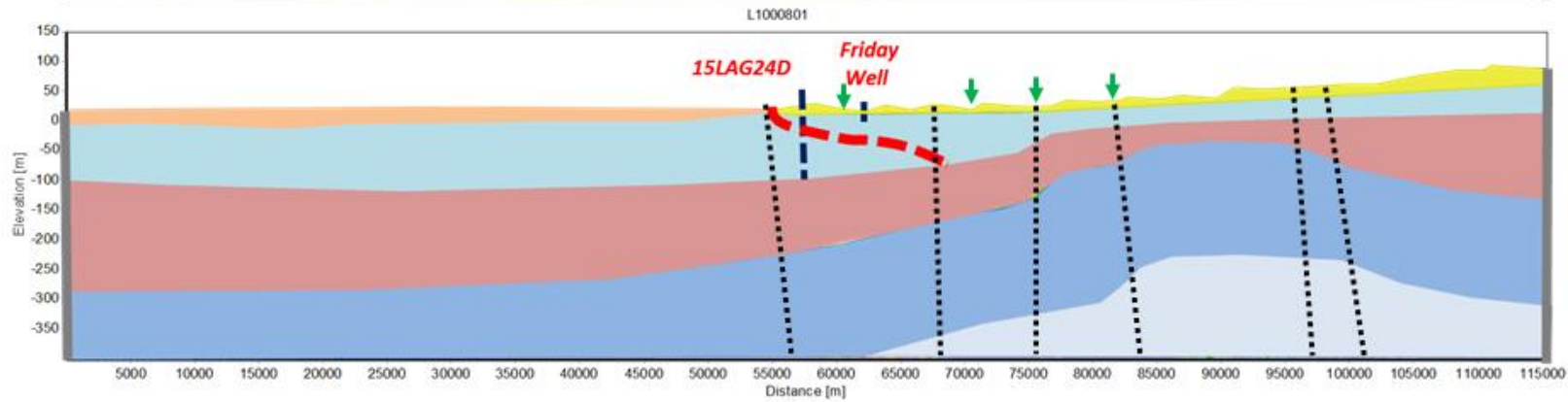
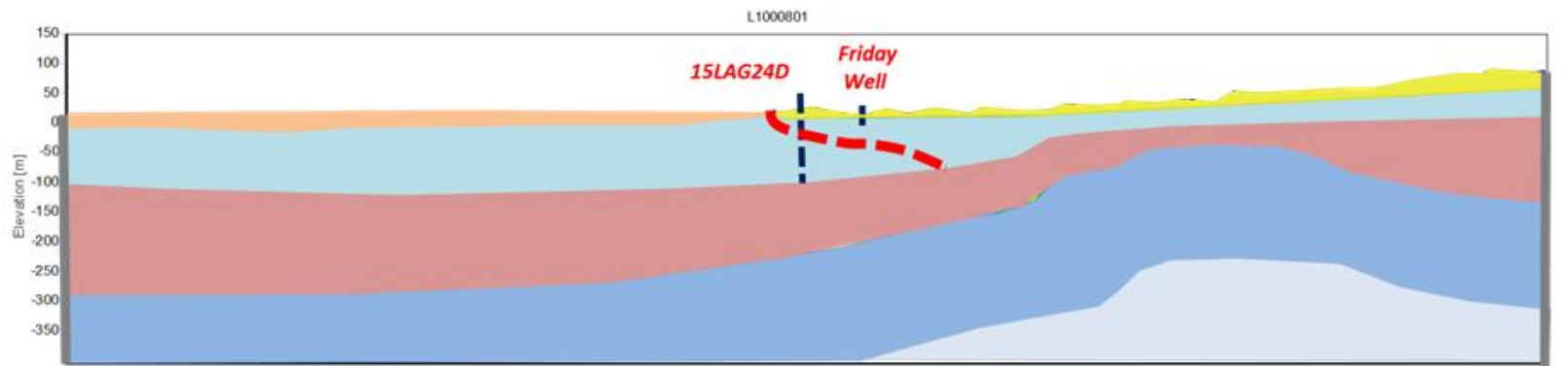
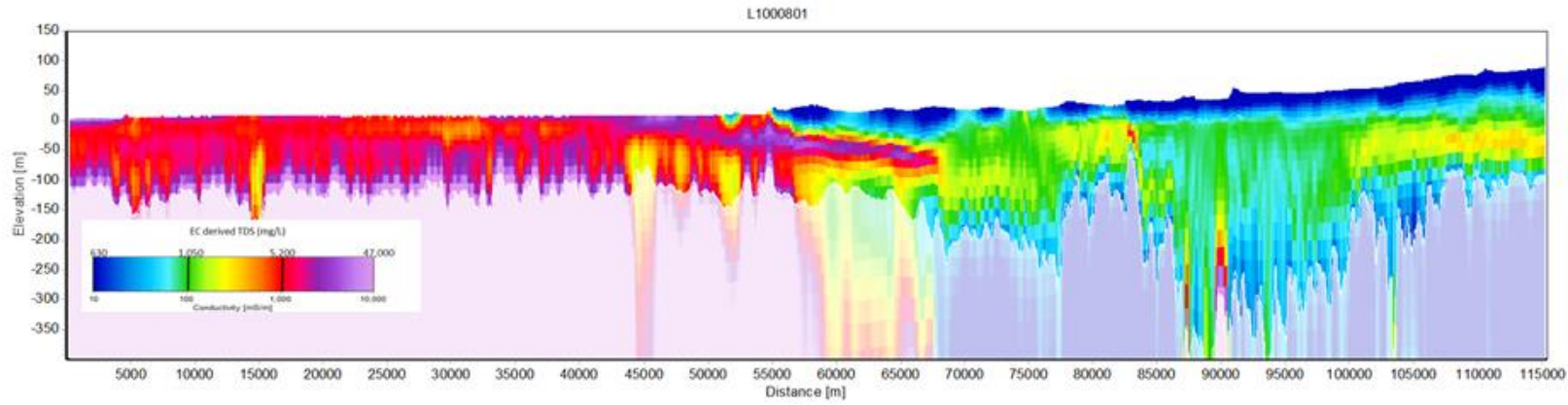


HYDROLOGICAL CONCEPTUALISATION OF THE WALYARTA MOUND SPRINGS

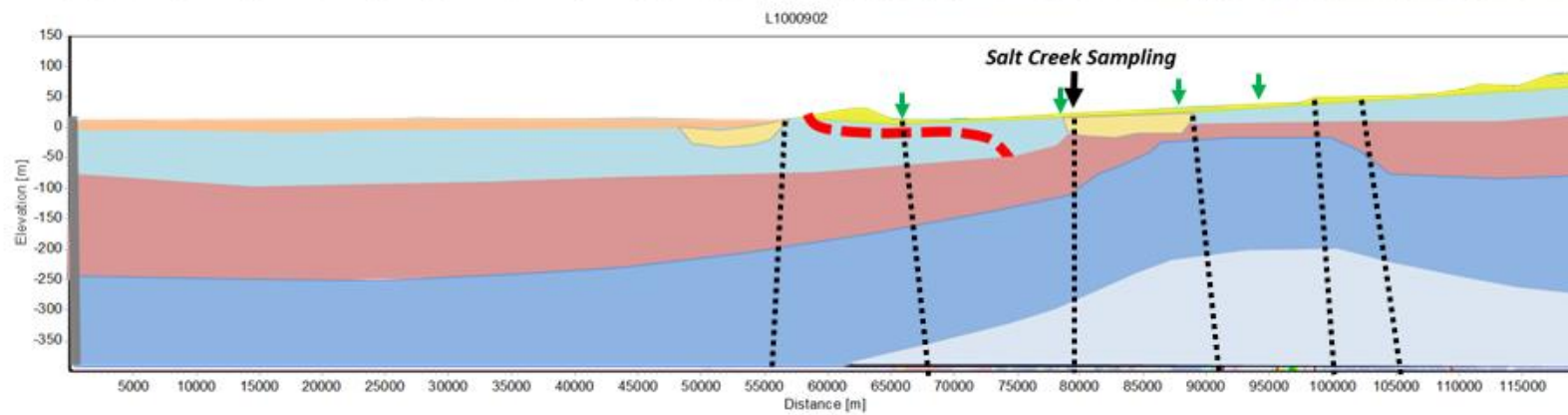
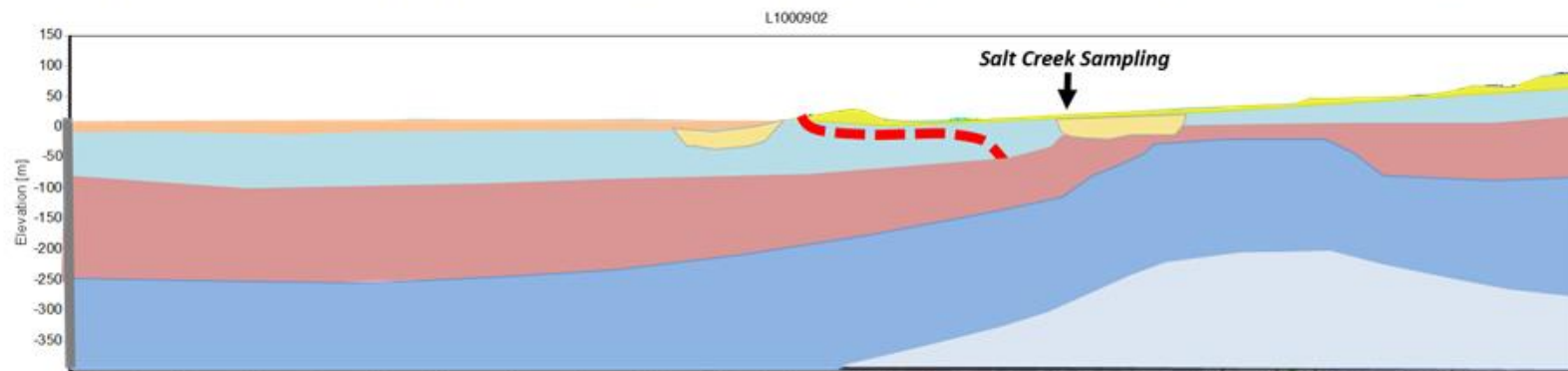
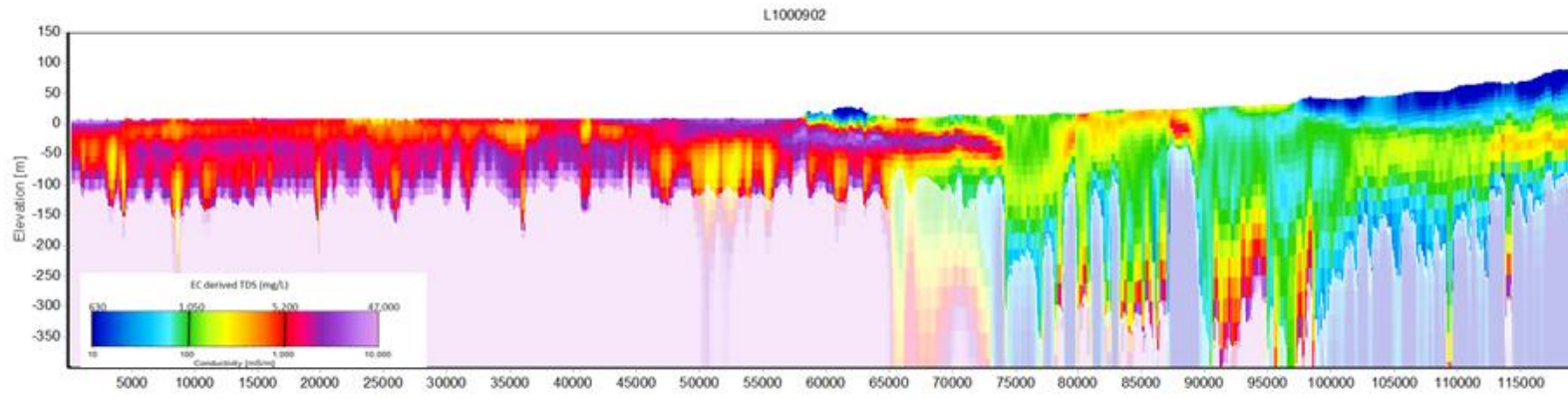




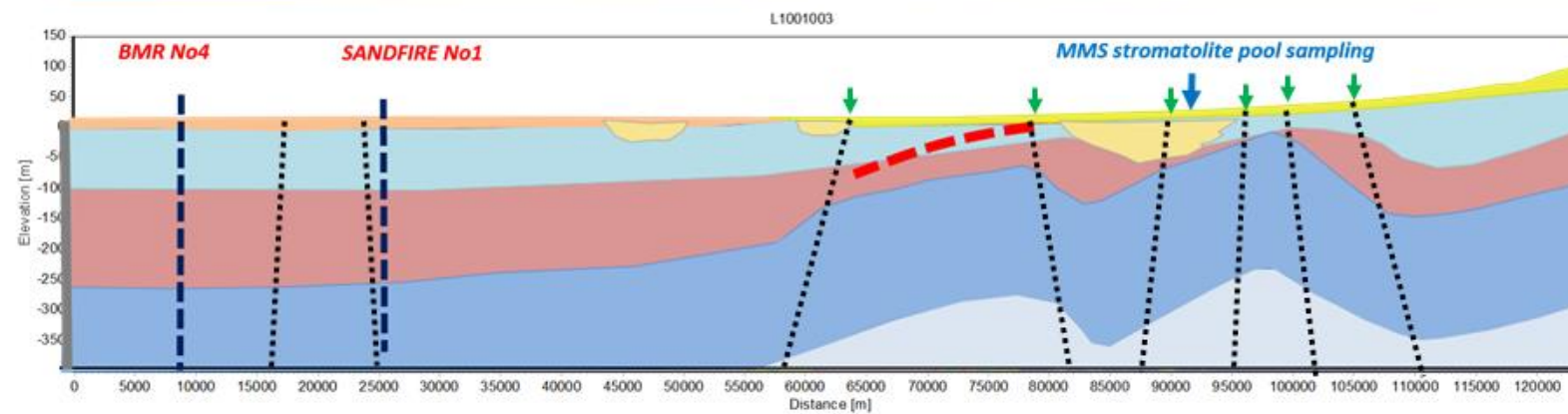
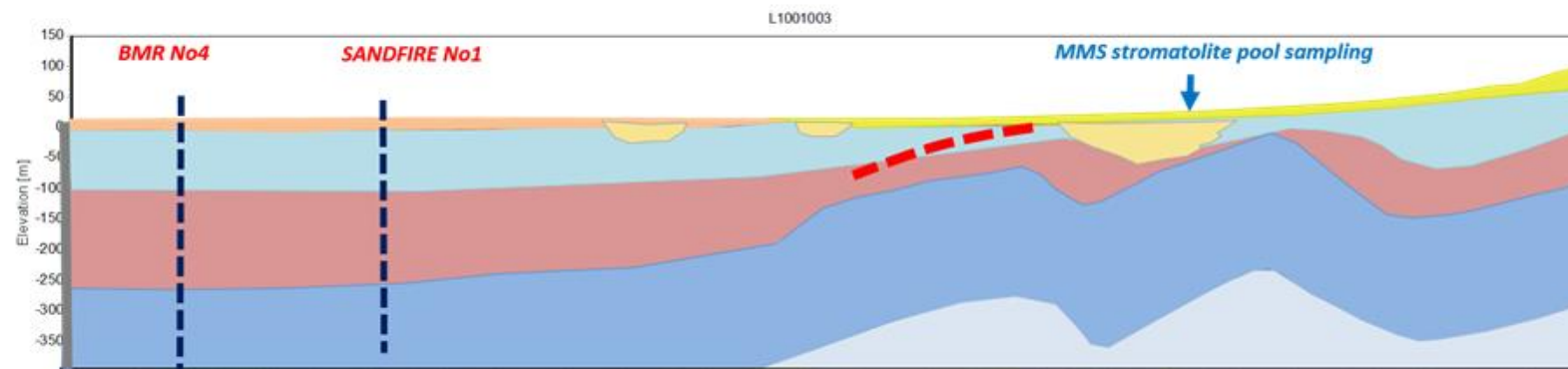
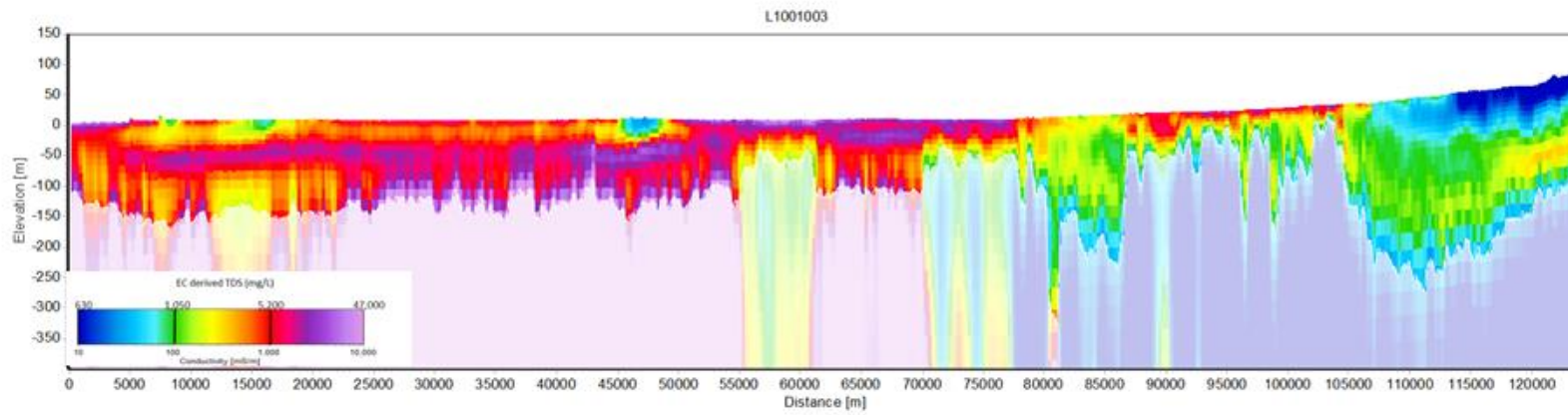
HYDROLOGICAL CONCEPTUALISATION OF THE WALYARTA MOUND SPRINGS



# HYDROLOGICAL CONCEPTUALISATION OF THE WALYARTA MOUND SPRINGS

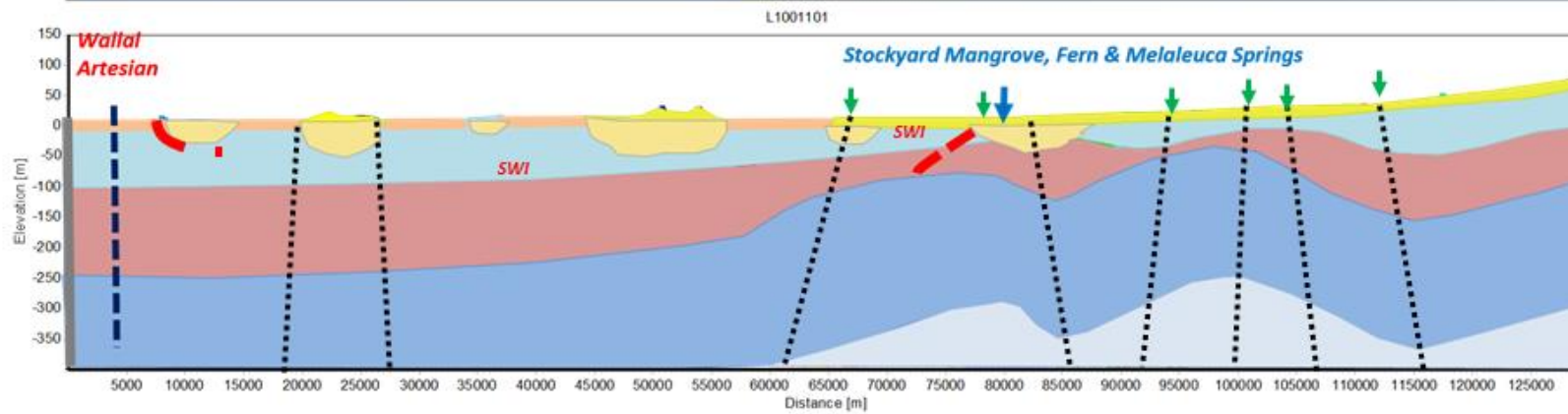
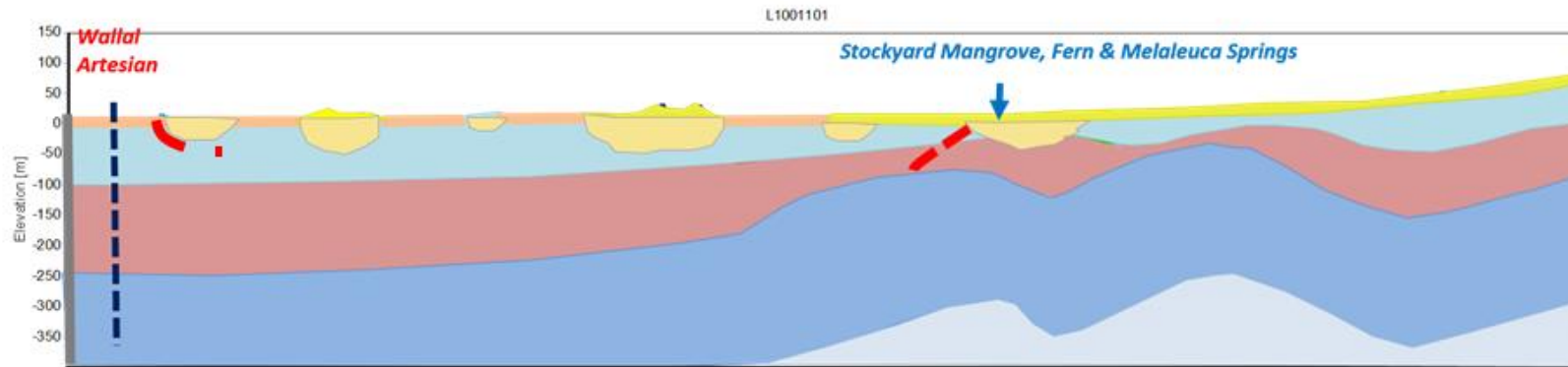
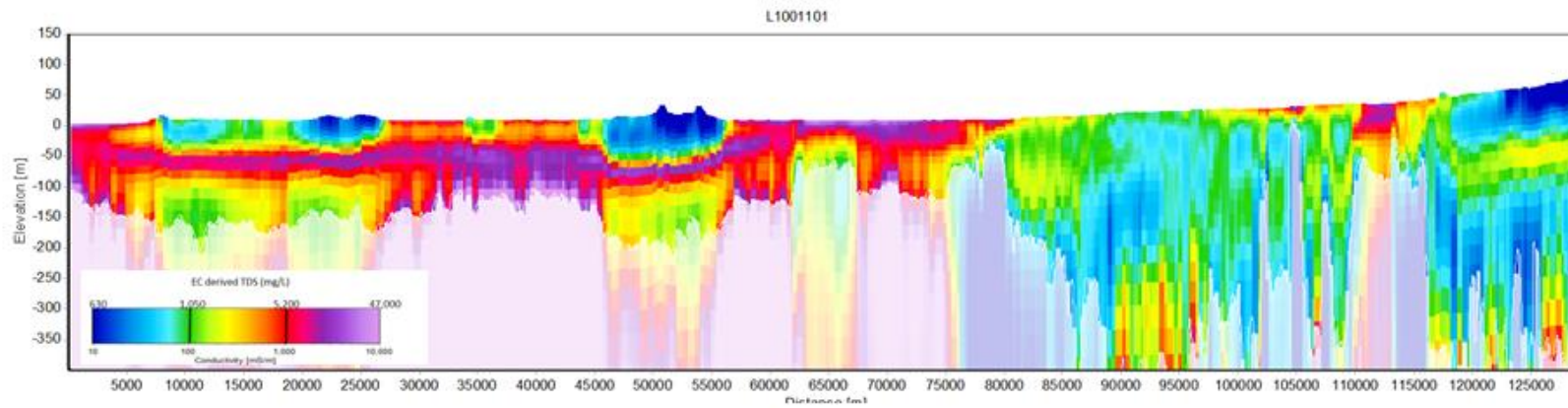


# HYDROLOGICAL CONCEPTUALISATION OF THE WALYARTA MOUND SPRINGS



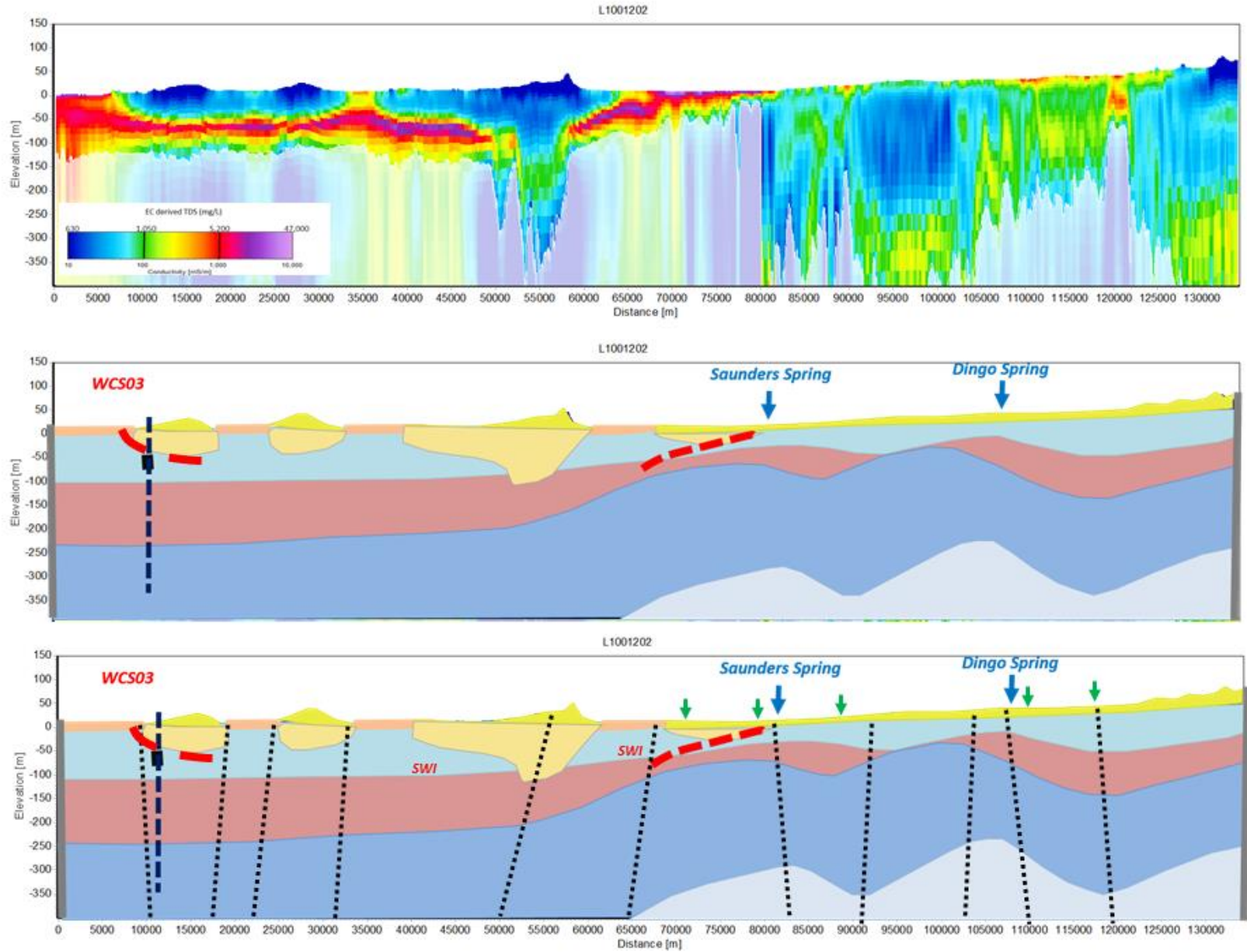


HYDROLOGICAL CONCEPTUALISATION OF THE WALYARTA MOUND SPRINGS

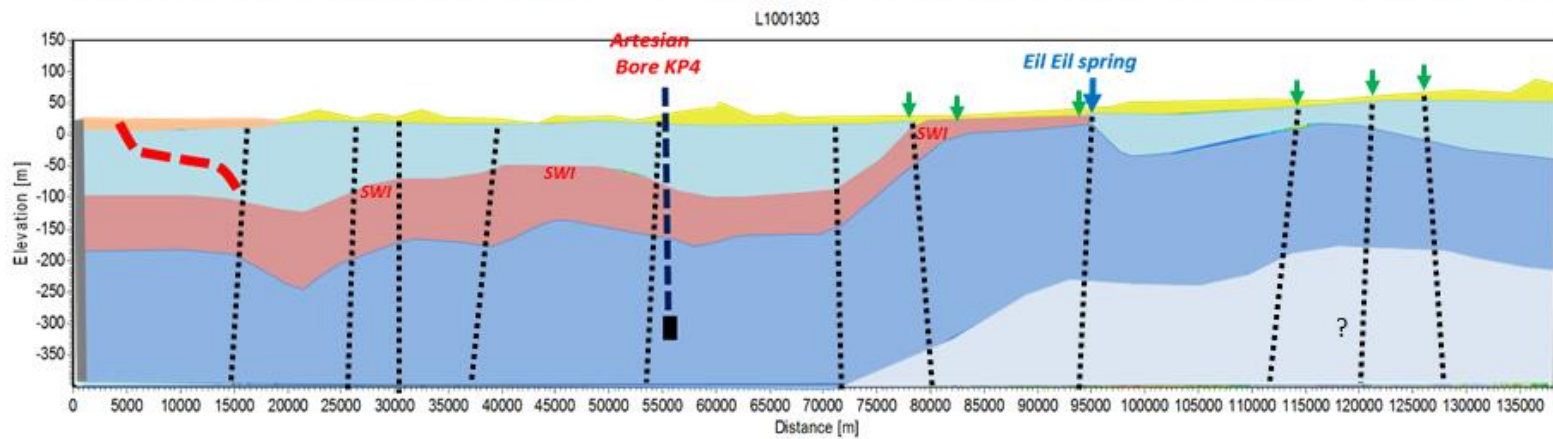
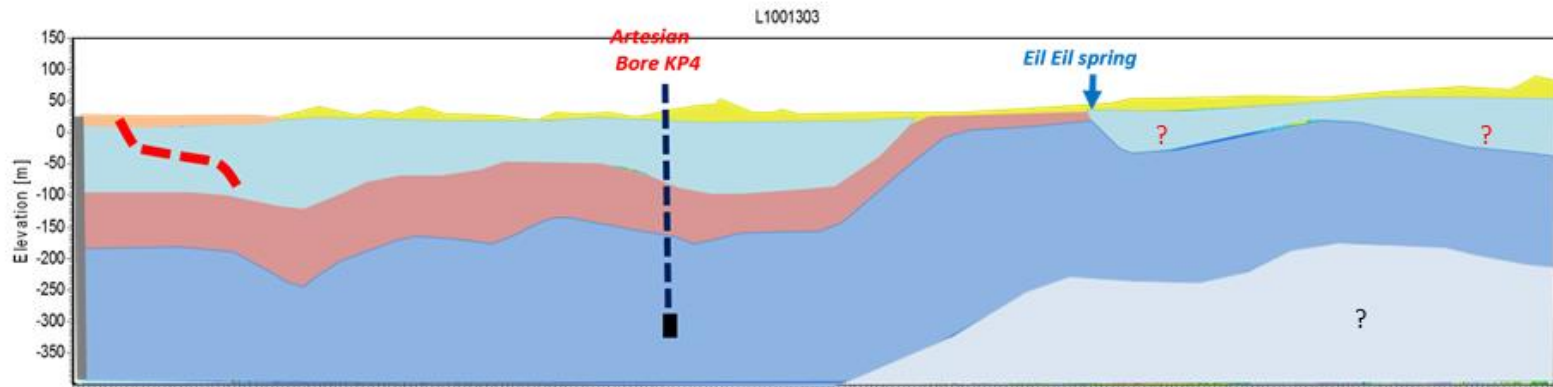
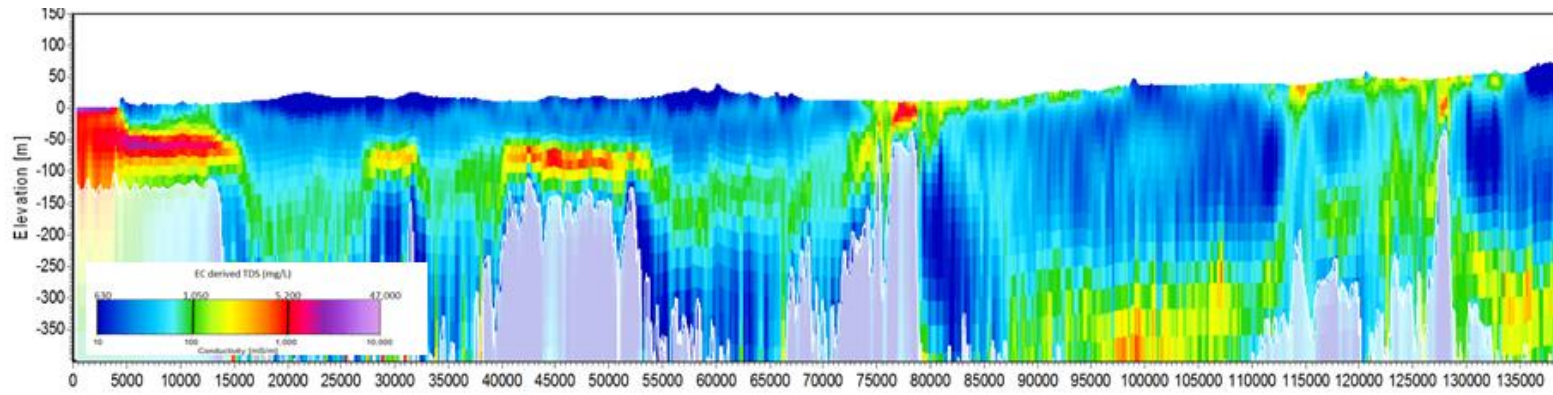




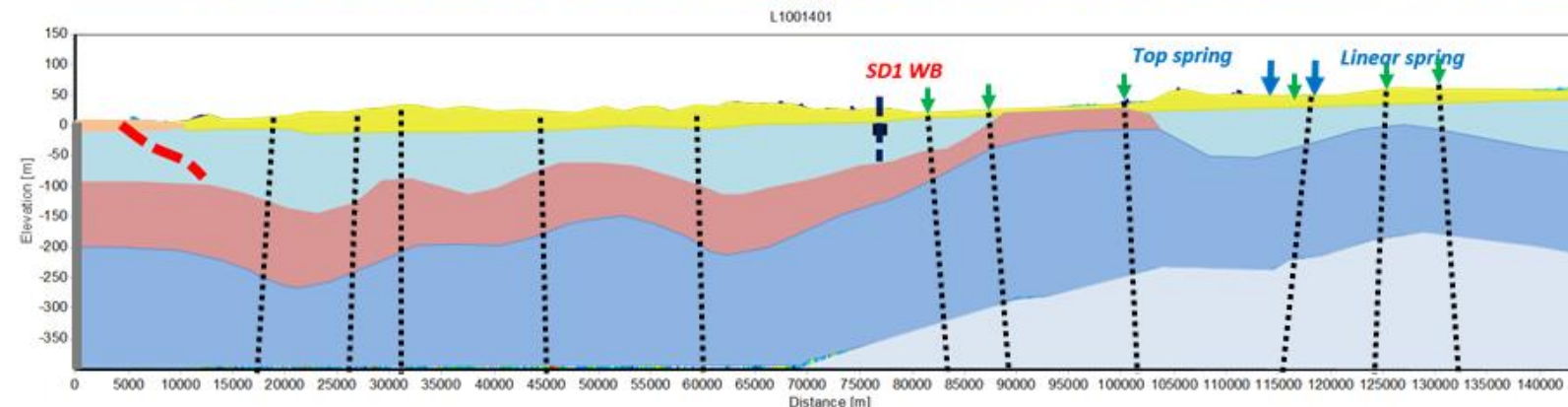
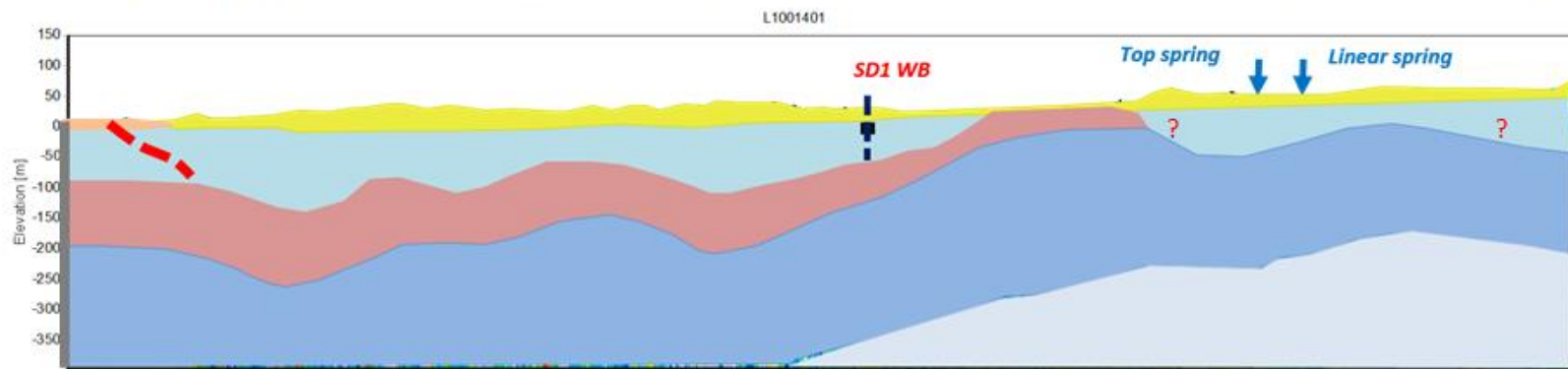
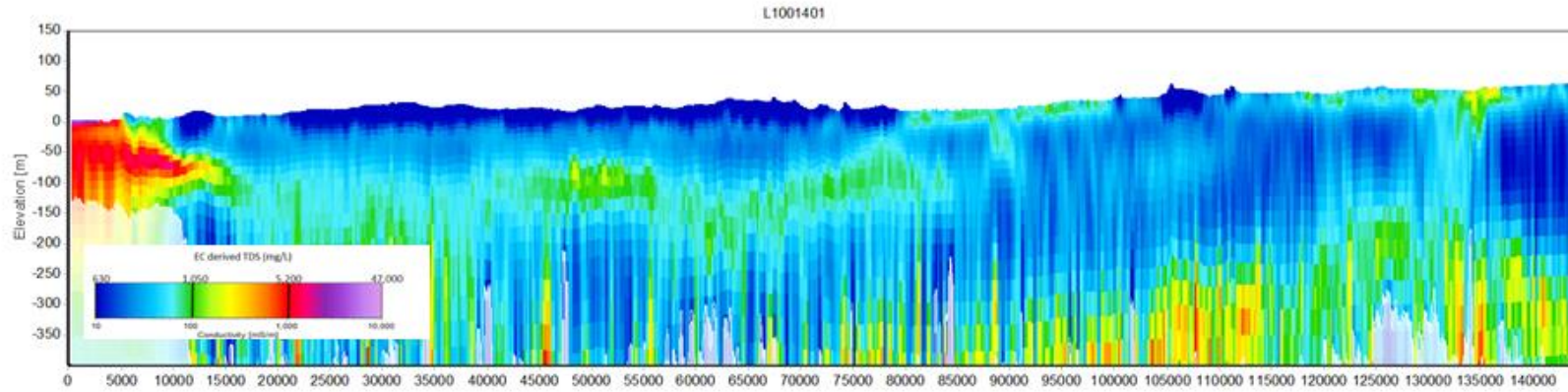
# HYDROLOGICAL CONCEPTUALISATION OF THE WALYARTA MOUND SPRINGS



HYDROLOGICAL CONCEPTUALISATION OF THE WALYARTA MOUND SPRINGS

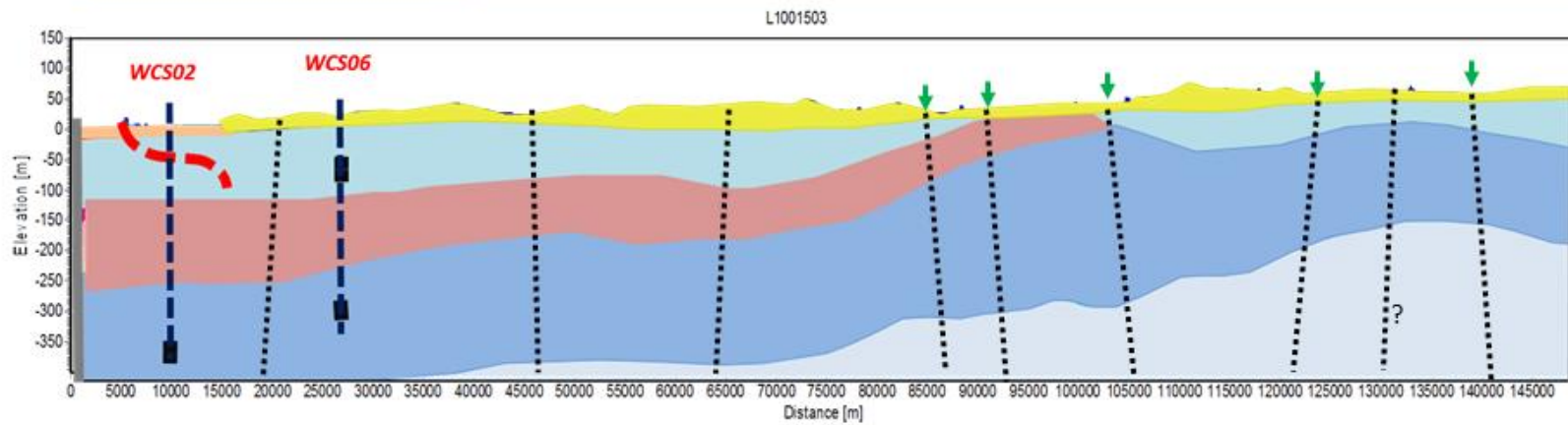
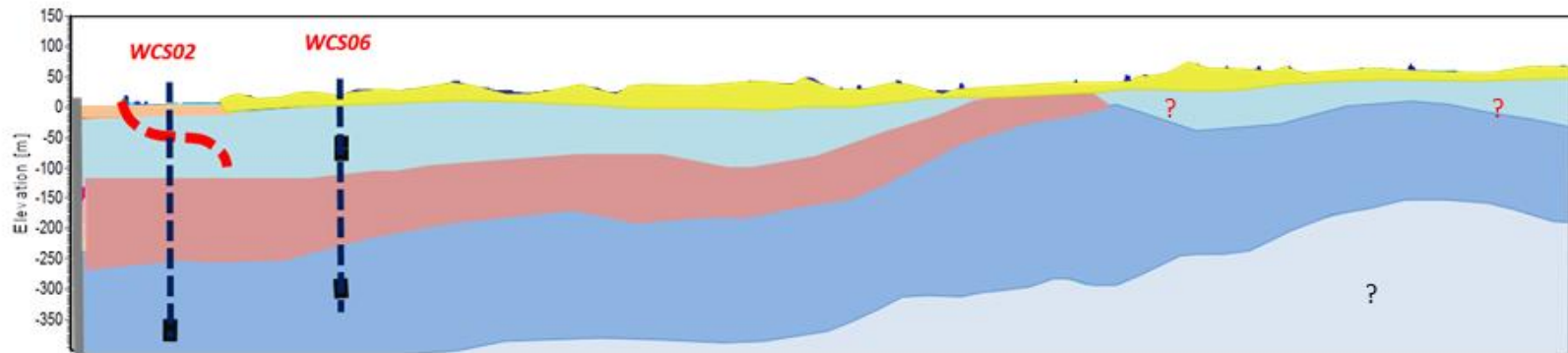
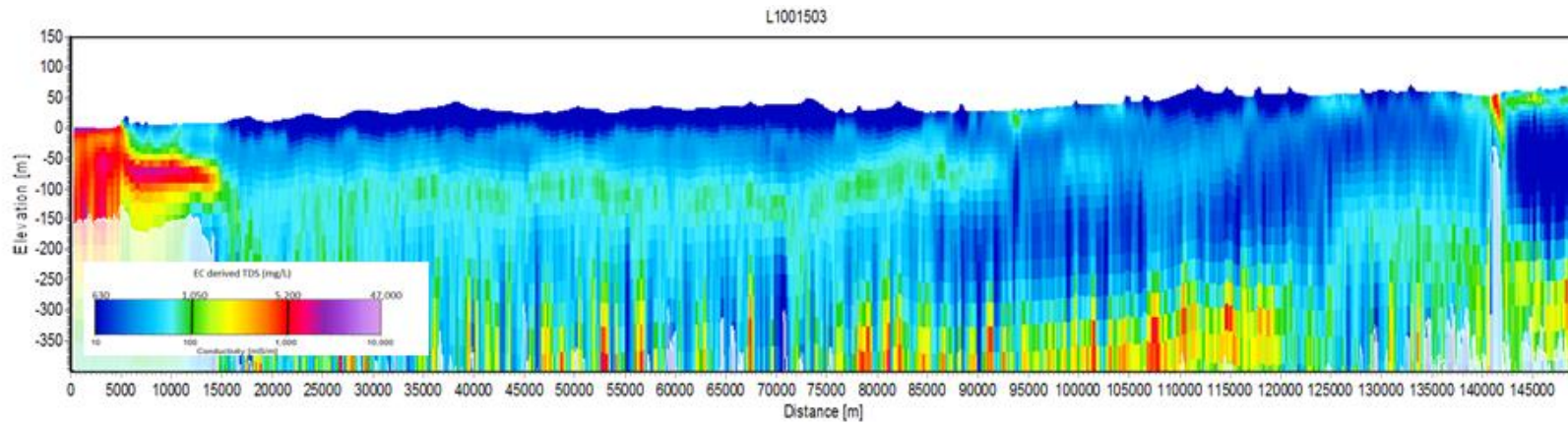


# HYDROLOGICAL CONCEPTUALISATION OF THE WALYARTA MOUND SPRINGS



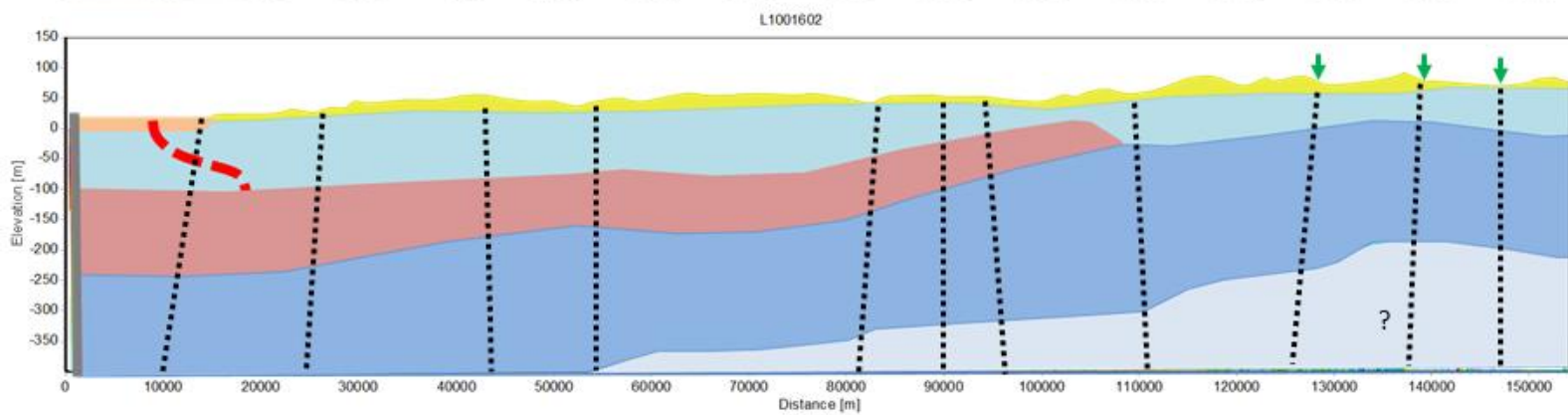
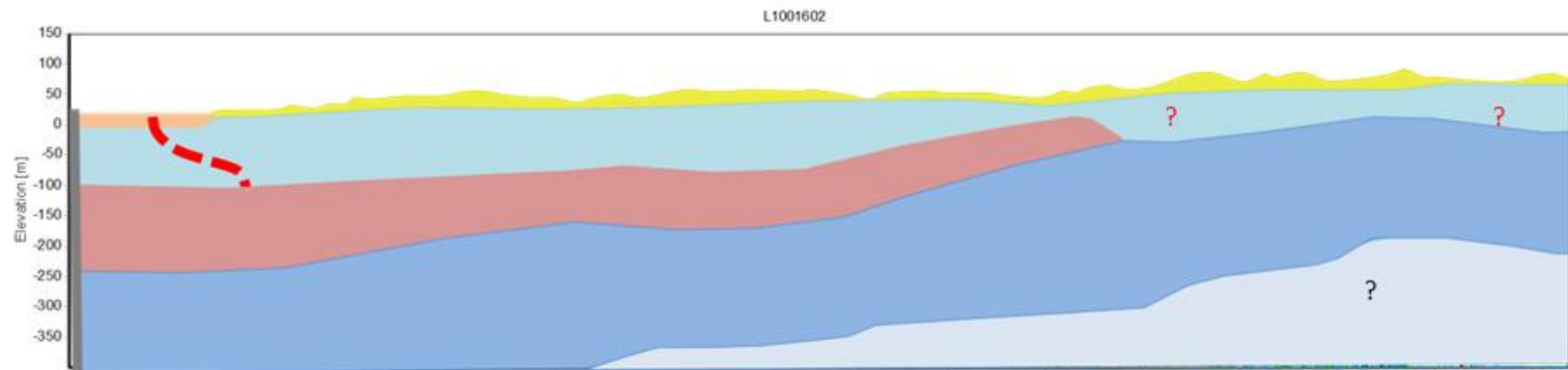
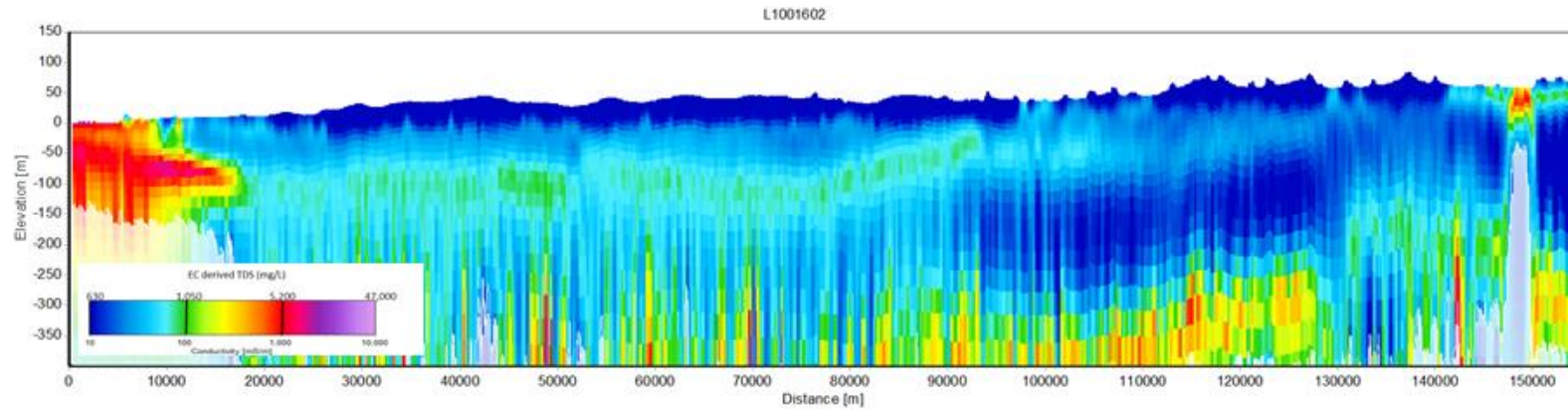


# HYDROLOGICAL CONCEPTUALISATION OF THE WALYARTA MOUND SPRINGS

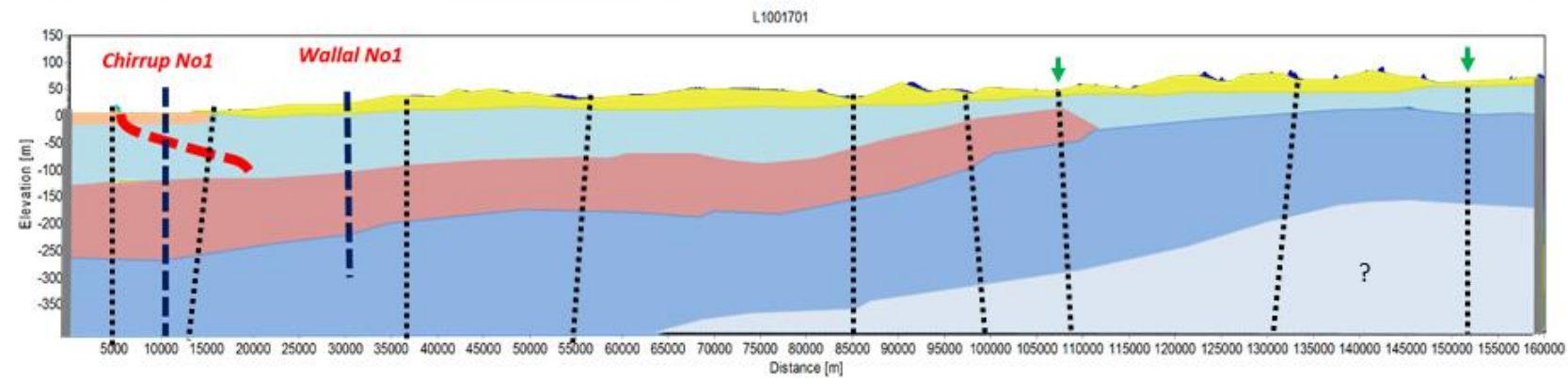
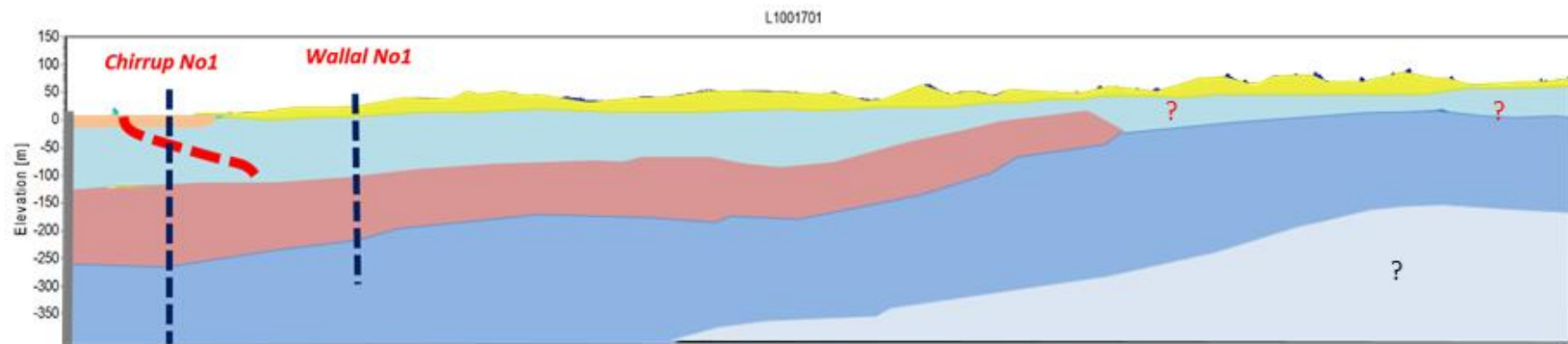
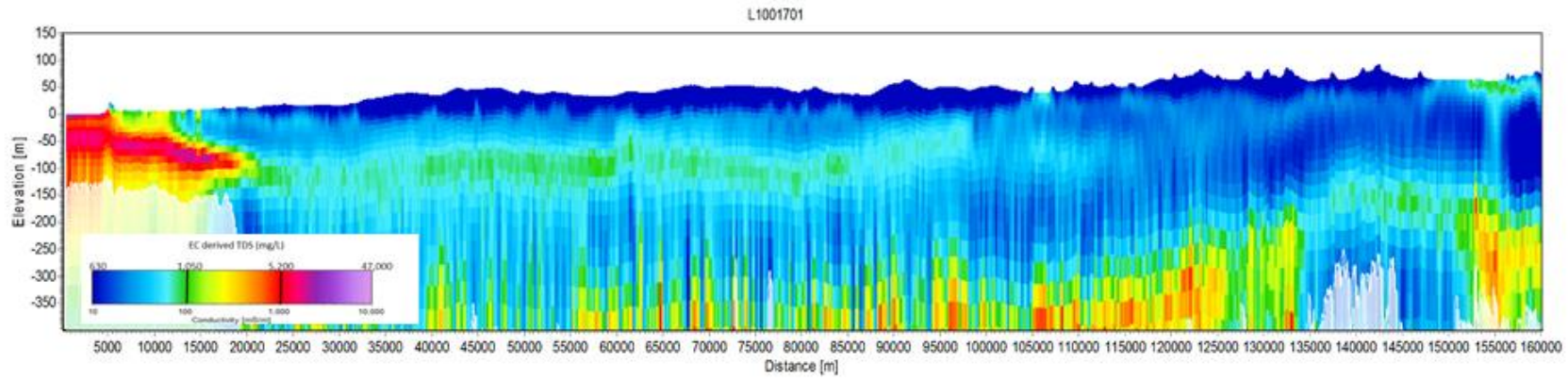




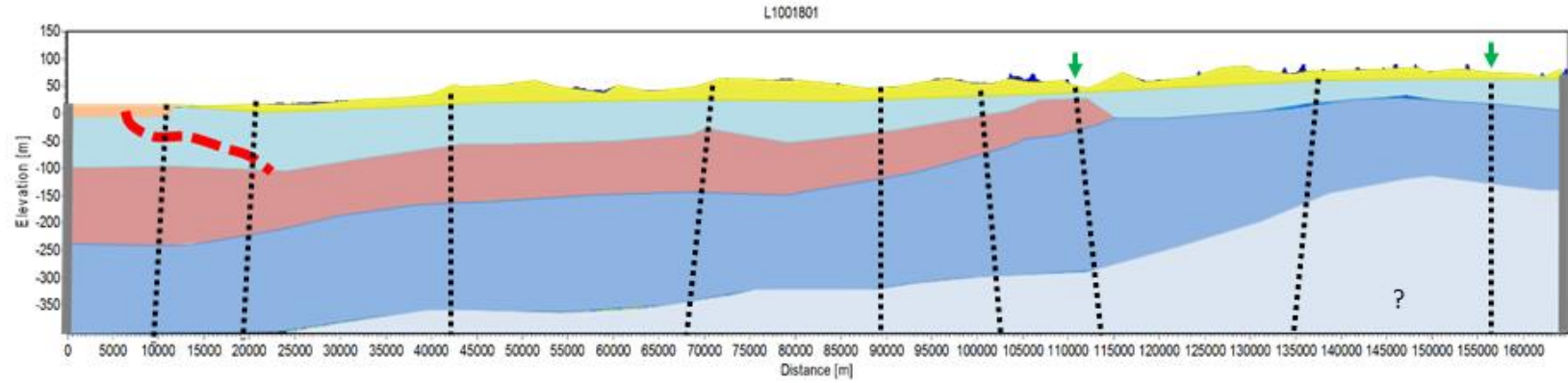
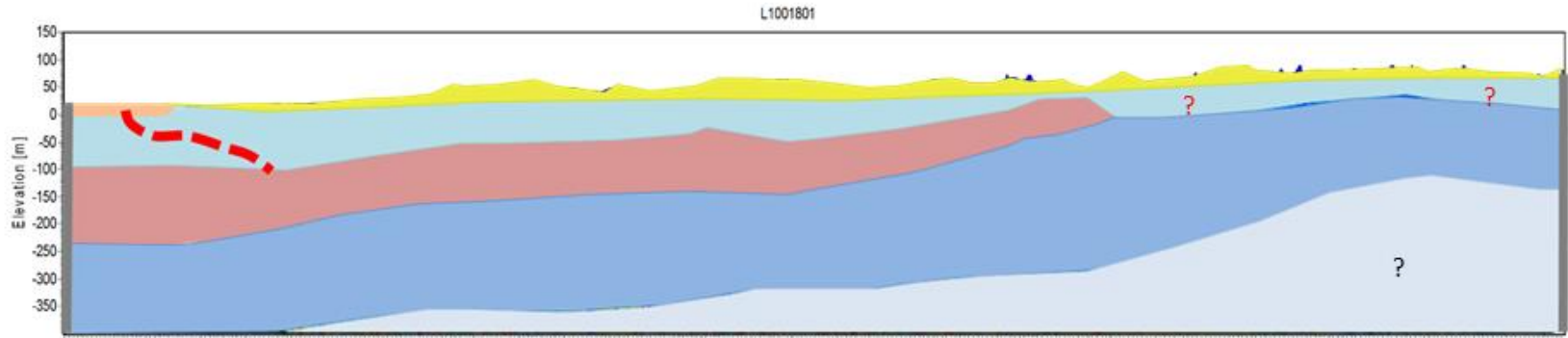
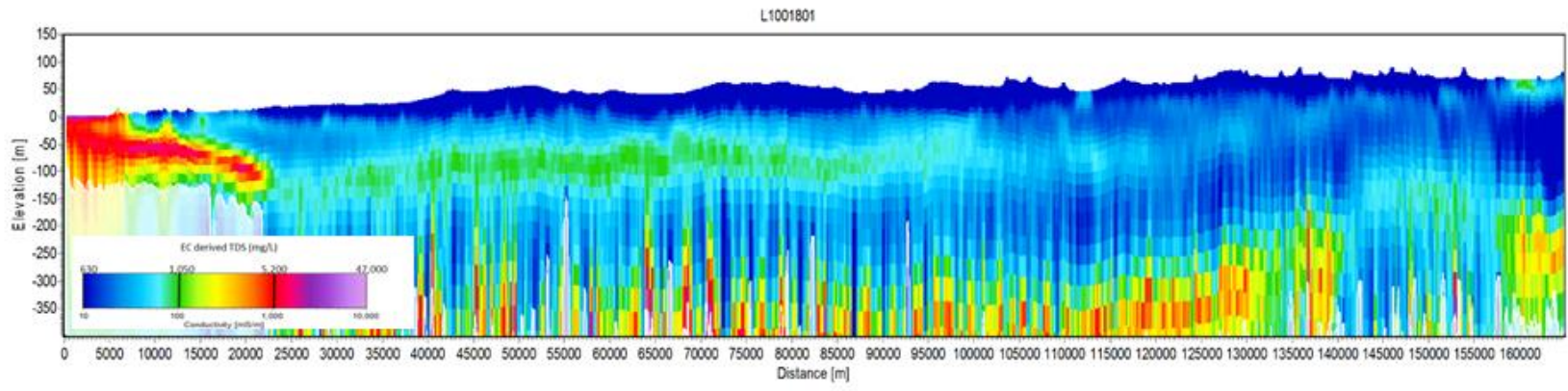
HYDROLOGICAL CONCEPTUALISATION OF THE WALYARTA MOUND SPRINGS



HYDROLOGICAL CONCEPTUALISATION OF THE WALYARTA MOUND SPRINGS

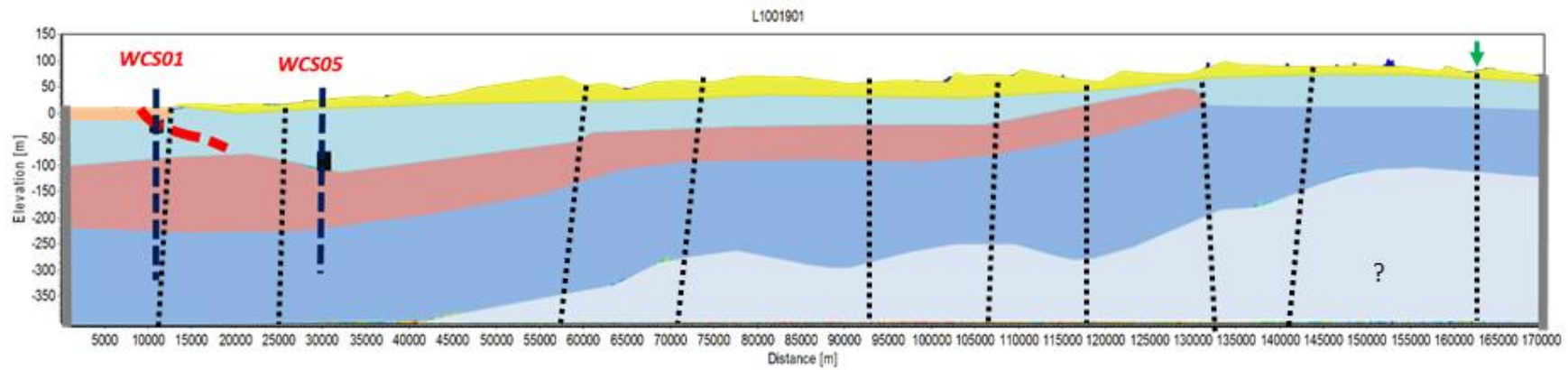
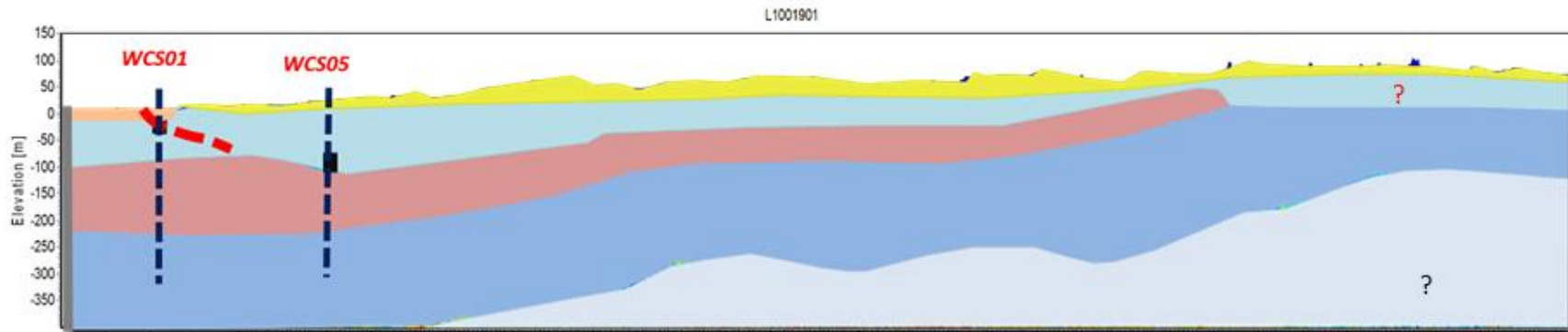
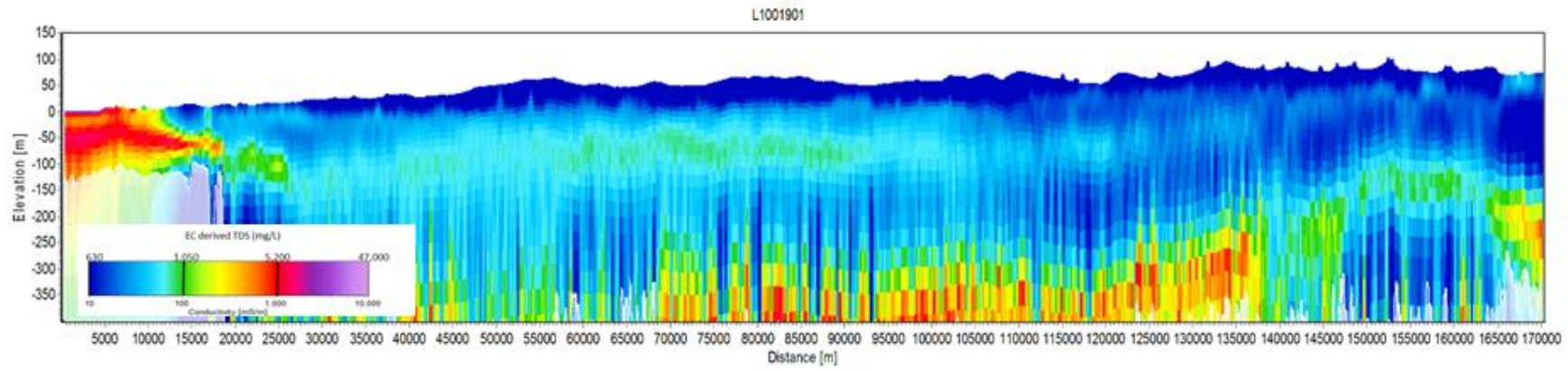


HYDROLOGICAL CONCEPTUALISATION OF THE WALYARTA MOUND SPRINGS





HYDROLOGICAL CONCEPTUALISATION OF THE WALYARTA MOUND SPRINGS





## Appendix 4 2015 Spring and Surface water Sampling Metadata

HYDROLOGICAL CONCEPTUALISATION OF THE WALYARTA MOUND SPRINGS

ID	Alt_ID	Date	Time	GPS point	Photo	X_MGA51	Y_MGA51	EC_mScm	pH	ORP_mV	Temp_oC	Total Alkalinity	Turbidity (text)	Colour (text)	Odour (text)	Sample depth_m	Overstorey veg	Understorey veg	Soil Desc	Surface moisture status	Estimated elevation	Underlying geology/hydrogeology	Creek/channel flow rate	SW/GW interaction	Site comments	Sample comments	Field WQ	Water Sampl ions	Major O	D/18	Nutrie nts	Fe2+	SiO2 (Reac +RE)	Metals Sr87/ Sr86	C14	Officer/sampler			
Bretts Open 1		2/09/2015	9:30:00 AM		3155-3177	337564.00	7810718.00	6.43	7.24		20.50														Bretts Spring, also known as Camp Swamp? (Val English).	Field WQ sampled from inflow at southern edge.	T	F	F	F	F	F	F	F	F	F	F	Lindsay Bourke/Glenn Harrington	
Bretts Open 1		2/09/2015	10:30:00 AM		3155-3177	337558.00	7810652.00	5.84	7.56		21.60	185	Medium	Grey/Black	None	0.05	Sesbania formosa	Typha sp.	BLACK to BROWN, Humic-rich peat at surface on mound	Saturated	-35mAHD	Unknown	N/A		Mound appears to be discharging to the north, very low flow rates, barely detectible.	Open water body ~0.10m deep. Mound <1m above surrounding area. Rushes present in water body. See Val English, Site also known as Camp Swamp. Significant cattle pugging in open water body.	Sample taken from area of groundwater discharge (very low rates of discharge) nearby Typha sp.	T	T	T	T	T	T	T	T	T	T	T	Lindsay Bourke/Glenn Harrington
Bretts Open 2		2/09/2015	12:12:00 PM		3178-3181	337438.00	7810870.00										Acacia sp.	Various grasses (species unknown)	GREY, sandy clay with swelling/cracking clays in depressions	Dry	-30 mAHD	Unknown	N/A		No SW present, likely area for SW accumulation during wet periods	Walked to Bretts Open 2, then back around to Bretts Open 1	N/A	F	F	F	F	F	F	F	F	F	F	Lindsay Bourke/Glenn Harrington	
Bretts Open 2		2/09/2015	12:12:00 PM		3182	337517.0	7817052.0										Acacia sp.				-30 mAHD	Unknown			Walked to Bretts Open 2, then back around to Bretts Open 1	N/A	F	F	F	F	F	F	F	F	F	F	Lindsay Bourke/Glenn Harrington		
Bretts Open 2		2/09/2015	12:20:00 PM		3183-2188	337498.0	7810687.0										Acacia sp.				-30 mAHD	Unknown			Walked to Bretts Open 2, then back around to Bretts Open 1	N/A	F	F	F	F	F	F	F	F	F	F	Lindsay Bourke/Glenn Harrington		
Centre of Typa @ Mangrove		4/09/2015						3.83	7.08		20.10														No site details documented. In the Stockyard suite.	N/A	T	F	F	F	F	F	F	F	F	F	F	Lindsay Bourke/Glenn Harrington	
Coolgardie Well		4/09/2015	7:50:00 AM		3344-3350	314056.0	7811227.0	0.78			22.10		Low	Clear	None	0.10	Melaleuca sp and Acacia sp.	absent	WHITE to GREY, Sandy clay with swelling/cracking clays in depressions	Dry	10mAHD	Unknown	N/A		No indication of SW/GW interactions	Heavily grazed area, particularly in stockyard.	Unable to obtain sample directly from pump, only tank overflow or trough. Unsuited for sampling. Field results from trough.	T	F	F	F	F	F	F	F	F	F	F	Lindsay Bourke/Glenn Harrington
Eastern Spring and Typha (east)		4/09/2015						3.66	8.92		25.80														No site details documented		T	F	F	F	F	F	F	F	F	F	F	Lindsay Bourke/Glenn Harrington	
Eastern Spring and Typha (west)		4/09/2015						3.11	7.40		29.60														No site details documented		T	F	F	F	F	F	F	F	F	F	F	Lindsay Bourke/Glenn Harrington	
Eil Eil		2/09/2015	3:00:00 PM		3221-3230	336933.0	7810320.0	8.58	8.37		33.30						N/A	Various rushes (species unknown)	GREY, clayey sand	Saturated	-35mAHD	Unknown	N/A		GW inflow from the south, southeast.	Area to the south of Eil Eil and open water body surrounded by Schlerophyll vegetation (Acacia sp. Etc). White Dragon Trees on banks of open water with high numbers of Corellas. Trees showing signs of grazing/pruning by birds.	Water quality measurement at open water body to the north of the mound. Sample point due south of XY coordinates	T	F	F	F	F	F	F	F	F	F	F	Lindsay Bourke/Glenn Harrington
Eil Eil		2/09/2015	3:20:00 PM		12 3221-3250	337150.0	7810263.0	4.27	7.87		25.50						N/A	Various rushes (species unknown)	GREY to BROWN, clayey sand	Saturated	-40mAHD	Unknown	N/A		GW inflow from the south.	Surface water present in open water body, also inundating significant area with Melaleuca sp. on the north-eastern edge of the open water body.	Field WQ sampled from open water (~0.02m) in shaded area.	T	F	F	F	F	F	F	F	F	F	F	Lindsay Bourke/Glenn Harrington
Eil Eil	Eil Eil Spring	2/09/2015	4:00:00 PM		14 3221-3250	337151.0	7810249.0	3.20	7.28		25.40	306	Medium	Brown	H2S	0.05	Melaleuca sp.	Typha sp.	BLACK to BROWN, Humic-rich peat at surface on mound	Saturated	-40mAHD	Unknown	N/A		Mound discharging to the north-east area of the open water body, although very low flow rates, barely detectible	Open water body ~0.10m deep. Mound <1m above surrounding area. Soil moisture is highly variable across the mound. Evidence of fire in the past (dead trees, stumps, black charred trunks etc)	Sampled from area with Typha sp. Sample taken from active discharge (very low rates of discharge).	T	T	T	T	T	T	T	T	T	T	T	Lindsay Bourke/Glenn Harrington
Fern		3/09/2015	1:56:00 PM		30 3308	331564.0	7813550.0	14.23			26.50						N/A	Typha sp. and rushes (species unknown)	GREY to BLACK, sandy clay	Saturated	-15mAHD	Unknown	N/A		SW present. GW discharge negligible, although likely to occur due to the presence of permanent water	GW inflow likely from the south along area of Typha sp.	Field WQ sampled from occurrence of Typha sp. occurring along likely GW discharge area to open water body (Fern Tail)	T	F	F	F	F	F	F	F	F	F	F	Lindsay Bourke/Glenn Harrington
Fern Peat		3/09/2015	2:00:00 PM		3313	331614.0	7813532.0	9.96	6.52		24.60	146	Low	Clear	None	0.10	Melaleuca sp.	Typha sp.	BLACK to BROWN, Humic-rich peat at surface on mound	Saturated	-17mAHD	Unknown	N/A		Mound likely to be discharging, although rate is indistinguishable	No visible surface water flow or active GW discharge.	Sample site surrounded by Typha sp., approx 3 x 6m (18m2), sample taken from excavated hole.	T	T	T	T	T	T	T	T	T	T	T	Lindsay Bourke/Glenn Harrington
Fern Tail		3/09/2015	1:10:00 PM		29 3301-3304	331586.1	7813633.3										N/A	Various grasses (species unknown)	WHITE to GREY, Clay to sandy clay								N/A	F	F	F	F	F	F	F	F	F	F	Lindsay Bourke/Glenn Harrington	
Fern tail		3/09/2015	2:25:00 PM		31 3301-3307; 3313-3316	331572.0	7813573.0	13.29	7.84		30.80	174	Low	Clear/Brown	None	0.05	N/A	Various grasses (species unknown)	WHITE to GREY, Clay to sandy clay	Evidence of drying from on margins	-15mAHD	Unknown	N/A		Open water body appears to be stagnant with no distinguishable outflow.	Surface crusting of precipitates on area surrounding Fern tail. Considerable cover by native/invasive perennial grasses (couch?) in damp areas surrounding water body	Sampled from open water body. No obvious evidence of SW outflow.	T	T	T	T	T	T	T	T	T	T	T	Lindsay Bourke/Glenn Harrington
Friday Well		31/08/2015	1:15:00 PM		3077-2080	326312.0	7819734.0	2.95	7.48	132.000	30.00	184	Low	Clear	None	N/A	Acacia sp.	None	WHITE to GREY Clayey sand, with silt	Dry	-10mAHD	Unknown	N/A		No SW present, likely area for SW accumulation during wet periods	Melaleuca sp. overstorey to the south of the well	Removed tank overflow @ 13:15 and sampled @ 14:20 Tank filled using solar submersible pump.	T	T	T	T	T	T	T	T	T	T	T	Lindsay Bourke/Glenn Harrington
Little Eil Eil		2/09/2015	1:00:00 PM		3193-3204	336691.0	7810703.0										Melaleuca sp. and Accacia sp.	Various grasses (species unknown)	WHITE to GREY Clayey sand, with silt	Dry	-32mAHD	Unknown	N/A		On margins of moat, likely to accumulate SW during wet periods	Located immediately south of the moat of Little Eil Eil. Transition from largely dry Schlerophyll (Acacia sp.) to wet vegetation (Melaleuca sp., Mangrove fern, Typha sp. etc). Photos also taken walking westwards, then south around moat.	N/A	F	F	F	F	F	F	F	F	F	F	Lindsay Bourke/Glenn Harrington	
Little Eil Eil		2/09/2015	1:20:00 PM		3204-3209	336615.0	7810690.0										Melaleuca sp. and Accacia sp.		WHITE to GREY Clayey sand, with silt	Dry, although some shallow pools present	-32mAHD	Unknown	N/A		SW largely absent, likely area for SW accumulation during wet periods	Large bare areas with clustered groups of very large (>20m) Melaleuca sp.	N/A	F	F	F	F	F	F	F	F	F	F	Lindsay Bourke/Glenn Harrington	
Little Eil Eil		2/09/2015	1:40:00 PM		3209-3216	336723.0	7810603.0										Melaleuca sp.	Mangrove fern (Scientific name unknown)	WHITE to GREY Clayey sand, with silt. Significant leaf litter on surface (Melaleuca litter)	Peak of mound dry	-35mAHD	Unknown	N/A		SW present in moat and isolated pockets.	North view of mound taken from the southern side of Little Eil Eil, nearby sample location	N/A	F	F	F	F	F	F	F	F	F	F	Lindsay Bourke/Glenn Harrington	
Little Eil Eil		2/09/2015	1:50:00 PM		3217-3220	336728.0	7810603.0	1.43	6.59	266.500	34.40	56	Low	Clear	None	0.10	Melaleuca sp.	None	BLACK to GREY, Humic-rich peat at surface on mound	Saturated	-35mAHD	Unknown	N/A		Moat around the entire mound with SW present ~70% of area	Mangrove fern (Latin name unknown) ceases abruptly at edge of mound	Sampled from likely groundwater discharge. Clear evidence of discharge and flow.	T	T	T	T	T	T	T	T	T	T	T	Lindsay Bourke/Glenn Harrington

HYDROLOGICAL CONCEPTUALISATION OF THE WALYARTA MOUND SPRINGS

ID	Alt_ID	Date	Time	GPS point	Photo	X_MGA51	Y_MGA51	EC_mScm	pH	ORP_mV	Temp_oC	Total Alkalinity	Turbidity (text)	Colour (text)	Odour (text)	Sample depth_m	Overstorey veg	Understorey veg	Soil Desc	Surface moisture status	Estimated elevation	Underlying geology/hydrogeology	Creek/channel flow rate	SW/GW interaction	Site comments	Sample comments	Field WQ	Water Major ions	D/18 O	Nutrie nts	Fe2+	SiO2 (Reac +RE)	Metals Sr87/Sr86	C14	Officer/sampler		
Lyngetts Well		31/08/2015	3:30:00 PM		3081-3085	338919.5	7820329.5												WHITE to GREY, Clayey, silty sand	Dry	-20mAHD	Unknown	NA	No SW present, likely area for SW accumulation during wet periods	Site located in a localised depression, between 2 x EW red sand dunes. Presence of Melaleuca sp. to south of site indicates likely presence of shallow water table.	Bore pump not operational. Unable to purge sample bore. Cattle trough empty. Well located in depression surrounded by melaleuca sp. Soils similar to Lyngetts, being clayey sand, white to grey with fine silt. Sand dune	F	F	F	F	F	F	F	F	F	Lindsay Bourke/Glenn Harrington	
Melaleuca Moat		3/09/2015	3:00:00 PM	32	3317-3322	331267.0	7813258.0										Melaleuca sp.	Various grasses (species unknown)	WHITE to GREY, Clayey, silty sand	Variable	-15mAHD	Unknown	NA	SW present in moat, although broader area dry. Likely area for SW accumulation in wet periods	Transition zone from dry sclerophyll vegetation (e.g. Acacia sp.), through a bare area to the mound and moat which are dominated by vegetation requiring wetter conditions (Melaleuca sp., Mangrove fern). Cattle pugging present in moat and bare areas.	NA	F	F	F	F	F	F	F	F	Lindsay Bourke/Glenn Harrington		
Melaleuca Moat		3/09/2015	3:04:00 PM	33	3322-3328	331264.8	7813224.7	14.38			24.40						Melaleuca sp.	Mangrove fern (Scientific name unknown)	BLACK to GREY, sandy clay	Saturated	-15mAHD	Unknown	NA	SW present in moat, although broader area dry. Likely area for SW accumulation in wet periods	Abrupt change in vegetation at edge of mound from Mangrove fern and Melaleuca sp. overstorey to only Melaleuca sp. Overstorey in the moat in places is in poor health and large bare areas occur further outside of the moat.	Field WQ sample taken from SW in moat, immediately adjacent to mound	T	T	T	T	T	T	T	T	T	Lindsay Bourke/Glenn Harrington	
Melaleuca Moat		3/09/2015	3:12:00 PM	34	3328-3331	331187.2	7813212.5	6.88			35.40						Melaleuca sp.	None	BLACK to GREY, sandy clay	Saturated	-15mAHD	Unknown	NA	SW present in moat, although broader area dry. Likely area for SW accumulation in wet periods	Abrupt change in vegetation at edge of mound from Mangrove fern and Melaleuca sp. overstorey to only Melaleuca sp. Overstorey in the moat in places is in poor health and large bare areas occur further outside of the moat.		T	F	F	F	F	F	F	F	Lindsay Bourke/Glenn Harrington		
Melaleuca Moat		3/09/2015	4:00:00 PM		3336	331191.0	7813212.0	6.97	9.14		33.50	123	Low	Clear	None	0.05	Melaleuca sp.	None	BLACK to GREY, sandy clay	Saturated	-15mAHD	Unknown	NA	Moat around the entire mound with SW present <30% of area	Standing water in some areas of the moat, but not all the way around. SW level -0.05m deep. Abrupt termination of vegetation on outer of moat with large bare area.	Sampled in area of dead Melaleuca sp, although with lowest observed salinity in moat area.	T	T	T	T	T	T	T	T	T	Lindsay Bourke/Glenn Harrington	
Melaleuca Peat		3/09/2015	3:30:00 PM	35	3332-3335	331223.0	7813231.0	12.00	6.53		23.50		High	Dark Brown	H2S	0.10	Melaleuca sp.	Mangrove fern (Scientific name unknown)	BLACK to BROWN, Humic-rich peat.	Saturated	-17mAHD	Unknown	NA	No obvious signs of GW discharge, although SW in moat indicates likely discharge.	Very little topographical relief on the mound. Roots and coarse organic material throughout top 0.10m. Clay content increasing rapidly with depth. Hole ceased at 0.3m. Very slow recovery in water levels after excavating hole to take water sample. Very dense understorey with significant leaf litter. Abrupt change in vegetation at the edge of mound.	Excavated hole to -0.30m, removed water and awaited for recovery then sampled. Unable to analyse Alkalinity or filter sample due to high suspended sediments. Froze nutrient samples and will request lab to attempt to filter. Sr sample not filtered on-site.	T	T	T	T	T	F	F	F	T	T	Lindsay Bourke/Glenn Harrington
No_ID_1		1/09/2015	9:00:00 AM		13086-3095, P90119 03-905	340888.8	7817500.3	82.50			21.60		Low	Clear	None	0.02	Mangrove (Avicennia marina)	None	RED to GREY, clayey sand	Damp	-20mAHD	Unknown	Very slow, rate unknown	Groundwater discharge from upgradient broad saline area, being channelled towards Salt Creek	Location where Adrian Pinder was bogged. Groundwater discharge at surface, contributing to Salt Creek. Surface crusting of salts across extensive area. Calcrete exposures immediately upgradient of sample location. Mangroves lining the more incised channel where samples taken. Acacia sp. and spinifex on sandier areas to the east and west of incised channel.	Sampled from shallow pool. Second WQ = 72.8 mS/cm, 23.5oC	T	F	F	F	F	F	F	F	F	Lindsay Bourke/Glenn Harrington	
No_ID_Salt_Creek		1/09/2015	1:40:00 PM		3105-3110	341436.0	7817254.0	59.40	7.91		24.40						Mangrove (Avicennia marina)	Spinifex and various grasses (species unknown)	WHITE to GREY, clayey sand	Dry	-20mAHD	Unknown	Negligible - No visible evidence of flow	No clear evidence of GW discharge, although likely contribution given presence of permanent water. Salt precipitates on bank.	To the east of Salt Creek Flow 1, Salt Creek, little or no visible flow, appears to be stagnant. Lots of fish. Large calcrete exposures upgradient of floodplain and incised channel. Very narrow (<5m) and shallow (<0.5m) in places.	Sampled from edge of Salt Creek.	T	F	F	F	F	F	F	F	F	Lindsay Bourke/Glenn Harrington	
Salt Creek Crossing		1/09/2015	3:15:00 PM		3130-3136	337776.0	7817267.0										Mangrove (Avicennia marina)	Spinifex and various grasses (species unknown)	WHITE to GREY, clayey sand	Damp	-20 mAHD	Unknown	Nil	SW on both sides of calcrete exposure at crossing. Flow is negligible. GW/SW interactions likely	Large calcrete slab crossing Salt Creek with no surface water flow. Shallow (<0.2m), broad (~20m) area with little topographical relief upgradient of Salt Creek. Salt crusting across broad flat area. Calcrete exposures present in Salt Creek further down gradient. Strong smell of H2S	NA	F	F	F	F	F	F	F	F	Lindsay Bourke/Glenn Harrington		
Salt Creek Flow 1		1/09/2015	2:00:00 PM		311-3116	341252.0	7817308.0	61.80	8.30		25.30						Mangrove (Avicennia marina)	Spinifex and various grasses (species unknown)	WHITE to GREY, clayey sand	Damp	-20 mAHD	Unknown	SW flow is negligible, appears stagnant	Calcrete exposure along both banks. Creek incised into calcrete. Little or no visible flow. Creek -15m wide -1.5-2.0m deep.	pHEC taken from northern bank. Sample not representative	T	F	F	F	F	F	F	F	F	Lindsay Bourke/Glenn Harrington		
Salt Creek Flow 3		1/09/2015	2:30:00 PM		3117-3120	339903.0	7817458.0	52.50	7.64		25.10						Mangrove (Avicennia marina)	Spinifex and various grasses (species unknown)	BROWN to WHITE, clayey sand	Dry	-20 mAHD	Unknown	Negligible - No visible evidence of flow	Negligible/little flow, high turbidity, brown. Too wide/deep to sample -15m wide 1.5-2.0m deep. Significant shading over Salt Creek.	Field WQ from shaded area on northern bank	T	F	F	F	F	F	F	F	F	Lindsay Bourke/Glenn Harrington		
Salt Creek Flow 4		1/09/2015	3:00:00 PM		3121-3129	337928.0	7817386.0	53.90	8.09		27.20						Mangrove (Avicennia marina)	Spinifex and various grasses (species unknown)	BROWN to WHITE, clayey sand. BROWN to WHITE Sand on upper areas.	Dry	-20 mAHD	Unknown	Negligible - No visible evidence of flow	Salt Creek is much deeper upgradient with more vigorous growth of mangroves. Calcrete fringing waters edge at sample point, almost crossing entire creek. Large calcrete slab further to the west at crossing. Strong smell of sulfides. Floodplain is very flat and broad with some erosion evident.	Field WQ from centre of Salt Creek.	T	F	F	F	F	F	F	F	F	Lindsay Bourke/Glenn Harrington		
Salt Creek Flow 6		1/09/2015	3:35:00 PM		3137-3142	335644.0	7817571.0	62.70	8.30		26.90		High				Mangrove (Avicennia marina)	Spinifex and various grasses (species unknown)	BROWN to WHITE, clayey sand. BROWN to WHITE Sand on upper areas.	Dry	-20 mAHD	Unknown	Negligible - No visible evidence of flow	High turbidity, light green -20m wide with unknown depth. Scetch of cross section in notes. No visible calcrete, very damp on banks -0.2m below top of bank. Mangrove density higher on northern bank.	Field WQ from edge of Salt Creek, not necessarily representative of whole water body.	T	F	F	F	F	F	F	F	F	Lindsay Bourke/Glenn Harrington		
Salt Creek Flow 7	Salt Creek 7	1/09/2015	4:25:00 PM		3143-3154	334121.0	7817347.0	68.80	8.49		28.40	106	Medium	Brown	H2S	1.00	Mangrove (Avicennia marina)	Various grasses (species unknown)	WHITE to GREY, Sandy clay. (Delta from southern inflow WHITE, clean sands)	Dry on banks, although saturated -0.2m below top on exposed bank	-15mAHD	Unknown	Negligible - No visible evidence of flow	No clear evidence of GW discharge, however likely due to presence of permanent water and saturation from -0.2m from top of banks to SW.	Vegetation on northern bank more dense than southern. Drainage line to the south (northerly inflow to creek) contains clean, white sands with Acacia sp (Photo DSC_3144-45). Contrasts with surrounding clay-rich, salt encrusted sapphire flats.	Water sample @ 1.0m, field WQ @ 0.25m. Unable to obtain field WQ parameters from same depth as water sample.	T	T	T	T	T	T	T	T	T	Lindsay Bourke/Glenn Harrington	

HYDROLOGICAL CONCEPTUALISATION OF THE WALYARTA MOUND SPRINGS

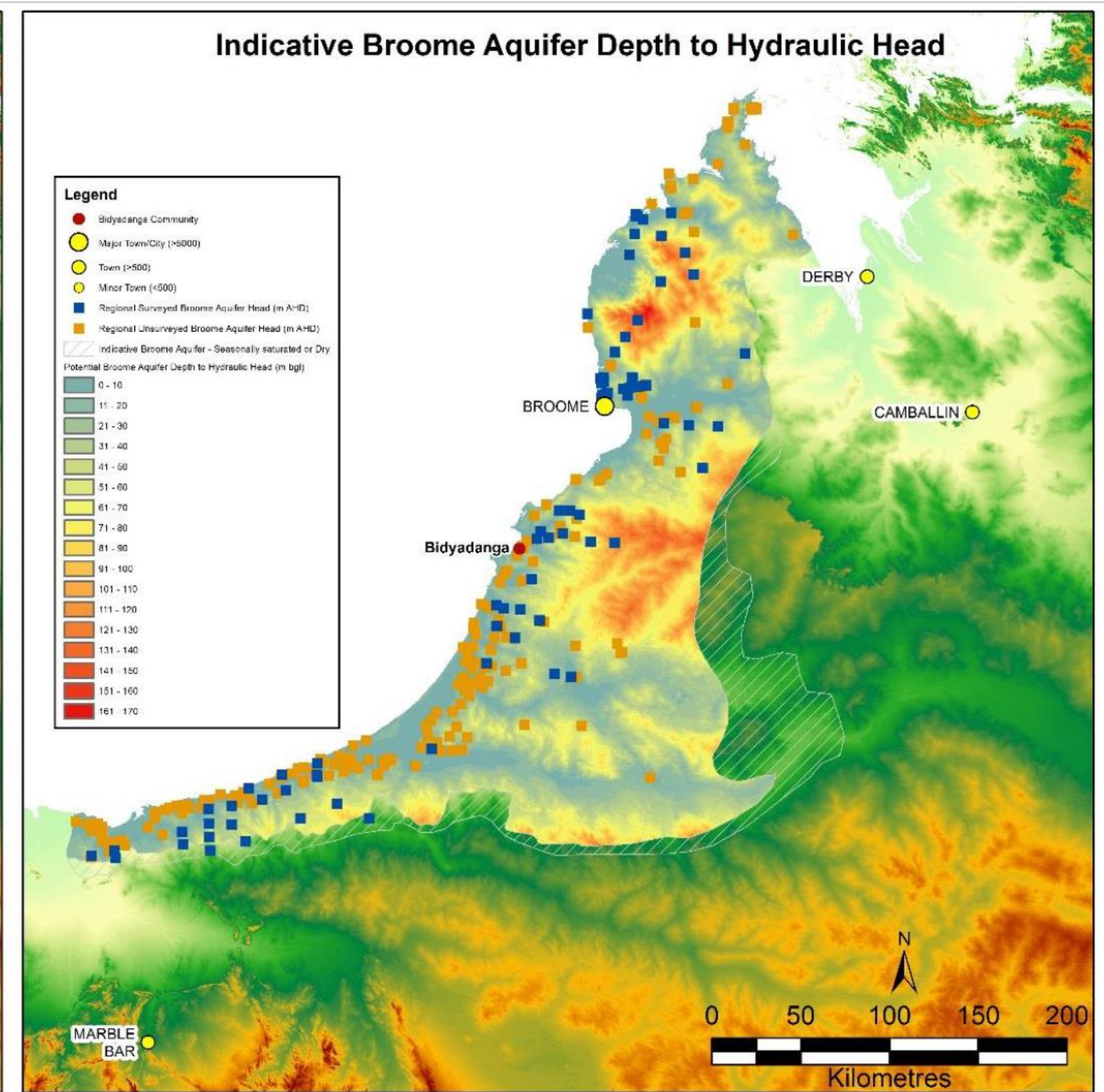
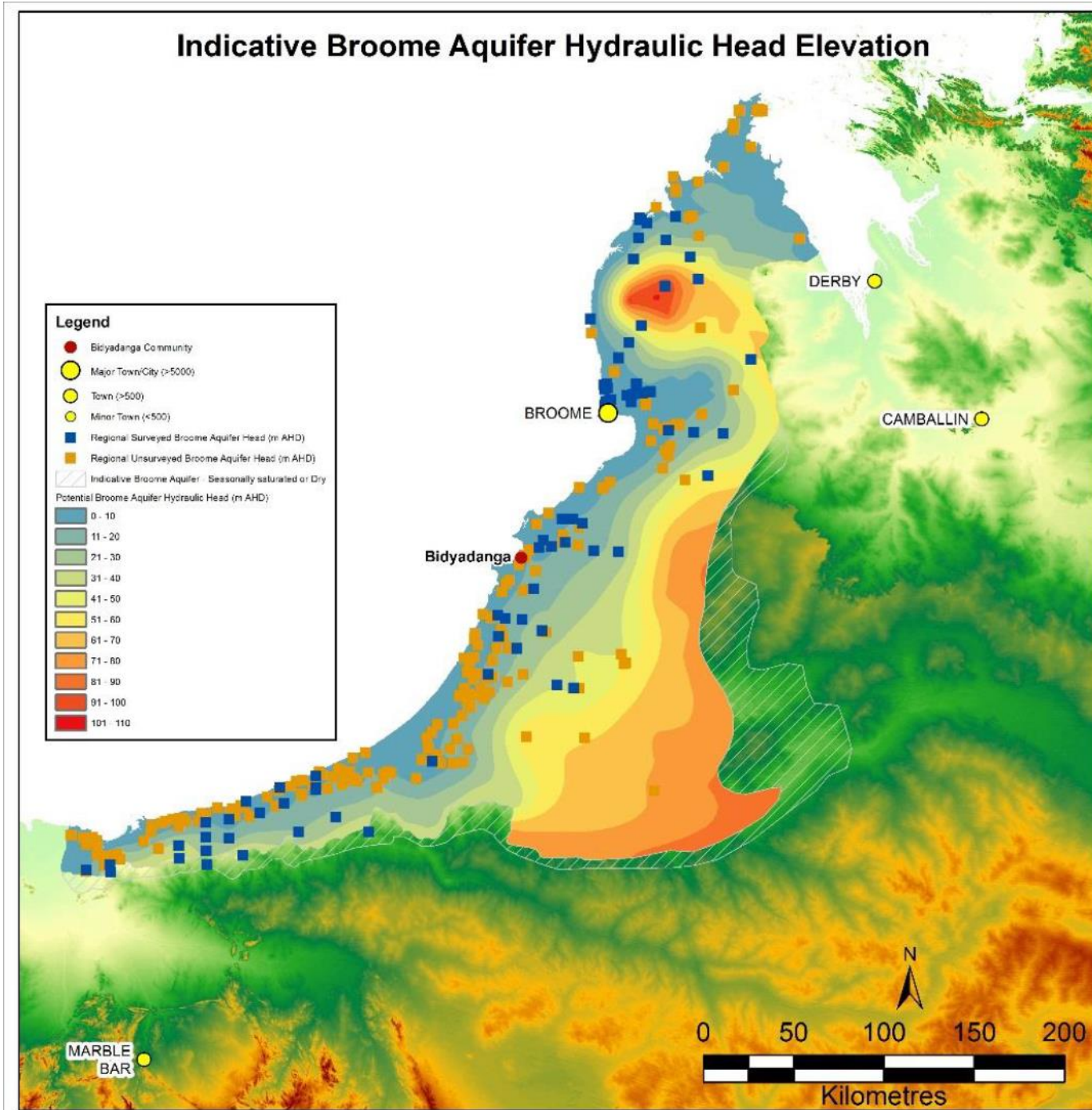
ID	Alt_ID	Date	Time	GPS point	Photo	X_MGA51	Y_MGA51	EC_mScm	pH	ORP_mV	Temp_oC	Total Alkalinity	Turbidity (text)	Colour (text)	Odour (text)	Sample depth_m	Overstorey veg	Understorey veg (Scientific name unknown)	Soil Desc	Surface moisture	Estimated elevation	Underlying geology/hydro	Creek/channel flow rate	SW/GW interaction	Site comments	Sample comments	Field WQ	Water Sampl ions	Major O	D/18	Nutrie nts	Fe2+	SiO2 (Reac +RE)	Metals Sr87/ Sr86	C14	Officer/sampler			
Saunders - DNA		4/09/2015	2:00:00 PM			326027.0	7811700.0				25.00						Sesbania formosa	Magrove fern (Scientific name unknown)								Peat sample taken for analysis of DNA in peat as part of the Global Peat Project.		F	F	F	F	F	F	F	F	F	F	Lindsay Bourke/Glenn Harrington	
Saunders East		3/09/2015	10:10:00 AM	26 3287-3289		326046.0	7811624.0	1.62	7.08		25.50	74	Low	Clear	None	0.02	Sesbania formosa	Typha sp.	BROWN, Humic-rich peat	Saturated	-17mAHd	Unknown	N/A	Obvious signs of GW discharge, rate unknown	A single stranded peat mound (~25m <sup>2</sup> ), very spongy underfoot. Ground moves (rebounds) when stepped on. Clear water with floating macrophyte/plant.	Water sampled directly from surface discharge of groundwater.		T	T	T	T	T	T	T	T	T	T	Lindsay Bourke/Glenn Harrington	
Saunders Open 1		3/09/2015	9:15:00 AM	24 3279-3283		325915.2	7811733.0	3.60	8.64		23.40						N/A	N/A	BROWN to GREY sandy clay	Saturated	-15mAHd	Unknown	N/A	Likely GW inflow from east, contribution from underlying sources unknown.	Shallow open water body. Broad area to the east with Typha sp. likely diffuse inflow to the open water body. Significant cattle pugging.	Water sampled from open water body (-centre).		T	F	F	F	F	F	F	F	F	F	Lindsay Bourke/Glenn Harrington	
Saunders Open 2		3/09/2015	10:50:00 AM	3291-3294		325700.0	7811778.0										None	Typha sp.	GREY to BLACK, sandy clay (swelling-cracking)	Damp	-15mAHd	Unknown	N/A	Upward discharge from groundwater likely to occur in vicinity of Typha sp.	See other comments for Saunders Open 2	N/A		F	F	F	F	F	F	F	F	F	Lindsay Bourke/Glenn Harrington		
Saunders Open 2		3/09/2015	10:53:00 AM	27 3291-3296		325744.6	7811784.7	1.98	8.79		26.60						None	Typha sp.	GREY to BLACK, sandy clay (swelling-cracking)	Saturated	-15mAHd	Unknown	N/A	Upward discharge from groundwater likely to occur in vicinity of Typha sp.	See other comments for Saunders Open 2	N/A		T	F	F	F	F	F	F	F	F	Lindsay Bourke/Glenn Harrington		
Saunders Open 2	Saunders 2	3/09/2015	11:15:00 AM	28 3291-3300		325720.0	7811795.0	1.26	9.22		28.50	70	Low	Clear	None	0.02	None	Typha sp.	GREY to BLACK, sandy clay (swelling-cracking)	Saturated	-15mAHd	Unknown	N/A	Surface water ponded around typha sp. Surrounding depression (open water body) dry	A stand of Typha sp. In the middle of a depression, likely to be an open water body during wet periods. Stock seen on wetland, residing in Typha sp (BFB). Significant area of cattle pugging. Depression bounded by Accacia sp.	Sample taken from standing SW at western edge of Typha sp.		T	T	T	T	T	T	T	T	T	T	T	Lindsay Bourke/Glenn Harrington
Saunders Open 2		3/09/2015	11:19:00 AM	3297-3298		325755.0	7811804.0	1.30	8.59		29.30						None	Typha sp.	GREY to BLACK, sandy clay (swelling-cracking)	Saturated	-15mAHd	Unknown	N/A	Surface water ponded around typha sp. Surrounding depression (open water body) dry	See other comments for Saunders Open 2	Sample taken from standing SW at eastern edge of Typha sp.		T	F	F	F	F	F	F	F	F	F	Lindsay Bourke/Glenn Harrington	
Saunders Peat		3/09/2015	8:40:00 AM	23 3275		325974.0	7811660.0	2.65	6.97		20.30	172	Low	Clear	None	0.02	Sesbania formosa	Typha sp. and Mangrove fern (Scientific name unknown)	BLACK to BROWN, Humic-rich peat.	Saturated	-17mAHd	Unknown	N/A	Obvious signs of GW discharge, rate unknown	Area of dense Mangrove Fern and small (<9m <sup>2</sup> ) area of Typha sp. Area tending towards middle slope of mound. Active GW discharge with westerly trend towards open water body.	Sampled next to Typha sp. where groundwater discharge obvious, discharge rate unknown. Central/southwestern extent of mound.		T	T	T	T	T	T	T	T	T	T	Lindsay Bourke/Glenn Harrington	
Saunders Spring		3/09/2015	7:21:00 AM	15 3251-3253		326021.0	7811557.0										Acacia sp.	None	BROWN to GREY clayey sand	Dry	-15mAHd	Unknown	N/A	SW present in depression. Likely GW contribution	This excavated depression (dirt spoils to the southeast) is located outside of the fenced area. SW depth <0.5m. Numerous cattle (>20) seen in the area over the period of the field trip. The Saunders peat mound is located immediately to the west.	N/A		F	F	F	F	F	F	F	F	F	Lindsay Bourke/Glenn Harrington		
Saunders Spring		3/09/2015	7:28:00 AM	16 3258-3259		325998.0	7811634.0										Sesbania formosa	Various rushes (species unknown)	BLACK to GREY, sandy clay with high organics	Saturated	-15mAHd	Unknown	N/A	SW present in depressions. Likely GW contribution	Saturated sandy clay, very boggy and difficult to traverse. Cattle pugging throughout lower lying areas. Little or no understorey in these areas. Very little exchange in relief in low-lying areas.	N/A		F	F	F	F	F	F	F	F	F	Lindsay Bourke/Glenn Harrington		
Saunders Spring		3/09/2015	7:40:00 AM	17 3265-3267		326035.0	7811649.0	4.40			17.00						Sesbania formosa	Magrove fern (Scientific name unknown)	BLACK to GREY, sandy clay with high organics	Saturated	-15mAHd	Unknown	N/A	SW present in depressions. Likely GW contribution	Very slow SW flow down gradient along moat in northerly direction towards open water body. Slight increase in elevation towards mound and increased proportion of Mangrove ferns.	Field WQ sample from standing SW.		T	F	F	F	F	F	F	F	F	F	Lindsay Bourke/Glenn Harrington	
Saunders Spring		3/09/2015	7:51:00 AM	18 3268		326057.0	7811705.0	4.16			18.20						Sesbania formosa	Typha sp.	BLACK to GREY, sandy clay with high organics	Saturated	-15mAHd	Unknown	N/A	GW discharge occurring from upgradient	Site located at northeast of Saunders peat mound. Very low volume of SW flow near Typha sp. Flow heads in north-westerly direction towards open water body	Field WQ sample from standing SW.		T	F	F	F	F	F	F	F	F	F	Lindsay Bourke/Glenn Harrington	
Saunders Spring		3/09/2015	8:10:00 AM	19 3270-3271		325993.0	7811712.0	5.99			18.60						Sesbania formosa	Magrove fern (Scientific name unknown) and Typha sp.	BLACK to GREY, sandy clay with high organics	Saturated	-15mAHd	Unknown	N/A	GW discharge occurring from upgradient	Site located at the northerly extent of Saunders peat mound, immediately down-gradient.	Field WQ sample from standing SW.		T	F	F	F	F	F	F	F	F	F	Lindsay Bourke/Glenn Harrington	
Saunders Spring		3/09/2015	8:21:00 AM	20 3272		325976.0	7811664.0	3.00			21.10						Sesbania formosa	Magrove fern (Scientific name unknown) and Typha sp.	BLACK to GREY, sandy clay with high organics	Saturated	-15mAHd	Unknown	N/A	GW discharge occurring from upgradient	Site located at the south-western extent of Saunders peat mound, immediately down-gradient.	Field WQ sample from standing SW.		T	F	F	F	F	F	F	F	F	F	Lindsay Bourke/Glenn Harrington	
Saunders Spring		3/09/2015	8:25:00 AM	21 3273		325973.0	7811657.0	2.68			19.60						Sesbania formosa	Magrove fern (Scientific name unknown)	BLACK to GREY, sandy clay with high organics	Saturated	-15mAHd	Unknown	N/A	GW discharge occurring from upgradient	Site located at the south-western extent of Saunders peat mound, immediately down-gradient.	Field WQ sample from standing SW within area dominated by Mangrove fern.		T	F	F	F	F	F	F	F	F	F	Lindsay Bourke/Glenn Harrington	
Saunders Spring		3/09/2015	8:28:00 AM	22 3274		325977.3	7811641.8	2.78			18.10						Sesbania formosa	Typha sp. and rushes (species unknown)	BLACK to GREY, sandy clay with high organics	Saturated	-15mAHd	Unknown	N/A	GW discharge occurring from upgradient	Site located at the south-western extent of Saunders peat mound, immediately down-gradient.	Field WQ sample from standing SW in open area nearby fallen Dragon Tree (Sesbania formosa).		T	F	F	F	F	F	F	F	F	F	Lindsay Bourke/Glenn Harrington	
Saunders Spring		3/09/2015	9:00:00 AM	3277-3278		325959.0	7811728.0										Acacia sp.	Typha sp. and rushes (species unknown)	BLACK to GREY, sandy clay with high organics	Saturated	-15mAHd	Unknown	N/A	GW discharge occurring from upgradient	Site located at the western extent of the peat mound, with GW discharging into the open water body.	N/A		F	F	F	F	F	F	F	F	F	Lindsay Bourke/Glenn Harrington		
Saunders West		3/09/2015	10:00:00 AM	25 3286		325934.0	7811717.0	1.79	7.10		20.00	186	Low	Clear	None	0.02	Sesbania formosa	Typha sp. and Mangrove fern (Scientific name unknown)	BLACK to BROWN humic-rich clay to sandy clay	Saturated	-15mAHd	Unknown	N/A	Obvious signs of GW discharge, rate unknown.	Area of less dense stand of Sesbania formosa with sparse (<10%) Mangrove Fern, Typha sp. and rushes (species unknown). Site discharges westwards to open water body	Sampled from Saunders outflow at Typha sp. Lower edge of mound.		T	T	T	T	T	T	T	T	T	T	Lindsay Bourke/Glenn Harrington	



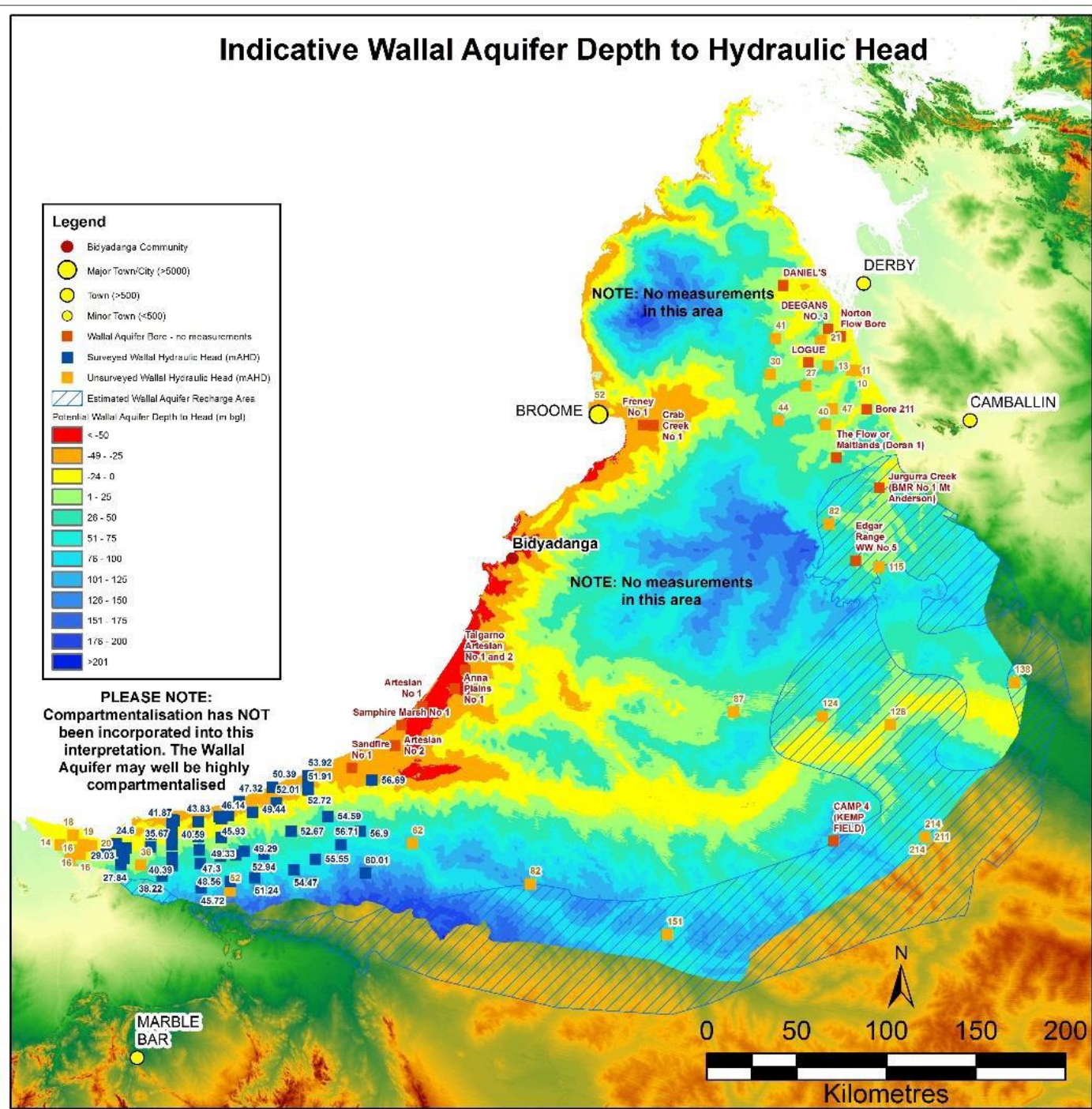
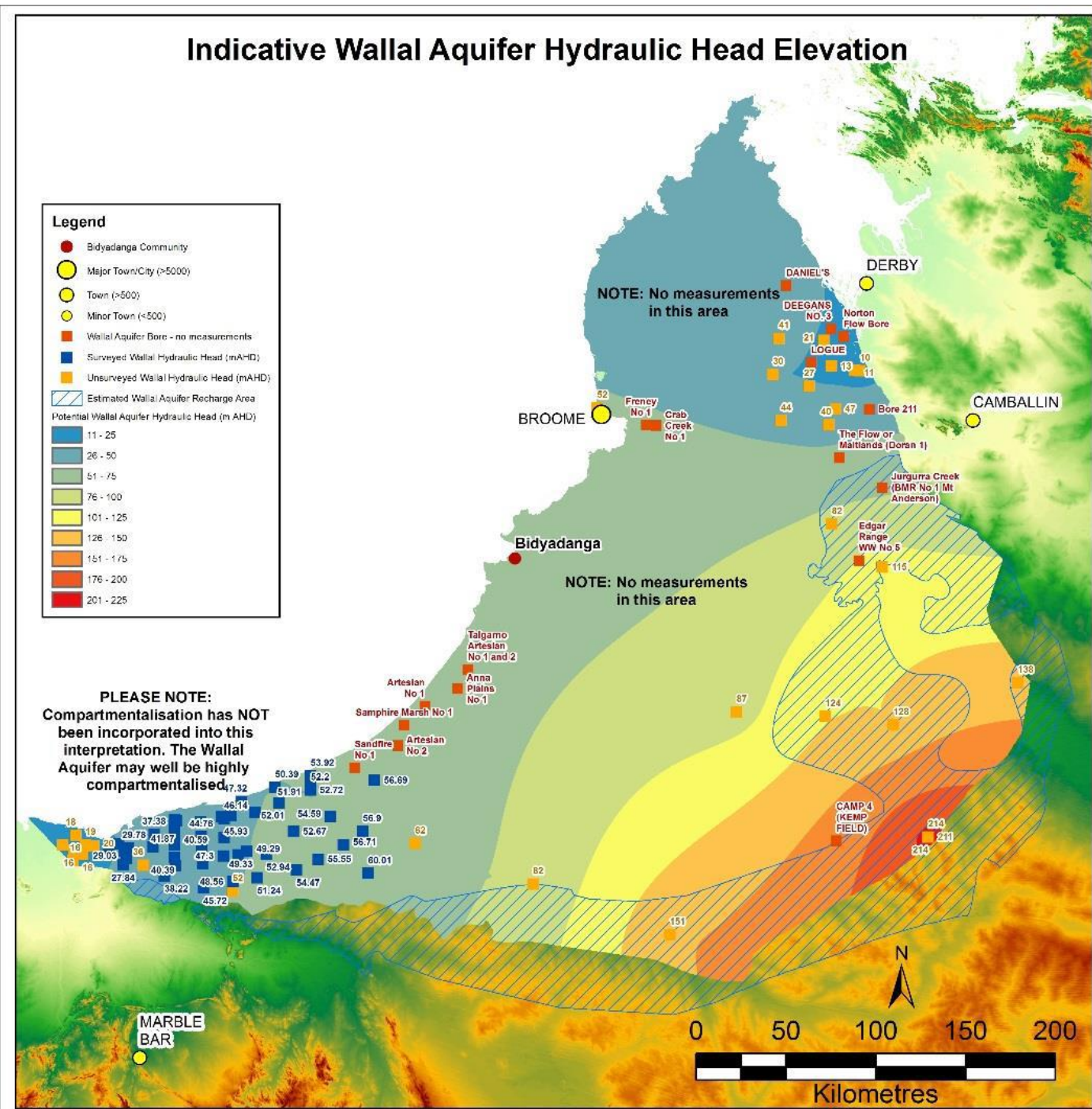
HYDROLOGICAL CONCEPTUALISATION OF THE WALYARTA MOUND SPRINGS

ID	Alt_ID	Date	Time	GPS point	Photo	X_MGA51	Y_MGA51	EC_mScm	pH	ORP_mV	Temp_oC	Total Alkalinity	Turbidity (text)	Colour (text)	Odour (text)	Sample depth_m	Overstorey veg	Understorey veg	Soil Desc	Surface moisture	Estimated elevation	Underlying geology/hydro	Creek/channel flow rate	SW/GW interaction	Site comments	Sample comments	Field WQ	Water Sampl ions	Major Ions	D/18 O	Nutrie nts	Fe2+	SiO2 (Reac +RE)	Metals Sr87/Sr86	C14	Officer/sampler		
Stockyard		4/09/2015	12:41:00 PM	37 1909-1910		331180.9	7814386.1										Sesbania formosa	Typha sp. and various grasses (species unknown) including a couch-like	WHITE to GREY clayey sand	Saturated	-15mAHd	Unknown	N/A	Obvious signs of GW discharge, rate unknown.	Spring ~200m south of track. Dragon flow trees and Typha sp.	N/A	F	F	F	F	F	F	F	F	F	F	Lindsay Bourke/Glenn Harrington	
Stockyard		4/09/2015	12:47:00 PM	38 1911-1913		331286.7	7814251.6										Melaleuca sp. and Acacia sp.	None	GREY to BLACK, sandy clay, with swelling cracking clays in depression	Damp	-15mAHd	Unknown	N/A	Damp soil in depression indicative of GW discharge	Bare area within depression with fringing Melaleuca sp. Some salt crusting in depression with swelling/cracking clays present in areas immediately upgradient of damp areas.	N/A	F	F	F	F	F	F	F	F	F	F	Lindsay Bourke/Glenn Harrington	
Stockyard Mangrove 2	SY Mangrove	4/09/2015	10:15:00 AM			331067.0	7814450.0	3.61	7.15		26.40	107	Low	Clear	None	0.02	Mangrove (Avicennia marina) and Sesbania formosa	Typha sp. and grasses (species unknown)	BROWN, Humic-rich peat with Sandy Clay	Saturated	-15mAHd	Unknown	N/A	Obvious signs of GW discharge, rate unknown.	Circular mound with Mangroves on the outer fringe and small (<5m) Sesbania formosa (White Dragon Tree) trees on mound. Sesbania formosa are in poor health. A moat is formed on the outer fringe of mound, although is very shallow (<0.05m) and extent of open water is low (<30%). Area to the north is a broad saline, clay-rich valley floor with samphire and other salt-tolerant vegetation.	Excavated hole to ~-0.20m. Sample obtained from GW discharge upgradient of hole.	T	T	T	T	T	T	T	T	T	T	Lindsay Bourke/Glenn Harrington	
Stockyard Mangrove West		4/09/2015	8:50:00 AM	3351-3353		330872.0	7814426.0	4.10	9.19		28.00						Mangrove (Avicennia marina)	Typha sp. and various grasses (species unknown) including a couch-like	GREY to WHITE sandy clay	Saturated	-15mAHd	Unknown	N/A	Groundwater discharge likely from central area with Typha sp. and Mangrove	A central mound (<0.2m above natural surface) with a stand of Mangroves. Stand of Typha sp. on northern and western edge of Mangrove stand. SW pooled around vegetation. Cattle pugging. Site immediately adjacent to broad, saline valley floor and lake Walyarta	Field WQ from shallow SW on eastern side of Typha sp.	T	F	F	F	F	F	F	F	F	F	F	Lindsay Bourke/Glenn Harrington
Stockyard Mangrove West		4/09/2015	8:50:00 AM			330872.0	7814426.0	4.13	8.44		23.40						Mangrove (Avicennia marina)	Typha sp. and various grasses (species unknown) including a couch-like	GREY to WHITE sandy clay	Saturated	-15mAHd	Unknown	N/A	Groundwater discharge likely from central area with Typha sp. and Mangrove	A central mound (<0.2m above natural surface) with a stand of Mangroves. Stand of Typha sp. on northern and western edge of Mangrove stand. SW pooled around vegetation. Cattle pugging. Site immediately adjacent to broad, saline valley floor and lake Walyarta	Field WQ from shallow SW on western side of Typha sp.	T	F	F	F	F	F	F	F	F	F	F	Lindsay Bourke/Glenn Harrington
Stockyard Typha		4/09/2015				330769.0	7814455.0	3.37	6.93		22.10							Typha sp.							Location estimated from GIS (uncertainty as to accuracy of coordinates). Small patch of Typha sp. Further west of Stockyard Mangrove West. Very few details documented.		T	F	F	F	F	F	F	F	F	F	Lindsay Bourke/Glenn Harrington	
Stromatolite Pool	MMS_19	1/09/2015	11:30:00 AM	3095-3104, P90119 06-908		347188.0	7816266.0	63.80	8.98	40.000	24.50	182	medium	Brown	Medium	1.20	Mangrove (Avicennia marina)	Various grasses (couch? species unknown) and samphire	GREY, Sandy clay	Dry on banks	-20mAHd	Unknown	Negligible - No visible evidence of flow	No clear evidence of groundwater discharge on banks, however likely groundwater contribution given presence of permanent water	Extensive calcrete exposure to the north of creek line (~200 m) with samphire and other salt-tolerant species in valley floor. Sand occurring on top of calcrete exposures with Acacia sp. and grasses. Mangroves on northern bank of creek line are larger and more numerous. Permanent water ceases to the west (Photo P9011906)	Sampled from centre of channel ~1.2m	T	T	T	T	T	T	T	T	T	T	T	Lindsay Bourke/Glenn Harrington

**Appendix 5 Indicative regional Broome and Wallal aquifer water levels: gradients (mAHD) and depth below ground level (mbgl) (from the DWER in prep)**



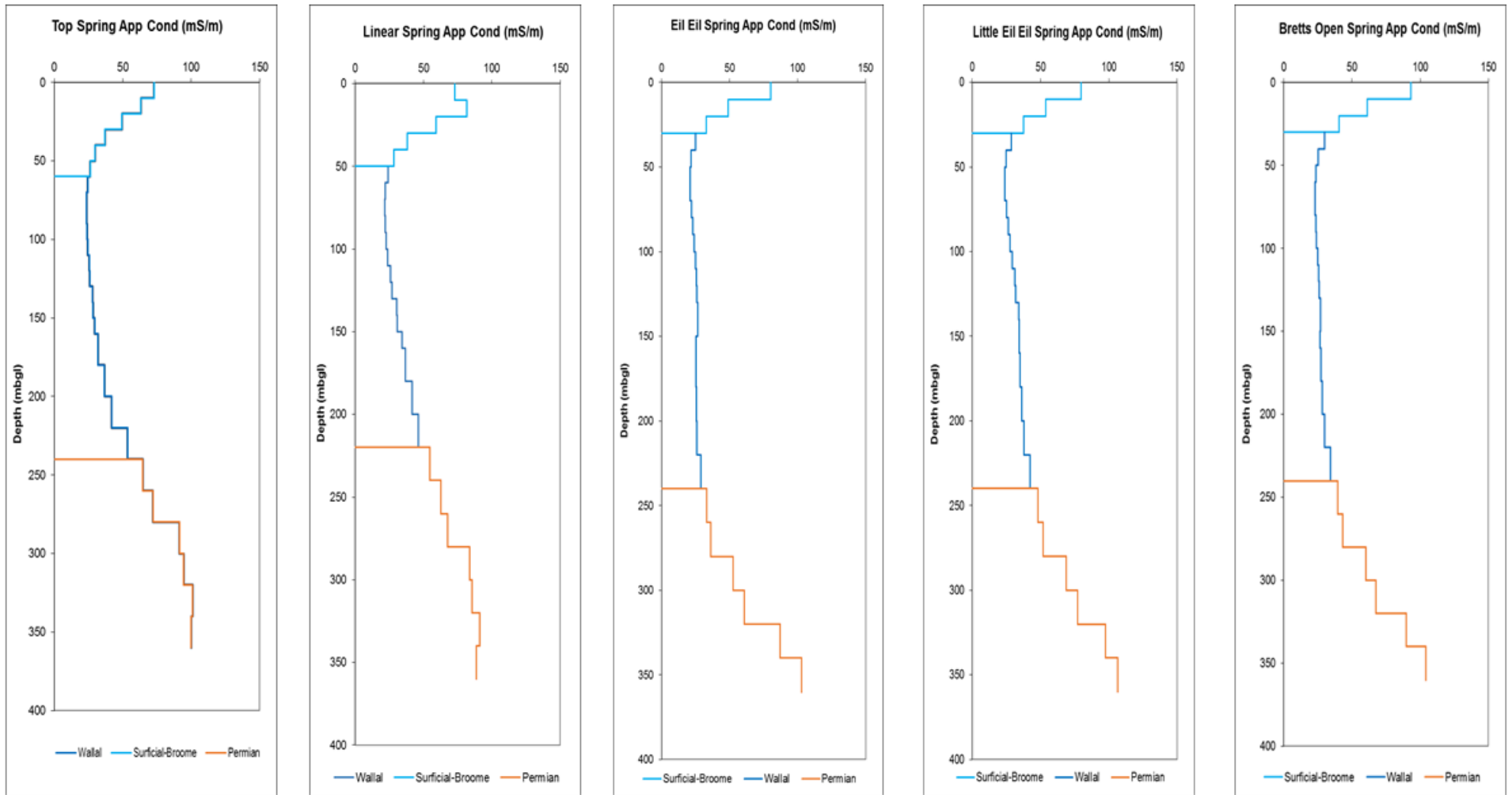




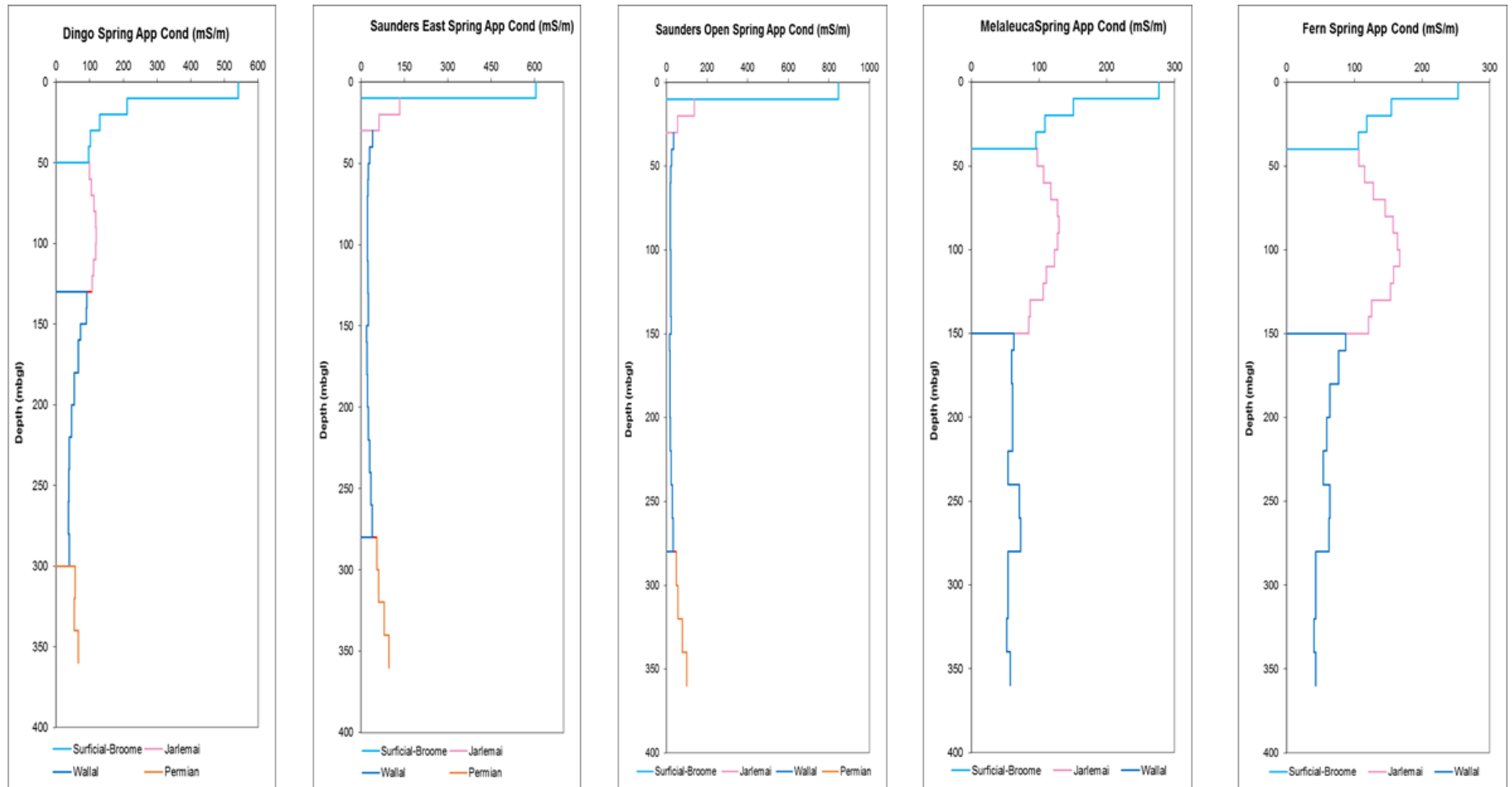


## Appendix 6 AEM conductivity depth profiles for major spring and surface water sites

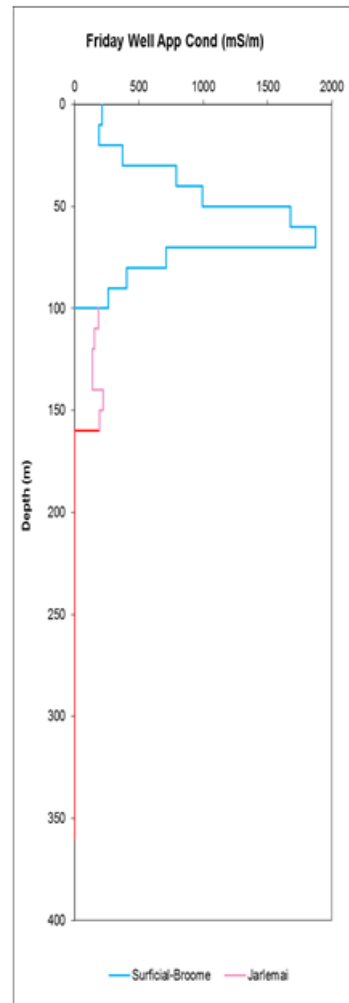
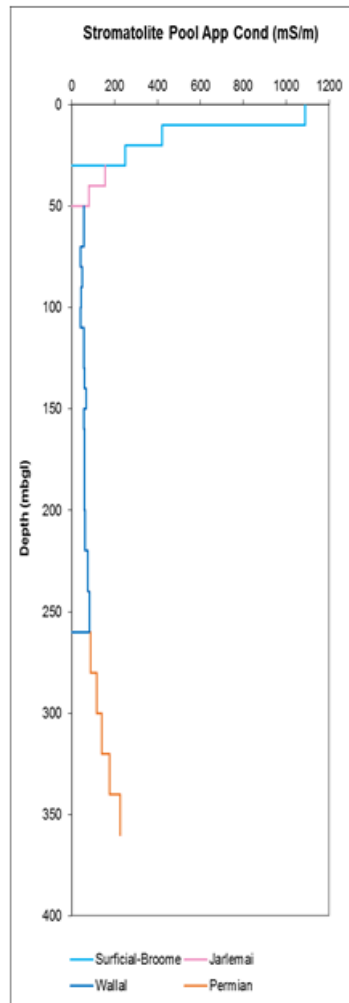
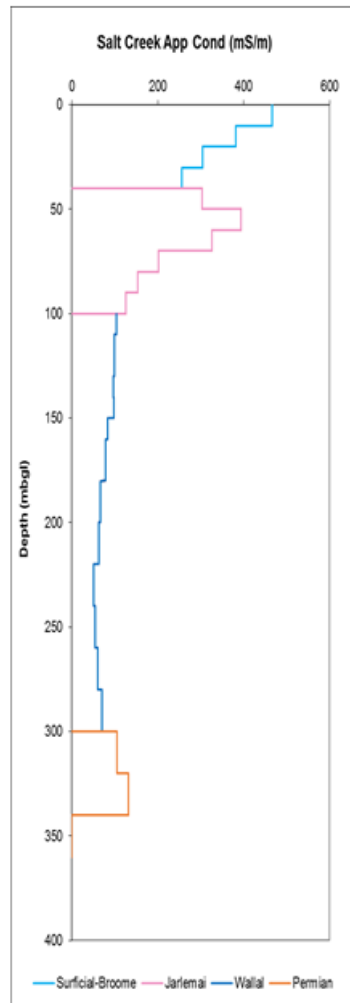
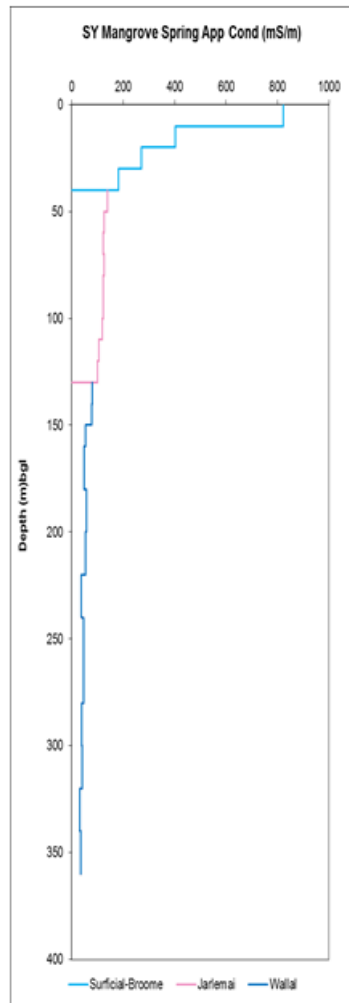
HYDROLOGICAL CONCEPTUALISATION OF THE WALYARTA MOUND SPRINGS



HYDROLOGICAL CONCEPTUALISATION OF THE WALYARTA MOUND SPRINGS



HYDROLOGICAL CONCEPTUALISATION OF THE WALYARTA MOUND SPRINGS





## Appendix 7 Hydrogeochemical Database

HYDROLOGICAL CONCEPTUALISATION OF THE WALYARTA MOUND SPRINGS

StationSampleID	Tectonic Element	Landscape/Flow path Position	Aquifer	Water Type	WIN_ID	Date Sampled	Data_Source	Alt/Report Bore Name	Bore Inlet_mbgf or EOH	Bore Inlet_TOS_mbgf	Bore Inlet_BOS_mbgf	Bore Inlet_MOS_mbgf	Easting_MGA51	Northing_MGA51	CBE %	pH lab	Br mg/L	Ca mg/L	Alk mg/L	Cl mg/L	HCO3 mg/L	CO3 mg/L	K mg/L	Mg mg/L	Na mg/L	NO3 mg/L	SiO2 mg/L	SO4 mg/L	TDS mg/L	Si Calcite	Si Gypsum	Si Dolomite	Si Chalcedony	Si Quartz	HCO3 / Cl	HCO3 / SiO2
WCB04B	1	Coast	Wallal	Na-Cl	23022644	4/12/2008	AnstoReport1		78.5-84.5	78.5	84.5	81.5	136332	7773562	0.0	6.2	1.4	86	47	760	56	0.007	18	45	430	<0.01	14	230	1640	-0.9	-1.4	-1.6	-0.2	0.3	0.1	4.0
WCB04B_R	1	Coast	Wallal	Na-Cl	23022644	8/06/2012	AnstoReport3	WCB04	78.5-84.5	78.5	84.5	81.5	136332	7773562	0.7	6.3	1.4	83	58	730	68	0.045	21	45	430	<0.05	13	240	1632	-0.8	-1.4	-1.4	-0.2	0.2	0.1	5.2
Mound Spring	1	Coast	Spring	Na-Cl		1973-1975	GSWALeech1979	Pardoo Mound Spring?					139332	7772796	-0.1	7.4		112	90	1060	110		25	68	564	<1	2	228	2169	-0.7	-1.4	-1.2	-0.9	-0.4	0.1	55.0
WCB04A	1	Coast	Wallal	Na-Cl	20070778	1973-1975	GSWALeech1979	4A	67.4-109.4	67.4	109.4	88.4	136373	7773577	-2.7	6.8		73	60	728	73		18	40	446	<1	15	243	1636	-1.0	-1.4	-1.9	0.0	0.5	0.1	4.9
WCB04B	1	Coast	Wallal	Na-Cl	23022644	19/03/2017	WCBsampling		78.5-84.5	78.5	84.5	81.5	136332	7773562	2.4	7.1	1.1	87	61	803	61		22	44	445	<0.01	14	259	1736	-0.9	-1.4	-1.8	0.0	0.4	0.1	4.2
PardooMoundSpring	1	Coast	Spring	Na-Cl		19/03/2017	WCBsampling	MoundSpring?					139332	7772796	6.0	7.9	1.0	115	112	952	112		19	62	599	<0.01	18	195	2073	-0.5	-1.4	-1.1	0.1	0.5	0.1	6.3
DeGrey1	1	Coast	Wallal	Na-Cl	20068699	18/08/1972	WIN/WIR		64.1-79.3	64.1	79.3	71.7	130675	7774380	7.1			67	65	692	77		19	35	410	1.0		178	1479	-1.0	-1.6	-1.9			0.1	
DeGreyStationBore7	1	Coast	Wallal	Na-Cl	20068700	17/10/1973	WIN/WIR		70-80	70	80	75	126325	7779571	7.8			82	50	776	59		19	44	437	1.0		206	1624	-1.0	-1.5	-2.0			0.1	
BanningarraSpring	1	Coast	Spring	Na-Mg-Cl		1973-1975	GSWALeech1979						153914	7782267	1.9	7.3		144	158	1620	192		42	137	791	6.0	2	240	3174	-0.4	-1.4	-0.5	-0.9	-0.4	0.1	96.0
WCB11A	1	Coast	Wallal	Na-Cl	20070796	1973-1975	GSWALeech1979	11A	61-85	61	85	73	144689	7770704	3.7	6.9		74	55	546	67		11	36	275	<1	20	114	1143	-1.0	-1.7	-1.9	0.1	0.6	0.1	3.4
WCB11Y	1	Coast	Wallal	Na-Ca-Cl		19/03/2017	WCBsampling		75.5 - 87.5	75.5	87.5	81.5	144753	7770687	3.2	7.2	0.8	77	39	582	39		12	36	262	<0.01	20	121	1150	-1.1	-1.6	-2.2	0.1	0.6	0.1	1.9
WCB09D	1	Coast	Wallal	Na-Cl	20070729	1973-1975	GSWALeech1979	9D	193-211	193	211	202	163655	7783915	9.5	7.0		63	67	528	82		11	33	306	<1	25	152	1200	-0.9	-1.6	-1.9	0.2	0.7	0.2	3.3
WCB09B	1	Coast	Wallal	Na-Ca-Cl	20070727	12/11/1973	WIN/WIR		74.4-95.4	74.4	95.4	84.9	163647	7783501	4.3			66	48	425	57		12	31	187	1.0		64	843	-1.0	-1.9	-2.1			0.1	
WCB17	1	Coast	Wallal	Na-HCO3-Cl	20070710	3/12/2008	AnstoReport1		220-244	220	244	232	809024	7784962	-5.1	6.5	0.6	20	203	140	245	0.060	6	11	150	<0.01	16	73	662	-0.7	-2.3	-1.2	-0.1	0.3	1.8	15.3
LambWell	1	Coast	Bossut	Na-Cl-HCO3		1973-1975	GSWALeech1979		7.95	7.95		4	185179	7787862	-0.5	7.9		43	336	291	409		8	12	313	47.0	69	60	1252	0.1	-2.3	0.0	0.7	1.1	1.4	5.9
WCB17B	1	Coast	Broome	Na-Ca-Cl-HCO3		1973-1975	GSWALeech1979	17B	64.0 - 70.0	64	70	67	181224	7784754	-0.6	7.5		49	190	211	232		8	18	172	12.0	59	80	841	0.0	-2.0	-0.1	0.6	1.0	1.1	3.9
WCB17C	1	Coast	Wallal	Na-Cl-SO4		17/11/2015	WCBsampling		130.75-148.75	130.75	148.75	139.75	181200	7784787	2.3		0.6	21	120	150	75		5	11	120	0.0		72	455	-1.1	-2.2	-2.1			0.5	
WCB17C_R	1	Coast	Wallal	Na-Cl-HCO3-SO4		20/03/2017	WCBsampling		130.75-148.75	130.75	148.75	139.75	181200	7784787	3.9	7.5	0.5	22	111	156	111		8	11	145	0.0	17	79	550	-1.1	-2.2	-2.2	0.1	0.5	0.7	6.5
WCB02A	1	Midflowpath	Wallal	Na-Ca-Mg-Cl	20068722	1973-1975	GSWALeech1979	2A	52-58	52	58	55	124727	7765223	3.1	7.6		156	248	718	302		12	91	276	55.0	65	71	1746	0.0	-1.7	0.0	0.6	1.1	0.4	4.6
WCB03A	1	Midflowpath	Wallal	Na-Cl	20068724	1973-1975	GSWALeech1979	3A	64.5-82.5	64.5	82.5	73.5	129992	7768714	-0.2	6.8		79	53	874	64		26	45	501	<1	16	216	1821	-1.0	-1.5	-2.0	0.0	0.5	0.1	4.0
DeGrey2	1	Midflowpath	Wallal	Na-Cl	20068711	18/08/1972	WIN/WIR		67.1-83.9	67.1	83.9	75.5	119092	7774086	2.2			268	65	3070	74		56	144	1590	1.0		382	5585	-0.6	-1.0	-1.1			0.0	
DeGreyStationBore8	1	Midflowpath	Wallal	Na-Cl	20068701	17/10/1973	WIN/WIR		70-80	70	80	75	125225	7771401	3.8			189	55	1760	63		38	107	871	1.0		305	3334	-0.7	-1.1	-1.4			0.0	
WCB02C	1	Midflowpath	Wallal	Na-Mg-Ca-Cl	20068723	9/10/1973	WIN/WIR		84-103	84	103	93.5	124690	7765231	0.3			272	253	1720	286		25	168	720	15.0		268	3474	0.1	-1.1	0.3			0.2	
WCB10A	1	Midflowpath	Wallal	Na-Cl	20070766	1973-1975	GSWALeech1979	10A	71-113	71	113	92	153470	7770770	-0.2	7.3		63	67	498	82		10	33	288	<1	22	159	1155	-0.9	-1.6	-1.9	0.2	0.6	0.2	3.7
WCB10B	1	Midflowpath	Wallal	Na-Cl	23022645	4/12/2008	AnstoReport1	WCB10	65-79.5	65	79.5	72.25	153468	7770768	-0.2	6.3	1.4	68	63	500	75	0.012	10	34	270	0.0	21	140	1119	-0.8	-1.6	-1.4	0.0	0.4	0.2	3.6
PB1_Ridley	1	Midflowpath	Wallal	Na-Cl	23059737	8/12/2008	Aquaterra_2009		52-102	52	102	77	154550	7770679	0.9			62	65	480	77		10	33	290			170	1122	-1.0	-1.6	-1.9			0.2	
WC-WCB4B/12	1	Midflowpath	Wallal	Na-Ca-Mg-Cl-HCO3	23059714		WorleyParsons2013		36.3-95.71	36.3	95.71	66.005	154442	7766710	3.3			53	216	143	216		6	21	99	27.1		12	577	-0.4	-2.7	-0.9			1.5	
WCB08C	1	Midflowpath	Wallal	Na-Cl-SO4	23022646	3/12/2008	AnstoReport1	WCB08	81-90	81	90	85.5	163700	7776416	-2.0	6.3	1.6	61	126	380	150	0.022	11	31	230	<0.01	17	160	1042	-0.5	-1.6	-0.9	-0.1	0.3	0.4	8.8
WCB09E	1	Midflowpath	Wallal	Na-Cl-SO4	23022647	3/12/2008	AnstoReport1	WCB09	129.5-142	129.5	142	135.75	163672	7783918	-2.0	6.2	1.0	64	46	450	55	0.007	10	32	210	<0.01	14	77	913	-0.9	-1.9	-1.6	-0.2	0.2	0.1	3.9
Pardoo-Chower	1	Midflowpath	Wallal	Na-Cl-HCO3-SO4		7/06/2012	AnstoReport3		133-151.7	133	151.7	142.35	169961	7780031	0.2	6.5	0.9	32	129	190	154	0.088	9	18	154	<0.05	17	99	675	-0.7	-2.0	-1.2	-0.1	0.3	0.8	9.0
Myadee Spring	1	Midflowpath	Spring	Na-Ca-Cl		1973-1975	GSWALeech1979						162564	7776789	6.4	7.0		67	110	389	134		12	34	220	<1	16	135	1007	-0.7	-1.6	-1.4	0.0	0.5	0.3	8.4
WCB07A	1	Midflowpath	Wallal	Na-Ca-HCO3-Cl	20070734	1973-1975	GSWALeech1979	7A	91.7-115.7	91.7	115.7	103.7	163872	7768911	-0.4	7.5		23	135	68	165		4	9	75	16.0	56	18	434	-0.9	-2.7	-2.0	0.6	1.0	2.4	2.9
WCB08A	1	Midflowpath	Wallal	Na-Cl-SO4	20070724	1973-1975	GSWALeech1979	8A	138.1-150.1	138.1	150.1	144.1	163805	7776214	-0.2	7.6		57	93	394	113		11	32	246	<1	21	170	1044	-0.8	-1.6	-1.7	0.2	0.6	0.3	5.4
WCB08B	1	Midflowpath	Wallal	Na-Cl-SO4	20070725	1973-1975	GSWALeech1979	8B	82.7-100.7	82.7	100.7	91.7	163838	7776216	5.0	7.2		57	110	364	134		12	31	237	<1	19	168	1022	-0.8	-1.6	-1.5	0.1	0.6	0.4	7.1
WC-WCB1B/12	1	Midflowpath	Wallal	Na-Cl-HCO3	23059707		WorleyParsons2013		60.8-151.39	60.8	151.39	106.09																								

HYDROLOGICAL CONCEPTUALISATION OF THE WALYARTA MOUND SPRINGS

StationSampleID	Tectonic Element	Landscape/Flo wpath Position	Aquifer	Water Type	WIN_ID	Date Sampled	Data_Source	Alt/Report Bore Name	Bore Inlet_mbgI	Bore Inlet_TOS_m bgl	Bore Inlet_BOS_m bgl	Bore Inlet_MOS_m bgl	Easting_ MGAS1	Northing_ MGAS1	CBE%	pH lab	Br mg/L	Ca mg/L	Alk mg/L	Cl mg/L	HCO3 mg/L	CO3 mg/L	K mg/L	Mg mg/L	Na mg/L	NO3 mg/L	SiO2 mg/L	SO4 mg/L	TDS mg/L	Si Calcite	Si Gypsum	Si Dolomite	Si Chalcedo ny	Si Quartz	HCO3 / Cl	HCO3 / SiO2
WCB22	2	Coast	Wallal	Na-Cl-HCO3	20073037	3/12/2008	AnstoReport1		278-296	278	296	287	196050	7787136	-1.5	6.4	0.8	30	171	170	206	0.04	8	14	160	0.0	16	92	697	-0.6	-2.0	-1.1	-0.1	0.3	1.2	12.9
WCB22C	2	Coast	Wallal	Na-Cl-HCO3-SO4	23022648	8/10/2014	GCS_GWMonitoring2015		138-150	138	150	144	196050	7787136	-3.8			27		170	185		11	12	150	0.5		98	654	-0.9	-2.0	-1.8			1.1	
WCB22B	2	Coast	Broome	Na-Ca-Cl-HCO3		1973-1975	GSWALeech1979	22B	49.0 - 55.0	49	55	52	196020	7787141	-1.0	7.6		38	138	106	168		2	14	81	19.0	54	27	509	-0.2	-2.5	-0.5	0.6	1.0	1.6	3.1
WCB22C	2	Coast	Wallal	Na-Cl-SO4-HCO3		18/03/2017	WCBSampling		138.5 - 150.5	138.5	150.5	145	196050	7787136	3.3	7.4	0.6	31	121	189	121		10	14	144	<0.01	16	101	627	-0.9	-2.0	-1.9	0.0	0.5	0.6	7.4
CooragooraPB1	2	Coast	Wallal	Na-HCO3		7/06/2012	AnstoReport3		202-277	202	277	240	212736	7790385	1.1	6.6	0.4	18	126	85	152	0.08	7	9	96	<0.05	15	44	425	-0.9	-2.5	-1.7	-0.2	0.2	1.8	10.5
WCB25X	2	Coast	Wallal	Na-Cl-HCO3	23047501	6/06/2012	208997		318-330	318	330	324	208997	7788943	-4.8	6.8	0.4	14	117	87	141	0.07	6	7	97	<0.05	14	41	408	-1.0	-2.6	-1.9	-0.2	0.2	1.6	9.9
WCB25Y	2	Coast	Wallal	Na-HCO3-Cl	23047502	6/06/2012	208997		256-268	256	268	262	208999	7788938	-1.0	7.0	0.3	13	125	62	151	0.08	6	5	87	<0.05	14	31	369	-1.0	-2.7	-2.0	-0.2	0.2	2.4	10.5
WCB25Z	2	Coast	Broome	Na-Ca-Cl-HCO3		6/06/2012	AnstoReport3		46.4 - 55.4	46.4	55.4	51	208988	7788930	-1.5	7.0	1.1	81	146	270	173	0.10	9	25	130	27.0	70	69	855	-0.3	-1.8	-0.6	0.5	0.9	0.6	2.5
WadesBore	2	Coast	Wallal	Na-Cl-SO4-HCO3	23060006	9/10/2014	GCS_GWMonitoring2015		120-150	120	150	135	207631	7790007	-3.6			38	115	240	140		14	19	160	0.5		120	732	-0.9	-1.8	-1.8			0.6	
WCB25C	2	Coast	Wallal	Na-HCO3-Cl	20073025	1973-1975	GSWALeech1979	25C	286-310	286	310	298	208995	7788968	-0.9	7.5		11	117	72	143		5	6	91	<1	16	36	380	-1.3	-2.7	-2.6	0.0	0.5	2.0	8.9
WCB25D	2	Coast	Broome	Na-Ca-Cl-HCO3		1973-1975	GSWALeech1979	25D	30.9 - 36.9	30.9	36.9	34	209001	7788964	9.1	7.6		89	195	261	238		6	20	151	35.0	82	46	928	0.3	-2.0	0.2	0.7	1.2	0.9	2.9
WCS01A	2	Coast	Wallal	Na-Cl-SO4		20/03/2017	WCBSampling		305.4-317.4	305.4	317.4	311	218618	7798430	2.7	7.6	0.9	45	92	308	92		12	20	195	0.0	15	137	825	-0.9	-1.7	-1.9	0.0	0.5	0.3	6.0
WCS01B	2	Coast	Broome	Na-Cl		20/03/2017	WCBSampling		29-35	29	35	32	218605	7798437	4.8	7.8	24.8	189	278	9670	278		252	479	5200	<0.01	26	1510	17629	-0.3	-0.9	0.1	0.3	0.7	0.0	10.6
WCS04A	2	Coast	Wallal	Na-Cl-HCO3		15/11/2015	WCBSampling		278-290	278	290	284	226151	7792448	2.7		0.5	19	110	120	133		11	9	120	0.0		59	471	-1.1	-2.3	-2.3			1.1	
WCS04A_R	2	Coast	Wallal	Na-Cl-HCO3		22/03/2017	WCBSampling		278-290	278	290	284	226151	7792448	7.6	7.6	0.4	20	107	121	107		8	10	139	<0.01	16	66	487	-1.1	-2.3	-2.3	0.0	0.5	0.9	6.9
WCB20Y	2	Midflowpath	Wallal	Na-Ca-HCO3-Cl	23047450	24/05/2013	196461		192-198	192	198	195	196461	7771429	-0.4	6.8	0.3	24	127	66	153	0.08	5	9	65	20.0	50	13	406	-0.8	-2.9	-1.5	0.4	0.8	2.3	3.1
WCB21Y	2	Midflowpath	Wallal	Na-Cl-HCO3	23046244	22/05/2013	211-223		211	223	217	217	196141	7778783	-5.7	6.4	0.3	18	102	73	123	0.06	4	8	74	12.0	42	27	381	-1.0	-2.7	-1.8	0.3	0.7	1.7	2.9
WCB20Z	2	Midflowpath	Broome	Na-HCO3-Cl		22/05/2012	AnstoReport3		52 - 58	52	58	55	196401	7771404	-0.8	6.9	0.3	19	236	91	285	0.16	4	6	142	12.0	57	17	632	-0.6	-2.9	-1.4	0.4	0.9	3.1	5.0
WCB21Z	2	Midflowpath	Broome	Na-Ca-HCO3-Cl		22/05/2012	AnstoReport3		35 - 41	35	41	38	196136	7778782	-0.5	7.0	0.4	36	147	86	176	0.09	5	14	68	24.0	62	14	486	-0.5	-2.7	-1.1	0.5	0.9	2.0	2.8
WCB20D	2	Midflowpath	Wallal	Na-Ca-HCO3-Cl	20073006	1973-1975	GSWALeech1979	20D	167-184	167	184	176	196448	7771310	-0.5	7.9		22	120	57	146		5	10	58	22.0	48	10	378	-1.0	-3.0	-2.0	0.5	1.0	2.6	3.0
WCB21A	2	Midflowpath	Wallal	Na-HCO3-Cl	20072997	1973-1975	GSWALeech1979	21A	200-224	200	224	212	196124	7778777	-0.8	7.3		16	108	72	131		5	8	79	12.0	41	31	395	-1.2	-2.6	-2.4	0.4	0.9	1.8	3.2
WCB21B	2	Midflowpath	Broome	Na-HCO3-Cl		1973-1975	GSWALeech1979	21B	30.0 - 39.0	30	39	35	196137	7778798	-1.0	7.8		10	133	69	162		5	5	102	<1	17	42	412	-0.2	-2.6	-0.5	0.6	1.0	2.3	9.5
WCB22A	2	Midflowpath	Wallal	Na-Ca-HCO3-Cl	20073037	1973-1975	GSWALeech1979	22A	278-296	278	296	287	196020	7787141	-1.2	7.8		34	153	81	186		2	14	73	20.0	58	20	488	-1.3	-2.7	-2.6	0.1	0.5	2.3	3.2
WCB23A	2	Midflowpath	Wallal	Na-Ca-Mg-HCO3-Cl	20072999	1973-1975	GSWALeech1979	23A	97-115	97	115	106	208399	7767996	-0.9	7.3		28	112	55	137		5	11	43	23.0	54	7	363	-0.9	-3.0	-1.9	0.6	1.0	2.5	2.5
WCB23B	2	Midflowpath	Wallal	Na-Ca-HCO3-Cl	20073000	25/05/2013	AnstoReport3		97-114.5	97	114.5	106	208484	7768015	2.7	6.4	0.2	27	108	54	130	0.07	4	10	46	<0.01	54	20	346	-0.8	-2.6	-1.5	0.4	0.8	2.4	2.4
WCB24Y	2	Midflowpath	Wallal	Na-HCO3-Cl	23046614	21/05/2013	208956		198-210	198	210	204	208956	7778334	-5.6	6.5	0.2	14	102	53	123	0.06	3	6	63	4.7	29	20	316	-1.0	-2.9	-2.0	0.1	0.5	2.3	4.2
WCB24Z	2	Midflowpath	Broome	Na-Ca-Cl-HCO3		21/05/2012	AnstoReport3		39.65 - 45.8	39.65	45.8	43	208946	7778341	-0.8	6.5	0.4	42	137	120	163	0.09	5	14	83	32.0	78	25	562	-0.5	-2.4	-1.1	0.6	1.0	1.4	2.1
WCB24A	2	Midflowpath	Wallal	Na-HCO3-Cl	20072992	1973-1975	GSWALeech1979	24A	170-179	170	179	175	208914	7778339	-1.2	7.8		13	105	49	128		4	5	65	1.0	25	24	314	-1.3	-2.8	-2.7	0.2	0.7	2.6	5.1
WCB24B	2	Midflowpath	Broome	Na-Ca-Cl-HCO3		1973-1975	GSWALeech1979	24B	34.0 - 40.0	34	40	37	208917	7778340	-0.3	7.5		49	133	127	162		5	11	88	37.0	49	22	550	-0.1	-2.5	-0.5	0.5	1.0	1.3	3.3
WC-WCB5B/12	2	Midflowpath	Wallal	Na-HCO3-Cl	23059716		WorleyParsons2013		109.4-249.4	109.4	249.4	179	208904	7778369	6.9			16	102	59	102		5	6	74	5.0	30	297	-1.2	-2.6	-2.5			1.7		
PB1	2	Upland	Wallal	Na-Mg-Cl-HCO3	23027497	2/12/2008	AnstoReport1		108-117	108	117	113	207921	7752149	2.1	6.5	0.5	21	83	110	100	0.02	5	14	70	5.7	61	15	402	-1.0	-2.9	-1.7	0.5	0.9	0.9	1.6
PB3	2	Upland	Wallal	Na-Ca-Mg-Cl-HCO3	23027499	2/12/2008	AnstoReport2		107.85-117	107.85	117	112	207273	7751532	7.2	6.2	0.2	15	52	60	63	0.01	3	9	40	1.7	58	<5	250	-1.3	-3.7	-2.4	0.4	0.8	1.1	1.1
PB3_R	2	Upland	Wallal	Na-Ca-Mg-Cl-HCO3	23027507	19/09/2000	BHPShayGapAssessment1998-99		107.85-117	107.85	117	112	207407	7751690	-1.8			14	45	75			3	8	32	12.0	10	199	-1.4	-3.1	-2.9			1.7		
PB4_R	2	Upland	Wallal	Na-Ca-Mg-Cl-HCO3	23030336	6/07/1998	BHPShayGapAssessment1998-99		94-97	94	97	96	207724	7752846	0.4	7.3		29		130	140		6	17	77		16	415	-0.9	-2.7	-1.8			1.1		
YB1	2	Upland	Wallal	Na-Mg-Cl-HCO3	23027422	26																														



HYDROLOGICAL CONCEPTUALISATION OF THE WALYARTA MOUND SPRINGS

StationSampleID	Tectonic Element	Landscape/Flow path Position	Aquifer	Water Type	WIN_ID	Date Sampled	Data_Source	Alt/Report Bore Name	Bore Inlet_EOH_mbgli	Easting_MGAS1	Northing_MGAS1	CBE %	pH lab	Br mg/L	Ca mg/L	Alk mg/L	Cl mg/L	Ca/Cl	HCO3 mg/L	CO3 mg/L	K mg/L	Mg mg/L	Na mg/L	NO3 mg/L	SiO2 mg/L	SO4 mg/L	SO4/Ca	TDS mg/L	SI Calcite	SI Gypsum	SI Dolomite	SI Chalcedony	SI Quartz	HCO3 / Cl	HCO3 / SiO2	
Boulder bore solar	4	TidalFlatMargin	Surficial-Broome	Na-Ca-Cl-HCO3			DPIRD		?	307861	7812088	8.8	6.9	0.2	18	59	57	0.32	72		3	7	48	5.3	73	11.1	0.6	501	-1.32	-2.99	-2.68	0.6	1.0	1.3	1.0	
Wonton bore new	4	TidalFlatMargin	Surficial-Broome	Na-Ca-Cl-HCO3			DPIRD		?	304968	7814555	6.1	7.2	0.4	41	126	92	0.45	154		4	11	71	6.8	92	13.8	0.3	747	-0.36	-2.64	-0.86	0.7	1.1	1.7	1.7	
Tank bore	4	TidalFlatMargin	Surficial-Broome	Na-Ca-Cl-HCO3			DPIRD		?	298876	7814288	-3.2	7.2	0.4	50	165	133	0.38	201		4	14	73	7.3	94	15.3	0.3	860	-0.18	-2.55	-0.50	0.7	1.1	1.5	2.1	
Coolgardie well	4	TidalFlatMargin	Surficial-Broome	Na-Mg-Ca-Cl-HCO3			DPIRD		2.7	314060	7811219	0.2	7.9	0.6	36	118	172	0.21	144		9	23	103	2.7	94	54	1.5	866	0.17	-2.18	0.54	0.7	1.1	0.8	1.5	
Moojan bore	4	TidalFlatMargin	Surficial-Broome	Na-Ca-HCO3-Cl			DPIRD		6.1	269122	7812147	-2.0	7.5	0.6	51	276	178	0.28	337		52	23	129	9.4	90	60	1.2	1139	0.27	-2.04	0.60	0.7	1.1	1.9	3.7	
Moogee bore	4	TidalFlatMargin	Surficial-Broome	Na-Ca-Cl-HCO3			DPIRD		?15.24	280425	7809480	2.7	6.7	0.6	44	113	186	0.24	138		4	14	114	7.1	88	21.6	0.5	859	-0.86	-2.46	-1.80	0.6	1.0	0.7	1.6	
House bore west	4	TidalFlatMargin	Surficial-Broome	Na-Ca-Cl-HCO3			DPIRD		?12.19	274267	7814855	-3.3	7.3	0.5	63	238	216	0.29	290		5	21	130	4.6	83	21	0.3	1064	0.15	-2.39	0.25	0.6	1.0	1.3	3.5	
Gravel Pit bore 1 (north)	4	TidalFlatMargin	Surficial-Broome	Na-Ca-Cl-HCO3			DPIRD		?	297419	7814550	-5.4	7.2	0.6	62	150	223	0.28	183		5	19	95	6.3	79	29.4	0.5	910	-0.19	-2.23	-0.52	0.6	1.1	0.8	2.3	
Dellas bore	4	TidalFlatMargin	Surficial-Broome	Na-Ca-Cl-HCO3			DPIRD		11.58	326488	7843452	0.8	6.9	0.7	54	136	226	0.24	166		11	23	113	5.2	88	25.8	0.5	950	-0.51	-2.35	-0.97	0.6	1.0	0.7	1.9	
Garden bore solar	4	TidalFlatMargin	Surficial-Broome	Na-Cl-HCO3			DPIRD		?15.24	286106	7813958	0.7	7.3	0.9	43	227	234	0.18	277		9	24	178	6.7	88	36	0.8	1123	-0.11	-2.33	-0.08	0.7	1.1	1.2	3.2	
House garden well	4	TidalFlatMargin	Surficial-Broome	Na-Cl-HCO3			DPIRD		?10.67	274031	7815387	-1.5	7.9	1.1	62	249	381	0.16	304		21	29	232	6.6	81	39	0.6	1361	0.65	-2.20	1.33	0.7	1.1	0.8	3.7	
Glugs bore	4	TidalFlatMargin	Surficial-Broome	Na-Cl-HCO3			DPIRD		?	276353	7814681	-4.3	7.1	1.4	51	201	513	0.10	245		15	35	275	6.1	79	36	0.7	1457	-0.24	-2.34	-0.22	0.6	1.0	0.5	3.1	
Nalgi well	4	TidalFlatMargin	Surficial-Broome	Na-Cl-HCO3			DPIRD		5.5	270687	7815001	-3.2	7.3	1.6	49	238	567	0.09	290		18	35	342	8.1	73	60	1.2	1603	-0.05	-2.16	0.18	0.6	1.0	0.5	4.0	
Widjubb Bore 2	4	TidalFlatMargin	Surficial-Broome	Na-Mg-Cl			DPIRD		4.4	324848	7841098	1.5	7.0	1.7	116	139	847	0.14	170		50	89	449	4.1	86	300	2.6	2069	-0.34	-1.27	-0.38	0.6	1.0	0.2	2.0	
MRD Sandfire #2	4	TidalFlatMargin	Wallal	Na-Cl			DPIRD		?	316016	7821782	-5.8	6.6	120.0	958	204	44900	0.02	249		1360	1870	23800	0.2	49	7500	7.8	73454	-0.14	-0.03	0.49	0.6	1.0	0.0	5.1	
MRD Anna Plains #3	4	Midflowpath	Surficial-Broome	Na-Ca-Mg-Cl-HCO3			DPIRD		?	333486	7841861	8.3	6.5	0.3	23	75	69	0.33	92		6	10	49	4.8	68	6.3	0.3	527	-1.49	-3.17	-2.91	0.5	0.9	1.3	1.3	
Joseph bore	4	Midflowpath	Surficial-Broome	Na-Ca-HCO3-Cl			DPIRD		?	328565	7838025	8.3	7.0	0.3	38	122	73	0.52	149		6	12	58	7.2	92	9.9	0.3	711	-0.57	-2.80	-1.23	0.7	1.1	2.0	1.6	
Teds bore	4	Midflowpath	Surficial-Broome	Na-Ca-Cl-HCO3			DPIRD		?	271948	7807904	4.3	6.6	0.3	25	74	76	0.33	90		3	8	50	5.0	73	8.1	0.3	549	-1.34	-3.01	-2.77	0.5	0.9	1.2	1.2	
Sandfire roadhouse bounda	4	Midflowpath	Surficial-Broome	Na-Ca-HCO3-Cl			DPIRD		?	299959	7812886	7.5	7.0	0.3	51	125	87	0.58	153		3	8	64	7.0	86	11.1	0.2	715	-0.49	-2.64	-1.36	0.6	1.0	1.8	1.8	
MRD Anna Plains #4	4	Midflowpath	Surficial-Broome	Na-Ca-Mg-Cl-HCO3			DPIRD		?	337979	7846074	5.3	6.9	0.3	26	91	89	0.29	111		8	13	58	4.2	73	13.2	0.5	601	-0.99	-2.83	-1.83	0.5	1.0	1.2	1.5	
Corbetts bore new	4	Midflowpath	Surficial-Broome	Na-Ca-Cl-HCO3			DPIRD		27.43	297883	7808650	2.7	6.7	0.3	43	115	102	0.42	140		4	9	64	7.8	75	11.1	0.3	669	-0.85	-2.71	-1.95	0.6	1.0	1.4	1.9	
Curly Bore	4	Midflowpath	Surficial-Broome	Na-Ca-Mg-Cl-HCO3			DPIRD		?	336351	7852499	5.7	6.8	0.4	43	121	108	0.40	148		9	15	65	6.1	81	13.5	0.3	719	-0.78	-2.65	-1.58	0.6	1.0	1.4	1.8	
MANDORA Bakers bore	4	Midflowpath	Surficial-Broome	Na-Ca-Cl-HCO3			DPIRD		?21.34	283328	7807074	8.5	6.9	0.4	45	123	112	0.40	150		5	13	82	14.0	90	13.5	0.3	781	-0.67	-2.63	-1.47	0.7	1.1	1.3	1.7	
Roscoe bore	4	Midflowpath	Surficial-Broome	Na-Ca-Mg-Cl-HCO3			DPIRD		?	322497	7821412	5.2	7.0	0.4	47	131	128	0.37	160		13	18	76	6.8	66	22.5	0.5	714	-0.52	-2.41	-1.04	0.5	0.9	1.2	2.4	
MRD Gravel pit bore	4	Midflowpath	Surficial-Broome	Na-Ca-Cl-HCO3			DPIRD		?	294938	7811468	-2.0	6.9	0.5	57	178	171	0.33	217		5	15	104	7.9	94	23.1	0.4	954	-0.43	-2.35	-1.03	0.7	1.1	1.3	2.3	
Sampson well	4	Midflowpath	Surficial-Broome	Na-Ca-Cl-HCO3			DPIRD		16.6	274425	7811222	-1.4	7.4	0.6	67	188	216	0.31	229		3	18	115	9.1	94	15	0.2	1035	0.11	-2.49	0.06	0.7	1.1	1.1	2.4	
Old Tafts bore	4	Midflowpath	Surficial-Broome	Na-Ca-Cl-HCO3			DPIRD		?	291191	7809179	-2.3	6.9	0.9	73	161	300	0.24	196		6	23	142	10.0	90	36	0.5	1111	-0.38	-1.82	-0.43	0.6	1.0	0.7	2.2	
Woolenappa bore	4	Midflowpath	Surficial-Broome	Na-Ca-Cl-HCO3			DPIRD		15.24	294713	7812109	2.6	7.2	1.4	80	347	362	0.22	423		9	30	286	6.7	105	45	0.6	1618	0.21	-2.07	0.40	0.7	1.1	1.2	4.0	
Friday bore	4	Midflowpath	Surficial-Broome	Na-Ca-Mg-Cl			DPIRD		?	326308	7819739	4.6	7.1	1.8	125	195	649	0.19	238		72	71	335	21.0	81	183	1.5	1839	-0.01	-1.40	0.14	0.6	1.0	0.4	2.9	
MRD Anna Plains #1	4	Midflowpath	Wallal	Na-Cl			DPIRD	KP3	?	320979	7826966	11.5	7.1	2.4	55	127	943	0.06	155		58	69	817	4.7	66	330	6.0	2370	-0.55	-1.56	-0.59	0.5	0.9	0.2	2.3	
Lyngetts well	4	Midflowpath	Surficial-Broome	Na-Cl			DPIRD		5.4	338919	7820329	4.7	7.3	3.8	178	244	1240	0.14	298		100	95	787	31.0	90	420	2.4	3092	0.33	-1.04	0.77	0.7	1.1	0.2	3.3	
Friday-Well	4	Midflowpath	Surficial-Broome	Na-Ca-Cl		31/08/2015	DBCA		?	326312	7819734	-2.7	7.9	1.6	115	187	696	0.17	227		<1	66	63	316	21.0	77	200	1.7	1783	0.31	-1.39	0.77	0.6	1.0	0.3	2.9
Tafts new bore	4	Midflowpath	Surficial-Broome	Na-Ca-Cl-HCO3			DPIRD		27.43	290944	7806391	1.6	6.8	0.5	37	81	153	0.24	99		4	12	82	10.0	81	15.6	0.4	722	-1.02	-2.63	-2.12	0.6	1.0	0.6	1.2	
MRD artesian bore	4	Midflowpath	Wallal	Na-Cl-SO4			DPIRD	Artesian Bore; KP4	300 - 310	292684	7810156	-1.2	6.1	1.0	28	58	306	0.09	71		8	16	201		16	126	4.5	694	-2.00	-1.96	-3.80	-0.1	0.3	0.2	4.5	
Dingo Spring	4	Midflowpath	Spring	Na-Cl		24/11/2016	DBCA		?	356553	7811878	0.8	7.0	1.9	108	61	1270	0.09	100		48	57	830	1.4	43	430	4.0	2889	-0.12	-1.19	-0.10	0.3	0.7	0.1	2.3	
Friday well	4	Midflowpath	Surficial-Broome	Na-Cl-HCO3		1/10/1999	Storeyetal2011		?	326023	7819514	-0.2	7.1		105	333	600	0.18	521		82	61	384	9.7	66	172	1.6	2519	0.14	-1.50	0.48	0.5	0.9	7.9	7.9	
Lyngett bore	4	Midflowpath	Surficial-Broome	Na-HCO3-Cl		1/10/1999	Storeyetal2011		5.4	338919	7820329	-0.4	7.2		74	355	570	0.13	507		61	40	463	16.0	75	206	2.8	2012	0.10	-1.54	0.32	0.6	1.0	4.1	4.1	
Bobs bore	4	Upland	Surficial-Broome	Na-Cl			DPIRD		?	341482	7827489	1.4	7.1	0.8	62	173	246	0.25	211		10	30	127	9.3	71	30	0.5	979	-0.21	-2.26	-0.31	0.5	0.9	0.9	3.0	
Walnut bore	4	Upland	Surficial-Broome	Na-Cl-HCO3			DPIRD		16.46	353808	7849436	0.2	7.5	0.8	47	259	302	0.16	316		24	22	239	5.1	98	66	1.4	1350	0.19	-2.07	0.47	0.7	1.1	1.0	3.2	
Camel bore	4	Upland	Surficial-Broome	Na-Mg-Cl			DPIRD		?	331812	7827801	-0.2	7.0	0.8	47	122	353	0.13	149		18	38	189	6.0	62	84	1.8	1048	-0.58	-1.98	-0.84	0.5	0.9	0.4	2.4	
Fern-Peat	4	Palaeovalley	Spring	Na-Cl		3/09/2015	DBCA		?	331614	7813532	0.5	7.1	3.5	177	152	2920	0.06	186		<1	81	99	1840	0.8	34	710	4.0	6052	-1.58	-0.96	-3.05	0.3	0.8	0.1	5.5
Fern-tail	4	Palaeovalley	Spring	Na-Cl		3/09/2015	DBCA		?	331572																										



## Appendix 8 Hydrogeochemistry – Correlation Matrices

HYDROLOGICAL CONCEPTUALISATION OF THE WALYARTA MOUND SPRINGS

Color map of correlations (Sheet1 in IC\_ICPmetalssummaryANSTO2013\_Wallal)

Variable	EC	T	Eh	pH	Meas.Alk	DO	Na	Ca	Mg	K	Cl	SO4	Rb	Sr	Br	F	Si	Mn	a18O	a2H	d13C_TDI C	d13C_DO C	87Sr/86Sr	14C	DIC	CBE	La	Ce	Nd	Dy	Y	Ho	Er
EC	1.000	-0.223	0.064	-0.475	-0.663	-0.284	0.993	0.935	0.958	0.982	0.997	0.981	0.979	0.987	0.957	-0.604	-0.428	0.040	0.456	0.368	-0.091	-0.163	0.407	-0.634	-0.493	-0.314	-0.197	-0.078	-0.079	-0.027	0.123	-0.043	-0.041
T	-0.223	1.000	-0.409	0.439	0.332	-0.586	-0.145	-0.434	-0.417	-0.199	-0.267	-0.078	-0.123	-0.295	-0.221	0.348	-0.552	0.133	0.071	0.183	0.108	0.243	0.383	-0.423	-0.031	-0.178	0.259	0.399	0.262	0.214	0.169	0.211	0.210
Eh	0.064	-0.409	1.000	-0.595	-0.515	0.705	-0.019	0.256	0.260	-0.030	0.103	-0.056	-0.088	0.166	0.073	-0.481	0.651	-0.063	-0.207	-0.238	0.011	-0.189	-0.461	0.526	-0.031	0.526	-0.263	-0.545	-0.444	-0.406	-0.400	-0.406	-0.398
pH	-0.475	0.439	-0.595	1.000	0.655	-0.056	-0.412	-0.578	-0.579	-0.380	-0.497	-0.426	-0.361	-0.527	-0.462	0.513	-0.194	-0.183	-0.248	-0.111	0.140	0.258	0.197	0.031	-0.144	0.094	0.222	0.367	0.310	0.254	0.179	0.255	0.253
Meas.Alk	-0.663	0.332	-0.515	0.655	1.000	-0.148	-0.621	-0.725	-0.729	-0.597	-0.708	-0.573	-0.608	-0.737	-0.515	0.590	-0.069	-0.043	0.081	0.187	0.518	0.378	0.114	0.125	0.639	-0.219	0.311	0.421	0.206	0.119	0.003	0.123	0.123
DO	-0.284	-0.586	0.705	-0.056	-0.148	1.000	-0.360	-0.050	-0.069	-0.331	-0.239	-0.438	-0.394	-0.187	-0.280	-0.148	0.841	-0.209	-0.452	-0.530	0.005	-0.215	-0.634	0.818	-0.074	0.703	-0.258	-0.507	-0.330	-0.297	-0.339	-0.288	-0.284
Na	0.993	-0.145	-0.019	-0.412	-0.621	-0.360	1.000	0.889	0.918	0.982	0.986	0.990	0.992	0.965	0.949	-0.561	-0.525	0.031	0.485	0.406	-0.055	-0.131	0.499	-0.704	-0.504	-0.381	-0.130	-0.002	-0.020	0.024	0.174	0.008	0.010
Ca	0.935	-0.434	0.256	-0.578	-0.725	-0.050	0.889	1.000	0.990	0.902	0.948	0.866	0.866	0.972	0.884	-0.703	-0.104	0.009	0.299	0.183	-0.216	-0.207	0.093	-0.375	-0.449	-0.074	-0.404	-0.312	-0.261	-0.193	-0.051	-0.206	-0.202
Mg	0.958	-0.417	0.260	-0.579	-0.729	-0.069	0.918	0.990	1.000	0.933	0.967	0.898	0.895	0.982	0.925	-0.702	-0.173	0.014	0.357	0.263	-0.161	-0.214	0.190	-0.426	-0.458	-0.112	-0.315	-0.233	-0.203	-0.141	0.002	-0.156	-0.152
K	0.982	-0.199	-0.030	-0.380	-0.597	-0.331	0.982	0.902	0.933	1.000	0.974	0.978	0.987	0.959	0.949	-0.579	-0.497	-0.019	0.491	0.398	-0.093	-0.154	0.491	-0.699	-0.502	-0.300	-0.129	-0.004	-0.047	-0.011	0.138	-0.028	-0.026
Cl	0.997	-0.267	0.103	-0.497	-0.708	-0.239	0.986	0.948	0.967	0.974	1.000	0.965	0.971	0.994	0.941	-0.622	-0.379	0.030	0.404	0.316	-0.134	-0.180	0.360	-0.588	-0.521	-0.275	-0.221	-0.119	-0.096	-0.039	0.113	-0.055	-0.052
SO4	0.981	-0.078	-0.056	-0.426	-0.573	-0.438	0.990	0.866	0.898	0.978	0.965	1.000	0.985	0.942	0.960	-0.552	-0.576	0.055	0.571	0.488	-0.021	-0.100	0.537	-0.763	-0.430	-0.415	-0.106	0.044	-0.011	0.028	0.172	0.010	0.013
Rb	0.979	-0.123	-0.088	-0.361	-0.608	-0.394	0.992	0.866	0.895	0.987	0.971	0.985	1.000	0.946	0.925	-0.541	-0.566	-0.015	0.488	0.382	-0.096	-0.132	0.528	-0.747	-0.533	-0.365	-0.105	0.021	0.000	0.041	0.191	0.024	0.025
Sr	0.987	-0.295	0.166	-0.527	-0.737	-0.187	0.965	0.972	0.982	0.959	0.994	0.942	0.946	1.000	0.924	-0.661	-0.299	0.032	0.349	0.258	-0.177	-0.207	0.280	-0.526	-0.525	-0.193	-0.279	-0.188	-0.159	-0.101	0.050	-0.116	-0.113
Br	0.957	-0.221	0.073	-0.462	-0.515	-0.280	0.949	0.884	0.925	0.949	0.941	0.960	0.925	0.924	1.000	-0.611	-0.441	0.054	0.623	0.574	0.123	-0.072	0.481	-0.633	-0.323	-0.364	-0.123	0.031	-0.045	-0.008	0.123	-0.027	-0.022
F	-0.604	0.348	-0.481	0.513	0.590	-0.148	-0.561	-0.703	-0.702	-0.579	-0.622	-0.552	-0.541	-0.661	-0.611	1.000	-0.105	0.513	-0.172	-0.085	-0.094	-0.168	-0.040	0.109	0.260	-0.234	0.099	0.171	0.147	0.122	0.035	0.140	0.125
Si	-0.428	-0.552	0.651	-0.194	-0.069	0.841	-0.525	-0.104	-0.173	-0.497	-0.379	-0.576	-0.566	-0.299	-0.441	-0.105	1.000	-0.110	-0.565	-0.595	-0.184	-0.079	-0.906	0.931	0.195	0.680	-0.419	-0.600	-0.406	-0.365	-0.427	-0.352	-0.349
Mn	0.040	0.133	-0.063	-0.183	-0.043	-0.209	0.031	0.009	0.014	-0.019	0.030	0.055	-0.015	0.032	0.054	0.513	-0.110	1.000	0.114	0.223	-0.257	-0.511	-0.068	-0.067	0.075	-0.260	-0.308	-0.148	-0.189	-0.165	-0.165	-0.152	-0.167
a18O	0.456	0.071	-0.207	-0.248	0.081	-0.452	0.485	0.299	0.357	0.491	0.404	0.571	0.488	0.349	0.623	-0.172	-0.565	0.114	1.000	0.853	0.520	0.166	0.631	-0.667	0.283	-0.568	0.036	0.177	-0.095	-0.108	-0.066	-0.123	-0.121
a2H	0.368	0.183	-0.238	-0.111	0.187	-0.530	0.406	0.183	0.263	0.398	0.316	0.488	0.382	0.258	0.574	-0.085	-0.595	0.223	0.853	1.000	0.563	0.344	0.696	-0.585	0.287	-0.639	0.170	0.407	0.134	0.109	0.130	0.092	0.096
d13C_TDIC	-0.091	0.108	0.011	0.140	0.518	0.005	-0.055	-0.216	-0.161	-0.093	-0.134	-0.021	-0.096	-0.177	0.123	-0.094	-0.184	-0.257	0.520	0.563	1.000	0.467	0.448	-0.071	0.496	-0.357	0.372	0.352	0.107	0.041	-0.003	0.029	0.040
d13C_DOC	-0.163	0.243	-0.189	0.258	0.378	-0.215	-0.131	-0.207	-0.214	-0.154	-0.180	-0.100	-0.132	-0.207	-0.072	-0.168	-0.079	-0.511	0.166	0.344	0.467	1.000	0.176	-0.033	0.293	-0.219	0.086	0.242	0.207	0.202	0.151	0.187	0.200
87Sr/86Sr	0.407	0.383	-0.461	0.197	0.114	-0.634	0.499	0.093	0.190	0.491	0.360	0.537	0.528	0.280	0.481	-0.040	-0.906	-0.068	0.631	0.696	0.448	0.176	1.000	-0.811	-0.124	-0.605	0.508	0.592	0.327	0.261	0.317	0.243	0.245
14C	-0.634	-0.423	0.526	0.031	0.125	0.818	-0.704	-0.375	-0.426	-0.699	-0.588	-0.763	-0.747	-0.526	-0.633	0.109	0.931	-0.067	-0.667	-0.585	-0.071	-0.033	-0.811	1.000	0.234	0.608	-0.216	-0.404	-0.222	-0.206	-0.299	-0.191	-0.189
DIC	-0.493	-0.031	-0.031	-0.144	0.639	-0.074	-0.504	-0.449	-0.458	-0.502	-0.521	-0.430	-0.533	-0.525	-0.323	0.260	0.195	0.075	0.283	0.287	0.496	0.293	-0.124	0.234	1.000	-0.297	0.160	0.121	-0.075	-0.129	-0.220	-0.126	-0.122
CBE	-0.314	-0.178	0.526	0.094	-0.219	0.703	-0.381	-0.074	-0.112	-0.300	-0.275	-0.415	-0.365	-0.193	-0.364	-0.234	0.680	-0.260	-0.568	-0.639	-0.357	-0.219	-0.605	0.608	-0.297	1.000	-0.279	-0.457	-0.337	-0.329	-0.368	-0.323	-0.319
La	-0.197	0.259	-0.263	0.222	0.311	-0.258	-0.130	-0.404	-0.315	-0.129	-0.221	-0.106	-0.105	-0.279	-0.123	0.099	-0.419	-0.308	0.036	0.170	0.372	0.086	0.508	-0.216	0.160	-0.279	1.000	0.875	0.779	0.694	0.668	0.690	0.694
Ce	-0.078	0.399	-0.545	0.367	0.421	-0.507	-0.002	-0.312	-0.233	-0.004	-0.119	0.044	0.021	-0.188	0.031	0.171	-0.600	-0.148	0.177	0.407	0.352	0.242	0.592	-0.404	0.121	-0.457	0.875	1.000	0.896	0.831	0.808	0.824	0.827
Nd	-0.079	0.262	-0.444	0.310	0.206	-0.330	-0.020	-0.261	-0.203	-0.047	-0.096	-0.011	0.000	-0.159	-0.045	0.147	-0.406	-0.189	-0.095	0.134	0.107	0.207	0.327	-0.222	-0.075	-0.337	0.779	0.896	1.000	0.989	0.970	0.988	0.988
Dy	-0.027	0.214	-0.406	0.254	0.119	-0.297	0.024	-0.193	-0.141	-0.011	-0.039	0.028	0.041	-0.101	-0.008	0.122	-0.365	-0.165	-0.108	0.109	0.041	0.202	0.261	-0.206	-0.129	-0.329	0.694	0.831	0.989	1.000	0.987	1.000	1.000
Y	0.123	0.169	-0.400	0.179	0.003	-0.339	0.174	-0.051	0.002	0.138	0.113	0.172	0.191	0.050	0.123	0.035	-0.427	-0.165	-0.066	0.130	-0.003	0.151	0.317	-0.299	-0.220	-0.368	0.668	0.808	0.970	0.987	1.000	0.985	0.985
Ho	-0.043	0.211	-0.406	0.255	0.123	-0.288	0.008	-0.206	-0.156	-0.028	-0.055	0.010	0.024	-0.116	-0.027	0.140	-0.352	-0.152	-0.123	0.092	0.029	0.187	0.243	-0.191	-0.126	-0.323	0.690	0.824	0.988	1.000	0.985	1.000	1.000
Er	-0.041	0.210	-0.398	0.253	0.123	-0.284	0.010	-0.202	-0.152	-0.026	-0.052	0.013	0.025	-0.113	-0.022	0.125	-0.349	-0.167	-0.121	0.096	0.040	0.200	0.245	-0.189	-0.122	-0.319	0.694	0.827	0.988	1.000	0.985	1.000	1.000

HYDROLOGICAL CONCEPTUALISATION OF THE WALYARTA MOUND SPRINGS

Color map of correlations (Sheet1 in IC\_ICPmetalsummaryANSTO2013\_input\_Broome)N=4 (Casewise deletion of missing data)>=

Variable	EC	T	Eh	pH	Meas.Alk	DO	Na	Ca	Mg	K	Cl	SO4	Ba	Rb	Sr	Br	F	NO3	Si	Mn	a18O	a2H	d13C_TDI C	d13C_DO C	87Sr/86Sr	14C	DIC	logPCO2	CBE	La	Ce	Pr	Nd	Sm	Eu	Gd	Tb	Dy	Y	Ho	Er	U
EC	1.000	0.289	0.754	0.078	-0.831	0.397	-0.178	0.952	0.982	0.901	0.820	0.809	-0.717	0.895	0.895	0.838	-0.687	0.797	0.698	-0.859	0.632	-0.046	0.107	0.977	0.905	-0.888	-0.843	-0.380	-0.036	0.661	0.857	0.498	0.836	0.805	0.364	0.553	-0.793	0.142	0.909	-0.682	0.366	-0.865
T	0.289	1.000	0.695	-0.865	-0.659	0.874	-0.681	0.025	0.100	-0.137	-0.165	-0.169	-0.612	0.040	0.154	-0.208	-0.115	0.803	0.838	-0.584	-0.077	-0.686	-0.613	0.201	0.165	0.081	-0.249	0.601	0.630	0.539	-0.221	0.518	0.515	-0.140	0.250	0.382	-0.552	0.096	-0.049	-0.612	0.090	0.142
Eh	0.754	0.695	1.000	-0.247	-0.992	0.892	-0.775	0.520	0.639	0.417	0.242	0.224	-0.989	0.396	0.435	0.278	-0.165	0.934	0.744	-0.982	0.031	-0.689	0.058	0.778	0.809	-0.620	-0.869	-0.152	0.624	0.961	0.333	0.901	0.573	0.221	-0.044	0.190	-0.983	-0.288	0.412	-0.982	-0.131	-0.323
pH	0.078	-0.865	-0.247	1.000	0.216	-0.535	0.328	0.258	0.248	0.407	0.310	0.302	0.134	0.140	0.011	0.398	0.131	-0.463	-0.659	0.121	0.034	0.387	0.901	0.226	0.315	-0.504	-0.257	-0.920	-0.350	-0.045	0.461	-0.039	-0.371	0.259	-0.450	-0.466	0.064	-0.405	0.276	0.132	-0.298	-0.339
Meas Alk	-0.831	-0.659	-0.992	0.216	1.000	-0.836	0.687	-0.623	-0.727	-0.523	-0.364	-0.347	0.971	-0.512	-0.547	-0.394	0.285	-0.952	-0.780	0.995	-0.158	0.590	-0.045	-0.842	-0.850	0.685	0.888	0.180	-0.518	-0.934	-0.443	-0.850	-0.660	-0.345	-0.053	-0.287	0.981	0.196	-0.524	0.959	0.023	0.439
DO	0.397	0.874	0.892	-0.535	-0.836	1.000	-0.931	0.098	0.232	-0.031	-0.187	-0.203	-0.876	-0.003	0.069	-0.169	0.130	0.829	0.681	-0.792	-0.300	-0.904	-0.153	0.411	0.470	-0.209	-0.588	0.183	0.859	0.854	-0.122	0.865	0.342	-0.196	-0.160	0.034	-0.817	-0.355	-0.017	-0.886	-0.298	0.116
Na	-0.178	-0.681	-0.775	0.328	0.687	-0.931	1.000	0.118	-0.039	0.207	0.415	0.434	0.811	0.272	0.229	0.364	-0.463	-0.596	-0.366	0.657	0.597	0.990	-0.112	-0.261	-0.397	0.142	0.548	-0.018	-0.977	-0.837	0.287	-0.912	0.006	0.440	0.508	0.334	0.734	0.660	0.242	0.837	0.627	-0.329
Ca	0.952	0.025	0.520	0.258	-0.623	0.098	0.118	1.000	0.987	0.987	0.952	0.945	-0.486	0.972	0.949	0.964	-0.790	0.590	0.534	-0.667	0.787	0.251	0.162	0.922	0.823	-0.891	-0.716	-0.469	-0.326	0.431	0.969	0.251	0.796	0.939	0.452	0.592	-0.587	0.275	0.992	-0.444	0.499	-0.976
Mg	0.982	0.100	0.639	0.248	-0.727	0.232	-0.039	0.987	1.000	0.965	0.890	0.880	-0.616	0.927	0.905	0.916	-0.700	0.667	0.562	-0.771	0.682	0.099	0.223	0.973	0.902	-0.935	-0.819	-0.507	-0.173	0.570	0.937	0.404	0.773	0.871	0.341	0.510	-0.707	0.142	0.958	-0.579	0.375	-0.931
K	0.901	-0.137	0.417	0.407	-0.523	-0.031	0.207	0.987	0.965	1.000	0.963	0.956	-0.399	0.950	0.907	0.985	-0.748	0.459	0.389	-0.580	0.776	0.341	0.280	0.890	0.804	-0.908	-0.687	-0.579	-0.405	0.359	0.996	0.187	0.696	0.944	0.384	0.506	-0.509	0.232	0.987	-0.359	0.456	-0.986
Cl	0.820	-0.165	0.242	0.310	-0.364	-0.187	0.415	0.952	0.890	0.963	1.000	1.000	-0.195	0.979	0.948	0.993	-0.880	0.370	0.398	-0.412	0.914	0.533	0.085	0.761	0.624	-0.762	-0.479	-0.409	-0.599	0.134	0.971	-0.056	0.748	0.998	0.592	0.667	-0.311	0.476	0.983	-0.149	0.668	-0.994
SO4	0.809	-0.169	0.224	0.302	-0.347	-0.203	0.434	0.945	0.880	0.956	1.000	1.000	-0.175	0.977	0.947	0.990	-0.889	0.359	0.395	-0.393	0.923	0.550	0.069	0.746	0.605	-0.745	-0.458	-0.393	-0.616	0.111	0.965	-0.079	0.749	0.999	0.608	0.678	-0.291	0.496	0.979	-0.128	0.685	-0.991
Ba	-0.717	-0.612	-0.989	0.134	0.971	-0.876	0.811	-0.486	-0.616	-0.399	-0.195	-0.175	1.000	-0.333	-0.356	-0.247	0.056	-0.870	-0.635	0.971	0.063	0.723	-0.197	-0.773	-0.835	0.651	0.905	0.264	-0.668	-0.991	-0.319	-0.951	-0.462	-0.165	0.184	-0.052	0.992	0.421	-0.371	0.999	0.260	0.286
Rb	0.895	0.040	0.396	0.140	-0.512	-0.003	0.272	0.972	0.927	0.950	0.979	0.977	-0.333	1.000	0.992	0.964	-0.912	0.545	0.576	-0.545	0.906	0.392	-0.033	0.819	0.674	-0.762	-0.546	-0.297	-0.470	0.256	0.940	0.059	0.863	0.981	0.644	0.749	-0.437	0.493	0.987	-0.286	0.688	-0.979
Sr	0.895	0.154	0.435	0.011	-0.547	0.069	0.229	0.949	0.905	0.907	0.948	0.947	-0.356	0.992	1.000	0.921	-0.936	0.613	0.668	-0.568	0.909	0.343	-0.149	0.799	0.642	-0.705	-0.520	-0.182	-0.427	0.267	0.890	0.068	0.920	0.957	0.707	0.816	-0.453	0.549	0.961	-0.308	0.732	-0.944
Br	0.838	-0.208	0.278	0.398	-0.394	-0.169	0.364	0.964	0.916	0.985	0.993	0.990	-0.247	0.964	0.921	1.000	-0.818	0.363	0.347	-0.450	0.859	0.490	0.201	0.804	0.690	-0.827	-0.553	-0.513	-0.552	0.199	0.993	0.018	0.697	0.982	0.490	0.578	-0.364	0.368	0.987	-0.204	0.574	-0.998
F	-0.687	-0.115	-0.165	0.131	0.285	0.130	-0.463	-0.790	-0.700	-0.748	-0.880	-0.889	0.056	-0.912	-0.936	-0.818	1.000	-0.436	-0.614	0.289	-0.982	-0.542	0.397	-0.538	-0.332	0.428	0.190	-0.072	0.619	0.052	-0.748	0.251	-0.887	-0.910	-0.900	-0.937	0.148	-0.805	-0.840	0.006	-0.924	0.840
NO3	0.797	0.803	0.934	-0.463	-0.952	0.829	-0.596	0.590	0.667	0.459	0.370	0.359	-0.870	0.545	0.613	0.363	-0.436	1.000	0.932	-0.925	0.282	-0.516	-0.257	0.744	0.695	-0.521	-0.719	0.096	0.432	0.798	0.377	0.694	0.799	0.372	0.305	0.514	-0.875	0.066	0.509	-0.851	0.205	-0.420
Si	0.698	0.838	0.744	-0.659	-0.780	0.681	-0.366	0.534	0.562	0.389	0.398	0.395	-0.635	0.576	0.668	0.347	-0.614	0.932	1.000	-0.733	0.455	-0.310	-0.567	0.574	0.456	-0.308	-0.449	0.374	0.221	0.529	0.317	0.401	0.898	0.424	0.600	0.754	-0.642	0.400	0.489	-0.607	0.492	-0.410
Mn	-0.859	-0.584	-0.982	0.121	0.995	-0.792	0.657	-0.667	-0.771	-0.580	-0.412	-0.393	0.971	-0.545	-0.568	-0.450	0.289	-0.925	-0.733	1.000	-0.176	0.551	-0.129	-0.882	-0.896	0.749	0.927	0.272	-0.481	-0.940	-0.504	-0.854	-0.644	-0.388	-0.022	-0.258	0.989	0.228	-0.570	0.958	0.040	0.490
a18O	0.632	-0.077	0.031	0.034	-0.158	-0.300	0.597	0.787	0.682	0.776	0.914	0.923	0.063	0.906	0.909	0.859	-0.982	0.282	0.455	-0.176	1.000	0.677	-0.282	0.499	0.300	-0.443	-0.140	-0.041	-0.743	-0.158	0.791	-0.353	0.791	0.939	0.856	0.868	-0.041	0.791	0.851	0.114	0.911	-0.869
a2H	-0.046	-0.686	-0.689	0.387	0.590	-0.904	0.990	0.251	0.099	0.341	0.533	0.550	0.723	0.392	0.343	0.490	-0.542	-0.516	-0.310	0.551	0.677	1.000	-0.052	-0.124	-0.264	0.003	0.425	-0.113	-0.996	-0.752	0.418	-0.847	0.093	0.554	0.529	0.379	0.634	0.655	0.371	0.754	0.655	-0.455
d13C_TDIC	0.107	-0.613	0.058	0.901	-0.045	-0.153	-0.112	0.162	0.223	0.280	0.085	0.069	-0.197	-0.033	-0.149	0.201	0.397	-0.257	-0.567	-0.129	-0.282	-0.052	1.000	0.304	0.466	-0.548	-0.480	-0.944	0.090	0.306	0.302	0.358	-0.445	0.019	-0.736	-0.683	-0.230	-0.747	0.125	-0.213	-0.632	-0.154
d13C_DOC	0.977	0.201	0.778	0.226	-0.842	0.411	-0.261	0.922	0.973	0.890	0.761	0.746	-0.773	0.819	0.799	0.804	-0.538	0.744	0.574	-0.882	0.499	-0.124	0.304	1.000	0.974	-0.955	-0.928	-0.542	0.053	0.743	0.848	0.605	0.702	0.732	0.163	0.365	-0.845	-0.059	0.865	-0.745	0.177	-0.823
87Sr/86Sr	0.905	0.165	0.809	0.315	-0.850	0.470	-0.397	0.823	0.902	0.804	0.624	0.605	-0.835	0.674	0.642	0.690	-0.332	0.695	0.456	-0.896	0.300	-0.264	0.466	0.974	1.000	-0.961	-0.985	-0.646	0.207	0.832	0.759	0.731	0.535	0.583	-0.065	0.147	-0.893	-0.286	0.749	-0.817	-0.052	-0.703
14C	-0.888	0.081	-0.620	-0.504	0.685	-0.209	0.142	-0.891	-0.935	-0.908	-0.762	-0.745	0.651	-0.762	-0.705	-0.827	0.428	-0.521	-0.308	0.749	-0.443	0.003	-0.548	-0.955	-0.961	1.000	0.905	0.762	0.048	-0.652	-0.886	-0.533	-0.504	-0.720	0.001	-0.174	0.735	0.186	-0.845	0.627	-0.056	0.826
DIC	-0.843	-0.249	-0.869	-0.257	0.888	-0.588	0.548	-0.716	-0.819	-0.687	-0.479	-0.458	0.905	-0.546	-0.520	-0.553	0.190	-0.719	-0.449	0.927	-0.140	0.425	-0.480	-0.928	-0.985	0.905	1.000	0.613	-0.373	-0.912	-0.633	-0.839	-0.455	-0.435	0.187	-0.037	0.943	0.412	-0.625	0.895	0.193	0.569
logPCO2	-0.380	0.601	-0.152	-0.920	0.180	0.183	-0.018	-0.469	-0.507	-0.579	-0.409	-0.393	0.264	-0.297	-0.182	-0.513	-0.072	0.096	0.374	0.272	-0.041	-0.113	-0.944	-0.542	-0.646	0.762	0.613	1.														



Color map of correlations (Sheet1 in IC_ICPmetalsummaryDPIRD2015_input)																																	
Variable	Alkalin	B	Ba	Br	Ca_dis	Ca	Cl_dis	Cr	Cu	ECond	Fe	Hardness	HCO3	K	Mg	Mg_dis	Na	N_Nox_dis	N_total_dis	pH	P_total	S	Si	Sr	TDS_grav	TDSsum	U	V	Zn	Temp	Eh_field	pH_field	Field_ALK
Alkalin	1.000	0.825	-0.217	0.810	0.161	0.294	0.838	-0.550	-0.045	0.872	-0.336	0.703	1.000	0.892	0.862	0.869	0.854	-0.207	-0.325	0.705	0.624	0.715	-0.777	0.555	0.877	0.871	0.881	0.788	0.012	-0.749	0.502	0.710	0.349
B	0.825	1.000	0.238	0.977	0.103	0.276	0.969	-0.022	-0.466	0.974	0.067	0.772	0.825	0.878	0.989	0.986	0.949	-0.021	-0.060	0.222	0.632	0.976	-0.921	0.733	0.973	0.970	0.858	0.938	-0.359	-0.407	0.045	0.302	0.302
Ba	-0.217	0.238	1.000	0.201	0.552	0.590	0.178	0.891	-0.277	0.139	0.966	0.498	-0.217	-0.179	0.222	0.193	0.015	0.769	0.873	-0.774	0.478	0.302	0.040	0.660	0.125	0.137	-0.197	0.357	-0.207	0.442	-0.853	-0.698	0.525
Br	0.810	0.977	0.201	1.000	0.035	0.237	0.997	-0.061	-0.365	0.993	-0.007	0.735	0.810	0.816	0.985	0.989	0.982	0.037	-0.040	0.190	0.543	0.983	-0.939	0.658	0.992	0.992	0.916	0.856	-0.235	-0.290	0.149	0.226	0.307
Ca_dis	0.161	0.103	0.552	0.035	1.000	0.972	0.074	0.203	0.381	0.085	0.618	0.702	0.161	-0.094	0.171	0.143	-0.095	0.699	0.703	-0.059	0.822	-0.009	0.278	0.727	0.077	0.086	-0.180	0.366	0.375	-0.204	-0.341	-0.073	0.912
Ca	0.294	0.276	0.590	0.237	0.972	1.000	0.277	0.193	0.359	0.281	0.596	0.823	0.294	0.016	0.355	0.331	0.105	0.754	0.724	-0.063	0.876	0.184	0.093	0.816	0.273	0.284	0.018	0.482	0.393	-0.176	-0.275	-0.093	0.977
Cl_dis	0.838	0.969	0.178	0.997	0.074	0.277	1.000	-0.109	-0.294	0.997	-0.030	0.759	0.838	0.808	0.988	0.992	0.982	0.061	-0.031	0.230	0.568	0.966	-0.923	0.666	0.997	0.998	0.926	0.850	-0.164	-0.314	0.195	0.251	0.355
Cr	-0.550	-0.022	0.891	-0.061	0.203	0.193	-0.109	1.000	-0.461	-0.155	0.893	0.075	-0.550	-0.361	-0.084	-0.110	-0.220	0.544	0.706	-0.931	0.071	0.092	0.180	0.295	-0.167	-0.160	-0.426	0.057	-0.421	0.647	-0.944	-0.824	0.104
Cu	-0.045	-0.466	-0.277	-0.365	0.381	0.359	-0.294	-0.461	1.000	-0.291	-0.241	-0.012	-0.045	-0.474	-0.329	-0.320	-0.337	0.382	0.219	0.248	0.010	-0.515	0.512	-0.187	-0.289	-0.275	-0.181	-0.445	0.984	0.027	0.489	0.028	0.462
ECond	0.872	0.974	0.139	0.993	0.085	0.281	0.997	-0.155	-0.291	1.000	-0.059	0.767	0.872	0.843	0.992	0.996	0.983	0.019	-0.072	0.291	0.590	0.957	-0.926	0.671	1.000	1.000	0.933	0.868	-0.169	-0.382	0.221	0.317	0.353
Fe	-0.336	0.067	0.966	-0.007	0.618	0.596	-0.030	0.893	-0.241	-0.059	1.000	0.400	-0.336	-0.284	0.041	0.007	-0.193	0.722	0.860	-0.751	0.458	0.100	0.238	0.594	-0.072	-0.063	-0.403	0.257	-0.215	0.382	-0.924	-0.657	0.489
Hardness	0.703	0.772	0.498	0.735	0.702	0.823	0.759	0.075	-0.012	0.767	0.400	1.000	0.703	0.539	0.821	0.805	0.637	0.472	0.422	0.125	0.953	0.692	-0.486	0.963	0.761	0.766	0.534	0.869	0.072	-0.380	-0.117	0.147	0.827
HCO3	1.000	0.825	-0.217	0.810	0.161	0.294	0.838	-0.550	-0.045	0.872	-0.336	0.703	1.000	0.892	0.862	0.869	0.854	-0.207	-0.325	0.705	0.624	0.715	-0.777	0.555	0.877	0.871	0.881	0.788	0.012	-0.749	0.502	0.710	0.349
K	0.892	0.878	-0.179	0.816	-0.094	0.016	0.808	-0.361	-0.474	0.843	-0.284	0.539	0.892	1.000	0.845	0.849	0.862	-0.458	-0.489	0.587	0.476	0.793	-0.886	0.481	0.848	0.834	0.837	0.834	-0.434	-0.723	0.290	0.690	0.015
Mg	0.862	0.989	0.222	0.985	0.171	0.355	0.988	-0.084	-0.329	0.992	0.041	0.821	0.862	0.845	1.000	0.999	0.958	0.059	-0.010	0.256	0.669	0.960	-0.898	0.751	0.991	0.990	0.885	0.921	-0.214	-0.405	0.122	0.303	0.404
Mg_dis	0.869	0.986	0.193	0.989	0.143	0.331	0.992	-0.110	-0.320	0.996	0.007	0.805	0.869	0.849	0.999	1.000	0.968	0.041	-0.035	0.272	0.646	0.960	-0.909	0.726	0.995	0.995	0.902	0.908	-0.204	-0.404	0.155	0.313	0.386
Na	0.854	0.949	0.015	0.982	-0.095	0.105	0.982	-0.220	-0.337	0.983	-0.193	0.637	0.854	0.862	0.958	0.968	1.000	-0.116	-0.213	0.326	0.440	0.949	-0.972	0.530	0.985	0.983	0.972	0.795	-0.216	-0.360	0.309	0.349	0.191
N_Nox_dis	-0.207	-0.021	0.769	0.037	0.699	0.754	0.061	0.544	0.382	0.019	0.722	0.472	-0.207	-0.458	0.059	0.041	-0.116	1.000	0.971	-0.604	0.419	0.033	0.284	0.491	0.007	0.029	-0.210	0.055	0.463	0.509	-0.441	-0.693	0.788
N_total_dis	-0.325	-0.060	0.873	-0.040	0.703	0.724	-0.031	0.706	0.219	-0.072	0.860	0.422	-0.325	-0.489	-0.010	-0.035	-0.213	0.971	1.000	-0.715	0.411	-0.005	0.346	0.505	-0.085	-0.066	-0.347	0.062	0.281	0.534	-0.641	-0.752	0.711
pH	0.705	0.222	-0.774	0.190	-0.059	-0.063	0.230	-0.931	0.248	0.291	-0.751	0.125	0.705	0.587	0.256	0.272	0.326	-0.604	-0.715	1.000	0.183	0.060	-0.297	-0.044	0.302	0.289	0.476	0.226	0.192	-0.879	0.786	0.969	-0.034
P_total	0.624	0.632	0.478	0.543	0.822	0.876	0.568	0.071	0.010	0.590	0.458	0.953	0.624	0.476	0.669	0.646	0.440	0.419	0.411	0.183	1.000	0.505	-0.295	0.954	0.585	0.587	0.331	0.824	0.044	-0.506	-0.207	0.234	0.827
S	0.715	0.976	0.302	0.983	-0.009	0.184	0.966	0.092	-0.515	0.957	0.100	0.692	0.715	0.793	0.960	0.960	0.949	0.033	-0.005	0.060	0.505	1.000	-0.936	0.661	0.955	0.954	0.849	0.861	-0.386	-0.209	-0.004	0.130	0.231
Si	-0.777	-0.921	0.040	-0.939	0.278	0.093	-0.923	0.180	0.512	-0.926	0.238	-0.486	-0.777	-0.886	-0.898	-0.909	-0.972	0.284	0.346	-0.297	-0.295	-0.936	1.000	-0.412	-0.928	-0.923	-0.937	-0.748	0.404	0.338	-0.264	-0.357	0.027
Sr	0.555	0.733	0.660	0.658	0.727	0.816	0.666	0.295	-0.187	0.671	0.594	0.963	0.555	0.481	0.751	0.726	0.530	0.491	0.505	-0.044	0.954	0.661	-0.412	1.000	0.663	0.667	0.376	0.879	-0.118	-0.310	-0.368	0.031	0.771
TDS_grav	0.877	0.973	0.125	0.992	0.077	0.273	0.997	-0.167	-0.289	1.000	-0.072	0.761	0.877	0.848	0.991	0.995	0.985	0.007	-0.085	0.302	0.585	0.955	-0.928	0.663	1.000	1.000	0.937	0.865	-0.169	-0.389	0.232	0.327	0.345
TDSsum	0.871	0.970	0.137	0.992	0.086	0.284	0.998	-0.160	-0.275	1.000	-0.063	0.766	0.871	0.834	0.990	0.995	0.983	0.029	-0.066	0.289	0.587	0.954	-0.923	0.667	1.000	1.000	0.935	0.860	-0.152	-0.372	0.230	0.310	0.359
U	0.881	0.858	-0.197	0.916	-0.180	0.018	0.926	-0.426	-0.181	0.933	-0.403	0.534	0.881	0.837	0.885	0.902	0.972	-0.210	-0.347	0.476	0.331	0.849	-0.937	0.376	0.937	0.935	1.000	0.671	-0.070	-0.408	0.525	0.458	0.132
V	0.788	0.938	0.357	0.856	0.366	0.482	0.850	0.057	-0.445	0.868	0.257	0.869	0.788	0.834	0.921	0.908	0.795	0.055	0.062	0.226	0.824	0.861	-0.748	0.879	0.865	0.860	0.671	1.000	-0.377	-0.535	-0.133	0.342	0.448
Zn	0.012	-0.359	-0.207	-0.235	0.375	0.393	-0.164	-0.421	0.984	-0.169	-0.215	0.072	0.012	-0.434	-0.214	-0.204	-0.216	0.463	0.281	0.192	0.044	-0.386	0.404	-0.118	-0.169	-0.152	-0.070	-0.377	1.000	0.094	0.496	-0.040	0.521
Temp	-0.749	-0.407	0.442	-0.290	-0.204	-0.176	-0.314	0.647	0.027	-0.382	0.382	-0.380	-0.749	-0.723	-0.405	-0.404	-0.360	0.509	0.534	-0.879	-0.506	-0.209	0.338	-0.310	-0.389	-0.372	-0.408	-0.535	0.094	1.000	-0.407	-0.946	-0.119
Eh_field	0.502	0.045	-0.853	0.149	-0.341	-0.275	0.195	-0.944	0.489	0.221	-0.924	-0.117	0.502	0.290	0.122	0.155	0.309	-0.441	-0.641	0.786	-0.207	-0.004	-0.264	-0.368	0.232	0.230	0.525	-0.133	0.496	-0.407	1.000	0.634	-0.129
pH_field	0.710	0.302	-0.698	0.226	-0.073	-0.093	0.251	-0.824	0.028	0.317	-0.657	0.147	0.710	0.690	0.303	0.313	0.349	-0.693	-0.752	0.969	0.234	0.130	-0.357	0.031	0.327	0.							







HYDROLOGICAL CONCEPTUALISATION OF THE WALYARTA MOUND SPRINGS

Color map of correlations (Sheet1 in IC\_ICP\_Springs\_metalsummary2016 input)

Variable	Acidity	Alkalinity	B	Ba	Br	Ca_dis	Ca	Cl_dis	Cr	Cs	Cu	ECond	Hardness	HCO3	K	K_dis	Li	Mg	Mg_dis	Mn	Mo	Na	Na_dis	N_NH3_dis	N_TK_dis	N_total_dis	Ni	pH	P	P_SR_dis	P_total	Rb	S	Se	Si	Si_dis	SiO2_dis	SO4_dis	SO4_S_dis	Sr	TDS_grav	TDSsum	V
Acidity	1.000	0.527	0.583	0.252	0.626	0.588	0.627	0.527	0.670	0.583	0.565	0.547	0.625	0.530	0.525	0.507	0.585	0.655	0.653	0.505	-0.068	0.552	0.541	0.058	0.492	0.502	0.208	-0.648	-0.436	0.220	0.362	0.600	0.480	0.623	0.373	0.394	0.394	0.453	0.487	0.669	0.554	0.552	0.183
Alkalinity	0.527	1.000	0.579	0.915	-0.122	0.056	0.050	-0.180	0.068	-0.085	-0.129	-0.142	0.079	1.000	-0.171	-0.161	-0.105	0.077	0.099	-0.107	-0.089	-0.152	-0.156	-0.176	-0.142	-0.229	-0.104	0.246	0.039	-0.209	-0.139	-0.120	-0.210	0.095	0.883	0.920	0.920	-0.207	-0.185	0.153	-0.116	-0.131	-0.318
B	0.583	0.579	1.000	0.379	0.484	0.733	0.718	0.547	0.730	0.641	0.574	0.584	0.753	0.580	0.592	0.611	0.610	0.751	0.769	0.179	-0.540	0.564	0.570	-0.158	-0.319	-0.307	0.658	-0.114	-0.170	-0.521	-0.336	0.595	0.557	0.607	0.551	0.575	0.575	0.568	0.587	0.780	0.601	0.596	0.455
Ba	0.252	0.915	0.379	1.000	-0.415	-0.228	-0.233	-0.472	-0.186	-0.375	-0.423	-0.436	-0.198	0.913	-0.442	-0.426	-0.401	-0.190	-0.171	-0.375	-0.071	-0.449	-0.452	-0.357	-0.298	-0.399	-0.201	0.446	0.180	-0.380	-0.374	-0.397	-0.488	-0.228	0.933	0.937	0.937	-0.477	-0.465	-0.120	-0.412	-0.428	-0.513
Br	0.626	-0.122	0.484	-0.415	1.000	0.913	0.941	0.966	0.925	0.920	0.972	0.966	0.910	-0.120	0.937	0.917	0.961	0.918	0.898	0.822	-0.419	0.972	0.964	-0.011	0.289	0.343	0.554	-0.675	-0.285	0.085	0.281	0.966	0.938	0.917	-0.265	-0.243	-0.243	0.909	0.922	0.906	0.969	0.960	0.725
Ca_dis	0.588	0.056	0.733	-0.228	0.913	1.000	0.992	0.946	0.976	0.929	0.949	0.965	0.996	0.058	0.963	0.966	0.950	0.984	0.986	0.590	-0.446	0.950	0.958	-0.155	-0.037	0.040	0.790	-0.526	-0.359	-0.202	-0.027	0.964	0.956	0.941	-0.033	0.002	0.002	0.954	0.961	0.981	0.969	0.967	0.854
Ca	0.627	0.050	0.718	-0.233	0.941	0.992	1.000	0.950	0.987	0.930	0.956	0.969	0.995	0.051	0.968	0.966	0.957	0.994	0.990	0.631	-0.490	0.957	0.961	-0.148	0.018	0.090	0.753	-0.571	-0.305	-0.183	0.009	0.978	0.958	0.927	-0.029	-0.003	-0.003	0.951	0.959	0.992	0.974	0.968	0.807
Cl_dis	0.527	-0.180	0.547	-0.472	0.966	0.946	0.950	1.000	0.935	0.977	0.998	0.997	0.936	-0.178	0.972	0.962	0.994	0.931	0.920	0.742	-0.414	0.999	0.999	0.053	0.180	0.248	0.676	-0.611	-0.376	0.005	0.189	0.978	0.975	0.924	-0.312	-0.285	-0.285	0.956	0.971	0.906	0.995	0.997	0.841
Cr	0.670	0.068	0.730	-0.186	0.925	0.976	0.987	0.935	1.000	0.936	0.945	0.952	0.987	0.070	0.955	0.952	0.951	0.995	0.990	0.605	-0.478	0.941	0.944	-0.179	0.056	0.125	0.768	-0.608	-0.376	-0.208	-0.023	0.972	0.933	0.900	0.020	0.034	0.034	0.923	0.936	0.984	0.955	0.952	0.782
Cs	0.583	-0.085	0.641	-0.375	0.920	0.929	0.930	0.977	0.936	1.000	0.981	0.973	0.926	-0.083	0.943	0.935	0.991	0.927	0.918	0.699	-0.427	0.978	0.975	0.127	0.196	0.249	0.681	-0.586	-0.436	-0.029	0.166	0.951	0.935	0.892	-0.216	-0.194	-0.194	0.912	0.939	0.897	0.970	0.976	0.792
Cu	0.565	-0.129	0.574	-0.423	0.972	0.949	0.956	0.998	0.945	0.981	1.000	0.995	0.941	-0.127	0.964	0.952	0.997	0.939	0.926	0.763	-0.438	0.999	0.996	0.043	0.195	0.251	0.657	-0.602	-0.366	0.000	0.194	0.976	0.964	0.934	-0.272	-0.245	-0.245	0.941	0.959	0.917	0.995	0.994	0.813
ECond	0.547	-0.142	0.584	-0.436	0.966	0.965	0.969	0.997	0.952	0.973	0.995	1.000	0.957	-0.140	0.984	0.976	0.993	0.952	0.944	0.711	-0.417	0.998	1.000	0.012	0.142	0.217	0.708	-0.617	-0.374	-0.032	0.150	0.987	0.985	0.930	-0.259	-0.231	-0.231	0.969	0.981	0.931	0.999	1.000	0.852
Hardness	0.625	0.079	0.753	-0.198	0.910	0.996	0.995	0.936	0.987	0.926	0.941	0.957	1.000	0.081	0.964	0.967	0.945	0.995	0.997	0.567	-0.454	0.941	0.949	-0.166	-0.025	0.056	0.798	-0.561	-0.363	-0.220	-0.043	0.968	0.951	0.920	0.015	0.043	0.043	0.949	0.957	0.991	0.961	0.959	0.830
HCO3	0.530	1.000	0.580	0.913	-0.120	0.058	0.051	-0.178	0.070	-0.083	-0.127	-0.140	0.081	1.000	-0.170	-0.159	-0.103	0.079	0.101	-0.105	-0.088	-0.150	-0.154	-0.173	-0.140	-0.226	-0.104	0.244	0.036	-0.207	-0.137	-0.118	-0.208	0.097	0.882	0.919	0.919	-0.206	-0.184	0.155	-0.114	-0.129	-0.317
K	0.525	-0.171	0.592	-0.442	0.937	0.963	0.968	0.972	0.955	0.943	0.964	0.984	0.964	-0.170	1.000	0.998	0.966	0.963	0.959	0.596	-0.392	0.973	0.980	-0.050	0.074	0.180	0.789	-0.667	-0.387	-0.104	0.056	0.993	0.996	0.877	-0.213	-0.194	-0.194	0.993	0.997	0.938	0.980	0.984	0.878
K_dis	0.507	-0.161	0.611	-0.426	0.917	0.966	0.966	0.962	0.952	0.935	0.952	0.976	0.967	-0.159	0.998	1.000	0.955	0.963	0.963	0.552	-0.382	0.961	0.972	-0.073	0.027	0.140	0.822	-0.649	-0.401	-0.140	0.011	0.986	0.994	0.870	-0.189	-0.170	-0.170	0.995	0.997	0.938	0.972	0.977	0.897
Li	0.585	-0.105	0.610	-0.401	0.961	0.950	0.957	0.994	0.951	0.991	0.997	0.993	0.945	-0.103	0.966	0.955	1.000	0.946	0.934	0.738	-0.444	0.996	0.993	0.070	0.193	0.251	0.672	-0.609	-0.381	-0.017	0.181	0.977	0.962	0.920	-0.238	-0.213	-0.213	0.940	0.960	0.923	0.992	0.993	0.804
Mg	0.655	0.077	0.751	-0.190	0.918	0.984	0.994	0.931	0.995	0.927	0.939	0.952	0.995	0.079	0.963	0.963	0.946	1.000	0.998	0.576	-0.483	0.939	0.944	-0.162	0.013	0.091	0.783	-0.597	-0.342	-0.221	-0.034	0.973	0.945	0.895	0.033	0.051	0.051	0.940	0.949	0.994	0.957	0.954	0.792
Mg_dis	0.653	0.099	0.769	-0.171	0.898	0.986	0.990	0.920	0.990	0.918	0.926	0.944	0.997	0.101	0.959	0.963	0.934	0.998	1.000	0.535	-0.450	0.927	0.935	-0.169	-0.016	0.069	0.806	-0.590	-0.372	-0.234	-0.058	0.965	0.941	0.893	0.059	0.081	0.081	0.941	0.949	0.992	0.947	0.946	0.807
Mn	0.505	-0.107	0.179	-0.375	0.822	0.590	0.631	0.742	0.605	0.699	0.763	0.711	0.567	-0.105	0.596	0.552	0.738	0.576	0.535	1.000	-0.380	0.750	0.719	0.221	0.540	0.483	0.036	-0.414	-0.063	0.386	0.600	0.660	0.613	0.752	-0.424	-0.392	-0.392	0.548	0.579	0.577	0.721	0.700	0.347
Mo	-0.068	-0.089	-0.540	-0.071	-0.419	-0.446	-0.490	-0.414	-0.478	-0.427	-0.438	-0.417	-0.454	-0.088	-0.392	-0.382	-0.444	-0.483	-0.450	-0.380	1.000	-0.427	-0.402	0.253	0.369	0.442	-0.339	-0.183	-0.535	0.611	0.359	-0.407	-0.386	-0.331	-0.124	-0.096	-0.096	-0.366	-0.369	-0.514	-0.447	-0.407	-0.209
Na	0.552	-0.152	0.564	-0.449	0.972	0.950	0.957	0.999	0.941	0.978	0.999	0.998	0.941	-0.150	0.973	0.961	0.996	0.939	0.927	0.750	-0.427	1.000	0.998	0.054	0.188	0.253	0.667	-0.616	-0.361	0.006	0.196	0.981	0.974	0.927	-0.286	-0.259	-0.259	0.954	0.969	0.917	0.997	0.997	0.824
Na_dis	0.541	-0.156	0.570	-0.452	0.964	0.958	0.961	0.999	0.944	0.975	0.996	1.000	0.949	-0.154	0.980	0.972	0.993	0.944	0.935	0.719	-0.402	0.998	1.000	0.036	0.160	0.234	0.698	-0.619	-0.387	-0.009	0.170	0.984	0.982	0.929	-0.281	-0.252	-0.252	0.966	0.979	0.920	0.998	0.999	0.852
N_NH3_dis	0.058	-0.176	-0.158	-0.357	-0.011	-0.155	-0.148	0.053	-0.179	0.127	0.043	0.012	-0.166	-0.173	-0.050	-0.073	0.070	-0.162	-0.169	0.221	0.253	0.054	0.036	1.000	0.572	0.549	-0.364	-0.141	-0.148	0.668	0.713	-0.056	-0.025	-0.070	-0.411	-0.389	-0.389	-0.057	-0.020	-0.199	0.002	0.022	-0.162
N_TK_dis	0.492	-0.142	-0.319	-0.298	0.289	-0.037	0.018	0.180	0.056	0.196	0.195	0.142	-0.025	-0.140	0.074	0.027	0.193	0.013	-0.016																								